International Journal of MECHANICAL SCIENCES

Volume 1, 1960

Vol. 1
1960

Editor-in-Chief

W. JOHNSON
(United Kingdom)

Regional Editors

W. RUPPERT
(Germany)

H. KUDO
(Japan)

PERGAMON PRESS

OXFORD • LONDON • NEW YORK • PARIS

INTERNATIONAL JOURNAL OF MECHANICAL SCIENCES

EDITORS

UNITED KINGDOM

W. Johnson (*Editor-in-Chief*), *Engineering Department, The University, Manchester* 13, *England*

GERMANY

W. Ruppert, *Frankfurt a. M., Glaubergstrasse* 22, *Germany*

JAPAN

H. Kudo, *Aeronautical Research Institute, University of Tokyo, Tokyo, Japan*

HONORARY EDITORIAL ADVISORY BOARD

C. B. Biezeno, *Delft*
P. F. Chenea, *Lafayette*
D. G. Christopherson, *London*
W. J. Duncan, *Glasgow*
R. H. Evans, *Leeds*
G. Ford, *Alberta*
A. M. Freudenthal, *Columbia*
S. Fukui, *Tokyo*
A. J. Gould, *Natal*
R. Grammel, *Stuttgart*
A. S. Hall, *Purdue*
J. P. den Hartog, *M. I. T.*
R. M. Haythornthwaite, *Ann Arbor*
P. G. Hodge, *Illinois Inst. Tech.*
N. J. Hoff, *Stanford*
J. H. Horlock, *Liverpool*
G. A. Horvay, *Schenectady*
J. A. Hrones, *Case*
C. F. Kettleborough, *Auckland*
J. Kolakowski, *Czestochowa*
J. Marin, *Penn. State*
D. Mordell, *McGill*
H. C. Rothbart, *New York*
B. W. Shaffer, *New York*
M. Shaw, *Queensland*
M. C. Shaw, *M. I. T.*
M. F. Spotts, *Northwestern*
W. T. Thomson, *UCLA*
L. C. Woods, *Sydney*

Sub-Editor: N. S. Barrett, *Journals Department, Pergamon Press Ltd., Headington Hill Hall, Oxford, England*

Publishing Offices: Headington Hill Hall, Oxford, England (Oxford 64881)

Published bi-monthly.

Subscriptions (including postage): (A) for libraries, government departments or industrial establishments, £7 0s. 0d. (U.S.A. $20.00) *per volume*; (B) for subscribers who write directly to the publisher certifying that the journal is for their personal use, £5 5s. 0d. (U.S.A. $15.00) *per annum*.

Single issues £2 10s. 0d. (U.S.A. $9.00) each.

Copyright © 1960 Pergamon Press Ltd.

PERGAMON PRESS LTD.

Headington Hill Hall, Oxford, England 122 East 55th Street, New York 22, N.Y.

LIST OF CONTENTS

Vol. 1
1960

Number 1

PAGE

G. T. VAN ROOYEN and W. A. BACKOFEN: A study of interface friction in plastic compression 1

R. I. TANNER and W. JOHNSON: Temperature distributions in some fast metal-working operations 28

R. R. ARCHER: Small vibrations of thin incomplete circular rings 45

H. KUDO: An upper-bound approach to plane-strain forging and extrusion—I 57

J. L. LIVESEY: Inertia effects in viscous flows 84

MILTON C. SHAW: The economics of stepless machine-tool drives 89

H. LIPPMANN: Elementary methods for the analysis of certain forging processes 109

J. HEYMAN: On the minimum-weight design of a simple portal frame 121

B. W. SHAFFER: A realistic evaluation of the factor of safety of a bolted bracket 135

Papers to be published in future issues 144

Numbers 2/3

J. C. CHAPMAN, BURTON ERICKSON and N. J. HOFF: A theoretical and experimental investigation of creep buckling 145

W. JOHNSON and H. KUDO: The use of upper-bound solutions for the determination of temperature distributions in fast hot rolling and axi-symmetric extrusion processes 175

P. B. NEAL: The "off" boundary condition in hydrodynamically lubricated convergent–divergent slider bearings 192

R. I. TANNER: Full-film lubrication theory for a Maxwell liquid 206

P. B. MELLOR: The ultimate strength of thin-walled shells and circular diaphragms subjected to hydrostatic pressure 216

H. KUDO: An upper-bound approach to plane-strain forging and extrusion—II 229

R. S. BENSON and W. A. WOODS: Wave action in the exhaust system of a supercharged two-stroke-engine model 253

S. KOBAYASHI, A. G. MACDONALD and E. G. THOMSEN: Some aspects of press forging 282

E. WHALLEY and R. F. MACKINNON: The design of pressure vessels subjected to thermal stress—III. Thermal shock 301

Book Reviews

Power Reactors 1959. (Reviewed by W. JOHNSON) 309

Proceedings of the Third U.S. National Congress of Applied Mechanics. (Reviewed by R. I. TANNER) 309

High Temperature Effects in Aircraft Structures. (Reviewed by W. JOHNSON) 310

First Steps in Heat Transfer, by J. SMALL. (Reviewed by W. JOHNSON) 311

Number 4

PAGE

L. C. Woods: On the theory of ventilated wind tunnels 313

A. A. Gvozdev: The determination of the value of the collapse load for statically indeterminate systems undergoing plastic deformation (translated from the Russian by R. M. Haythornthwaite) 322

W. Johnson and H. Kudo: The compression of rigid–perfectly-plastic material between rough parallel dies of unequal width 336

Ferdinand Freudenstein: On the dynamics of high-speed cam profiles 342

R. P. N. Jones: The effect of small changes in mass and stiffness on the natural frequencies and modes of vibrating systems 350

J. F. Ely and O. C. Zienkiewicz: Torsion of compound bars—A relaxation solution 356

Hideaki Kudo: An upper-bound approach to plane-strain forging and extrusion—III 366

E. Whalley and S. Morris: The design of pressure vessels subjected to thermal stress—IV. Multilayer vessels 369

E. Whalley: The design of pressure vessels subjected to thermal stress (Review) 379

Letters to the Editor:

F. R. E. Crossley and U. Germen: On the response of the singly free linear oscillator 396

R. I. Tanner: Comment on "Small vibrations of thin incomplete circular rings" 397

Book Reviews:

Steam Power Plants, by Charles Donald Swift. (Reviewed by D. J. Riley) 398

Industrial Thermal Insulation, by A. C. Wilson. (Reviewed by A. Williams) 398

Energy Principles in Applied Statics, by T. M. Charlton. (Reviewed by M. G. Derrington) 399

Problems in Strength of Materials, by R. S. Paradise and G. A. Church. (Reviewed by M. G. Derrington) 400

Principles and Use of Surveying Instruments, by J. Clendinning. (Reviewed by S. Raymond) 400

AUTHOR INDEX

(B.R. indicates a Book Review)

Archer R. R. 45
Backofen W. A. 1
Benson R. S. 253
Chapman J. C. 145
Crossley F. R. E. 396
Derrington M. G. (B.R.'s) 399, 400
Ely J. F. 356
Erickson B. 145
Freudenstein F. 342
Germen U. 396
Gvozdev A. A. 322
Haythornthwaite R. M. 322
Heyman J. 121
Hoff N. J. 145
Johnson W. 28, 175; (B.R.'s) 309, 310, 311; 336
Jones R. P. N. 350
Kobayashi S. 282
Kudo H. 57, 175, 229, 336, 366
Lippman H. 109
Livesey J. L. 84
MacDonald A. G. 282
Mackinnon R. F. 301
Mellor P. B. 216
Morris S. 369
Neal P. B. 192
Raymond S. (B.R.) 400
Riley D. J. (B.R.) 398
Rooyen G. T. van 1
Shaffer B. W. 135
Shaw Milton C. 89
Tanner R. I. 28, 206; (B.R.) 309; 397
Thomsen E. G. 282
Whalley E. 301, 369, 379
Williams A. (B.R.) 398
Woods L. C. 313
Woods W. A. 253
Zienkiewicz O. C. 356

Vol. 196

Int. J. Mech. Sci. Pergamon Press Ltd. 1960. Vol. I. pp. 1–27. Printed in Poland

A STUDY OF INTERFACE FRICTION IN PLASTIC COMPRESSION

G. T. VAN ROOYEN * AND W. A. BACKOFEN †

(*Received* 25 *February* 1959)

Summary—An experimental study was made of friction over the interface between a cylindrical specimen and loading platen during plastic compression. The variations of normal pressure, shear stress, and friction coefficient were determined using a pair of pressure-sensitive pins installed in a platen so that at least one was oblique to the interface. Experiments were made on aluminum, primarily, with some carried out on copper and iron. Lubricant coverage included an absence of lubrication, solid films (lead foil, molybdenum disulphide, soap, teflon), and liquids (mineral oil with and without fatty-acid additions).

A simple calculation of the friction hill assuming constant friction coefficient, or a lubricant film of constant shear strength, and homogeneous compression, was valid only for the restricted conditions of low coefficient (or low shear strength) and small reduction. With increasing reduction, deformation became non-homogeneous and ubricant-film breakdown began at the periphery of the specimen. It was concluded that failure started as a consequence of increasing interface area and abrasion from displacement over the platen face.

For different conditions of lubrication, friction coefficient was found to vary, below a maximum of approximately 0·5, with both reduction and location in the interface. The results could be rationalized in terms of relative changes in interface shear stress and material flow pressure.

Vol. 1
1960

INTRODUCTION

BOTH the theory and practice of plastic-working operations can benefit from improved understanding of conditions in the tool-metal interface. In the study of this problem, however, it is important that information be obtained in a direct experimental manner without reliance upon a previous theoretical analysis of the mechanics of a particular operation. In previous work the normal pressure and its variation over a tool-metal interface have been determined experimentally using the pressure-sensitive pin technique.[1–6] Recent work has also led to mean values of friction coefficient directly from measurement of forces on the tools.[7–9]

An earlier paper described a study of cold rolling in which the distribution of normal pressure, interface shear stress, and friction coefficient over the contact arc were determined for limited conditions of testing with a procedure using a pair of pressure-sensitive pins mounted in a roll, one normal and the other inclined to the interface.[10] The method has

* National Mechanical Engineering Research Institute, South African Council for Scientific and Industrial Research, Pretoria.

† Massachusetts Institute of Technology, Cambridge 39, Massachusetts.

now been refined, simplified, and made more precise. Results of further and more extensive study under experimentally less complex conditions are reported in this paper.

EXPERIMENTAL PROCEDURES

Basis of Measurement

A cylindrical specimen is positioned on a platen fitted with normal and oblique pins so that both pins make contact at the same radius. During compression, therefore, the normal pressure and the tangential, or friction-induced, shear stress are the same on each pin. Fig. 1 shows schematically the forces acting on the pins, and Table 1 contains definitions of important symbols. As noted below, the pins are elastically less stiff than the platen. Accordingly, since each is generally pressed against the wall of its recess, a friction force, directed as shown in Fig. 1, acts along the pin axis.

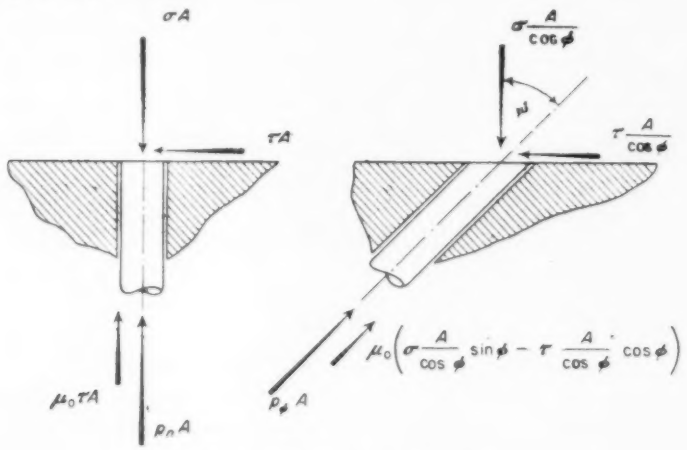

Fig. 1. Forces acting on pins.

A consideration of equilibrium along each pin axis indicates how the determination of p_n and p_φ is translated into a friction coefficient. For the normal pin

$$\frac{p_n}{\sigma} = 1 - \mu_0\mu . \tag{1}$$

For the oblique pin, with $\mu < \tan\varphi$,

$$\frac{p_\varphi}{\sigma} = 1 + \tan\varphi(\mu - \mu_0) + \mu_0\mu . \tag{2}$$

Finally,

$$\frac{p_\varphi}{p_n} = \frac{1 + \tan\varphi(\mu - \mu_0) + \mu_0\mu}{1 - \mu_0\mu} . \tag{3}$$

TABLE 1. DEFINITION TERMS

σ = normal pressure between specimen and platen at any point in the interface; also, the hydrostatic pressure in calibration tests.
τ = friction-induced shear stress in the interface at any point where the normal pressure = σ.
μ = friction coefficient, τ/σ; definition used regardless of whether sticking or sliding occurs over the interface.
A = cross-sectional area of a pin.
p_n = stress in the normal pin.
p_φ = stress in the oblique pin inclined at angle φ to platen normal towards center of compression specimen, as shown in Fig. 1.
p_φ^* = stress in the oblique pin inclined at angle φ to platen normal in the direction opposite to that shown in Fig. 1.
$\bar{p}$ = mean pressure over specimen-platen interface; (total load)/(area of interface).
μ_0 = friction coefficient between pin and platen.
σ_y = yield stress in homogeneous compression.
τ_y = yield stress in shear.
σ_h = hydrostatic stress at any point in the interface, representing the friction hill.
h = thickness
d = diameter
r = radius
R = reduction in thickness, $(h_0-h)/h_0$
Subscript 0 indicates initial dimensions.

which forms the basis of a measurement of μ. Equations (1) and (2) are represented graphically in Fig. 2 for various values of μ and μ_0 with $\varphi = 45°$.

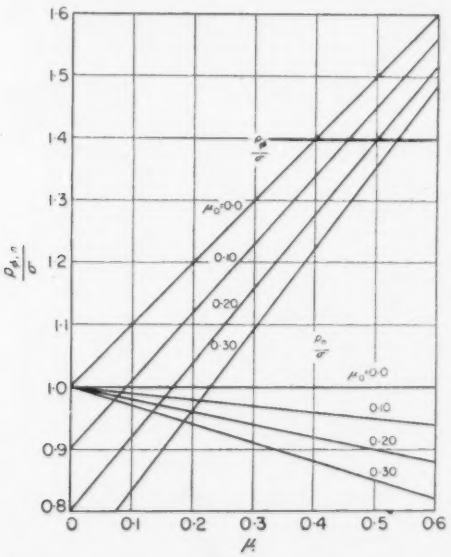

Fig. 2. Graphical solutions of equations (1) and (2) for different values of μ_0, with $\varphi = 45°$.

An alternative pin arrangement, with certain advantages to be described later, consists of two oblique pins contacting the specimen at

the same radius. One is inclined at angle φ towards the center of a specimen (Fig. 1), while the other is also inclined at angle φ but in the opposite direction. A derivation similar to the above requires equation (2) and, for $\mu < 1/\tan\varphi$,

$$\frac{p_\varphi^*}{\sigma} = 1 - \tan\varphi(\mu + \mu_0) - \mu_0\mu \tag{4}$$

which gives

$$\frac{p_\varphi}{p_\varphi^*} = \frac{1 + \tan\varphi(\mu - \mu_0) + \mu_0\mu}{1 - \tan\varphi(\mu + \mu_0) - \mu_0\mu}. \tag{5}$$

Apparatus

Pin design. The design finally evolved for an oblique-normal pair is shown in Fig. 3. Both pin diameters were 1/8 in., $\varphi = 45°$, and centers in the

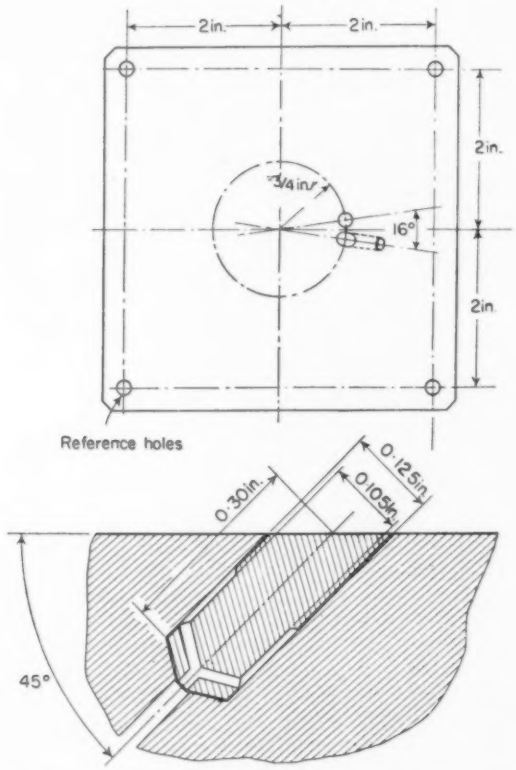

Fig. 3. Location of pins in platen with a cross-sectional view of an oblique pin.

platen surface lay on a circle of 3/4-in. radius around the mid-point of the platen. Four reference holes in the platen permitted accurate positioning of a specimen relative to the location of the pins. The alternative pair of oblique pins had diameters of 3/32 in. with $\varphi = 30°$; the planes

of the platen normal and pin axes were parallel, with pin centers in the platen surface spaced 3/16 in. apart.

Platens and pins alike were made from a machinable grade of hardened and tempered steel of Rockwell hardness C 30. All pins were lapped into position to obtain a precision fit with maximum diametral clearance of 0·0001 to 0·0002 in.; larger clearance was avoided to prevent the possibility of specimen material extruding into the annular space between pin and platen. After fitting, the pins were loaded to the highest anticipated level, and then the pin-platen assembly was ground flush over the pressing surface.

Axial force on the pin was measured with a wire-resistance strain gage. A conventional SR-4 type gage was disassembled by immersing in acetone, and enamelled copper-lead wire was soldered to the ends of the resistance element. The wire was then wrapped and glued on a thin paper base around the reduced section of the pin. A 3/32 in. diameter oblique pin ($\varphi = 30°$) is shown in Fig. 4 with the gage glued in place.

Vol. 1
1960

Fig. 4. Oblique pin showing strain gage in position; ×12.

Instrumentation. A commercial Speedomax unit was used for the graphical recording of all electrical signals. The gage on each pin of a pair was connected with three others of conventional type mounted on a cantilever to form a Wheatstone bridge which could be balanced initially by deflect-

ing the cantilever. The end of a third cantilever, fitted with two active gages joined with two dummy gages to form another bridge, was brought into contact with the moving platen to measure distance between platens. During an experiment, the three signals were placed on the same record with a circuit in which all bridges were connected in parallel with a common power supply, while three small relays were used to deliver, in turn, the output of each bridge to the recorder. The three relays were operated at such speed that each bridge was connected to the recorder for about 2 sec. With an average pressing speed of approximately 0·02 in./min, there was ample time for a clear indication of bridge output. Accordingly, all signals passed through the same d.c. amplifier (chopper stabilized) to the same recorder. During hydrostatic calibration of the pins, described in the following section, a load cell for measurement of the hydrostatic pressure was substituted for the cantilever measuring platen displacement; otherwise, an identical procedure was followed in using the recording equipment.

Calibration of pins. The calibration served two purposes. It provided the value of μ_0 for an oblique pin, and it correlated the chart record with pin pressure: p_n, p_φ, p_φ^*.

Initially, both normal and oblique pins were calibrated in the platen by loading in a direction normal to the platen surface through a strain-gage dynamometer fitted with a small projection placed on the pins. Procedure was essentially the same as that previously described.[10] Because of the frictional force along the oblique-pin axis, a given signal or strain in the pin was associated with load p_1 upon direct loading and load $p_2 < p_1$ during unloading. Therefore

$$\mu_0 = \frac{p_1 - p_2}{(p_1 + p_2)\tan\varphi}. \tag{6}$$

The value of μ_0 so determined applied rigorously only to the oblique pin, for which precision in μ_0 is especially important as made clear by consideration of equation (2) or its graphical representation in Fig. 2. Therefore, in experiments with pairs of oblique and normal pins, the same value of μ_0 had to be taken for both pins. Because of the great similarity between the pin installations, such an assumption was considered reasonable over a broad range of experimental conditions.

Only when μ was large was the assumption of identical μ_0 no longer so tenable. To handle such conditions, the pin-platen assembly incorporating two oblique pins was constructed with which μ_0 could be measured for each pin. However, the very close agreement between μ values obtained with the two pieces of apparatus will be seen to give much support to the assumption of a common μ_0 for normal and oblique pins.

A potentially serious disadvantage to calibration by direct pin loading arose from the circumstance that both pin and platen faces were under

load during an experiment. The possibility existed, therefore, of a force system different from that shown in Fig. 1 if there was any binding interaction caused by elastic strain simultaneously in pin and platen. To insure that any complications of this kind were not overlooked, the pins were further calibrated extensively under hydrostatic pressure applied over an area on the platen comparable to that covered by a specimen.

A sectional view of the pressure chamber is shown in Fig. 5. Water containing a corrosion inhibitor filled the cavity, and was prevented

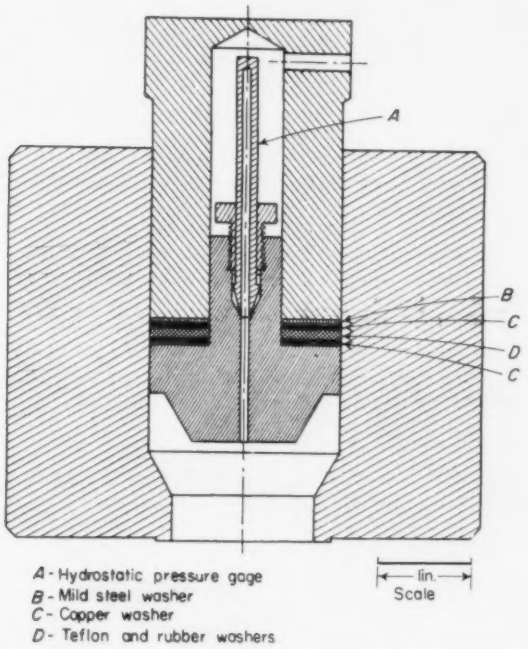

Fig. 5. Hydrostatic pressure cylinder.

from entering between pin and platen by covering the platen with a sheet of thin aluminum foil and another of plastic cloth. The gasket assembly tightly sealed the top of the chamber, since it transmitted all load between the two parts of the piston and was subjected to pressure higher than the hydrostatic level in the chamber. In similar fashion, the bottom was sealed to the platen by a design providing a contact pressure higher than the water pressure. Maximum pressure in calibration was approximately 60,000 p.s.i. A thick-walled tube, secured to the lower part of the piston assembly and fitted with two circumferentially mounted SR-4 strain gages served as a pressure indicator.

The procedure for evaluating μ_0 in hydrostatic calibration was basically that underlying the development of equation (6); for any given oblique-pin output, while loading and unloading along linear paths, substitution of

Vol. 1
1960

the outputs from either normal pin or hydrostatic pressure gage yielded the value of μ_0. Typical results of hydrostatic calibration testing with a normal and oblique ($\varphi = 45°$) pin, for widely different values of μ_0, are shown in Fig. 6. These plots illustrate that the pins were elastically less stiff than the platen, being depressed relative to the platen under

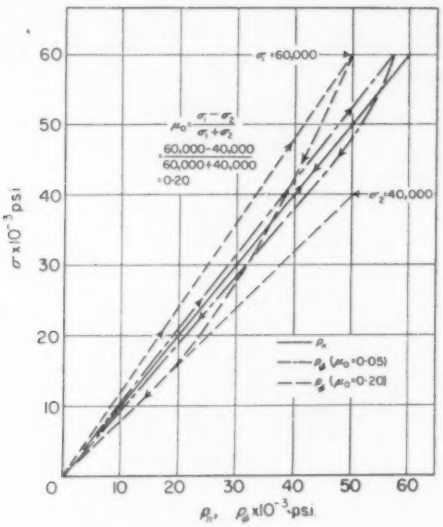

Fig. 6. Hydrostatic calibration results for normal and oblique pins ($\varphi = 45°$), showing method for evaluating μ_0.

load, and that there was no binding interaction between normal pin and platen when both were under load. The absence of binding between pins and platen was further confirmed by the compression of a specimen in which holes were drilled at the pin locations so that only the platen was under load; no pin response was detected, in contrast to the findings in previous work with such pins.[2,4,10] Thus experimental support is given the analysis based on the force systems represented in Fig. 1.

The curves for the oblique pin in Fig. 6, with $\mu_0 = 0{\cdot}20$, are representative of those obtained in the absence of any lubricant in the interface between pin and platen. After preliminary testing with liquid lubricants however, μ_0 decreased and became somewhat erratic due to the presence of test lubricant at the pin-platen interface. It was found that an application of MoS_2 in a resin carrier over the cylindrical surface of the pin resulted in a μ_0 value of approximately 0·05 which remained remarkably constant throughout all experiments. Removal of pins after a large number of experiments showed that the MoS_2 film was still intact. Accordingly, this practice of pin lubrication was generally followed; then experimental calibration points for plots such as those in Fig. 6 did not

deviate from a straight line by more than 1/4 per cent and the resulting value of μ_0 could be used with much confidence.

To estimate the accuracy with which μ was measured, uncertainty in μ can be taken as nearly the same as that in μ_0 so that error in μ will vary inversely with its magnitude. For a conservative estimate, uncertainty in μ_0 was 0·003. Consistent with this figure, for well-defined lubrication from solid films, μ was easily reproduced within 5 per cent at an average level of about 0·1. For an average of 0·01 (teflon film), the estimated error is 30 per cent, and, in experiment, μ could readily be reproduced within this figure. With fluid lubricants, values under nominally identical conditions could differ by greater amounts than estimated. For an average μ of 0·1, the variation now could rise to 15 per cent. But it is felt that the larger variation was not as much a consequence of experimental method as it was of local variations in friction over the interface. In compression with liquid and boundary-lubricant films, irregular and local departures from a cylindrical shape were occasionally observed which could only be explained by small-scale changes in friction.

Vol. 1
1960

Test Materials

The principal experimental material was Al of commercial purity, designation 1100F, obtained as rolled bar of 2 in. dia. Macro-etching revealed uniform, fine grain size, and the hardness across the section was essentially uniform at a level of Rockwell H 67. Any texture in the rod was highly symmetrical about the rod axis, so that upon compression parallel to the axis there was little deviation from round; after 30 per cent reduction, the deviation was not more than 0·010 to 0·015 in. in an initially 2-in.-dia. specimen. A true yield stress vs. reduction curve was obtained by axial compression of a 3-in. length of rod. The specimen was frequently re-lubricated, and after a reduction of 30 per cent was turned to a diameter of 1-3/8 in. before compressing further.

Most test specimens were prepared as discs of 0·500-in. thickness and 2-in. dia. by cutting directly from the rod. For reference purposes, such specimens are hereafter designated as of $d_0/h_0 = 4$. Other experiments were performed on discs of 0·10 in. thickness and 2·5-in. diameter, hereafter indicated with $d_0/h_0 = 25$. The latter were obtained by sectioning and turning after some of the 2-in.-dia. rod was compressed until a diameter slightly greater than 2·5 in. was produced.

Final surface preparation consisted of turning followed by polishing on 240 grit emery cloth, etching for approximately 5 min in Keller's reagent, then rinsing in hot water and drying in a clean hot-air blast. The ends of the finished specimens were parallel to within 0·0005 in., while thickness was maintained to $\pm 0{\cdot}0005$ in.

Some experiments were also made with annealed copper and Armco

iron specimens of $d_0 = 2$ in. and $h_0 = 0{\cdot}500$ in. ($d_0/h_0 = 4$). Details of preparation are noted in connection with the presentation of results.

The various lubricants examined are listed in Table 2.

Testing Details

To insure reproducible experimental conditions, the platen surfaces were abraded before each experiment with a fresh piece of emery cloth folded around a flat block and applied by hand with a circular motion. A random pattern of scratch marks was produced with a surface finish of 12 to 13 r.m.s. microinches. After abrading, the platen surface was wiped with a clean, dry cloth if no lubricant or solid lubricant was to be used, or wiped with a cloth dampened in the liquid lubricant to be tested.

TABLE 2. LUBRICATION

Lubricant	Remarks
Lead	Used as foil of 0·002 in. thickness overlapping the specimen.
MoS_2	Carried in resin base; sprayed onto specimen and air dried.
Soap	Specimen chemically treated to produce a chromate-phosphate base; then dipped into hot molten soap and air dried.
Teflon	Carried in resin base; brushed onto specimen and air dried.
Mineral oil	medicinal grade; poured on in excess.
5% oleic acid in mineral oil	Poured on in excess.
1% lauric acid in mineral oil	Poured on in excess.

Chart records of pin response to reduction were obtained only for the particular radius at which the pins were positioned. An additional test was required for information about any other location on the interface. Under all conditions, measurements at the 3/4-in.-radius position were made; for many, testing was also done at the 1/4-in., 1/2-in., and 9/10-in. positions.* Two or more tests were frequently carried out at the same location.

* Rigorously, equation (3) applies only when the pins contact a specimen at the 3/4-in. radius. With location at any other radius, the value of μ from equation (3) is in some error. The error will be found to increase with decreasing or increasing radius and increasing difference between μ and μ_0. Taking some extreme conditions for the present work, μ from equation (3) will be low by 3·5 per cent at the 1/4-in. position with $\mu = 0{\cdot}2$ and $\mu_0 = 0{\cdot}1$. No corrections were actually made, however, because of the negligible size of the error. Equation (5) holds at all radii if μ_0 is the same for both pins. The actual values of μ_0 proved to be approximately 0·05 and 0·07, sufficiently alike that correction was again avoided.

All experiments were conducted in a hydraulic testing machine of 200,000 lb capacity. When average platen pressure, $\bar{p}$, was compared with a value derived by integrating the normal pressure distribution records, agreement was within 5 per cent. Due to the small size of the pins in relation to the interface, no pressure correction was necessary for the finite size of the pins. Hydrostatic calibration was carried out at least after every third test and frequently after every second, so that any effect of lubricant on pin behavior would not be overlooked.

EXPERIMENTAL RESULTS

Effect of Pins on Metal Flow at the Interface

Only if pins and platen were equally stiff under all loads would the pins remain flush with the platen surface, and thus would be eliminated much of any possible interference with metal flow. From an experimental viewpoint, such a design appeared difficult, and the pins in the present work were depressed under load relative to the platen surface; by measurement with a microscope on a heavily compressed specimen, a depression (elevation on the specimen surface) of 0·0001 to 0·0002 in. or approximately 0·01 per cent of the pin diameter was found. No systematic study was made of the effects of various amounts of pin depression, for the aim was rather to minimize it.

Slight depression is least objectionable with no relative displacement, or sticking, between specimen and platen, or with a solid lubricant providing a continuous film over the interface. In the case of a M_0S_2 film, for example, the location of the pins on a specimen could not be detected after compression and removal of the film. With fluid lubricants, however, pin location could be found from a marking on the surface.

To observe any effect on deformation in the vicinity of a pin, specimens were compressed with oleic acid in mineral oil after a spiral V-groove had been machined across the specimen surface. Figure 7(a) is a photograph of the surface around an oblique pin following a reduction of 35 per cent. Although some trace of the pin can be seen, the lines are continuous with no distortion in the area of the pin. To show the effect of local variations in friction, a small spot of teflon to provide low friction was applied on a grooved surface which was then coated with mineral oil. The result, after only 15 per cent reduction, is pictured in Fig. 7(b); the distortion is clear, with greater surface displacement over the light area representing the teflon spot. Figure 7(c) shows the result of a small, high-friction spot, obtained by covering a specimen with lead sheet in which a hole had been cut; after the 15 per cent reduction, much distortion is observed with essentially no displacement having occurred over the light area representing the hole in the sheet.

The absence of distortion in experiments of the type producing Fig. 7(a) is considered reasonable evidence that pin depression, even

(a) (b) (c)

Fig. 7. Surfaces prepared with circular grids before compression under different conditions: ×15.
(a) area in contact with an oblique pin after a reduction of 35 per cent with oleic acid in mineral oil as lubricant, showing absence of distortion in circular grid marks.
(b) distortion around a low-friction teflon spot on a surface lubri cated with mineral oil.
(c) distortion around a high-friction bare spot on a surface other wise covered with lead foil.

Vol. 1
1960

in the presence of liquid lubricants, does not seriously influence local frictional conditions and deformation patterns. As further support, specimens compressed in pin tests with liquid lubricants increased uniformly in diameter with no movement of the original center point on the surface; if frictional variations were intentionally introduced, a change in position of the original center point could be observed.

Analytical Considerations of the Friction Hill

An analysis by Siebel,[11] incorporating assumptions of constant friction coefficient and homogeneous compression, is available for the prediction of pressure requirements during the reduction of a circular disc. Such calculations have been made, and values of μ for various lubricants have also been computed on this basis from measurements of mean tool pressure.[12] Although highly convenient, application is limited, and the restricted conditions of small reduction and low μ under which the analysis is valid are well illustrated with present data. Excellent agreement with experiment is found in Fig. 8 where normal pressure, σ, and μ are plotted as a function of radius for a 2 per cent reduction on specimens

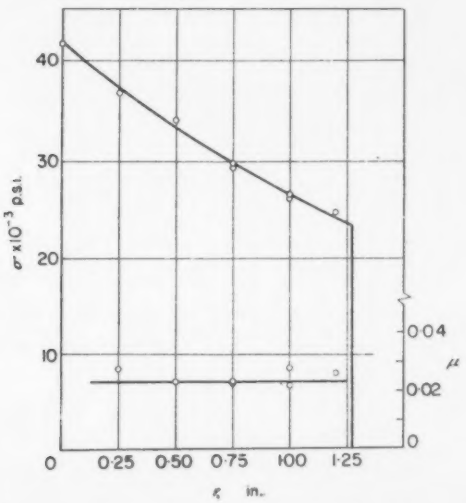

Fig. 8. Distribution of normal pressure and friction coefficient for 2 per cent reduction using soap on aluminum prepared with a chromate-phosphate base; $d_0/h_0 = 25$. Plotted points are from experiment while curve is drawn according to Siebel analysis for $\mu = 0{\cdot}022$.

of $d_0/h_0 = 25$ using the soap lubrication. The predicted normal pressure distribution is given by

$$\sigma = \sigma_y e^{\mu(d_0-2r)/h}$$

which yields the curve drawn in the figure for $\mu = 0{\cdot}022$. The fit to

experimental points, using a measured value of μ, gives further support to the reliability of the experimental method.

Another simple prediction for a lubricant film of low constant shear strength, τ, follows from the same analysis by substituting τ for the friction-induced interface shear stress, $\mu\sigma$. The equation is

$$\sigma = \sigma_y + \frac{\tau(d_0 - 2r)}{h}.$$

The data of Fig. 9 were obtained under conditions for which such an analysis could be expected to hold: lubrication with lead foil sticking to both platen and specimen surface for a 4 per cent reduction and $d_0/h_0 = 25$. Measured pressure is seen to increase linearly from the edge

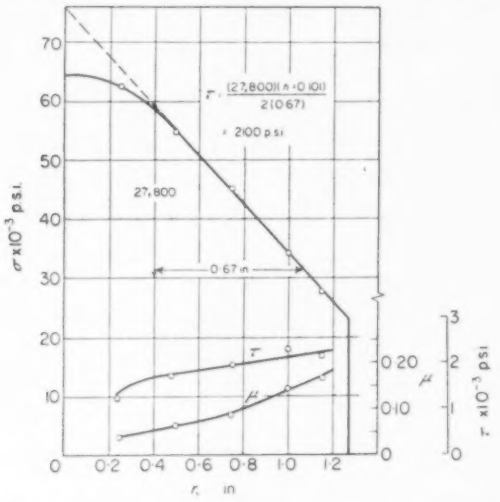

Fig. 9. Distribution of normal pressure, interface shear stress and friction coefficient for 4 per cent reduction with lead foil on aluminum; $d_0/h_0 = 25$.

as predicted, while the slope of this friction hill gives a value for $\tau = -(d\sigma/dr)(h/2)$ or 2100 p.s.i., both generally reasonable and in good agreement with the measured shear stress over a substantial distance from the edge. The increase with radius of the measured τ may be rationalized through some strain hardening, shear strain in the lead increasing with radius, and possibly a strain-rate effect, as the rate of straining would also increase along the radius.

If the analysis of Siebel were generally valid, all curves relating mean tool pressure to reduction for the different lubricants on specimens of given geometry would be expected to form an homologous family; two members of the family are shown as the dashed curves in Fig. 10, calculated using the yield stress curve for the aluminum with constant μ of 0·1 and 0·2. After small reductions, however, test results also presented

in Fig. 10 exhibit marked departures from such a prediction. Curve intersections do occur and friction coefficients deduced by matching experimental and calculated curves are in substantial variance with

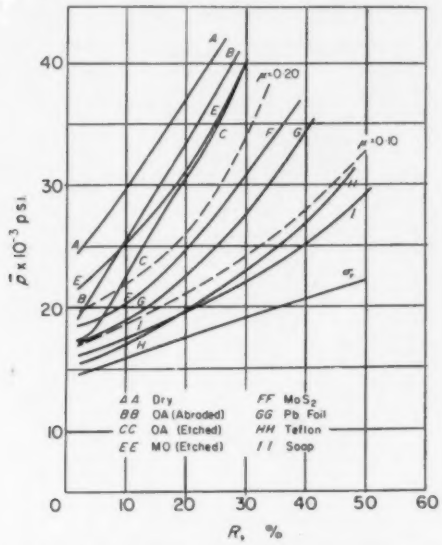

Fig. 10. Dependence of average platen pressure on reduction for various lubricants on Al; $d_0/h_0 = 4$. Curves drawn with dashed lines, are calculated from Siebel analysis. Curve *BB* relates to a test in which the specimen surface was abraded on emery cloth immediately before lubrication.
MO = mineral oil; OA = oleic acid in mineral oil.

local measurements. Discrepancies to be found are reasonably attributed to such analytical simplifications as invariant μ, unbroken lubricant film, and homogeneous compression.

Local Measurements

A finding of broad application for the type of loading under consideration is a variation in μ with both location in the interface and reduction. In presenting data which give the details of this finding, the conditions of lubrication are considered in terms of three general classes.

(i). *Solid films*

Lead foil. A relatively low and constant shear-strength film was established between specimen and platen due to the surface preparation resulting in foil sticking to each throughout the compression. Normal pressure and shear stress distributions are plotted for specimens of $d_0/h_0 = 4$ at several reductions in Fig. 11. *Vertical lines are drawn on the abscissa in all plots of this general type, and, in each case, a line indicates the radius to the edge after a particular reduction while the height represents the corresponding yield stress under homogeneous compression.*

Vol. 1
1960

Following compression, an annular region devoid of lead foil was found at the periphery of all surfaces. Its origin was associated with the initially overlapping foil having been cut off by the specimen under load at an early stage. During continued deformation, barreling occurred

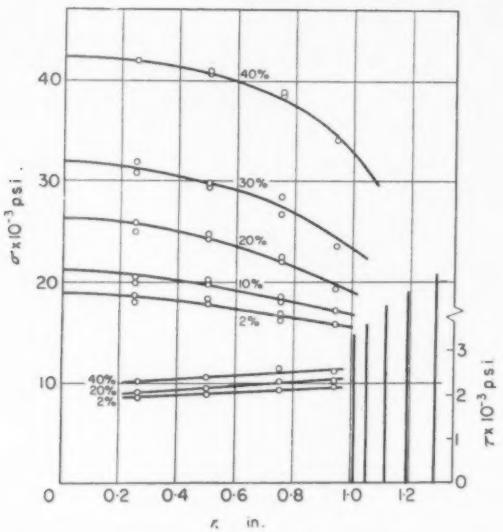

Fig. 11. Distribution of normal pressure and interface shear stress with lead foil as lubricant on Al for the different reductions noted; $d_0/h_0 = 4$.

with the barreled surface becoming part of the plane surface and the annular region of direct contact between Al and platen growing in extent. The effect of this film breakdown on normal pressure is illustrated in Fig. 12 with the distribution for a 41·5 per cent reduction and for an additional 1 per cent after recovering the surface with foil.*

Three zones could be distinguished on the surface subsequent to the continuous reduction. Throughout zone I the foil was intact and adhering tightly to the specimen. Zones II and III were indistinguishable to the eye, both blending as a region bare of foil. Abutting the visible foil, however, in zone II, Al was present only as a thin film, being folded over a sub-surface layer of lead easily revealed by peeling away the covering of Al. In zone III, lead was entirely absent.

Direct contact between Al and platen led to high friction coefficient and rapidly increasing normal pressure, not only confined to this region (zones II and III), however, but extending far in over the interface

* The slope of the friction hill over the relubricated specimen of Fig. 11, treated like that of Fig. 9, also yields a value of τ_y for lead of approximately 2100 p.s.i. Conditions here are similarly reasonable for assuming an essentially constant shear strength film over the interface.

covered by lead (zone I). The friction coefficient in zones II and III must have been high; from reference to other experiments with no lubrication, it would have been approximately 0·5. A consequence was highly non-homogeneous deformation which must also have contributed to this form of normal pressure distribution. To reveal the nature of the deformation, specimens were prepared with fine spiral grooves making

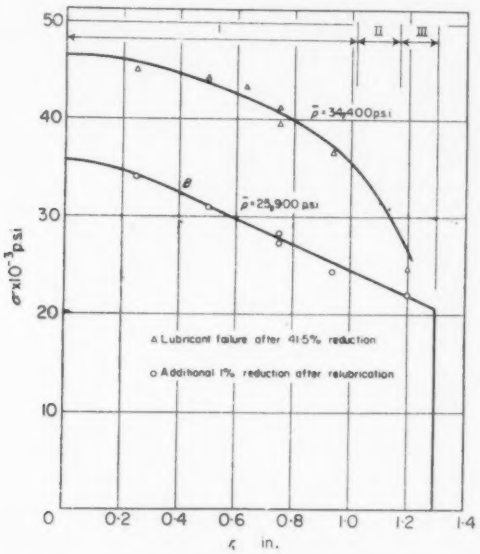

Fig. 12. Normal pressure distribution with lead foil on Al ($d_0/h_0 = 4$) for continuous reduction of 41·5 per cent and after recovering with foil for an additional reduction of 1 per cent. Numerals I, II and III refer to surface zones discussed in text.

equally spaced reference marks, as those described in connection with Fig. 7, covered with lead foil, and then compressed. Measurements of groove spacing after different reductions are summarized in Fig. 13. They show clearly that there was very little surface displacement, or essentially a condition of sticking prevailed, at the boundary of the area where the lead foil terminated (zone III) and friction was high. With increasing reduction, the spacing in this vicinity actually decreased after an initial increase. In effect, the surface was compressed against a high-friction barrier. Upon crossing into zone I, the spacing reached a maximum. Material from this location was required to move over the more or less rigid barrier, consistent with the observed fold formation on the surface (zone II). Then constant spacing was found, which increased with reduction about as rapidly as required for homogeneous compression. Finally, a marked drop was observed which could also be associated with non-homogeneous deformation in the form of a relatively non-plastic central zone.

Vol. 1
1960

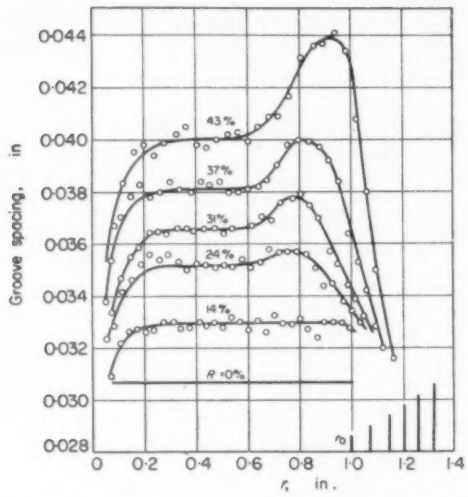

Fig. 13. Radial variation of spacing between spiral-cut grooves, initially equidistant, on specimens compressed, different amounts after lubrication, with lead foil. Vertical lines on abscissa represent the radius after each reduction.

Molybdenum disulphide. Variation in μ with both reduction and location is demonstrated in Fig. 14, with an explanation for some of the trends found in Fig. 15. For the range of reductions in Fig. 15, the shear stress in the film was, on the whole, measured to be even slightly higher than the strength in shear of the lead foil (Fig. 11). Peripheral

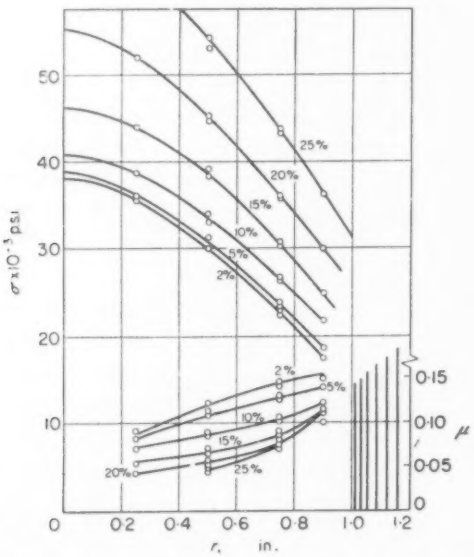

Fig. 14. Distribution of normal pressure and friction coefficient at different reductions on Al with MoS_2 as lubricant; $d_0/h_0 = 10$.

breakdown with fold formation was again observed. Well removed from this region, however, at radii of 1/4 in. and 1/2 in., the stress in the film decreases approximately 30 per cent to the maximum reduction. Due

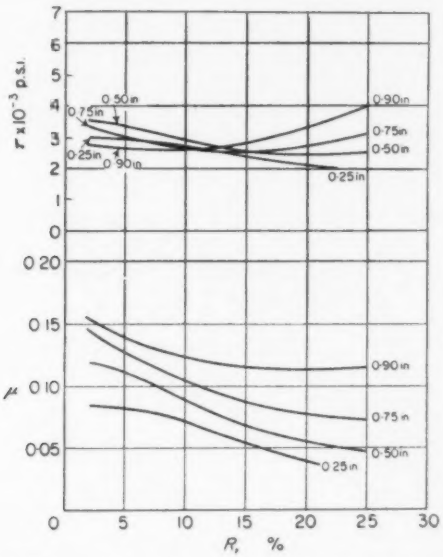

Fig. 15. Variation with reduction of interface shear stress and friction coefficient at different radii with MoS_2 as lubricant on Al; $d_0/h_0 = 10$.

to film failure, the decrease occurred only to about 15 per cent reduction at 3/4 in., and was almost negligible at the 9/10-in. radius. Such a film-strength characteristic is attributed to the hexagonal structure of the MoS_2. With film movement over the platen, the particles are thought to have become oriented with the easy-shearing basal planes parallel to the interface. Then, as the extent of alignment increased with the displacement accompanying increased reduction, the shear stress supported by the film could be expected to decrease in the observed manner.

(ii). *Unlubricated conditions*

Unlubricated specimens and platens provided a set of complex, but at least moderately well-defined, test conditions. From surface-marker studies, essentially no displacement of the specimen surface relative to the platens was found to occur, or, a condition of sticking prevailed. Variations in normal pressure and μ across the interface under such conditions are shown in Fig. 16. These data were obtained in experiments using an oblique pair of pins for reason of the generally high friction. However, other tests with an oblique-normal pair at the 3/4-in.-*radius* position produced essentially the same findings. Dependence of τ in Fig. 17 on both reduction and position indicates plastic shearing over the interface,

although at a stress higher than τ_y, taken to be one-half the homogeneous compression yield stress.

Solutions for normal pressure distribution when complete sticking exists are available only for the condition of plane strain. The prediction by Prandtl[13] of a linear increase with distance inward from the free edge

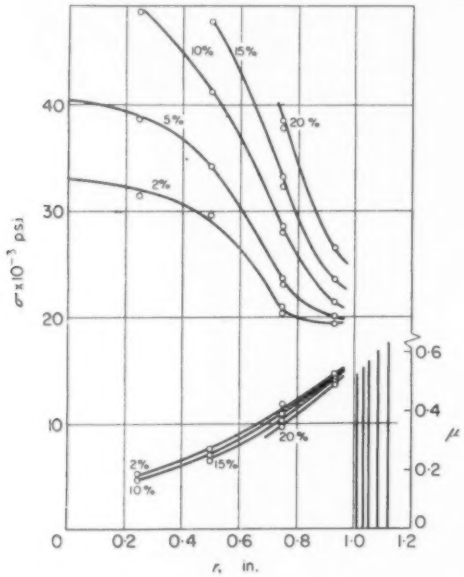

Fig. 16. Distribution of normal pressure and friction coefficient for various reductions on unlubricated aluminum; $d_0/h_0 = 4$.

is a considerable departure from the distributions in Fig. 16. The observed plateau near the edge for the 2 per cent reduction, however, is a characteristic of the solution by Hill, Lee and Tupper.[14] According to the latter, the plateau pressure level is given by $\tau_y(1+\pi/2)$. Application of this solution is admittedly tenuous for reasons of the small d_0/h_0 and absence of plane strain. Yet, if τ_y is taken to be $0{\cdot}5\sigma_y$, the calculated pressure at the edge for 2 per cent reduction is 19,000 p.s.i., compared with the measured value of 19,400 p. s. i.

The generally large differences in Fig. 17 between measured interface shear stress and τ_y from homogeneous compression may be rationalized to a considerable extent at least by the marked departure from homogeneous compression. Microhardness-traverses along normals to the surface at different radii and for a reduction of 20 per cent (Fig. 18) showed the surface layers at the larger radii to have been strain-hardened to a greater extent than the bulk of the specimen. At the low radius of 0·23 in., hardness increased with distance below the surface, suggesting the existence in this region of a relatively non-plastic zone. Over this

zone, as Fig. 17 shows, measured interface shear stress is below τ_y at the lower reductions.

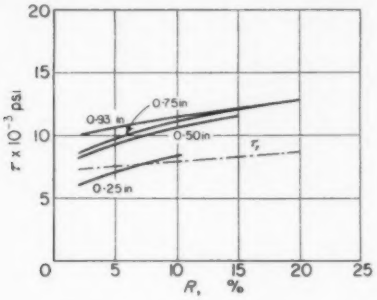

Fig. 17

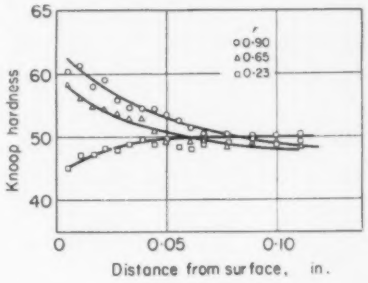

Fig. 18

Fig. 17. Variations of interface shear stress with reduction at different radii in the compression of unlubricated Al; $d_0/h_0 = 4$. $\tau_y = 0{\cdot}5\sigma_y$ for homogeneous compression.

Fig. 18. Microhardness variation along a direction normal to the interface at different radii in an aluminum specimen compressed 20 per cent without lubricant; $d_0/h_0 = 4$.

(iii). *Liquid lubricants*

Detailed tests were made with oleic acid in mineral oil on Al which gave results summarized in Figs. 19 and 20. A number of experiments were also made with Al in which data were obtained only at the 3/4-in.-radius position on specimens of $d_0/h_0 = 4$. Such was the practice for straight

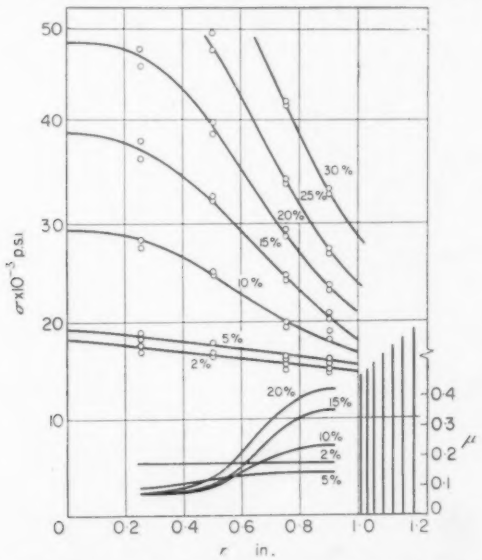

Fig. 19. Distribution of normal pressure and friction coefficient at different reductions on Al lubricated with oleic acid in mineral oil; $d_0/h_0 = 4$. Due to the close proximity of curves no experimental points for μ are shown.

Vol. 1
1960

mineral oil, lauric acid in mineral oil, and oleic acid in mineral oil used with specimens abraded on emery cloth (in contrast to the usual final etch) before lubricating. The reduction dependence of τ and μ from these experiments is plotted in Fig. 21 along with results for the 3/4-in.-radius position from various other tests.

All data in Figs. 19, 20 and 21 for liquid lubricants on Al were obtained with an oblique-normal pair of pins. Experiments were also made at a 3/4-in. radius using the oblique pair, with no significant difference in results.

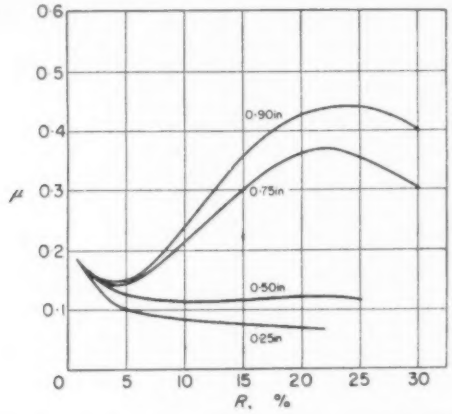

Fig. 20. Friction coefficient vs. reduction at different radius positions with oleic acid in mineral oil on Al; $d_0/h_0 = 4$.

Fig. 22 contains the results of limited testing on Armco iron and copper ($d_0/h_0 = 4$), similarly at the 3/4-in.-radius position. All specimen surfaces were abraded with 240-grit emery cloth in preparation. Those to be tested with oleic acid in mineral oil were also oxidized by heating in air: copper for 15 min at 300°C, and iron for 15 min at 450°C. In all experiments, use was made of an oblique pair of pins.

By far the most marked dependence of μ on both reduction and position was encountered under conditions of boundary lubrication with fatty acids in mineral oil. From the combined data in Figs. 19–22, the variation with reduction seems logically regarded as involving three stages.

Stage I. The value of μ, effectively uniform over the interface initially, dropped as reduction began. Tests with both oleic acid and lauric acid on an etched Al surface (Figs. 19, 20 and 21) provided the strongest ndication of such behavior; the lowering of μ was sufficiently abrupt to result in a noticeable drop in platen load at the onset of deformation. Although less marked, a similar decrease in μ occurred with lauric acid and oleic acid on abraded surfaces of copper and iron (Fig. 22).

This first stage appeared much influenced by surface preparation; it was absent at the 3/4-in. radius with oleic acid on abraded Al (Fig. 21), while it was more extensive for oleic acid on iron that had been thermally

oxidized prior to testing, yet was absent again in the case of copper lubricated with oleic acid after a thermal treatment (Fig. 22). A reasonable basis for explanation would seem to be the importance, established by rider-and-plate studies,[15] of oxide films in the reaction of fatty acids with metal surfaces to produce effective boundary lubrication. The

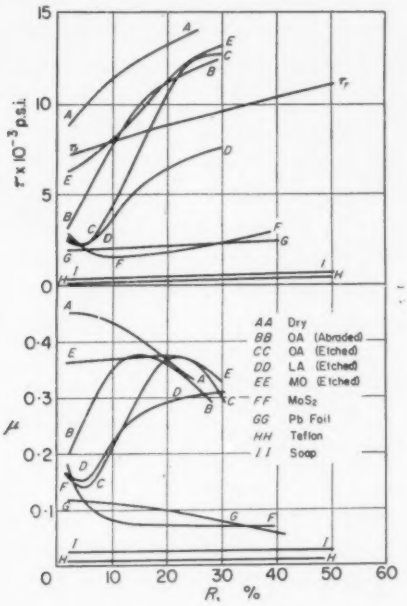

Fig. 21

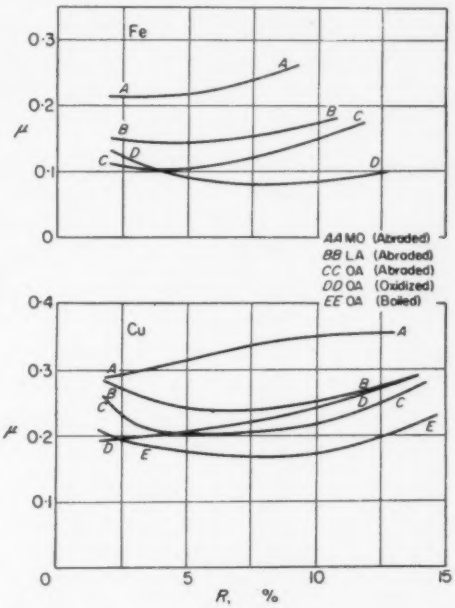

Fig. 22

Fig. 21. Variation with reduction of interface shear stress and friction coefficient at 3/4-in.-radius position for various lubricants on Al; $d_0/h_0 = 4$.

MO = mineral oil
OA = oleic acid in mineral oil
LA = lauric acid in mineral oil

Fig. 22. Friction coefficient at 3/4-in.-radius position vs. reduction for iron and copper; $d_0/h_0 = 4$. Boiled sample immersed in boiling water for 5 min before test.

MO = mineral oil
OA = oleic acid in mineral oil
LA = lauric acid in mineral oil.

observations may correlate with some removal of oxide from the Al, a thickening of the oxide on iron, and the production of a weakly adherent oxide on the copper.

Stage I appeared further to result from the presence of fatty acid, being absent when the acid was omitted under conditions otherwise associated with its occurrence (Figs. 21 and 22). The origin may well be found in the beginning of deformation, enlarging surface area and thus facilitating penetration of lubricant and its reaction with the surface.

Stage II. Depending upon position at the interface, μ either remained essentially constant with further reduction, giving a stage II range (1/4- and 1/2-in. radius, Fig. 20), or passed through a more or less flat minimum to give a narrower and less well-defined range (3/4- and 9/10-in.-radius position, Figs. 20 and 22), a characteristic in rather sharp contrast to the insensitivity of stage I to location. By machining fine spiral grooves over the surface before lubrication, the total reduction dictated by testing-machine capacity, and the reduction range for stage II behaviour, could be substantially increased. Although an experiment on a gross scale, it did indicate the importance of surface condition in a mechanical sense. The experiment with oxidized, as opposed to abraded, iron surfaces showed an increase in stage II (Fig. 22); the nature of the oxide contribution is not clear, but if it functioned to any extent as a mechanical carrier of lubricant, then the fine grooving may have represented an appropriate model of a thick and tenacious oxide coating.

Effective boundary lubrication would appear to be the principal reason for stage II.

The values of μ for boundary lubrication on copper, in particular, might be considered high but not in any important disagreement with what has been reported from rider-and-plate studies, where surfaces of copper required abrasion under water or a treatment in boiling water before effective lubrication resulted.[15] In some degree consistent with that work, copper specimens treated in boiling water for 5 min in the present experiments showed lowest friction coefficient (curve *EE*, Fig. 21).

Stage III. Only tests at 3/4-in. radius and larger illustrate this stage in which friction coefficient rose rapidly with increasing reduction, finally passing through a maximum. Reference to Fig. 21 shows that the interface shear stress accompanying the maximum had exceeded τ_y with the result of sticking and the plastic shearing of surface layers. Film breakdown was associated with stage III, and, as noted earlier for solid lubricants, failure began over the periphery of the specimen with findings being made of fold formation.

DISCUSSION AND CONCLUSIONS

A definition of friction coefficient as $\mu = \tau/\sigma = \tau/(\sigma_y + \sigma_h)$ sets an upper limit on possible values of μ, in the presence of bulk plastic deformation, of approximately 0·5. A maximum in μ would be realized with $\sigma_h = 0$, which occurs at the periphery of a test specimen, and highest possible τ; the latter could hardly exceed the bulk shear strength of the experimental material so that $\tau_{max} = \tau_y \cong 0{\cdot}5\sigma_y$, depending upon yielding theory and with regard for the circumstance that σ_y would correspond to the particular condition of strain at the place of measurement. Consistent with such an argument, values of μ of about 0·5–0·6 were found near the periphery of unlubricated discs (Fig. 16).

Vol. 1
1960

The definition also suggests that strong departures from Amontons' law could be observed, as in fact they were. Terms in the denominator are variable with both reduction and interface position, but, for given test material, σ_y would be reasonably reproducible and predictable, while for fixed geometry as well, σ_h would vary only as a consequence of changes in lubricating action. Therefore, departures from that law would logically be sought in variations in film characteristics, influencing the value of τ.

The data have demonstrated dependence of μ on both reduction and position of measurement. Three trends with increasing reduction may be singled out.

1. μ *decreasing* (Figs. 11, 14, 15, 16 and 21). It is necessary only that τ become larger at a lesser rate than $(\sigma_y + \sigma_h)$. This condition was realized in the case of lead foil of low shear strength, increasing only slightly with reduction (Fig. 11), and has also been discussed by Bowden and Tabor [16] in terms of data from rider-and-plate-type experiments with increasing loads in which soft metal films were interposed between the rubbing parts. It was found also for MoS_2 films, which experiment has shown may even result in decreasing τ (Fig. 15). In absence of lubrication, or with no relative displacement between specimen and platen (sticking), μ must again decrease, for $\tau = \tau_y$ will increase only in proportion to σ_y (as approximately $0{\cdot}5\sigma_y$) and at a lesser rate than $(\sigma_y + \sigma_h)$ (Fig. 16).

2. μ *increasing.* Examples are given only by measurements with mineral oil and mineral oil with fatty acid at the 3/4-in.- (or greater) radius position. Now, the rate of increase of τ must be greater than that of $(\sigma_y + \sigma_h)$ and, further, must be attributed to film deterioration producing a growing amount of metal-to-metal contact. Finally $\tau = \tau_y \cong 0{\cdot}50\sigma_y$ when τ continues to rise, but less rapidly, and μ passes through a maximum value; $\mu_{max} \cong 0{\cdot}5$ only when $\sigma_h = 0$ at the periphery. Of the several observations at positions within the interface, $\mu_{max} < 0{\cdot}5$ because $\sigma_h > 0$. Thus the liquid lubricants at sufficiently high reductions also give examples of the previously noted trend in μ.

3. μ *constant.* Amontons' law is satisfied with τ/σ remaining constant and independent of reduction and position only in a limited number of measurements with soap and teflon films, which gave extremely low values of μ. For reasons not physically clear, τ increased in proportion to σ and so constant μ was preserved. More detailed experiments, including variations in test geometry, will be useful in developing an explanation.

Except for the few data on soap films, there is a clear influence on μ of position of measurement. For a constant reduction, μ decreased with movement from the periphery towards the center (Figs. 9, 11, 14, 16 and 19). Much of this trend, particularly at low reduction, may be attributed to the increase in σ_h along the same direction. It is also clear, however, that high μ near the periphery can result from film breakdown beginning at this location. Thus, for conditions of the present experiments,

Vol. 1
1960

normal pressure on the lubricant film is not a criterion for failure, which actually started where the pressure was lowest. The most striking example is given by oleic acid in mineral oil with which marked stage-II behavior occurred at the 1/4- and 1/2-in.-radius locations but spanned a negligible range of reduction at positions nearer the periphery.

Two other considerations in a film-failure criterion are:

1. Enlargement of interface area, effecting a film "dilution" and final rupturing.

2. Displacement of points in the original interface over the rigid platen serving to abrade and so disrupt the film.

If compression is regarded as homogeneous, then the first is not a sufficient reason for failure since the onset of stage III in Fig. 20 is dependent upon location, yet all elements in the interface should undergo the same area change for a given reduction. As regards the second, displacement of any point, Δ, at initial radius r_0, for reduction R is given by

$$\Delta = r_0 \left(\frac{1}{\sqrt{1-R}} - 1 \right)$$

and thus increases with radial position, being a maximum at the periphery. But again, on the basis of homogeneous compression, this cannot be a sole cause of breakdown even though it involves the peripheral region in a unique way; examination of Fig. 20 shows that points at interior locations (1/4- and 1/2-in. radius) may undergo displacement greater than near the periphery yet without the breakdown.

Further study of conditions for failure is in order, and should include measurements of surface distortion using inert markers not functioning as lubricant reservoirs like the grooves. Borrowing from Fig. 13, however, the important detail to be understood is that of a departure from homogeneous deformation. The data show clearly that enlargement of surface area may in fact change with position, being much greater in the peripheral region, and that displacement as well may be in variance with homogeneous compression. Accordingly, both increase in surface area and displacement will likely be found essential to a failure criterion when allowance is made for non-homogeneity of deformation.

The results of such experiments make clear the importance, in plastic-working lubrication, of strong film adherence to preserve continuity and resist disruption. The difficulties, in a practical evaluation of lubricants through behavior in more or less simple tests and in various operations, are generally acknowledged. An important reason would seem to lie in the nature of the deformation — whether continuous or non-steady state; the extent and type of non-homogeneity — and its bearing on film failure. The non-steady-state compression of a disc between overlapping platens, involving a broad range of displacement with non-homogeneous de-

Vol. 1
1960

formation, appears to represent a particularly searching test of the resistance of a film to failure.

Finally, the work has demonstrated that a technique of measurement with inclined and normal pins, although complex, can provide rather clear insight into lubrication and friction in plastic-working operations. It should make possible some new and direct approaches to the study of problems in this field.

Acknowledgment – The Al test material was generously supplied by the Aluminum Company of America.

REFERENCES

1. E. Siebel and W. Lueg, *Mitt. K.-Wilh.-Inst. Eisenforch.* **15**, 1 (1933).
2. C. L. Smith, F. H. Scott and W. Sylwestrowicz, *J. Iron St. Inst.* **170**, 347 (1952).
3. I. G. Astakhow, *Inst. Stali im. I. V. Stalina, SSSR.* Symposium No. 30, 147, (1951).
4. C. W. MacGregor and R. B. Palme, *J. Appl. Mech.* **70**, 297 (1948).
5. J. T. Bergen and G. W. Scott, *Trans. Amer. Soc. Mech. Engrs.* **73**, 101 (1951).
6. J. Frisch. and E. G. Thomsen, *Trans. Amer. Soc. Mech. Engrs.* **76**, 599 (1954).
7. P. W. Whitton and H. Ford, *Proc. Inst. Mech. Engrs., Lond.* **169**, 123 (1955).
8. J. G. Wistreich, *Proc. Inst. Mech. Engrs., Lond.* **169**, 654 (1955).
9. H. Majors, Jr., *Trans. Amer. Soc. Mech. Engrs.* **78**, 79 (1956).
10. G. T. van Rooyen and W. A. Backofen, *J. Iron St. Inst.* **186**, 235 (1957).
11. E. Siebel, *Stahl u. Eisen, Duaseldorf* **43**, 1295 (1923).
12. W. Schroeder and D. A. Webster, *J. Appl. Mech.* **16**, 289 (1949).
13. L. Pramdtl, *Z. angew. Math. Mech.* **3**, 401 (1923).
14. R. Hill, E. H. Lee and S. J. Tupper, *J. Appl. Mech.* **18**, 46 (1951).
15. E. D. Tingle, *Trans. Faraday Soc.* **46**, 93 (1950).
16. F. P. Bowden, and D. Tabor, *The Friction and Lubrication of Solids* p. 119. Oxford University Press (1954).

Vol. 1
1960

Int. J. Mech. Sci. Pergamon Press Ltd. 1960. Vol. I, pp. 28–44. Printed in Poland

TEMPERATURE DISTRIBUTIONS IN SOME FAST METAL-WORKING OPERATIONS

R. I. TANNER AND W. JOHNSON
Department of Mechanical Engineering, University of Manchester

(*Received* 6 *February* 1959)

Summary—A short discussion of the basic equations concerned with heat generation and flow in a plastically deforming body is given and criteria are established for neglecting body forces and accelerations. A "thermal Mach number" is evidenced, being the ratio of heat diffusion to a typical velocity in the system. It is next shown that the space rate of heat diffusion upstream of a tangential velocity discontinuity in plane plastic flow is negligible for practical purposes when the speed normal to the discontinuity is more than about 2 in/sec.

Examples are given of the determination of the approximate temperature distribution in some fast plane-strain extrusion processes, using graphical techniques; solutions requiring dead metal zones are seen to require melting of the extruded metal. Some non-steady motion problems are referred to.

Vol. 1
1960

NOTATION

DIMENSIONLESS or normalized variables are denoted by a bar, deviatoric quantities by an asterisk, e.g. σ^*_{ij}

A dot denotes total derivative, e.g. $\frac{\partial}{\partial t} + u\frac{\partial}{\partial x} + v\frac{\partial}{\partial y} + w\frac{\partial}{\partial z}$ in Cartesian co-ordinates.

A comma, followed by an index denotes covariant differentiation. (In Cartesian co-ordinates this is simply the partial derivative with respect to the ith co-ordinate.) All quantities have been expressed in consistent mechanical units, hence the scaling factors J and g_c do not appear in the equations.

a^i	acceleration vector component
$d_{ij} = \frac{1}{2}\left(\frac{\partial u_i}{\partial x_j} + \frac{\partial u^j}{\partial x^i}\right)$	the rate of deformation tensor
E	Young's modulus
f^i	component of body force per unit mass
g^{ij}	the metric tensor
G, K	rigidity modulus and bulk modulus respectively
q^i	heat flux vector component
t	time
T	temperature
u^i	velocity vector component
v_n or $v_{n:AB}$	normal velocity across a shock AB
x^i	co-ordinates

a a numerical factor $1 \geqslant a \geqslant 0$
β coefficient of linear thermal expansion
λ a scalar quantity
ν Poisson's ratio
ϱ mass per unit volume at temperature T
σ^{ij} stress tensor
g characteristic body force
J mechanical equivalent of heat
$\dot{E}$ time rate of change of internal energy of system

INTRODUCTION

The work dissipation due to the plastic deformation of a metal results in a temperature rise which, under certain conditions, may be of considerable importance. For instance, it is well known that in order to avoid hot shortness in extrusion operations, restrictions must be placed on the speed and temperature of the operation because the phenomenon depends on temperatures attained; also, recent interest in the temperature developed in an extruded calot has been stimulated by the necessity to hot-form radioactive materials which undergo deleterious phase changes at too high temperatures. Problems involving the calculation of temperatures generated in plasticity problems do not appear to have been the subject of intensive investigation; in fact from the point of view of theoretical applied mechanics, the paper by Bishop[1] would seem to be unique. Interest in the measurement of bulk temperature due to imposed plastic deformation first appeared in a paper by Farren and Taylor,[2] when investigating the temperatures achieved in a simple tensile test. There has been a certain amount of interest in temperature distribution in dies during wire-drawing,[3] and in machining.[4] Of late a major experimental investigation has been made by Watkins, Ashcroft and McKenzie[5] to determine the temperature attained at various points inside an extruded cylindrical slug of material.

Bishop's original paper gives the isotherms associated with the plane-strain extrusion of a perfectly plastic-rigid material through a square die of fractional reduction two-thirds, the die face and container wall being perfectly smooth. The slip-line field solution for this case is shown in Fig. 1 and consists of a circular quadrant and an isosceles triangle; it is a simple solution amenable to analytical treatment. Bishop shows how, by employing relaxation methods, isotherms may be determined for a slug initially at the temperature of its environment from a calculation of the amount of plastic work put into each element of it, regard being paid to heat exchanges by conduction, due to the temperature variation throughout the mass of the slug. This single solution is, unfortunately, of limited value for engineers. It treats of only a simple slip-line field which is analytically tractable and use is made of mathematical techniques

beyond the knowledge of most engineers. For these two reasons, and because of the aforesaid increasing practical interest in temperature rises, the authors were stimulated towards investigating the prediction of temperature distribution in plane-strain problems, particularly those requiring slip-line field solutions of the more complicated kind.

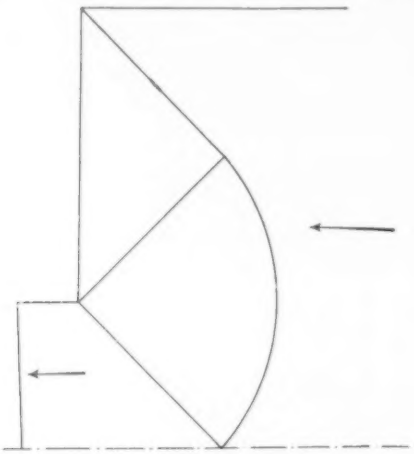

Fig. 1. Half slip-line field for plane-strain extrusion through a square die when the die face and container wall are both perfectly smooth.

It will be shown that in metal-working operations which proceed at speeds of in/sec, where the die, the tools and the container are non-conducting, conduction within the slug itself has little effect in tending to equalize temperatures throughout the bulk of material. Since for most metal-working operations the theoretical assumptions are only approximately valid, for a good first approximation, neglect of the conduction factor is justifiable. This leaves the way open to employ a well-known graphical technique for finding the temperature distribution which is highly suitable for engineers.[6]

GENERAL EQUATIONS AND DISCUSSION OF TEMPERATURE DISTRIBUTION

Basic equations

The motion of any continuum satisfies the following equations.[7]

(a) Equation of continuity of matter

$$\frac{\partial \varrho}{\partial t} + (\varrho v^i)_{,i} = 0 \tag{1}$$

(b) Equations of equilibrium

$$\sigma^{ij}{}_{,j} + \varrho f^i = \varrho a^i \tag{2a}$$

$$\sigma^{ij} = \sigma^{ji} \tag{2b}$$

(c) The conservation of energy equation

$$\dot{E} = \sigma^{ij} d_{ij} - q^i{}_{,i} \,. \tag{3}$$

It will be assumed that such temperature alterations as occur do not affect the physical properties of the material.

Equation (1) assumes that there are no voids in the material, e.g. in the case of plastic flow it is supposed that no "defects" are developed.[8] The equations (2) are true (except perhaps at isolated points or lines) in all practical cases, though it is possible to imagine materials in which it is not so.[9]

So far eight equations containing seventeen unknowns have been proposed. The remaining nine are given by assuming specific material properties. For plastic flow *in the absence of appreciable vorticity*[10,11] the Prandtl-Reuss equations are applicable

$$d^*_{ij} = \sigma^*_{ij} \lambda + \dot{\sigma}^*_{ij}/2G \tag{4}$$

$$d_{ii} = (1-2\nu)\dot{\sigma}_{ii}/E \,. \tag{5}$$

The equations (4) and (5) relate to an isotropic material. The scalar quantity λ may be eliminated by use of the yield criterion

$$\sigma^{*i}{}_j \sigma^{*j}_i = 2Y^2/3 \tag{6}$$

Y, the yield stress in simple tension, is principally a function of the plastic work done on the specimen, the rate of straining, and the temperature.

So far six more equations have been found. The remaining three relate to the internal energy and indirectly the heat flux vector q^i.

The heat flux vector is in many cases related to the temperature by Fourier's Law

$$q_i = -k^j_i T_{,j} \,. \tag{7a}$$

Only isotropic materials will be considered and hence

$$q_i = -k\delta^j_i T_{,j} = -kT_{,i} \tag{7b}$$

k being the familiar coefficient of thermal conductivity and δ^j_i the Kronecker delta symbol.

Fig. 2 represents schematically an extrusion process conceived as a thermodynamic system in which the punch does work on a mass of metal, causing it to pass through *rigid* dies. The system is the mass of metal within the indicated boundary. This being a steady-state open system, the General Energy Equation is, for unit mass throughout,[12]

$$\Sigma Q = \Sigma w + \frac{(v_2^2 - v_1^2)}{2} + g(z_2 - z_1) + (p_2 V_2 - p_1 V_1) + (E_2 - E_1) \tag{8a}$$

Vol. 1
1960

ΣQ the heat transfer across the boundary is zero: the boundaries are supposed non-conducting. Σw the work done by the system is zero: the dies and container are rigid and immovable. $(v_2^2 - v_1^2)/2$, where v_2 and v_1 are the speeds of the metal at exit and entrance to the system, is neglected, being thought to be small in comparison with other terms; this also applies to the $g(z_2 - z_1)$ term, the alteration in the "potential energy"

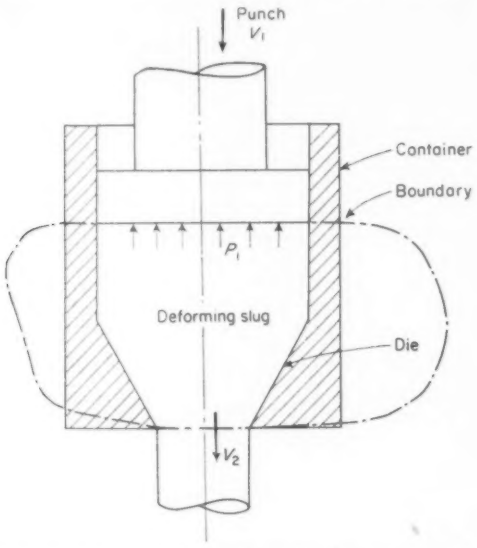

Fig. 2. An extrusion schematically represented.

of the metal. $(E_2 - E_1)$ denotes the alteration in the total internal energy of the system. The terms p_2V_2 and p_1V_1, where p_1 and p_2 are the pressures and V_1 and V_2 the volumes per unit mass at entry and exit to the system, are the usual flow-work terms of thermodynamics. For simplicity it will be assumed that $V_2 = V_1$, thus neglecting any changes in the volume of the metal due to pressures p_1 and p_2. p_2 is here to be taken as zero, so that p_1 is the extrusion pressure. Equation (8a) thus reduces to

$$E_2 - E_1 = p_1V_1 . \tag{8b}$$

Now $(E_2 - E_1)$ may be considered to be made up of two portions which manifest themselves as (i) a temperature rise and (ii) an alteration in the crystal lattice structure; in effect (ii) is a form of energy storage. The former will now be denoted by U_{thermal} and the latter by U_{lattice}. It appears from the experimental work of Farren and Taylor[2] that U_{thermal} and U_{lattice} are of nearly different magnitudes, indeed they found that a variable percentage (usually about 90 per cent) of the mechanical work done in plastic flow reappeared as heat. An input of work clearly had a different effect from that of an input of an equivalent quantity of heat, the lattice of the material being left in a work-hardened or strained state.

It would seem that if the metal is worked above its recrystallization temperature, then provided the process is slow enough one would presumably recover all the work as heat since the metal lattice would be left in its initial state due to self-annealing.

The above indicates that the thermodynamics of a plastically working solid is not simple. For a discussion of temperatures reached in processes involving plastic flow, however, it will be assumed that the fraction $(1-\alpha)$ is absorbed or stored in the lattice alteration and the remainder produces heat and so an increase in temperature, thus

$$E_1 - E_2 = U_{\text{lattice}} + U_{\text{thermal}} . \tag{9}$$

Hence

$$\dot{U}_{\text{lattice}} = (1-\alpha)\,\sigma^{ij} d^*_{ij} \tag{10}$$

$$\dot{U}_{\text{thermal}} = \alpha\sigma^{ij} d^*_{ij} + (k g^{ij} T_{,i})_{,i} . \tag{11}$$

Vol. 1
1960

The expression (10) also includes, in general, some of the work done elastically. (11) is the form assumed by Bishop[1] who expressed it as

$$\dot{U}_{\text{thermal}} = \varrho c T \tag{12}$$

where c is the specific heat at constant volume. If the lattice is unchanged by the deformation then equation (12) is strictly true, and this will be assumed to be the case henceforth. Equation (11) may then be written

$$d(\varrho c T)/dt = \alpha\sigma^{ij} d_{ij} + (k g^{ij} T_{,i})_{,j} . \tag{11a}$$

If k and c are both constant, then (11a) may be written out in Cartesian co-ordinates,

$$\begin{aligned} &\partial T/\partial t + u\partial T/\partial x + v\partial T/\partial y + w\partial T/\partial z - T(\partial u/\partial x + \partial v/\partial y + \partial w/\partial z) \\ &\quad = (\alpha/\varrho c)\{d^*_{ij}\sigma^{ij}\} + (k/\varrho c)(\partial^2 T/\partial x^2 + \partial^2 T/\partial y^2 + \partial^2 T/\partial z^2) . \end{aligned} \tag{11b}$$

For an incompressible material this reduces to Bishop's[1] expression.

The equation of state is, approximately,

$$\varrho/\varrho_0 = (1 + p/K)/(1 + 3\beta T) \tag{13}$$

ϱ_0 is the density when $T = 0$ and p the hydrostatic stress about the point.

Thus, in general, the temperature field will react with the strains and hence the velocities, via the stress-strain relations (4) and (5) and the continuity equation (1). However, these disturbances will only be of the order of the elastic strains. Neglecting these thermal expansion effects is compatible with assuming a plastic-rigid material. In any case equation (13) shows that the effects of pressure and temperature tend to cancel out.

If the assumptions of rigidity and incompressibility are made, equations (1) and (2) reduce to

$$v^i{}_{,j} = 0 \tag{1a}$$

$$\sigma^{ij}{}_{,j} + \varrho_0 f^i = \varrho_0 a^i . \tag{2a}$$

For steady slow flow and in the absence of body forces equation (2a) becomes

$$\sigma^{ij}{}_{,j} = 0 . \tag{2c}$$

If v is taken as a characteristic speed, L as a characteristic length, and g as a characteristic body force magnitude, then (2a) may be written

$$Y\bar{\sigma}^{ij}{}_{,j}/L + \varrho_0 g\bar{f}^i = \varrho_0 v^2 \bar{a}^i/L . \tag{2d}$$

Hence equation (2c) is appropriate if

(a)

$$1 \geqslant \varrho_0 gL/Y$$

(b)

$$1 \geqslant \varrho_0 v^2/Y .$$

A short calculation shows that (a) will be satisfied unless gL has a magnitude of at least 10^3 ft^2/sec^2. Body forces and acceleration forces are generally quite weak and (short of near impact operations) few industrial processes are likely to require the consideration of body forces in plastic problems. But if the theory was to be applied to geophysical problems such as glacier flow or earth stability problems with characteristic dimensions of tens of feet, then body forces would clearly require to be taken into account.

Consider two typical industrial instances, (i) the cold extrusion of (a) aluminium and (b) pure lead at speeds of 15 in/sec, (ii) the (a) cold and (b) hot rolling or drawing of mild steel sheet at 3000 and 6000 ft/min. For case (i), (a) $\varrho_0 \simeq 0{\cdot}1$ lb/in^3, $Y \simeq 16$ tons/in^2 and thus $\varrho_0 v^2/Y \simeq 10^{-6}$; (b) $\varrho_0 = 0{\cdot}4$ lb/in^3, $Y \simeq 1{\cdot}5$ tons/in^2 and $\varrho_0 v^2/Y \simeq 10^{-4}$. For case (ii), $\varrho_0 \simeq 0{\cdot}28$ lb/in^3, $v = 600$ in/sec; thus if for cold rolling, $Y \simeq 16$ tons/in^2 then at the lower speed $\varrho_0 v^2/Y \simeq 0{\cdot}01$, whilst for hot rolling with $Y \simeq 4$ tons/in^2 at the higher speed $\varrho_0 v^2/Y \simeq 0{\cdot}1$. It is evident that from the point of view developed above, the application of the ordinary quasi-static stress analyses to extremely fast hot metal-working operations must lead to sizeable errors.

In the following the simple form of equation (2c) is used as is customary in plasticity theory. For an incompressible, plastic-rigid material with constant specific heat and thermal conductivity, the energy equation in steady flow may be written

$$(k/\varrho c)(g^{ij}T_{,i})_{,j} - u^i T_{,i} + (a/\varrho c) d_{ij}\sigma^{ij} = 0 . \tag{11c}$$

The factor a should be unity for a perfectly plastic material, but since the temperature everywhere is directly proportional to a, (11c) being a linear equation, no assumptions as to its value need be made until the end of the calculation.

The equation (11c) is not easy to solve even supposing that the stresses and velocities are given. Assuming continuity of the velocity

Vol. 1
1960

field (discontinuous solutions will be considered later), normalize equation (11c) to give

$$(k/\varrho cL^2)(g^{ij}\bar{T}_{,i})_{,j}-(v/L)\bar{u}^i\bar{T}_{,j}+(aYv/L\varrho cT_0)\bar{d}_{ij}\bar{\sigma}_{ij}=0\,. \qquad (11d)$$

It appears permissible to neglect the first term in equation (11d) in comparison with the second if

$$v\varrho cL/k \geqslant 1\,.$$

This may be thought of as a thermal Mach number, expressing the ratio of the rate of diffusion of heat to a typical velocity in the system.

Typical values of $k/\varrho c$ are given in Table 1, together with values of a for common metals.

Typical values of Lv for extrusion and drawing are 30–100 ft²/hr. Thus it seems that neglecting the first term in equation (11d) is fairly well justified for steel and lead, except in regions where the heat flux vector is nearly perpendicular to the velocity vector. This condition will occur mainly around the edges of the material where it is in contact with the dies or tools. In most cases errors of the order of 1 per cent for steel and of 5 per cent for copper may be expected. In view of other gross assumptions made in plasticity theory, these errors are tolerable.

Bishop's work[1] gives support to the view that the assumptions of steady flow and zero conductivity enable an accurate estimate of the temperature distribution to be made in many cases.

TABLE 1

Material	$k/\varrho c$ (ft²/hr)	a(%)
Silver	6·6	—
Copper	4·4	92
Aluminium	3·7	93
Mild Steel	0·48	87
Lead	0·94	—

The temperature distribution in steady flow will give the maximum deviation from the original temperature profile. Thus there seems to be ample justification for neglecting the higher order terms or considering a steady state in a preliminary investigation.

So far continuous fields of the variables have been considered. At a line of velocity discontinuity the temperature undergoes a sudden increase (if the conductivity is zero) of amount

$$(\Delta T)_0=\frac{Y}{\sqrt{3}}\,\frac{a}{\varrho c}\left(\frac{\Delta v_T}{v_n}\right) \qquad (14)$$

Δv_T being the discontinuity in the tangential velocity, and v_n the velocity of flow across the discontinuity. The actual solution, taking into account

Vol. 1
1960

conductivity, can be found by considering the problem shown in Fig. 3. A discontinuity of value Δv_T occurs at $x = 0$. Using equation (11c)

$$(k/\varrho c)d^2T/dx^2 - v_n dT/dx = 0 \tag{15}$$

with

$$T_\infty - T_{-\infty} = Y a(\Delta v_T)/\sqrt{3}\varrho c v_n \equiv (\Delta T)_0 .$$

The solution of equation (15) is

$$\left.\begin{aligned} 0 > x \quad & T - T_{-\infty} = (\Delta T)_0 \exp(v_n \varrho c/k) \\ x \geqslant 0 \quad & T - T_{-\infty} = (\Delta T)_0 \end{aligned}\right\} \tag{16}$$

This solution is represented in Fig. 3 for various materials.

For mild steel and lead, the temperature rise 0·05 in. upstream of the shock will be less than 2 per cent of the total rise if the normal

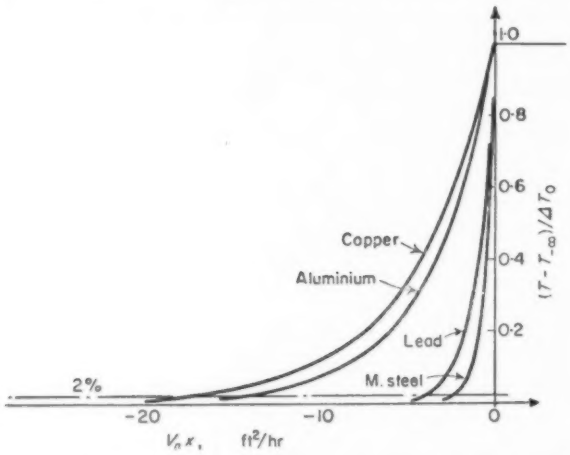

Fig. 3. Temperature distribution upstream of a velocity discontinuity.

velocity across the shock is greater than 2·8 in/sec. Since a velocity discontinuity will not in fact be perfectly sharp in a real material, it is clear that neglect of conduction in a shock leads to inappreciable error.

So far we have only considered cases where the yield stress in constant. In many industrial processes a heated billet is used and consequently the yield stress of the material varies from point to point due to differential cooling effects.

For these problems an upper-bound solution for pressures may be found by assuming the same velocity field as in the corresponding solution for constant yield stress and assuming the local stresses to be reduced in the proportion of the local yield strength to the yield strength when cold. This will give correct boundary conditions for problems in which the velocity is prescribed over parts of the boundary and zero stresses over the remainder, and is therefore applicable to extrusion, drawing,

rolling and also to punch indentation and wedge problems. It is thus permissible to write

$$\sigma^{ij} = Y(T)(\sigma^{ij})_0/Y_0 . \tag{17}$$

This will satisfy the yield condition equation (6) and the stress-strain relations equation (4) for a plastic-rigid material. However, the equilibrium equations (2b) are not satisfied. Hence the pressures calculated will constitute an upper bound and the rate of working will be everywhere greater than the true solution. It may be noted that an extremum principle has been taken and used for a non-homogeneous material. This is permissible because each element of (approximately) constant yield value may be considered as a separate plastic problem. Therefore, the local rate of working in the assumed state is greater everywhere than that in the real solution, and thus the external rate of working and the pressures are also an upper bound. This process could also be applied to find the correction to the temperatures obtained using equation (11c), due to softening of the material by self-heating. However, it hardly seems worthwhile, since, in most cases it is not likely to be the largest source of error.

Vol. 1
1960

When conductivity is neglected the temperature field may be found relatively easily by graphical methods for steady flow processes, and if the slip-line field is approximated to by a series of shock lines, a good approximation to the temperature distribution in the emerging slug is usually obtained.

For problems involving the "unit diagram" [13] one would have to consider that the material had reached a steady state before the actual configuration was reached, and while temperatures may be found as for steady-flow problems, it is doubtful if the calculated temperatures will represent reality.

A better solution taking the conductivity into account may be found by assuming a solution

$$T = T_1 + (k/\varrho c)\, T_2 + (k/\varrho c)^2 T_3 + \ldots \tag{18}$$

and substituting in equation (11c). T_1 is the solution for zero conductivity, and T_2 satisfies the equation

$$u\partial T/\partial x + v\partial T/\partial y + w\partial T/\partial z = V^2 T_1 . \tag{19}$$

The right-hand side is a known function. However, the fundamental error inherent in ignoring higher-order terms in a differential equation is not removed by this method, as equation (19) only requires boundary conditions like the reduced equation with zero conductivity.

The reduced equation and equation (19) only need the initial temperature conditions on a curve, whereas the full equation (11c) requires the temperature to be given round a closed boundary. Solutions of

equation (19) seem to be harder to obtain than was the first solution for T_1 and the practical value of the method is open to doubt.

Lastly, it may be noted that, if the temperature profile in the emerging slug is given, it is easy to calculate the induced stresses in cooling if the slug at exit is assumed stress-free. In many extrusions, and short of estimating the residual stresses (created because the largest temperature rise occurs in the outside of the product), there will also be a tendency for fracture to occur on the outside.

TEMPERATURE DISTRIBUTION IN SWITFLY WORKED METALS

In the previous section a criterion was established whereby the temperature equalization tendency, brought about by conduction, could be estimated; it was shown that it may be safely neglected for most metals when the speed of extrusion is measured in in/sec. On this assumption a simple procedure may be built up for predicting the temperature distribution in a slip-line field region.

For simplicity, the method will be exemplified by reference to the simple case depicted in Fig. 1. First, the slip-line field is approximated using chords in place of circular arcs or triangles replacing sectors. The degree of coarseness acceptable in a replacement of the slip-line field by a system of chords is a matter of the degree of inaccuracy tolerable. In this instance, three 30° isosceles triangles replace a circular quadrant, see Fig. 4. This procedure gives a "kinematically admissable velocity field" for this particular problem, which can be used for estimating the

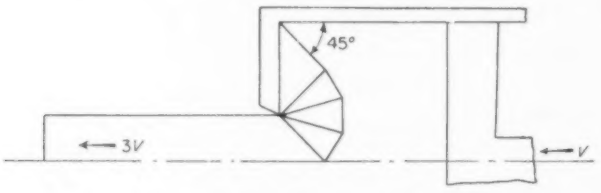

Fig. 4. A kinematically admissable velocity field obtained by coarsely approximating the slip-line field of Fig. 1.

ram pressure necessary to effect extrusion, by using an extremum principle due to Hill[13] or one of the Limit Theorems due to Drucker, Greenberg and Prager[14]. It can easily be proved that in the limit the velocity field described can be so finely constructed as to yield an estimate of the extrusion load differing as little as we please from that given by the slip-line field and the employment of the Hencky equations. Second, construct the hodograph to Fig. 4; this is shown in Fig. 5. This latter diagram enables the velocity of any particle, which is part of the extrusion, to be stated. Define a number of stream tubes — four in this case — by

the "horizontal" lines meeting the bounding entry line at its points of discontinuity, A, B, C and D in Fig. 6. The stream lines of particles passing through these points are easily obtained using the hodograph. All the material moving within a given tube undergoes a similar history of deformation; the progress of each of the four tubes through the deformation zone is now as indicated by the dotted lines. If there is concern

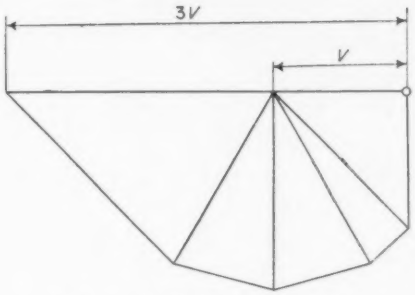

Fig. 5. Hodograph to Fig. 4.

with the pattern of temperature distribution only, all material constants, e.g. the actual value of the yield stress of the material, may be omitted from the calculations. Consider stream tube II. If material approaches AB at unit speed, the work done per unit time is proportional to the tangential velocity discontinuity across $AB \times$ length AB; but this work is expended on volume t and hence the temperature rise on crossing AB is proportional to V^*_{AB}. $AB/t = V^*_{AB}/V_{N:AB}$ where $V_{N:AB}$ is the speed normal to AB. This quotient is easily obtained by use of the hodograph. The material in AA_1B is rigid and remains at constant temperature until it crosses A_1B where, for a second time, it undergoes a sudden change in direction. The temperature of the material moving into $BA_1A_2B_1$ jumps by an amount $V^*_{A_1B}/V_{N:A_1B}$. $V_{N:A_1B}$ is the speed normal to A_1B. Again this quotient is obtainable from the hodograph. Further temperature jumps occur on crossing A_2B_1 and A_3B_2. The final temperature of the material is the sum of the separate jumps to some factor of proportionality. Similar calculations are made for each of the three remaining stream tubes. The largest value of the temperature has been converted to 100 and the value in each section of the diagram increased in proportion. The approximate temperature distribution is now clear and is depicted in Fig. 6. Its accuracy can be increased by using a finer net of lines, but even at this level of coarseness, comparison with the isotherms given by Bishop[1] is very reasonable.

This method may be used for complicated slip-line fields of the form indicated in Fig. 7(a) and (b) and for which cases temperature distributions are shown. The calculations were made on small-scale diagrams and whilst they are not thought to be correct to more than about 4 per

Vol. 1
1960

cent, they are more than adequate for indicating qualitative distributions of temperature.

Of special interest are extrusions involving the deposition of zones of dead metal, see Fig. 8(a) and (b). The energy dissipation due to shearing which takes place along the boundary of the dead zones, OA and OBC, is not accounted for in the magnitudes quoted; indeed, this work causes virtually no temperature rise in the body of the flowing

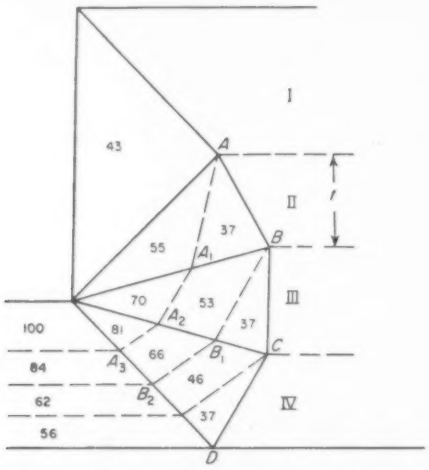

Fig. 6. Temperature distribution as calculated using the field in Fig. 4.

material, since there is no material flow across the boundary. This implies that the infinitely thin boundary layer assumes an infinitely high temperature, or, more realistically, that melting takes place. Obviously, in a slug of considerable length, even though the extrusion be fast, a fraction of the heat must be conducted into the dead metal zone and part involved in phase changes. This simple physical consideration leads to the perhaps naive conclusion that once a dead metal zone is established in a fast extrusion, the condition of shearing along the dead metal zone soon ceases to operate and is superceded by a "lubrication" along the zone with molten material, theb oundary friction it provides being determined by its viscosity at some high temperature.

Fig. 9(a)[13] shows one half of a diagram in which a punch indents a wide block of material constrained to deform in plane strain. The methods described above can be adapted to this instance. The temperatures calculated and presented in the figure only occur along the line to which they are assigned; they do *not* apply to a whole region as in the preceding steady-state cases and the distribution is not continuous throughout the slip-line field. This is because the given slip-line field applies only at the instant of deformation and changes from moment

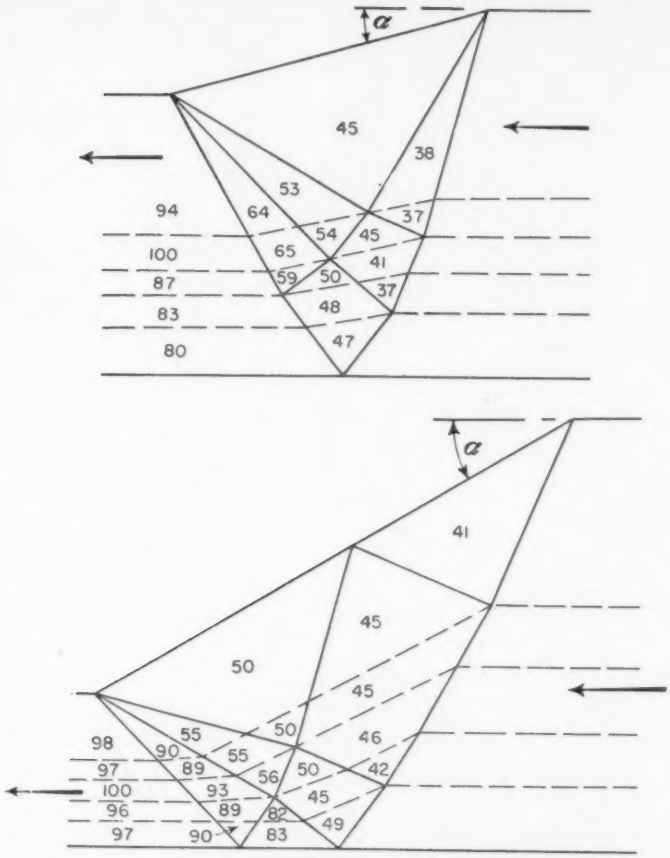

Fig. 7. Calculated temperature distribution for extruding or drawing through smooth wedge-shaped dies when
(a) $r < 2\sin\alpha/(1+2\sin\alpha)$; $\alpha = 15°$, $r = 0{\cdot}24$
(b) $r > 2\sin\alpha/(1+2\sin\alpha)$; $\alpha = 30°$, $r = 0{\cdot}64$

to moment with finite indentation. Fig. 9(b) and (c) are also unsteady motion problems and are to be interpreted similarly.[15,16] In these two instances, the predicted distributions are only likely to be substantially true where there are strong velocity discontinuities.

CONCLUSIONS

It has been shown that within the limitations of the assumptions made for fast metal-working processes in which the temperature of the material to be worked is about the same as that of its surroundings, i.e. in a quasi-cold operation, the calculation of temperature distributions due to plastic work dissipated in deforming a body, is well approximated by neglecting the effects of conduction. Realization of this fact means that calculations of this kind for operations whose speeds are industrially

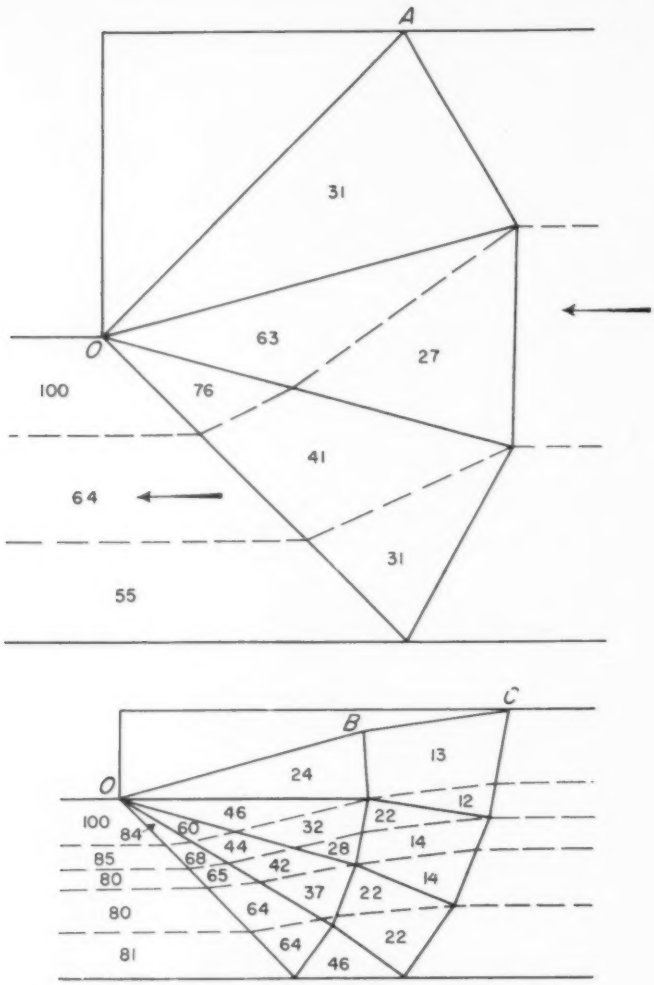

Fig. 8. Calculated temperature distribution for extruding through square dies when zones of dead metal are deposited
(a) $r = 0{\cdot}50$ and container wall smooth;
(b) $r < 0{\cdot}5$ and container wall rough.

realistic, are easy and straightforward. Especially is this the case for all plane-strain problems when use is made of the extremum principle which provides an upper bound to the load in conjunction with the substitution of a system of tangential velocity discontinuities for the appropriate slip-line field.

The method described is applicable to all plane-strain problems to which slip-line field solutions are normally applied, e.g. to steady-state problems such as sheet-drawing through wedge-shaped dies and rolling, using Alexander's solution.[17] In principle the method is also applicable

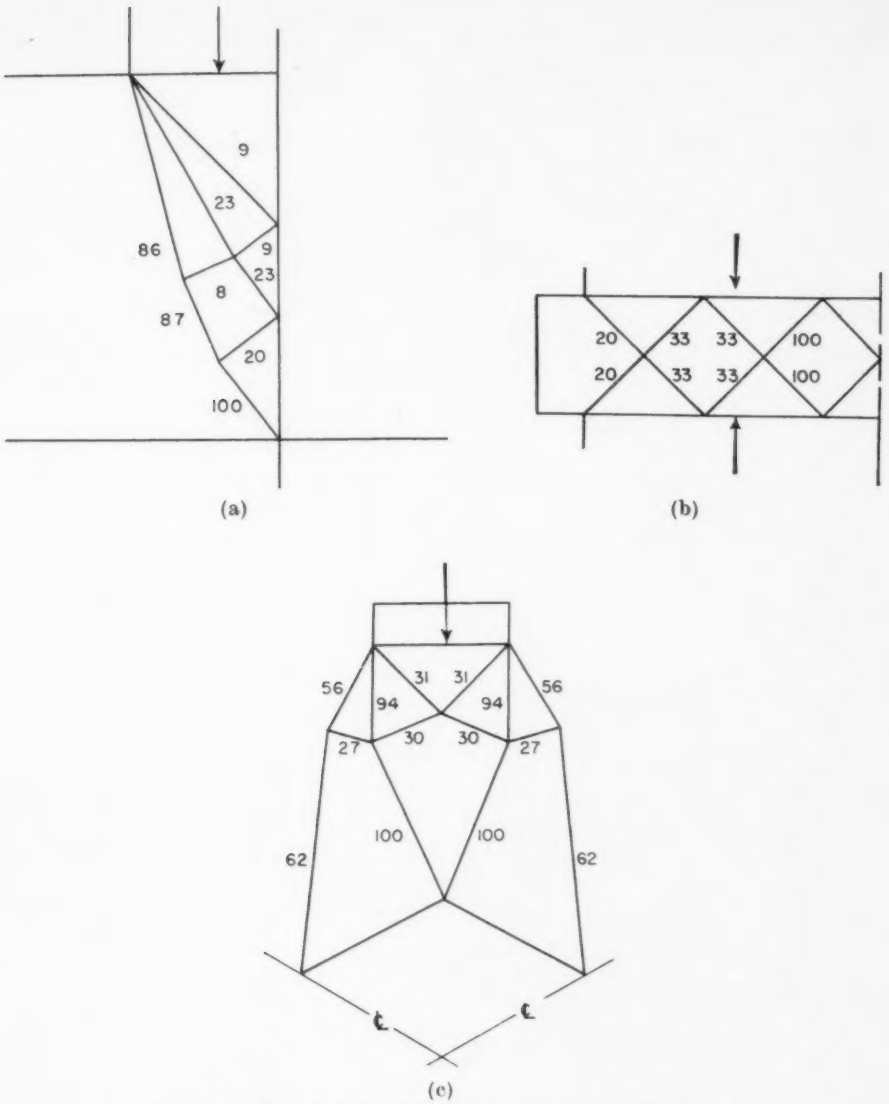

Fig. 9. Half diagram showing an "approximated slip-line field" and the instantaneous temperature rises across the discontinuities for plane strain

(a) flat punch indentation of a semi-infinite medium
(b) compression between perfectly smooth platens
(c) forging of a block of material with three equal-size, symmetrically inclined punches: only one third of whole diagram is shown.

to unsteady-state problems though they would be extremely laborious to calculate, and to non-steady-motion problems such as involve the unit diagram.

Two particular classes of three-dimensional problems amenable to the approach described above are those of indenting and piercing, the solutions being similar to that given by Drucker and Shields[18] and the extrusion of round rods or tubes due to Kudo[19]. The solutions for some of these latter instances are of industrial value and it is intended to produce them in subsequent papers.

REFERENCES

1. J. F. W. BISHOP, *Quart. J. Mech.* **9**, 236 (1956).
2. W. S. FARREN and G. I. TAYLOR, *Proc. Roy. Soc.* A **107**,422 (1925).
3. J. G. WISTREICH, Wire-drawing *J. Inst. Met., Metallurgical Reviews* (1958).
4. A. C. RAPIER, *Brit. J. Appl. Phys.* **5**, 400 (1954).
5. M. T. WATKINS, K. ASHCROFT and J. MCKENZIE, Conference in technology of engineering manufacture *Proc. Inst. Mech. Engrs., Lond.* Preprint (1958).
6. W. JOHNSON, Estimation of upper bound loads for extrusion and coining extrusions *Proc. Inst. Mech. Engrs., Lond.* Preprint (1958).
7. A. M. FREUDENTHAL and H. GEIRINGER, Mathematical theory of the inelastic continuum *Handbuch der Physik*, Bd. 6, Teil 9. Springer, Berlin (1956).
8. W. JOHNSON, *Appl. Sci. Res., Hague* **8** A, 52 (1959).
9. J. LARMOR, *Proc. Lond. Math. Soc.* **23**, 127 (1891).
10. T. Y. THOMAS, *Proc. Nat. Acad. Sci., Wash.* **41**, 716 (1955).
11. T. Y. THOMAS, *Proc. Nat. Acad. Sci., Wash.* **41**, 720 (1955).
12. J. H. KENNAN, *Thermodynamics.* John Wiley, NewYork (1954).
13. R. HILL, *Mathematical Theory of Plasticity.* Clarendon Press, Oxford. (1950).
14. D. C. DRUCKER, H. J. GREENBERG and W. PRAGER, *J. Appl. Mech.* **18**, 371 (1951).
15. A. P. GREEN, *Phil. Mag.* **42**, 900 (1951).
16. W. JOHNSON, *Engineer, Lond.* **205**, 348 (1958).
17. J. M. ALEXANDER, *Proc. Inst. Mech. Engrs., Lond.* **169**, 1021 (1955)
18. D. C. DRUCKER and R. T. SHIELDS, *J. Appl. Mech.* **20**, 453 (1953).
19. H. KUDO, A computation of required pressure for the extrusion-forging of a circular shell. *Proceedings of the Seventh Japanese Congress on Applied Mechanics*, p. 57 (1957).

Int. J. Mech. Sci. Pergamon Press Ltd. 1960. Vol. I, pp. 45–56. Printed in Poland

SMALL VIBRATIONS OF THIN INCOMPLETE CIRCULAR RINGS

ROBERT R. ARCHER *
Massachusetts Institute of Technology

(*Received* 9 *March* 1959)

Summary—The in-plane inextensional vibrations of an incomplete circular ring of small cross section are studied by means of the classical equations of motion. Natural frequencies and modes are found for rings with clamped ends and subtended angles between 180° and 360°. A solution is given for the problem of an incomplete ring clamped at one end and given a prescribed, time-dependent displacement at the other end.

Vol. 1
1960

INTRODUCTION

IN THIS paper a mathematical study of the in-plane inextensional vibrations of an incomplete circular ring of small cross section is carried out starting with the basic equations of motion as given in Love with the addition of terms to represent damping effects.[1]

With a view to an application of this analysis to a problem connected with a gyroscopic instrument, the problem of an incomplete circular ring clamped at one end and given a prescribed (time-dependent) displacement at the other end is considered in detail.[2] In particular, equations are developed for determining the transient response of a semi-circular ring caused by a small "step motion" of one support relative to the other. This solution is given in terms of the natural frequencies and modes of motion of the ring. In the Appendix a considerable amount of information about these modes and frequencies is obtained with the help of machine computation through the integration of the differential equation for the problem, together with the appropriate boundary conditions. In particular the first four natural frequencies for the clamped incomplete ring are determined which serves to improve and extend the earlier approximate solution found by den Hartog using energy techniques.[3]

BASIC EQUATION OF MOTION

This analysis is carried out for the case of a plane circular ring of constant symmetrical cross section whose dimensions are small compared with the radius of the center-line of the ring. Body forces are neglected and only in-plane forces are considered.

* This paper was part of a report prepared for the Instrumentation Laboratory of the Massachusetts Institute of Technology under the auspices of DSR Project 52—140, sponsored by the Weapons Guidance Laboratory of the Wright Air Development Center, through USAF contract AF 33(616)—3892, Air Force Task Number 50518. The author is grateful for permission granted by the Instrumentation Laboratory to publish these results.

For an element of the ring as shown in Fig. 1, let N, T and M be the internal shear force, normal force and bending moment, respectively.

With these forces the equation of motion in the radial direction takes the form

$$\frac{\partial N}{\partial \theta} + T = mr\frac{\partial^2 u}{\partial t^2} + Kr\frac{\partial u}{\partial t} \tag{1}$$

where m is the mass per unit length, r the radius of the center-line, K the viscous damping coefficient, and u the inward radial displacement for the ring.

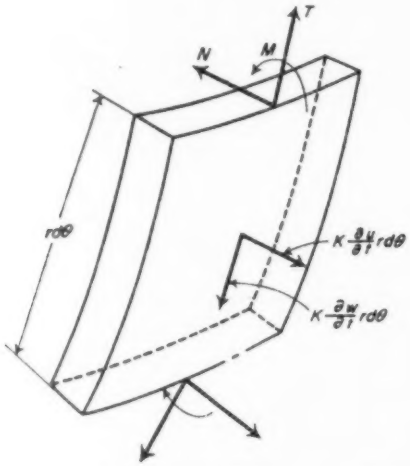

Fig. 1. Element of ring showing force and moment resultants.

In the tangential direction the equation of motion takes the form

$$\frac{\partial T}{\partial \theta} - N = mr\frac{\partial^2 w}{\partial t^2} + Kr\frac{\partial w}{\partial t} \tag{2}$$

where w is the displacement in the sense of increasing θ.

If rotatory inertia * is neglected, the moment equation takes the form

$$\frac{\partial M}{\partial \theta} + Nr = 0\,. \tag{3}$$

We have neglected terms involving shear deformation but Timoshenko has shown that the effect is unimportant for rings where the wavelength of the vibration is at least 10 times the depth of the cross section.[4]

Following Love we simplify the analysis by restricting attention to problems where there is no extension of the center-line, this condition requires that w and u are related by

$$u = \frac{\partial w}{\partial \theta}\,. \tag{4}$$

* See (1) for a more detailed derivation.

Vol. 1
1960

Finally, to complete the set of equations we have the bending moment related to the change in curvature in the form

$$M = \frac{EI}{r^2}\left(\frac{\partial^2 u}{\partial \theta^2} + u\right). \tag{5}$$

The substitution of (4) into (5), (5) into (3), and (1) and (3) into (2) leads to a single sixth order partial differential equation for w in the form

$$\frac{EI}{r^4}\left(\frac{\partial^6 w}{\partial \theta^6} + 2\frac{\partial^4 w}{\partial \theta^4} + \frac{\partial^2 w}{\partial \theta^2}\right) = m\frac{\partial^2}{\partial t^2}\left(w - \frac{\partial^2 w}{\partial \theta^2}\right) + K\frac{\partial}{\partial t}\left(w - \frac{\partial^2 w}{\partial \theta^2}\right). \tag{6}$$

PRODUCT SOLUTION

We seek solutions of (6) in the form

$$w(\theta, t) = W(\theta)\,T(t) \tag{7}$$

which leads to a separation of (6) into

$$\frac{EI}{mr^4}\left(W^{(vi)} + 2W^{(iv)} + W''\right) = \omega^2(W'' - W) \tag{8}$$

$$\ddot{T} + K/m\dot{T} + w^2 T = 0 \tag{9}$$

where

$$(\,)' = \frac{d}{d\theta}(\,), \qquad \dot{(\,)} = \frac{d}{dt}(\,).$$

If we now restrict attention to rings with clamped edges at $\theta = 0$ and $\theta = a$ then the boundary conditions take the form

$$w = 0, \qquad u = \frac{\partial w}{\partial \theta} = 0, \qquad \frac{\partial^2 w}{\partial \theta^2} + w = 0, \tag{10}$$

or

$$W(0) = W'(0) = W''(0) = W(a) = W'(a) = W''(a) = 0. \tag{11}$$

Let $\{\varphi_n(\theta)\}$ represent a set of eigenfunctions and $\{\omega_n\}$ a set of eigenvalues with the property that

$$\varphi_n^{(vi)} + 2\varphi_n^{(iv)} + \varphi_n'' = \lambda_n^2(\varphi_n'' - \varphi_n) \tag{12}$$

where

$$\lambda_n^2 = \omega_n^2 \frac{mr^4}{EI} \tag{13}$$

and the $\{\varphi_n\}$'s satisfy the boundary conditions

$$\varphi_n(0) = \varphi_n'(0) = \varphi_n''(0) = \varphi_n(a) = \varphi_n'(a) = \varphi_n''(a) = 0\ *. \tag{14}$$

We have solutions of (6) in the form

$$w(\theta, t) = \sum_n \varphi_n(\theta)\,T_n(t) \tag{15}$$

* See the Appendix for solutions of this problem.

Vol. 1
1960

where

$$T_n(t) = e^{-\frac{K}{2m}t}\left\{a_n \cos\omega_n \sqrt{1-\left(\frac{K}{2m\omega_n}\right)^2}\, t + b_n \sin\omega_n \sqrt{1-\left(\frac{K}{2m\omega_n}\right)^2}\, t\right\} \tag{16}$$

for

$$\omega_n > K/2m$$

and

$$T_n(t) = \left\{a_n \exp\left[-\frac{K}{2m}\left(1+\sqrt{1-\left(\frac{2m\omega_n}{K}\right)^2}\right)\right]t + b_n \exp\left[-\frac{K}{2m}\left(1-\sqrt{1-\left(\frac{2m\omega_n}{K}\right)^2}\right)\right]t\right\} \tag{17}$$

for

$$K/2m > \omega_n\,.$$

VIBRATIONS PRODUCED BY A PRESCRIBED MOTION OF SOME CROSS SECTION OF THE RING *

As an example of the motion resulting from the prescribed motion of a cross section of the ring let the tangential motion of the end $\theta = 0$ be prescribed in the form

$$w(0,t) = F(0)f(t)\,. \tag{18}$$

We write the solution of (6) in the form

$$w(\theta,t) = f(t)F(\theta) + \sum_n A_n(t)\varphi_n(\theta) \tag{19}$$

where $F(\theta)$ is the statical deflection curve obtained by neglecting all the time-dependent terms in (6). Thus $f(t)F(\theta)$ would be the solution for a quasi-static prescribed motion of the end of the ring.

Substitution of (19) into (6) leads to the equation

$$\ddot{A}_n + K/m\,\dot{A}_n + \omega_n^2 A_n = -c_n(\ddot{f} + K/m\dot{f}) \tag{20}$$

where c_n is defined by

$$F(\theta) = \sum_n c_n\varphi_n(\theta)\,. \tag{21}$$

Now for a given $f(t)$ and initial values of w and $\frac{\partial w}{\partial t}$ (19) gives the resulting motion.

SOLUTION FOR A PARTICULAR END MOTION

Consider the problem of a semi-circular ring clamped at each end and at rest in a damping medium. Suppose one end ($\theta = 0$) initially, is displaced tangentially by a small amount $R\varepsilon$ and the slope at this

* The procedure used here was used by Mindlin and Goodman for beam vibrations.[5]

Vol. 1
1960

end makes an angle ε with the slope in the undeformed state. Now let the end return to its natural position according to the motion

$$w(0,t) = R\varepsilon e^{-at} \qquad (t>0)\,. \tag{22}$$

The statical deflection curve is taken as the solution of the equation

$$w^{(vi)} + 2w^{(iv)} + w'' = 0 \tag{23}$$

subject to the conditions

$$w(0) = R\varepsilon \qquad w'(0) = 0 \qquad w''(0) + w(0) = r\varepsilon \tag{24}$$

$$w(\pi) = 0 \qquad w'(\pi) = 0 \qquad w''(\pi) + w(\pi) = 0 \tag{25}$$

The solution of (23) which also satisfies (24) and (25) is

$$F(\theta) = \left\{ r\left(\frac{\pi^2-4}{\pi^2-8}\right) - \frac{\pi r}{\pi^2-8}\theta + \left[R - r\left(\frac{\pi^2-4}{\pi^2-8}\right)\right]\cos\theta \right.$$
$$\left. + \left[\frac{R-2r}{\pi} + \frac{2r}{\pi}\left(\frac{\pi^2-4}{\pi^2-8}\right)\right]\sin\theta - \frac{2r}{\pi^2-8}\theta\sin\theta + \frac{1}{\pi}(r-R)\theta\cos\theta \right\}\varepsilon\,. \tag{26}$$

The coefficients c_n are computed from the equation

$$c_n = \frac{\int_0^\pi [\varphi_n(\theta) - \varphi_n''(\theta)]F(\theta)\,d\theta}{\int_0^\pi [\varphi_n(\theta) - \varphi_n''(\theta)]\varphi_n(\theta)\,d\theta}\,. \tag{27}$$

For this example equation (20) takes the form

$$\ddot{A}_n + K/m\dot{A}_n + \omega_n^2 A_n = c_n a(K/m - a)e^{-at} \tag{28}$$

and the initial conditions

$$F(\theta) = w(\theta,0)\,, \quad \frac{\partial w}{\partial t}(\theta,0) = 0 \tag{29}$$

lead to the conditions

$$A_n(0) = 0\,, \qquad \dot{A}_n(0) = ac_n\,. \tag{30}$$

As indicated in equations (16) and (17), the form of the solutions of (28) depends on a comparison of $K/2m$ and ω_n. We will write out the solution for the case when the A_n's of interest are related to ω_n's having the property $\omega_n < K/2m$. For this case we can solve (28) for $A_n(t)$ and then write the complete solution in the form

$$w(\theta,t) = \sum_n c_n\varphi_n(\theta)\left\{K_n^+ \exp\left[-\frac{K}{2m}\left(1+\sqrt{1-\left(\frac{2m\omega_n}{K}\right)^2}\right)t\right]\right.$$
$$+K_n^- \exp\left[-\frac{K}{2m}\left(1-\sqrt{1-\left(\frac{2m\omega_n}{K}\right)^2}\right)t\right]$$
$$\left. + Q_n \exp[-at]\right\} + F(\theta)e^{-at} \tag{31}$$

where

$$K_n^+ = \frac{ma}{K\sqrt{1-\left(\frac{2m\omega_n}{K}\right)^2}}\left[-(1+Q_n)+\frac{K}{2ma}\left(1-\sqrt{1-\left(\frac{2m\omega_n}{K}\right)^2}\right)Q_n\right] \quad (32)$$

$$K_n^- = \frac{ma}{K\sqrt{1-\left(\frac{2m\omega_n}{K}\right)^2}}\left[1+Q_n-\frac{K}{2ma}\left(1+\sqrt{1-\left(\frac{2m\omega_n}{K}\right)^2}\right)Q_n\right] \quad (33)$$

$$Q_n = \frac{a(K/m-a)}{a^2-aK/m+\omega_n^2}. \quad (34)$$

All quantities of physical interest can be found from equations (1) through (5) using (31) through (34).

Acknowledgements—The author would like to take this opportunity to thank Miss Barbara O'Connell and Mrs Gisela Thomas of the Mathematics Section of the Instrumentation Laboratory of the Massachusetts Institute of Technology for assistance in the numerical computations involved in this paper.

APPENDIX

Computation of the natural frequencies and modes of motion for a clamped incomplete ring.

1. *Statement of the problem*

Given the differential equation

$$y^{(vi)}+2y^{(iv)}+y''=\lambda^2(y''-y) \qquad (\ )'=\frac{d}{d\theta}(\ ) \quad (A\text{-}1)$$

together with the boundary conditions

$$y(0)=y'(0)=y''(0)=y(a)=y'(a)=y''(a)=0\,, \quad (A\ 2)$$

we seek solutions of equation (A-1) which also satisfy the conditions (A-2).

2. *General solution*

Take

$$y(\theta)=\sum_{k=1}^{3} A_k\cos\sigma_k\theta+B_k\sin\sigma_k\theta \quad (A\text{-}3)$$

then substitution into (A-1) gives

$$\sigma_k^6-2\sigma_k^4+\sigma_k^2(1-\lambda^2)-\lambda^2=0 \quad (A\text{-}4)$$

as the equation for the σ_k which makes (A-3) a solution of (A-1).

For

$$0<\lambda^2<0{\cdot}113401$$

it turns out that there are solutions to the boundary value problem only for $a>2\pi$.

For

$$0{\cdot}113401 < \lambda^2 < 17{\cdot}6366$$

(A-3) takes the form

$$y(\theta) = A_1 \cos\sigma_1\theta + A_2 \cos\mu\theta \cosh\nu\theta + A_3 \cos\mu\theta \sinh\nu\theta + B_1 \sin\sigma_1\theta + B_2 \sin\mu\theta \sinh\nu\theta + B_3 \sin\mu\theta \cosh\nu\theta \qquad \text{(A-5)}$$

where σ_1^2 is the real root and σ_2^2 and σ_3^2 are the conjugate complex roots of (A-4) with

$$\sqrt{\sigma_2^2} = \mu + i\nu$$

and

$$\sqrt{\sigma_3^2} = \mu - i\nu .$$

For

$$17{\cdot}6366 < \lambda^2 < \infty$$

(A-3) becomes

$$y(\theta) = A_1 \cos\sigma_1\theta + A_2 \cosh\sigma_2\theta + A_3 \cosh\sigma_3\theta + B_1 \sin\sigma_1\theta + B_2 \sinh\sigma_2\theta + B_3 \sinh\sigma_3\theta \qquad \text{(A-6)}$$

where σ_1^2, $-\sigma_2^2$ and $-\sigma_3^2$ are the real roots of (A-4).

The satisfaction of (A-2) for

$$0{\cdot}113401 < \lambda^2 < 17{\cdot}6366$$

requires that the determinant D_1 given by equation (A-7) (p. 55) be equal to zero. While for

$$17{\cdot}6366 < \lambda^2 < \infty$$

the satisfaction of (A-2) requires that D_2 given by equation (A-8) (p. 55) be equal to zero.

The values λ_n which satisfy (A-7) and (A-8) for particular values of α are given in Table A-1, and in Fig. A-1 for α between π and 2π.

For $\alpha = \pi$ the characteristic functions φ_1, φ_2 and φ_3 corresponding to the characteristic values λ_1, λ_2 and λ_3 are given along with their first three derivatives in Figs. A-2, A-3 and A-4. The deflection modes for the "natural" vibrations of the clamped semi-circular ring are sketched in Figs. A-5, A-6 and A-7.

It is seen that the deflection modes for any particular value of α can be obtained by taking the value of σ_n (or μ, ν) from Table A-1, and substituting into (A-7) or (A-8). The resulting degenerate system of equations permits a solution for certain of the constants A_n and B_n in terms of one remaining constant (or several of them). Substituting into (A-5) or (A-6) gives the characteristic modes φ_n for that particular value of α.

The numerical results given in table A-1 were calculated using the IBM 650 at the Massachusetts Institute of Technology Instrumentation Laboratory. For $n = 1$ and 2 the fourth decimal place is probably not

Vol. 1
1960

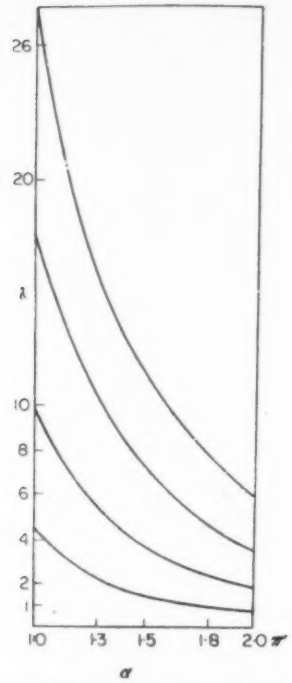

Fig. A-1. Natural frequencies for the incomplete ring.

TABLE A-1. λ_n'S WHICH SATISFY (A-7) OR (A-8) FOR PARTICULAR VALUES OF α.

α	λ^2	σ_1^2		σ_2^2			σ_3^2	
			Real		Imag	Real		Imag
3·1416	19·22	5·7504		− 2·291			−1·459	
3·1416	93·15	11·0775		− 8·030			−1·047	
3·1416	321·5	19·3858		−16·373			−1·013	
3·1416	756·3	28·9720		25·967			−1·005	
4·0841	4·552	3·4252	− ·7126		·9063	− ·7126		−·9063
4·0841	26·68	6·5463		− 3·318			−1·229	
4·0841	97·86	11·3202		− 8·276			−1·045	
4·0841	242·9	17·0346		−14·018			−1·017	
4·7124	1·946	2·6381	− ·3191		·7974	− ·3191		−·7974
4·7124	12·85	4·9318	−1·4659		·6762	−1·4659		−·6762
4·7124	49·58	8·4466		− 5·349			−1·097	
4·7124	126·6	12·6867		− 9·653			−1·034	
5·6549	·6220	1·9685	·01576		·5619	·01576		−·5619
5·6549	4·733	3·4693	− ·7347		·9081	− ·7347		−·9081
5·6549	19·97	5·8365		− 2·426			−1·410	
5·6549	55·15	8·8356		− 5·750			−1·086	
6·2832	0·3208	1·7128	·1436		·4083	·1436		−·4083
6·2832	2·545	2·8538	− ·4269		·8423	− ·4269		−·8423
6·2382	11·46	4·7257	−1·363		·7530	−1·363		−·7530
6·2832	33·06	7·1396		− 3·974			−1·165	

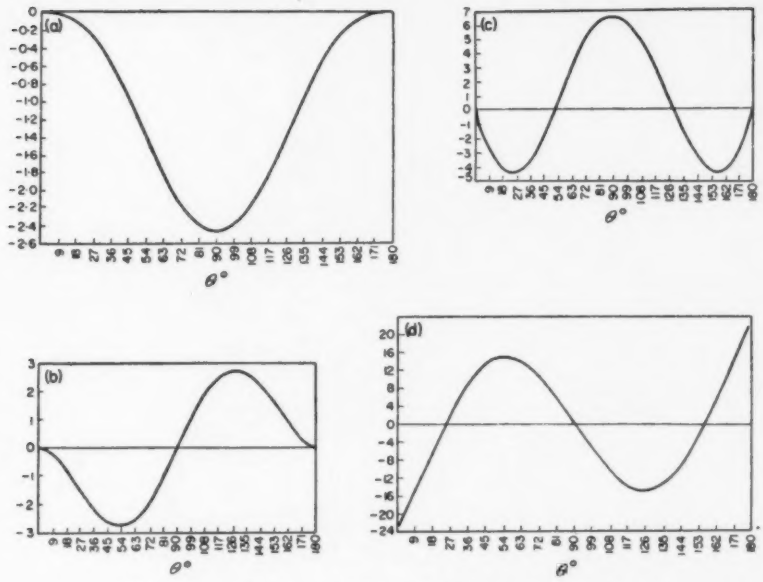

Fig. A-2. Graph of (a) φ_1, (b) φ_1', (c) φ_1'', (d) φ_1'''.

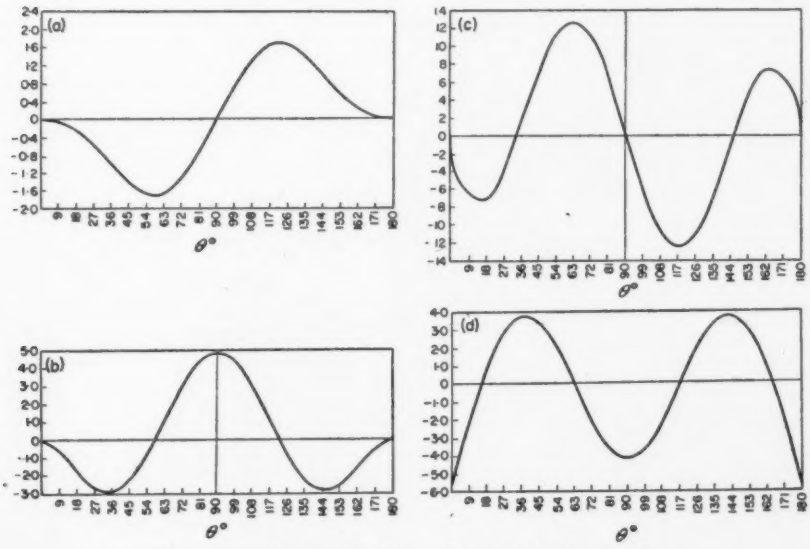

Fig. A-3. Graph of (a) φ_2, (b) φ_2', (c) φ_2'', (d) φ_2'''.

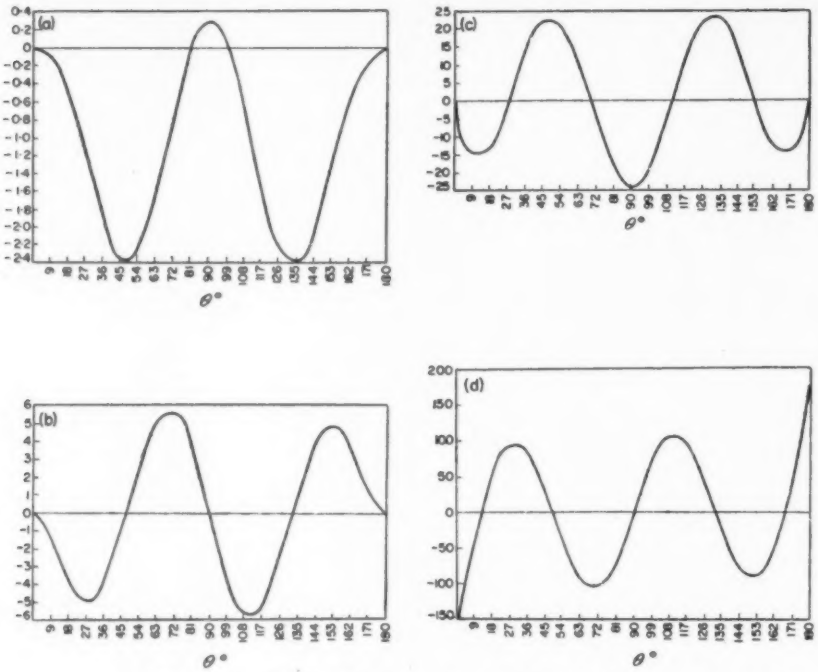

Fig. A-4. Graph of (a) φ_3, (b) φ_3', (c) φ_3'', (d) φ_3'''.

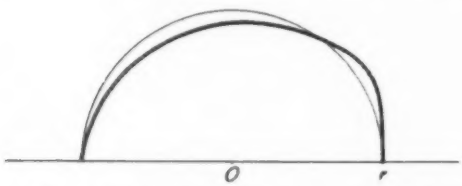

Fig. A-5. Sketch of first (fundamental) mode of vibration.

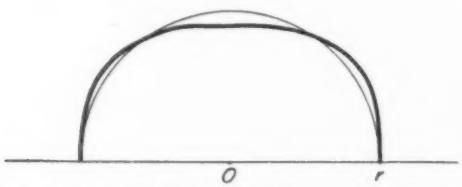

Fig. A-6. Sketch of second mode of vibration.

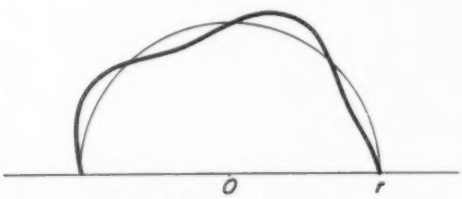

Fig. A-7. Sketch of third mode of vibration.

Vol. 1
1960

$$
D_1 = \begin{vmatrix}
1 & 1 & 0 & 0 & 0 & 0 \\
0 & 0 & \nu & \sigma_1 & 0 & \mu \\
-\sigma_1^2 & \nu^2-\mu^2 & 0 & 0 & 2\nu\mu & 0 \\
\cos\sigma_1 a & \cos\mu a\cosh\nu a & \cos\mu a\sinh\nu a & \sin\sigma_1 a & \sin\mu a\sinh\nu a & \sin\mu a\cosh\nu a \\
-\sigma_1\sin\sigma_1 a & -\mu\sin\mu a\cosh\nu a + \nu\cos\mu a\sinh\nu a & -\sin\mu a\sinh\nu a + \nu\cos\mu a\cosh\nu a & \sigma_1\cos\sigma_1 a & \mu\cos\mu a\sinh\nu a + \nu\sin\mu a\cosh\nu a & \mu\cos\mu a\cosh\nu a + \nu\sin\mu a\sinh\nu a \\
-\sigma_1^2\cos\sigma_1 a & (\nu^2-\mu^2)\cos\mu a\cosh\nu a - 2\mu\nu\sin\mu a\sinh\nu a & (\nu^2-\mu^2)\cos\mu a\sinh\nu a - 2\mu\nu\sin\mu a\cosh\nu a & -\sigma_1^2\sin\sigma_1 a & (\nu^2-\mu^2)\sin\mu a\sinh\nu a + 2\mu\nu\cos\mu a\cosh\nu a & (\nu^2-\mu^2)\sin\mu a\cosh\nu a + 2\mu\nu\cos\mu a\sinh\nu a
\end{vmatrix} \tag{A-7}
$$

$$
D_2 = \begin{vmatrix}
1 & 1 & 1 & 0 & 0 & 0 \\
0 & 0 & 0 & \sigma_1 & \sigma_2 & \sigma_3 \\
-\sigma_1^2 & \sigma_2^2 & \sigma_3^2 & 0 & 0 & 0 \\
\cos\sigma_1 a & \cosh\sigma_2 a & \cosh\sigma_3 a & \sin\sigma_1 a & \sinh\sigma_2 a & \sinh\sigma_3 a \\
-\sigma_1\sin\sigma_1 a & \sigma_2\sinh\sigma_2 a & \sigma_3\sinh\sigma_3 a & \sigma_1\cos\sigma_1 a & \sigma_2\cosh\sigma_2 a & \sigma_3\cosh\sigma_3 a \\
-\sigma_1^2\cos\sigma_1 a & \sigma_2^2\cosh\sigma_2 a & \sigma_3^2\cosh\sigma_3 a & -\sigma_1^2\sin\sigma_1 a & \sigma_2^2\sinh\sigma_2 a & \sigma_3^2\sinh\sigma_3 a
\end{vmatrix} \tag{A-8}
$$

reliable while for $n = 3$ and 4 the third decimal place is probably not reliable.

It may be noted here that the results of den Hartog for the lowest natural frequency of clamped incomplete rings with included angles between $\theta = \pi$ and 2π are in agreement to the number of decimal places which were retained in his calculations.[3]

REFERENCES

1. A. E. H. LOVE, *A Treatise on the Mathematical Theory of Elasticity* (4th Ed.). Dover (1927).
2. R. R. ARCHER, *Massachusetts Institute of Technology, Laboratory Report.* R-148. (1957).
3. J. P. DEN HARTOG, *Phil. Mag.* **5** (Series 7), 400 (1928).
4. S. TIMOSHENKO, *Vibration Problems in Engineering* (3rd Ed.). Van Nostrand, New York (1955).
5. R. L. MINDLIN and L. E. GOODMAN, *J. Appl. Mech.* **17**, 377 (1950).

Vol. 1
1960

Int. J. Mech. Sci. Pergamon Press Ltd. 1960. Vol. I, pp. 57–83. Printed in Poland

AN UPPER-BOUND APPROACH TO PLANE-STRAIN FORGING AND EXTRUSION—I

HIDEAKI KUDO *
Aeronautical Research Institute, Tokyo University

(*Received* 17 *December* 1958)

Summary — To calculate the load required to perform certain kinds of plastic working operations and to account approximately for the modes of flow encountered, a description of a new upper-bound approach is first presented. To facilitate the calculation of good upper bounds, the concept of a unit region is introduced. After finding that the type of velocity field which consists of several rigid triangular parts is the most suitable for the present study, the lowest rate of energy dissipation and the related form of rigid-triangle velocity field are determined for each of the unit rectangular deforming regions having various height-width ratios and frictional boundary conditions. On analysing a particular working problem, the work-piece is supposed to be composed of several unit regions and the lowest upper bound for the working pressure, as well as the most suitable velocity field inside the material, is obtainable directly from those determined for unit regions.

There follows from this method applied to several forging problems with open-dies—(a) Results on the compression of a plate between two flat parallel dies and on the indentation of a flat punch into a semi-infinite or a finite body and these are in close agreement with slip-linesolutions by other investigators. (b) The working pressures and the modes of deformation in open-die extrusion-forging are obtained and they explain some empirically known facts. (c) The working pressure and the mode of deformation in heading are estimated. Some of these results are compared with slip-line solutions and found to be in good agreement. (d) The indentation of a flat punch into a work-piece held in a container is analysed and the upper bound for punch pressure, mode of deformation and distortion of material are related to the dimensions of the working tool and the work-piece, as well as to the conditions of lubrication.

From these results, the upper-bound approach method proposed here seems to offer a fairly accurate and simple means in analysing plane-strain forging problems.

NOTATION

A	= surface area of cross-section
a	= height-width ratio of unit rectangular deforming region
B	= width of work billet
$\dot{E}$	= internal rate of energy dissipation
e	= coefficient of internal energy dissipation
f	= slip-resistance ratio on the surface of tangential velocity discontinuity
G	= depth of plastically deforming region in work-piece
H	= depth of die impression
k	= yield stress of material in shear
$\bar{p}$	= upper bound for mean working pressure
R	= fractional reduction
Rt	= total fractional reduction in area
r	= sign representing "rough" surface ($f = \frac{1}{2}$)

* Now on leave of absence and at Manchester University.

s = sign representing "smooth" surface ($f = 0$)
T = height of work-piece
$\dot{U}$ = flow speed of material through orifice
$\dot{V}$ = die working speed
W = width of working tool
W_c, W_e, W_p = width of container, extrusion die orifice and piercing punch

INTRODUCTION

INSTEAD of the laborious analyses of forging and extrusion processes by means of slip-line field theory, several attempts have already been made to analyse these problems by obtaining upper-and lower-bound solutions.

In many forging and extrusion processes most of the work-piece surface is rigidly constrained by the tools during the deformation. In such cases, good upper bounds or sufficiently low upper bounds could easily be obtained from considerations of geometrical configuration only. The upper-bound approach is of special value in the analysis of complicated problems. In the present paper, therefore, only upper-bound solutions are treated. This upper-bound approach method has recently been adopted also by Johnson *et ali.* [1–6] and used in treating several extrusion and forging problems independently of the author.

Vol. 1
1960

In order to obtain a best solution, i.e. the lowest upper bound, several types of admissible velocity fields have been first examined. It is generally found that the best type of velocity field is composed of rigid triangular parts, their interfaces being surfaces of velocity discontinuity. With such a velocity field sufficiently low upper bounds are obtained with little labour.

To obtain upper-bound solutions for complicated problems easily, the concept of "unit rectangular deforming region" is introduced. Preparing diagrams of the coefficient of energy dissipation for various unit regions of different height-width ratios and boundary frictional conditions and dividing the deforming material into several unit regions, good upper bounds for working pressure in many working problems have been calculated. The problems treated below are those of compression, open-die extrusion-forging, heading, indentation, extrusion, piercing, extrusion-forging, several special types of extrusion and extrusion-forging and closed-die coining. Comparison of the upper bounds for working pressure obtained in this way and the slip-line field solutions already reported by other investigators for several particular problems have been made and it has been found that the method developed in the present work results in a close approximation to that given by the exact solutions.

Rigid–triangle velocity fields which yield minimum upper bounds are also found to be in good agreement with velocity fields derived from slip-line field theory and with flow patterns obtained experimentally using lead specimens.

ANALYTICAL BACKGROUND

For the sake of analytical simplicity, the material is assumed non-work-hardening and rigid-plastic, and to follow the Mises yield criterion and the Lévy-Mises stress-strain-rate relations or the Tresca yield criterion and related stress-strain-rate relations.

According to one of the Limit Theorems, the true rate at which the work is done by applied tractions is not larger than the internal rate of energy dissipation derived from an admissible velocity field in the material. The internal rate of energy dissipation in plane-strain problems $\dot{E}$ is [7]

$$\dot{E} = \sqrt{2}\,k \int_V \sqrt{\dot{\varepsilon}_x^2 + \dot{\varepsilon}_y^2 + \tfrac{1}{2}\dot{\gamma}_{xy}^2}\, dV + 2k \int_S f\dot{s}\, dS \tag{1}$$

for the Lévy–Mises material, or

$$\dot{E} = 2k \int_V |\dot{\varepsilon}|_{\max} dV + 2k \int_S f\dot{s}\, dS \tag{2}$$

for the Tresca material.[8] k is the yield shear stress of the material in plane strain: the other symbols have their usual meanings in plasticity theory. The first integration of each equation is carried out throughout the entire volume of the material which deforms continuously, and the second over the whole surface over which a tangential velocity discontinuity occurs both inside the material and on the boundary between the material and the tool. In the above equations, f denotes the shear or frictional resistance on the discontinuity surface, divided by the plane-strain compressive yield stress $2k$ of the material, and $\dot{s}$ denotes the rate of relative slip of the surface.

For the types of velocity field examined below, the above two equations become one, the only difference existing in the relation of k to the uniaxial yield stress of the material.

When a work-piece is deformed by a rigid tool advancing at a speed of $\dot{V}$, the upper bound $\bar{p}$, for the mean pressure in the direction of tool travel over the projected area A of the working surface on to the plane perpendicular to the direction of working, is derived from

$$\frac{\bar{p}}{2k} = \frac{\dot{E}}{2kA\dot{V}} \tag{3}$$

In the following discussion, the expression on the left-hand side of (3) will be termed the "upper bound for the mean working-pressure ratio". In this paper only problems with tools having working surfaces perpendicular to the direction of tool travel are treated.

To facilitate the analysis of complicated problems, the concept of a "unit rectangular deforming region" is introduced. The region 1234,

Fig. 1, has a height-width ratio a and is surrounded by rigid bodies each of which may be considered to be either a rigid tool or a rigid part of the material. The region is assumed to deform in such a manner that its top surface 13 descends vertically due to an external force which causes the right-hand side surface, 34, to move outwards as a straight line.

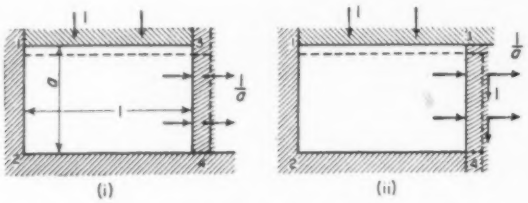

Fig. 1. Unit rectangular deforming regions.

Three different conditions on the surface 34 will be examined. In the first there is nothing outside the surface and it is entirely free from constraint. In the second case, the outside rigid body moves in the horizontal direction without any external resistance and keeps overall contact with the deforming material. In the third, a vertical movement of the outside body, whose speed is the same as that of the top surface, is superposed on the second case by an external force. Henceforth the latter two cases will be called boundary conditions (i) and (ii) respectively.

ADMISSIBLE VELOCITY FIELDS AND THEIR INTERNAL RATE OF ENERGY DISSIPATION

Inside the unit rectangular region various types of admissible velocity fields can be considered to accommodate the velocity boundary conditions described above. However, after comparing several types of velocity field such as "a homogeneous velocity field", "a centred-fan", "a rigid-triangle velocity field" and others, it was found that the third was best for the present purpose because it usually yielded a lower rate of energy dissipation than the others and the calculation of that rate was relatively simple to make. In the following, therefore, velocity fields embodying rigid triangles will be used exclusively.

In this work the value of slip-resistance ratio f was assumed to be constant over each constraining surface and to be either zero or one half. For convenience, a non-dimensional magnitude e will be introduced. This is the internal rate of energy dissipation divided by the product of yield stress of the material, top surface area and its speed of downwards movement. The magnitude e will be called "the coefficient of internal energy dissipation" in subsequent discussion.

The types of rigid-triangle field which were examined are shown in Figs. 2, 3, 4, 5 and 6. The internal rate of energy dissipation for such fields are obtained from equations (1) or (2) for which the first integration

vanishes. Every coefficient of internal rate of energy dissipation thus derived has, except for Fig. 4(b), a form

$$e = g \cdot a + c\frac{1}{a} \tag{4}$$

where g and c are algebraic functions of given boundary conditions f_{ij} and of position and inclination of discontinuity surface, α, β or δ. In most cases the inclination, which makes e a minimum and accordingly e also, is easily calculated.

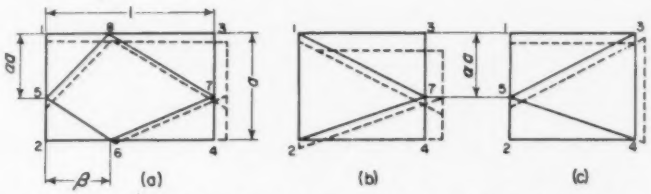

Fig. 2. Rigid-triangle velocity fields for the unit region.

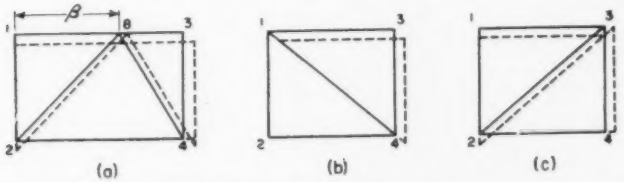

Fig. 3. Simpler rigid-triangle velocity fields for the unit region.

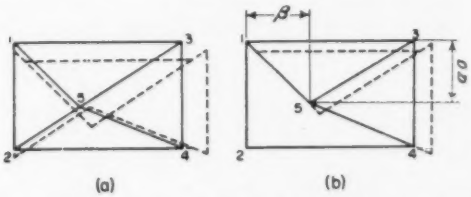

Fig. 4. Some modified types of rigid-triangle velocity fields for unit regions.

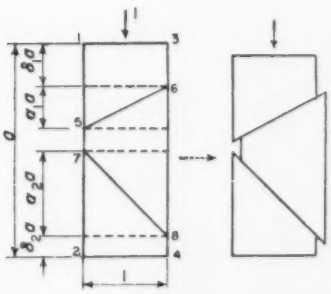

Fig. 5

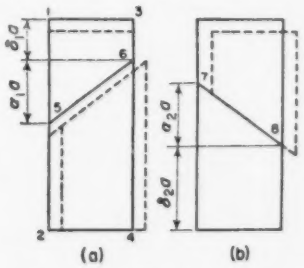

Fig. 6

Fig. 5. Rigid-triangle velocity field for a slender unit region.

Fig. 6. Simpler rigid-triangle velocity fields for a slender unit region.

Vol. 1
1960

When the height-width ratio a is very small compared with unity, it is found that the types of velocity fields which are composed of a series of unit cells, Figs. 7 and 8, yield a lower rate of internal energy dissipation. It can be proved that e is a minimum when the lines of velocity discon-

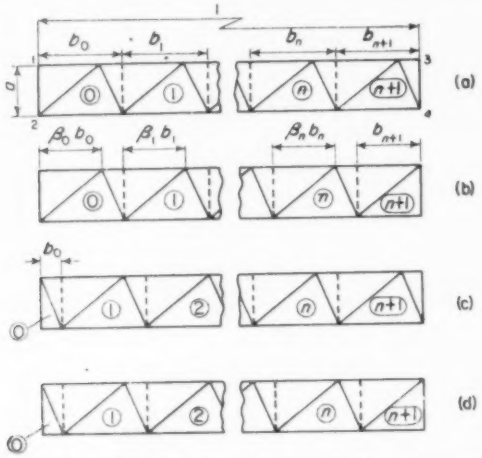

Fig. 7. Combined rigid-triangle velocity fields (from Fig. 3) for a flat rectangular deforming region.

tinuity belonging to each particular group run parallel, as is seen in Figs. 7 and 8. The selection of the most suitable velocity field, i.e. that which yields the lowest energy dissipation, depends on the boundary

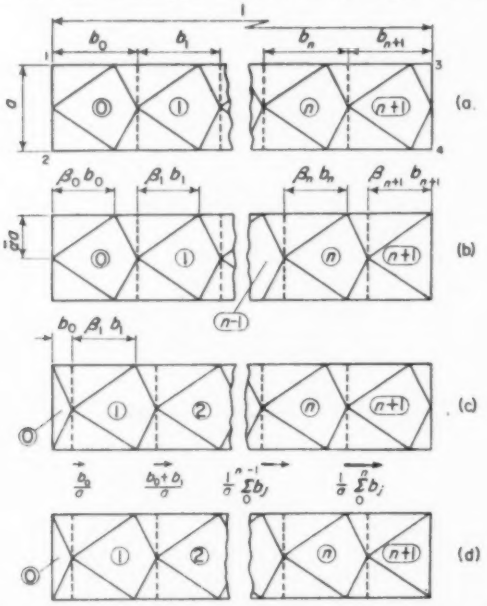

Fig. 8. Combined rigid-triangle velocity fields (from Fig. 2) for a flat rectangular deforming region.

conditions imposed and can be done analytically. It is to be noted that a velocity field, in which the line of discontinuity comes to an end on the free side surface 34, does not give the least energy dissipation except when both top and bottom boundary surfaces are smooth.

When $a \gg 1$ and the surface 34 is free, the velocity fields of the types shown in Figs. 5 and 6 give the lowest value of e. These fields result in an uneven surface on one or both sides of the rectangular region.

The most suitable types of velocity field and their related expressions for the coefficient of internal rate of energy dissipation for each set of boundary conditions and for various magnitudes of height-width ratios a are summarised in Table 1. The derivation of these results is described in detail elsewhere.[9] In the Table, the notation on the left-hand side represents the set of boundary conditions. Thus, "s" denotes the smooth surface, while "r" the rough, and the signs are arranged in order of surface 12, 13, 24 and 34. The number in the parentheses following the surface-roughness notation distinguishes the two conditions possible on the right-hand boundary surface of the rectangular region following Fig. 1. The value of the roman number in parenthesis in the expression for e may be identified thus

$$\text{I} \equiv \frac{1}{2}\left(nH + \frac{1}{nH}\right)$$

$$\text{II} \equiv \left(n - \frac{1}{2}\right)H + \frac{n + \frac{1}{2}}{4n - 1}\,\frac{1}{H}$$

$$\text{III} \equiv \left(n - \frac{1}{2}\right)H + \frac{n}{4n - 3}\,\frac{1}{H}$$

$$\text{IV} \equiv nH + \frac{n + \frac{3}{4}}{4n}\,\frac{1}{H}$$

$$\text{V} \equiv \frac{1}{4}\sqrt{16 - a^2} + \frac{1}{4}a$$

$$\text{VI} \equiv \frac{\sqrt{7}}{8}\sqrt{16 - a^2} + \frac{3}{8}a\,.$$

The most suitable types of velocity field and the positions and inclinations of the lines of velocity discontinuity will be understood from the figures in Table 1.

By preparing graphs of e against a, the numerical calculations associated with particular metal-working problems are greatly facilitated.

TABLE 1. MOST SUITABLE RIGID-TRIANGLE VELOCITY FIELDS AND THE MINIMUM COEFFICIENTS OF ENERGY DISSIPATION $\dot{E}$ FOR UNIT RECTANGULAR DEFORMING REGIONS HAVING VARIOUS SETS OF BOUNDARY FRICTIONAL CONDITIONS AND VARIOUS HEIGHT-WIDTH RATIOS. *

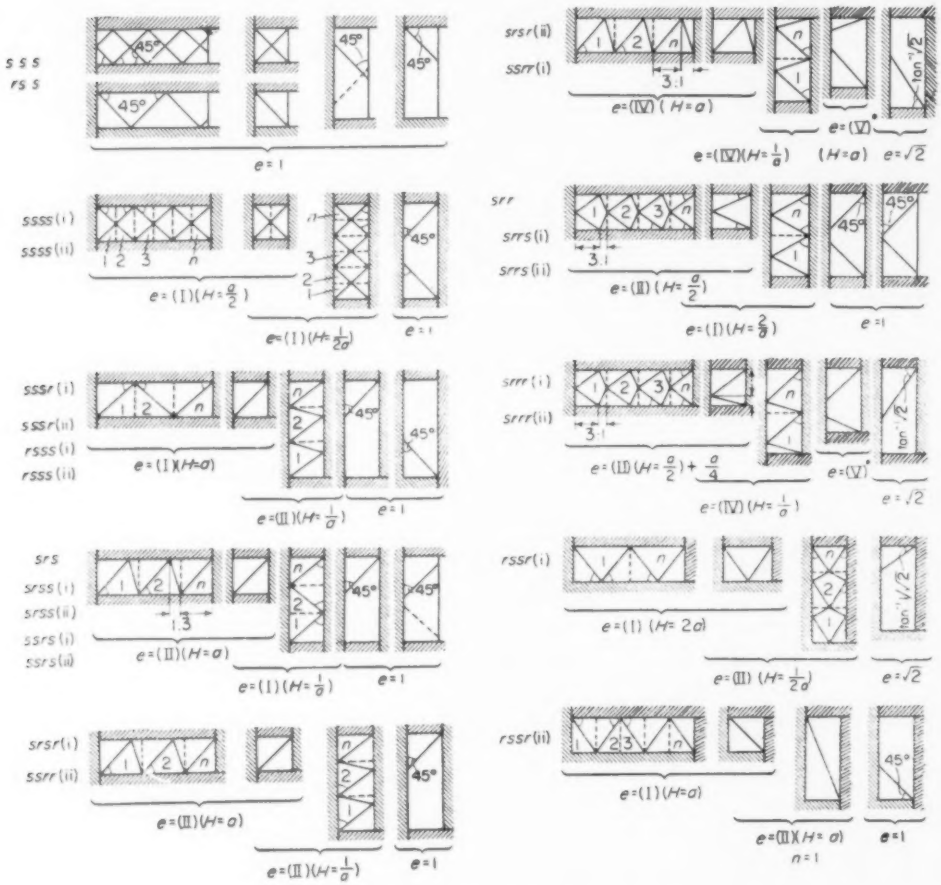

COMPRESSION

The process of plane-strain compression between two parallel flat dies has already been analysed extensively. It will, however, be of interest to apply the rigid-triangle velocity field to this problem in order to examine the effectiveness of the present upper-bound-approach method as well as the suitability of the rigid-triangle velocity field.

When the width of the perfectly smooth die $2W$ is wider than that of $2B$ (Fig. 9(a)) from *sss*, Table 1, the upper bound $\overline{p}/2k$ for the mean compression pressure is 1, since in this case $\overline{p}/2k = e$. An identical result is also obtained from considerations of the homogeneous velocity field in this case. The value of the upper bound obtained here agrees of course

* Under $e = (\mathrm{I})$ $(H = a)$ should be inserted: n is odd.

Vol. 1
1960

TABLE 1 (CONTD) *

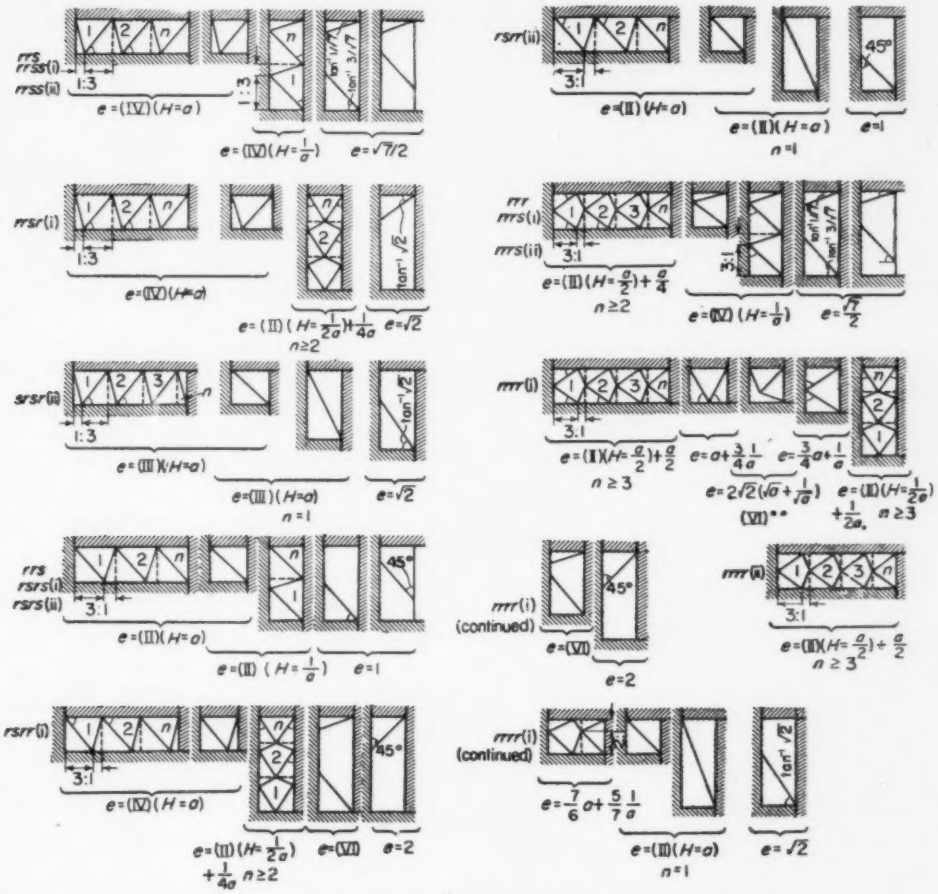

with the exact solution. The rigid-triangle velocity field, however, is quite different (see Fig. 9(b) and (c)).

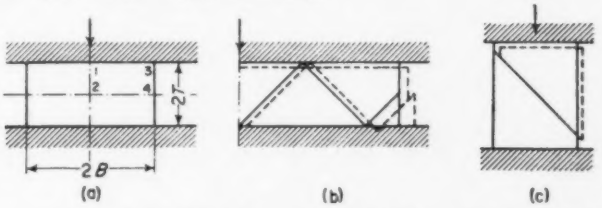

Fig. 9. Compression of a rectangular work-piece between flat dies, having a width wider than the work-piece.

For rough tools, since the right-hand half of the work-piece corresponds to *srr* from symmetry, Table 1, or since the boundary condition of the

* In third group on the right read $n \geq 2$ for $n \geq 3$. (Twice). In fifth group on right read *rrrr* (ii) and $e = (\mathrm{III})\ (H = a)$.

first quarter of the work-piece is represented by *srs*, the upper-bound ratio is

$$\frac{\bar{p}}{2k} = \left(n - \frac{1}{2}\right)\frac{T}{B} + \frac{n+\frac{1}{2}}{4n-1}\frac{B}{T}, \qquad n = 1, 2, \ldots \tag{5}$$

and n is chosen so as to minimise $\bar{p}/2k$. Its calculated value is represented in Fig. 10. It is seen that the upper bound exceeds the slip-line solution of Prandtl [10] and Ross [11] by not more than 5 per cent. The most suitable rigid-triangle velocity fields are illustrated in Fig. 11 and are evidently in agreement in character with that of Prandtl.

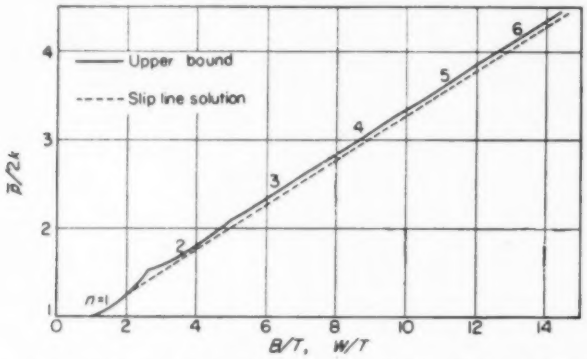

Fig. 10. Comparison of upper-bound and slip-line field solutions for the mean compression pressure with flat rough dies.

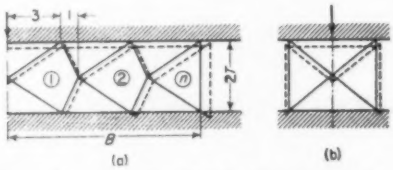

Fig. 11. Most suitable velocity fields for compression between flat rough dies.

When the width of the die is narrower than that of the work-piece, Fig. 12, the boundary condition of the first quarter 1234 of the parts of material lying between the dies can be regarded as *sssr* (i) or *srsr* (i),

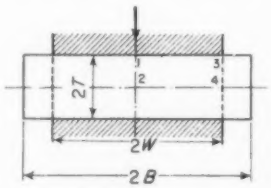

Fig. 12. Compression of a flat work-piece between flat dies having widths narrower than the work piece.

(Table 1), according to the surface, smooth or rough, of the die. This follows from the assumption that the part of the material which does not lie between dies is rigid. For smooth dies, the resulting upper bound is Hill's upper bound introduced by Green[12].

In the case of rough dies, the least upper bound for $W/T \geqslant 1$ is also given by equation (5), and the corresponding velocity field is as shown in Fig. 11. The slip-line field solutions given by Hill [13] and Alexander [14] are also represented in Fig. 10 and again it is seen that the present upper bound lies well within the vicinity of the exact solution.

The most suitable rigid-triangle velocity field obtained here is similar to that obtained by slip-line analysis as well as that indicated by the experiments of Hodge[15] and Nye[16]. The maximum ratio of W/T at which a single rigid wedge adheres to the whole surface of the die, however, is 2·6 by the present analysis, whilst it is 3·64 using slip-line analysis.

The upper bounds obtained above are also applicable after a finite deformation by substituting for T the instantaneous distance between the dies, the boundary conditions for the deforming region remaining unchanged.

Vol. 1
1960

OPEN-DIE EXTRUSION-FORGING

Consider a rectangular work-piece forged between two parallel wide dies, one being flat, the other being provided with an orifice at its centre, Fig. 13. This process is similar to that of an extrusion-forging which will be discussed later, except that in the present case there is no constraint on the side surfaces of the work-piece.

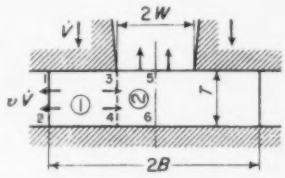

Fig. 13. Open-die extrusion and the division of the work-piece into two unit deforming regions (smooth dies) for analysis.

For smooth tools, it is convenient to assume that the left half of the work-piece is composed of two unit rectangular deforming regions [1] and [2], the former being pressed down by the top die and the latter being squeezed by the moving boundary plane 34. The plane 34 is assumed to remain flat during deformation. From a geometrical consideration for height-width ratios a_1 and a_2, pressing speeds $\dot{V}_1$ and $\dot{V}_2$ and pressing areas A_1 and A_2 for both regions, there being unit thickness perpendicular to the plane of flow, Table 2 can be prepared. Denote the speed of the top die and the bulging-out speed of the left-hand side surface 12 by $\dot{V}$ and $v\dot{V}$

respectively. The total internal rate of energy dissipation is generally given by

$$\dot{E} = 2k \sum_{i=1}^{n} e_i A_i \dot{V}_i \tag{6}$$

TABLE 2. HEIGHT-WIDTH RATIO, PRESSING AREA AND SPEED FOR INDIVIDUAL UNIT RECTANGULAR DEFORMING REGIONS IN OPEN-DIE EXTRUSION WITH SMOOTH TOOLS.

Region	Height-width ratio a_i	Pressing area A_i	Pressing speed $\dot{V}_i$
(1)	$\frac{T}{B-W}$	$B-W$	$\dot{V}$
(2)	$\frac{W}{T}$	T	$\left(\frac{B-W}{T}-v\right)\dot{V}$

where e_i represents the coefficient of energy dissipation for region [1]. The upper bound for the mean working-pressure ratio over the surface of the work-piece is then

$$\frac{\bar{p}}{2k} = \frac{\dot{E}}{2kB\dot{V}} = e_1\left(1-\frac{W}{B}\right)+e_2\left(1-\frac{W}{B}-\frac{T}{B}v\right) \tag{7}$$

If a very thin rigid layer of material is supposed to exist between the two unit regions and if it is supposed to move only in the horizontal direction, then in Table 1, regions [1] and [2] correspond to *rss* and *srs* respectively. When a certain amount of material has been extruded through the top die orifice, region [2] may be considered to correspond to *srsr* (i), since the extruded part will again become rigid.

It is easily shown that $\bar{p}/2k$ as given by equation (7) takes the least value

$$\frac{\bar{p}}{2k} = 1-\frac{W}{B} \tag{8}$$

when

$$v = \frac{B-W}{T}. \tag{9}$$

Thus, for smooth dies, region [2], which lies beneath the orifice, does not deform at all, the only deformation being the compression of region [1]. Fig. 14. illustrates the most suitable velocity fields.

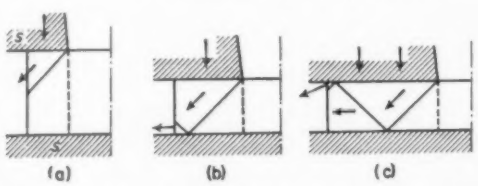

Fig. 14. Most suitable velocity fields in open-die extrusion with smooth dies.

For a rough top die and a smooth bottom die, a "neutral plane" on which the horizontal velocity component is zero, will be considered, Fig. 15(a). Its position for the axes of symmetry is denoted by ϱB. Three unit regions [1], [2] and [3] are considered, their height-width

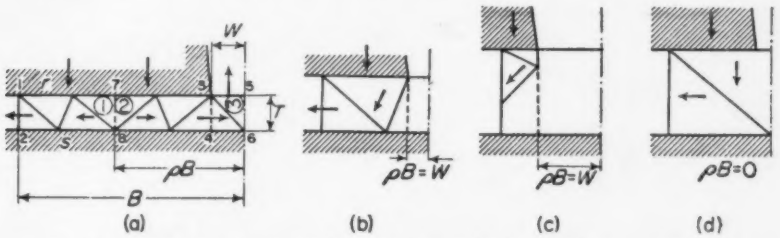

Fig. 15. Division of the work piece for analysis and the most suitable velocity fields in an open-die extrusion with a rough top die and a smooth bottom die.

ratios, pressing areas and pressing speeds being listed in Table 3. The upper bound for the mean working pressure is, from equation (6) and Table 3,

$$\frac{\bar{p}}{2k} = e_1(1-\varrho) + (e_2+e_3)\left(\varrho - \frac{W}{B}\right). \tag{10}$$

TABLE 3. HEIGHT-WIDTH RATIO, PRESSING AREA AND SPEED FOR INDIVIDUAL UNIT RECTANGULAR DEFORMING REGIONS IN OPEN-DIE EXTRUSION WITH A ROUGH TOP DIE AND A SMOOTH BOTTOM DIE.

Region	Height-width ratio a_i	Pressing area A_i	Pressing speed $\dot{V}_i$
(1)	$\dfrac{T}{(1-\varrho)B}$	$(1-\varrho)B$	$\dot{V}$
(2)	$\dfrac{T}{\varrho B - W}$	$\varrho B - W$	$\dot{V}$
(3)	$\dfrac{W}{T}$	T	$(\varrho B - W)\dfrac{\dot{V}}{T}$

If a velocity field is adopted so that no relative slip between regions [1] and [2] occurs, the boundary conditions for the three regions are expressed by *srs*, *srsr* (i) and *srs* (or *srsr* (i) at an intermediate stage), Table 1. An example of the velocity field is shown in Fig. 15(a). Taking the values for e_1, e_2 and e_3 from the diagrams described already and minimizing equation (10) with respect to ϱ, the upper-bound ratios are obtained numerically.

For comparatively large ratios of T/B, the velocity fields of the type shown in Fig. 15(b), (c) and (d) yield lower values than does the type (a).

In types (b) and (c), the part of the material immediately below the orifice does not deform, while in type (d) the work-piece is compressed as a whole.

The least upper bound obtained in this way is plotted in Fig. 16 against T/B with W/B as a parameter. For values of T/B up to those

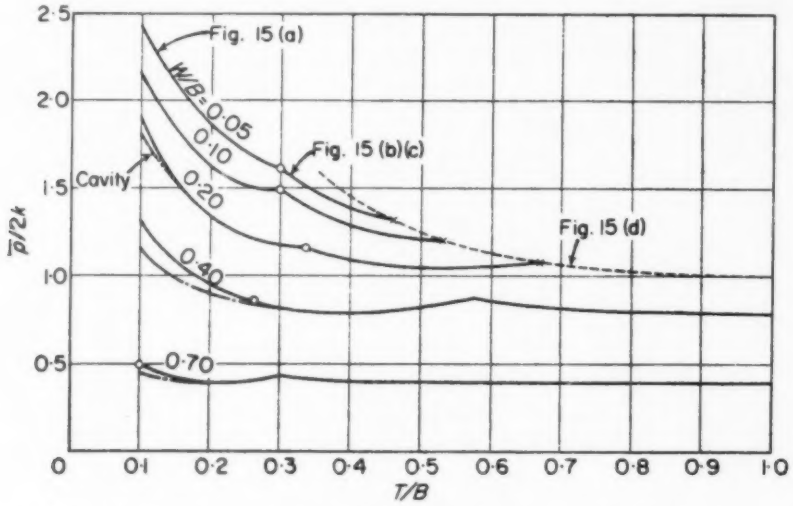

Fig. 16. Upper bounds for the mean working-pressure over ratios the work-piece in open-die extrusion with a rough top die and a smooth bottom die.

indicated by the hollow-circle point on the solid-line curve, the velocity field Fig. 15 (a) gives the least upper bound; for larger values of T/B, the fields (b) and (c) give the smaller values. For values of T/B larger than those indicated by the crosses, the field (d) gives the least upper bound, shown by the broken-line curve. The dash-dot-line curve in Fig. 16 represents the upper bound when part of the bottom surface is allowed to separate from the bottom die. This lifting-up results in the formation of a cavity on the bottom surface of the work-piece; it will be treated later in greater detail with regard to the extrusion-forging problem.

The location of the neutral plane in the most suitable velocity field is determined by ϱ, values for which are shown in Fig. 17. The relative rate of flow of material through the orifice to the top die is given by

$$\dot{U} = \varrho \frac{B}{W} \dot{V} . \tag{11}$$

The above results provide an explanation of the experimental results of Pomp, Muenker and Lueg [17] for axi-symmetrical forging with smooth and rough dies. The working pressure required to produce a part having a "T" section using equation (8) and Fig. 16, is found to be much lower

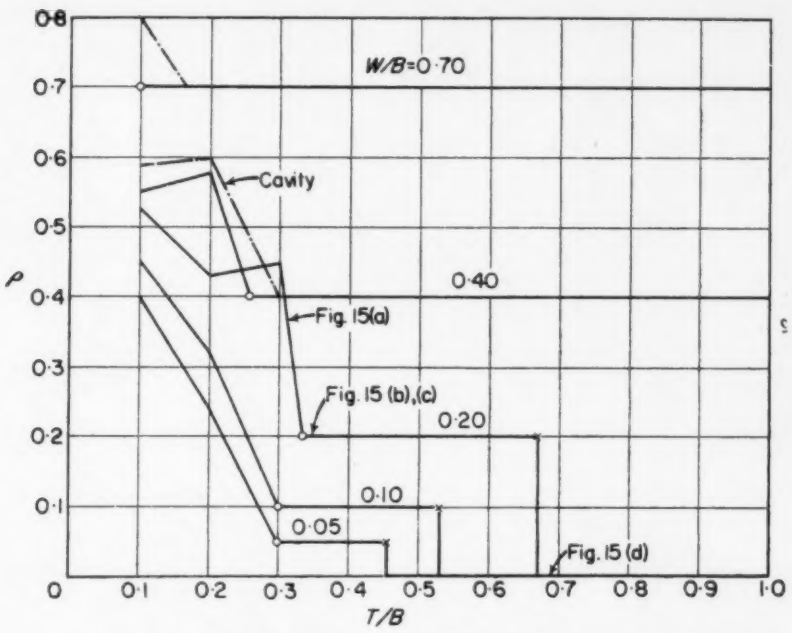

Fig. 17. Most suitable position of the neutral plane 78 during open-die extrusion with a rough top die and a smooth bottom die.

in the open-die forging method than that in the extrusion-forging method with closed dies, discussed below. However, other factors such as buckling, cracking of the work-piece and irregularity of product would cause difficulties in open-die forging.

HEADING

Products having a "*T*"-shaped section are also frequently produced by heading operations. A projected and unsupported part of the work-piece, which is fitted into a die cavity, is compressed or upset between a top and bottom die, Fig. 18. This problem has already been treated by Ross [11] using slip-line theory for a smooth top die and a rough bottom die.

The simplest way of treating the problem by the methods of this paper is to regard the part of the material below the face of the bottom die 2356 as rigid, Fig. 18(a). The resulting solution is then equivalent to that of the normal compression of a rectangular work-piece between two parallel dies, the bottom die 25 being rough. In fact, it was found that this mode of deformation was best for a small width-to-clearance ratio B/H. The slip-line analysis following Ross, indicated the occurrence of plastic deformation in part of the material below the line 25.

An attempt is made to obtain an upper bound by dividing the whole work-piece into three unit rectangular deforming regions in Fig. 18(b).

Vol. 1
1960

The boundary planes 456 and 25 are assumed to remain straight during deformation, the distance of the former from the orifice of the die being denoted by ξB. The height-width ratio, pressing area and speed for each

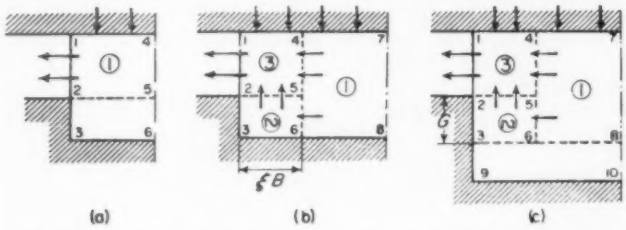

Fig. 18. Three ways of dividing a work-piece into unit rectangular deforming regions and rigid regions for the upper-bound analysis of a heading process.

unit region are given in Table 4. The two different pressing speeds given for region [3] correspond to the upward movement of boundary 25 and the downward movement of the top die respectively. For some cases,

TABLE 4. HEIGHT-WIDTH RATIO, PRESSING AREA AND SPEED FOR INDIVIDUAL UNIT RECTANGULAR DEFORMING REGIONS IN HEADING.

Region	Height-width ratio a_i	Pressing area A_i	Pressing speed $\dot{V}_i$
(1)	$\dfrac{T}{(1-\xi)B}$	$(1-\xi)B$	$\dot{V}$
(2)	$\dfrac{\xi B}{T-H}$	$T-H$	$\dfrac{(1-\xi)B}{T}\dot{V}$
(3)	$\dfrac{H}{\xi B}$	ξB	$\dfrac{(1-\xi)(T-H)}{\xi T}\dot{V}$
	$\dfrac{H}{\xi B}$	ξB	$\dot{V}$

it was found that better results were obtained by using different velocity fields in region [3] according to these two pressing actions.

The upper bound for the mean working pressure to initiate flow is, from equation (6),

$$\frac{\bar{p}}{2k} = e_1(1-\xi) + (e_2+e_3)(1-\xi)\left(1-\frac{H}{T}\right) + e_3'\xi + f_{17}\xi(1-\xi)\frac{B}{T} \qquad (12)$$

where e_3 and e_3' are the coefficients of the internal rate of energy dissipation in region [3] corresponding to the two different modes of deformation stated above. Selecting proper velocity fields for each unit region from Table 1 and substituting the corresponding value e_i, the value of ξ which

Vol. 1
1960

makes equation (12) minimum and the related minimum value of $\bar{p}/2k$ can be obtained numerically. In the present problem, the selection of a velocity field could not be done uniquely since the boundary conditions of individual unit regions at the intersurfaces depend on the combination of velocity fields for three unit regions. Moreover, using the velocity fields from Table 1, it was necessary to add a certain correction term of small amount to equation (12) in order to take into account an inevitable relative slip on the boundary 456. The right-hand side of Fig. 19 shows an example of the most suitable velocity field for a smooth top die and

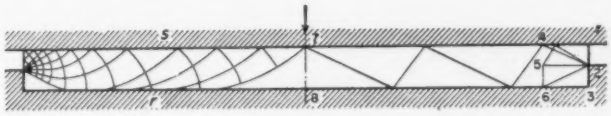

Fig. 19. Comparison between slip-line field and most suitable rigid-triangle velocity field in heading with a smooth top die and a rough bottom die.

a rough bottom die. Figs. 20(a), (b) and 21(a) illustrate the most suitable velocity fields for a smooth top and bottom die and for a rough top and bottom die respectively.

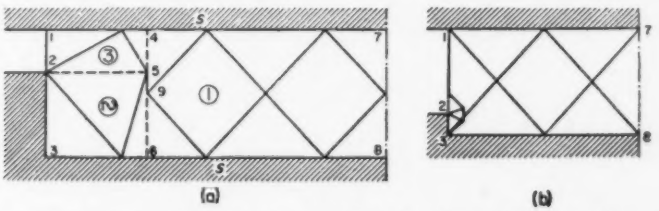

Fig. 20. Most suitable velocity fields in heading with smooth tools.

When the bottom die is rough, for a given value of B/H with T/H increasing, Fig. 22(a), $\bar{p}/2k$ decreases to a certain minimum (solid circle) and thereafter increases. It is found that for T/H larger than this mini-

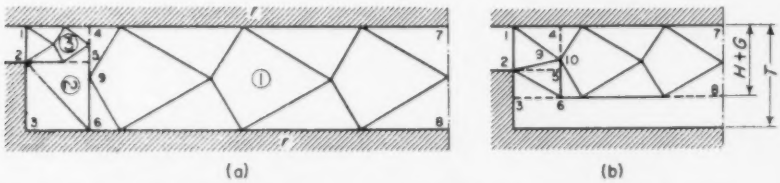

Fig. 21. Most suitable velocity fields for heading with rough tools.

mum, the deformation mode such as is shown in Fig. 18(c) in which a lower part of work-piece 368910 remains undeformed, gives a lower rate of energy dissipation. The corresponding upper bound is then independent of the

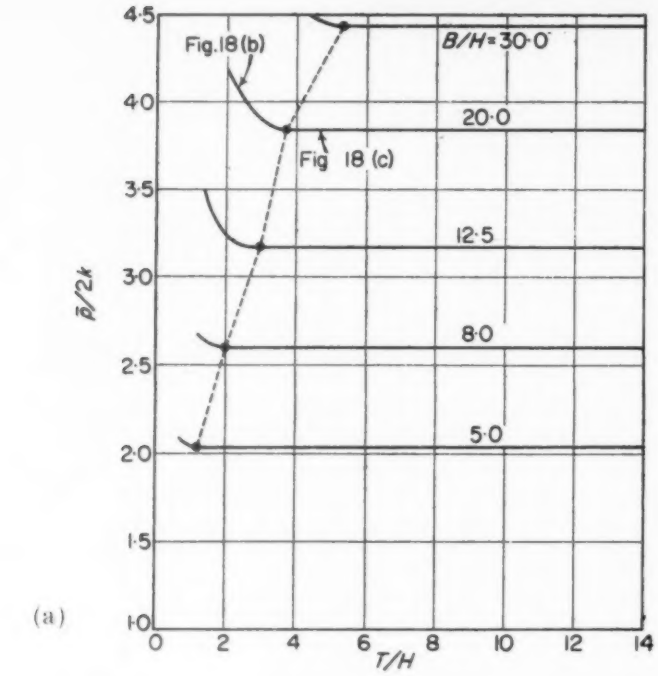

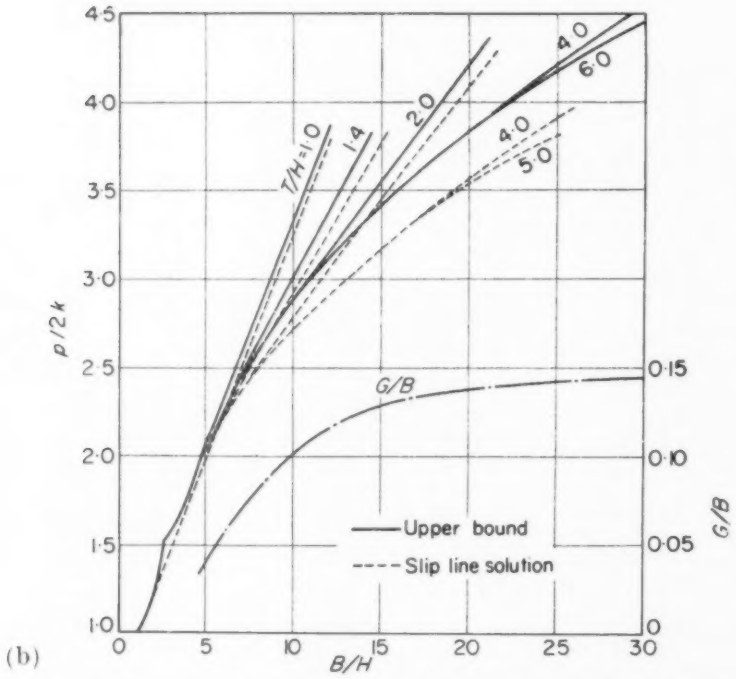

Fig. 22. Upper bounds for the mean heading pressure at incipient flow with a smooth top die and a rough bottom die.

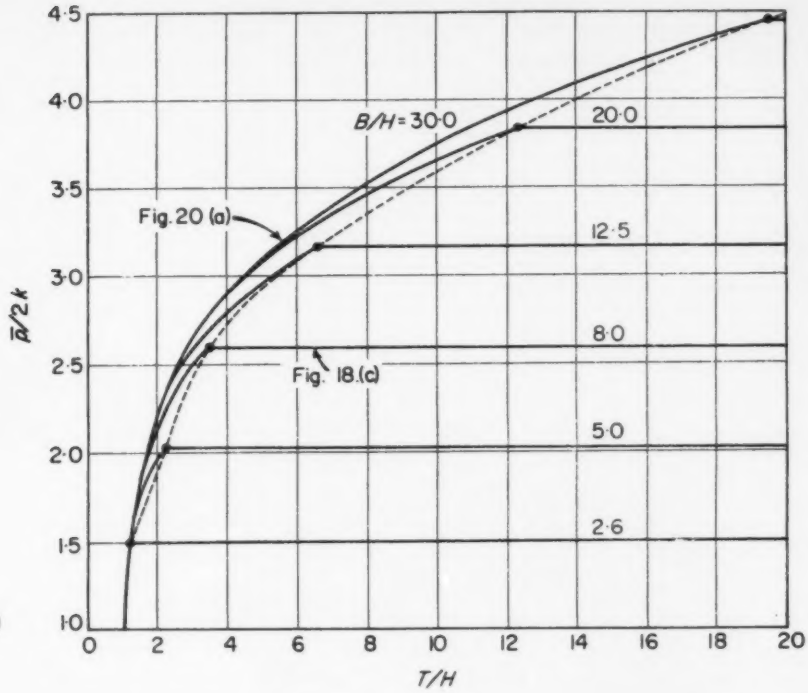

(a)

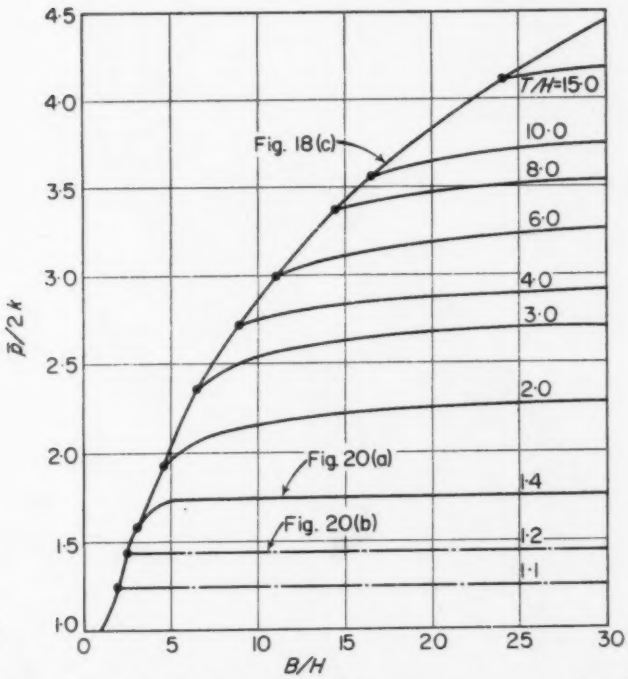

(b)

Fig. 23. Upper bounds for mean heading pressure at incipient flow with smooth tools.

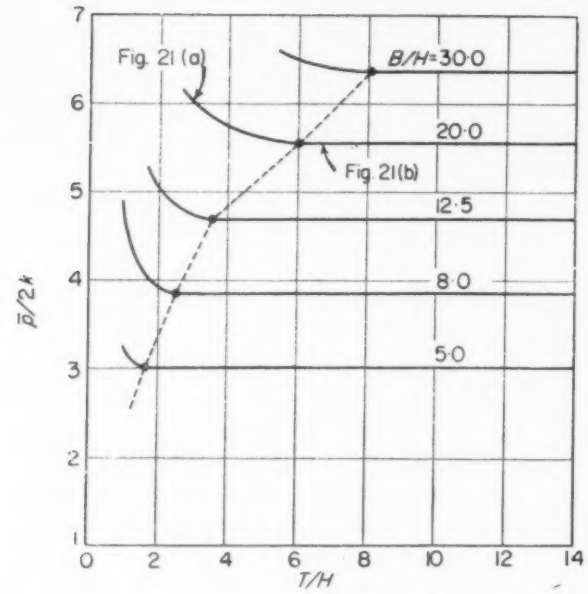

(a)

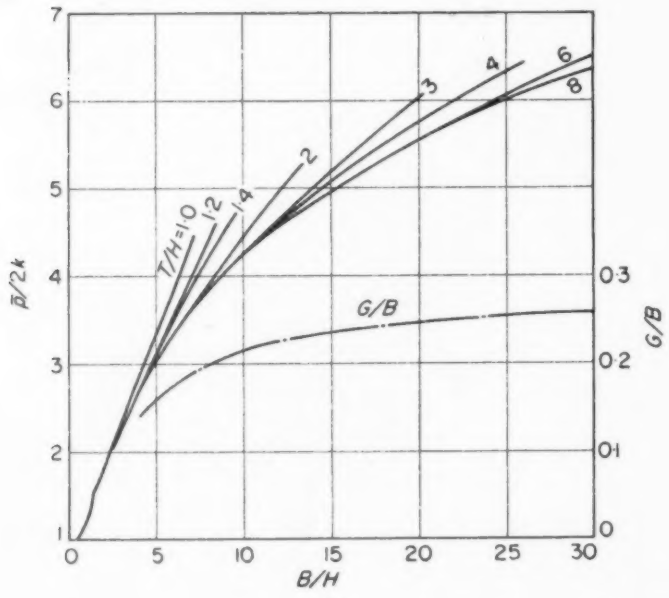

(b)

Fig. 24. Upper bounds for the mean heading pressure at incipient flow with rough tools.

depth of cavity T and is given by the horizontal line in Figs. 22(a) and 24(a). When the top and bottom dies are both smooth, $\bar{p}/2k$ increases with T/H, Fig. 23(a), the deformation mode being of the type shown in Fig. 18(b). In this case also, the deformation mode in Fig. 18(c) gives a better upper bound after a certain critical point (solid circle) is exceeded. It is clear that the ordinate of a horizontal line in Fig. 23(a) is equal to that of the horizontal line in Fig. 22(a) having the same value of B/H.

Figs. 22(b), 23(b) and 24(b) are the cross plotting of Figs. 22(a), 23(a) and 24(a) respectively. In Figs. 22(b) and 24(b), curves for given values of T/H also provide upper bounds for work-pieces having larger values of T/H. In these figures, the depth of the deforming region from bottom die face G for very deep work-pieces is shown by a dash-dot line. In Fig. 23(b), the dash-dot line indicates that the most suitable velocity field is of the type shown in Fig. 20(b), in which part of the free surface of the work-piece bulges out.

Vol. 1
1960

Ross's slip-line results for a smooth top die and rough bottom die, are reproduced in Fig. 22(b). The difference between the present upper bound and the slip-line field solution is seen to be small, the maximum difference being about 10 per cent for the range of conditions analysed. A comparison between the most suitable rigid-triangle velocity field and the slip-line field given by Ross, Fig. 19, shows them to be very similar in character.

The above results hold also for an inverse heading process, in which the distance between the top and bottom die faces is kept constant and the work-piece is pushed by the bottom die up against the top one, the side surface of the bottom die orifice being smooth.

INDENTATION

In this section problems in which a flat punch is forced into a flat surface of material resting on a flat bottom die are treated.

The indentation of a semi-infinite body, Fig. 25, was first treated by Prandtl [18] and recently, in a more general form, by Hill,[13] using slip-line theory. The problem was also investigated by Shield and Drucker [8] using the Limit Theorems. All results for the indenting pressure were identical and equal to $(2+\pi)k$; the slip-line fields used are reproduced on the right-hand side of the axis of symmetry in Fig. 26(a) and (b).

For the purpose of examining the accuracy and convenience of the present method, the rigid-triangle velocity field will be applied. Two unit rectangular deforming regions [1] and [2] in the material near the indentation punch, Fig. 25, are assumed. The height-width ratio, pressing area and pressing speed for each are tabulated in Table 5. The upper bound for punch pressure is from equation (6),

$$\frac{\bar{p}}{2k} = e_1 + e_2 . \tag{13}$$

Assuming that the material in region [1] does not move upward, and that in region [2] does not move downward during deformation, the frictional boundary conditions for the two regions can then be regarded as *ssrr* (i) and *rrr* Table 1, when the punch is smooth.

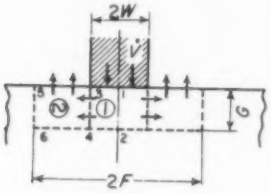

Fig. 25

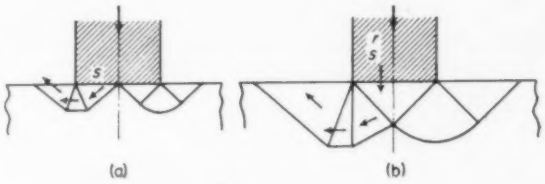

Fig. 26

Fig. 25. Indentation of a semi-infinite body and the division of the work-piece into unit deforming regions and a rigid region.

Fig. 26. Comparisons of the most suitable rigid-triangle velocity fields with the slip-line field in the indentation of a semi-infinite body.

In the present problem, since there is no restriction on the height-width ratios for the two regions, the minimum values of e_1 and e_2 taken from the e versus a diagrams can be substituted into equation (13) which becomes

$$\frac{p}{2k} = \frac{\sqrt{7}}{2} + \frac{\sqrt{7}}{2} = 2{\cdot}65 \tag{14}$$

when

$$\frac{G}{W} = \frac{\sqrt{7}}{4} \quad \text{or} \quad \frac{4}{\sqrt{7}}, \qquad \frac{F-W}{G} = \frac{4}{\sqrt{7}}. \tag{15}$$

The corresponding velocity fields are shown on the left-hand side of Figs. 26(a) and (b). For both the punch pressure and the velocity field the disparity between the present results and those of the slip-line solution will be seen to be very small.

When the punch is rough, it is found from Table 1, that the minimum upper bound is also given by equation (14), while the most suitable velocity field is of the type (b), Fig. 26, only.

TABLE 5. HEIGHT-WIDTH RATIO, PRESSING AREA AND SPEED FOR INDIVIDUAL UNIT RECTANGULAR DEFORMING REGIONS IN INDENTATION.

Region	Height-width ratio a_i	Pressing area A_i	Pressing speed $\dot{V}_i$
(1)	$\frac{G}{W}$	G	$\dot{V}$
(2)	$\frac{F-W}{G}$	W	$\frac{W}{G}\dot{V}$

When the height of the work-piece is reduced below a certain limit, the deforming region is considered to penetrate through the whole height of the work-piece, Fig. 27. A good upper bound for the indenting pressure

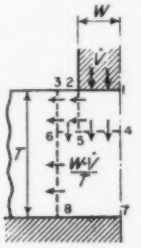

Fig. 27. Division of work-piece into unit deforming regions and a rigid part for the upper-bound analysis of the indentation of a flat work-piece having a finite height.

Vol. 1
1960

is then easily obtained from the results already derived for the heading process when the bottom flat die is smooth. If the top free surface and the bottom surface of the work-piece are assumed to remain flat and if their distance apart is assumed to remain constant, the most suitable velocity field, as obtained above for the heading process for a long work-piece with a smooth top die, is the same as regards velocity boundary conditions for the present problem. The only real difference between the indentation and heading cases lies in the sign of the velocity. Fortunately, the velocity field for heading leads to neither unevenness of the surface 12 nor relative slip between the punch and material.

With this velocity field, therefore, the corresponding upper bound for the mean punch pressure for indentation can be proved to be equal, to the upper bound for the mean heading pressure as given in Fig. 22(b), irrespective of the punch roughness. In Fig. 28, the relation between

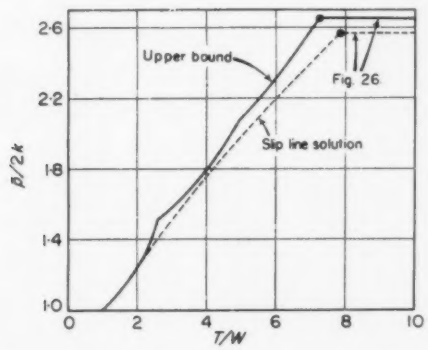

Fig. 28. Relations between incipient indentation pressure and the height of the work-piece as determined from the rigid-triangle velocity field and slip-line theory.

the upper bound and T/W is represented by a solid line. For T/W larger than 8·3, $\bar{p}/2k$ derived from the deformation mode of Fig. 27 exceeds 2·65. It can then be considered that for $T/W \geqslant 8{\cdot}3$, the deformation mode will change into the semi-infinite-body type of deformation. The corresponding curve given by Hill [13] is also reproduced in Fig. 28. Fig. 29 compares the velocity field of the present method and the corresponding slip-line field. * The upper bound velocity field holds also after a finite deformation.

When the width of the work-piece is not much larger than that of the punch width, a rigid-triangle velocity field such as shown in Fig. 30 is found to yield a good upper bound $(B+W)/2W$ for $T \geqslant B+W$.

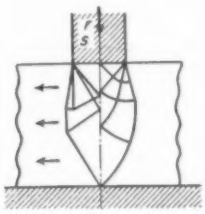

Fig. 29

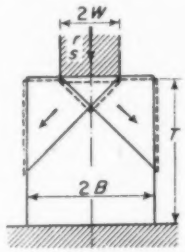

Fig. 30

Fig. 29. Comparison between the most suitable rigid-triangle velocity field and the slip-line field for the indentation of a flat work-piece.

Fig. 30. Most suitable velocity field for the indentation of a work-piece having a relatively narrow width.

To prevent the undesirable distortion of a work-piece having a comparatively narrow width resulting from indentation, it is usual to constrain the work-piece in a container, Fig. 31.

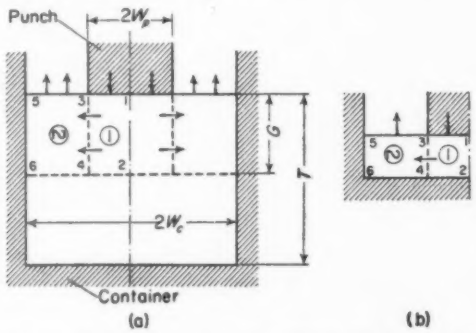

Fig. 31. Division of work-piece into several unit deforming regions and a rigid region for the upper-bound analysis of the constrained indentation of a work-piece in a container.

* It was pointed out by Hill [19] that the type of slip-line field, Fig. 29, is correct only when the indentation is done symmetrically on the top and bottom surface of the work-piece.

If the work-piece is relatively high and if the two unit rectangular deforming regions are assumed as shown in Fig. 31(a), an upper bound for the mean punch pressure at the beginning of flow is also given by equation (13). In the present problem, however, there exists a relation

$$a_2 = \frac{1-R}{R} \cdot \frac{1}{a_1} \tag{15}$$

between the height-width ratios $a_1 = G/W_p$ and $a_2 = (W_c - W_p)/G$, where $R = W_p/W_c$. When the punch and container are both smooth, the boundary conditions for regions [1] and [2] are, according to Table 1, *ssrr* (i) and *rrs* respectively. When the punch and container are both rough, they are represented by *srrr* (i) and *rrr* respectively.

Reading the values e_1 and e_2 from the e versus a diagrams and minimizing equation (13) with respect to G, the minimum upper bound for the punch-pressure ratio, as well as the related depth of the deforming region G, is numerically obtained. As a special case, when the punch and container are smooth and the value of R is relatively large, the analytical expressions for e_1 and e_2 are identical functions of a. Since the function has the form of equation (4) and since $g > e$ for the present conditions, it can be proved that equation (13) has a minimum value when

$$a_1 = a_2 = \sqrt{\frac{1-R}{R}}. \tag{16}$$

In Figs. 32 and 33, the upper bound is indicated by a horizontal straight line.

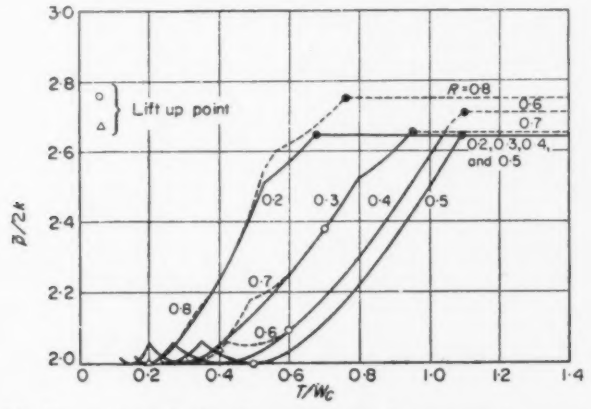

Fig. 32. Upper bounds for the mean punch pressure in constrained indentation with smooth tools.

For a comparatively short work-piece it is more reasonable to assume that the whole body of the material deforms plastically, For the two unit regions in Fig. 31(b), the height-width ratios are uniquely determined

when the values of R and T/W_c are given. The upper bound is also calculated from equation (13) and is shown in Figs. 32 and 33. The solid circle in the figures indicates the transition point between the two modes

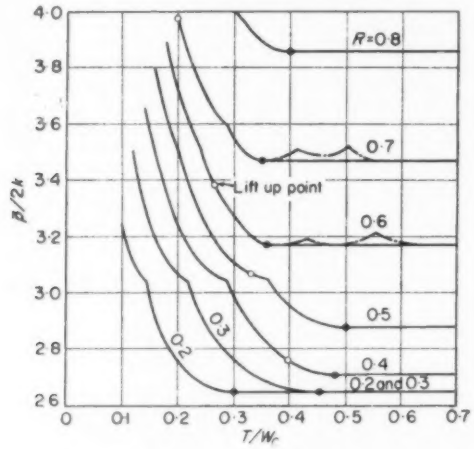

Fig. 33. Upper bounds for the mean punch pressure in constrained indentation with rough tools.

of deformation given by Fig. 31(a) and (b) respectively. The dash-dot line in Fig. 33 indicates that the upper bound for the deformation mode (b) of Fig. 31, exhibits more than one minimum, their values being identical as far as the accuracy of the present calculations permit.

The most suitable velocity fields are illustrated in Figs. 34 and 35. In the velocity fields shown by Figs. 34(c), (d) and 35(c), part of the bottom surface of the work-piece separates from the bottom die. This

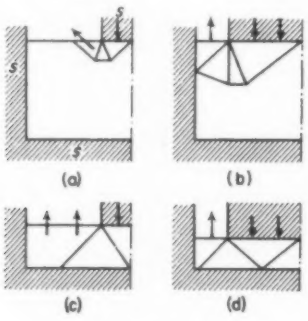

Fig. 34

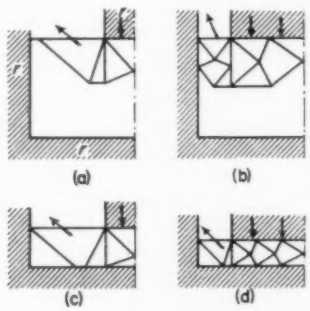

Fig. 35

Fig. 34. Most suitable velocity fields for constrained indentation with smooth tools.

Fig. 35. Most suitable velocity fields for constrained indentation with rough tools.

Vol. 1
1960

phenomenon is often observed in practice and the hollow circle and triangle in Figs. 32 and 33 indicate the critical point for the onset of this lifting-up.

REFERENCES

1. W. Johnson, *Appl. Sci. Res. Hague* **7A**, 437 (1958).
2. W. Johnson, *Third. U. S. Congress Applied Mechanics* p. 571 (1958).
3. W. Johnson, *Appl. Sci. Res., Hague* **8A**, 52 (1959).
4. W. Johnson, *Proc. Inst. Mech. Engrs., Lond*, **173**, 61 (1958).
5. W. Johnson, *Appl. Sci. Res., Hague* **8A**, 228 (1959).
6. W. Johnson, P. B. Mellor and D. M. Woo, *J. Mech. Phys. Solids*, **6**, 203 (1958).
7. W. Prager and P. G. Hodge, *Theory of Perfectly Plastic Solids*. John Wiley, New York (1951).
8. R. T. Shield and D. C. Drucker, *J. Appl. Mech.* **20**, 453 (1953).
9. H. Kudo, *Kokenshuko, Univ. Tokyo* **1**, 37 (1958). In Japanese.
10. L. Prandtl, *Z. angew. Math. Mech.* **3**, 401 (1923).
11. E. W. Ross, *J. Appl. Mech.* **24**, 457 (1957).
12. A. P. Green, *Phil. Mag.* **42** (Series 7), 900 (1951).
13. R. Hill, *The Mathematical Theory of Plasticity*. Clarendon Press, Oxford (1950).
14. J. M. Alexander, *J. Mech. Phys. Solids* **3**, 233 (1955).
15. P. G. Hodge, *J. Appl. Mech.* **17**, 257 (1950).
16. J. F. Nye, *J. Appl. Mech.* **19**, 337 (1952).
17. A. Pomp, T. Muenker and W. Lueg, *Mitt. K.-Wilh.-Inst. Eizenforsch* **20**, 265 (1938).
18. L. Prandtl, *Goettinger Nachr. Math.-Phys. Kl.* **74** (1920).
19. R. Hill, *J. Mech. Phys. Solids* **1**, 265 (1953).

Vol. 1
1960

Int. J. Mech. Sci. Pergamon Press Ltd. 1060. Vol. I, pp. 84–88. Printed in Poland

INERTIA EFFECTS IN VISCOUS FLOWS

J. L. LIVESEY
Mechanical Engineering Department, Manchester University

(*Received* 11 *March* 1959)

Summary — Certain well-known formulae in viscous flow neglect the inertia terms in the equation of motion. A method for including the inertia effects by solving the equation of motion approximately, in its integral form, is demonstrated with reference to the particular problem of radial flow between parallel plates. It is shown that the significance of the inertia effects may readily be estimated.

NOMENCLATURE

r, y, θ = cylindrical co-ordinates
u = velocity along r direction
u = mean velocity along r direction
ϱ = density
μ = coefficient of viscosity
ν = kinematic viscosity
r_1, r_2 = typical radii, $r_1 < r_2$
Q = gross volume flow per unit time
$2h$ = gap between parallel plates
U, R, h = typical magnitudes of u, r, y.
p = static pressure

INTRODUCTION

THE literature of so-called viscous flows contains many examples of the solution of the Reynolds equation

$$\frac{\partial p}{\partial r} = \mu \frac{\partial^2 u}{\partial y^2} . \tag{1}$$

This equation ignores inertia effects completely and represents, simply, a balance between pressure forces and viscous shear forces. In many low Reynolds number flows accelerations are present and inertia effects may be significant. The magnitude of these inertia effects should be estimated carefully before solutions derived from (1) are applied.

The most common field in which equation (1) is applied is that of hydrodynamic lubrication. Recent work in this field has focussed attention on inertia forces, and several workers have indicated methods of analysing the viscous flow which include inertia effects.[1–4] The methods described amount to solving the equation of motion approximately, in its integral form, as first suggested by Karman in his momentum-equation approach to boundary layer theory.

An order of magnitude analysis, applied to the equation of motion, yields a value for the Reynolds number, in terms of the geometry of the problem, for which the inertia effects are significant.[3]

The methods mentioned above will now be applied to the solution of a particular well known problem in viscous flow.

RADIAL FLOW BETWEEN PARALLEL PLATES

Referring to Fig. 1, consider the steady radial flow of a viscous incompressible fluid between two parallel plates of infinite extent. Assuming the flow to be purely radial, we are left with the Navier-Stokes equation for the r direction

$$\varrho u \frac{\partial u}{\partial r} = -\frac{\partial p}{\partial r} + \mu \left(\frac{\partial^2 u}{\partial r^2} + \frac{1}{r} \frac{\partial u}{\partial r} - \frac{u}{r^2} + \frac{\partial^2 u}{\partial y^2} \right). \tag{2}$$

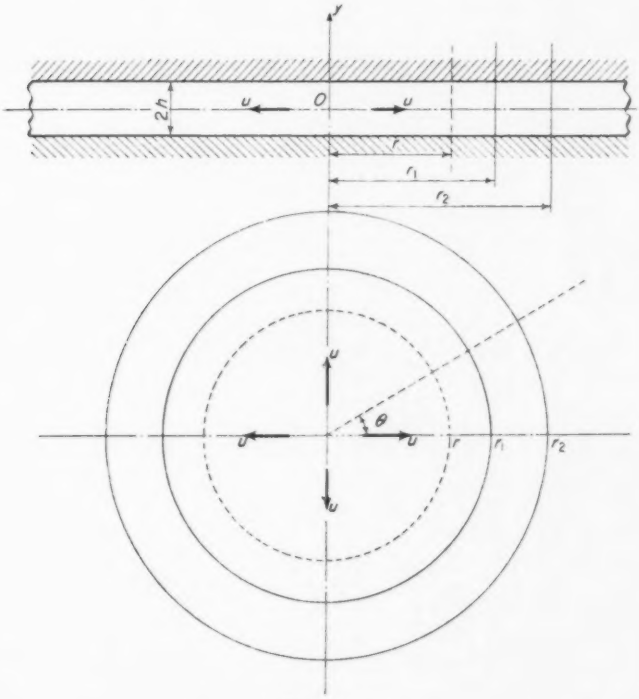

Fig. 1

The continuity equation is

$$\frac{\partial u}{\partial r} + \frac{u}{r} = 0 \tag{3}$$

again assuming velocities identically zero in the y and θ directions. Equation (3) enables equation (2) to be reduced to

$$\varrho u \frac{\partial u}{\partial r} = -\frac{\partial p}{\partial r} + \mu \frac{\partial^2 u}{\partial y^2} \tag{4}$$

Comparison of equations (4) and (1) indicates that the full equation (4) differs from the Reynolds equation (1) by the term $\varrho u \frac{\partial u}{\partial r}$ on the left-hand side. This term involves the inertia force due to the convective acceleration $u \frac{\partial u}{\partial r}$.

An exact solution to (4) for the boundary conditions in Fig. 1 has never been obtained, and would, in fact, involve departure from a purely radial flow. The introduction of the Navier-Stokes equation for the y-direction would be necessary and this would then be solved simultaneously with (4). However, the departure from radial flow must be slight and an approximate solution to (4) may be attempted as follows.

A parabolic velocity distribution

$$u = \frac{3Q}{8\pi r h^3}(h^2 - y^2) \tag{5}$$

is assumed following the known two-dimensional solution.

This distribution is of the form

$$u \propto \frac{1}{r} f(y)$$

and thus satisfies the continuity equation (3).

Equation (4) may now be integrated across the film thickness at any radius r as follows:

$$\varrho \int_0^h u \frac{\partial u}{\partial r}\, dy = -\int_0^h \frac{\partial p}{\partial r}\, dy + \mu \int_0^h \frac{\partial^2 u}{\partial y^2}\, dy \tag{6}$$

i.e. the momentum equation will be satisfied only in its integral form for the finite width of the film. This is essentially the approach used by Karman in his momentum-equation solutions to the boundary layer problem.

Substituting (5) in (6) and integrating yields

$$-\frac{3Q^2\varrho}{40\pi^2 h} \cdot \frac{1}{r^3} = -h\frac{\partial p}{\partial r} - \frac{3\mu Q}{4\pi h^2} \cdot \frac{1}{r} \tag{7}$$

this is now integrated along r between two limits, say, r_1 and r_2, where $r_1 < r_2$ yielding

$$p_1 - p_2 = \frac{3\mu Q}{4\pi h^3} \ln\left(\frac{r_2}{r_1}\right) - \frac{3\varrho Q^2}{80\pi^2 h^2}\left[\frac{1}{r_1^2} - \frac{1}{r_2^2}\right] \tag{8}$$

as the expression for the pressure difference between any two points r_1 and r_2.

The term $\frac{3\mu Q}{4\pi h^3} \ln\left(\frac{r_2}{r_1}\right)$ is the contribution to the pressure change due to viscous effects and is to be found quoted widely in the literature of viscous flows.

Vol. 1
1960

The term $-\dfrac{3\varrho Q^2}{80\pi^2 h^2}\left[\dfrac{1}{r_1^2}-\dfrac{1}{r_2^2}\right]$ is the contribution to the pressure change due to inertia effects and is usually ignored. Note that for the *outward* radial flow considered this term is of opposite sign to the viscous pressure drop. It will be shown shortly that for quite moderate velocities the inertia effects may be more important than the viscous effects and the sign of the radial pressure gradient may be changed.

RELATIVE MAGNITUDE OF THE INERTIA EFFECTS

Referring to equation (4), the viscous effects and the inertia effects will be of the same order of magnitude when

$$\left[\varrho u\frac{\partial u}{\partial r}\right]=0\left[\mu\frac{\partial^2 u}{\partial y^2}\right] \tag{9}$$

taking U, R, h as typical magnitudes we get from (9)

$$\left(\varrho\frac{Uh}{\mu}\right)=0\left(\frac{R}{h}\right),$$

i.e.

$$R_e=0\left(\frac{R}{h}\right),$$

i.e. if the Reynolds number for the regime is of the order of R/h the two effects will be equally significant.

For the particular problem solved here we may equate the terms in their integral form, as they appear in equation (7), and this yields

$$\left(\frac{\varrho\bar{u}h}{\mu}\right)=\frac{5}{2}\frac{r}{h}$$

as the criterion for equal significance of the two effects.

Taking as an example the flow of air under normal conditions of temperature and pressure where $\nu=1{\cdot}59\times10^{-4}$ ft²/sec and assuming the gap between the plates is 0·1 in. then, at a radius of 5 in.,

$$\frac{\bar{u}h}{\nu}=250$$

i.e. a Reynolds number for which viscous flow would usually be assumed. The mean flow-velocity

$$\bar{u}=250\times1{\cdot}59\times10^{-4}\times12\times20=10\text{ ft/sec}$$

If water is considered the velocity is reduced to less than 1 ft/sec. Hence significant inertia effects may be encountered at low velocity levels.

CONCLUSIONS

The significance of inertia effects in viscous flows may readily be estimated.

Approximate solution of the equation of motion, in its integral form, as first suggested by Karman, enables the inertia effects to be calculated.

For the particular case of outward radial flow, the inertia effects are shown to be large enough to change the sign of the radial pressure gradient at quite low Reynolds numbers.

REFERENCES

1. A. FOGG, *Proc. Inst. Mech. Engrs. Lond.* **155**, 49 (1946).
2. W. KAHLERT, *Ingen.-Arch.* **16**, 321 (1947).
3. R. S. BRAND, *J. Appl. Mech.* **77**, 363 (1955).
4. J. F. OSTERLE, Y. T. CHOU and E. A. SAIBEL, *J. Appl. Mech.* **79**, 494 (1957).

Vol. 1
1960

Int. J. Mech. Sci. Pergamon Press Ltd. 1960. Vol. I, pp. 89–108.Printed in Poland

THE ECONOMICS OF STEPLESS MACHINE-TOOL DRIVES

MILTON C. SHAW
Massachusetts Institute of Technology

(*Received* 29 *January* 1959)

Summary — General analyses are presented for the expenditures justified for automatically controlled stepless machine-tool drives for use on machine-tools designed for turning and for facing operations. A stepless speed drive is found to be more important for facing operations than for straight turning. Such drives are also found to be more important for machines designed for use with high-speed steel-tooling than for machines using carbide or ceramic tools.

The cost optimum procedure for using a facing lathe equipped with a finite number of spindle speeds obtained by use of change gears is also presented and compared with representative practice.

Vol. 1
1960

INTRODUCTION

WHEN the average engineer is called upon to compare the machining characteristics of two steels, or the relative performance of two machining methods he will usually adopt improvement in tool life, or the greater number of parts that may be produced per hour, as his basis of comparison. In reality, these quantities are merely components of the variable of ultimate importance, which is *unit machining cost*. Very frequently a new tool or substitute work material having better machining characteristics will cost more, and the question which then naturally arises is should the new idea be introduced. The question that should immediately arise in such a case is whether the savings involved more than offset the added cost. Strange as it may seem a careful comparison of the new and old unit costs are rarely made. Instead, the engineer will usually devote all of his attention to tool life or production rate and make his final decision on the basis of an intuitive feeling that the improvement he observes will pay off.

There seems to be an inherent tendency for engineers to be uncomfortable with analyses that employ cost as the main dependent variable. In our engineering schools we teach engineers to design rationally with regard to stresses, deflections, efficiencies of energy conversion and utilization, but cost analysis is not logically developed. There is a tendency on the part of many engineering teachers to consider any problem involving cost to lie in the province of the business man, and hence, to be something on which the engineering student should not waste his time. Nothing could be further from the truth and it is hoped that this attitude can be corrected in the future.

The specific problem that is to be discussed here is that of the infinitely variable machine tool drive. We will consider why such a drive

should be used and when it is economically feasible. In the past, discussions of this problem have been limited to facing problems and the main emphasis has been upon the saving of time.[1]

There is still another area in which a stepless drive may sometimes be justified, but this does not involve a saving in time and hence will be overlooked unless unit cost is the basis of comparison adopted. In straight-bar turning there is an optimum cutting speed for which the unit cost will be a minimum. If the machine is operated above this speed, tool cost will be higher than it should be, while labor and over-head cost will be too high if the cutting speed is below the optimum. For a machine that has change gears, only certain speeds are available, and if the cost optimum speed does not correspond to one of the available speeds, the machining cost will be higher than it should be. Whether a stepless drive should be used depends, of course, upon whether the additional costs incurred in not having such a device over the life of the machine will more than offset the additional price that is asked for this feature. This particular problem will be discussed first, but before this is done it is convenient that we briefly review the economics of single-point turning.

MACHINING COSTS

The costs associated with a straight-turning operation include:

1. Direct labor and machine cost (xT_c), where x is the value of the machine and operator with overhead (cents/min) and (T_c) the machining time per part:

$$T_c = \frac{\pi dl}{12Vt} = \frac{L}{V} \tag{1}$$

where d = work diameter, in.
l = axial length machined, in.
t = feed, in/rev
V = cutting speed, ft/min
L = helical length machined $= \dfrac{l\pi d}{t12}$, ft.

2. Tool changing cost per part $\left(xT_d \dfrac{T_c}{T}\right)$

where T_d = time to change and set a tool, min
T = tool life, min

3. Tool cost per part $\left(y \dfrac{T_c}{T}\right)$ where y is the mean value of a single cutting edge.

The total machining cost per part is then

$$c = xT_c + (xT_d + y)\frac{T_c}{T} \tag{2}$$

The tool life (T) may be expressed in terms of cutting speed (V) to a good approximation by the Taylor equation as follows:

$$VT^n = C \tag{3}$$

where n and C are constants for a given tool, work material and feed. An average value of n for an HSS tool is 0·1, while $n = 0{\cdot}2$ for carbide and $n = 0{\cdot}4$ for a ceramic tool (see Fig. 1[2]).

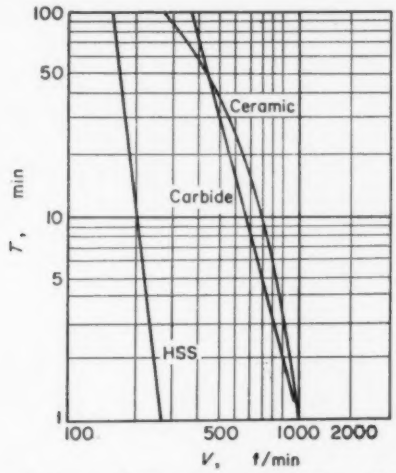

Fig. 1. Representative tool-life curves for HSS, carbide and ceramic tools when cutting AISI 4340 steel.

If equations (1) and (3) are substituted into equation (2), then the minimum unit cost may be found by setting the derivative of c with respect to V equal to zero $\left(\frac{\partial c}{\partial V} = 0\right)$. When this is done the tool life to give minimum cost (T^*) is found to be

$$T^* = \left(\frac{xT_d + y}{x}\right)\left(\frac{1}{n} - 1\right) = R\left(\frac{1}{n} - 1\right), \text{ min} \tag{4}$$

where

$$R = \frac{xT_d + y}{x}, \text{ min} \tag{5}$$

The corresponding cutting speed is then

$$V^* = \frac{C}{(T^*)^n} = \frac{C}{\left[R\left(\frac{1}{n} - 1\right)\right]^n} \tag{6}$$

and if this value is substituted into equation (2) we obtain the following expression for the minimum machining cost per part

$$c^* = \frac{xT_c^*}{1 - n} \tag{7}$$

The foregoing analysis is to be found at several points in the literature (for example, see Gilbert[3]) and a practical method of finding exponent (n) in the workshop is outlined by Shaw[4]. Equation (6) should be used to determine the optimum cutting speed for minimum unit cost in straight turning operations and if possible the machine should be operated at the speed indicated.

TURNING WITH A STEPLESS SPEED CHANGER

Most modern lathes are constructed with a geared head and may be operated at a finite number of speeds which differ one from the next by a constant ratio $(1+K)$, where K is usually from 0·2 to 0·4. Since all possible speeds cannot be obtained with such a machine, it will rarely happen that the exact speed desired to provide minimum unit cost (V^*) can be utilized. If in a given instance the speed corresponding to minimum cost per part (c^*) is V^* then the maximum discrepancy in speed due to the lack of a stepless speed changer will be $\left(\pm\frac{K}{2}V^*\right)$, while the average discrepancy will be $\left(\pm\frac{K}{4}V^*\right)$. The ideal cost per part when V^* can be realized is given by equation (7). The cost per part with the average discrepancy present (i.e., when $V_1 = V^*\left(1\pm\frac{K}{4}\right)$ will be

$$c_1 = xT_{c1}\left(1+\frac{R}{T_1}\right) \tag{8}$$

$$= \frac{xT_c^*}{1\pm\frac{K}{4}}\left[1+\frac{R\left(1\pm\frac{K}{4}\right)^{\frac{1}{n}}}{T^*}\right] \tag{9}$$

$$= \frac{xT_c^*}{1\pm\frac{K}{4}}\left[1+\frac{n\left(1\pm\frac{K}{4}\right)^{\frac{1}{n}}}{1-n}\right] \tag{10}$$

The average additional cost per part when a stepless speed changer is not used will be

$$c_1 - c^* = xT_c^*\left[\frac{1}{1\pm\frac{K}{4}}+\frac{n}{1-n}\left(1\pm\frac{K}{4}\right)^{\frac{1}{n}}-1-\frac{n}{1-n}\right] \tag{11}$$

$$= xT_c^*\left\{\frac{\mp\frac{K}{4}}{1\pm\frac{K}{4}}+\frac{n}{1-n}\left[1\pm\frac{K}{4}\right]^{\frac{1}{n}-1}-1\right\} \tag{12}$$

Vol. 1
1960

If P_T parts are to be made the during the entire life of the machine, then the total saving associated with the stepless speed changer is

$$S = P_T(c_1 - c^*) = P_T T_c^* x \left\{ \frac{\mp \frac{K}{4}}{1 \pm \frac{K}{4}} + \frac{n}{1-n}\left[\left(1 \pm \frac{K}{4}\right)^{\frac{1}{n}-1} - 1\right] \right\} \quad (13)$$

The quantity $P_T T_c^*$ is the total time the machine will be making useful parts. If E is the *machine efficiency*, (where $(1-E)$ is the ratio of the nominal production time the machine is inoperative for maintenance, breakdown, or other unavoidable delays) F is the *use factor* on straight turning (i.e., the fraction of the floor-to-floor time that is actually used for the straight long turning operation), and M is the nominal total number of minutes the machine will be in service during its entire useful life, then

$$P_T T_c^* = EFM \quad (14)$$

In evaluating equation (13) the average between the solutions with the plus and minus signs should be taken since each is equally likely, and hence

$$S = \frac{EFMx}{2} \left\{ \frac{2\left(\frac{K}{4}\right)^2}{1 - \left(\frac{K}{4}\right)^2} + \frac{n}{1-n}\left[\left(1 + \frac{K}{4}\right)^{\frac{1}{n}-1} + \left(1 - \frac{K}{4}\right)^{\frac{1}{n}-1} - 2\right] \right\} \quad (15)$$

When the quantities $\left(1 + \frac{K}{4}\right)^{\frac{1}{n}-1}$ and $\left(1 - \frac{K}{4}\right)^{\frac{1}{n}-1}$ are expressed as binomial expansions and higher order terms are ignored and it is noted that $\left(\frac{K}{4}\right)^2 << 1$, then equation (15) may be written

$$S = \frac{EFMxK^2}{32n} \quad (16)$$

The total saving associated with the stepless speed changer is thus seen to be directly proportional to the effective value of the machine, operator and overhead during the entire effective useful life of the machine ($EFMx$) on the operation in question, directly proportional to the square of the gear ratio (K^2) and inversely proportional to the exponent of the Taylor tool-life equation (n). Strangely enough the total saving does not depend upon the details of the operation such as the feed rate, the work material, the length or diameter of cut or upon the tool cost or tool design.

Example

The following example illustrates the use of equation (16) for a simple long-turning operation:

$EF = 0{\cdot}8$

Vol. 1
1960

Life of machine, $M = 2{\cdot}4 \times 10^6$ min (2 shifts, 5 days per week for 10 years)
Value of machine labor and overhead, $x = 10$ cents/min
Gear ratio, $K = 0{\cdot}3$

From equation (16) the results of Table 1 are obtained

TABLE 1

n	S, \$
0·1	5400
0·2	2700
0·4	1350

Let A be the additional amount we are justified in paying for the infinitely variable speed changer when the lathe is new. If only HSS tooling is used ($n = 0{\cdot}1$) the amount of benefit to be derived from the speed changer in 10 years will be \$5400, or \$540 per year. Let the value of invested capital be 10 per cent per year and let 5 per cent of the initial investment be allowed for maintenance of the speed changer each year.

At the end of the first year the net investment in the speed changer will be $(1{\cdot}10A + 0{\cdot}05A - 540)$. At the end of the second year the net investment becomes: $(1{\cdot}10A + 0{\cdot}05A - 540)\ 1{\cdot}1 + 0{\cdot}05A - 540$, while at the end of the yth year the net investment would be

$$(1{\cdot}1)^y A + (0{\cdot}05A - 540) \sum_{z=0}^{y-1} (1{\cdot}1)^z$$

In the present problem the value of A should be such that this quantity is just zero when $y = 10$, and therefore,

$$A = \frac{540 \sum_{z=0}^{9} (1{\cdot}1)^z}{(1{\cdot}1)^{10} + 0{\cdot}05 \sum_{z=0}^{9} (1{\cdot}1)^z} = \frac{540(15{\cdot}94)}{2{\cdot}59 + 0{\cdot}05(15{\cdot}94)} = \$2540$$

Thus, if the machine considered is to be used with HSS tools ($n = 0{\cdot}1$) for 10 years and is to have a negligible value at the end of this time, the additional amount we may pay for the speed changer when it is new and just break even is \$2540. If this machine were to be used with carbide tooling, for which the average value of n would be about 0·2, then the yearly saving would be $\frac{2700}{10} = \$270$ and the amount that could be paid for the speed changer (A) would be $\left(\frac{270}{540}\right)(2540)$ or \$1270. Similarly, for ceramic tooling, n might be closer to 0·4 (Fig. 1) and (A) would then be but \$635. These results are summarized in Table 2.

Vol. 1
1960

TABLE 2

Tool material	n	A, $ For 10-yr life
HSS	0·1	2540
Carbide	0·2	1270
Ceramic	0·4	635

While the additional amount that we would be justified in spending for an infinitely variable drive for a straight turning operation is not great, such a drive is relatively simple and need not be automatically regulated.

FACING

When a facing cut is taken at constant rev/min (N) the cutting speed (V) will vary with the radial distance (r) from the centerline of the workpiece. A cut will begin at some minimum radius (r_1) and end at some maximum radius (r_2). In facing at constant rev/min (N) we may consider the cutting speed (V) to be constant and equal to ($2\pi rN$) when cutting an infinitesimal distance $dL_c = rd\theta$, where $d\theta$ is a very small angular rotation of the workpiece.

Tool-life equation (3) may be written in terms of the length of work traversing the cutting edge (L) as follows:

$$V\left(\frac{L}{V}\right)^n = C = V^{1-n}L^n \tag{17}$$

It is convenient to consider an equivalent distance L_c' passing the cutting edge at constant speed $V_1 = 2\pi r_1 N$, which will give the same amount of tool wear as actual distance L_c passing the cutting edge at variable speed ($2\pi rN$). From equation (17) it is evident that

$$(2\pi r_1 N)^{1-n}(dL_c')^n = (2\pi rN)^{1-n}(dL_c)^n = (2\pi rN)^{1-n}(rd\theta)^n \tag{18}$$

If the radial feed/rev is (t), then

$$r = r_1 + \frac{\theta}{2\pi}t \tag{19}$$

where θ is the angle the work turns through from the beginning of the cut when $r = r_1$.

Hence, from equations (18) and (19)

$$dL_c' = \frac{\left(r_1 + \dfrac{\theta}{2\pi}t\right)^{\frac{1}{n}}}{r_1^{\frac{1-n}{n}}}\,d\theta \tag{20}$$

The value of the equivalent length (L_c') for the entire cut from radius r_1 to radius r_2 may be found by integrating the above equation between the limits $\theta = 0$ and $\theta = \dfrac{2\pi(r_2 - r_1)}{t}$.

$$L_c' = \int_{\theta=0}^{\frac{2\pi(r_2-r_1)}{t}} \frac{\left(r_1 + \dfrac{\theta}{2\pi}t\right)^{\frac{1}{n}}}{r_1^{\frac{1-n}{n}}} d\theta = 2\pi r_1 \left(\frac{r_2 - r_1}{t}\right) Z \tag{21}$$

where

$$Z = \frac{n}{1+n} \frac{\left(\dfrac{r_2}{r_1}\right)^{\frac{1}{n}+1} - 1}{\dfrac{r_2}{r_1} - 1} \tag{22}$$

The actual length traversed (L_c) at variable speed V is

$$L_c = \int_{\theta=0}^{2\pi\left(\frac{r_2-r_1}{t}\right)} \left(r_1 + \frac{\theta}{2\pi}t\right) d\theta = 2\pi \left(\frac{r_2 + r_1}{2}\right)\left(\frac{r_2 - r_1}{t}\right) \tag{23}$$

The time it takes to make the cut at constant rev/min is

$$T_{cN} = \frac{r_2 - r_1}{Nt} \tag{24}$$

If the lathe is provided with a device for varying the rev/min automatically and continuously with the radial tool position, so as to maintain the cutting speed constant at (V), then the time it will take to complete a cut will be

$$T_{cV} = \frac{L_c}{V} = 2\pi \left(\frac{r_2 + r_1}{2}\right)\left(\frac{r_2 - r_1}{Vt}\right) \tag{25}$$

From equation (2), the cost per part when machining at constant rev/min will be

$$c_N = xT_{cN} + \frac{Rx}{P} \tag{26}$$

where $T_{cN} =$ time to complete a cut $= \dfrac{r_2 - r_1}{Nt}$

$P =$ number of parts per cutting edge

$$P = \frac{\text{tool life expressed as distance cut at } V = V_1}{L_c'}$$

From equations (17) and (21)

$$P = \frac{C^{\frac{1}{n}}}{(2\pi r_1 N)^{\frac{1-n}{n}} 2\pi r_1 \left(\dfrac{r_2 - r_1}{t}\right) Z} \tag{27}$$

Vol. 1
1960

Therefore,

$$c_N = x\left[\frac{r_2-r_1}{Nt} + R\left(\frac{2\pi r_1}{C}\right)^{\frac{1}{n}}\frac{r_2-r_1}{t}ZN^{\frac{1-n}{n}}\right] \tag{28}$$

When $\frac{\partial c_N}{\partial N}=0$, the cost per part will be a minimum and this gives

$$N^* = \frac{\frac{C}{2\pi r_1}}{\left[R\left(\frac{1}{n}-1\right)Z\right]^n} \tag{29}$$

which is the constant rotational speed (N) counterpart of equation (6).

Substituting equation (29) back into equation (28) gives

$$c_N^* = x\left(\frac{r_2-r_1}{t}\right)(RZ)^n\left(\frac{2\pi r_1}{C}\right)\left[\left(\frac{1-n}{n}\right)^n+\left(\frac{n}{1-n}\right)^{1-n}\right] \tag{30}$$

From equations (7), (6) and (23)

$$c_V^* = \frac{x\frac{L_c}{V_c^*}}{1-n} = x\left(\frac{r_2-r_1}{t}\right)R^n\frac{2\pi}{C}\left(\frac{r_2+r_1}{2}\right)\left[\left(\frac{1-n}{n}\right)^n\frac{1}{1-n}\right] \tag{31}$$

and

$$\frac{c_N^*}{c_V^*} = \left(\frac{2r_1}{r_1+r_2}\right)Z^n \tag{32}$$

The saving per part when cutting at constant (V) as opposed to cutting at constant (N) will be

$$c_N^*-c_V^* = \left(\frac{c_N^*}{c_V^*}-1\right)c_V^* = \left[\left(\frac{2r_1}{r_1+r_2}\right)Z^n-1\right]\frac{xT_c^*}{1-n} \tag{33}$$

and for P_T parts the total saving will be

$$S = P_T T_c^* x\frac{\left[\frac{2}{1+\frac{r_2}{r_1}}Z^n-1\right]}{1-n} = P_T T_c^* xQ \tag{34}$$

where Q is the quantity in brackets, which is shown plotted in Fig. 2 for different values of r_2/r_1 and n.

If E is the machine efficiency (where $(1-E)$ is the ratio of the nominal production time the machine is inoperative for maintenance, breakdown or other unavoidable delays), F is the use factor on facing (i.e., the fraction of the floor-to-floor time that is actually used for the facing

Vol. 1
1960

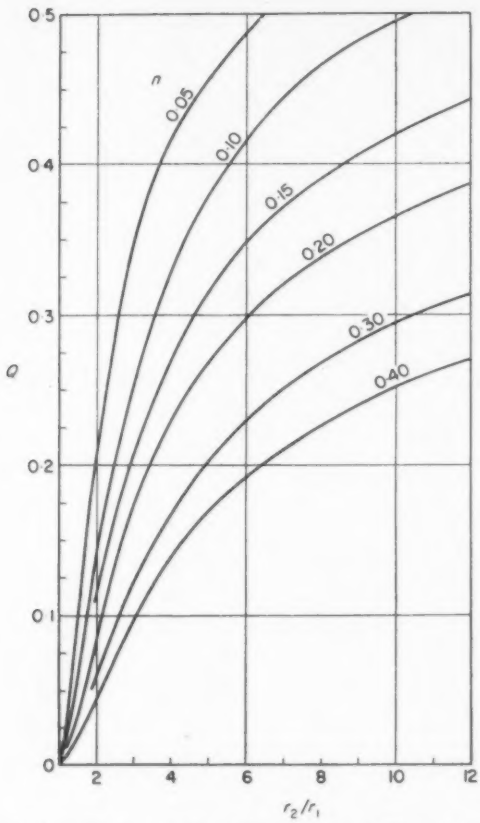

Fig. 2. Variation of factor Q with r_2/r_1 for different values of n.

operation) and M is the total number of minutes the machine will be in service during its entire useful life, then

$$S = EFMxQ \tag{35}$$

Example

In the initial example we will assume that no speed change is made during the entire cut from radius r_1 to radius r_2.

In the machining of a compressor-wheel face from AISI 4340 steel the following conditions pertain:

Machine efficiency, $E = 0{\cdot}8$

Use factor, $F = 0{\cdot}6$

Life of machine, $M = 2{\cdot}4 \times 10^6$ min (2 shifts, 5 days per week for 10 years)

Value of machine, labor and overhead, $x = 15$ cents/min

$r_1 = 2$ in.

$r_2 = 12$ in.

Equation (35) is evaluated in Table 3 for three values of n.

TABLE 3

n	S, \$
0·1	72,000
0·2	51,500
0·4	33,200

If the value of the machine is considered zero at the end of the ten-year period, the value of the invested capital is taken at 10 per cent, while 5 per cent of the initial investment is allowed for maintenance per year, then the amount that could be spent for the variable speed changer to break even (A) would be as follows for the case where $n = 0{\cdot}1$.

$$A = \frac{\frac{72{,}000}{10}\sum_{z=0}^{9}(1{\cdot}1)^z}{(1{\cdot}1)^{10} + 0{\cdot}05\sum_{z=0}^{9}(1{\cdot}1)^z} = \$33{,}800$$

Vol. 1
1960

If the machine is to be used with HSS tooling, this is the value we could afford to spend for the variable speed feature at the time the lathe is purchased. When other types of tooling are used the values given in Table 4 pertain:

TABLE 4

Tool material	n	A, \$ For 10-year life
HSS	0·1	33,800
Carbide	0·2	24,200
Ceramic	0·4	15,600

The sort of lathe that might be used for the job considered here is shown in Fig. 3. The cost of this machine is about \$40,000 (with change gears to provide 24 spindle speeds), but without the automatic speed-changing attachment, which would cost an additional \$10,000. It is seen from Table 4 that the additional \$10,000 cost is justified in all cases and particularly for HSS tooling. Actually, in the foregoing example the value of (F) used for all tools was based on carbide tooling. We should expect (F) to decrease somewhat when machining at the much higher speeds used with ceramic tools and if such a correction were to be made in the analysis, the \$15,600 value in Table 4 should be replaced by a lower value.

CHOICE OF FACING SPEED

The problem of finding the best speed (V) when facing with a lathe *having an automatically controlled spindle speed* is very similar to that of finding the optimum speed in turning. In both cases the best speed

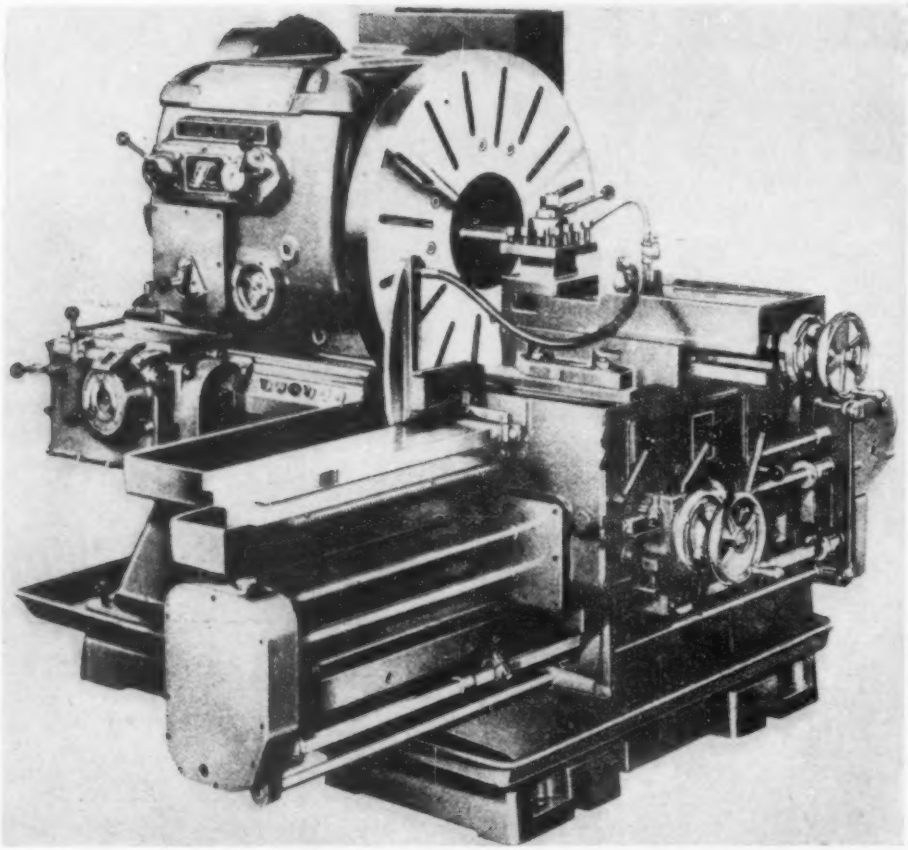

Fig. 3. Representative facing lathe of 60-in. capacity and equipped with automatic stepless speed drive.

is that giving the minimum cost per part, and this may be readily found from equation (6) if the constants n and C are known together with the cost data involved in computing (R). The values of n and C may be found by facing or turning tool life tests at two values of constant speed (V) with all other conditions maintained the same as in the actual facing operation (i.e. feed, fluid, tool, work material, etc.). By plotting tool life (T) versus cutting speed (V) on log-log coordinates, values for n and C may be readily found and the value of V^* computed.

If V^* is known for a facing operation performed at constant surface speed, then the cost optimum rev/min (N^*) for facing at constant rotational speed may be computed from this as follows. From equation (29)

$$2\pi r_1 N^* = \frac{C}{\left[R\left(\frac{1}{n} - 1\right)Z\right]^n} \tag{36}$$

for constant N machining, while from equation (6)

$$V^* = \frac{C}{\left[R\left(\frac{1}{n} - 1\right)\right]^n} \tag{37}$$

for constant V machining. From these two equations it is evident that

$$2\pi r_1 N^* = \frac{V^*}{Z^n} \tag{38}$$

Thus, the starting surface speed for constant rev/min machining should be $\left(\frac{1}{Z^n}\right)$ times the constant V machining velocity (V^*).

Values for (Z^n) may be conveniently obtained from Fig. 4 for use in equation (38).

In the previously considered facing problem, the value of V^* (cost optimum facing speed for constant surface speed machining) is 300 ft/min for a carbide tool for which $n = 0{\cdot}2$, then the cost optimum rev/min for constant rotational speed machining (N^*) would be from equation (38) and Fig. 4.

$$\frac{2\pi 2 N^*}{12} = \frac{300}{4{\cdot}35}$$

or

$$N^* = 66 \text{ rev/min}$$

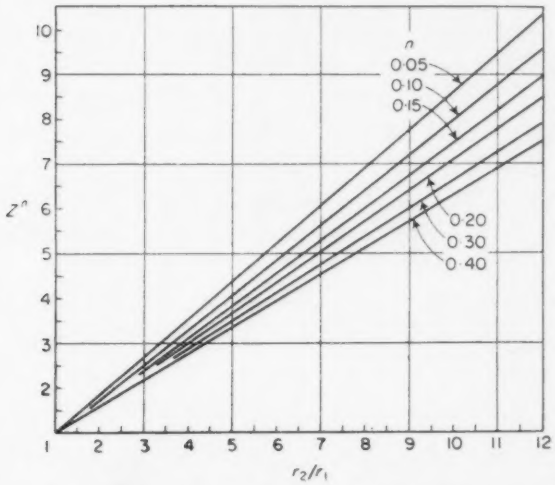

Fig. 4. Variation ot quantity Z^n with r_2/r_1 for different values of n.

In this case the rotational speed would be maintained constant at 66 rev/min for the entire cut. The surface speed at r_1 would be $\frac{2\pi 2(66)}{12}$ or 69 ft/min, while the surface speed at the end of the cut would be 6 times this value or 414 ft/min.

It is to be expected that some difficulty may be experienced with the finish at the lower cutting speeds in the vicinity of r_1. This will largely depend upon the feed that is used, the material machined, the tool geometry, and the cutting fluid that is employed. Should the finish be unacceptable for the lower surface speeds it would then be necessary to divide the cut into at least two parts with a speed change part way between r_1 and r_2, and how this is best done is discussed in the next section.

It is immediately evident that a lathe which enables a facing cut to be taken at constant surface speed (V) is almost indispensable where finish is critical and (r_2/r_1) is large.

OPTIMUM SPEED-CHANGING PROCEDURE

When facing on a lathe having a finite number of change speeds it may be desirable to change the rev/min one or more times during the cut in going from a radius of r_1 to a radius r_2 for one or more of the following reasons:

1. To avoid low surface speeds that may give poor finish.
2. To avoid very low or very high surface speeds where the tool life may fall off. Low-speed trouble is likely for carbide tools and even more likely for ceramic tools. High-speed overheating is more apt to be experienced with HSS tools.
3. To enable a reduction in cost per part.

When the cut is divided into two parts for any reason, it should be done in such a way that the cost per part will be a minimum. If the speed is to be maintained constant from r_1 to r_a at N_1 and then shifted to N_2, where it will be maintained from r_a to the end of the cut (r_2), the first problem is to find the best value for r_a.

From equation (35) it is evident that the saving associated with constant-speed machining is proportional to Q. We should, therefore, divide our cut into two parts in such a way that the sum of the Q's for the two cuts will be a minimum. From Fig. 2 it is evident that this will be the case when $\left(\frac{r_a}{r_1}+\frac{r_2}{r_a}\right)$ is a minimum. The value of r_a required to make $\left(\frac{r_a}{r_1}+\frac{r_2}{r_a}\right)$ a minimum may be found by equating the derivative of this quantity with respect to (r_a) to zero as follows:

$$\frac{\partial\left(\frac{r_a}{r_1}+\frac{r_2}{r_a}\right)}{\partial r_a}=\frac{1}{r_1}-\frac{r_2}{r_a^2}=0 \tag{39}$$

or

$$r_a=\sqrt{r_1 r_2} \tag{40}$$

From which it is evident that

$$\frac{r_a}{r_1} = \frac{r_2}{r_a} = \sqrt{\frac{r_2}{r_1}} \tag{41}$$

The best way of dividing a facing cut into two parts is thus seen to be in such a way that the two ratios of radii are the same and equal to $\sqrt{\frac{r_2}{r_1}}$.

If two speed-changes are to be made, the best procedure for making these can be found in a similar way. In this case r_a and r_b are the intermediate values of radii at which the changes in speed will be made. The operation will now be accomplished at minimum cost when

$$\frac{\partial\left(\frac{r_a}{r_1}+\frac{r_b}{r_a}+\frac{r_2}{r_b}\right)}{\partial r_a} = \frac{1}{r_1} - \frac{r_b}{r_a^2} = 0 \tag{42}$$

$$\frac{\partial\left(\frac{r_a}{r_1}+\frac{r_b}{r_a}+\frac{r_2}{r_b}\right)}{\partial r_b} = \frac{1}{r_a} - \frac{r_2}{r_b^2} = 0 \tag{43}$$

From which it is found

$$r_a = \sqrt[3]{r_1^2 r_2} \tag{44}$$

$$r_b = \sqrt[3]{r_1 r_2^2} \tag{45}$$

and

$$\frac{r_a}{r_1} = \frac{r_b}{r_a} = \frac{r_2}{r_b} = \sqrt[3]{\frac{r_2}{r_1}} \tag{46}$$

Similarly for three speed-changes at r_a, r_b, and r_c

$$r_a = \sqrt[4]{r_1^3 r_2} \tag{47}$$

$$r_b = \sqrt[4]{r_1^2 r_2^2} \tag{48}$$

$$r_c = \sqrt[4]{r_1 r_2^3} \tag{49}$$

and

$$\frac{r_a}{r_1} = \frac{r_b}{r_a} = \frac{r_c}{r_b} = \frac{r_2}{r_c} = \sqrt[4]{\frac{r_2}{r_1}} \tag{50}$$

It should always be advisable to divide a facing cut into two or more parts each having a different constant value of (N) if the changes in speed could be accomplished at no cost. Actually, it will take a time T_g (min) to change the speed, and the cost associated with this will be (xT_g). Whether or not it is advisable to change speed from the stand-

Vol. 1
1960

point of cost depends upon whether the saving associated with the speed change is greater than the cost of making it. From equation (34) it may be seen that the saving *per part* associated with (s) speed changes will be

$$c_S = T_c^* x(Q_o - (s+1)Q_s) - sxT_g \tag{51}$$

where Q_o is the value of Q when there is no speed change and may be found from Fig. 2 when the ratio of radii $= \frac{r_2}{r_1}$

Q_s is the value of Q for each constant speed increment when there are s speed changes. Q_s is the value from Fig. 2 corresponding to a ratio of radii of $\sqrt[s]{\frac{r_2}{r_1}}$.

When the value c_S is positive then it costs less to divide the cut into parts, whereas when c_S is negative, then it costs more to change the speed than the resulting saving.

The saving to be gained by use of an automatic speed changer over a machine operating with (s) speed changes will be

$$S = EFMx\left(Q_o - \frac{c_S}{T_c^*}\right) \tag{52}$$

Example

In the problem previously considered we may ask whether one, two or more speed changes will result in a reduction in cost. Before answering, however, we must specify two more pieces of data concerning the process, namely (T_c^*) and (T_g). For the machine considered (Fig. 3), the feed can be disengaged, the speed changed, and the feed reengaged in a time of 0·4 min, and therefore T_g is 0·4 min. For a value of V^* of 300 ft/min, and a feed of 0·02 in/rev, T_c^* may be found from equation (25) as follows:

$$T_c^* = 2\pi\left(\frac{12+2}{2}\right)\left[\frac{(12-2)}{300(12)(0{\cdot}02)}\right] = 6{\cdot}1 \text{ min}$$

For a cut without speed change $\frac{r_2}{r_1} = 6$ and Q_0 is found to be 0·297 in Fig. 2 for $n = 0{\cdot}2$ (carbide tool). When a single speed-change is made at $r_a = \sqrt{r_1 r_2} = 4{\cdot}90$ in., the ratio of radii is $\sqrt{\frac{r_2}{r_1}} = \sqrt{6} = 2{\cdot}45$ and Q_1 is found to be 0·128 from Fig. 2. Substituting into equation (51) we find

$$c_S = \{(6{\cdot}1)[0{\cdot}297 - 2(0{\cdot}128)] - 0{\cdot}4\}x = -0{\cdot}15x\,.$$

This means that it will cost $0{\cdot}15x$ *more* per part when machining with the cut divided into two parts at a radius of 4·90 in.

The values of N_1^* (for $r = 2$ to 4·9 in.) and N_2^* (for $r = 4{\cdot}9$ to 12 in.) that should be used in such a case may be found from equation (38)

as follows, where $Z^n = 1{\cdot}9$ is the value corresponding to a ratio of radii of $\sqrt{6} = 2{\cdot}45$, from Fig. 4

$$N_1^* = \frac{300(12)}{2\pi(2)(1{\cdot}9)} = 151 \text{ rev/min}$$

$$N_2^* = \frac{300(12)}{2\pi(4{\cdot}9)(1{\cdot}9)} = 61{\cdot}5 \text{ rev/min}$$

These values of rev/min will give surface speeds that vary from 158 to 388 ft/min for each of the two cuts. The value 158 ft/min is much more apt to give trouble free operation from the standpoint of surface finish than the 69 ft/min value for the case with no speed change. Likewise, the 388 ft/min top speed is much less apt to give trouble due to overheating the tool than the 414 ft/min top speed for the case with no speed change. These advantages are obtained at the slight added cost per part of $0{\cdot}15x$.

Vol. 1
1960

It is of interest to see if a reduction in cost can be had by using two speed changes. These speed changes should be made at the following radii:

$$r_a = \sqrt[3]{r_1^2 r_2} = \sqrt[3]{2^2(12)} = 3{\cdot}63 \text{ in.}$$

$$r_b = \sqrt[3]{r_1 r_2^2} = \sqrt[3]{2(12)^2} = 6{\cdot}60 \text{ in.}$$

and the ratios of radii for all three cuts would be $\sqrt[3]{\frac{r_2}{r_1}}$ of 1·82. From Fig. 2 the value of Q_2 corresponding to this ratio and $n = 0{\cdot}2$ is found to be 0·065. The value of c_S is then as follows for a 0·02 in/rev feed:

$$c_S = \{6{\cdot}1[0{\cdot}297 - 3(0{\cdot}065)] - 2(0{\cdot}4)\}x = -0{\cdot}178x$$

This time the cost per part is *increased* a greater amount than when the cut is divided into but 2 parts.

The speeds to be used in this case follow:

$$N_1^* (\text{for } r = 2 \text{ to } 3{\cdot}63) = \frac{300(12)}{2\pi(2)(1{\cdot}50)} = 191 \text{ rev/min}$$

$$N_2^* (\text{for } r = 3{\cdot}63 \text{ to } 6{\cdot}60) = \frac{191}{1{\cdot}82} = 105 \text{ rev/min}$$

$$N_3^* (\text{for } r = 6{\cdot}60 \text{ to } 12) = \frac{105}{1{\cdot}82} = 58 \text{ ft/min}$$

and these values would result in a range of surface speeds from 200 to 365 ft/min for each of the three cuts.

The cutting times in each of these cases would be

For first cut: $T_{c1} = 0{\cdot}427$ min.

For second cut: $T_{c2} = 1{\cdot}42$ min.

For third cut: $T_{c3} = 4{\cdot}65$ min.

Since the cutting time for the shortest of these cuts (0·42 min) is just about equal to the time required to change speeds, it does not seem practical to increase further the number of speed changes. If four or more changes should be used on such an operation the operator would undoubtedly be kept too busy and as a result the time to make a speed change would probably begin to rise.

The value of S for $n = 0{\cdot}2$ given in Table 3 when there is no speed change in cutting from r_1 to r_2 will be as follows for a single speed change (from equation 52)

$$S = (0{\cdot}8)(0{\cdot}6)(2{\cdot}4 \times 10^6)(0{\cdot}15)(0{\cdot}297 + \frac{0{\cdot}15}{6{\cdot}1} = \$56{,}400$$

and the corresponding value of A in Table 4 becomes \$26,200.

All of the quantities previously derived for the example involving an n of 0·2 are collected in Table 5 for comparison. The second column of this table (s) corresponds to the number of speed changes used in making the facing cut, while column (6) gives the total time to make the cut including the time to change speeds. The other items may be readily identified. When the facing cut is made at constant surface speed it will take 6·1 min, while at a constant rev/min (66 rev/min) the total cutting time is 7·57 min and the amount that is justified for purchase of an automatic stepless speed changer (A) is \$24,200. If the cut is divided into two parts ($s = 1$), the entire cut will take less time (7·18 min), but the cost justified for the stepless speed changer increases to \$26,600 and hence, the operation is a more expensive one. When two speed changes are used the value of A is still higher (\$26,600).

Corresponding values are also given in Table 5 for a feed of 0·01 in/rev. Here, it is seen that values of (A) become progressively lower for 1 and 2 speed changes respectively.

TABLE 5

t (in/rev)	s	V (ft/min)	r (in.)	N	$\Sigma(T_c + sT_g)$ (min)	A (\$)
0·02	∞	300	2–12	VAR.	6·10	—
	0	69–414	2–12	66	7·57	24,200
	1	158–338	2–4·9	151	7·18	26,200
			4·9–12	62		
	2	200–365	2–3·63	191	7·30	26,600
			3·63–6·60	105		
			6·60–12	58		
0·01	∞	300	2–12	VAR.	12·20	—
	0	69–414	2–12	66	15·14	24,200
	1	158–387	2–4·9	151	13·96	23,600
			4·9–12	62		
	2	200–365	2–3·63	191	13·80	21,200
			3·63–6·60	105		
			6·60–12	58		

The general observation that may be made is that the value of (A) is changed very little by stepwise changes in speed during a cut. It follows, at the same time, that changes in speed during a cut result in very little saving (or loss), and such changes do not appear justified except when single-speed operation is troublesome due to the extreme speeds being too low or too high. Therefore, use of equation (35) without speed change will give results of sufficient accuracy for estimating the saving to be gained by use of an automatic speed changer even in cases where the machine will actually be used with one or more speed changes during the cut.

CURRENT PRACTICE

When the operating rules that are currently in use in industry are applied to the facing example we have been considering (feed = 0·02 in/rev),

TABLE 6

r (in)	N (rev/min)	V (ft/min)	T_c (min)
2–4	139	145–300	·719
4–8	70	145–300	2·86
8–12	34	145–220	5·88
	Time for 2 speed-changes		·8
		Total	10·26

the values given in Table 6 are obtained. The total machining time is seen to be far longer than the corresponding optimum value of 7·30 min given in Table 5. Current practice is seen to err in two principal ways:

1. In not dividing the cut properly with regard to the radii at which the speed is changed. The ratio of radii should be $\sqrt[4]{6} = 1{\cdot}57$ in all cases, whereas a value of 2·00 pertains for the first two speed-changes in Table 6 and a value of 1·50 is used for the third.

2. In not going to a high enough speed at the end of each cut. Instead of making the maximum speed (V) for constant rev/min machining the same as the value that would be used when machining at constant surface speed (300 ft/min), the range of speeds pertaining should straddle this optimum value (300 ft/min).

The cost of the operation when performed in accordance with Table 6 will be significantly greater than performed under the optimum conditions of Table 5. The magnitude of this difference, which constitutes the penalty for operating according to the currently accepted rules, may be readily computed by use of techniques already discussed.

CONCLUSION

Two types of problems associated with stepless speed machine tool drives are identified and considered from an economic point of view.

Vol. 1
1960

The amount justified for a stepless speed drive for a straight turning machine is found to vary directly as K^2 (where $(1+K)$ is the gear-change ratio) and inversely with the coefficient of the Taylor tool life equation. For average conditions the additional amount justified at time of purchase for a stepless speed drive on a turning machine will vary from about \$1000 to \$2500. The higher value is more apt to pertain for HSS tools, whereas the lower value is more likely for carbide tooling. When ceramic tools are used the additional purchase price justified becomes less than \$1000.

A variable speed drive is found to be far more important for facing operations. Many lathes designed for facing are equipped with a finite number of speeds obtained by change gears. The matter of choosing cost-optimum facing speeds, the radii at which speed should be changed, as well as the number of speed changes for minimum cost is considered in detail for such a lathe. The saving in cost associated with an automatic variable speed drive operated under cost optimum conditions is determined for the expected life of a facing lathe. It is found that under average conditions the additional cost at time of purchase that is justified for an automatic speed changer on a facing lathe is apt to be in excess of \$30,000 for HSS tooling, in excess of \$20,000 for carbide tooling, but somewhat less for ceramic tooling. These values assume that both the finite speed and stepless speed machines are operated under conditions to yield optimum machining cost per part. They do not, however, attempt to evaluate the value of the improved finish possible with a machine having a stepless speed drive.

Acknowledgement—The author would like to express his appreciation to the Shell Oil Company for the research grant that was used in connection with this study.

REFERENCES

1. M. KRONENBERG, *Tool Engr.* **39**, 93 (1957).
2. M. C. SHAW, *Industrie-Anzeiger* **79**, 282 (1957).
3. W. W. GILBERT, *Machining Theory and Practice* p. 465. ASM, Cleveland, Ohio (1950).
4. M. C. SHAW, *Industrie-Anzeiger* **79**, 847 (1957).

Int. J. Mech. Sci. Pergamon Press Ltd. 1960. Vol. I, pp. 109–120. Printed in Poland

ELEMENTARY METHODS FOR THE ANALYSIS OF CERTAIN FORGING PROCESSES

H. LIPPMANN
Institut für Mechanik, Techn. Hochschule Hannover, Germany

(*Received* 2 *April* 1959)

Summary — An elementary method of determining the pressure in plane strain press forging between dies with engravings of small inclination is given. The last part of the paper shows, with the help of an elementary model how to compute the energy needed in forging and the efficiency of the operation.

Vol. 1
1960

INTRODUCTION

THE elementary method of computing the force P needed for the plane-strain plastic compression of a bar between rough plane plates with coefficient of friction μ is as follows; (see Fig. 1) let q be the average value of $-\sigma_x$, p of $-\sigma_y$ along the y-direction and l the width of the bar perpendicular to the xy-plane. Equilibrium of forces in the x-direction gives

$$hl\,dq = -2(\operatorname{sgn} x)\mu p\,dx\,,$$

μp being the shear stress due to friction and $\operatorname{sgn} x = 0,\ \pm 1$ for $x = 0,\ \gtrless 0$. If h/b does not exceed a certain number B, then it may be assumed that σ_x, σ_y are everywhere principal stresses. The theory of plane plastic strain indicates that the principal stress normal to the xy-plane of Fig. 1 is $(\sigma_x+\sigma_y)/2$ (cf. Hill,[1] p. 129). Tresca's yield criterion is therefore $|\sigma_x-\sigma_y| = Y$, where Y is the uniaxial yield stress, which is constant for a rigid-perfectly plastic material. Thus for plastic compression of the bar,

$$p-q = Y\,. \tag{2}$$

Combining (1) and (2) it follows,

$$\frac{dp}{dx} + 2\operatorname{sgn} x\,\frac{\mu p}{h} = 0\,;$$

$p|_{x=b/2} = p|_{x=-b/2} = Y$ because of (2) and $q = 0$, therefore

$$p = Y\exp 2\frac{\mu}{h}\left(\frac{b}{2} - |x|\right) \quad \text{for} \quad -\frac{b}{2} \leq x \leq \frac{b}{2}\,. \tag{3}$$

A second integration over the upper (or lower) surface of the specimen gives the force P:

$$P = 2l\int_0^{b/2} p\,dx = blY\,\frac{e^{2\mu\frac{b}{h}}-1}{2\mu\frac{b}{h}} \approx blY\left(1+\frac{\mu}{2}\,\frac{b}{h}\right). \tag{4}$$

With less accuracy (3) is also valid for cylindrical specimens.[2]

Formulae derived from (4) are the only useful theoretical ones for certain problems in press-forging practice. The methods utilizing slip lines besides being troublesome lead only to lower bounds for the force,[3] and exact values are unlikely. In the same way, velocity fields yield only upper bounds.[4] The approaches of Körber and Eichinger[5] (viscous fluid)

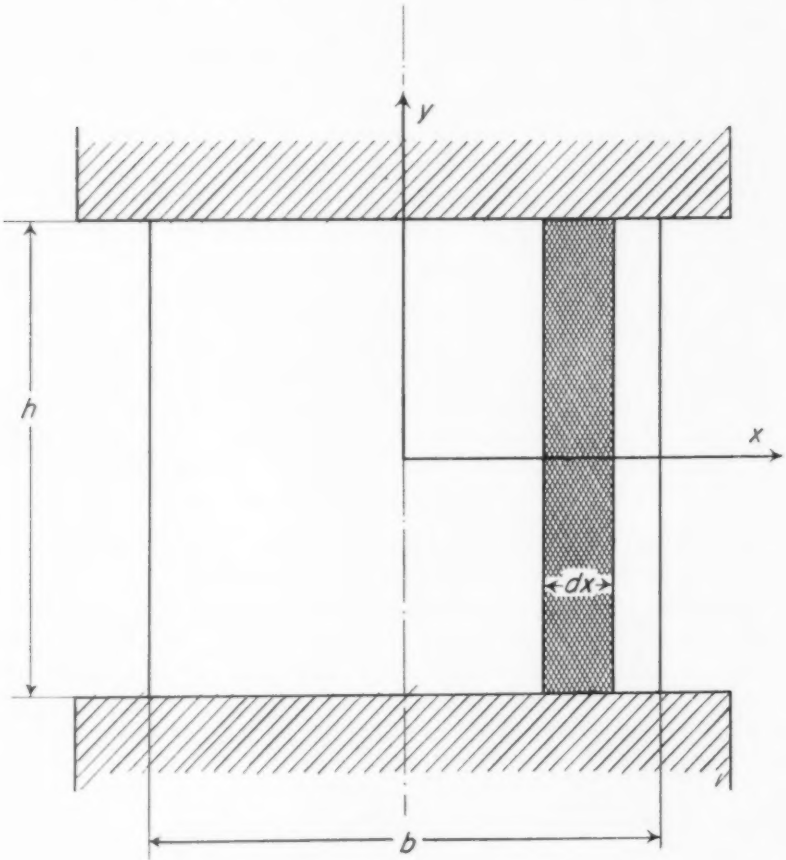

Fig. 1. Plane-strain compression between flat plates.

or Eichinger and Pomp[6] contain errors, and a complete solution for the stresses and strains based for instance on the Levy-Mises equations seems to be impossible if it is desired to fulfil all the boundary conditions.[1] Therefore at present only the Siebel-v.Karman elementary method can be expected to give useful results under complicated circumstances. Reicherter[7] attempted to compute forces in the case of engraved dies, but Lippmann and Neuberger[8] showed his method to be in error. In the following section another method is to be described. It is the counterpart to the method of Kobayashi *et al*[10] which seems to be successful in the case of steep engravings.[11] The approach of Dietrich

and Ansel [12] seems to partake of both methods. It is based on different assumptions which are useful for theories of drawing and pressing, but there is no indication when it will be exact.

DERIVATION OF THE STRESS p AND THE LOAD P

To extend the elementary method, similar assumptions must be made as in Section 1; (see Fig. 2.)

(i) The condition is that of plane strain; i.e. $l \gg b, H$ (l being the width of the specimen).

(ii) The slope of the upper and lower boundary curves is small at all points.

(iii) Material does not adhere to the dies. At the die faces there is Coulomb friction and there is only one section of no flow at $x = x_0$.

(iv) b/H has at least the value $1/B$ (cf. Section 1); B being a suitably chosen constant; the smaller B, the better the solution.

Vol. 1
1960

From assumptions (ii) and (iv) it is seen that σ_y, σ_x can be regarded as the extreme principal stresses, and neither vary greatly in the y-direction. To compute the stresses near the right-hand end of the cross-section take co-ordinates as shown in Fig. 2. The x-axis is arbitrary (and in this instance is equidistant from both dies); the y-axis is at the left end of

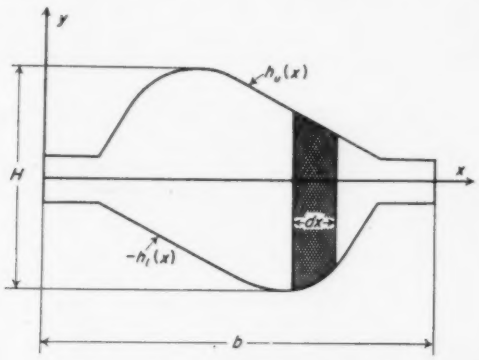

Fig. 2. Compression between engraved dies.

the cross-section. The upper curve $h_u(x)$ and the lower one $-h_l(x)$ are supposed given. All the derivatives of h_u and h_l as well as the total height, $h(x) = h_u(x) + h_l(x)$, together with their derivatives, are also known. p, q are the average values of $-\sigma_y$, $-\sigma_x$ respectively, along the vertical direction as before. Then – and this is characteristic of the elementary approach – the equilibrium conditions at a strip of breadth dx are set up; Fig. 3 shows the upper part of an element, only. The width l is without influence.

If p_u is the stress normal to the upper surface, then $p_u \Delta s_u$ is the force acting on the unit width of the upper surface. The force due to friction, R_u,

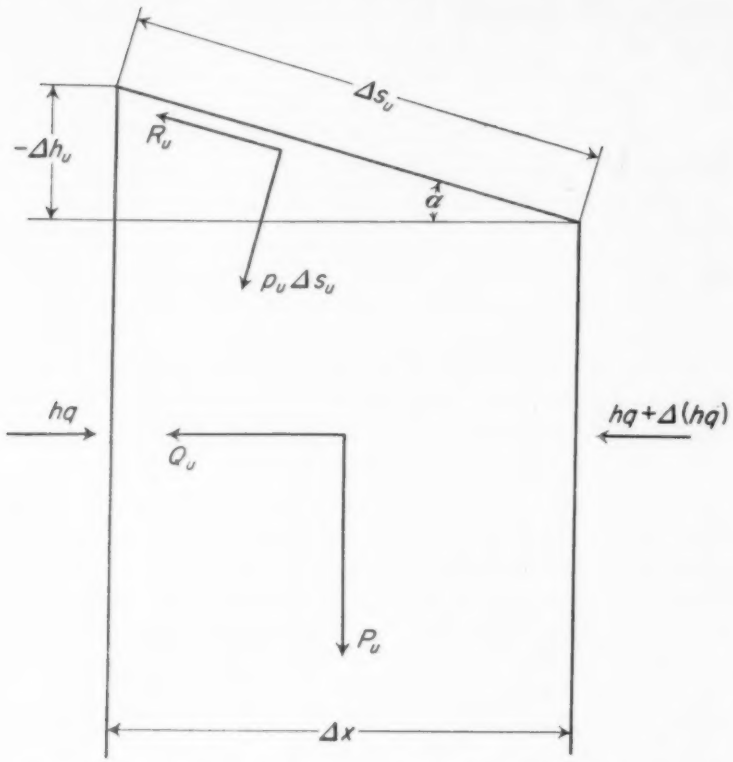

Fig. 3. Forces acting on the upper part of an element of material.

has the direction shown, only for the indicated direction of flow. e.g. near the right-hand end of the cross-section;

$$R_u = \mu p_u \Delta s_u .$$

The resulting force in the horizontal direction is,

$$Q_u = p_u \Delta s_u(\sin\alpha + \mu\cos\alpha) = p_u(-\Delta h_u + \mu\Delta x);$$

and in the vertical direction

$$P_u = p_u \Delta s_u(\cos\alpha - \mu\sin\alpha) = p_u(\Delta x + \mu\Delta h_u) .$$

Similarly for the lower part

$$Q_l = p_l(-\Delta h_l + \mu\Delta x) , \quad \text{and}$$
$$P_l = p_l(\Delta x + \mu\Delta h_l) .$$

The condition of equilibrium gives

$$\begin{aligned} Q_u + Q_l + \Delta(hq) &= 0 , \\ P_u &= P_l . \end{aligned} \tag{5}$$

Equations (5) are a generalization of equation (1) for the right-hand

part of the cross-section and reduce to equation (1) for $\Delta h_u = \Delta h_l = 0$. Because of assumption 2, $(\Delta x + \mu \Delta h_l) > 0$, and

$$p_l = p_u \frac{\Delta x + \mu \Delta h_u}{\Delta x + \mu \Delta h_l},$$

so that

$$p_u \left\{ \mu \Delta x - \Delta h_u + \frac{(\Delta x + \mu \Delta h_u)(\mu \Delta x - \Delta h_l)}{\Delta x + \mu \Delta h_l} \right\} = -(hq).$$

Hence,

$$\frac{d(hq)}{dx} = \frac{(1-\mu^2)\frac{dh}{dx} - 2\mu\left(1 - \frac{dh_u}{dx}\frac{dh_l}{dx}\right)}{1 + \mu \frac{dh_l}{dx}} p_u .$$

But

$$p_u = \frac{P}{\Delta x + \mu \Delta h_u} = \frac{\frac{P_u}{\Delta x}}{1 + \mu \frac{\Delta h_u}{\Delta x}},$$

and $\frac{P_u}{\Delta x} = p$; and since $p - q = Y$,

$$\frac{d(h[p-Y])}{dx} + p \frac{2\mu(1 - h'_u h'_l) - (1-\mu^2)h'}{(1+\mu h'_u)(1+\mu h'_l)} = 0;$$

$'$ denoting $\frac{d}{dx}$, then $p' + p \frac{h' + f}{h} - \frac{(hY)'}{h} = 0$, where

$$f(x) = \frac{2\mu(1 - h'_u h'_l) - (1-\mu^2)h'}{(1+\mu h'_u)(1+\mu h'_l)}. \tag{6}$$

At the right-hand boundary, $x = b$ and $p = Y$. The definite integral is

$$p(x) = \exp \int_x^b \frac{h' + f}{h}\, dx \left\{ Y - \int_x^b \frac{(hY)'}{h} \left[\exp - \int_x^b \frac{h' + f}{h}\, dx \right] dx \right\}, \tag{7}$$

which reduces to (3) when $h' = h'_u = h'_l = 0$, if suitable co-ordinates are chosen. Note that (7) remains valid even if Y is not constant but any given function $Y = Y(x)$. In every case equation (7) can be evaluated numerically, and — see the following example — analytical integration is sometimes possible.

Let E be the plane $y = 0$ normal to Fig. 2 and F the projection of the specimen on to E. $|\mathrm{F}| = bl$ is the area of E. If df is an area-element of F, it is found by a second integration that the force

$$P = \int^{(\mathrm{F})} p\, df . \tag{8}$$

Taking a circular surface for F and following Siebel [2] the case of axial symmetry could be approximated to by means of (7) and (8). Here however attention is confined to plane strain and (7) is correct only for the right-hand part of the cross-section (Fig. 2). Reflecting the co-ordinates at a vertical axis and fixing them at the rigth-hand boundary of the specimen,

Vol. 1
1960

equations can be taken over for the left-hand part of the cross-section. Thus, formulating p from both sides, exactly one line $x = x_0$ will exist with $p_{\text{left}} = p_{\text{right}}$ (assumption 3). To the right of x_0, the first solution for p will be correct and to the left, the second one. As will be seen in the following example, this procedure will be simpler in the special case of a symmetrical specimen. But first write down the term $\frac{h'+f}{h}$, with (6) substituted, for small derivatives, products being neglected.

$$\frac{h'+f}{h} \approx \frac{\mu}{h}\left[1+\frac{1}{1+\mu h'}\right] \tag{9}$$

For typical dies we can assume $h' \leq 0$. Substituting this and equation (9) into equation (7) we find for $Y = \text{const.}$

$$p \geq Y \exp 2\mu \int_x^b \frac{dx}{h} ,$$

i.e., neglecting the slope of the engravings a lower bound is found for the stress p. In the proof of an expression equivalent to the last, Lippmann and Neuberger [8] were previously in error. *

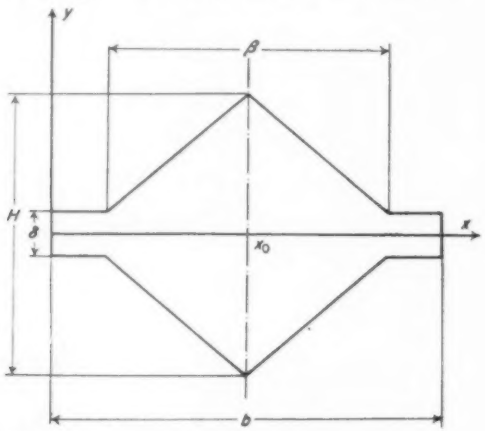

Fig. 4. Cross-section chosen as an example.

Example (See Hoffman and Sachs[13] for a simplified approach)

As an example consider a symmetrical specimen of width l whose cross-section is shown in Fig. 4. Y will be assumed constant. With $x_0 = b/2$ known, equation (7) is correct for $x_0 = \frac{b}{2} \leq x \leq b$. Hence

$$h_u = h_l = \frac{1}{2}h = \begin{cases} \dfrac{H}{2} - \dfrac{H-\delta}{\beta}\left(x - \dfrac{b}{2}\right) & \text{for} \quad \dfrac{b}{2} \leq x \leq \dfrac{b+\beta}{2} \\ \dfrac{\delta}{2} \quad \text{for} \quad \dfrac{b+\beta}{2} \leq x \leq b , \end{cases}$$

* For this hint, the author is indebted to Prof. Bredendick, Dresden.

and

$$h'_u = h'_l = \frac{1}{2}h' = \begin{cases} -\dfrac{H-\delta}{\beta}; & \dfrac{b}{2} < x < \dfrac{b+\beta}{2} \\ 0; & \dfrac{b+\beta}{2} < x < b\,. \end{cases}$$

According to equation (6),

$$f = \text{const} = \frac{2\mu\left(1-\left(\dfrac{H-\delta}{\beta}\right)^2\right)+2(1-\mu^2)\dfrac{H-\delta}{\beta}}{\left(1-\mu\dfrac{H-\delta}{\beta}\right)^2}. \tag{10}$$

Put

$$M = \frac{f-2\dfrac{H-\delta}{\beta}}{2\dfrac{H-\delta}{\beta}} = \frac{f}{2\dfrac{H-\delta}{\beta}} - 1\,. \tag{11}$$

Then $M=-1$ for $f=0$ only; i.e. $\left(\dfrac{H-\delta}{\beta}\right)^2 - \dfrac{1-\mu^2}{\mu}\dfrac{H-\delta}{\beta} - 1 = 0$. The unique non-negative solution is $\dfrac{H-\delta}{\beta} = \dfrac{1}{\mu}$; i.e. the denominator of equation (10) disappears also. L'Hospital's rule gives $\lim\limits_{(H-\delta)/\beta \to 1/\mu} \pm f = \pm\infty$; i.e. $\lim M = \pm\infty$: $M=-1$ is impossible and $|M| = \infty$ could appear only for $(H-\delta)/\beta = 1/\mu$, which implies large inclinations which are not under consideration. Suppose

$$\frac{H-\delta}{\beta} \leqslant \frac{1}{\mu}. \tag{12}$$

Then $M=0$ is impossible too. Indeed this equation together with (11) and (10) would give $\left(\dfrac{H-\delta}{\beta} - \dfrac{1}{\mu}\right)\left(\left(\dfrac{H-\delta}{\beta}\right)^2 + 1\right) = 0$, i.e. $(H-\delta)/\beta = 1/\mu$ again.

Write down equation (7) and evaluate the integrals, noting that there is a corner in the curve of h at $x=(b+\beta)/2$. The result is

$$p(x) = \begin{cases} Y\exp\dfrac{2\mu}{\delta}(b-x) & \text{for} \quad \dfrac{b+\beta}{2} \leq x \leq b \\ Y\left\{\delta^{-M}\left(\exp\dfrac{\mu}{\delta}[b-\beta]+\dfrac{1}{M}\right)\left(H-2\dfrac{H-\delta}{\beta}\left[x-\dfrac{b}{2}\right]\right)^M - \dfrac{1}{M}\right\} \\ \qquad\qquad \text{for} \quad \dfrac{b}{2} \leq x \leq \dfrac{b+\beta}{2}. \end{cases} \tag{13}$$

Because $h = H - 2\dfrac{H-\delta}{\beta}\left(x-\dfrac{b}{2}\right) > \delta$, $\left(\dfrac{b}{2} \leq x < \dfrac{b+\beta}{2}\right)$, it is found that $p \to \infty$ as $\dfrac{H-\delta}{\beta} \to \dfrac{1}{\mu}$, so that equation (12) is a definite requirement

Vol. 1
1960

for the validity of the formulas. If equation (12) is not satisfied the method of Kobayashi *et al.*[10] would give better results.

Equation (13) together with (10) and (11) gives $p(x)$, see, for instance, Fig. 5. From a second integration the force P using (8) is obtained noting the symmetry of the cross section.

$$P = 2l\left\{\int_{\frac{b}{2}}^{\frac{b+\beta}{2}} p\,dx + \int_{\frac{b+\beta}{2}}^{b} p\,dx\right\}$$

$$= 2Yl\left\{\frac{\delta^{-M}}{2^{\frac{H-\delta}{\beta}}}\left(\exp\frac{\mu}{\delta}[b-\beta]+\frac{1}{M}\right)\frac{H^{M+1}-\delta^{M+1}}{M+1} - \frac{\beta}{2M} + \frac{\exp\frac{\mu}{\delta}[b-\beta]-1}{2\frac{\mu}{\delta}}\right\} \quad (14)$$

For the example in Fig. 5: $P/Yl = 1200$ cm.

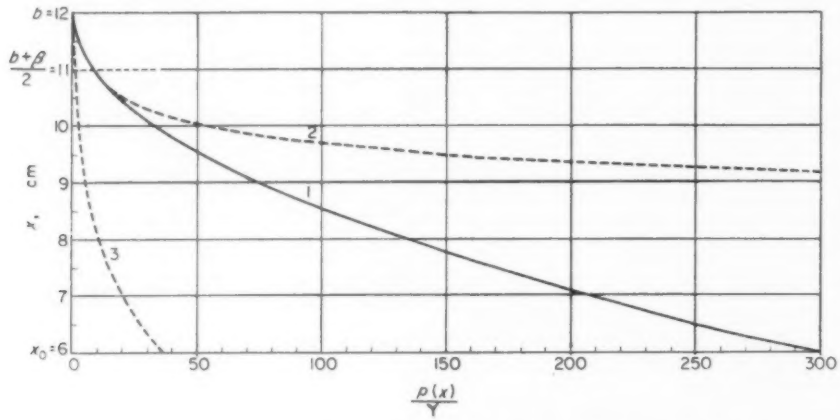

Fig. 5. Stress-ratios p/Y versus x for three types of cross-section with $\mu = 0{\cdot}3$. Curve 1: Fig. 4 with $H = 2$ cm; $b = 12$ cm; $\beta = 10$ cm; $\delta = 0{\cdot}3$ cm. Curve 2: Rectangular section, Fig. 1, following equation (3) with $h = 0{\cdot}3$ cm and $b = 12$ cm. Curve 3: Rectangular section, Fig. 1, following equation (3) with $h = 1$ cm and $b = 12$ cm.

ENERGY AND EFFICIENCY OF FORGING PROCESS

Real forging is a fast process and consequently acceleration forces should be considered. But in the elementary theory these are neglected and at most a higher value for Y is taken. Here instead of the force, the energy required in the tup or the punch for forging is obtained. If h_0 denotes the initial height of a cylindrical specimen, h its final height and V its volume, the Finck equation,[2]

$$A_{id} = V\,Y \ln\frac{h_0}{h} \quad (15)$$

is frequently used to give the "ideal" work, i.e. A_{id} without friction or other losses. The real work is

$$A = \frac{1}{\eta} A_{id}$$

where η is the efficiency which in general is unknown. Several attempts have been made to obtain η, see for instance Geleji[9]. But these attempts seem to be fragmentary. A method is now developed for computing η, based on a well defined model. Suppose that

(i) The total force, $P(h)$, for a specimen of total height h is given, friction included. (For instance, P can be computed by the method of Section 2, or P is given experimentally.)

(ii) For every stroke $\Delta h = (h_0 - h)$ is small, i.e. $P \sim$ constant.

(iii) The total foundation, i.e. the lower die and surrounding earth etc., can be considered as a system, composed of a spring without mass, coefficient c, and a rigid mass M; see Fig. 6.

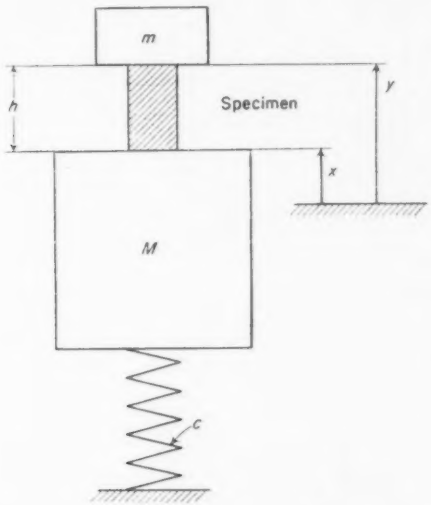

Fig. 6. Forging model.

For simplicity, and because the mass M involved is large, damping is neglected.

(iv) The mass of the specimen is small and negligible.

Let m be the mass of the forging tup or punch so that its energy at the instant of impact is

$$A = \frac{1}{2} m v_0^2 .$$

v_0 is the velocity computed, for instance, from the initial height H of the tup, i.e. $v_0 = \sqrt{2gH}$ in free fall, g being the acceleration due to gravity.

Describe the movement of M by x, the movement of m by y, see Fig. 6, and choose the initial co-ordinate to be $x = 0$. While the specimen is loaded, $y - x = h$, h being taken to be variable. The movement of m ($\cdot \equiv$ derivative with respect to time t) is

$$P - mg = m\ddot{y} \; ;$$

the movement of M:

$$-P - Mg - cx = M\ddot{x}$$

for

$$\dot{h} < 0 \, .$$

Because $\dot{x} = x = 0$ when $t = 0$, the following integrals are obtained

$$x = -\frac{2M}{c}\left(\frac{P}{M} + g\right) \sin^2 \sqrt{\frac{c}{M}} \frac{t}{2} \tag{17a}$$

$$h = h_0 - v_0 t + \left(\frac{P}{m} - g\right)\frac{t^2}{2} + 2\,\frac{M}{c}\left(\frac{P}{M} + g\right) \sin^2 \sqrt{\frac{c}{M}} \frac{t}{2} \tag{17b}$$

$$\dot{h} = -v_0 + \left(\frac{P}{m} - g\right) t + \sqrt{\frac{M}{c}}\left(\frac{P}{m} + g\right) \sin \sqrt{\frac{c}{M}}\, t \, . \tag{17c}$$

From given values f, M, v_0 and equation 17(c) compute a time $t = t_1$ so, that $\dot{h}(t_1) = 0$, i.e. when deformation is complete. But if A has been dissipated already during $\dot{h} < 0$, a time $t = t_2$ has to be considered. Thus, $A = -\int_0^{t_2} P\dot{y}\, dt = -P\,(y(t_2) - y(0)) = P\,(h_0 - h(t_2) - x(t_2))$, and because of equations (17a, b), $A = P\left(v_0 t_2 - \left(\frac{P}{m} - g\right)\frac{t_2^2}{2}\right) = \frac{1}{2}\, m v_0^2$. The solution must fulfil the condition $A = 0$ for $t_2 = 0$, i.e.

$$t_2 = \frac{v_0}{\dfrac{P}{m} - g}\left\{1 - \sqrt{\frac{1}{2}\left(1 + \frac{mg}{P}\right)}\right\} . \tag{18}$$

The correct time of deformation is then $t_d = \min(t_1, t_2)$. Then equation 17(b) gives $\Delta h = (h_0 - h)$, and the work dissipated in the specimen itself is

$$A_{id}^* = P\Delta h \, . \tag{19}$$

The meaning is altered by comparison with (15), when friction is considered; therefore write A_{id}^* instead of A_{id}, so that

$$\eta^* = \frac{A_{id}^*}{A} \tag{20}$$

where η^* replaces η. If one stroke more is given, the computation must be repeated and yields

$$\eta^* = \frac{\sum A_{id}^*}{\sum A}. \tag{20a}$$

This is illustrated in the following example.

Numerical example

For a cylindrical specimen in free-forging use the well-known simplified Siebel formula

$$P = FY\left(1 + \frac{\mu}{3}\frac{d}{h}\right). \tag{21}$$

This is analogous to equation (4), but now $F = \frac{\pi}{4}d^2$ where d is the diameter. Assume that,

Weight of the forging-tup: 100 kp $\left(m = 10{\cdot}2\,\frac{\text{kp}\dagger\,\text{sec}^2}{\text{m}}\right)$

Weight of the foundation: 5000 kp $\left(M = 5{\cdot}10\,\frac{\text{kp}\,\text{sec}^2}{\text{m}}\right)$

$c = 0{\cdot}333 \times 10^5$ kp m^{-1}; $Y = 20 \times 10^6$ kp m^{-2}, making some allowance for high speed; $\mu = 0{\cdot}3$; $h_0 = 0{\cdot}08$ m; initial diameter $d_0 = 0{\cdot}04$ m. Suppose it is required to forge it to $h = h_2 = 0{\cdot}06$ m, i.e. $d = d_2 = 0{\cdot}0462$ m

(a) by one stroke (free fall from the altitude H),

(b) by two strokes, first down to $h = h_1 = 0{\cdot}07$ m and then down to h_2, i.e. altitudes H_1, H_2.

It is required to find H, H_1, H_2 and η_a^*, η_b^* for (a) and (b) respectively. For (a): From equation (21) $P = 3{\cdot}04 \times 10^4$ kp, which is for the average height 0·07 m. From equation (17c) with $\dot{h} = 0$

$$v_0 = 2{\cdot}97 \times 10^3 t_1 + 8{\cdot}59 \sin 8{\cdot}08 t_1 .$$

t_1 can be expected to be of magnitude of 10^{-2}sec and therefore $\sin 8{\cdot}08 t_1 \approx 8{\cdot}08 t_1$ and $v_0 = 3039 t_1$. With the same simplification and $\Delta h = 0{\cdot}02$m, using equation (17b), it is found that $t_1 = 3{\cdot}63 \times 10^{-3}$sec. From equations (18) and (17b) in the same way $t_2 = 1{\cdot}58 \times 10^{-3}$sec, and hence

$$t_d = t_2 = 1{\cdot}58 \times 10^{-3}\text{sec} .$$

From equation (18), $v_0 = 16{\cdot}08\text{m}\,\text{sec}^{-1}$; thus

$$H = v_0^2/2g = 13{\cdot}1\text{m} .$$

This height in general, cannot be effected technically. From equation (20)

$$\eta_a^* = 0{\cdot}462 = 46{\cdot}2 \text{ per cent.}$$

† 1 kp is the force due to gravity acting upon a mass of 1 kg.

Vol. 1
1960

For (b): Stroke 1: For the average height 0·075m from equation (21) $P = 2{\cdot}83 \times 10^4$ kp. In the same way as above, $t_d = t_2 = 1{\cdot}142 \times 10^{-3}$sec and $v_0 = 10{\cdot}30\,\mathrm{m\,sec^{-1}}$, thus

$$H_1 = 5{\cdot}40\mathrm{m}\,.$$

Stroke 2: Analogous computation leads to $t_d = t_2 = 1{\cdot}03$sec and $v_0 = 11{\cdot}39\,\mathrm{m\,sec^{-1}}$, with

$$H_2 = 6{\cdot}60\mathrm{m}\,.$$

Because of equation (20a), $\eta_b^* = 0{\cdot}510 = 51$ per cent.
Two strokes are thus seen to be better than one; both strokes for instance from the height $H = \frac{1}{2}(H_1 + H_2) = 6{\cdot}00$m. For more exact values the computation would have to be repeated, improving Y and expressing it in terms of the determined velocities v_0.

For every fixed forging aggregate, c and M must be determined by experiments. The dimensions of the real foundation give only very coarse values.

Acknowledgements — The author wishes to express his gratitude to Mr W. Johnson and Mr J. B. Haddow for their help in preparing the paper for publication.

REFERENCES

1. R. HILL, *The Mathematical Theory of Plasticity*. Oxford, Clarendon Press (1956).
2. E. SIEBEL, *Grundlagen der bildsamen Formänderung*. Stahl und Eisen, Verlag, Düsseldorf (1932).
3. V. V. SOKOLOVSKIJ, *Theorie der Plastizität*. Übers. aus d. Russ., Verlag Technik, Berlin (1955).
4. H. KUDO, *J. Inst. Aero. Res., Tokyo* **1**, 37 (1958).
5. F. KÖRBER and A. EICHINGER, *Mitt. K.-Wilh.-Inst. Eisenforsch.* **22**, 57 (1940).
6. A. EICHINGER and A. POMP, *Arch. Eisenhüttenw.* **14** 1 (1940).
7. K. REICHERTER, *Werkstattstechnik u. Masch.-Bau* **46**, 89 (1956).
8. H. LIPPMANN and F. NEUBERGER, *Werkstattstechnik u. Masch.-Bau* **48**, 449 (1958).
9. A. GELEJI, *Die Berechnung der Kräfte und des Kraftbedarfes bei der Formgebung im bildsamen Zustande der Metalle*. Akadémiai Kiado, Budapest (1952).
10. S. KOBAYASHI, R. HERZOG, J. T. LAPSLEY and E. G. THOMSEN, *Theory and Experiments of Press Forging Axisymmetric Parts of Aluminium and Lead*. ASME Paper No. 58-A-154 (1958).
11. S. KOBAYASHI and E. G. THOMSEN, *Approximate Solutions to a Problem of Press Forging*. ASME Paper No. 58-A-140 (1958).
12. R. L. DIETRICH and G. ANSEL, *Trans. Amer. Soc. Metals* **38**, 709 (1947).
13. D. HOFFMAN and G. SACHS, *Introduction to the Theory of Plasticity*. McGraw-Hill, New York (1953).

Int. J. Mech. Sci. Pergamon Press Ltd. 1960. Vol. I, pp. 121–135. Printed in Poland

ON THE MINIMUM-WEIGHT DESIGN OF A SIMPLE PORTAL FRAME

JACQUES HEYMAN
Deportment of Engineering, University of Cambridge

(*Received* 16 *March* 1959)

Summary — Simple plastic theory is used to investigate the minimum-weight design of a rectangular portal frame under various loadings. Two designs under slightly different conditions are made according to the Foulkes theory [1] for frames with prismatic members; the results are then compared with the corresponding absolute minimum-weight design.

For the simple problem discussed, the general results are presented graphically, and calculations are made for three specific frames.

Vol. 1
1960

INTRODUCTION

WHEN the loads acting on a frame composed of mild-steel members are slowly increased, collapse occurs when sufficient plastic hinges are formed to turn the frame into a mechanism of one degree of freedom. Given the dimensions and centre-lines of a frame, and the values of the loads acting (which may incorporate a suitable load factor), a *design* of the frame will be achieved when material is assigned to the members so that the frame is just collapsing.

Material can be assigned subject to various restrictions; the most common is that members should be prismatic between joints. Foulkes [1] studied *minimum-weight design* under these conditions. If several members of a frame are required to have the same (prismatic) section, or to bear constant ratios to each other, then they will be referred to as a *span*. Foulkes showed that if a frame has N spans to be designed, then minimum material consumption will occur when the frame is capable of collapsing in a mechanism of (at least), N degrees of freedom. The design of the N spans consists in determining N values of full plastic moment; thus for the degenerate case $N = 1$, when the problem can more correctly be referred to as one of analysis, since one value of full plastic moment will determine the complete design, the frame will collapse in a mechanism of one degree of freedom. (Extra degrees of freedom may sometimes occur under certain load combinations, but do not affect the general propositions.)

The theorems established by Foulkes give no rules for finding the actual minimum-weight design for a specific example. The problem can be treated by the methods of linear programming;[2] alternatively, a different computing technique has recently been evolved.[3,4,5] In the present

paper, the rectangular portal frame is treated analytically on the assumption (*a*) that the two columns of the frame are compelled to have the same section, possibly different from that of the beam, (*b*) that the two columns may take unequal sections, thus implying an extra degree of freedom in the collapse mechanism.

The use of prismatic members can be justified practically for small frames on the count of cheapness of fabrication. For a large frame, however, using made-up sections, the designer can vary the cross-section of a member within a span at no great expense. The study of minimum-weight design using tapering members is therefore of interest. A recent paper [6] has shown that if the members of a frame are varied continuously so that the "strength" of the frame follows the bending-moment diagram, then, providing the bending-moment diagram is determined in a certain way, the frame will have *absolute minimum weight.*

Thus, for a simply supported beam subjected to a uniformly distributed load, having a parabolic bending-moment diagram, absolute minimum-weight design will occur when the beam is tapered so that the full plastic moment varies parabolically from a maximum at the centre to zero at the ends. For a statically indeterminate frame, infinitely many equilibrium bending-moment distributions may be constructed for a given loading, and the problem is more complicated. To fix the bending-moment diagram (i.e. to determine the values of the redundancies) use may be made of the theorem [6] which states that absolute minimum weight will occur for that design which is capable of deforming with the members bent in *constant* (positive or negative) curvature.

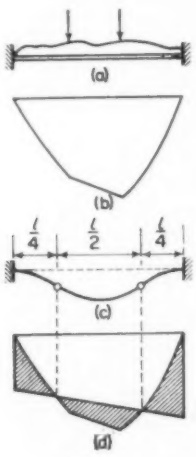

Fig. 1

For example, the fixed-ended beam carrying the (reasonable) loads in Fig. 1(a) has a (convex) free bending-moment diagram as shown in Fig. 1(b). A reactant line due to the redundancies must be superimposed

on this diagram. Now simple geometrical considerations show that the only way in which the beam can deform into arcs of constant curvature is for the central portion of length $l/2$ to have positive curvature, the two end portions of length $l/4$ having negative curvature. Since the bending moments must be *compatible* in sign with these curvatures, inflexion points must occur at quarter span, and the reactant line can be fixed as in Fig. 1(d). If the cross-section of the beam is varied so that the full plastic moment at each section is given by the shaded area in Fig. 1(d), then the beam will have absolute minimum weight.

Note that the position of the inflexion points is independent of the loading on the beam. Fig. 2 illustrates an important special case, when the beam is acted upon by a single load located within $l/4$ of a support.

Vol. 1
1960

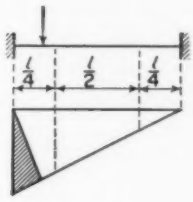

Fig. 2

The reactant line coincides with the right-hand line of the free bending-moment diagram, and the absolute minimum-weight design is a cantilever whose full plastic moment decreases linearly from the support to zero at the loading point. Such degenerate cases occur for more complex problems.

It is only for the simplest frames that the inflexion points can be located independently of the loading system. For the rectangular portal frame considered below, the positions of the inflexion points depend both on span-to-height ratio and the values of the loads. However, general slope-inflexion equations can be set up, and it may be shown that it is always possible to find a mode of deformation with arcs of constant curvature compatible in sign with the bending-moment distribution.

SLOPE-INFLEXION EQUATIONS

Fig. 3 shows a beam of length L bent into arcs of constant curvature having no, one, or two points of inflexion within its length. Taking the

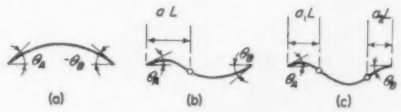

Fig. 3

constant curvature equal to unity, the following relations obtain for rotations at the ends of the beam:

No inflexion point: $\theta_A = L[\frac{1}{2}]$, $\theta_B = L[-\frac{1}{2}]$ (1a)

One inflexion point: $\theta_A = L[\frac{1}{2}-(1-a)^2]$, $\theta_B = L[\frac{1}{2}-a^2]$ (1b)

Two inflexion points: $\theta_A = L[\frac{1}{2}-(1-a_1)^2+a_2^2]$, $\theta_B = L[-\frac{1}{2}+(1-a_2)^2-a_1^2]$ (1c)

These three cases suffice for the solution of most problems. (The solution for the fixed-ended beam treated above, Fig. 1, can be seen immediately from equations (1c). Setting $\theta_A = \theta_B = 0$, then $a_1 = a_2 = 1/4$.)

RECTANGULAR PORTAL FRAME

The frame to be designed is shown in Fig. 4, and carries a side load H and a central-beam load V. All values of the ratios l/h and Hh/Vl will be considered. Designs will first be made, and the analysis presented,

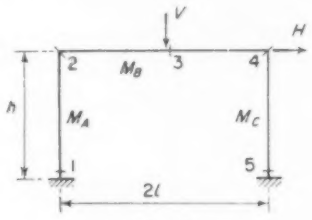

Fig. 4

for $H = 0$. The designs for $H \neq 0$ will not be presented so fully, but the results given graphically. Finally, three numerical examples are worked.

A. *Prismatic members: columns equal*

The columns 12 and 54 in Fig. 4 have the same uniform full plastic moment M_A, and the beam has the uniform full plastic moment M_B. There are two spans to be designed, and therefore the minimum weight design must be capable of collapsing in a mechanism of two degrees of freedom. This was a problem considered by Foulkes,[1] who also showed that the sum of the absolute values of hinge rotations in each span must be proportional to the length of that span.

For the side load $H = 0$, suppose the frame is of uniform section throughout, $M_A = M_B = M$, so that a mechanism of two degrees of freedom can be formed as shown in Fig. 5. (An extra degree of freedom is possible for this special case if the joints at the top of the columns are allowed to rotate independently.) The total hinge rotation in the columns is $2\theta_1$, so that, taking the constant of proportionality as unity,

$$2\theta_1 = 2h \tag{2a}$$

and, similarly for the beam,

$$4\theta_2 - 2\theta_1 = 2l \tag{2b}$$

Thus

$$\theta_1 = h \tag{3}$$
$$\theta_2 = \tfrac{1}{2}l + \tfrac{1}{2}h$$

Equilibrium at the joints will be satisfied only if the hinge rotations are positive as drawn in Fig. 5; $(\theta_2 - \theta_1) \geqslant 0$ gives, from equations (3), $l \geqslant h$, or

$$\frac{l}{h} \geqslant 1 \tag{4}$$

The mode sketched in Fig. 5 is possible only if inequality (4) is satisfied; considering equilibrium of the beam,

$$M_A = M_B = \frac{Vl}{4}. \tag{5}$$

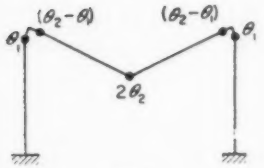

Fig. 5

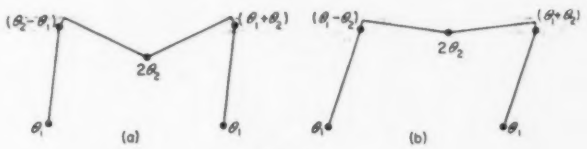

Fig. 6

For $l/h \leqslant 1$, the two modes sketched in Fig. 6(a) and (b) occur. For both modes, equilibrium gives

$$\left.\begin{aligned} M_A &= 0 \\ M_B &= \frac{Vl}{2} \end{aligned}\right\} \tag{6}$$

and both modes are combinations of beam collapse and side-sway. Summing the hinge rotations in Fig. 6(a)

$$\left.\begin{aligned} 2\theta_1 + 2\theta_2 &= 2h \\ 2\theta_2 &= 2l \end{aligned}\right\} \tag{7}$$

i.e.

$$\left.\begin{aligned} \theta_1 &= h - l \\ \theta_2 &= l \end{aligned}\right\} \tag{8}$$

and the conditions $\theta_1 \geqslant 0$ and $\theta_2 \geqslant \theta_1$ give

$$\frac{1}{2} \leqslant \frac{l}{h} \leqslant 1 \tag{9}$$

Similarly, consideration of Fig. 6(b) leads to

$$\left.\begin{aligned}\theta_1 &= \frac{h}{2}\\ \theta_2 &= l\end{aligned}\right\} \tag{10}$$

and the condition $\theta_1 \geqslant \theta_2$ gives

$$\frac{l}{h} \leqslant \frac{1}{2} \tag{11}$$

For $H \neq 0$, the collapse modes drawn in Fig. 5 for $M_A = M_B$ and in Fig. 6 for $M_A < M_B$ occur providing the ratio Hh/Vl is limited; modes similar to those in Fig. 6, but for $M_A > M_B$ can also occur, as can the other two basic modes for a uniform frame. The complete design field is covered by seven different modes, displayed in Fig. 7.

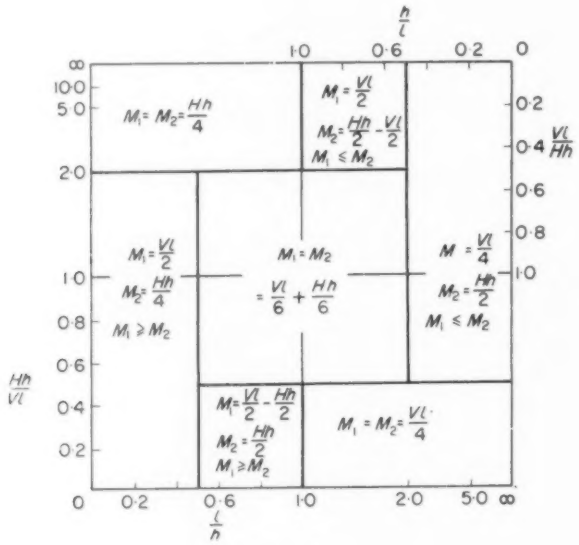

Fig. 7

B. *Prismatic members: columns unequal*

There are three spans to be designed; column 12 of length h and full plastic moment M_A, beam 24 ($2l$ and M_B), and column 54 (h and M_C). Eight modes cover the design field as shown in Fig. 8. Some of these modes are not unique; for example, a mode can be found for $M_A = M_B \leqslant M_C$ which exactly superimposes on the region for mode 6 ($M_A \geqslant M_B = M_C$). The values of full plastic moments are given in Table 1.
Note the "disappearance" of column 12 for modes 1 and 2; the side load is carried entirely by the right hand column. For a "practical" minimum-weight design in which zero-section columns are not permitted, it is simple

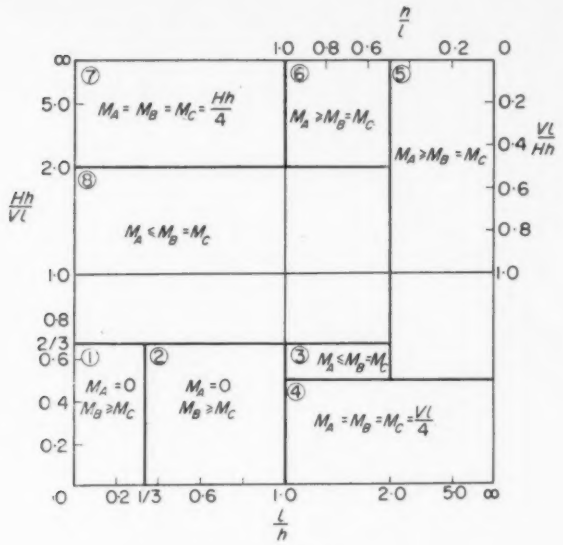

Fig. 8

TABLE 1

Mode	M_A	M_B	M_C	
1, 2	0	$\frac{Vl}{2} - \frac{Hh}{4}$	$\frac{Hh}{2}$	$M_B \geqslant M_C$
3	$Vl - \frac{3Hh}{2}$	$\frac{Hh}{2}$	M_B	$M_A \leqslant M_B = M_C$
4	$\frac{Vl}{4}$	M_A	M_A	$M_A = M_B = M_C$
5	$Hh - \frac{Vl}{4}$	$\frac{Vl}{4}$	M_B	$M_A \geqslant M_B = M_C$
6	$Hh - \frac{3Vl}{2}$	$\frac{Vl}{2}$	M_B	$M_A \geqslant M_B = M_C$
7	$\frac{Hh}{4}$	M_A	M_A	$M_A = M_B = M_C$
8	$\frac{3Hh}{8} - \frac{Vl}{4}$	$\frac{Vl}{4} + \frac{Hh}{8}$	M_B	$M_A \leqslant M_B = M_C$

to use the Foulkes principles with assigned minimum sections. If minimum sections are assigned to all N spans, and if the minimum weight design has M spans with the assigned minimum sections, there are $(N-M)$ independent mechanisms of collapse. (Obviously, if $M = N$, the frame is not collapsing, and has effectively been designed by methods other than plastic.)

Vol. 1
1960

C. *Absolute minimum-weight design*

There are three different configurations, referred to briefly as modes, for absolute minimum-weight design; the modes occupy the regions shown in Fig. 9.

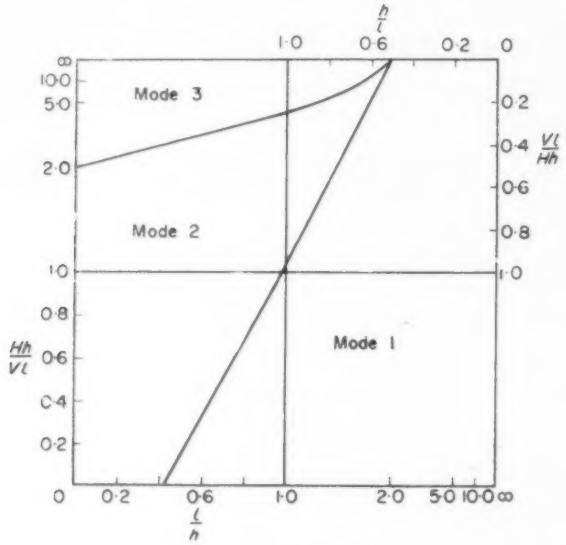

Fig. 9

Mode 1. A mode of deformation involving constant curvature of the members of the portal frame is shown in Fig. 10. The mode is specified in terms of the four points of inflexion by means of the parameters a_1, a_2, b_1, b_2; the deformations can be specified in terms of the two rotations θ_2 and θ_4 of the joints, and the rotation φ measuring the side-sway. Two slope-inflexion equations (equations (1)) can be written for each member, and the rotations θ_1, θ_2 and φ eliminated, leading to the three equations

$$\left.\begin{aligned} 1 &= (1-a_1)^2+(1-a_2)^2 \\ 1-2a_1 &= \frac{l}{h}[-1+2(1-b_1)^2-2b_2^2] \\ 1-2a_2 &= \frac{l}{h}[-1+2(1-b_2)^2-2b_1^2] \end{aligned}\right\} \qquad (12)$$

These three equations are of course insufficient to determine the positions of the four inflexion points, and a further equation must be found by considering the bending-moment diagram.

Fig. 11 gives a sketch of the bending moments. Since the frame has three redundancies, there must be two equilibrium equations linking the

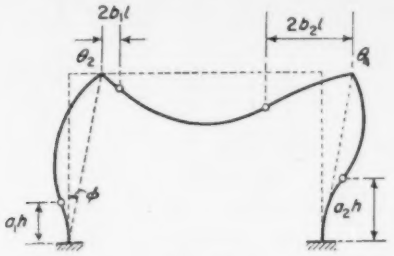

Fig. 10

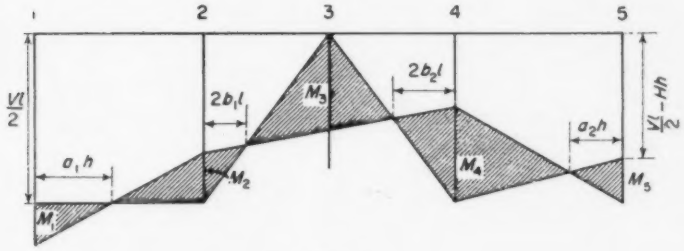

Fig. 11

value of the five bending moments M_1 to M_5; these can be written conveniently

$$\left.\begin{aligned} M_2+2M_3+M_4 &= Vl \\ -M_1-M_2+M_4+M_5 &= Hh \end{aligned}\right\} \tag{13}$$

Further, geometrical consideration of Fig. 11 gives the relationships

$$\left.\begin{aligned} M_2 &= \frac{2b_1}{1-2b_1}\cdot M_3 \\ M_1 &= \frac{a_1}{1-a_1}\cdot\frac{2b_1}{1-2b_1}\cdot M_3 \\ M_4 &= \frac{2b_2}{1-2b_2}\cdot M_3 \\ M_5 &= \frac{a_2}{1-a_2}\cdot\frac{2b_2}{1-2b_2}\cdot M_3 \end{aligned}\right\} \tag{14}$$

and equations (13) and (14) combine to give

$$\frac{Hh}{Vl}(1-b_1-b_2) = \left[\frac{b_2(1-2b_1)}{(1-a_2)} - \frac{b_1(1-2b_2)}{(1-a_1)}\right] \tag{15}$$

Equations (12) and (15) are now sufficient to determine the positions of the inflexion points, and hence to fix the bending-moment diagram from equations (14) and (13). Note that the mode is dependent on the value of the ratio Hh/Vl, that is, upon the loading, whereas the mode for the fixed-ended beam, Fig. 1, did not depend on the loading.

Vol. 1
1960

Equations (12) and (15) cannot be solved explicitly, but a straightforward numerical solution is possible, not involving trial and error. The analysis is valid for $b_1 \geqslant 0$; the limit $b_1 = 0$ is shown as the dividing line between modes 1 and 2 in Fig. 9. For all designs to the right of this dividing line, the values of a_1, a_2, b_1, and b_2 are compatible with the mode sketched in Fig. 10.

For the particular case $H = 0$, when, by symmetry, $a_1 = a_2$ and $b_1 = b_2$, equation (15) is satisfied identically, and equations (12) contract to

$$\left.\begin{aligned} 1 &= 2(1-a)^2 \\ 1-2a &= \frac{l}{h}(1-4b) \end{aligned}\right\} \tag{16}$$

from which

$$\left.\begin{aligned} a &= 1-\frac{1}{\sqrt{2}} \\ b &= \frac{1}{4}\left[1-(\sqrt{2}-1)\frac{h}{l}\right] \end{aligned}\right\} \tag{17}$$

Now b must be positive; thus

$$\frac{l}{h} \geqslant (\sqrt{2}-1) \tag{18}$$

For $H = 0$ and $\dfrac{l}{h} \leqslant (\sqrt{2}-1)$, mode 2 occurs.

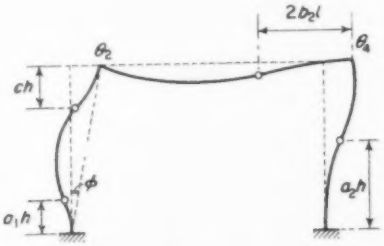

Fig. 12

Mode 2. The minimum-weight collapse configuration for mode 2 is shown in Fig. 12. Comparing with Fig. 10, the inflexion point near the left-hand knee of the frame has moved from the beam into the column. As before, three equations can be obtained from the slope-inflexion equations:

$$\left.\begin{aligned} 1+c^2 &= (1-a_1)^2+(1-a_2)^2 \\ (1-2a_1-2c) &= \frac{l}{h}[1-2b_2^2] \\ (1-2a_2) &= \frac{l}{h}[2(1-b_2)^2-1] \end{aligned}\right\} \tag{19}$$

Vol. 1
1960

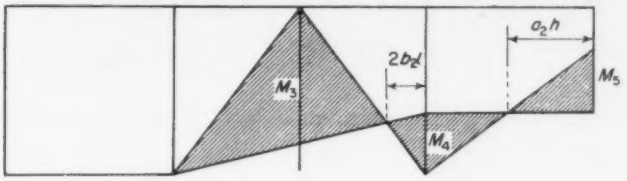

Fig. 13

Since two inflexion points occur in the left-hand column, the column section must degenerate to zero; the bending-moment diagram is sketched in Fig. 13. Consideration of this diagram leads to the fourth equation.

$$\frac{Hh}{Vl}(1-a_2)(1-b_2) = b_2 \tag{20}$$

The equations are valid providing $c \geqslant 0$, and providing $a_1 \geqslant 0$. The first condition gives the dividing line between modes 1 and 2 in Fig. 9; the second the dividing line between modes 2 and 3. (Equations (19) with $c = 0$ are identical with equations (12) with $b_1 = 0$, and similarly for equations (20) and (15).)

For the particular case again $H = 0$, equation (20) gives $b_2 = 0$, and both columns have zero section.

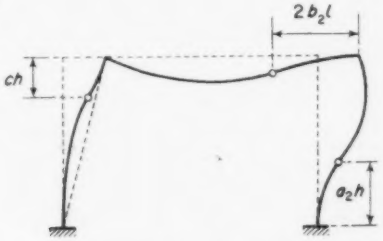

Fig. 14

Mode 3. A mode involving *three* inflexion points is sketched in Fig. 14; the slope-inflexion equations are therefore sufficient to determine the parameters a_2, b_2, and c. The figure has been drawn badly; by symmetry it is clear that $b_2 = \frac{1}{2}$, and that a_2 and c are complementary ($a_2 + c = 1$). Indeed, writing the equations, it is found that

$$\left.\begin{aligned} a_2 &= \frac{1}{2} + \frac{1}{4}\frac{l}{h} \\ c &= \frac{1}{2} - \frac{1}{4}\frac{l}{h} \\ b_2 &= \frac{1}{2} \end{aligned}\right\} \tag{21}$$

and the bending-moment diagram is as sketched in Fig. 15. Using the equilibrium equations

$$\begin{aligned} M_4 - M_2 &= Vl \\ M_1 + M_2 + M_4 + M_5 &= Hh \end{aligned} \tag{22}$$

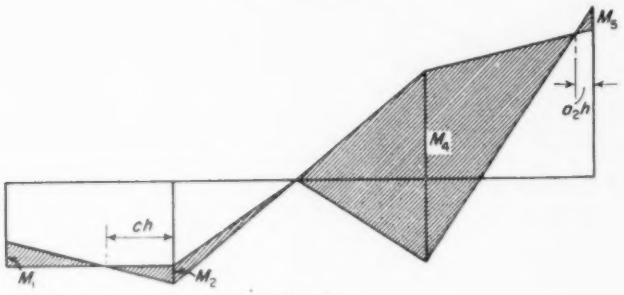

Fig. 15

the values of the bending moments are found to be

$$\left.\begin{aligned} M_1 &= \frac{1-c}{c} M_2 \\ M_5 &= \frac{a_2}{1-a_2} M_4 \\ M_2 &= -\frac{Vl}{2} + \frac{1}{2} cHh \\ M_4 &= \frac{Vl}{2} + \frac{1}{2} cHh \end{aligned}\right\} \tag{23}$$

Now $M_2 \geqslant 0$; hence

$$\frac{Hh}{Vl} \geqslant \frac{1}{c} = \frac{4}{2 - l/h} \tag{24}$$

Equality (24) is the dividing line between modes 2 and 3 in Fig. 9.

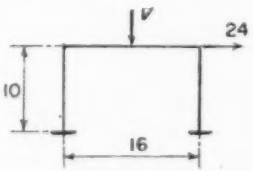

Fig. 16

Numerical examples

The frame shown in Fig. 16 ($l/h = 0{\cdot}8$) will be designed for the three loads $V = 75$, 30 and 6 ($Hh/Vl = 0{\cdot}4$, 1 and 5). From Figs. 7, 8 and 9 it will be seen that the three design conditions have different minimum-weight solutions; in particular, modes 1, 2 and 3 are represented in the

absolute minimum-weight design. The bending-moment diagrams at minimum weight are drawn in Figs. 17, 18 and 19 for $V = 75$, 30 and 6 respectively; in each figure (*a*) corresponds to prismatic members with equal columns and (*b*) with unequal columns, while (*c*) is the absolute minimum-weight design.

Making the assumption (on which the Foulkes theorems are based) that weight of a structure is proportional to the product of full plastic moment and length, Table 2 gives, to an arbitrary scale, the total material consumption for the various designs.

TABLE 2

V	(a) Prismatic, equal columns	(b) Prismatic unequal columns	(c) Absolute minimum weight
75	5280 (2424)	5040 (2360)	2310
30	2880 (1440)	2640 (1440)	1233
6	2160 (1135)	—	984

Vol. 1
1960

It may be noted that if *any* equilibrium bending moment is drawn (i. e. an arbitrary reactant line superimposed on a free bending-moment

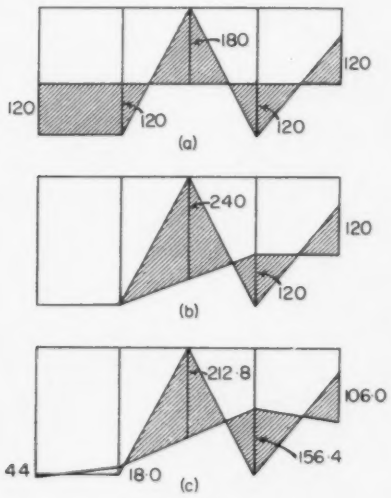

Fig. 17

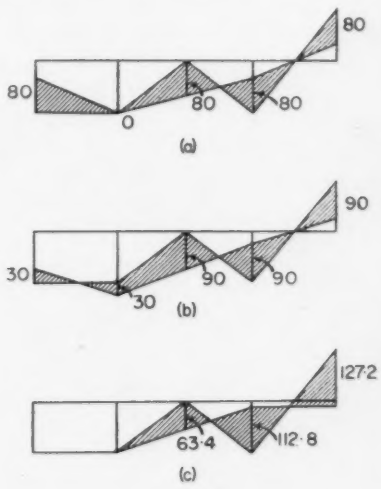

Fig 18

diagram) and material assigned so that the strength of a cross-section is just equal to the value of the bending moment at that section, then a *design* of the frame has been made. Using tapering instead of prismatic members for the bending-moment distributions sketched in (*a*) and (*b*) of Figs. 17, 18 and 19, frames will be designed, not of minimum weight, which will just collapse under the given loads. The corresponding weights

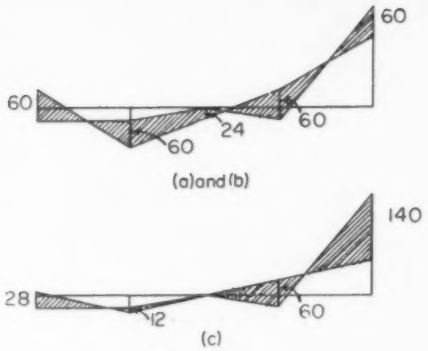

Fig. 19

are given in brackets in Table 2, and these are not much higher (2, 17 and 15 per cent for designs (*b*)) than the absolute minima.

REFERENCES

1. J. FOULKES, *Proc. Roy. Soc.* A, **223**, 482 (1954).
2. R. K. LIVESLEY, *Quart. J. Mech.* **9**, 257 (1956).
3. J. HEYMAN and W. PRAGER. *J. Franklin Inst.* **266**, 339 (1958).
4. J. HEYMAN, *Min. Proc. Instn. Civ. Engrs.* **12**, 39 (1959).
5. J. HEYMAN, *Proc. Amer. S. Civ. Engrs.* **84**, 1790 (1958).
6. J. HEYMAN, *Quart. J. Mech.* **12**, 314 (1959).

Int. J. Mech. Sci. Pergamon Press Ltd. 1960. Vol. I, pp. 135–143. Printed in Poland

A REALISTIC EVALUATION OF THE FACTOR OF SAFETY OF A BOLTED BRACKET*

BERNARD W. SHAFFER
New York University
New York, N. Y.

(*Received* 25 *March* 1959)

Summary — A bolted bracket is analyzed when it is subjected to a pure bending moment of sufficient intensity to induce first an elastic, then an elastic-plastic, and finally a fully plastic stress distribution within the supporting set of bolts. It is shown that when the bracket is held in place by three equally spaced bolts, it can resist at least 28 per cent more load than a conventional elastic analysis of the problem indicates. This percentage is even larger when more bolts are used. In view of the widely differing results that are obtained by analyzing the problem from the conventional and the proposed points of view, it is suggested that the factor of safety be defined as the ratio of the load-carrying capacity of the unit, computed by including the effect of plastic flow, to the maximum specified external load.

Vol. 1
1960

INTRODUCTION

IN EVALUATING the factor of safety of a bolted bracket, it is customary[1–3] to compare the yield stress of the material with the maximum stress in the most highly loaded bolt, computed on the basis of an elastic analysis. This procedure is based on the supposition that once the yield stress is reached, plastic flow begins and the bracket becomes structurally useless. Current practice neglects the effect of contained plastic flow, during which additional loading of the structure can take place before deformations become unreasonably large. Consequently, some of the load-carrying capacity of the bolted bracket is overlooked and an unrealistic factor of safety is calculated.

It is the purpose of the present paper to present a complete analysis of a bracket, which is subjected to an externally applied moment of such magnitude that the supporting bolts are stressed beyond their elastic limit. The analysis will reveal the additional load-carrying capacity of the structure, overlooked in the usual computations. It will also show why and how the present procedure for evaluating the factor of safety in the bolted bracket should be changed to include the effect of plastic flow. Furthermore, since plastic-flow analysis is relatively new to many

* The current paper was included in an introductory lecture on plasticity presented at the Allegany Ballistics Laboratory of the Hercules Powder Company in Cumberland, Maryland, July 23 and 24, 1957. It was prepared in the course of research for the Bureau of Ordnance, Department of the Navy, under Contract No. NOrd-16497 with New York University.

design engineers, the present paper may also help serve as an introduction to the subject, a field of study which has made enormous gains during the past few years.[4–10]

BASIC CONSIDERATIONS

The stress-strain relation of most bolt materials may be approximated reasonably well by the diagram shown in Fig. 1. The elastic portion of the diagram is a straight line whose slope is equal to E, the modulus

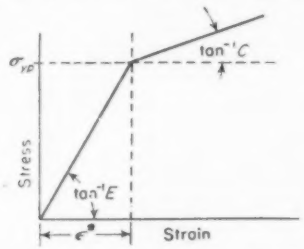

Fig. 1. The stress-strain relationship.

of elasticity of the material. The plastic portion is also a straight line. It starts at the yield stress σ_{yp}, and has a slope equal to C. The slope C is smaller than the slope E, so that an increment of stress required to produce an increment of strain is less within the plastic region than it is within the elastic region. A material for which C vanishes is called perfectly plastic; for such a material indefinite plastic flow can occur with no increase in stress. A material for which C is greater than zero is said to work-harden; it does not permit an increase in strain without an increase in stress.

Most of the subsequent analysis is concerned with a bracket supported by bolts made of a perfectly plastic material. The assumption of perfect plasticity is reasonable for many of the common bolt materials. Furthermore, the assumption leads to considerable simplification of the mathematical details associated with the analysis without obscuring the salient features of the plastic-flow study.

The bracket to be analyzed is shown displaced from its unloaded position in Fig. 2. It is subjected to a bending moment M and supported by three bolts of equal length, of equal cross-sectional area A, and having identical material properties. The bolts are located at distances d_1, d_2, and d_3 from the foot of the bracket. The bracket itself is assumed to be sufficiently stiff so that the surface (om) originally in contact with the retaining wall, always remains plane. Thus, the elongation of each bolt under load is proportional to the distance between the bolt and the foot of the bracket; i.e. if e_i denotes the elongation of the ith bolt,

$$\frac{e_1}{d_1} = \frac{e_2}{d_2} = \frac{e_3}{d_3} = \vartheta \tag{1}$$

Vol. 1
1960

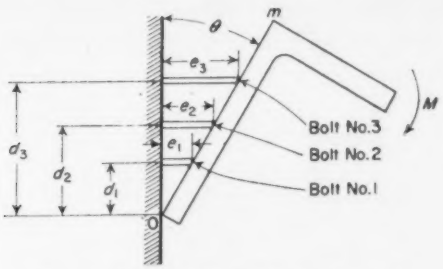

Fig. 2. Deformation of the bracket.

where θ denotes the small angle through which the bracket rotates when the load is applied.

In the analysis to follow, the stresses in the set of bolts and the resulting rotation of the bracket are evaluated for increasing bending moments M. The analysis is first concerned with the fully elastic, the elastic-plastic, and the fully plastic stress distributions within a set of bolts made of a perfectly plastic material. The effect of work-hardening is then discussed separately.

ELASTIC SOLUTION

Let P_1, P_2 and P_3 denote the forces within the first, second and third bolt, respectively. If the applied bending moment is small enough so that all of the resulting stresses are within the elastic range, Hooke's Law applies, and one may express the relationship between the forces and the elongation of the bolts as

$$\frac{e_1}{P_1} = \frac{e_2}{P_2} = \frac{e_3}{P_3} = \frac{l}{AE} \tag{2}$$

where l is the active length of each bolt, A is its cross-sectional area, and E is the modulus of elasticity of the bolt material. The same value of l/AE applies for each bolt since the bolts are assumed to be identical. One may write, therefore, in view of equation (1), that

$$\frac{P_1}{d_1} = \frac{P_2}{d_2} = \frac{P_3}{d_3}\,. \tag{3}$$

Equilibrium requires the applied bending moment to be equal to the resisting moment, or

$$M = P_1 d_1 + P_2 d_2 + P_3 d_3\,. \tag{4}$$

In view of equation (3), and the fact that the force in bolt No. 3 is equal to $\sigma_3 A$, where σ_3 is its stress, one may also write the foregoing expression as

$$M = \frac{\sigma_3 A}{d_3}\,(d_1^2 + d_2^2 + d_3^2)\,. \tag{5}$$

According to equation (3), the force in each bolt is proportional to its distance from the foot of the bracket. Thus, bolt No 3 is the most highly stressed. Its stress is prescribed for a given applied bending moment M by equation (5). This relationship remains valid only as long as the applied bending moment is small enough so that σ_3 does not exceed the yield stress σ_{yp}. Thus the largest moment for which equation (5) holds is, equal to

$$M_1 = \frac{\sigma_{yp} A}{d_3} (d_1^2 + d_2^2 + d_3^2) . \tag{6}$$

The rotation of the bracket corresponding to this moment is, in view of equations (1) and (2), equal to

$$\theta_1 = \frac{e_3}{d_3} = \frac{1}{d_3}\left(\frac{l\sigma_{yp}}{E}\right) \tag{7}$$

As the applied bending moment increases beyond the value M_1 the bracket enters the first stage of the elastic-plastic solution.

FIRST STAGE OF THE ELASTIC-PLASTIC SOLUTION

During the first stage of the elastic-plastic solution, bolt No. 3 flows plastically. In keeping with the assumption of a perfectly plastic bolt material, its stress is a constant equal to σ_{yp}, the yield stress of the material. Thus the force in bolt No. 3, namely P_3, is a constant and equal to $\sigma_{yp}A$, and one may write the equilibrium equation for this case as

$$M = P_1 d_1 + P_2 d_2 + \sigma_{yp} A d_3 . \tag{8}$$

Even though plastic flow occurs in bolt No. 3, the remaining bolts are still within the elastic range of the material, and subject to Hooke's Law. The forces in these bolts, therefore, are related to their elongations by the expression

$$\frac{e_1}{P_1} = \frac{e_2}{P_2} \tag{9}$$

Since the bracket remains rigid during the entire loading program, the deformation of each bolt is proportional to its distance from the foot of the bracket, regardless of whether the stresses in the bolts are completely elastic, elastic-plastic or completely plastic. In view of equations (1) and (9) one may thus write

$$\frac{P_1}{d_1} = \frac{P_2}{d_2} , \tag{10}$$

which permits the equlibrium condition to be rewritten as

$$\begin{aligned} M &= P_2 \frac{d_1^2}{d_2} + P_2 d_2 + \sigma_{yp} A d_3 \\ &= \frac{\sigma_2 A}{d_2} (d_1^2 + d_2^2) + \sigma_{yp} A d_3 \end{aligned} \tag{11}$$

where σ_2 denotes the stress in bolt No. 2.

As the intensity of applied moment M increases, so does the stress in bolt No. 2 and eventually the yield stress of the material, σ_{yp}, is reached. This occurs at a bending moment M_2 which, in view of equation (11) is given by

$$M_2 = \frac{\sigma_{yp} A}{d_2} (d_1^2 + d_2^2 + d_3 d_2) \tag{12}$$

The bracket rotation corresponding to this bending moment is, in view of Equations (1) and (2), given by the expression

$$\theta_2 = \frac{e_2}{d_2} = \frac{1}{d_2}\left(\frac{l\sigma_{yp}}{E}\right). \tag{13}$$

Second stage of the elastic-plastic solution

When the applied bending moment exceeds M_2, yielding occurs in both the second and third bolts, so that

$$P_2 = P_3 = \sigma_{yp} A \tag{14}$$

and the equilibrium condition becomes

$$M = P_1 d_1 + \sigma_{yp} A d_2 + \sigma_{yp} A d_3 = \sigma_1 A_1 d_1 + \sigma_{yp} A (d_2 + d_3) \tag{15}$$

where σ_1 is the stress in bolt No. 1. The latter relationship between stress and applied bending moment, which is valid in the second stage of the elastic-plastic solution, remains applicable until yielding also starts in the first bolt. This situation occurs when the stress in the first bolt is equal to σ_{yp} and the applied bending moment is

$$M_3 = \sigma_{yp} A (d_1 + d_2 + d_3) \tag{16}$$

The bracket rotation corresponding to M_3 in view of equations (1) and (2), is

$$\theta = \frac{e_1}{d_1} = \frac{1}{d_1}\left(\frac{l\sigma_{yp}}{E}\right) \tag{17}$$

When the bending moment reaches M_3, all three bolts are within the plastic range, and their deformations become large even without an increase in applied load. At this stage the bracket becomes structurally useless.

MAXIMUM LOAD-CARRYING CAPACITY

It was shown in the previous section that according to elastic theory, the maximum bending moment to which the bracket can be subjected is given by the expression

$$M_1 = \frac{\sigma_{yp} A}{d_3} (d_1^2 + d_2^2 + d_3^2) \tag{6}$$

By including the effect of contained plastic flow, it was observed that the bracket can resist a bending moment equal to

$$M_3 = \sigma_{yp} A (d_1 + d_2 + d_3) \tag{16}$$

before the deformations become large enough to make the unit structurally useless. Since all the bolts were identical, in the previous analysis, the ratio of the expressions for M_3 and M_1 may be written

$$\frac{M_3}{M_1} = \frac{\frac{d_1}{d_3} + \frac{d_2}{d_3} + 1}{\left(\frac{d_1}{d_3}\right)^2 + \left(\frac{d_2}{d_3}\right)^2 + 1} \tag{18}$$

This ratio, which depends only on the geometry of the problem, shows the effect of including plastic flow in the analysis of the bracket.

In order to evaluate the significance of equation (18), consider the particular case where the bolts are uniformly spaced. For this configuration $d_2 = 2d_1$, $d_3 = 3d_1$ and the ratio of bending moments expressed in equation (18) equals 1·28. This shows that the load-carrying capacity of the bracket computed by including the effect of plastic flow is 1·28 times the bending moment computed by means of an entirely elastic analysis. The bracket with three bolts can therefore carry 28 per cent more load than indicated by the conventional approach.

If the calculation is repeated for four evenly spaced bolts, it is found that the unit can carry 33 per cent more load than that indicated by a completely elastic solution. Additional bolts lead to even greater percentages of load increase, but with a perfectly plastic material the 50 per cent figure cannot be exceeded.

INFLUENCE OF WORK-HARDENING

It is also of interest to study the effect of work-hardening on the maximum load-carrying capacity of the bolted bracket. In the present section we will consider only the particular case in which the stress in bolt No. 1 is at the yield stress of the material. If one studies other cases, one is led to more intricate analyses, but to similar conclusions.

When a bolt is loaded within the plastic range, it is convenient to express its total elongation as

$$e = e^* + f \tag{19}$$

where e^* is the elongation corresponding to the yield stress of the material (i.e. the elastic component of elongation) and f is the plastic component of elongation. Similarly, it is convenient to express the force in each bolt as

$$P = \sigma_{yp} A + Q \tag{20}$$

where $\sigma_{yp} A$ is the force corresponding to the yield stress and Q is the additional force sustained by the bolt. For a work-hardening material

whose stress-strain curve is shown in Fig. 1, the slope within the elastic range is related to the stress and elongation at the yield point by the expression,

$$E = \frac{l\sigma_{yp}}{e^*} \tag{21}$$

and similarly, the slope within the plastic portion of the curve is related to the force and elongation components in the plastic range by the expression

$$C = \frac{lQ}{fA} \tag{22}$$

The strain distribution within the set of bolts made of a work-hardening material can be evaluated by examining Fig. 3. This diagram shows the bracket with an applied bending moment M, which is sufficiently

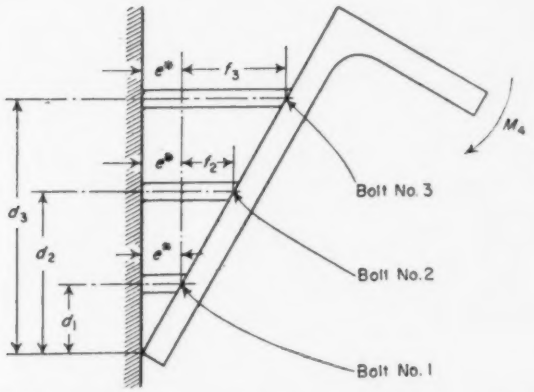

Fig. 3. Deformation of the bracket supported by work-hardening bolts.

large to cause the elongation in bolt No. 1 to equal e^*, the elongation at the yield stress of the material. The plastic elongations in bolts No. 2 and No. 3 are seen to be proportional to the distance from these bolts to bolt No. 1; or, in terms of the dimensions appearing in the figure,

$$\frac{f_2}{d_2 - d_1} = \frac{f_3}{d_3 - d_1} \tag{23}$$

In view of equation (22), and since the bolts are taken to be physically identical, one may rewrite the previous expression as

$$\frac{Q_2}{d_2 - d_1} = \frac{Q_3}{d_3 - d_1} \tag{24}$$

Within the work-hardening range, therefore, the plastic components of the forces in bolts No. 2 and No. 3 are proportional to the distances of these bolts from the bolt in which the yield stress is reached.

Equilibrium considerations and the assumption that bolt No. 1 is at the yield stress of the material lead to the expression

$$M_4 = \sigma_{yp} A d_1 + P_2 d_2 + P_3 d_3 , \tag{25}$$

which, in view of equation (20) becomes

$$M_4 = \sigma_{yp} A (d_1 + d_2 + d_3) + Q_2 d_2 + Q_3 d_3 . \tag{26}$$

This equation may also be expressed in terms of the yield stress and the plastic force component Q in bolt No. 2 by introducing equation (24) to obtain

$$M_4 = \sigma_{yp} A (d_1 + d_2 + d_3) + Q_2 \left[\frac{d_2^2 + d_3^2 - d_1(d_2 + d_3)}{d_2 - d_1} \right] \tag{27}$$

When the plastic component of force in bolt No. 2 is equal to zero (corresponding to an analysis in which the bolts are made of a perfectly plastic material, i. e. slope $C = 0$), the expression for bending moment M_4 is identical to that for M_3, given in equation (16). Furthermore, since Q_2 is a positive number for any work-hardening material, the added term in equation (27) is positive definite, and M_4 is therefore always greater than M_3. Thus, a bracket supported by a set of bolts made of a work-hardening material can carry more load than one made of a perfectly plastic material. The amount of additional load that can be supported depends upon the slope of the plastic portion of the stress-strain curve and may not be significant for small slopes.

CONCLUSION

It has been demonstrated that the load-carrying capacity of a bolted bracket is significantly larger than an elastic analysis indicates. With three uniformly spaced bolts made of a perfectly plastic material, 28 per cent more load can be sustained than that computed by conventional methods. Should the bolts be made of a work-hardening material, then the increase in the load-carrying capacity of the structure is even greater than the aforementioned value.

In evaluating the factor of safety of the bracket, one is interested in comparing the maximum load-carrying capacity of the unit with the maximum load to which the structure is subjected. When confining one's attention to an entirely elastic solution, the ratio of loads is identical to a ratio of the yield stress of the material to the maximum stress induced in the most highly loaded bolt. However, when the bolts are made of a perfectly plastic material and all but at least one are at the yield stress, one can continue to load the structure, even though the maximum stress remains constant. The stress ratio is then no longer related to the factor of safety as it was in the elastic range. The true meaning of the factor of safety continues to be the ratio of the load-carrying

capacity of the structure, computed as a problem in plasticity, to the specified maximum external load.

A design engineer is naturally concerned with the maximum deflections that may be expected in a structure stressed beyond the elastic limit. It is worth while, therefore, to calculate the strains associated with the present problem by assuming the bolts to be made of mild steel, whose yield stress $\sigma_{yp} = 30{,}000$ in/in^2 and whose modulus of elasticity E is 30×10^6. (These bolts yield at a strain ε^* of 0·001 in/in). The maximum strain occurs in bolt No. 3 and is equal to $3\varepsilon^*$. For mild steel this corresponds to a strain of 0·003 in/in. In service the bolt strain is even less, because of the factor of safety. One should agree that these strains are not excessively large and can be tolerated in many applications.

The previous discussion holds for work-hardening as well as perfectly plastic materials. Although detailed analyses for many different structures are feasible for the former case, generally they tend to be inherently more intricate than the latter case. It is convenient, therefore, to base structural computations for work-hardening materials on the assumption of a perfectly plastic material. This assumption always leads to a conservative estimate of the factor of safety. The estimate is much more realistic than one which is obtained from a conventional elastic analysis of the problem.

Vol. 1
1960

REFERENCES

1. A. Vallance and V. L. Doughtie, *Design of Machine Members* p. 162. McGraw-Hill, New York, (1951).
2. V. M. Faires, *Design of Machine Elements* p. 280. Macmillan, New York (1949).
3. S. J. Berard, E. O. Waters and C. W. Phelps, *Principles of Machine Design* p. 86. Ronald Press, New York (1955).
4. A. M. Freudenthal, *The Inelastic Behavior of Engineering Materials and Structures*. John Wiley, New York (1950).
5. A. Nadai, *Theory of Flow and Fracture of Solids*. McGraw-Hill, New York (1950).
6. R. Hill, *The Mathematical Theory of Plasticity*. Oxford University Press (1950).
7. W. Prager and P. G. Hodge, Jr., *Theory of Perfectly Plastic Solids*. John Wiley, New York (1951).
8. O. Hoffman and G. Sachs, *Introduction to the Theory of Plasticity for Engineers*. McGraw-Hill, New York (1953).
9. A. Phillips, *Introduction to Plasticity*. Ronald Press, New York (1956).
10. P. G. Hodge, Jr., *Plastic Analysis of Structures*. McGraw-Hill, New York (1959).

PAPERS TO BE PUBLISHED IN FUTURE ISSUES

J. C. Chapman, B. Erickson and N. J. Hoff: A theoretical and experimental investigation of creep buckling.

W. Johnson and H. Kudo: The use of upper-bound solutions for the determination of temperature distribution in fast hot-rolling and axi-symmetric extrusion processes.

P. B. Neal: The "off" boundary condition in hydrodynamically lubricated, convergent-divergent slider bearings.

R. I. Tanner: Film-lubrication theory for a Maxwell fluid.

P. B. Mellor: The ultimate strength of thin-walled sheets and circular diaphragms subjected to hydrostatic pressure.

H. Kudo: An upper-bound approach to plane-strain forging and extrusion (Parts II and III).

R. S. Benson and W. A. Woods: Wave action in the exhaust system of a supercharged two-stroke-engine model.

S. Kobayashi, A. G. MacDonald and E. G. Thomsen: Some aspects of press forging.

E. Whalley and R. F. Mackinnon: The design of pressure vessels subjected to thermal shock.

L. C. Woods: On the theory of ventilated wind tunnels.

A. A. Gvozdev: The determination of the value of the collapse load for statically indeterminate systems undergoing plastic deformation (Translated from the Russian by R. M. Haythornthwaite).

W. Johnson and H. Kudo: The compression of rigid-perfectly plastic material between rough, parallel dies of unequal width.

F. Freudenstein: On the dynamics of high-speed cam profiles.

R. P. N. Jones: The effect of small changes in mass and stiffness of the natural frequencies and modes of vibrating systems.

J. F. Ely and O. C. Zienkiewicz: Torsion of compound bars — A relaxation solution.

E. Whalley and S. Morris: The design of multilayer pressure vessels subjected to thermal stress.

P. F. Morgan and A. Saunders: An experimental investigation of inertia effects in viscous flow.

J. H. Horlock: Review — Losses and efficiences in axial-flow turbines.

E. Whalley: Review — The design of pressure vessels subjected to thermal stress.

I. I. Levitskii and K. K. Shakhvazian: The synthesis of four-element space mechanisms with lower pairs (Translated from the Russian by F. Freudenstein).

F. R. G. Crossley and U. German: On the response of the singly-free linear oscillator

A. S. Kobayashi and P. R. Trumpler: Elastic stresses in a rotating disc of general profile.

Int. J. Mech. Sci. Pergamon Press Ltd. 1960. Vol. 1, pp. 145–174. Printed in Poland

Vol. 1
1960

A THEORETICAL AND EXPERIMENTAL INVESTIGATION OF CREEP BUCKLING†

J. C. CHAPMAN,‡ BURTON ERICKSON§ and N. J. HOFF¶

(*Received* 22 *April* 1959)

Summary – This paper describes a practical, graphical and numerical procedure for the determination of the collapse time of pin-ended aluminum alloy columns subject to creep. A "critical deflection" is found at which the bending rigidity of the column is reduced to such an extent that the column becomes unstable under the constant load applied to it. To eliminate some of the unessential complexities of the problem, the analysis is carried out on the assumption that the actual column can be replaced by an idealized two-flange column which deflects sinusoidally up to failure. The flexural stiffness is taken as constant along the length of the column and equal to the mid-point stiffness, which is determined from the stress–strain curve of the material. The corresponding "critical time" is then calculated by using the creep-strain vs. time curves of the material. The method gives good agreement with experimental results obtained at the Polytechnic Institute of Brooklyn and at the Battelle Memorial Institute.

NOTATION

y	= deflection of column
ϱ	= radius of gyration
$a = y/\varrho$	= non-dimensional deflection at center of column
a_{00}	= non-dimensional initial deflection amplitude
a_0	= non-dimensional deflection amplitude immediately after application of load
a_{crit}	= non-dimensional deflection amplitude at which buckling occurs
a_{creep}	= non-dimensional deflection amplitude due to creep
a_{inst}	= non-dimensional elastic or plastic deflection amplitude which is caused by increased bending moment arising from creep deflection
L	= length of column
I	= second moment of area of column cross section
M	= bending moment
σ_c	= stress at concave flange
σ_t	= stress at convex flange
$\sigma_m = P/A$	= mean stress
σ_{crit}	= critical stress
A	= Area

† The results presented in this paper were obtained in the course of research carried out at the Polytechnic Institute of Brooklyn under Contract Nonr. 839(18) with the O.N.R.

‡ Imperial College of Science and Technology, London.
§ Politechnic Institute of Brooklyn, New York.
¶ Stanford University, Stanford, California.

h	= depth of section
P	= Load
$P_E = \pi^2 EI/L^2$	= Euler's buckling load
$P^* = \pi^2 E_{\text{red}} I/L^2$	= buckling load when limit of proportionality has been exceeded
E	= Young's modulus of material, found at the proper temperature
E_c	= tangent modulus in concave flange
E_t	= tangent modulus in convex flange or Young's modulus depending on loading conditions
$E_{\text{red}} = 2E_cE_t/(E_c + E_t)$	= reduced modulus
ε_c	= strain in concave flange
ε_t	= strain in convex flange
ε_{cc}	= strain in concave flange due to creep
ε_{tc}	= strain in convex flange due to creep
δ	= deflection of beam
Δ	= small increment

INTRODUCTION

Vol. 1
1960

WHEN a load is applied to an initially slightly curved column, the bending moment resulting from the eccentricity of the line of thrust with respect to the centroidal axis causes an instantaneous elastic and possibly plastic increase of curvature. Because of the bending moment the stresses at the concave and convex surfaces of the column are different in magnitude, and the two surfaces are therefore subject to different rates of creep – that is, under constant load the surface strains change with time at different rates. There results a continuing deflection of the column for constant load, with a consequent increase in bending moment; this increase in bending moment produces a corresponding increase in stress at the concave face of the column and a decrease at the convex face, resulting in changes in the creep rates.

Thus the column continues to deflect at an increasing rate under constant load, and since the stress–strain curve of the material of the column is not straight at high stresses, there comes a time when the decrease in effective flexural rigidity causes the column to collapse. The present paper describes in some detail an approximate method of determining the collapse or "critical" time for a column under a given load.

Most methods which have been put forward for determining the behavior of columns subject to creep have made use of the assumption that the relation between strain, time and stress for a given material and temperature can be expressed by some convenient mathematical law. The method now described makes use of a basic stability concept in order to determine the magnitude of the deflection at which the column collapses; this approach was proposed in three recent papers.[1,2,3] A graphical and numerical procedure which makes use of the actual creep and stress–strain curves for the material of the column is then employed to find the time corresponding to this collapse or "critical" deflection.

THEORY

Basic assumptions

For simplicity it is assumed that the section of the column can be replaced by an equivalent section consisting of two concentrated flanges spaced apart at a distance equal to twice the radius of gyration of the actual section, and having a total area equal to the actual area.

It is also assumed that at any instant the flexural stiffness of the column is constant along its length and is equal to the stiffness at the center section, even though the variation in bending stress along the column may be such that the tangent modulus in the flanges near the center of the column differs appreciably from that near the ends. Given the further assumption that any initial curvature of the column and eccentricity of loading can be jointly represented by a concentric load acting on a column having an initially sinusoidal shape, it is then consistent in these respects to assume that the deflected shape of the column remains sinusoidal throughout its life, although the relation between creep rate and stress does not support this assumption.

It is believed that these assumptions are justified in view of the intrinsic difficulty of specifying the creep properties of aluminum alloys at elevated temperatures, and in view of the extreme sensitivity of these properties to very small changes in temperature.

Determination of critical deflection

When a load P is applied to a column, the initial amplitude y_{00} of the deviations from straightness increases instantaneously to y_0; thereafter the deflection and the concave surface stress increase under constant load because of creep.

The stress–strain curve of the material of the column is not indefinitely linear, and the tangent modulus of the material decreases as the stress increases, so that the flexural stiffness of the column also decreases. There comes a time when the stiffness of the column is diminished to such an extent that the constant load P becomes equal to the Euler buckling load for a column having this reduced stiffness, and at that stage the column must collapse. Thus instead of defining a critical value of load, it is possible to define a critical value of stiffness, and this stiffness corresponds to a certain critical deflection.

Consider the section of the column to be one having two concentrated flanges such that the total cross sectional area A and the moment of inertia I are preserved. The non-dimensional deflection a is defined as

$$a = y/\varrho = 2y/h$$

where y is the total deflection at the center of the column and $\varrho = h/2$ is the radius of gyration. The stresses on the concave and convex side respectively are then given by statics:

$$\left.\begin{aligned}\sigma_c &= \sigma_m(1+a)\\ \sigma_t &= \sigma_m(1-a)\end{aligned}\right\} \tag{1}$$

where σ_m is the mean stress P/A. If the deflection of the column is caused to increase an infinitesimal amount under constant load, the compressive strain in the concave flange increases in proportion to the tangent modulus E_c corresponding to the instantaneous value of σ_c. At the same time the strain in the convex flange changes in proportion to the modulus E_t and the effective bending rigidity of the column is proportional to the reduced modulus for a section having two concentrated flanges

$$E_{\text{red}} = 2E_tE_c/(E_t+E_c)\,. \tag{2}$$

E_t is equal to Young's modulus E when the stress σ_t in the convex flange is compressive but decreasing; it is still equal to E when the deflection is sufficiently large for σ_t to be tensile but less than the elastic limit of the material; and finally, it is the tangent modulus in tension when σ_t exceeds the elastic limit in tension. From the instantaneous stress–strain diagram for the material, determined at the proper temperature, the value of the tangent modulus can be found for any value of σ (Fig. 1).

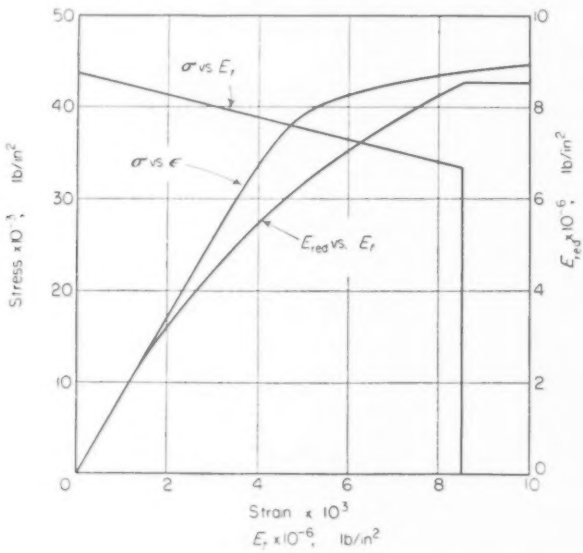

FIG. 1. Corrected stress–strain curve as determined from instantaneous bending tests at 500° F. $\frac{1}{2}$ in. × $\frac{1}{4}$ in. section Al alloy 2024–T 4.

Subsequently σ_c and σ_t can be calculated from equations (1) for a prescribed value of σ_m and for varying values of a and in this way the variation of E_t and E_c with a can be established. Then corresponding

values of E_{red} can be computed from equation (2). Finally the quantity σ_m/E_{red} can be plotted against a (Fig. 2).

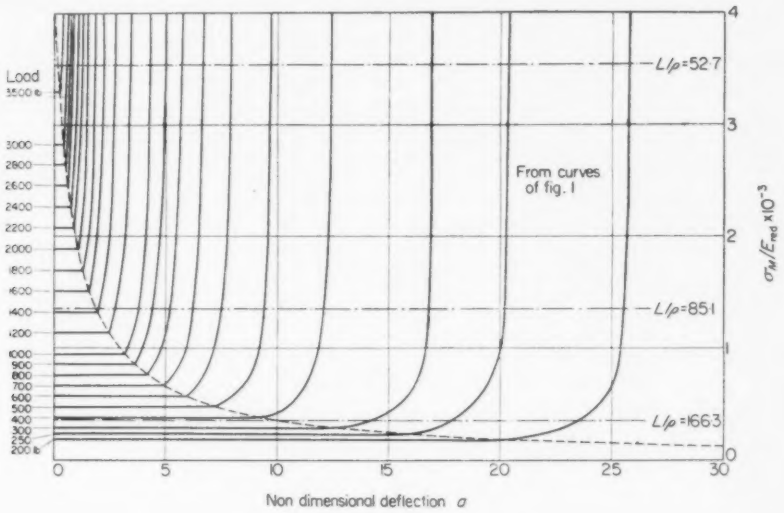

FIG. 2. Determination of a_{crit}.

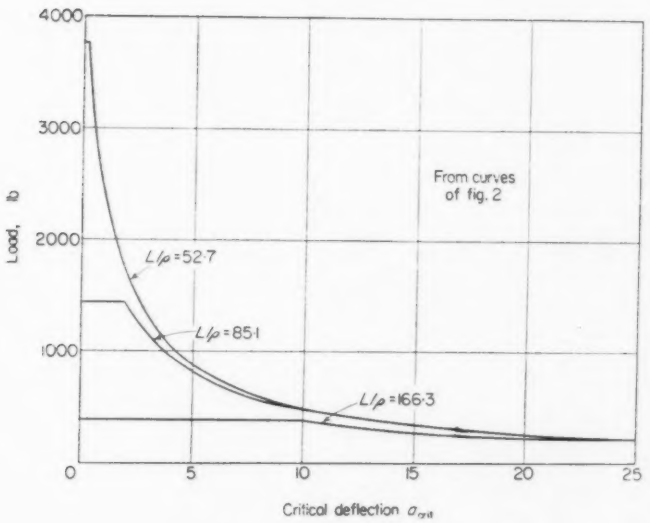

FIG. 3. a_{crit} vs. load.

The critical stress is given by

$$\sigma_{cr} = \pi^2 E_{red}/(L/\varrho)^2, \tag{3}$$

so that buckling occurs at that deflection for which

$$\sigma_m/E_{red} = \sigma_{cr}/E_{red} = \pi^2/(L/\varrho)^2. \tag{4}$$

Vol. 1
1960

This value of $a = a_{crit}$ can be found for a given σ_m and L/ϱ from the graph of Fig. 2. Fig. 3 presents load values plotted against a_{crit} for the three column sizes provided for originally in the experimental program; they were calculated in the manner just described. It remains then to find the time at which a_{crit} is reached.

Determination of critical time

When a load is applied to a column having an initial non-dimensional amplitude of deviation from straightness a_{00}, an instantaneous additional deflection occurs. If the column remains elastic the total non-dimensional central deflection is given by

$$a_0 = a_{00}/[1-(P/P_E)]\,. \tag{5}$$

If the deflection a_0 is so large that the proportional limit of the material is significantly exceeded, a_0 must be found by a process which will be described later.

Next, reference is made to the creep strain vs. time curves for the material obtained at different stress levels. These curves should be plotted exclusive of the instantaneous elastic or plastic strain which occurs when the specimen is loaded (see, for example, Fig. 4). Then for the value

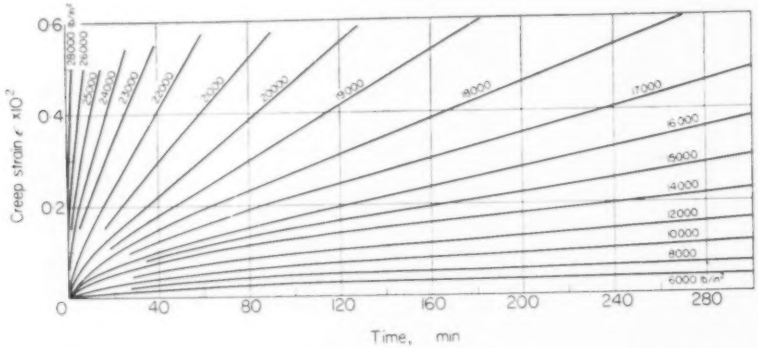

FIG. 4. Adjusted creep strain vs. time for given values of σ (lb/in²).

of a_0 given by equation (5) we can find σ_c and σ_t from equations (1). From the creep curves the amount of creep strain occurring during a small interval of time at each of these two stress levels can be found. Since the deflection at failure, a_{crit}, is already known, it is possible to determine an increment of time corresponding to an increment of strain which is some suitably small fraction of the total strain corresponding to a_{crit}.

The strain increment in the two flanges corresponds to an increment of curvature and consequently an increment of deflection, which is given by

$$\Delta a_{\text{creep}} = L^2(\Delta\varepsilon_{cc} - \Delta\varepsilon_{tc})/2\pi^2\varrho^2. \tag{6}$$

This increment in the amplitude of the non-dimensional sinusoidal deflection results in a simultaneous increment of bending moment which is

$$\Delta M = P\varrho\Delta a_{\text{creep}}. \tag{7}$$

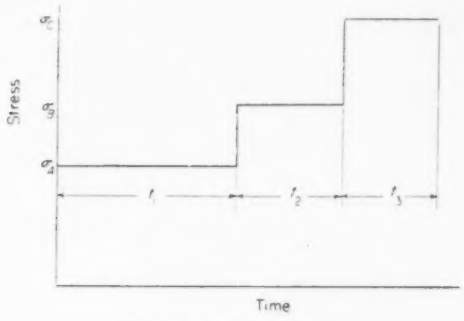

FIG. 5. Stress history.

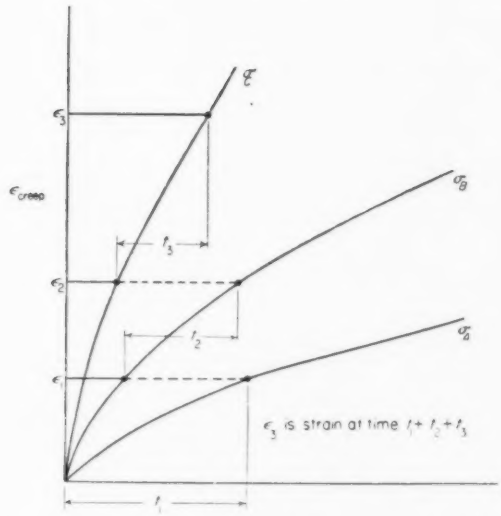

FIG. 6. Creep strain curve corresponding to stress history of Fig. 5.

Due to this increment of bending moment there is an instantaneous increment of curvature given by

$$\Delta(1/R) = P\varrho\Delta a_{\text{creep}}/E_{\text{red}}I, \tag{8}$$

and the corresponding increment in deflection is

$$\Delta a_{\text{inst}} = \Delta a_{\text{creep}} PL^2/\pi^2 E_{\text{red}} I = \Delta a_{\text{creep}} P/P^*, \tag{9}$$

where

$$P^* = \pi^2 E_{\text{red}} I/L^2. \tag{10}$$

Thus the instantaneous elastic or plastic increase in deflection corresponding to an increment of creep deflection can be calculated. New values of σ_c and σ_t corresponding to the total deflection $a_0 + a_{\text{creep}} + a_{\text{inst}}$ can then be found from equations (1) and the additional creep strain occurring during a further increment of time can be found from the creep strain curves. In doing this it is assumed that when transferring from one stress level to another (Fig. 5) there is continuity of creep strain (Fig. 6). As the calculation proceeds, the total creep strain which has occurred should be recorded separately.

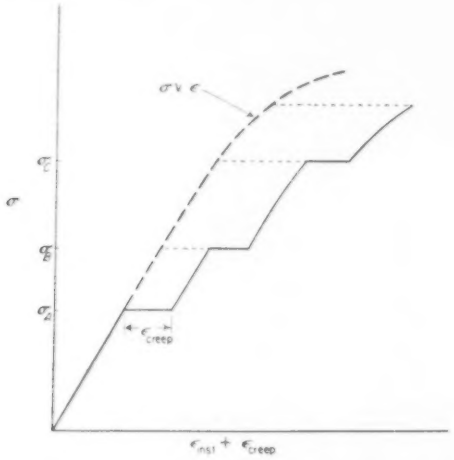

FIG. 7. Stress strain curve corresponding to stress history of Fig. 5.

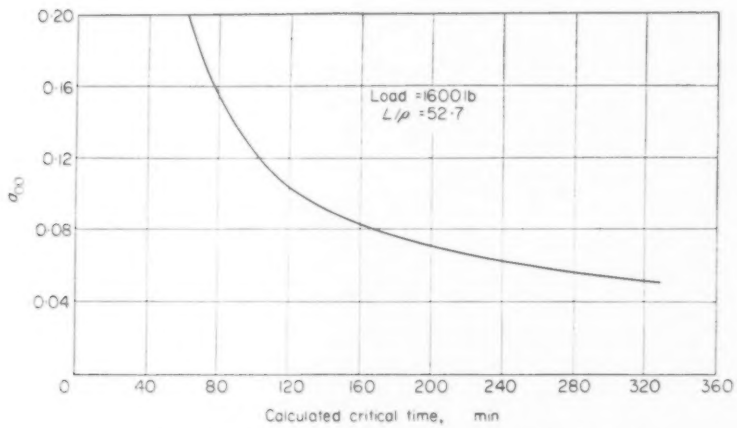

FIG. 8. Variation of critical time with initial eccentricity.

It is also assumed that the instantaneous increment in strain corresponding to an increment in stress is given by the stress–strain curve at the appropriate stress level and that this is unaffected by any inter-

vening creep strain which may have occurred (see Fig. 7). Having found the creep strain increments corresponding to the second increment of time as appropriate to the revised values of σ_c and σ_t, the associated instantaneous elastic and possibly plastic response can again be found. In this way a plot of the deflection a vs. time is obtained. The time corresponding to a_{crit} is the "critical" or failure time of the column. An example of this calculation is given in Appendix 1. The variation of critical time with initial eccentricity is shown in Fig. 8.

Calculation of instantaneous deflection and failure load in the absence of creep

When load is applied to the column an instantaneous elastic and possibly plastic deflection occurs. If the load is sufficiently large to cause the deflection to reach the critical value a_{crit}, then failure occurs instantaneously without any creep having taken place, and the critical time is zero. Where the critical time is other than zero, the first step in its determination is to find the elastic and possibly plastic deflection which occurs when the load is applied, as has already been observed.

Up to the elastic limit of the material of the column the deflection is given by

$$a_0 = a_{00}/[1-(P/P_E)]\,.$$

After the elastic limit has been appreciably exceeded, the deflection can be determined graphically, making use of the stress–strain curve of the material. The amplitude corresponding to ε_c and ε_t, for a sinusoidal deflection, is

$$a_0 = a_{00} + L^2(\varepsilon_c - \varepsilon_t)/2\pi^2\varrho^2\,. \tag{11}$$

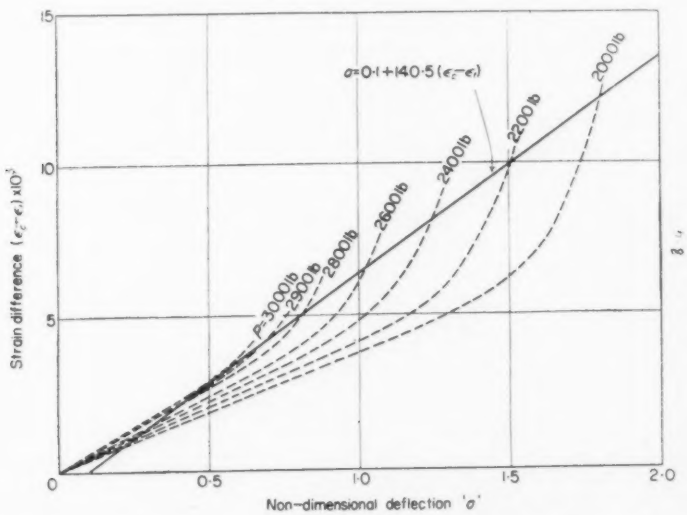

FIG. 9. Relation between strain difference and instantaneous column deflection ($L/\sigma = 52{\cdot}7$).

This equation defines the relation between strain and deflection and makes it possible to plot $(\varepsilon_c - \varepsilon_t)$ against a_0 for given values of a_{00} and L/ϱ. A further relation between load, strain and deflection is found in equations (1) and the stress–strain curve for the material. Therefore curves of $(\varepsilon_c - \varepsilon_t)$ against a_0 can be plotted for specified values of $\sigma_m = P/A$ (Fig. 9). The intersections of these curves with the straight line given by equation (11) give points on the load–deflection curve (Fig. 10). The

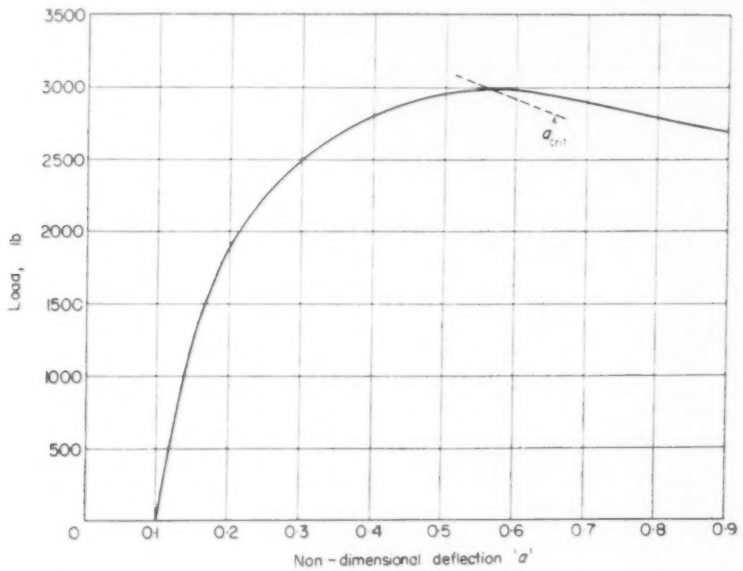

FIG. 10. Instantaneous load-deflection curve for column calculated from stress-strain curve of material ($L/\varrho = 52{\cdot}7$).

second intersection of a curve, corresponding to the larger deflection, represents a point on the unstable part of the load–deflection curve. The value of P for which the second curve is tangential to the line of equation (11) is the instantaneous failure load for the column. The maximum load corresponds to a deflection $a = a_{\text{crit}}$. An example of the above calculation is given in Appendix 2 which also outlines a simplified procedure suitable for columns in which σ_t remains within the elastic limit.

EXPERIMENTS

Determination of stress–strain curve for material in the absence of creep

Load–deflection curves were obtained for beams each having a 12 in. test length, which was subjected to a uniform bending moment. The material was 2024–T4, and the cross section of the beams, which were bent about the longer axis, was $\frac{1}{2}$ in. $\times$ $\frac{1}{4}$ in. The maximum deflection

Vol. 1
1960

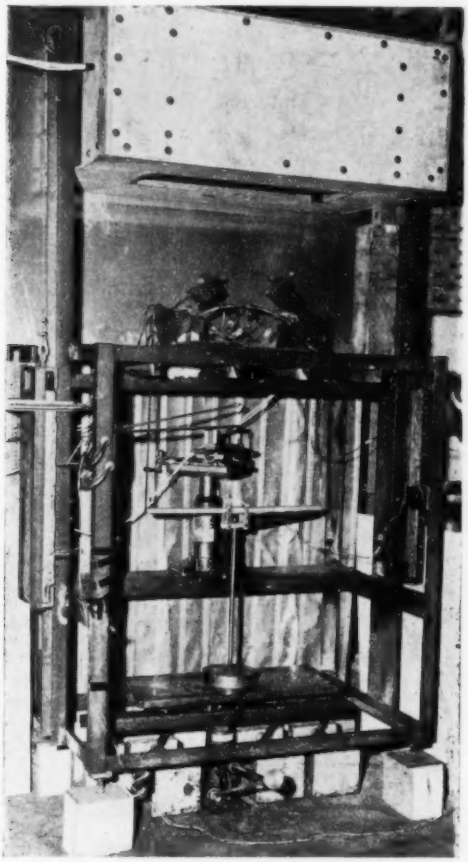

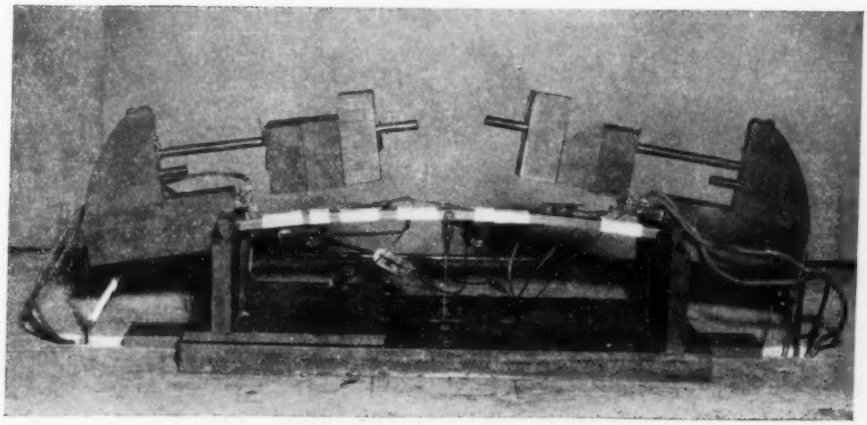

FIG. 11. Creep bending oven.

permitted by the loading rig was 1·4 in. which corresponded to a strain on the surface of the beam of 0·0057.

The loading rig is shown in Fig. 11. The load was applied by weights through an aluminum spreader beam to phosphor-bronze straps which were suspended from cantilevers at each end of the test beam. The bearing surfaces between the phosphor-bronze straps and the cantilevers were each provided with a radius so that the lever arms should remain constant during the deflection of the beam. The knife edge at one end of the test beam was mounted on a plate which ran on ball bearings so that end restraint to the beam was minimized. The base of the loading rig was sufficiently stiff to prevent relative movement between the ends of the beam and the reference point from which the deflection of the beam was measured. The dead weight of the aluminum spreader beam, the end cantilevers and the loading straps was counterbalanced by weights which were inserted before the test began. The load on the hanger was supported by the ram of a hydraulic jack and the load was applied by allowing the ram to fall. In order to achieve a practically constant velocity during the application of the load the ram was loaded by additional weights totalling 200 lb. (The maximum load carried by the specimen was 150 lb.) As the ram fell the load on the hanger was gradually transmitted to the specimen.

Four electric resistance strain gauges were fixed at the center of the aluminum spreader beam and wired into opposing arms of a Wheatstone Bridge. The output from the bridge was fed to a Honeywell recorder, and in this way a plot of load against time was obtained. The load on the hanger was more than sufficient to cause failure of the beam, so that when the load hung free of the ram the end cantilevers were in contact with the base of the loading rig. In this free hanging condition the load on the hanger was fully supported by the aluminum spreader beam and the load measurement system was therefore self-calibrating since the load on the hanger was known. So that the range of the recorder could be suitably adjusted before a test, a steel safety bar was inserted across the specimen between the end fittings and the load could then be hung from the spreader beam without being transmitted to the specimen. The valve which controlled the flow of oil from the jack cylinder was turned to an adjustable stop, and in this way a chosen velocity could be maintained.

In the first experiments the deflection at the center of the beam was measured by means of a differential transformer. The core of the transformer was suspended from a chain which was fixed to a U-clamp at the center of the specimen. To cover the range of deflection of the beam, it was necessary to use the full travel of the core, on both sides of the central null point. It was found that the deflection vs. response curve of the transformer was very flat around the null point (see Fig. 12).

To overcome this difficulty one side of the primary coil of the transformer was connected to one side of the secondary, and the flat portion of the curve was then eliminated. In spite of this refinement the differential transformer was not wholly satisfactory, partly because the oscillator

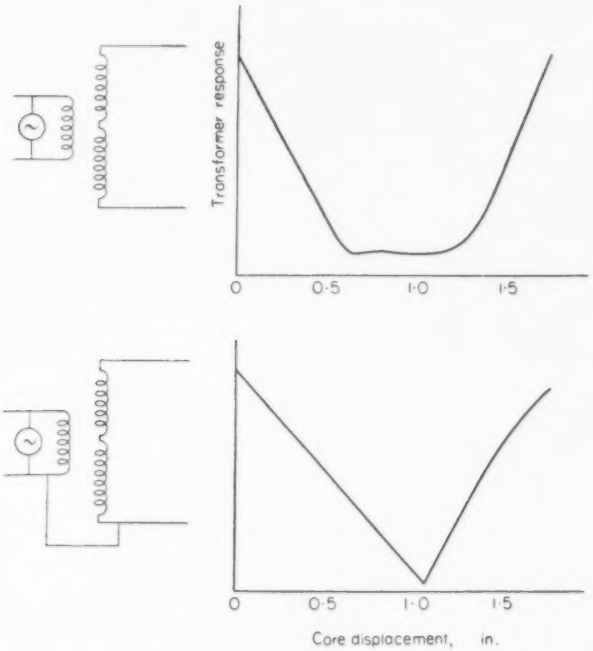

FIG. 12. Output-characteristics of differential transformer.

which supplied the high-frequency voltage was unreliable and partly because the conversion from chart reading to deflection was tedious. Furthermore, a separate calibration covering the whole deflection range had to be made for each test since the calibration curve was liable to vary.

Subsequently, therefore, another device was used for measuring the deflection of the beam. The device consisted of a thin aluminum strip which was clamped against rotation at one end and fixed to a light aluminum tube at the other. The free end of the tube was suspended from the chain which was fixed to the center of the beam. Four strain gauges were fixed to the surfaces of the aluminum strip and formed the arms of a Wheatstone Bridge, the output of which was fed into a recorder. The rigidity of the aluminum tube was very large compared with that of the strip and therefore all the curvature necessitated by the deflection of the cantilever was, so to speak, concentrated at the aluminum strip. This not only increased the sensitivity of the device but also eliminated "whip" from the system.

Having a curve of load vs. time and also of deflection vs. time it is

then possible to plot load against deflection. In most of the tests load was applied for about 2 sec. In order to find whether this rate of loading was sufficiently rapid to eliminate the effects of creep, further tests were run with a loading time of 8 sec. No significant difference in the load–deflection curves for the two loading speeds was observed, and it seems reasonable to assume therefore that the 2 sec tests were sufficiently rapid to be considered instantaneous for practical purposes.

The lid of the oven, which could be raised for access to the specimen, was lined with strip heaters of 1500 W total capacity. Auxiliary 100 W heaters were provided within the end loading cantilevers. Five thermocouples were spaced along the length of the beam for observing temperature and three additional thermocouples were connected to a controller which governed the power to the strip heaters. The auxiliary end heaters were separately controlled manually by powerstats.

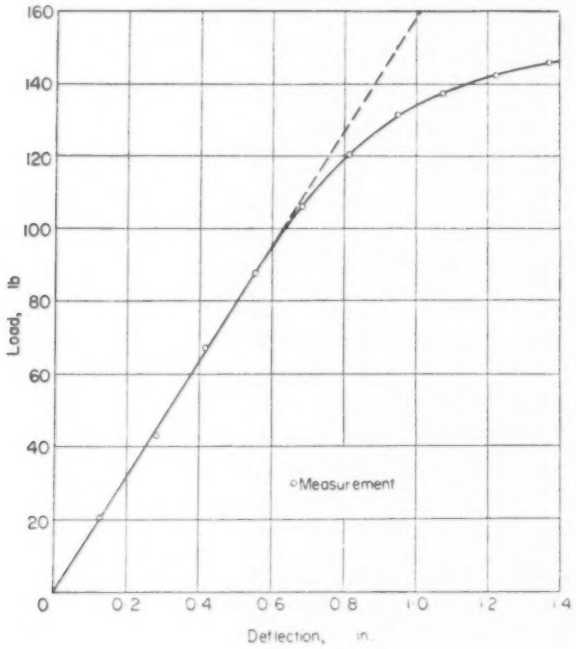

FIG. 13. Typical load–deflection curve for beam.

To test the measuring technique some tests were run on cold specimens, so that the load–deflection curves so obtained could be compared with a load–deflection curve which was obtained by incremental loading and direct measurement of deflection by means of a dial gauge.

From the fourteen load–deflection curves obtained (Fig. 13) a mean curve was drawn (Fig. 14). To convert the deflection to strain it was

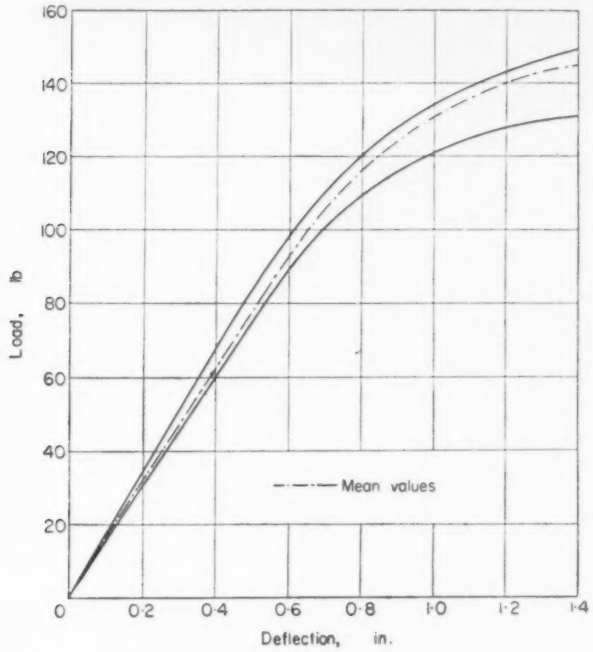

FIG. 14. Envelope of fourteen instantaneous bending test results (500°F).

assumed, for the purpose of these tests, that the surface strain is given by

$$\varepsilon = 4\delta h/L^2. \tag{12}$$

The error involved in this assumption is examined in Appendix 3 and shown in Fig. 15.

To find the relation between load and stress involves a more complicated procedure, owing to the non-linear distribution of stress over the depth of the section. After the limit of proportionality has been exceeded a first approximation to the stress–strain curve can be found on the assumption that

$$\sigma = Mh/2I. \tag{13}$$

The load–deflection curve can therefore be considered to be a first approximation to the stress–strain curve to some scale. The strain is proportional to the distance from the neutral axis, so the stress–strain curve can also be taken as the stress distribution over the depth of the beam. Referring to Fig. 16, the stress under the straight line EC would produce a moment in equilibrium with the applied bending moment, since the stress at point C was calculated on the assumption that the stress distribution was linear. The stress under the curved line EABC therefore would not be in equilibrium with the applied moment and requires correction. A convenient numerical procedure for deriving the stress–strain curve is outlined in Appendix 4.

Vol. 1
1960

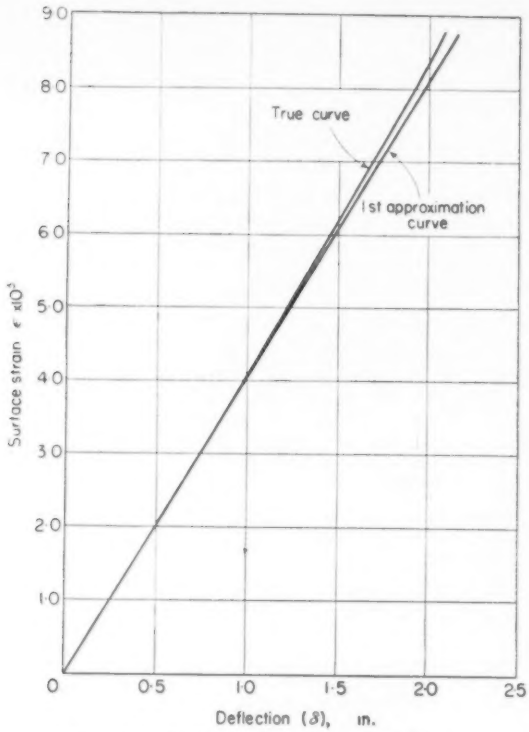

FIG. 15. Surface strain vs. deflection.

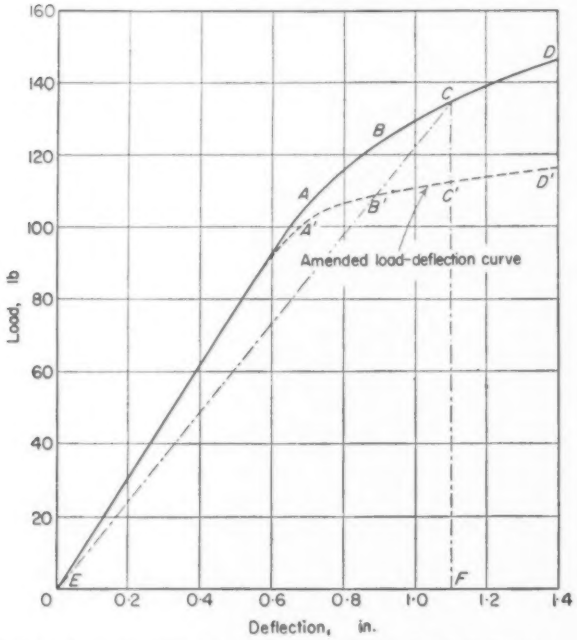

FIG. 16. Derivation of stress-strain curve from load-deflection curve of beam.

Creep bending tests

The beams were loaded in the same way as for the instantaneous bending tests. The load was applied over a period of about 5 sec, since a more rapid application of load could have resulted in additional deflection owing to impact at the moment when the load became fully supported by the beam. Loads ranging from 27 lb to 144 lb were applied and these corresponded to a flange stress σ in the equivalent beam ranging from 6000 to 32,000 lb/in^2. The deflection was measured by the aluminum strip device which was used for the instantaneous bending tests, and the instant when the load was fully supported by the specimen was indicated by a sharp kink in the deflection vs. time curve. Ideally the deflection for which the kink occurs should be given for the applied load by the load–deflection curve found from the instantaneous tests. The deflections determined from the kinks of the deflection vs. time curves of the creep tests have been superimposed on the instantaneous load–deflection curve in Fig. 17, and the correspondence between these separate experimental

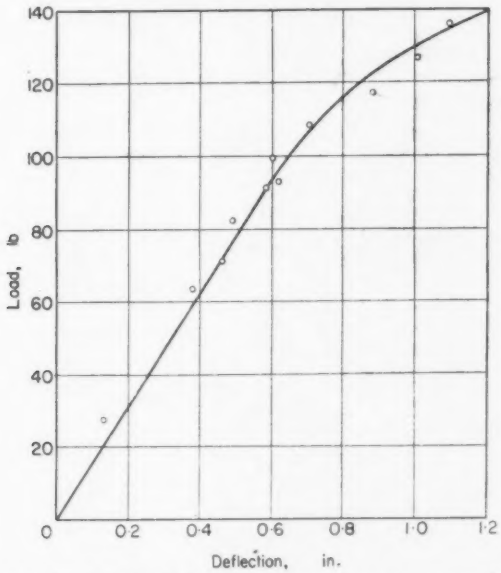

FIG. 17. Average load–deflection curve from instantaneous bending tests with corresponding points from creep bending tests.

points and the mean instantaneous curve gives confidence that the creep deflections measured were inclusive of primary creep and exclusive of instantaneous deflection. The deflection was also measured relative to the zero load condition by means of a direct scale reading at the end of the cantilever; this observation could not, of course, be made during the very early stages of primary creep due to the rapid deflection of the beam.

For the creep tests the end pillars of the loading rig were increased in height so that a maximum central deflection of 2 in. was attained when the end cantilevers reached the base of the loading rig. The tests were run until this deflection had been reached or until 6 hr had elapsed, whichever occurred first. In general, the temperature as indicated by the thermocouples remained within $\pm 1°$F of 500°F throughout the test.

The deflection curves are shown in Fig. 18. Four tests were run for a value of $\sigma = 22{,}000$ lb/in², and it can be seen that there was considerable scatter. One of the four specimens was soaked for 6 hr at 500°F, and allowed to cool before testing; the deflection vs. time curve obtained for this specimen lay within the range covered by the other three speci-

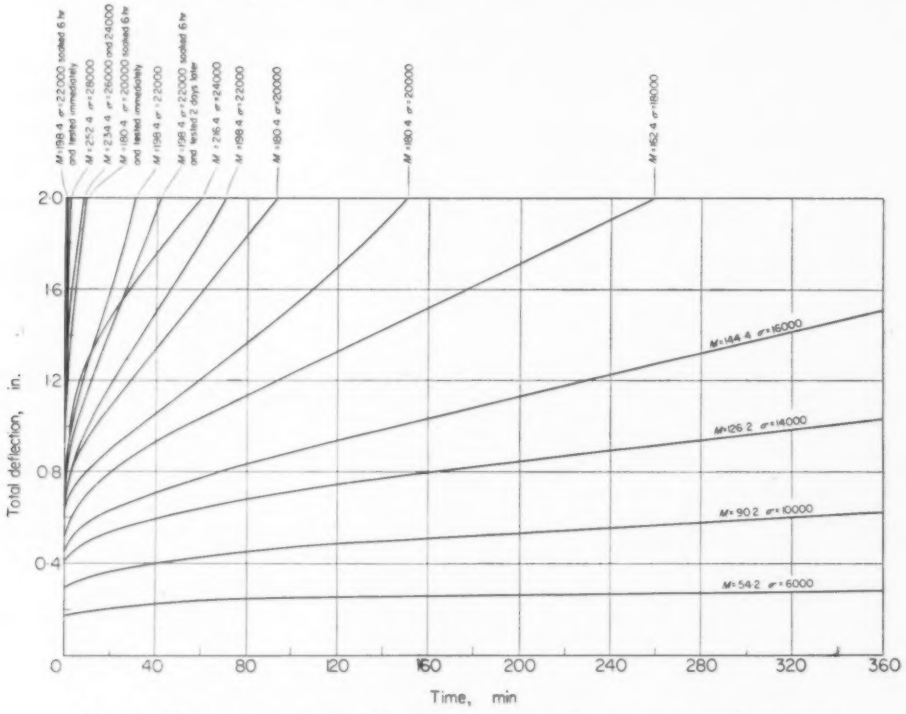

FIG. 18. Unadjusted total deflection vs. time from creep bending tests (500°F) Al alloy 2024–T4.

mens. Two specimens which were soaked for 6 hr and then immediately tested at $\sigma = 20{,}000$ lb/in² and $\sigma = 22{,}000$ lb/in², respectively, were found to creep much more rapidly than specimens tested at the same stresses without prior soaking.

When the deflection of the beam approaches 2 in. the use of equation (12) to determine strain from deflection results in an appreciable error, particularly when it is remembered that to obtain the creep strain the elastic strain must be subtracted from the total strain. A more ac-

curate relation is therefore given in Appendix 3 and Fig. 15, and this was used for converting deflection to strain. The load–deflection curves of Fig. 18 were adjusted by an interpolation process, and the curves of Fig. 4 were derived by converting from deflection to equivalent flange strain. These creep curves are believed to be sufficiently accurate for the purposes of the present investigation but it is considered that an insufficient number of tests has been made for the curves to be used as standards of reference.

Column tests

The columns were loaded by dead weight through the lever system shown in Fig. 19. Load was transferred to the column by allowing the ram of the supporting jack to fall: the rate of load application could be measured by means of strain gauges fixed to the upper and lower flanges of the loading lever, the output being fed into a recorder. The load was applied to the column through knife-edges which incorporated a device for adjusting the eccentricity. The knife-edges had cylindrical seatings, to minimize bending moments about the major axis.

Vol. 1
1960

In the first tests the eccentricity was adjusted by trial, by observing elastic strain differences due to load at room temperature. For this purpose electric resistance strain gauges were fixed to the column faces at the center and at the third points. At elevated temperatures the deflection was measured at one third point by a differential transformer.

In later tests the eccentricity was adjusted by observing deflections measured by 0·0001 in. dial gauges at the center, at the third points and at the ends of the column. To minimize the spring pressure of the dial gauges, the action of one of the internal springs was reversed so that the spindle came to rest at the center of its travel. The dial gauges were connected to the column by a friction device which was designed to prevent damage to the dial gauges at the moment of failure of the column.

In all tests the initial eccentricity was set so that the elastic strain differences or deflection due to a load applied at room temperature was that which would be expected for a column having an initial sinusoidal amplitude of one tenth of the radius of gyration.

Experiments were performed on columns having an overall length of 3·80 in.; this length corresponds to an L/ϱ ratio of 52·7. Deflections were read until the column deflected so rapidly that this was no longer possible – that is, until a few seconds before final collapse.

Figs. 20 and 21 show deflection vs. time and load vs. critical time curves for three column lengths for several loads as calculated. It will be remembered that although the theoretical calculation gives the amplitude of the column at any time, the sinusoidal shape is an inherent assumption.

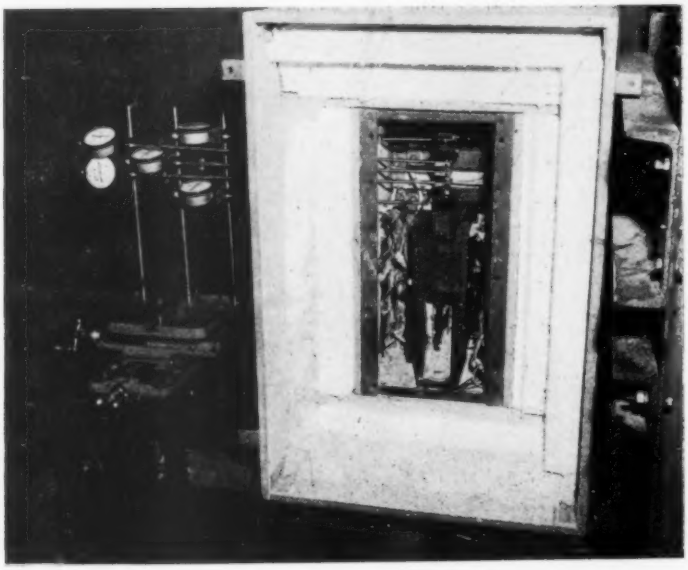

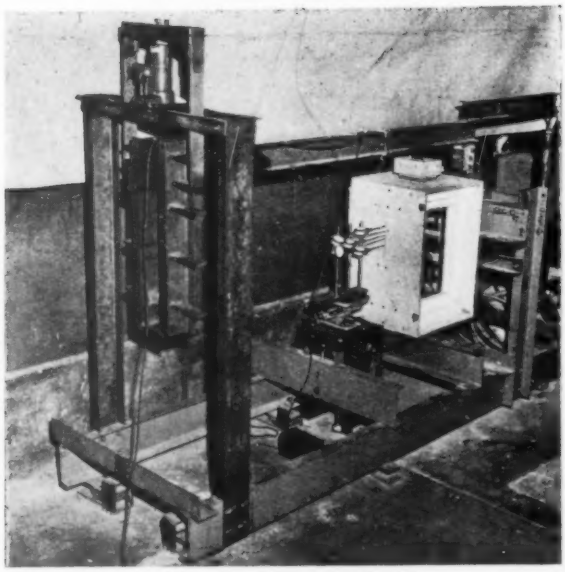

FIG. 19. Column creep oven.

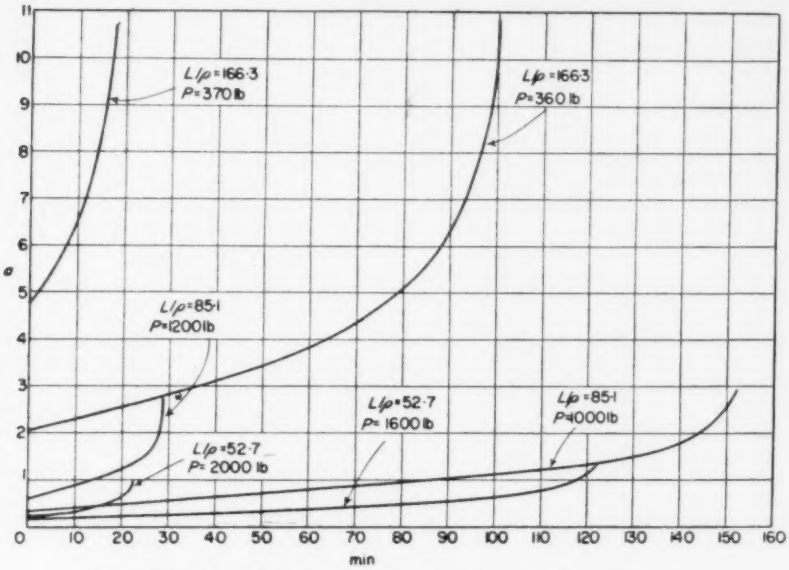

FIG. 20. Typical deflection vs. time curves for columns.

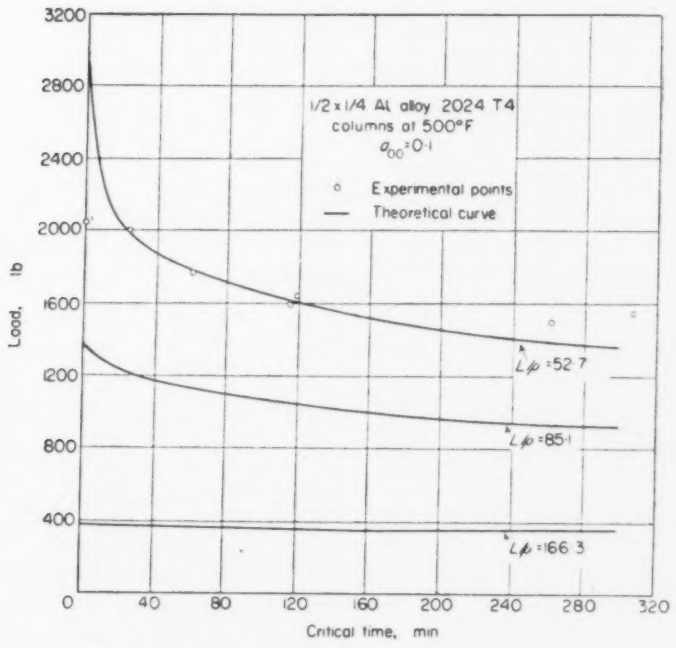

FIG. 21. Calculated and measured critical time.

Vol. 1
1960

Correlation with tests of CARLSON *and* MANNING

The results of an extensive series of tests have been published by the above authors [4], and an attempt has therefore been made to correlate the present theory with these earlier results. Some difficulty was encountered since the creep curves published in the above paper cover only a limited range of stress and strain.

A comparison between measured and calculated failure times is shown in Fig. 22.

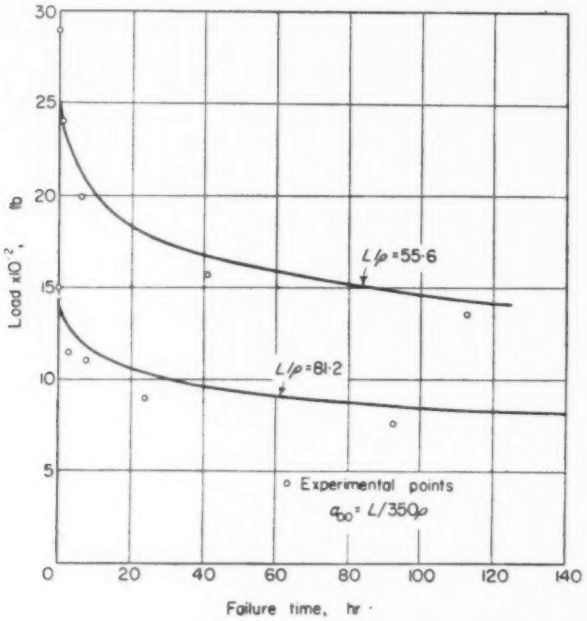

FIG. 22. Comparison of theory with CARLSON and MANNING's experimental results.

CONCLUDING REMARKS

A method has been presented for the calculation of the critical deflection of a column whose material is subject to instantaneous elastic and plastic deformations and to creep. If sufficient information on the behaviour of the material in creep is available, the critical time, that is the time necessary to reach the critical deflection, can be determined analytically, graphically or numerically. At the critical deflection the velocity of the lateral deflection of the column becomes infinite if inertia effects are disregarded.

When the stress–strain curve of the material has no horizontal tangent, the reduced modulus has a minimum value different from zero. If the load applied to the column is smaller than the critical load corresponding to the minimal reduced modulus, a critical deflection does not exist and

the theory here presented does not apply. It has been shown theoretically that in such a case buckling occurs when the lateral deflection tends to infinity. For practical purposes, failure may be deemed to have occurred when the lateral displacement becomes unacceptably large. However, in most cases of interest in missile design the conditions are such that the present theory is valid. This was borne out by an analysis of tests carried out at the Polytechnic Institute of Brooklyn and at the Battelle Memorial Laboratory.

Acknowledgements – The authors wish to acknowledge their indebtedness to Mr. BRIAN M. LEMPRIÈRE and Mr. VASANT D. WAGLE who carried out the preliminary tests and contributed to the development of the equipment and test techniques. They are particularly grateful to Mr. THOMAS J. LARDNER for the care and devotion with which he ran most of the final tests and carried out the numerical analysis necessary for a comparison between theory and experiment.

Vol. 1
1960

APPENDIX 1

DETERMINATION OF CRITICAL TIME

The following example is presented as a more detailed illustration of the procedure outlined in the text for the calculation of the time which has elapsed when the deflection a_{crit} is reached. This time is the collapse or "critical" time for the column.

Length $L = 3{\cdot}80$ in.
Cross section $= 1/2$ in. $\times$ $1/4$ in.
Radius of gyration $\varrho = 0{\cdot}07217$ in.
$L/\varrho = 52{\cdot}7$
Initial deflection $a_{00} = 0{\cdot}1$
Elastic modulus at 500°F $= 8{\cdot}5 \times 10^6$ lb/in²
Constant applied load $P = 2000$ lb
Mean stress $\sigma_m = 16{,}000$ lb/in²
From Fig. 3, $a_{crit} = 1{\cdot}5$
Euler buckling load at 500°F, $P_E = \pi^2 EI/L^2 = 3782$ lb

For a stress less than 33,500 lb/in², (or for a less than 1·09), the stress–strain curve is approximately linear, and

$$P/P^* = P/P_E = 0{\cdot}529$$

The instantaneous deflection which occurs when the load is applied is given by

$$a_0 = a_{00}/[1-(P/P_E)] .$$

With the values given, $a_0 = 0{\cdot}212$. This value is less than 1·09, and the above formula is therefore appropriate.

At time $t = 0$, therefore, the deflection $a = 0{\cdot}212$ and the flange stresses are found from equations (1):

$$\sigma_c = 16{,}000 \times 1{\cdot}212 = 19{,}400 \text{ lb/in}^2$$
$$\sigma_t = 16{,}000 \times 0{\cdot}788 = 12{,}600 \text{ lb/in}^2 .$$

For this stress level a suitable increment of time is about 5 min. From the curves most nearly appropriate to the above stresses in Fig. 4, the creep strains corresponding to a time interval of 5 min can be found, starting from the zero strain level.

Then for the time increment $t = 0$ to $t = 5$ min the increments of creep strain are

$$\Delta\varepsilon_{cc} = 0{\cdot}047 \times 10^{-2}$$
$$\Delta\varepsilon_{tc} = 0{\cdot}013 \times 10^{-2}$$

These strains are also the total creep strains at $t = 5$.

The increment in central deflection due to the incremental creep strain can be found from equation (6):

$$\Delta a_{\text{creep}} = L^2(\Delta\varepsilon_{cc} - \Delta\varepsilon_{tc})/2\pi^2\varrho^2$$

so that for $t = 0$ to $t = 5$ the increment of deflection is

$$\Delta a_{\text{creep}} = 140{\cdot}5(0{\cdot}047 - 0{\cdot}013)\,10^{-2} = 0{\cdot}048\,.$$

The increment of deflection due to creep gives rise to an instantaneous increment of deflection given by equation (9):

$$\Delta a_{\text{inst}} = \Delta a_{\text{creep}} P/P^*\,.$$

So for the time interval $t = 0$ to $t = 5$ the instantaneous increment of deflection is

$$\Delta a_{\text{inst}} = 0{\cdot}048 \times 0{\cdot}529 = 0{\cdot}025\,.$$

The total deflection a at $t = 5$ is therefore

$$a_{t=5} = a_{t=0} + \Delta a_{\text{creep}} + \Delta a_{\text{inst}} = 0{\cdot}212 + 0{\cdot}048 + 0{\cdot}025$$
$$a_{t=5} = 0{\cdot}285\,.$$

The flange stresses σ_c and σ_t should now be re-calculated

$$\sigma_c = 16{,}000 \times 1{\cdot}285 = 20{,}600 \text{ lb/in}^2$$
$$\sigma_t = 16{,}000 \times 0{\cdot}715 = 11{,}400 \text{ lb/in}^2\,.$$

Next, the creep curves of Fig. 4 are again used to find the increments of creep strain which occur at these two stress levels during an additional time interval of 5 min. It is important to note that the strain increments must be found for a time interval of 5 min starting from the strain levels

$$\varepsilon_{cc} = 0{\cdot}047 \times 10^{-2}$$
$$\varepsilon_{tc} = 0{\cdot}013 \times 10^{-2}$$

In this way the total creep strains at $t = 10$ are found to be

$$\varepsilon_{cc} = 0{\cdot}080 \times 10^{-2}$$
$$\varepsilon_{tc} = 0{\cdot}020 \times 10^{-2}$$

and the creep strain increments are

$$\Delta\varepsilon_{cc} = 0{\cdot}033 \times 10^{-2}$$
$$\Delta\varepsilon_{tc} = 0{\cdot}007 \times 10^{-2}\,.$$

The corresponding increment of deflection is

$$\Delta a_{\text{creep}} = 140{\cdot}5(0{\cdot}033 - 0{\cdot}007)\,10^{-2} = 0{\cdot}037$$

and the instantaneous response is

$$\Delta a_{\text{inst}} = 0{\cdot}037 \times 0{\cdot}529 = 0{\cdot}020\,.$$

The total deflection at $t = 10$ is therefore

$$a_{t=10} = 0{\cdot}285 + 0{\cdot}037 + 0{\cdot}020 = 0{\cdot}342 .$$

The flange stresses are then

$$\sigma_c = 16{,}000 \times 1{\cdot}342 = 21{,}500 \text{ lb/in}^2$$
$$\sigma_t = 16{,}000 \times 0{\cdot}658 = 10{,}500 \text{ lb/in}^2 .$$

From the curves of Fig. 4, at the appropriate stress levels, it is found that during a further 5 min interval the total creep strains increase from

$$\varepsilon_{cc} = 0{\cdot}080 \times 10^{-2}$$
$$\varepsilon_{tc} = 0{\cdot}020 \times 10^{-2}$$

to

$$\varepsilon_{cc} = 0{\cdot}135 \times 10^{-2}$$
$$\varepsilon_{tc} = 0{\cdot}025 \times 10^{-2} ,$$

and the creep strain increments are

$$\Delta\varepsilon_{cc} = 0{\cdot}055 \times 10^{-2}$$
$$\Delta\varepsilon_{tc} = 0{\cdot}005 \times 10^{-2} .$$

The increment of creep deflection is

$$\Delta a_{\text{creep}} = 140{\cdot}5\,(0{\cdot}055 - 0{\cdot}005)\,10^{-2} = 0{\cdot}070 ,$$

and

$$\Delta a_{\text{inst}} = 0{\cdot}070 \times 0{\cdot}529 = 0{\cdot}037 .$$

The total deflection after 15 min is

$$a_{t=15} = 0{\cdot}342 + 0{\cdot}070 \times 0{\cdot}037 = 0{\cdot}449 ,$$

and the flange stresses are

$$\sigma_c = 16{,}000 \times 1{\cdot}449 = 23{,}200 \text{ lb/in}^2$$
$$\sigma_t = 16{,}000 \times 0{\cdot}551 = 8{,}800 \text{ lb/in}^2 .$$

During a further 5 min interval at these stress levels the creep strains increase from

$$\varepsilon_{cc} = 0{\cdot}135 \times 10^{-2}$$
$$\varepsilon_{tc} = 0{\cdot}025 \times 10^{-2}$$

to

$$\varepsilon_{cc} = 0{\cdot}210 \times 10^{-2}$$
$$\varepsilon_{tc} = 0{\cdot}025 \times 10^{-2} ,$$

the creep strain increments being

$$\Delta\varepsilon_{cc} = 0{\cdot}075 \times 10^{-2}$$
$$\Delta\varepsilon_{tc} = 0 .$$

Then

$$\Delta a_{\text{creep}} = 140{\cdot}5\,(0{\cdot}075 - 0)\,10^{-2} = 0{\cdot}105$$
$$\Delta a_{\text{inst}} = 0{\cdot}105 \times 0{\cdot}529 = 0{\cdot}055$$
$$a_{t=20} = 0{\cdot}449 + 0{\cdot}105 + 0{\cdot}055 = 0{\cdot}609$$
$$\sigma_c = 16{,}000 \times 1{\cdot}609 = 25{,}700 \text{ lb/in}^2$$
$$\sigma = 16{,}000 \times 0{\cdot}391 = 6{,}300 \text{ lb/in}^2 .$$

The rate of deflection now is such that the time interval should be reduced. Then proceeding as before

Vol. 1
1960

$$\text{At } t = 22 \text{ min} \qquad \varepsilon_{cc} = 0{\cdot}310 \times 10^{-2}$$
$$\varepsilon_{tc} = 0{\cdot}025 \times 10^{-2}$$
$$\Delta\varepsilon_{cc} = 0{\cdot}100 \times 10^{-2}$$
$$\Delta\varepsilon_{tc} = 0$$
$$\Delta a_{\text{creep}} = 140{\cdot}5\,(0{\cdot}100 - 0)\,10^{-2} = 0{\cdot}140$$
$$\Delta a_{\text{inst}} = 0{\cdot}140 \times 0{\cdot}529 = 0{\cdot}074$$
$$a_{t=22} = 0{\cdot}609 + 0{\cdot}140 + 0{\cdot}074 = 0{\cdot}823$$
$$\sigma_c = 16{,}000 \times 1{\cdot}823 = 29{,}200 \text{ lb/in}^2$$
$$\sigma_t = 16{,}000 \times 0{\cdot}177 = 2{,}800 \text{ lb/in}^2$$
$$\text{At } t = 22\tfrac{1}{2} \text{ min} \qquad \varepsilon_{cc} = 0{\cdot}390 \times 10^{-2}$$
$$\varepsilon_{tc} = 0{\cdot}025 \times 10^{-2}$$
$$\Delta\varepsilon_{cc} = 0{\cdot}080 \times 10^{-2}$$
$$\Delta\varepsilon_{tc} = 0$$
$$\Delta a_{\text{creep}} = 140{\cdot}5\,(0{\cdot}080 - 0)\,10^{-2} = 0{\cdot}112$$
$$\Delta a_{\text{inst}} = 0{\cdot}112 \times 0{\cdot}529 = 0{\cdot}059$$
$$a_{t=22\frac{1}{2}} = 0{\cdot}823 + 0{\cdot}112 + 0{\cdot}059 = 0{\cdot}994$$
$$\sigma_c = 16{,}000 \times 1{\cdot}994 = 31{,}900 \text{ lb/in}^2$$
$$\sigma_t = 16{,}000 \times 0{\cdot}006 = 100 \text{ lb/in}^2 .$$

The creep rate for a stress of 31,900 lb/in² is so large that failure ensues almost immediately, and the failure time may be taken as

$$t_{\text{crit}} = 22\tfrac{1}{2} \text{ min}$$

APPENDIX 2

DETERMINATION OF INSTANTANEOUS FAILURE LOAD FOR COLUMN, MAKING DIRECT USE OF THE STRESS–STRAIN CURVE FOR THE MATERIAL

It is required to find the load which will cause failure at $t = 0$, and to plot the load–deflection curve for the column.

The relation between total deflection and strain difference for a column with a sinusoidal deflection is

$$a = a_{00} + L^2(\varepsilon_c - \varepsilon_t)/2\pi^2\varrho^2 . \tag{11}$$

The relations between stress and total deflection are

$$\left.\begin{aligned} \sigma_c &= \sigma_m(1+a) \\ \sigma_t &= \sigma_m(1-a) \end{aligned}\right\}$$
$$(\text{in which } \sigma_m = P/A) . \tag{1}$$

The relation between stress and strain for the material is given in Fig. 1.

For a given value of $\sigma_m = P/A$ it is possible to find σ_c, σ_t, $(\varepsilon_c - \varepsilon_t)$ and a from the above four relations.

For $L = 3{\cdot}8$ in. $\varrho = 0{\cdot}07217$ in. $a_{00} = 0{\cdot}1$,

equation (11) becomes

$$a = 0{\cdot}1 + 140{\cdot}5(\varepsilon_c - \varepsilon_t),$$

and this expression is plotted in Fig. 9.

Then for specified values of P, equations (1) and the stress–strain curve make it possible to plot $(\varepsilon_c - \varepsilon_t)$ against a.

For example, if $P = 2000$ lb, $\sigma_m = 16{,}000$ lb/in², and for chosen values of a the stress and strains are

a	σ_c	σ_t	$\varepsilon_c \times 10^3$	$\varepsilon_t \times 10^3$	$(\varepsilon_c - \varepsilon_t) \times 10^3$
1	32,000	0	3·8	0	3·8
1·2	35,200	− 3,200	4·2	−0·4	4·6
1.4	38,400	− 6,400	4·8	−0·8	5·6
1·6	41,600	− 9,600	6·1	−1·1	7·2
1·7	43,200	−11,200	7·7	−1·3	9·0
1·8	44,800	−12,800	10·4	−1·5	11·9

Intersections occur at $a = 0{\cdot}21$ and at $a = 1{\cdot}81$, so these are the two possible values of a corresponding to a load of 2000 lb.

Proceeding in the same way for further values of P, the curves of Fig. 9 and the load–deflection curve of Fig. 10 are constructed.

It often happens that the stress σ_t falls within the linear part of the stress–strain curve. Then

$$\varepsilon_t = \sigma_t / E$$

From equations (1),

$$\sigma_t = 2\sigma_m - \sigma_c$$

so that

$$\varepsilon_t = (1/E)(2\sigma_m - \sigma_c)$$

Also from (1)

$$\lambda = (\sigma_c/\sigma_m) - 1$$

Substitution of these expressions for ε_t and a in (11) results in

$$(\sigma_c/\sigma_m) - 1 - a_{00} = (L^2/2\pi^2\varrho^2)[\varepsilon_c - (2\sigma_m/E) + (\sigma_c/E)].$$

Since $P_E = \pi^2 E A \varrho^2 / L^2$, this can be written as

$$\varepsilon_c = (\sigma_c/E)[2(P_E/P) - 1] - 2(\sigma_m/E)[(1 + a_{00})(P_E/P) - 1]. \qquad (14)$$

This expression represents a linear relation between ε_c and σ_c; for any given value of σ_m the corresponding value of σ_c is given by the intersection of the curve representing equation (14) with the stress–strain curve for the material.

Then the deflection is given by

$$a = (\sigma_c/\sigma_m) - 1.$$

For the column chosen in the example $P_E = 3782$ lb, and if $P = 2000$ lb, equation (14) becomes

$$E\varepsilon_c = 2{\cdot}782\sigma - 34{,}500$$

$$\varepsilon_c = 0{\cdot}328 \times 10^{-6}\sigma_c - 4{\cdot}06 \times 10^{-3}.$$

This gives intersections with the stress–strain curve at $\sigma_c = 19{,}200$ lb/in² and $\sigma_c = 44{,}700$ lb/in² corresponding to $a = 0{\cdot}20$ in. and $a = 1{\cdot}80$ in. respectively (Fig. 23). The first intersection occurs within the linear part of the curve, and the deflection could have been obtained directly from the equation for the deflection of an elastic column.

The second intersection represents a point on the unstable part of the load–deflection curve. The value of σ_t corresponding to this deflection is $-12{,}800$ lb/in^2, so that the assumption that $\sigma_t = E\varepsilon_t$ was valid in this case.

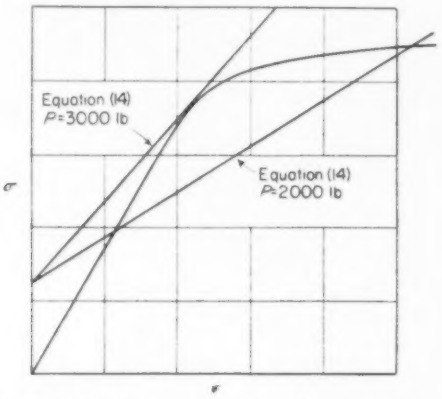

FIG. 23. Relation between load and compressive stress.

The curve of equation (14) for $P = 3000$ lb (Fig. 23) does not intersect the stress–strain curve, and this indicates that this load exceeds the carrying capacity of the column. The load for which equation (14) is tangential to the stress–strain curve is the maximum load which the column can carry.

When both stresses σ_c and σ_t fall within the linear part of the stress–strain curve, the strains are given by

$$\varepsilon_c = \sigma_c/E$$
$$\varepsilon_t = \sigma_t/E$$

so

$$(\varepsilon_c - \varepsilon_t) = (\sigma_c - \sigma_t)/E\,,$$

and from equation (1)

$$(\sigma_c - \sigma_t)/E = 2aP/AE\,.$$

Substitution in equation (11) gives

$$a = a_{00} + aPL^2/\pi^2 EA\varrho^2 = a_{00} + aP/P_E$$

or

$$a = \frac{a_{00}}{1 - (P/P_E)}\,,$$

which is the usual expression for the deflection of an elastic column.

Appendix 3

RELATION BETWEEN STRAIN AND DEFLECTION FOR BEAM WITH UNIFORM CURVATURE

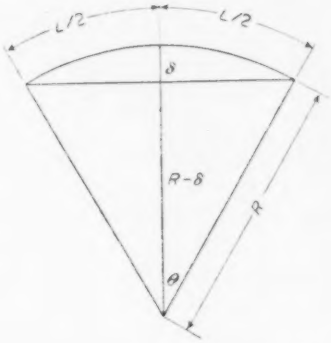

Fig. 24. Geometry of deflected beam.

From the geometry of Fig. 24

$$\delta(2R-\delta) = (R\sin\Theta)^2$$

and

$$\Theta = L/2R\,,$$

so

$$\delta(2R-\delta) = [R\sin(L/2R)]^2\,. \tag{15}$$

The surface strain is given by

$$\varepsilon = h/2R\,,$$

and equation (15) therefore makes it possible to plot ε against δ (Fig. 15).

If δ is small compared with R, and if $R\sin\Theta \approx L/2$, equation (15) becomes

$$2R\delta = L^2/4$$

and

$$\varepsilon = 4\delta h/L^2\,.$$

Appendix 4

DETERMINATION OF STRESS–STRAIN CURVE FROM LOAD–DEFLECTION CURVE FOR BEAM

The full line of Fig. 16 is the mean measured load–deflection curve for the beams tested. Points A, B, C, D have been corrected successively to give points A', B', C', D'.

Consider the correction of point C. Let the ordinate FC represent to some scale the stress at the surface of the beam if the distribution over the depth were linear; then the moment of resistance of the stress under triangle EFC is proportional to the actual moment acting on the beam. Therefore the position of the point C must be changed to some position C' such that the moment of the $EFC'B'A'$ is the same as that of the triangle EFC.

The moment of the triangle EFC is approximately proportional to

$$(1{\cdot}1 \times 135) + (1{\cdot}0 \times 122) + (0{\cdot}9 \times 110) + \ldots\ldots (0{\cdot}1 \times 11) = 617 .$$

The moment of the area $EFCBA$ is proportional to

$$(1{\cdot}1 \times 135) + (1{\cdot}0 \times 130) + (0{\cdot}9 \times 123) + \ldots\ldots (0{\cdot}1 \times 11) = 673 .$$

If C is moved to a position C' such that the ordinate $FC' = 111$, the moment of the area $EFC'B'A'$ is proportional to

$$(1{\cdot}1 \times 111) + (1{\cdot}0 \times 110) + (0{\cdot}9 \times 109) + \ldots\ldots (0{\cdot}1 \times 11) = 628 .$$

$C'$is therefore approximately the corrected position of C.

The deflection scale is readily converted to surface strain by the approximate expression

$$\varepsilon = 4\delta h/L^2 ,$$

where h is the depth of the beam and δ the deflection, or alternatively by the more accurate relation of Appendix 3.

The load scale is converted to surface stress by applying the formula

$$\sigma = Mh/2I$$

to a point on the linear part of the curve.

REFERENCES

1. N. J. HOFF, *Effets thermiques dans le Calcul de la Résistance des Structures d'Avions et d'Engins*, Advisory Group for Aeronautical Research and Development (AGARD) of NATO, No. 52 (1956).
2. B. FRAEIJS DE VEUBEKE, *High Temperature Effects in Aircraft Structures* (Edited by N. J. HOFF) Chap. 13, p. 267. Pergamon Press, London (1958).
3. N. J. HOFF, *J. Roy. Aero. Soc.* **61**, 756 (1957).
4. R. L. CARLSON and G. K. MANNING, *Investigation of Compressive Creep Properties of Aluminum Columns at Elevated Temperature (Stability Problems)*. Wright Air Development Center Technical Report 52-251, Part 2 (1954).

Int. J. Mech. Sci. Pergamon Press Ltd. 1960. Vol. 1, pp. 175–191 Printed in Poland

THE USE OF UPPER-BOUND SOLUTIONS FOR THE DETERMINATION OF TEMPERATURE DISTRIBUTIONS IN FAST HOT ROLLING AND AXI-SYMMETRIC EXTRUSION PROCESSES

W. JOHNSON * and H. KUDO †

(*Received* 23 *April* 1959)

Summary – By using realistic upper-bound solutions it is possible to estimate instantaneous temperature distributions throughout a mass of material which is fast being plastically deformed.

For a particular hot rolling process an estimate of this distribution has been made and, in part to justify the use of the method employed, the results of calculations of the deformation of an initially square grid and a calculation of the necessary roll torque and roll pressure distribution are given.

Two particular instances of axi-symmetric processes are examined, both of 0·75 reduction. Firstly, for extrusion through a square die two forms of velocity field are presented and the results predicted therefrom are compared. Secondly, extrusion through a smooth conical die is examined.

Vol. 1
1960

INTRODUCTION

IN A previous paper[1] TANNER and JOHNSON considered some of the aspects concerning temperature rise which occur when a metal is rapidly plastically deformed, particularly under conditions of plane strain, by reference to extrusion processes. Their work extended the original work of BISHOP[2]. Their analysis indicated that for fast metal-working processes (a criterion of fastness was given) conduction could be neglected, and on the further assumption that all the work of plastic deformation reappeared as heat, it became possible, by approximating a given slip-line field solution and so treating it as an upper bound, to determine the distribution of temperature throughout the deforming mass. This approach is subject to a certain amount of inexactitude, because amongst other features, an upper-bound solution provides loads which overestimate the true load. However, two categories of solution are available:

(i) plane-strain solutions for which a slip-line field solution exists

(ii) solutions which are analytical or graphical, plane strain or otherwise.

For category (i), slip-line fields, though they give upper-bound solutions and are not unique, have yet been shown to give reliable information for many diverse problems. Upper-bound solutions which consist

* Department of Mechanical Engineering, University of Manchester.

† Aeronautical Research Institute, Tokyo University.

of a system of fictional tangential velocity discontinuities, can be made to approximate slip-line field solutions as close as required, and, assuming a slip-line solution to be the most accurate solution, it follows that the degree of inexactitude in these cases can be made extremely small.

To category (ii) belong the classes of problem for which no exact solution has been found; in particular there is neither a slip-line solution for every given plane-strain circumstance nor for metal-working problems is there a fully satisfactory solution for axi-symmetric processes. In these instances, the employment of an upper-bound solution becomes something of an expedient. It will give a magnitude for the load to perform a certain operation which exceeds that which is certainly required, and, if other methods for load estimation are lacking, then short of highly empirical approaches, it offers a rational approach to the problem. To effect a solution of this kind requires one to discover a "kinematically admissible velocity field", and this of itself is often a matter of considerable difficulty. If this can be done, then it is usually possible to minimise the over-estimate of load; it will be shown elsewhere that good upper bounds for indenting and extrusion operations are available. (Work to be published by KUDO *et al.*) Knowledge of these solutions can be utilised to give further information such as grid deformation and temperature distribution. Information derived in this way is of course open to criticism, but, when it is not available to engineers by any other means, it is entirely reasonable to employ the approach, feeding into the situation to be investigated such realistic background knowledge as may be available.

Two problems, each of great industrial importance are examined below and they are representative of the two categories of solution described above. Firstly, a slip-line field for the hot rolling process as originally given by ALEXANDER[3] is used, and, by "rationalising" this field in a manner earlier described (TANNER and JOHNSON)[1], the temperature distribution through the roll-gap has been evaluated; the predicted mode of deformation of the material as it passes through the gap is also presented. The analysis is completed by showing the pressure distribution over the contact roll surface and by drawing some interesting comparisons with earlier technological theory. The second problem is concerned with axi-symmetric extrusion through square and conical dies. It employs analytical expressions for the velocities first obtained by KUDO[4]. For the case of extrusion through a square die, two proposed solutions are compared and, though they differ in assumed form, the predicted temperature distributions in the outgoing stock do not differ greatly.

The assumptions concerning the material, i. e. its rigid–perfectly plastic nature, its temperature independent properties, etc., are precisely the same as those adopted in the paper by TANNER and JOHNSON[1]. The

results of their analysis are also assumed to carry over to these investigations.

THE HOT ROLLING PROCESS

The fast hot rolling of wide sheet is examined, this being an extremely important industrial operation. It is well known that the temperature of sheet which is being rolled is largely maintained at a fairly high level, despite the temperature drop due to heat loss through conduction to the manipulator rolls and by radiation whilst waiting between passes; the input of work which is dissipated as heat is generated concurrently by the process of plastic deformation. The maintenance of a high temperature ensures a low yield stress in the material throughout the whole of the rolling process. In the example below, the sheet is assumed to be rolled under conditions of plane strain so that the only known available slip-line field solution is applicable.

Vol. 1
1960

(i) *Temperature profiles through a roll gap*

To exemplify the application of the graphical technique referred to in Section (i) above, a particular rolling example will be analysed. The discontinuous velocity field assumed was derived by adapting the slip-line field solution originally given by ALEXANDER[3]. ALEXANDER examined the hot rolling of a plastic–rigid material under the assumption that the shear stress along the boundary between the roll and the material attains the yield shear stress of the material. His solution required the occurrence of a very thin slice of rigid material adjacent to the roll surface at the entry point; this feature is omitted in the discussion below.

The case examined (see Fig. 1) is that in which the length of the arc of contact AB is 1·14 in., the roll radius 15 in., entry thickness 0·259 in., exit thickness 0·173 in., the total fractional reduction being 1/3. This figure shows the adaptation of ALEXANDER's solution; the discontinuous velocity field in the physical plane is obtained by approximating the curved slip-lines and the roll contour with chords. The corresponding hodograph, shown in Fig. 2, was similarly drawn, and a check on its accuracy showed it to be correct to better than 3 per cent.

The increment of work done per unit volume of the material ΔW when crossing a line of velocity discontinuity is,

$$\Delta W = k\dot{s}/\overline{V}_n \tag{1}$$

where $\dot{s}$ is the rate of relative slip across a surface of velocity discontinuity and $\overline{V}_n$ is the speed of the material element normal to the discontinuity surface, as determined from the hodograph. In Fig. 3 is plotted $\Sigma\Delta W/2k$ for each stream line. Fig. 4 shows the distribution of $\Sigma\Delta W/2k$ in the sheet, in and after passing through the roll-gap, it being assumed that the whole operation is performed adiabatically. The

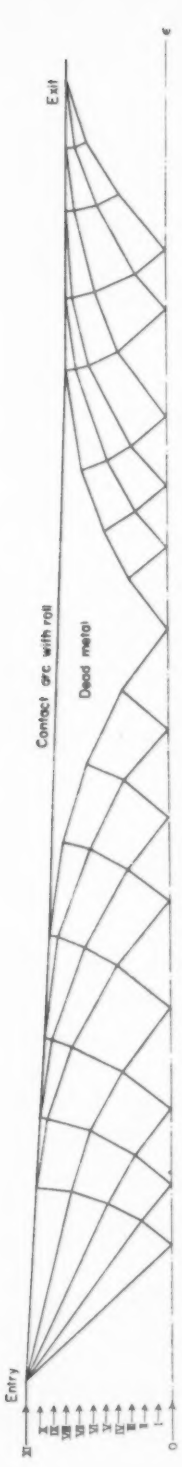

FIG. 1. Approximated discontinuous velocity field for hot rolling.

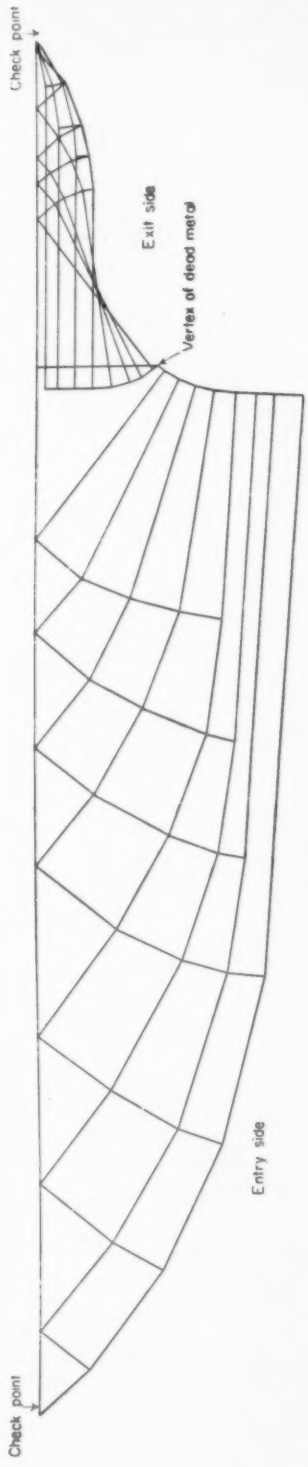

FIG. 2. Hodograph for Fig. 1.

temperature at each point in the material is simply proportional to $\Sigma \Delta W/2k$. Temperature increases ΔT are estimated by multiplying $\Sigma \Delta W/2k$ by a factor c, i. e.

$$\Delta T = c \frac{\Sigma \Delta W}{2k} \,^{\circ}\mathrm{C} \,. \tag{2}$$

c is 60–80 for aluminium, 110–140 for copper and 120–220 for steel, at

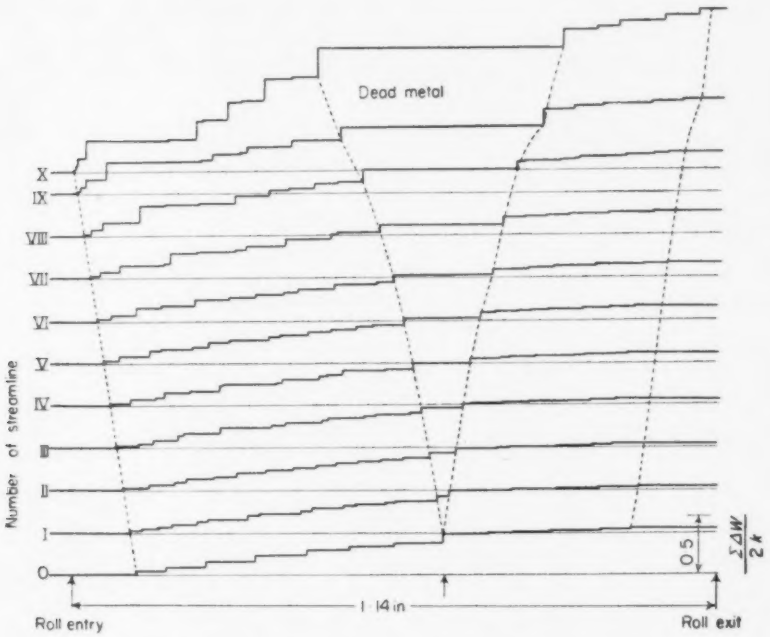

FIG. 3. $\Sigma \Delta W/2k$ along each stream line in rolling.

about room temperature, these ranges being determined primarily by the possible range in yield stress of the metal. Fig. 4 thus shows the temperature profile at five sections through the gap.*

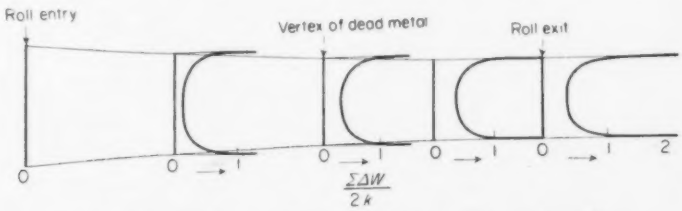

FIG. 4. Temperature profile at various sections in rolling.

* A brief examination of the temperature rise through the roll gap in cold rolling, derived from an elementary technological analysis, has been made by LIPPMAN and JOHNSON and is to be published in *Appl. Sci. Res., Hague.*

(ii) *Distortion of a square grid*

Suppose it is required to determine the distortion of a grid of lines square before entering the roll gap, as it passes between the rolls. The horizontal lines are the stream lines, and since the problem is a steady-state one, the horizontal position l of a particle after a time t, which moves along a stream line is

$$t = \int_0^t dl/u \tag{3}$$

u being the horizontal component of the velocity of the particle, obtained from the hodograph. In the discontinuous velocity field used here, u is constant in a rigid zone and the t versus l graph for a stream line consists of substantially straight-line sections. This is given in Fig. 5. The point

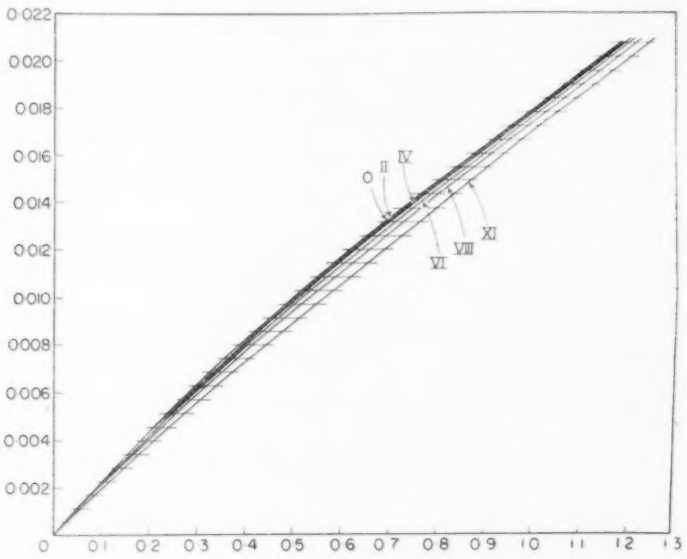

FIG. 5. Time-advance curve along each stream line.

of intersection of the $t-l$ curves and the horizontal lines from the prime ordinate, after a fixed interval $\Delta t = \delta/u_{\text{entry}}$ facilitates calculation of the initially vertical lines; δ is the horizontal distance between the grid lines. The distortions of the grid lines between the rolls, and then as far as the exit, are thus obtained; the results of the calculation are displayed in Fig. 6. The general retardation of the centre of the sheet with respect to its outer surfaces increases till the "dead metal zone" is reached; in the "dead metal zone" there is no further distortion and between leaving this zone and finally emerging from the gap, there is a small reversal of the distortion. The general shape of the deformed grid is seen to

be similar to that obtained experimentally by cold rolling, as per ALEXANDER's paper[5].

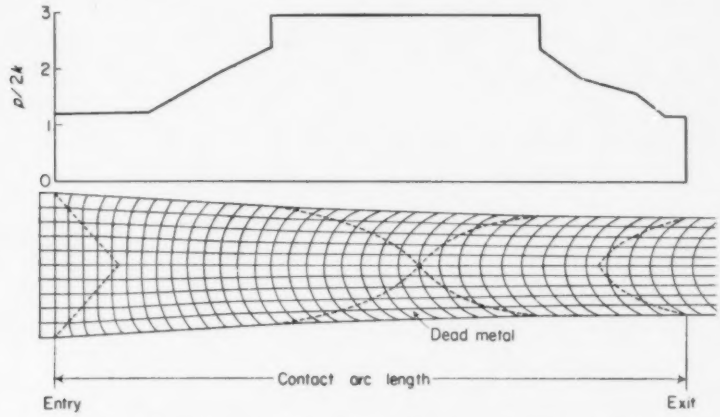

FIG. 6. Distorted grid for rolling and pressure distribution.

(iii) *Total work done and roll torque*

The rate of energy dissipation $\dot{e}$ is obtained by summing the quantities

$$\dot{e} = k.d.\dot{s} \tag{4}$$

at all surfaces of discontinuity, including the boundary surfaces between the roll and the material. d is the length across which the velocity discontinuity occurs; k is the plane strain yield shear stress.

The roll torque T is

$$\omega T = \Sigma \dot{e} \tag{5i}$$

where ω is the angular velocity of the rolls.

For this particular example,

$$T = \Sigma \dot{e}/\omega = 2{\cdot}8k \tag{5ii}$$

per in. thickness perpendicular to the rolling plane. The mean work done per unit volume of the rolled sheet is

$$\Sigma \dot{e}/h \times u_{\text{entry}} = 1{\cdot}99k \simeq 1{\cdot}00 \times 2k \tag{6}$$

(iv) *Pressure distribution over the roll contact surface*

Fig. 1 shows the modified α and β lines of the slip-line field system and employing the Hencky equations and calculating the rotations from point to point in the field, the pressure at various points throughout the roll-gap may be determined. Fig. 6 shows the pressure at particular points on the roll contact surface and over the internal boundary of the dead metal surface. The mean pressure p_m between the dead metal region and the roll only is ascertainable; in this instance $p_m = 2{\cdot}96 \times 2k$.

In calculating the pressures it was assumed that the slip-line at entry

Vol. 1
1960

was at 45° to the centre line of the sheet. The pressure at the common single point N of the two dead metal zones then follows easily. If this pressure is calculated from the exit side of the gap, it is first necessary to consider an equilibrium condition because the exit slip-lines are curved. In this case p_N calculated from exit side is $3{\cdot}17 \times 2k$ and from the entry side $3{\cdot}12 \times 2k$.

From Alexander's stress plane, p_N is $3{\cdot}07 \times 2k$.

(v) *Comparison with approximate solution*

The usual technological approach to the rolling problem proceeds by first finding the position of the neutral point. The equilibrium equation on the exit side of the gap, see Fig. 7, is

$$h dp - k(\cot\alpha + 2)dh = 0 \tag{7}$$

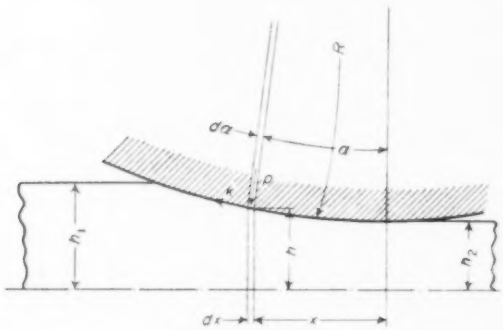

FIG. 7. Figure for approximate analysis of rolling.

Since

$$h \simeq h_2 + k\alpha^2/2$$

and

$$\tan\alpha \simeq \alpha \simeq \sqrt{2(h-h_2)/R}$$

equation (7) thus becomes

$$dp = k\left[\sqrt{\frac{R}{2}}\frac{1}{h}\frac{dh}{\sqrt{h-h_2}} + \frac{2}{h}dh\right]. \tag{8}$$

Integrating (8) and noting that $p = 2k$ at $h = h_2$

$$p_2 = 2k\left[\sqrt{\frac{k}{2h_2}}\tan^{-1}\sqrt{\frac{h-h_2}{h_2}} + \ln\frac{h}{h_2} + 1\right]. \tag{9}$$

A similar procedure on the entry side gives, when $p = 2k$ at $h = h_1$

$$p_1 = 2k\left[\sqrt{\frac{R}{2h_2}}\left(\tan^{-1}\sqrt{\frac{h_1-h_2}{h_2}} - \tan^{-1}\sqrt{\frac{h-h_2}{h_2}} + \ln\frac{h}{h_1} + 1\right)\right]. \tag{10}$$

The neutral point position is given by $p_1 = p_2$ and thus

$$\sqrt{\frac{R}{2h_2}}\left\{2\tan^{-1}\sqrt{\frac{h_N-h_2}{h_2}}-\tan^{-1}\sqrt{\frac{h_1-h_2}{h_2}}\right\}+\ln\frac{h_1}{h_2}=0 \tag{11}$$

Substituting the particular values of this instance, gives

$$\left.\begin{aligned}\frac{h_N}{h_2}-1 &= 0{\cdot}0830 \simeq \frac{1}{2h_2R}X_N^2\\ \text{and thus}\qquad X_N &= 0{\cdot}464 \text{ in.}\end{aligned}\right\} \tag{12}$$

The position of N as determined from the slip-line field is $X_N = 0{\cdot}483$.

The roll torque becomes

$$T = k(L-2X_N)R = 3{\cdot}18k \tag{13}$$

where L is the length of the contact arc. This value of T exceeds that obtained from the discontinuous velocity field by about 13 per cent.

Vol. 1
1960

AXI-SYMMETRIC EXTRUSION PROCESSES

No exact solutions to the problem of axi-symmetric extrusion have yet been obtained and it is therefore reasonable to seek close upper bounds. KUDO[4] has made extensive and seemingly comparatively successful investigations into various axi-symmetric processes using this upper-bound approach and it was therefore decided to examine the temperature increase in extruding material as predicted by his solutions, particularly since an exact mathematical analysis is unlikely. The approximate nature of this particular investigation is well appreciated by the authors, but it is presented here in the belief that even an approximate analysis may be of use for engineering research and development purposes.

An upper bound to the extrusion pressure $\bar{p}$ is, following HILL's[6] extremum principle or using DRUCKER, GREENBERG and PRAGER's upper-bound theorem, given by

$$\frac{\bar{p}}{Y} = \frac{1}{\sqrt{3}}\int_S \dot{s}\,dS + \int_{\bar{V}} \dot{\bar{\varepsilon}}\,d\bar{V} \tag{14}$$

if the material yields in accordance with Mises criterion. The first term on the right-hand side of (14) is the sum of all work done at the boundary of a continuously deforming region; S is the surface area across which the tangential velocity discontinuity $\dot{s}$ occurs. The second term on the right in equation (14) is the work done in steady deformation; $\dot{\bar{\varepsilon}}$ is the equivalent strain rate at a point of an element of volume $d\bar{V}$.

The detailed results of the application of (14) to this case and as applied to axi-symmetric extrusion are quoted in full, since they will be new to many.

(i) *Homogeneous velocity field for a square die*

(a) *Stream lines.* Fig. 8(a) shows a homogeneous velocity field con-

sisting of an annulus [2] and an inner cylinder [1]. Let the reduction in radius of the bar be from unity to b.

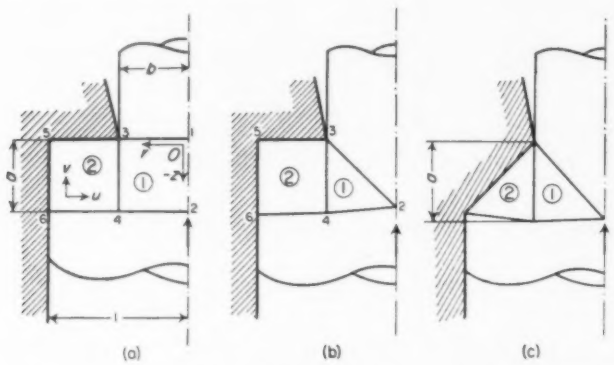

FIG. 8(a). Homogeneous velocity field for straight die extrusion.
FIG. 8(b). Homogeneous–triangular velocity field.
FIG. 8(c). Triangular–triangular velocity field for conical die extrusion.

The assumed velocity field in region [2] is, for unit speed of the ram,

$$u = -(1-r^2)/2ar \quad \text{and} \quad v = -z/a \tag{15}$$

the meaning of the various symbols being obvious on reference to the figure. The equation of the stream lines in this annulus is given by

$$dr/dz = u/v = (1-r^2)/2rz\,. \tag{16}$$

The depth of the velocity field a is so chosen that the extrusion pressure is a minimum; in this instance, $a = 0{\cdot}51$.

Solving (16) and noting that $z = -a$ at $r = r_0$, equation (16) gives

$$z(1-r^2) + a(1-r_0^2) = 0\,. \tag{17}$$

This equation holds for $r \geqslant b$.

The assumed velocity field in region [1] is

$$u = -\frac{Ar}{2a} \quad \text{and} \quad v = \frac{Az}{a} + A + 1 \tag{18}$$

where $A = (1-b^2)/b^2$, so that u and v are correct at the boundary of the regions.

Thus the stream lines $r_0 \leqslant b$ in this region, are easily shown to be given by

$$r^2[Az + a(A+1)] = ar_0^2 \tag{19}$$

For the stream lines $r_0 \geqslant b$ in region [1], equation (19) may be re-written as

$$r^2(1-b^2)\{Az + a(A+1)\} = ab^2\{A(r_0^2 - b^2) + 1 - b^2\} \tag{20}$$

The stream lines are shown in Fig. 9, for the particular case of a 75 per cent reduction, i. e. $b = 1/2$.

(b) *Temperature increase.* The work input to unit volume of material across surface 46, see Fig. 8, is

$$W_{46} = \frac{Y}{\sqrt{3}} \frac{u}{1} = \frac{Y(1-r^2)}{2\sqrt{3}ar} \tag{21}$$

The rate of work done per unit volume of material in region [2] is

$$\dot{W}_{[2]} = Y\dot{\bar{\varepsilon}} \tag{22}$$

where

$$\dot{\bar{\varepsilon}} = \frac{1}{\sqrt{3}a}\left(3+\frac{1}{r^4}\right)^{1/2} \tag{23}$$

Noting that $u = dr/dt = -(1-r^2)/2ar$, equation (22) becomes

$$dW_{[2]} = -\frac{Y}{\sqrt{3}}\left(3+\frac{1}{r^4}\right)^{1/2}\frac{2r\,dr}{1-r^2} \tag{24}$$

and thus

$$W_{[2]} = -Y\left[\ln\left(\sqrt{r^4+\frac{1}{3}}-r^2\right)-\frac{1}{\sqrt{3}}\ln\left(\frac{\sqrt{r^4+\frac{1}{3}}+\frac{1}{\sqrt{3}}}{r^2}\right)+\right.$$

$$\left.+\frac{2}{\sqrt{3}}\ln\left(\frac{\sqrt{r^4+\frac{1}{3}}+\frac{2}{\sqrt{3}}}{1-r^2}-\frac{\sqrt{3}}{2}\right)\right]_{r=r_0}^{r} \tag{25}$$

Hence in region [2] where $r_0 \geqslant b$, the total work done for a material element of unit volume which came from the undeforming region is the sum of W_{46} and $W_{[2]}$.

The work done on a unit volume of material which crosses surface 34 is given by

$$W_{34} = \frac{Y}{\sqrt{3}}\frac{\dot{s}_{34}}{u_{34}} \tag{26}$$

where

$$\dot{s}_{34} = |v_{[1]34} - v_{[2]34}| = (1+A)(1+z/a) \tag{27}$$

using equations (15) and (18). Thus equation (27) becomes

$$W_{34} = \frac{Y}{\sqrt{3}}\frac{(1+A)(1+z/A)}{bA/2a}. \tag{28}$$

The time rate of work done in region [1] is

$$\dot{W}_{[1]} = Y\dot{\bar{\varepsilon}} = Y\dot{\varepsilon}_z = Y\,dv/dz = YA/a. \tag{29}$$

Thus, $dW_{[1]} = YAdt/a = YAdz/(zA+aA+a)$ using (18) and hence

$$W_{[1]} = Y\int Adz/(Az+aA+a) = Y[\ln(z+a+a/A)]_{z=-a \text{ or } z'}^{z} \qquad (30)$$

where, from equation (17)

$$z' = -a(1-r_0^2)/(1-b^2)\,. \qquad (31)$$

For material in region [1] which has entered via region [2] it follows that

$$W = \frac{Y(1-r_0^2)}{2\sqrt{3}\,ar_0} - Y\left[\ln\left(\sqrt{r^4+\frac{1}{3}}-r^2\right) - \frac{1}{\sqrt{3}}\ln\left(\frac{\sqrt{r^4+\frac{1}{3}}+\frac{1}{\sqrt{3}}}{r^2}\right)+\right.$$

$$\left.+\frac{2}{\sqrt{3}}\ln\left(\frac{\sqrt{r^4+\frac{1}{3}}+\frac{2}{\sqrt{3}}}{1-r^2}-\frac{\sqrt{3}}{2}\right)\right]_{r=r_0}^{b} + \frac{2Y(1+A)(a+z')}{\sqrt{3}\,bA} +$$

$$+Y[\ln(z+a+a/A)]_{z=z'}^{z}\,. \qquad (32)$$

The work done per unit volume on crossing surface 24 is

$$W_{24} = YrA/2\sqrt{3}a \qquad (33)$$

and on crossing surface 13,

$$W_{13} = YrA/2\sqrt{3}a(1+A)\,. \qquad (34)$$

Thus, adding W_{24} from equation (33) and $W_{[1]}$ from equation (30), the total work done on material in region [1] which has entered initially across 24, is found. The final total work done on unit volume of material in the extruded product is obtained by adding to the total of the work done on the material in region [1], that done at exit across surface 31 as given by equation (34).

(ii) *Triangular velocity field for a square die*

The shape of this type of velocity field is shown in Fig. 8(b). Annulus [2] is of the same form as with the homogeneous type velocity field, whilst the triangular region [1] is bounded by planes 24 and 34 across which tangential velocity discontinuities of constant magnitude exist. Discontinuity 24 has at best a slight inclination of 0·05, while the depth of the deforming region is $a = 0{\cdot}51$. In the calculations below it has been assumed that plane 24 is perpendicular to the axis.

Again assuming the punch speed to be unity, the speed normal to 34 is $(1-b^2)/2ab$ and thus in region [1]

$$\left.\begin{aligned} u &= -(1-b^2)/2ab \equiv -B \\ v &= 1+B(a+z)/r \end{aligned}\right\} \qquad (35)$$

Equations (35) are compatible with the rigid body motion of the extruded bar along the boundary surface 32, defined by $r/b-2/a = 1$.

The equation of the stream lines is given by

$$r^2+2Br(a+z)=r_0^2, \qquad r_0 \leqslant b \tag{36i}$$

and

$$r^2+2Br(a+z)=b^2+2bB(a+z'), \qquad r_0 \geqslant b \tag{36ii}$$

where z' is again given by equation (31).

In region [2] the work done per unit volume of the material on crossing surface 46 is given by equation (21) and that done in region [2] by (25).

Across surface 34 the tangential velocity discontinuity $\dot{s}_{34}$ is

$$\dot{s}_{34}=1+B(a+z)/b+z/a\,. \tag{37}$$

The work done per unit volume on crossing 34 is W_{34} and

$$W_{34}=Y(1+b^2)(a+z)/\sqrt{3}b(1-b^2)\,. \tag{38}$$

Vol. 1
1960

In region [1]

$$\dot{\bar{\varepsilon}}=2B\{r^2+(a+z)^2/4\}^{1/2}/\sqrt{3}r^2 \tag{39}$$

and

$$dW_{[1]}=2Y\{r^2+(a+z)^2/4\}^{1/2}dr/\sqrt{3}r^2\,. \tag{40}$$

Expression (40) is evaluated numerically along a stream line and when $r_0 \leqslant b$,

$$W_{[1]}=\frac{2Y}{\sqrt{3}}\int_1^{\xi}\frac{\sqrt{\xi^4+(1/4B)^2(1-\xi^2)^2}}{\xi^3}d\xi\,, \qquad 1 \leqslant \xi \leqslant b \tag{41}$$

where $\xi = r/r_0$. Accordingly, $W_{[1]}$ can be determined as a function of r/r_0.

Referring to Fig. 10, the work done per unit volume on crossing surface 24 is

$$W_{24}=YB/\sqrt{3} \tag{42}$$

and on crossing surface 23, because the tangential velocity jump is $\dot{s}_{23}=B\sec\theta$, is

$$W_{23}=YB(a^2+b^2)/\sqrt{3}\,. \tag{43}$$

Equation (41), together with equations (42) and (43), implies that for $r \leqslant b$, the total work done along each stream line is constant.

(iii) *Triangular velocity field for a conical die*

For a smooth die of semi-angle 45° calculations may be made in a manner similar to those for the square die. The field chosen is clear from Fig. 8(c); the derivation of the appropriate expressions and the calculations present no difficulty. The optimum value of a is 0·55.

(iv) *Axi-symmetric bar extrusion results*

For the particular example of an 0·75 reduction detailed calculations have been made and the results are as follows for extrusion through a square die with smooth tools:

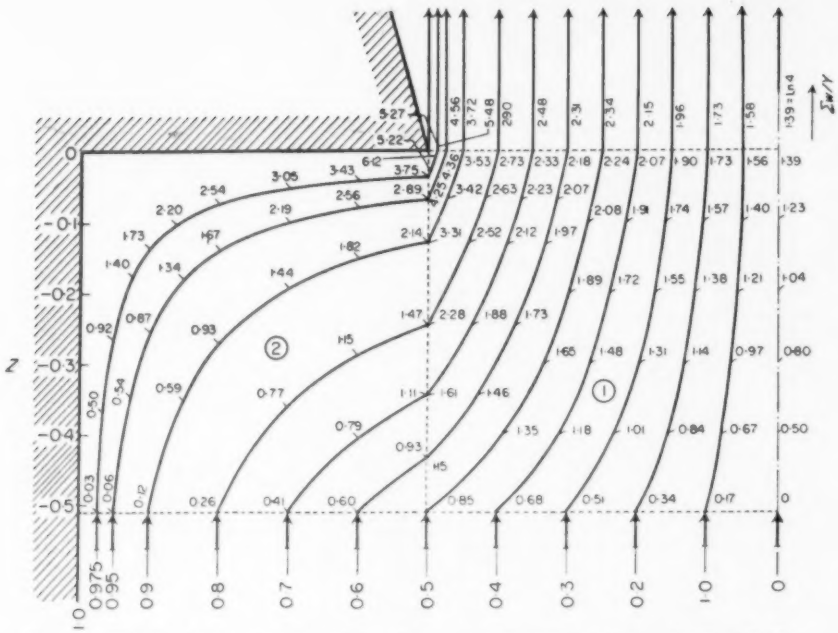

FIG. 9. Work done along stream lines for homogeneous velocity field.

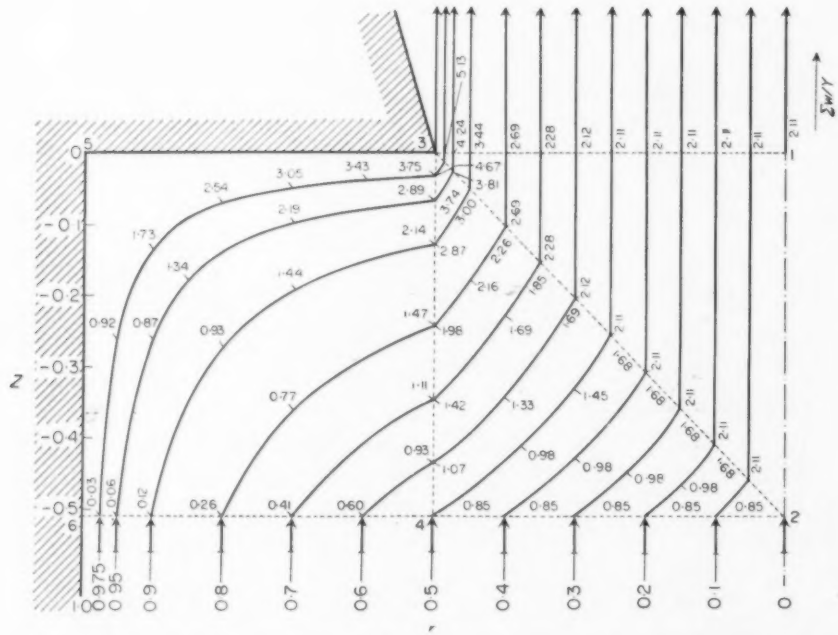

FIG. 10. Work done along stream lines for homogeneous-triangular velocity field.

(a) *Entirely homogeneous velocity field.* Fig. 9 shows the calculated stream lines; the numbers at particular points on the lines give the ratio, work done to Y, and are proportional to the temperature rise. The temperature profile at exit is also shown; note that the temperature goes to infinity as the time approaches infinity at the surfaces of the extruded bar. Fig. 12(a) shows the predicted form of a square grid, for $t = 1$, using this particular expression for the velocity field. In this type of velocity field, it is to be noted that the longitudinal lines on a billet are not necessarily identical with the stream lines unless the time is infinite. The predicted extrusion pressure, $\bar{p}$, is $\bar{p} = 2{\cdot}87\,Y$.

(b) *Homogeneous triangular velocity field.* Fig. 10 shows the stream lines, predicted temperature distribution and the final temperature profile. Fig. 12(b) drawn for $t = 1$ shows the form that would be taken up by a square grid flowing under the influence of this velocity field. The predicted extrusion pressure required, $\bar{p}$, is $\bar{p} = 2{\cdot}85\,Y$, being slightly smaller than that required by the homogeneous velocity field.

The final temperature profiles in the extruded bar, as predicted by (i) and (ii), are compared in Fig. 11, the temperature approaching infinity on the outside of the bar in both cases. The broad similarity of the profiles is evident. To a radius four-fifths that of the emerging bar the tem-

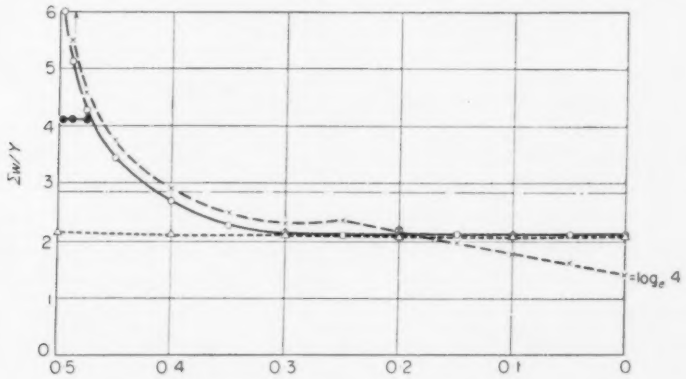

Fig. 11. Temperature distribution for extrusion.

- - × - - Homogeneous–homogeneous: square die.
—⊖— Homogeneous–triangular after $t = \infty$, square die (i. e steady state).
—●— Homogeneous–triangular at $t = 1$, square die.
---△--- Conical die.
— · — Mean value for square die.

perature in both instances is less than the bulk mean; the rapid rise in temperature on the outside of the bar is clear.

(c) Similar calculations to those described above have been made for extrusion through a smooth conical die of 0·75 reduction and results are

given in Figs. 11 and 12(c). In this case $\bar{p}/Y = 2{\cdot}065$. The absolute temperature rise is given by equation (2), since Y is nearly equal to $2k$.

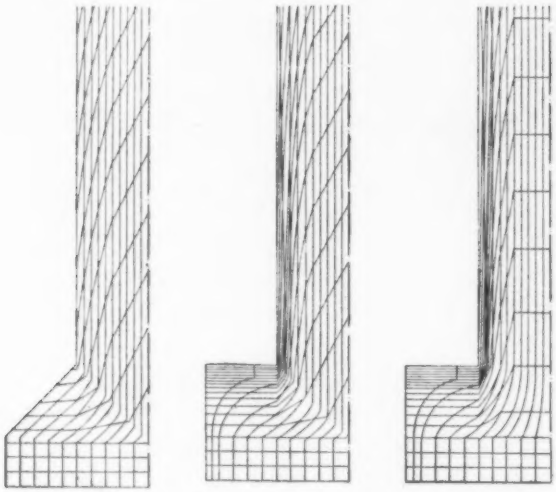

FIG. 12. Distorted grid for extrusion.
(a) Homogeneous velocity field.
(b) Homogeneous–triangular velocity field.
(c) Triangular–triangular velocity field.

CONCLUSIONS

During a fast working process, heat loss to external surroundings by radiation and conduction may be neglected if the processed material is originally at about the same temperature as the surroundings; temperature equalization throughout the body in the deforming region is also negligible if this too occupies only a short space of time. On these assumptions, the local temperature rise in a small volume of the material at a point is proportional to the plastic work expended on the element. Thus the temperature rise at each point in the deforming region is calculable if the local rate of work input is calculable, and in the problems investigated above, this is so. This rate of work input is an assumed one, or, more precisely, one which has to be guessed, the guess being circumscribed by various boundary requirements and an appeal to a principle of minimum total work input.

The results of the calculations presented take no account of such real features as roll distortion, radiation losses, conduction losses to dies or rolls, variation of yield stress with temperature, and the working of a non-homogeneous medium. There are also many other features of these metal-working processes which, for real as well as exact estimation, would need to be examined.

The authors have examined the major feature of these processes and presented results which were easy to obtain by obvious methods.

REFERENCES

1. R. Tanner and W. Johnson, *Int. J. Mech. Sci.* **1**, 28 (1959).
2. J. W. F. Bishop, *Quart. Appl. Math.* **9**, 236 (1956).
3. J. M. Alexander, *Proc. Inst. Mech. Engrs., Lond.* **169**, 1021 (1955).
4. H. Kudo, *Int. J. Mech. Sci.* **1**, 57 (1959).
5. J. M. Alexander, *Proc. Inst. Mech. Engrs., Lond.* (1958).
6. R. Hill, *Mathematical Theory of Plasticity*. Clarendon Press, Oxford (1950).

Vol. 1
1960

Int. J. Mech. Sci. Pergamon Press Ltd. 1960 Vol. 1. pp. 192–205. Printed in Poland

THE "OFF" BOUNDARY CONDITION IN HYDRODYNAMICALLY LUBRICATED CONVERGENT–DIVERGENT SLIDER BEARINGS

P. B. NEAL

Department of Mechanical Engineering, University of Sheffield

(*Received* 23 *April* 1959)

Summary — The application of hydrodynamical theory to convergent–divergent slider-bearing lubrication meets with difficulties in the choice of the necessary "off" film boundary condition due to the negative pressures which are in general predicted, in the divergent region, if hydrodynamic continuity is assumed throughout the bearing interspace. Pertinent theoretical and experimental evidence, as to the correct boundary conditions, is reviewed and leads to the conclusion that two criteria must be satisfied, viz. stability and continuity. New experimental evidence is put forward which suggests that flow continuity is the overriding criterion and that stability must be satisfied within the restriction imposed by the condition of continuity.

NOTATION

(See Figs. 1 and 6)

c = bearing radial clearance
h = film thickness
H = defined in Fig. 6
p = film pressure
P = bearing load per unit width
q = lubricant flow rate per unit width
U = sliding velocity
x = co-ordinate in direction of sliding
z = co-ordinate in plane of film and normal to sliding
η = viscosity
ε = eccentricity (ratio)
Φ = angular co-ordinate (origin at position of maximum film thickness)
$\pi \pm \alpha$ = values of Φ for $\dfrac{dp}{d\Phi} = 0$
ψ = attitude angle (angle between load line and line of centres)
Δ = load criterion $\left(= \dfrac{P}{\eta U} \cdot \dfrac{c^2}{R^2}\right)$

Subscripts

m = refers to section of maximum film pressure
0 = refers to section of minimum film thickness
1 = "on" boundary (i. e. beginning of continuous film)
2 = "off" boundary (i. e. end of continuous film)

Vol. 1
1960

INTRODUCTION

THE key to the mechanism whereby an oil film may transmit a load between a pair of relatively moving surfaces, as in a slider bearing, was provided by the chance observation by BEAUCHAMP TOWER[1] that the pressure within the film could greatly exceed the average bearing pressure. TOWER was conducting an investigation, promoted by the Institution of Mechanical Engineers, into frictional losses in journal bearings. That the journal and bearing of such an assembly could be completely separated by a finite film of oil, and that the pressure in such a film could be measured, does not appear to have been previously recognised – or if it had been recognised it was evidently not considered to be of significance. TOWER's observation was made whilst attempting to prevent leakage of oil from the bearing through an oil hole situated in the crown of a half-bearing. TOWER[2] subsequently measured the pressure at a number of points and was able to show that the bearing load was equilibrated by the integrated film pressures.

Recognising that the pressure distribution obtained by TOWER was due to hydrodynamic action within the oil film, OSBORNE REYNOLDS[3] successfully applied the theory of hydrodynamics to explain the pressure generation. REYNOLDS showed that, on the basis of constant fluid properties, pressure variation in the lubricant film was due to the fluid being dragged into a space varying in thickness in the direction of motion of one surface relative to the other, and governed by equation (1):

$$\frac{\partial}{\partial x}\left(h^3\frac{\partial p}{\partial x}\right)+\frac{\partial}{\partial z}\left(h^3\frac{\partial p}{\partial z}\right)=6\eta U\frac{\partial h}{\partial x}\,. \tag{1}$$

In the journal bearing the necessary film geometry is provided by the displacement of the journal centre from the centre of curvature of the bearing, that is, by an eccentricity, which in general results in a convergent–divergent film shape. Neglecting lubricant flow in the axial (z) direction, and putting $h = c(1+\varepsilon\cos\Phi)$, equation (1) then becomes

$$\frac{\partial}{\partial\Phi}\left((1+\varepsilon\cos\Phi)^3\frac{\partial p}{\partial\Phi}\right)=\frac{-6\eta U}{c^2}\varepsilon\sin\Phi\,. \tag{2}$$

The series solution adopted by REYNOLDS for equation (2) converged only for values of eccentricity up to about 0·5. Applying his solution to the particular case of a centrally-loaded half (approx.)-bearing, REYNOLDS found that, at an eccentricity of 0·5, the pressures near the outlet or "off" end of the film were beginning to show negative values. REYNOLDS drew attention to this but emphasised that the problem of obtaining solutions for eccentricities greater than 0·5 was associated with the integration of equation (2) and not in the negative pressures themselves. Remarking that "... the amount of negative pressure which the oil will bear depends upon circumstances which are uncertain ...", he suggested that, for

a bearing operating at an eccentricity such as would predict negative pressures, the "off"-end limit of integration would have to be the point of theoretical minimum pressure, i. e. the point at which $p = \frac{d\Phi}{dp} = 0$, but he was not explicit in the choice of this condition. (It is worth noting that, although there appears to be no evidence of large negative pressures having existed in bearings, such tensile stresses are possible in fluids. REYNOLDS[4] maintained mercury and water under tensions of up to 3 atm for long periods under static undisturbed conditions. More recently, BRIGGS[5] has reported tensions of up to 277 atm in water contained in a glass tube subject to a centrifugal field.)

In accordance with the unlikelihood of lubricants sustaining negative pressure, the regions for which negative pressures were predicted were associated with rupture of the oil-film. REYNOLDS recognised that, in the case of the half-bearing which he evaluated, any rupture of the film, due to the onset of negative pressures, would not occur at the thinnest part of the film and that, therefore, the journal would still be entirely separated from the bearing by an oil film. He was of the opinion, however, that the value of eccentricity for which negative pressures were first predicted in the bearing, represented the maximum value under which lubrication could be considered certain, and the corresponding load the limit of the safe working load. Had he considered the complete (360°) journal bearing as well, REYNOLDS would almost certainly have concluded otherwise.

THE JOURNAL BEARING – SINCE REYNOLDS

The difficulties of integration experienced by REYNOLDS were overcome by SOMMERFELD[6] who showed how equation (2) could be solved for a journal bearing of any arc, and without restriction on the eccentricity, on the assumption of film continuity throughout the length of the arc. For the complete (360°) bearing, SOMMERFELD's solution gave a pressure distribution around the bearing antisymmetric about the line of centres of the journal and the bearing. In consequence of this the line of centres set itself at 90° to the direction of the applied load for all values of the eccentricity. The obvious objection to the complete and continuous film postulated was that large negative pressures were predicted in the divergent region unless the lubricant were supplied either at high pressure or at the (variable) point of minimum film pressure. JAKOBSSON & FLOBERG[7] have shown that the straight line journal-centre locus predicted by SOMMERFELD is realisable in practice. Their experimental results, obtained for a very lightly loaded bearing in which side-leakage was prevented, are shown in Fig. 2. Under normal practical conditions the journal centre locus has been shown, by NÜCKER[8], CLAYTON and JAKEMAN[9], and others, to follow a roughly semicircular path from O to A, Fig. 2.

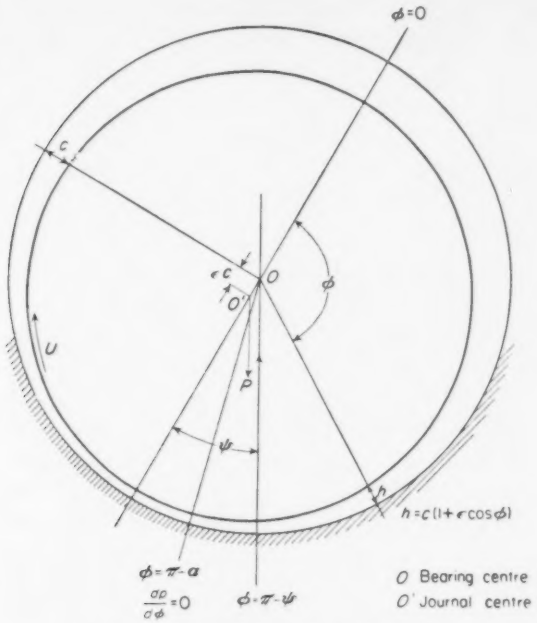

FIG. 1. Journal bearing notation.

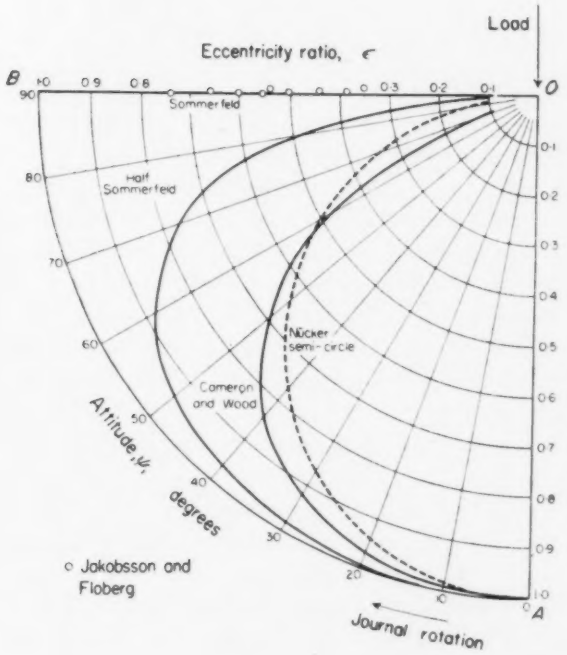

FIG. 2. Attitude–eccentricity curves. 360° journal bearing.

SOMMERFELD's solution applied to the centrally loaded half-bearing (the case considered by REYNOLDS) predicts the journal-centre locus *OPQRB* shown in Fig. 3. This was shown by SWIFT[10] to lead to unstable operation

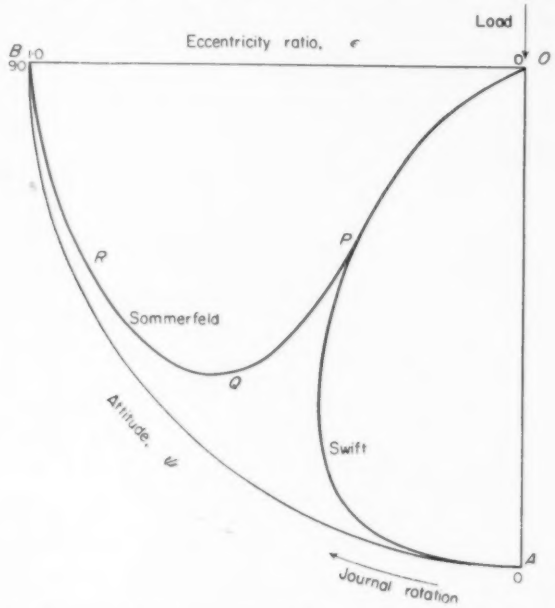

FIG. 3. Attitude-eccentricity curves. 180° centrally loaded journal bearing.

over the rising part *QB* of the locus, that is for eccentricity greater than about 0·9. This by itself does not necessarily invalidate the SOMMERFELD locus since operation in this region might well prove to be unstable if the fluid could sustain the necessary negative pressures, or if the lubricant were supplied at such a location and pressure as to maintain the pressure positive everywhere. However, neither of these conditions is normally met, whilst in practice half-bearings have operated successfully at eccentricities greater than 0·9. Furthermore, as anticipated by REYNOLDS, experiment has shewn that, as with the 360° bearing, the journal centre converges on the point *A*, which is furthest in the direction of the applied load, for high values of eccentricity.

The discrepancy between the performance predicted on the basis of the SOMMERFELD theory and that of common experience, stems from the SOMMERFELD assumption of a complete and continuous film throughout the bearing arc. Visual evidence of cavitation in the divergent part of the oil film has been given by VOGELPOHL[11] and COLE and HUGHES[12] for 360° journal bearings, and by DOWSON[13] for spherical sliders. As far as the predicted negative pressures are concerned, it might at first sight be thought reasonable simply to ignore them and to assume that a state of cavitation exists at constant pressure throughout the region for which

the negative pressures are predicted. This artifice has been used by GÜMBEL[14] and has the advantage of mathematical simplicity (especially in certain cases of two-dimensional flow) but, as shewn by STIEBER[15], violates the necessary condition of flow continuity.

The flow continuity and stability criteria referred to above are quite independent criteria as applied by their authors and will, therefore, first be considered separately.

CAVITATION AND FLOW CONTINUITY

The requirements of flow continuity in a cavitating lubricant film may be considered most simply by examining the pressure distribution and flow of lubricant between a curved stationary slider of infinite width and a plane surface which moves with constant velocity in its own plane, Fig. 4. Subject to the usual assumptions, that the lubricant property

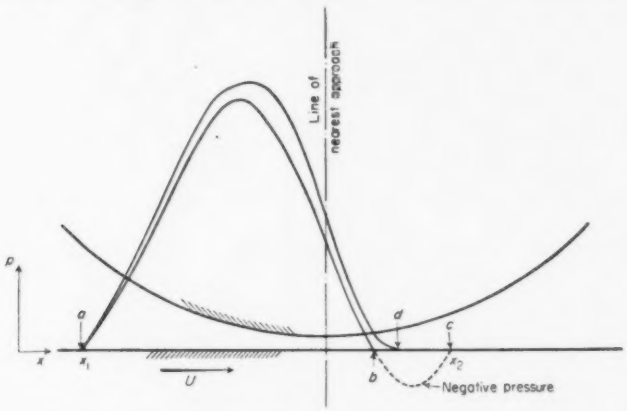

FIG. 4. Pressure distribution under a curved slider.

values are constant throughout the thickness of the film and that inertia effects are negligible, equation (1) may be integrated directly to give

$$\frac{dp}{dx} = 6\eta U \frac{(h-h_m)}{h^3}, \tag{3}$$

where h_m is the value of h at the section of maximum film pressure. Since there is zero flow in the z direction, the continuity relationship for the film is

$$q = \frac{Uh}{2} - \frac{h^3}{12\eta}\frac{dp}{dx} = \text{constant}. \tag{4}$$

Equations (3) and (4) must apply at every section in the film at which the fluid is homogeneous.

Applying the appropriate boundary conditions that $p = 0$, at $x = x_1$ and x_2, in equation (3), the pressure distribution obtained is of the general

form shown in Fig. 4. If the lubricant is unable to sustain the negative pressures predicted in the divergent part of the film, then the lubricant there will no longer be homogeneous and the negative pressures predicted will be invalid since the governing equation will no longer be equation (3). Furthermore, the positive pressures predicted are also invalidated since they were determined on the assumption that the film was homogeneous between the prescribed endpoints x_1 and x_2. Thus, if negative pressures are to be discounted, x_1 and x_2 cannot be chosen arbitrarily but must be compatible. It is evident from Fig. 4 that the choice of the point b, for a zero-pressure boundary condition, is valid since the fluid between a and b would be everywhere at positive pressure and, therefore, subject to equation (3). Accordingly, the point b may be specified as far to the right as point d, at which the pressure and pressure gradient assume zero values simultaneously. If the slider terminates before the point d then, of course, no problem arises. Now if a fluid will not support a negative pressure it is the release of vapour or dissolved air which prevents it from doing so. Thus, if negative pressures are, in fact, discounted, the pressure in the film, having fallen to zero or near zero, will remain constant, or nearly so, throughout the remainder of the divergent region.

Considering now the flow of lubricant in the film, as did STIEBER, the lubricant flow, per unit width of the slider, at section b, Fig. 4, is

$$q = \frac{Uh_b}{2} - \frac{h_b^3}{12\eta}\left(\frac{dp}{dx}\right)_b . \tag{4. i}$$

At a section immediately to the left of b, $\frac{dp}{dx}$ has a negative value so that the flow due to the slider velocity is supplemented by a positive quantity equal to $\left|\frac{h^3}{12\eta}\frac{dp}{dx}\right|_b$. At a section immediately to the right of b, there is zero pressure gradient and, therefore, no pressure induced flow. STIEBER assumed that the flow here would be simply $Uh/2$ and that, therefore, there is a greater quantity of fluid fed to the section than the section can carry. Although the fluid to the right of the section b would not be homogeneous under the postulated circumstances and a linear velocity distribution through the film thickness would not, therefore, be necessarily correct, the flow continuity condition at b could be maintained only if the fluid in the cavitated region were of completely stratified liquid–vapour form and of negligible effective viscosity. Only in this way could the parabolic velocity distribution to the left of b persist into the cavitation region without an attendant pressure gradient. Such an idealised form of cavitation would seem to be unlikely. In view of this the only "off" boundary condition tenable, within the length of the slider, is that which allows the pressure gradient to have a zero value at the point at which the pressure of the lubricant falls to the cavitation value. The

actual pressure at which this would occur depends upon the nature of the lubricant, and upon the fact that a finite time may be required for the release of the vapour or gas. Pressures below the ambient are, therefore, not excluded, but only in exceptional circumstances would truly negative pressures be expected.

STABILITY

The stability approach to the question of the correct "off" boundary condition uses the criterion that, of all possible equilibrium states of a system, the one with which is associated a position of minimum potential energy is one of stable equilibrium.

The stability criterion appears first to have been applied to the problem of oil-film extent by SWIFT[10] for the case of the journal half-bearing, the Sommerfeld journal-centre locus for which is shown in Fig. 3. SWIFT argued as follows against the part QB of this locus. The pressures in the film would be equilibrated by the externally applied load when the journal operates in equilibrium at any such point R between Q and B. Should the journal-centre be disturbed from the point R in the direction of B, then the integrated film pressures would exceed the applied load and the journal-centre would move further towards B. Similarly, an initial disturbance in the direction of Q would result in further movement towards Q. Thus operation over the part QB of Sommerfeld's locus is unstable. With the knowledge that half-bearings could in fact operate in a stable manner over that range of eccentricity shown by the Sommerfeld theory to be unstable, and limiting the integration of equation (2) to that part of the bearing arc for which the pressure is positive, SWIFT sought the necessary "off" boundary condition to satisfy the criterion of minimum potential energy of the journal. It is clear that to satisfy this condition the value of $\varepsilon\cos\psi$ must be a maximum, where ε is the eccentricity (ratio) and ψ the angle between the load line and the line of centres of journal and bearing. For the particular case considered (180° bearing) SWIFT showed that his criterion corresponded to an "off" boundary condition $p = \dfrac{dp}{d\Phi} = 0$ at some point $\Phi = \pi + a$, where a is dependent upon the eccentricity.

CAMERON and WOOD[16] attempted to apply the same stability criterion to the 360° bearing analytically. Assuming that the film pressure begins to build up from the section of maximum film thickness, i. e. $p = 0$ at $\Phi = 0$, they showed that for a given eccentricity the attitude angle ψ is a minimum when $p = \dfrac{dp}{d\Phi} = 0$ at the "off" boundary. Their conclusion that this boundary condition corresponds to minimum potential energy of the journal was, therefore, not proven. Nevertheless, using these boundary conditions, they determined journal-centre loci and other useful

Vol. 1
1960

data for a number of different length/diameter ratios. Cameron and Wood's journal-centre locus for an infinitely long bearing, i. e. no side-leakage, is plotted in Fig. 2. Shown in the same diagram is the locus based on the Sommerfeld theory but with negative pressures neglected, i. e. $p = 0$ at $\Phi = 0, \pi$. The general shape of Cameron and Wood's locus is in closer agreement with experimental data than the "half"-Sommerfeld curve. Fig. 5 shows

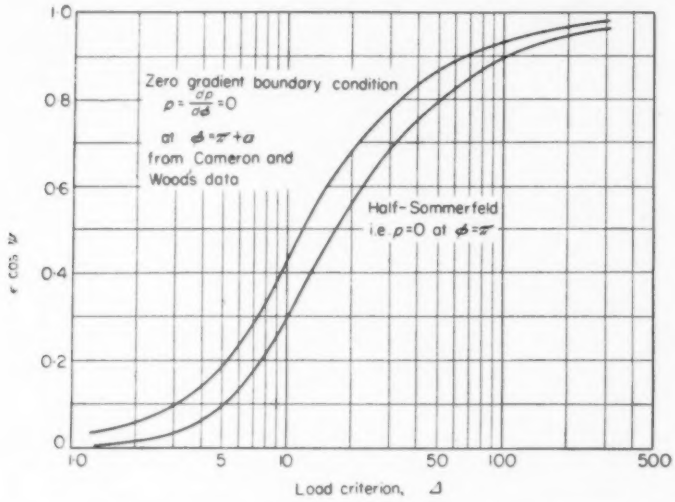

FIG. 5. Vertical displacement of journal for infinite 360° journal bearing. Film assumed to commence at $\Phi = 0$.

the value of $\varepsilon \cos\psi$ plotted against the load criterion for the two cases. It is clear that for any given load, within the range calculated, the zero-gradient boundary condition permits operation at a lower potential energy. It cannot be concluded, however, that this necessarily corresponds to a minimum.

OTHER CONVERGENT-DIVERGENT BEARING FORMS

The problem of the "off" boundary condition is by no means confined to journal bearings, since it is the convergent–divergent shape of the oil film which presents it. Any slider bearing of convergent–divergent form will, therefore, pose the same problem. Whilst for the 180° journal bearing the zero-gradient boundary condition has been shown to follow from both flow continuity and stability criteria, the criteria themselves appear to be physically unrelated. The flow continuity criterion has been considered without reference to any particular bearing form so long as both surfaces are mathematically continuous. The stability criterion, as applied, does, on the other hand, involve the particular bearing geometry, e. g. an eccentricity in the case of the journal bearing, and, in view of this,

two further cases of different bearing forms, for which experimental data are available, are considered.

THE PIVOTED RADIUSED PAD

Fig. 6 shows a thrust pad having a cylindrical working surface and pivoted about a line parallel to a generator of the pad surface and normal to the direction of sliding. It is clear that the pad must set itself in such

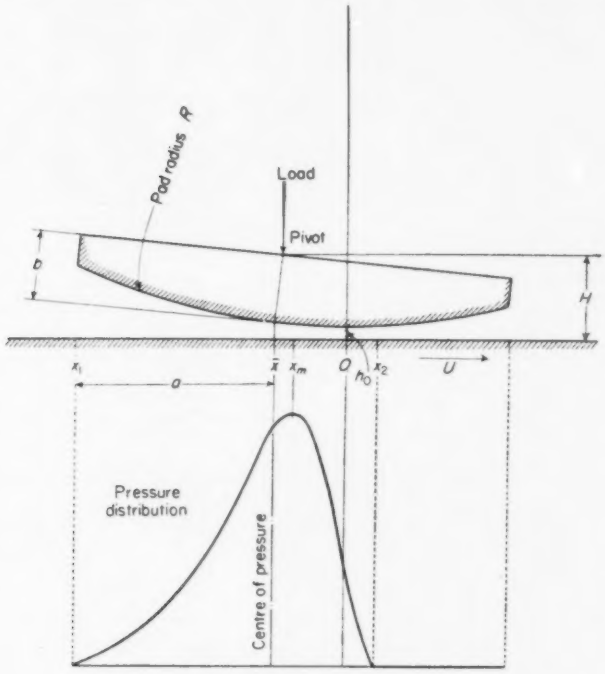

FIG. 6. Pivoted radiused pad.

a way that the pressure resultant on the pad passes through the pivot. (In common with SWIFT's treatment of the 180° journal bearing, the effect of viscous traction on the pad surface is neglected.) On the basis of no side-leakage, the pressure distribution, pressure resultant, and height of the point of application of the load to the pad, were determined for a number of values of minimum film thickness and a range of assumed positions of the maximum pressure in the film. Owing to the nature of the problem and the degrees of freedom involved, particular values of the pad dimensions were used. The dimensions were chosen to correspond to a pad for which experimental data were available.

The technique of computation was as follows, with reference to Fig. 6. A value of h_0, the minimum film thickness, at $x = 0$, was taken. A value of x_m, the point corresponding to maximum film pressure, was selected

and the resulting pressure distribution determined. The pressure distribution was then adjusted so as to give $p = 0$ at $x = x_1$, the entry point under the pad, the position of which was at this stage known only approximately. Provided that the pressure returned to zero in the divergent region, the pressures were integrated over the positive pressure region, i. e. from x_1 to x_2, and the position $\bar{x}$ of the pressure resultant determined. In general, some further adjustment was necessary to ensure that $x_1 - \bar{x} = a$, which is fixed for a given pivot position. Values of x_m for which the pressure in the divergent region did not become zero were, of course, discarded. The range of values of x_m used were such as to cover the range of "off" boundary condition from $p = 0$ at $x = 0$, to $p = \dfrac{dp}{dx} = 0$ at $x = -x_m$. A range of values of minimum film thickness was also taken so as to investigate the effect of different impressed boundary conditions for a given value of load.

Applying the stability criterion to the present case, it is evident that the height of the point of application of the load to the pad, i. e. H, should be a minimum for a given value of the load. This height is given by

$$H = h_0 + b + \frac{(R-b)}{2R^2}(\bar{x})^2 .$$

For the particular pad considered, $R = 100$ in., $b = 2$ in., the least value of H was found to correspond to the boundary condition $p = \dfrac{dp}{dx} = 0$ at such a value of $x = -x_m$ compatible with the film geometry. These conditions are identical to those found by SWIFT for the 180° centrally loaded journal bearing. This conclusion is not general, however, since it was also found that at some larger value of b (about 10 in.) a reversal occurred and, for b greater than this, H was least for the $p = 0$, $x = 0$ boundary condition.

EL-SISI[17] has investigated experimentally the pressure distribution under a pivoted radiused pad to the dimensions quoted above. Using very small search holes and moving the load line through small distances relative to these search holes, he paid particular attention to the pressure distribution near the end of the pressure film. Over a wide range of operating conditions EL-SISI found that the pressure fell to atmospheric and the pressure gradient became zero simultaneously at the "off" film boundary which was always downstream from the point of nearest approach.

RIGID THRUST PAD OF SINUSOIDAL PROFILE

A thrust pad, having a sinusoidal profile in the direction of sliding, presents the same film geometry as does a complete journal bearing, with the exception that the minimum film thickness is not limited as it is, by the radial clearance, in a journal bearing. Since the film geometry is the same, the pressure distribution is of the same general form ABC,

Fig. 7, where the end-points A and C are conditioned by the value of the boundary pressure.

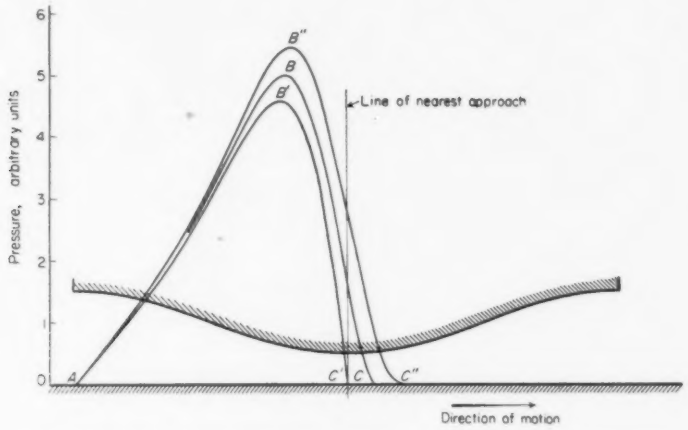

FIG. 7. Effect of assumed "off" boundary condition on the resulting pressure distribution for sinusoidal-profile pad.

Applying Swift's stability (minimum potential energy) criterion, the correct pressure distribution will be that, of all possible distributions, which permits the applied load to be carried with the thinnest film, since the pad is non-tilting. If, as for the journal bearing, possible pressure distributions are understood to include all those having the end-point C between C', the point of nearest approach of the two surfaces, and C'', the point at which $\frac{dp}{dx} = 0$, then it is clear that the pressure distribution $AB'C'$ permits any given load to be carried with a thinner film than any other distribution. This is so since any other distribution ABC shows a greater integrated load than $AB'C'$ for the same film thickness and would, therefore, support the specified load with a thicker film. This is in direct contrast to the case of the journal bearing for which it was shown that the pressure distribution $AB''C''$ permits a lower position of the loaded journal than the distribution $AB'C'$.

Thus, for the case under consideration, the stability criterion, as applied by Swift, does not lead to the same "off" boundary condition as does the requirements of flow continuity. Indeed, this would be found to be so for any non-tilting convergent–divergent thrust pad. Such a pad, therefore, offers a convenient means of distinguishing between the two criteria.

Using a thrust bearing comprising sector pads of sinusoidal profile, the circumferential pressure distribution has been investigated. The bearing comprised three equally spaced pads each subtending an angle of 60° at the bearing centre. The double amplitude of the profile was 0·0028 in., the pads being symmetrical about the line of nearest approach.

Vol. 1
1960

A number of small search holes, Fig. 8, were provided opening on to the working surface of one of the pads, at mid-radius. The search holes

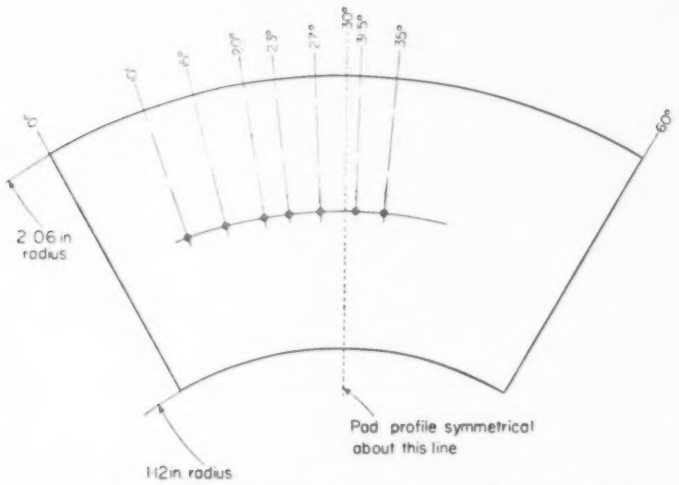

FIG. 8. Location of pressure search holes in sinusoidal pad. Search holes 0·03 in. diameter.

were each connected to a calibrated pressure gauge of suitable range. In order to reduce to a minimum the time of response of the gauges, these were evacuated and subsequently oil filled.

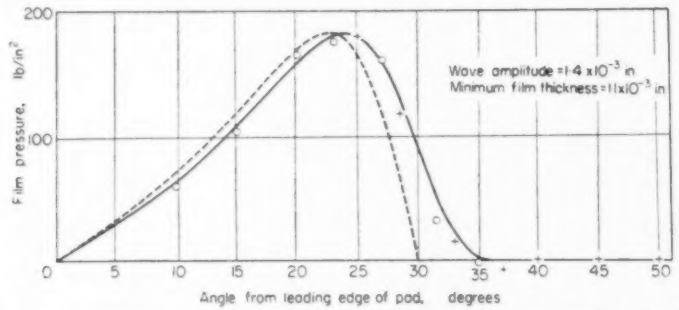

FIG. 9. Sinusoidal pad—theoretical and experimental pressure distributions.

○ + experimental pressure readings

○ forward running

\+ reverse running

– – – – stability ——— flow continuity

Both theoretical curves have been scaled to give the same peak pressure as experimental results.

Fig. 9 shows a typical pressure distribution obtained, together with theoretical distributions according to the stability and flow continuity criteria. The theoretical curves are both based on no side-leakage and on the value of minimum film thickness, 0·0011 in., to which the experi-

mental curve relates. They are, however, both scaled down to give the same value of maximum film pressure as was obtained experimentally so that the shape of the experimental distribution can be directly compared with the two theoretical curves. It is clear that the experimental points are more closely related to the curve derived from the zero-gradient "off" boundary condition, i. e. that appropriate to the flow-continuity criterion.

CONCLUSIONS

The criteria, of stability and flow continuity, which have been invoked are both fundamental concepts. They are, however, mutually independent and as such must both be satisfied simultaneously. Thus there is no question of a choice between the two criteria, as would appear to be the case from consideration of the rigid convergent–divergent thrust pad.

The experimental pressure distribution obtained for the sinusoidal thrust pad appears, on first sight, to contravene stability. On further consideration, however, it would appear that it is the application of the criterion of stability that is really at fault. The stability criterion requires that, of all possible equilibrium positions, that associated with a minimum potential energy will be one of stable equilibrium. The flow continuity criterion in fact limits the number of possible films to those which satisfy flow continuity. Thus, whilst stability must be satisfied under steady conditions of operation, it is necessary that it should be so satisfied within the limitations imposed by flow continuity. Since, in the problem under consideration, there appears to be only one film which satisfies flow continuity, the stability criterion, being limited to only one possibility, appears to be superfluous.

REFERENCES

1. B. Tower, *Proc. Inst. Mech. Engrs., Lond.* **34**, 632 (1883).
2. B. Tower, *Proc. Inst. Mech. Engrs., Lond.* **36**, 58 (1885).
3. O. Reynolds, *Phil. Trans.* **177** (Pt. 1), 157 (1886).
4. O. Reynolds, *Collected Papers* (1877 and 1880) Vol. I. Cambridge (1901).
5. L. J. Briggs, *J. Appl. Phys.* **21**, 721 (1950).
6. A. Sommerfeld, *Z. Math. Phys.* **50**, 97 (1904).
7. B. Jakobsson and L. Floberg, *Lubrication and Wear.* Proc. Inst. Mech. Engrs., Lond. Conference, p. 753 (1957).
8. W. Nucker, *Z. Ver. dtsch. Ing.* 352 (1932).
9. D. Clayton and C. Jakeman, *Proc. Instn. Mech. Engrs., Lond.* **134**, 437, (1936).
10. H. W. Swift, *Min. Proc. Inst. Civ. Engrs.* **233**, 267 (1932).
11. G. Vogelpohl, *Z. Ver. dtsch. Ing.* 386 (1937).
12. J. A. Cole and C. J. Hughes, *Proc. Inst. Mech. Engrs., Lond.* **170**, 499 (1956).
13. D. Dowson, *Lubrication and Wear.* Proc. Inst. Mech. Engrs., Lond. Conference, p. 93 (1957).
14. L. Gümbel, *Jb. Schiffbautech. Gesellsch.* **18** (1917).
15. W. Stieber, *Das Schwimmlager.* V. D. I., Berlin (1933).
16. A. Cameron and W. L. Wood, *Proc. Inst. Mech. Engrs., Lond.* **161**, 59 (1949).
17. S. I. El-Sisi. Ph. D. Thesis, University of Sheffield (1953).

Int. J. Mech. Sci. Pergamon Press Ltd. 1960. Vol. 1. pp. 206–215. Printed in Poland

FULL-FILM LUBRICATION THEORY FOR A MAXWELL LIQUID

R. I. TANNER

Departament of Mechanical Engineering, The University, Manchester

(*Received* 3 *April* 1959)

Summary — Present theories of viscoelastic lubrication are based on a stress-deformation law which is more appropriate to a near-solid than a near-liquid. Utilizing the concept of the absolute time derivative in the formulation of the stress-deformation law, a plane flow theory of viscoelastic lubrication is constructed. Linearization of the equations permits solution for slightly viscoelastic fluids, such as ordinary lubricating oils. As an example, the load and drag of rollers with a given separation are worked out. It is shown that the load capacity of a given film of lubricant is lowered and the coefficient of friction is increased by viscoelastic effects.

NOTATION

d_{ij} = deformation-rate tensor
D_1, D_2 = diameter of rollers
D = drag force per unit width
D^* $\equiv D/(\eta U/\sqrt{h_1 K})$
G = shear modulus
h = film thickness
h_1 = minimum film thickness
h_0 = thickness of film where $\frac{dp}{dx} = 0$
K = total curvature of rolling surfaces $\equiv \left(\frac{1}{D_1} + \frac{1}{D_2}\right)$
N = load per unit width
N^* $\equiv N/(\eta U/h_1 K)$
p = pressure
p^* $\equiv p/(\eta U/h_1\sqrt{h_1 K})$
T = relaxation time η/G
u, v = fluid velocities in x, y directions
U = surface speed of rollers
$\overline{xx}, \overline{xy}, \overline{yy}$ = deviatoric-stress components in x–y plane
μ = coefficient of friction
η = viscosity
σ_{ij} = deviatoric-stress tensor
w = local-rotation rate in x–y plane

INTRODUCTION

THE theory of lubrication has developed mainly along the lines laid down by REYNOLDS[1]. In a classic paper, he analysed the isothermal flow of an incompressible Newtonian fluid in a rigid bearing. Recently, interest has been shown in the effects which appear when some of Reynolds'

assumptions are discarded. The effects of temperature and viscosity variations, oil compressibility, and bearing deflexions have been examined by various authors, and BLOK[2] has reviewed these results. The effects of deviations from ideal Newtonian fluid behaviour have also been investigated by various authors (MILNE[3], KOTOVA[4] for greases, MILNE[5] for Maxwell liquids).

These new assumptions are necessary to explain the mechanism of lubrication in highly loaded elements such as cams, gears and rolling bearings. CAMERON[6] suggests that viscoelasticity may be important in explaining the high load capacity of thin oil films. Measurements made by LAMB[7] show that ordinary lubricating oils may be closely represented as a Maxwell fluid with a single relaxation time. MILNE[5] following BROER's work[8], has analysed a typical case of lubrication by a simple Maxwell liquid and finds that, contrary to CAMERON's suggestion, the capacity of the oil film is reduced from the simple Newtonian case.

Vol. 1
1960

The above analyses used stress-deformation laws of the form

$$\sigma_{ij}/2\eta + (D\sigma_{ij}/Dt)/2G = d_{ij}\,, \tag{1}$$

where D/Dt is the Stokesian derivative $\partial/\partial t + u_k \partial/\partial x^k$. σ_{ij} is the deviatoric stress, and $d_{ij} \equiv \frac{1}{2}\left(\frac{\partial u_i}{\partial x^j} + \frac{\partial u_j}{\partial x^i}\right)$ is the deformation-rate tensor. This is more appropriate to a near-solid, in which deformations and vorticities are small, than to a near-liquid. These conditions are fulfilled in BROER's first problem, relating to unsteady laminar flow in a tube, but not in the second problem or in general in problems of lubrication.

It appears to the author that the stress-deformation law due to NOLL[9], utilizing the result of THOMAS[10], is more appropriate to a theory of lubrication than the law expressed by equation (1). THOMAS's formulation ensures that a rigid rotation does not alter the stress state relative to axes fixed in the body. This is clearly a fundamental property of any realistic stress-deformation law. Equation (1) does not possess this property.

NOLL uses equation (1) with the Stokesian derivative replaced by the absolute time derivative, which will be discussed briefly in Section 2. It has been shown by FROMM[11] that NOLL's formulation leads to unrealistic predictions when a material is sheared at rates comparable with $G/2\eta$, and various modifications to the simple stress-deformation law have been proposed to deal with this. In the following analysis we use equation (1) with D/Dt replaced by the absolute time derivative and suppose that the shear rate is considerably less than $G/2\eta$. This is not very restrictive when applied to lubricating oils. The results obtained broadly confirm MILNE's observation that the load capacity of a viscoelastic lubricant film is less than that of an equivalent Newtonian fluid film.

STRESS-DEFORMATION RELATIONS

In the general case the absolute time derivative $(D/Dt)_A$ of a tensor a_{ij} is given by THOMAS[10]

$$(Da_{ij}/Dt)_A = Da_{ij}/Dt - \omega_{ix}a_{xj} + \omega_{xj}a_{ix} \tag{2}$$

where repeated suffices denote summation and the w_{ij} are the components of vorticity

$$w_{ij} = \frac{1}{2}\left(\frac{\partial u_i}{\partial x^j} - \frac{\partial u_j}{\partial x^i}\right). \tag{3}$$

The following analysis will be concerned with two-dimensional flow, and it seems worth while to give an elementary derivation of (2) for this case.

The motion of a small element consists of translation, rotation and deformation. Only the deformation may influence the stress state, otherwise a rigid-body motion will significantly alter the stress pattern, even when inertia and body forces are neglected. To ensure that rotation and translation play no part in the stress-deformation equations, we may take individual co-ordinate axes for each element that translate and rotate with the element. This co-ordinate system is termed the kinematically preferred system. An observer in this frame of reference would see only deformations, and would be able to infer the correct stress-deformation laws for any element. Rotation and translation would not enter into his relations. A similar situation exists in terrestrial mechanics, where the rotation and translation of the earth do not enter into the equations of motion.

We suppose that equation (1) is the true law in the kinematically preferred co-ordinate system. Clearly, this co-ordinate system is not useful for solving problems, and the law would be better expressed in ordinary Eulerian co-ordinates. Consider the shear component $d_{x'y'}$ in two-dimensional flow. Related to the kinematically preferred co-ordinates, this is

$$d_{x'y'} = \overline{x'y'}/2\eta + (D\overline{x'y'}/Dt)/2G\,. \tag{4}$$

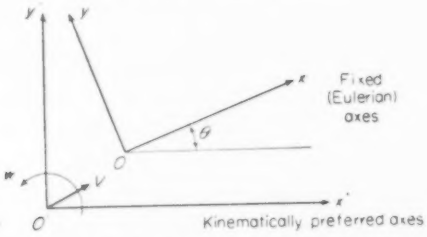

FIG. 1. System of co-ordinates.

Relative to these axes the Eulerian co-ordinates are translating with a velocity $-(V)$ and rotating with an angular speed $-(w)$ (Fig. 1). Consider the translation first. The components of stress and deformation are un-

altered in form when the axes are changed without rotation. Hence equation (4) remains true and the translation may be disregarded.

Using this result we may now consider the effect of a simple rotation of axes about the point under discussion, that is, with 0 and 0′ coincident (Fig. 1). The components of stress and deformation transform according

FIG. 2. Film geometry.

to well-known rules, HILL[12]. When the axes are rotated through $-(\theta)$

$$\overline{x'y'} = -(-\overline{xx}+\overline{yy})\frac{\sin 2\theta}{2}+\overline{xy}\cos 2\theta\,. \tag{5}$$

The unprimed quantities refer to fixed Eulerian co-ordinates. Equation (5) and the corresponding expression for $d_{x'y'}$ may be substituted in (4), giving the stress-deformation law in terms of the Eulerian quantities. The quantity $D\overline{x'y'}/Dt$ becomes

$$\frac{\sin 2\theta}{2}\frac{D}{Dt}(\overline{xx}-\overline{yy})+\cos 2\theta\frac{D}{Dt}\overline{xy}+(\overline{xx}-\overline{yy})\cos 2\theta\left(\frac{d\theta}{dt}\right)-2\overline{xy}\sin 2\theta\left(\frac{d\theta}{dt}\right). \tag{6}$$

Viewed from the fixed axes, from which θ is measured, $d\theta/dt$ is positive and equal to w, the local rate of rotation. If we now put $\theta = 0$ the axes instantaneously coincide, and equation (6) becomes

$$\frac{D}{Dt}(\overline{x'y'}) = \frac{D\overline{xy}}{Dt}+w(\overline{xx}-\overline{yy})\,. \tag{7}$$

The left-hand side, by definition, is the absolute time derivation of $\overline{x'y'}$. Hence the form taken by the x–y component of equation (1) when the absolute time derivative is used, is, in Eulerian co-ordinates,

$$d_{xy} = \frac{\overline{xy}}{2\eta}+\left[\frac{D\overline{xy}}{Dt}+w(\overline{xx}-\overline{yy})\right]\Big/2G\,. \tag{8}$$

Similarly it may be shown that

$$d_{xx} = \frac{\overline{xx}}{2\eta}+\left[\frac{D\overline{xx}}{Dt}-2w\overline{xy}\right]\Big/2G \tag{9}$$

$$d_{yy} = \frac{\overline{yy}}{2\eta}+\left[\frac{D\overline{yy}}{Dt}+2w\overline{xy}\right]\Big/2G \tag{10}$$

where

$$w = \frac{1}{2}\left(\frac{\partial u}{\partial y}-\frac{\partial v}{\partial x}\right).$$

These are the equations which will be used in the following work. Note that only for irrotational flow do they reduce to the form used by MILNE, BROER, and others.

THE THEORY OF LUBRICATION

We make the usual assumptions of film lubrication theory, i. e. that inertia forces are negligible and the film is thin. These assumptions are discussed by SOMMERFELD[13], for example. We consider flow in the x–y plane and neglect the velocity parallel to $y \equiv (r)$ compared with that parallel to $x \equiv (u)$.

In steady flow the equations (8), (9) and (10) approximate to

$$\frac{\partial u}{\partial y} = \frac{\overline{xy}}{\eta} + \frac{1}{G}\left\{u\frac{\partial \overline{xy}}{\partial x} + \frac{1}{2}\frac{\partial u}{\partial y}(\overline{xx} - \overline{yy})\right\} \tag{11}$$

$$\frac{\partial u}{\partial x} \approx 0 \approx \frac{\overline{xx}}{2\eta} + \frac{1}{2G}\left\{u\frac{\partial \overline{xx}}{\partial x} - \frac{\partial u}{\partial y}\overline{xy}\right\} \tag{12}$$

$$\frac{\partial v}{\partial y} \approx 0 \approx \frac{\overline{yy}}{2\eta} + \frac{1}{2G}\left\{u\frac{\partial \overline{yy}}{\partial x} + \frac{\partial u}{\partial y}\overline{xy}\right\}. \tag{13}$$

$\overline{xx}, \overline{yy}$ are small compared with $\overline{xy}$, hence

$$\overline{xx} \approx \frac{\eta}{G}\overline{xy}\frac{\partial u}{\partial y} \tag{14}$$

$$\overline{yy} \approx -\frac{\eta}{G}\overline{xy}\frac{\partial u}{\partial y}. \tag{15}$$

The ratio η/G is the relaxation time T. The above steps are true only if (UT/h) is small compared with unity; this is assumed throughout the subsequent analysis. Using the results (14) and (15) in equation (11) shows that the term $u\frac{\partial \overline{xy}}{\partial x}$ is small compared with the other bracketed term, hence (11) becomes, approximately,

$$\eta\frac{\partial u}{\partial y} = \overline{xy}\left[1 + T^2\left(\frac{\partial u}{\partial y}\right)^2\right]. \tag{16}$$

Order-of-magnitude studies of the equilibrium equations show that they reduce to the single equation

$$\frac{dp}{dx} = \frac{\partial \overline{xy}}{\partial y} \tag{17}$$

where p is the pressure. PASLAY[14] has derived equations similar to (16) and (17) for the problem of calendering of a viscoelastic material. He solves the equations by a numerical procedure; we shall develop an approximate analytical theory valid when (UT/h) is small compared with unity.

Substituting for $\overline{xy}$ and neglecting terms of order $(T\partial u/\partial y)^4$ gives

$$\frac{dp}{dx} = \eta\frac{\partial^2 u}{\partial y^2}\left[1-3T^2\left(\frac{\partial u}{\partial y}\right)^2\right]. \tag{18}$$

At this point it may be valuable to compare (18) with the corresponding equation in MILNE's analysis, which is

$$\frac{dp}{dx} = \eta\frac{\partial^2 u}{\delta y^2} - UT\frac{d^2p}{dx^2}. \tag{19}$$

The last term is of the order of (UT/L) times the others, L being the film length. Since h/L is of the order of 10^{-2} at most, it is clear that this term is very small compared with $3T^2\eta(\partial u/\partial y)^2\partial^2 u/\partial y^2$ in equation (18), unless $UT/h <$ about 10^{-2}, when the theory differs negligibly from the Newtonian case. Thus omission of the term UTd^2p/dx^2 seems to be less serious than the omission of the last term of (18).

Vol. 1
1960

Integration of (18), or, alternatively, integration of (17) and substitution from (16), gives

$$\frac{y}{\eta}\frac{dp}{dx} + C_1 = \frac{\partial u}{\partial y}\left\{1-T^2\left(\frac{\partial u}{\partial y}\right)^2\right\} \tag{20}$$

or, neglecting terms of order $(T\partial u/\partial y)^4$,

$$\frac{\partial u}{\partial y} \simeq \left(\frac{y}{\eta}\frac{dp}{dx}+C_1\right)\left\{1+T^2\left(\frac{y}{\eta}\frac{dp}{dx}+C_1\right)^2\right\}. \tag{21}$$

Integrating again

$$u = \frac{y^2}{2\eta}\frac{dp}{dx} + C_1 y + C_2 + \frac{\eta T^2}{4\dfrac{dp}{dx}}\left(\frac{y}{\eta}\frac{dp}{dx}+C_1\right)^4. \tag{22}$$

For continuity of flow we must have

$$\int_0^h u\,dy = \text{constant} \equiv (u_1+u_2)h_0/2. \tag{23}$$

The functions C_1 and C_2 are found from the boundary conditions, $u = U_1$ on $y = 0$, $u = U_2$ on $y = h$.

$$U_1 = C_2 + \eta T^2 C_1^4 \Big/ 4\left(\frac{dp}{dx}\right) \tag{24}$$

$$U_2 = \frac{h^2}{2\eta}\frac{dp}{dx} + C_1 h + C_2 + \eta T^2\left(\frac{h}{\eta}\frac{dp}{dx}+C_1\right)^4 \Big/ 4\left(\frac{dp}{dx}\right). \tag{25}$$

Equation (23) yields

$$(U_1+U_2)h_0/2 = (h^3/6\eta)\frac{dp}{dx} + C_1h^2/2 + C_2h + \\ + \left\{\eta^2T^2/20\left(\frac{dp}{dx}\right)^2\right\}\left[\left(h\frac{dp}{dx}+C_1\right)^5 - C_1^5\right]. \tag{26}$$

From these three equations we may eliminate C_1 and C_2, thus giving a single equation for p in terms of h_0 and a constant of integration.

The boundary conditions for this equation are similar to those of the ordinary theory of lubrication. There the pressure is given at one point and the flow is assumed to cavitate in such a way that the dissipation of energy is minimized. Similarly, the dissipation of energy should be minimized for the viscoelastic problem. It seems probable that this will give the correct flow. The theory is applied, in Section 4, to the problem of two cylinders rolling without slipping. The classical solution to this problem was derived by MARTIN[15].

APPLICATION TO THE PROBLEM OF ROLLING

We consider two cylinders rolling together without slipping. Their diameters are D_1 and D_2 and the gap $h(x)$ may be expressed as

$$h = h_1 + Kx^2 \tag{27}$$

where h_1 is the minimum film thickness and

$$K \equiv \frac{1}{D_1} + \frac{1}{D_2}. \tag{28}$$

The common surface speed of the rollers is $-U$. From equations (24) and (25) we find, on neglecting T^4 in comparison with T^2,

$$C_1 = -\frac{h}{2\eta}\frac{dp}{dx} \tag{29}$$

$$C_2 = -U - \frac{T^2}{64}\frac{h^4}{\eta^3}\left(\frac{dp}{dx}\right)^3. \tag{30}$$

Substituting in equation (25) and rearranging

$$\frac{dp}{dx} = \frac{12\eta U}{h^3}(h_0 - h)\left\{1 - \frac{1728 T^2 U^2}{80}\left(\frac{h_0 - h}{h^2}\right)^2\right\}. \tag{31}$$

Equation (31) shows that the magnitude of dp/dx is everywhere less than in the Newtonian case. Starting from $p = 0$ at $x = \infty$ it is clear that the maximum pressure will be less and the load capacity will also be less.

It will be assumed that the pressure and its gradient fall to zero at the same value of $x(\equiv x_0)$ and the film tears at this point. This gives the minimum drag or dissipation.

By integrating (31) one may show that the point x_0 is very close to the Newtonian value, $x_0 = -0{\cdot}475\sqrt{\frac{h_1}{K}}$. The actual value depends on

(TU/h_1), but since the theory is not valid for $(TU/h_1) > 0{\cdot}3$ at the most, it may be shown that the separation point x_0 occurs for

$$-0{\cdot}475\sqrt{\frac{h_1}{K}} > x_0 > -0{\cdot}478\sqrt{\frac{h_1}{K}}\,. \tag{32}$$

Using the Sommerfeld transformation for convenience,

$$x = \sqrt{\frac{h_1}{K}}\tan\Phi \tag{33}$$

equation (31) may be integrated for various values of h_0. As an example, the pressure distribution for $h_0/h_1 = 1{\cdot}2285$ is given by

$$\begin{aligned} p\Big/\left(\frac{\eta U}{h_1\sqrt{h_1 K}}\right) \equiv p^* &= 3{\cdot}685\cos^3\Phi\sin\Phi - 0{\cdot}472\,\{\cos\Phi\sin\Phi + \Phi - \pi/2\} \\ &+ (TU/h_1)^2\{40{\cdot}046\cos^{11}\Phi\sin\Phi - 73{\cdot}302\cos^9\Phi\sin\Phi \\ &+ 36{\cdot}944\cos^7\Phi\sin\Phi - 0{\cdot}099\cos^5\Phi\sin\Phi \\ &- 0{\cdot}124\cos^3\Phi\sin\Phi - 0{\cdot}186\,(\cos\Phi\sin\Phi + \Phi - \pi/2)\} \end{aligned} \tag{34}$$

To satisfy the condition $p = 0$, $dp/dx = 0$ when $\Phi = \tan^{-1}(-0{\cdot}478)$, $(TU/h_1)^2$ must have the value 0·112. This is expected to be the maximum value of $(TU/h_1)^2$ to which the theory applies. Fig. 3 compares this case

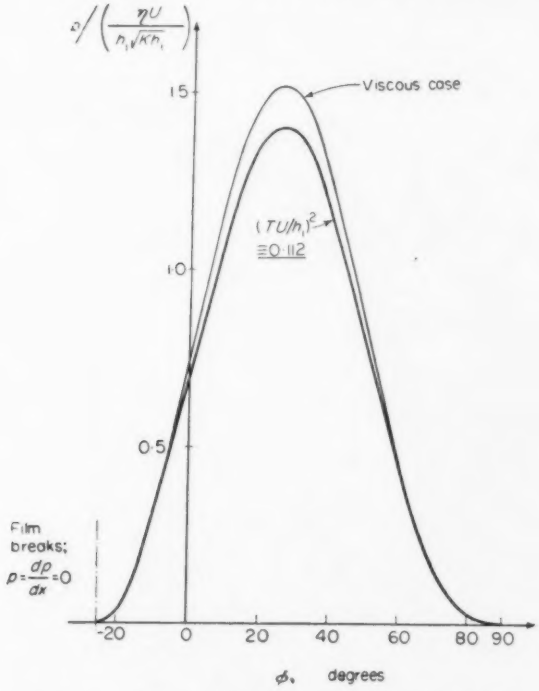

FIG. 3. Pressure distribution between rollers.

with the viscous theory. Similarly other curves may be drawn for various values of $(TU/h_1)^2$ if required.

Integration gives the load per unit width (N) equal to $\int_{x_0}^{\infty} p\,dx$.

$$N\Big/\left(\frac{\eta U}{h_1 K}\right) \equiv N^* = \int_{x_0=x}^{\infty} p^* \sec^2\Phi\, d\Phi\,. \tag{35}$$

Now

$$p^* = p^*[\Phi, (TU/h_1)^2]$$

$$x_0 = x_0[(TU/h_1)^2]\,.$$

Hence $N^* = N^*[(TU/h_1)^2]$. Using a McLaurin series expansion and retaining only the first two terms (in uniformity with the previous procedure)

$$N^* = N_0^* + a_1(TU/h_1)^2\,. \tag{36}$$

Now $N_0^* = 2{\cdot}45$, and computation of a_1 gives the following expression for N^*

$$N^* = 2{\cdot}45\,\{1 - 0{\cdot}5(TU/h_1)^2\}\,. \tag{37}$$

Similarly the drag D per unit width may be computed

$$D = \int_{x_0}^{\infty} \overline{xy}|_{y=0}\,dx\,. \tag{38}$$

From equations (17) and (20)

$$\overline{xy}|_{y=0} = \eta C_1 = -\frac{h}{2}\frac{dp}{dx}\,. \tag{39}$$

Evaluation of the integral (38) for the case $x_0\Big/\sqrt{\frac{h_1}{K}} = -0{\cdot}477$ and for the viscous case gives

$$D^* \equiv D\Big/\left(\frac{\eta U}{\sqrt{h_1 K}}\right) = 3{\cdot}24\,\{1 + 0{\cdot}22(TU/h_1)^2\}\,. \tag{40}$$

Therefore the coefficient of rolling friction (μ) is given by

$$\mu = 1{\cdot}32\sqrt{h_1 K}\,(1 + 0{\cdot}72(TU/h_1)^2)\,. \tag{41}$$

DISCUSSION

The use of the absolute time derivative complicates considerably the theory of viscoelastic flow. However, in calculations where the vorticity is of the same order of magnitude as the deformation it seems essential to use this derivative. This argument also applies to plastic flow, as pointed out by THOMAS.

The theory leads to a non-linear relation between the pressure gradient

and velocity. This has been linearized, assuming departures from MARTIN's theory are small when $(TU/h_1)^2$ is small. The resulting non-linear differential equation for $p(x)$ (equation 26) is of the first order. Hence the boundary conditions needed are the same as those in the classical theory. MILNE's theory, by contrast, introduces extra boundary conditions. The qualitative agreement between the two theories is not as surprising as it might first appear. The introduction of the elastic term corresponds to allowing elastic deformation of the oil film to take place. Intuitively one would then expect that a given load would produce a thinner film, because the film is "softer".

The theory proposed is only valid for values of TU/h_1 up to about 0·3. A typical value of T for lubricating oils appears to be about 10^{-8} sec. h_1 may be about 10^{-5}–10^{-6} ft, so the theory is valid up to rolling speeds of the order of 100 ft/sec. This seems to be adequate for practical purposes.

The observation by CROOK[16], that measured film thicknesses between lightly loaded rollers are only half those predicted by the classical theory, cannot be due to viscoelastic effects. The value of TU/h_1 in his experiment was about 0·04 or so, (assuming $T = 10^{-8}$ sec). Deviations from the Newtonian behaviour would not amount to more than about 0·1 per cent (equation 35).

It is believed that the above analysis is not very sensitive to the exact form of the viscoelastic stress deformation law assumed, provided it is properly invariant. For higher values of (TU/h_1), where linearization is inapplicable, a closer estimation of the properties of real materials would be essential, especially if numerical analysis is resorted to.

REFERENCES

1. O. REYNOLDS, *Phil. Trans.* Part I. **177**, 157 (1886).
2. H. BLOK, *Ann. N. Y. Acad. Sci.* **53**, 779 (1951).
3. A. A. MILNE, On grease lubrication of a slider bearing. *Lubrication and Wear.* Proc. Inst. Mech. Engrs., Lond. Conference (1957).
4. L. I. KOTOVA, *J. Tech. Phys., Moscow* **27**, 1424 (1957).
5. A. A. MILNE, Theory of rheodynamic lubrication for a Maxwell liquid. *Lubrication and Wear.* Proc. Inst. Mech. Engrs., Lond. Conference (1957).
6. A. CAMERON, *J. Inst. Petrol. Tech.* **40**, 191 (1954).
7. J. LAMB, *Proc. Roy. Soc.* A **253**, 52 (1959).
8. L. J. F. BROER, *Appl. Sci. Res., Hague* (A) **6**, 226 (1957).
9. W. NOLL, *J. Rat. Mech. Anal.* **4**, 1 (1954).
10. T. Y. THOMAS, *Proc. Nat. Acad. Sci., Wash.* **41**, 716 (1948).
11. H. FROMM, *Z. angew. Math. Mech.* **28**, 43 (1948).
12. R. HILL, *Mathematical Theory of Plasticity*, Appendix IV, p. 349. Clarendon Press, Oxford (1950).
13. A. SOMMERFELD, *Mechanics of Deformable Bodies*, p. 253. Academic Press, New York (1950).
14. P. R. PASLAY, *Calendering of a Visco-Elastic Material.* ASME 57-APM-1 (1957).
15. H. M. MARTIN, *Engng. Mag.* **102**, 116 (1916).
16. A. W. CROOK, *Phil. Trans.* A **250**, 387 (1958).

Int. J. Mech. Sci. Pergamon Press Ltd. 1960. Vol. 1, pp. 216–228. Printed in Poland

THE ULTIMATE STRENGTH OF THIN-WALLED SHELLS AND CIRCULAR DIAPHRAGMS SUBJECTED TO HYDROSTATIC PRESSURE

P. B. MELLOR

Department of Mechanical Engineering, University of Liverpool

(*Received* 15 *May* 1959)

Summary – The ultimate strength of thin-walled cylinders, spherical shells and circular diaphragms subjected to hydrostatic pressure is investigated for materials whose strain-hardening characteristics can be fitted by the empirical equation $\bar{\sigma} = A(B+\bar{\varepsilon})^n$. Experimental values of maximum pressure obtaining in the deforming of circular diaphragms of initially cold-worked materials are shown to be in good agrement with a theoretical treatment by Hill.

INTRODUCTION

THE simple tensile test is the most convenient and the most widely used method of determining strain-hardening characteristics of metals, and the ultimate tensile strength is the principal material property obtained from the test. The U. T. S. corresponds to the maximum load attained in the test which in turn marks the end of uniform straining. After the maximum load condition the stress distribution in the "neck" of the specimen is complex and cannot be predicted theoretically.

Similar conditions may arise in shells subjected to slowly increasing internal pressure. What errors are involved if the maximum pressures are calculated on a basis of U. T. S. alone? This question is investigated for thin-walled cylinders and spherical shells where plastic flow takes place under uniform stress until the maximum pressure is reached.

If a flat circular metal diaphragm is clamped around its periphery and subjected on one side to increasing fluid pressure, plastic flow takes place under a non-uniform stress distribution. However, the maximum stress and strain occur at the centre of the diaphragm and the stress and strain ratios at this point remain constant throughout the straining. The maximum pressures reached in a series of experiments will be compared with a special solution by HILL[1].

The first assumption to be made is that the material is rigid-work-hardening. That is, no straining occurs until first yield and the relation between plastic strain increment and deviatoric stress is given by the Lévy–Mises equation,

$$\frac{d\varepsilon_1}{\sigma_1-\sigma_m} = \frac{d\varepsilon_2}{\sigma_2-\sigma_m} = \frac{d\varepsilon_3}{\sigma_3-\sigma_m} \qquad (1)$$

where $\sigma_1 > \sigma_2 > \sigma_3$ are the principal stresses, $d\varepsilon_1$, $d\varepsilon_2$ and $d\varepsilon_3$ are the corresponding principal strain increments, and $\sigma_m = (\sigma_1 + \sigma_2 + \sigma_3)/3$, the mean stress.

Again, since various stress and strain conditions are to be compared, the following equations defining generalized stress $\bar{\sigma}$ and strain $\bar{\varepsilon}$ will be adopted:

$$\bar{\sigma} = 1/\sqrt{2}[(\sigma_1 - \sigma_2)^2 + (\sigma_2 - \sigma_3)^2 + (\sigma_3 - \sigma_1)^2]^{1/2} \tag{2}$$

$$d\bar{\varepsilon} = \sqrt{2}/3[(d\varepsilon_1 - d\varepsilon_2)^2 + (d\varepsilon_2 - d\varepsilon_3)^2 + (d\varepsilon_3 - d\varepsilon_1)^2]^{1/2} \tag{3}$$

Also, in all problems to be considered the metal thickness is so small compared with the radius of curvature of the member that bending and shearing stresses can be disregarded and the stress σ_3, normal to the surface, is negligible. Therefore, putting $\sigma_3 = 0$ and $\sigma_2 = x\sigma_1$, where x will be referred to as the stress ratio, equations (1), (2) and (3) become

$$\frac{d\bar{\varepsilon}}{2(1-x+x^2)^{1/2}} = \frac{d\varepsilon_1}{2-x} = \frac{d\varepsilon_2}{2x-1} = -\frac{d\varepsilon_3}{1+x}, \tag{4}$$

$$\bar{\sigma} = \sigma_1(1-x+x^2)^{1/2}, \tag{5}$$

$$d\bar{\varepsilon} = d\varepsilon_1 \cdot \frac{2}{2-x}(1-x+x_2)^{1/2}. \tag{6}$$

In the following work, only cases where the principal axes of stress remain fixed and the stress ratio remains constant will be considered, so that equation (4) can be expressed in total strains.

$$\frac{\bar{\varepsilon}}{2(1-x+x^2)^{1/2}} = \frac{\varepsilon_1}{2-x} = \frac{\varepsilon_2}{2x-1} = \frac{-\varepsilon_3}{1+x}. \tag{7}$$

Thus the Lévy–Mises equation reduces to the Hencky equation or plastic deformation law and the strain-hardening characteristics may be expressed by the empirical equation,

$$\bar{\sigma} = A(B+\bar{\varepsilon})^n. \tag{8}$$

This equation was suggested by SWIFT[2]. It is useful for a general discussion to think of a material whose strain-hardening characteristic varies only with its initial state B. The constants A and n are constants for that particular metal, independent of the initial work-hardening. This equation was fitted to stress–strain curves obtained by measurements on circular diaphragms of various sheet metals of deep drawing quality and values are given in Table 1 (MELLOR[3]). Ideally, $B = 0$ for a fully annealed material. When $B = 0$ the equation becomes identical with Ludwik's equation, which may be expressed as $\bar{\sigma} = C\bar{\varepsilon}^m$. Care must be taken not to confuse the constants A and C or the indices n and m which are only

identical if $B = 0$. The two empirical equations will be compared later in the article.

TABLE 1

Metal	$\bar{\sigma} = A(B+\bar{\varepsilon})^n$ (lb/in²)
Soft copper	$\bar{\sigma} = 62{,}200(0{\cdot}016+\bar{\varepsilon})^{0{\cdot}3}$
Half-hard copper	$\bar{\sigma} = 62{,}200(0{\cdot}114+\bar{\varepsilon})^{0{\cdot}3}$
Soft brass	$\bar{\sigma} = 106{,}000\bar{\varepsilon}^{0{\cdot}48}$
Half-hard brass	$\bar{\sigma} = 106{,}000(0{\cdot}127+\bar{\varepsilon})^{0{\cdot}48}$
Soft aluminium	$\bar{\sigma} = 22{,}200\bar{\varepsilon}^{0{\cdot}25}$
Half-hard aluminium	$\bar{\sigma} = 22{,}200(0{\cdot}222+\bar{\varepsilon})^{0{\cdot}25}$
Killed steel	$\bar{\sigma} = 91{,}000\bar{\varepsilon}^{0{\cdot}2}$
Stainless steel	$\bar{\sigma} = 222{,}000(0{\cdot}016+\bar{\varepsilon})^{0{\cdot}5}$

THE SIMPLE TENSILE TEST

If P is the load, X the current cross-sectional area and l the current gauge length, then the true stress σ, is given by

$$P = \sigma X . \tag{9}$$

Neglecting the small elastic change in volume the material may be assumed to be incompressible and

$$X_0 l_0 = Xl \tag{10}$$

where X_0 is the original cross-sectional area and l_0 the original gauge length.

At the maximum load, $dP = 0$ and from equation (9)

$$\sigma dX + X d\sigma = 0 . \tag{11}$$

Also, from the condition for constancy of volume

$$l dX + X dl = 0 . \tag{12}$$

From equations (11) and (12) the point of maximum load at instability condition is given by

$$\frac{d\sigma}{\sigma} = \frac{dl}{l} = d\varepsilon$$

where the logarithmic strain $\varepsilon = \int \frac{dl}{l}$ or

$$\frac{d\sigma}{d\varepsilon} = \sigma . \tag{13}$$

The stress ratio x, in this case, is zero and equation (13) can therefore be written

$$\frac{d\bar{\sigma}}{d\bar{\varepsilon}} = \bar{\sigma} .$$

Introducing the empirical equation (8) from which $\frac{d\bar{\sigma}}{d\bar{\varepsilon}} = \frac{n\bar{\sigma}}{(B+\bar{\varepsilon})}$ the effective strain at instability $\bar{\varepsilon} = n-B$. The instability strains for a number of stress systems have been evaluated previously on the basis of the empirical equation (MELLOR[4]).

The condition $B \geqslant n$ implies that instability arises before any general elongation or thinning has occurred. This is a useful guide to the behaviour of a material under a given stress system but any assessment of the instability strain in this region must take into account the elastic strains.

From equation (7) the principal strains at instability are

$$\varepsilon_1 = -2\varepsilon_2 = -2\varepsilon_3 = (n-B)$$

and the longitudinal stress is, from equation (8),

$$A(n)^n = \frac{P_m}{X_m}$$

where P_m is the maximum load and X_m the corresponding cross-sectional area of the specimen. The relation between the current and original cross-sectional areas is determined by considering the strains.

$$ln\frac{X_m}{X_0} = ln\frac{l_0}{l_m} = -\varepsilon_1 = -(n-B)$$

$$\text{or} \quad X_m = X_0 \exp(B-n)\,.$$

Therefore

$$A(n)^n = \frac{P_m}{X_0}\exp(n-B)$$

and the ultimate tensile strength

$$\frac{P_m}{X_0} = A(n)^n \exp(B-n)\,. \tag{14}$$

This relation, in terms of the constants of the empirical law $\bar{\sigma} = A(B+\bar{\varepsilon})^n$, is valid as long as $n \geqslant B$. For ease of reference the stresses and strains in terms of these constants are set down in Table 2.

TABLE 2. SUMMARY OF RESULTS

Loading System	$\bar{\varepsilon}$	ε_1	ε_2	$\varepsilon_3 = ln\frac{t}{t_0}$	$\frac{\bar{\sigma}}{A}$	$\frac{\sigma_1}{A}$	$\frac{\sigma_2}{A}$
Simple tension	$(n-B)$	$(n-B)$	$-\frac{1}{2}(n-B)$	$-\frac{1}{2}(n-B)$	$(n)^n$	$(n)^n$	0
Cylindrical shell	$\left(\frac{n}{\sqrt{3}}-B\right)$	$\frac{\sqrt{3}}{2}\left(\frac{n}{\sqrt{3}}-B\right)$	0	$-\frac{\sqrt{3}}{2}\left(\frac{n}{\sqrt{3}}-B\right)$	$\left(\frac{n}{\sqrt{3}}\right)^n$	$\frac{2}{\sqrt{3}}\left(\frac{n}{\sqrt{3}}\right)^n$	$\frac{1}{\sqrt{3}}\left(\frac{n}{\sqrt{3}}\right)^n$
Spherical shell	$\left(\frac{2n}{3}-B\right)$	$\frac{1}{2}\left(\frac{2n}{3}-B\right)$	$\frac{1}{2}\left(\frac{2n}{3}-B\right)$	$-\left(\frac{2n}{3}-B\right)$	$\left(\frac{2n}{3}\right)^n$	$\left(\frac{2n}{3}\right)^n$	$\left(\frac{2n}{3}\right)^n$

Vol. 1
1960

THIN-WALLED PIPE OR CYLINDER

If p is the internal pressure, the hoop stress $\sigma_1 = pr/t$ and the longitudinal stress $\sigma_2 = pr/2t$, where r and t are the current values of cylinder radius and wall thickness respectively. The stress ratio $x = \frac{1}{2}$ and at instability, $dp = 0$

$$\frac{d\sigma_1}{\sigma_1} = \frac{d\sigma_2}{\sigma_2} = \frac{dr}{r} - \frac{dt}{t}$$

where $dr/r = d\varepsilon_1$, the hoop strain increment, and $dt/t = d\varepsilon_3$, the incremental thickness strain.

Substituting the value $x = \frac{1}{2}$ into equation (4), $d\bar{\varepsilon} = \frac{2}{\sqrt{3}} d\varepsilon_1 = -\frac{2}{\sqrt{3}} d\varepsilon_3$; $d\varepsilon_2 = 0$ and from equation (5) $\bar{\sigma} = \frac{\sqrt{3}}{2}\sigma_1$. The condition for maximum pressure or instability is therefore

$$\frac{d\bar{\sigma}}{d\bar{\varepsilon}} = \sqrt{3}\sigma = \frac{n\bar{\sigma}}{(B+\bar{\varepsilon})}$$

and the instability strain $\bar{\varepsilon} = \left(\frac{n}{\sqrt{3}} - B\right)$. For all practical cases the maximum principal strain is much less than the maximum principal strain in simple tension (see Table 2).

The maximum principal stress σ_1, at instability, is determined by substituting the effective strain in equation (8) and the stress ratio $x = \frac{1}{2}$ in equation (5). This gives

$$\sigma_1 = A \cdot \frac{2}{\sqrt{3}} \left(\frac{n}{\sqrt{3}}\right)^n .$$

The dimensionless quantities $\bar{\sigma}/A$ are plotted in Fig. 1.

It is now necessary to relate the maximum internal pressure to the initial wall thickness t_0 and the initial mean radius of the cylinder r_0. The strains are

$$\varepsilon_1 = \ln \frac{r}{r_0} = \frac{\sqrt{3}}{2}\left(\frac{n}{\sqrt{3}} - B\right); \qquad -\varepsilon_3 = \ln \frac{t_0}{t} = \frac{\sqrt{3}}{2}\left(\frac{n}{\sqrt{3}} - B\right)$$

giving

$$r = r_0 \exp \tfrac{1}{2}(n - \sqrt{3}B); \qquad t = t_0 \exp \tfrac{1}{2}(\sqrt{3}B - n) .$$

The pressure at instability is

$$p = \frac{\sigma_1 t}{r} = \frac{t_0}{r_0} \cdot A \cdot \frac{2}{\sqrt{3}} \left(\frac{n}{\sqrt{3}}\right)^n \exp(\sqrt{3}B - n) . \tag{15}$$

The term $A \cdot \frac{2}{\sqrt{3}} \left(\frac{n}{\sqrt{3}}\right)^n \exp(\sqrt{3}B - n)$ is the conventional instability stress;

that is the stress based on the initial dimensions of the cylinder. Let this quantity be denoted by S_1. What error is involved if the U. T. S. (the

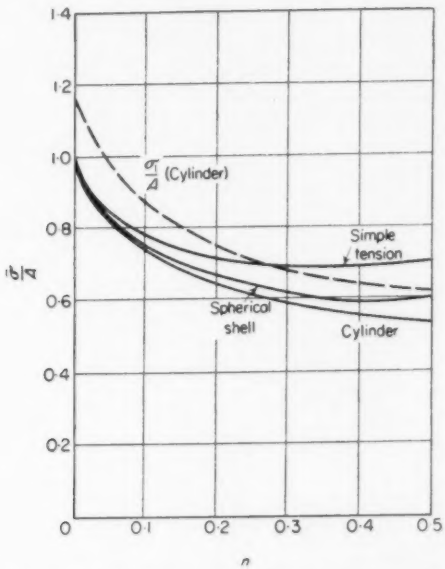

FIG. 1. Variation of effective instability stress with index n.

conventional instability stress in tension) is used in equation (15) instead of S_1? The ratio

$$\frac{S_1}{(\text{U. T. S.})} = \frac{2}{(\sqrt{3})^{n+1}} \exp B(\sqrt{3}-1) = K_1 \quad \text{(say)}$$

and the pressure at instability can be written

$$p = K_1(\text{U. T. S.})\frac{t_0}{r_0}. \tag{16}$$

The variation of K_1 with n and B is shown in Fig. 2. The condition $n = 0$ refers to an ideally plastic material and instability occurs at yielding, giving $K_1 = 1{\cdot}155$. For cases where K_1 is greater than unity, basing the instability pressure on the U. T. S. alone would under-estimate the strength of the material. The reverse is true for cases where K_1 is less than unity. Depending on the value of n it is possible to under-estimate the maximum pressure by 13 per cent or over-estimate it by 15 per cent. The effects of initial work-hardening (increasing B) is to increase the value of K_1, but, of course, the value of the instability strain decreases.

As an example consider a thin-walled cylinder constructed in aluminium (see Table 1). For soft aluminium $B = 0$ and $n = 0{\cdot}25$ giving, from Fig. 2, $K_1 \simeq 1$. Therefore in this case basing the design on the U. T. S. alone

Vol. 1
1960

would give the correct maximum pressure. However, considering the half-hard aluminium, where $B = 0{\cdot}222$ and $n = 0{\cdot}25$, instability arises

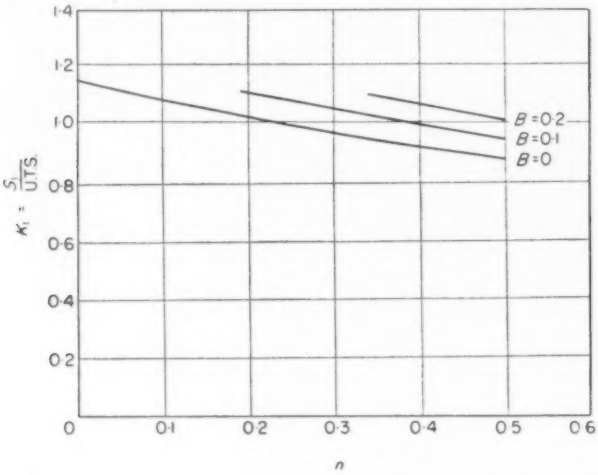

FIG. 2. Variation of ratio (conventional instability stress/ultimate tensile strength) for thin-walled cylinder.

before any general elongation has taken place. In this case it would seem preferable to design on the basis of the yield criterion of the metal.

SPHERICAL SHELL

The procedure is the same as for the thin-walled cylinder. The tangential stresses are $\sigma_1 = \sigma_2 = pr/2t$, the stress ratio $x = 1$ and the strain increment $d\bar{\varepsilon} = 2d\varepsilon_1 = 2d\varepsilon_2 = -d\varepsilon_3$. The maximum pressure at instability condition is given by $dp = 0$ and

$$\frac{d\sigma_1}{\sigma_1} = \frac{d\sigma_2}{\sigma_2} = \frac{dr}{r} - \frac{dt}{t} = d\varepsilon_1 - d\varepsilon_3 .$$

At instability therefore

$$\frac{d\bar{\sigma}}{d\bar{\varepsilon}} = \frac{3}{2}\bar{\sigma} = \frac{n\bar{\sigma}}{(B+\bar{\varepsilon})}$$

and the instability strain $\bar{\varepsilon} = \left(\frac{2n}{3} - B\right)$ (see Table 2).

The maximum principal stress σ_1, at instability, is determined by substituting the effective strain in equation (8). This gives $\sigma_1 = A\left(\frac{2n}{3}\right)^n$.

The strains $\varepsilon_1 = \varepsilon_2$ and ε_3 in terms of the dimensions of the shells are

$$\varepsilon_1 = \varepsilon_2 = \ln\frac{r}{r_0} = \frac{1}{2}\left(\frac{2n}{3} - B\right); \qquad -\varepsilon_3 = \ln\frac{t_0}{t} = \left(\frac{2n}{3} - B\right)$$

giving

$$r = r_0 \exp \frac{1}{2}\left(\frac{2n}{3} - B\right); \quad t = t_0 \exp\left(B - \frac{2n}{3}\right).$$

The pressure at instability is

$$p = \frac{2\sigma_1 t}{r} = 2\frac{t_0}{r_0} A \left(\frac{2n}{3}\right)^n \exp\left(\frac{3}{2}B - n\right).$$

The term $A\left(\frac{2n}{3}\right)^n \exp\left(\frac{3}{2}B - n\right)$ is therefore the conventional instability stress. Let this be denoted by S_2. The ratio $\frac{S_2}{(\text{U. T. S.})} = \left(\frac{2}{3}\right)^n \exp\frac{B}{2} = K_2$ (say) and the pressure at instability can be written

$$p = 2K_2(\text{U. T. S.}) \cdot \frac{t_0}{r_0}. \tag{18}$$

The variation of K_2 with n and B is shown in Fig. 3. It is seen that K_2 is always less than unity. This means that if the maximum attainable

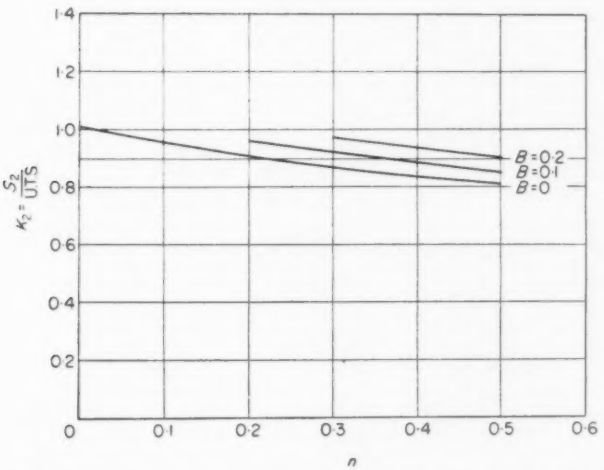

FIG. 3. Variation of ratio (conventional instability stress/ultimate tensile strength) for spherical shell.

pressure is calculated on the basis of U. T. S. alone it will always be over-estimated. For a material with $n = 0{\cdot}5$ and $B = 0$ this would lead to an over-estimation of approximately 22 per cent in the maximum pressure.

CIRCULAR DIAPHRAGM

The distribution of stress and strain in a plastically deforming circular diaphragm is now well understood. HILL[1] put forward a theory for a material having a linear strain-hardening characteristic and this was

Vol. 1
1960

shown to be in good agreement with experimental results on half-hard aluminium (MELLOR[3]). Following the work of HILL, THOMAS[5] took the particular case of soft copper and obtained a solution by a method of successive approximations which was in fairly good agrement with experimental work. However, the solution is lengthy and if only the maximum pressure and instability are required a special solution by HILL[1] is worth investigating. It has been shown, MELLOR[4], that this special solution agrees fairly well with experimental results for instability strains if the equation $\bar{\sigma} = A(B+\bar{\varepsilon})^n$ can be fitted to the experimentally determined strain-hardening characteristic.

It is known from experiment that with an annealed metal a maximum occurs in the pressure, and that fracture follows, under decreasing pressure, in the region of the pole. The relation between pressure and polar curvature, ϱ, is $p = 2\sigma_1 t/\varrho$ where $\sigma_1 = \sigma_2$ the surface stresses at the pole, and t is the current sheet thickness at the pole. At instability $dp = 0$ and

$$\frac{d\sigma_1}{\sigma_1} = \frac{d\varrho}{\varrho} - \frac{dt}{t}$$

or

$$\frac{1}{\sigma_1} \cdot \frac{d\sigma_1}{d\varepsilon_1} = 1 + \frac{1}{\varrho} \cdot \frac{d\varrho}{d\varepsilon_3} \tag{19}$$

where the through thickness strain ε_3 is now defined as the positive quantity $\ln \frac{t_0}{t}$, t_0 being the initial thickness of the sheet.

In this special solution HILL assumes that the particles in the diaphragm describe circular paths which are orthogonal to the momentary profile. On this assumption

$$\varepsilon_3 = 2\ln\left(1+\frac{h^2}{a^2}\right); \quad \frac{\varrho}{a} = \left(1+\frac{h^2}{a^2}\right)\Big/\frac{2h}{a} \tag{20}$$

where h is the polar height and a is the die radius. Relation (20) is independent of the properties of the metal and it is a better approximation for the work-hardened materials, Fig. 4. However, the accuracy of the theoretical instability strains depends on the term $1/\varrho \cdot d\varrho/d\varepsilon_3$ in equation (19).

Two experimentally determined values of this are compared in Fig. 5, with theoretical values from equation (20). The accuracy with which the instability strains can be determined depends on the correlation between experimental and theoretical values of $1/\varrho \cdot d\varrho/d\varepsilon_3$.

From equations (19) and (20) the point of instability occurs when

$$\frac{1}{\sigma_1} \cdot \frac{d\sigma_1}{d\varepsilon_3} = \frac{3}{2} - \frac{\varrho}{2h}.$$

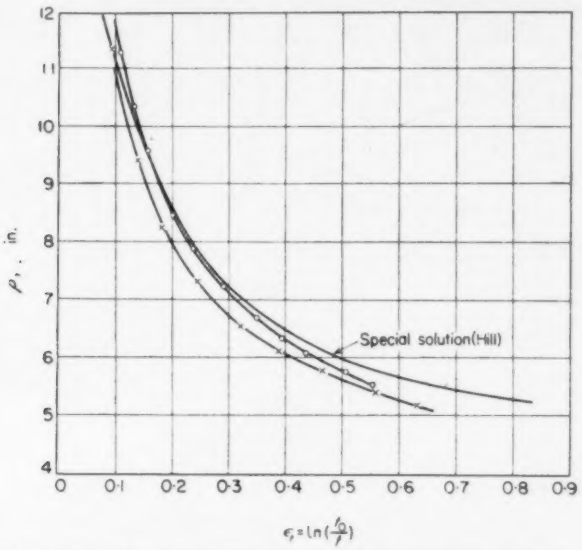

FIG. 4. Variation of polar radius of curvature with polar thickness strain.
—○—○— Half-hard copper.
—×—×— Soft brass.

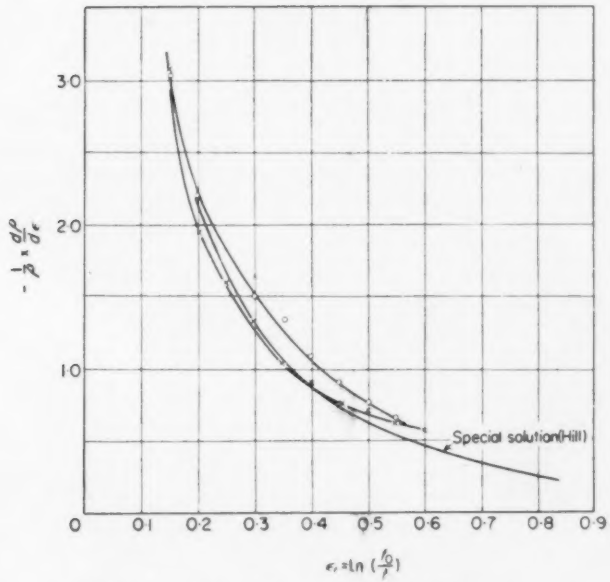

FIG. 5. —○—○— Half-hard copper.
—×—×— Soft brass.

On expanding in powers of ε_3 this reduces to

$$\frac{1}{\sigma_1}\cdot\frac{d\sigma_1}{d\varepsilon_3}\simeq\frac{11}{8}-\frac{1}{2\varepsilon_3}.$$

If then the stress–strain curve is fitted by the relation $\bar{\sigma}=A(B+\bar{\varepsilon})^n$ the polar thickness strain at maximum pressure is given by the quadratic equation

$$11\varepsilon_3^2+\varepsilon_3(11B-8n-4)-4B=0\,. \tag{21}$$

The stress-ratio, $x=1$, and the polar stress at instability is given by

$$\sigma_1=A(B+\varepsilon_3)^n\,. \tag{22}$$

Knowing ε_3 and σ_1, the polar height and polar radius of curvature can be determined from equation (20) and hence the maximum pressure.

Theoretical and experimental results are compared in Table 3. Some materials fractured without a decisive maximum in oil pressure and in

TABLE 3. INSTABILITY CONDITIONS IN CIRCULAR DIAPHRAGMS

Metal	t/t_0 Instability		Oil pressure (lb/in²)		Polar height (in.)		Polar radius of curvature (in.)		Polar stress (lb/in²)	
	Experiment	Theory	Experiment	Theory	Experiment	Theory	Experiment	Theory	Experiment	Theory
Soft copper	0·555	0·563	408	378	3·30	2·88	5·25	5·78	53,000	53,000
Half-hard copper	0·59	0·581	404	396	2·85	2·79	5·65	5·86	52,900	54,800
Soft brass	0·50 F	0.498	610 F	590	4·18 F	3·22	5·05 F	5·50	84,900 F	89,100
Half-hard brass	0·51 F	0·518	650 F	633	3·66 F	3·12	5·10 F	5·57	90,500 F	94,300
Soft aluminium	0·565	0·580	148	138	3·20	2·80	5·35	5·86	19,200	19,100
Half-hard aluminium	0·65 F	0·613	150 F	148	2·43 F	2·63	6·35 F	6·06	20,400 F	20,400
Killed steel	0·56	0.603	602	555	3·23	2·68	5·20	6·00	80,500	79,500
Stainless steel	0·52	0·487	1260	1240	3·90	3·28	5·00	5·45	168,500	190,300

(i) F denotes that the material fractured under increasing pressure.
(ii) The radius of the die was 5 in. and the initial nominal thickness of the metal 0·036 in.

these cases experimental results for fracture are presented. It is seen that theory under-estimates the polar height and over-estimates the radius of curvature at instability. The maximum oil pressure attained is under-estimated for all materials and there is better correlation for the more work-hardened materials. For the annealed materials the pressure at instability is under-estimated by between 5 and 8·5 per cent. This is a consequence of equation (20) which is not such a good approximation for the annealed materials as it is for the work-hardened materials. All theoretical results are of course dependent on the accuracy with which the empirical law $\bar{\sigma}=A(B+\bar{\varepsilon})^n$ can be fitted to the experimentally determined strain-hardening characteristics.

EMPIRICAL EQUATIONS TO REPRESENT THE STRESS–STRAIN CURVE

The most widely used equation to represent a stress–strain curve is of the form $\bar{\sigma} = C\bar{\varepsilon}^m$ where C and m are constants for a particular material. The value of the constant m depends on the degree of initial work-hardening, small values indicating a cold-worked material.

WEIL[6] and SVENSSON[7] have investigated the bursting pressures of thin-walled cylinders and spherical shells using this equation and have obtained equations (15) and (17) for the case $B = 0$, when $n = m$. Curves $b = 0$, Figs. 1 and 2, may be discussed for the equation $\bar{\sigma} = C\bar{\varepsilon}^m$ where work-hardened materials having low values of $m = n$ have the higher K values.

The equation $\bar{\sigma} = A(B+\bar{\varepsilon})^n$ has the advantage in a general discussion that the forming capability and the difference between, for example, soft brass and soft aluminium in this respect is emphasized (see Tables 1 and 2). Once the best metal (high value of n) has been chosen, the effect of initial work-hardening on forming capability can be studied. A further advantage of the equation is that it provides a much better fit to stress–strain curves of work-hardened materials. This is illustrated in Fig. 6

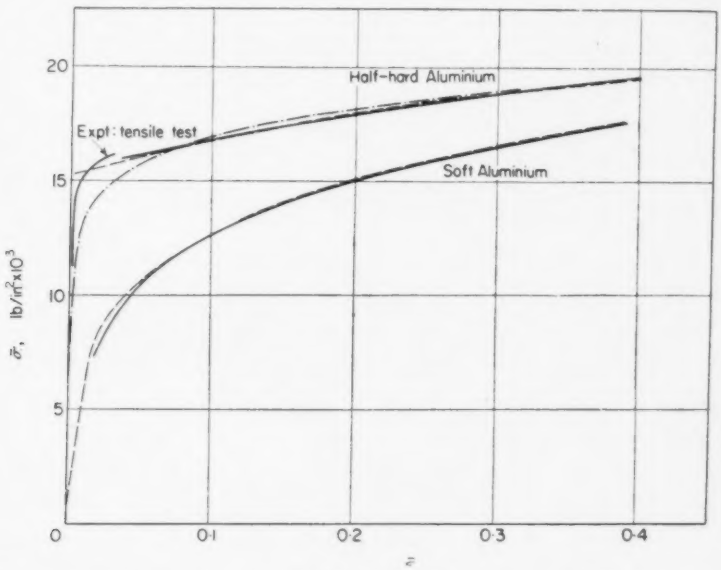

FIG. 6. Empirical curves to strain-hardening characteristics of aluminium.

. . . . . $\bar{\sigma} = A(B+\bar{\varepsilon})^n$

— · — · — $\bar{\sigma} = 21{,}400\bar{\varepsilon}^{0\cdot1}$.

which shows the stress–strain curves for two tempers of aluminium. The experimental results to high strain values were obtained by taking readings from a plastically deforming circular diaphragm. A stress–strain curve for the half-hard aluminium up to the necking-point in simple tension

is also included in the figure. The curve for half-hard aluminium to large strains can be fitted either by the equation $\bar{\sigma} = 22{,}200(0{\cdot}222 + \bar{\varepsilon})^{0{\cdot}25}$ or $\bar{\sigma} = 21{,}400\bar{\varepsilon}^{0{\cdot}1}$. Taking the latter expression, the theoretical value of thickness ratio at instability of a circular diaphgram is 0·646, which is in very good agreement with the experimental value. However, the latter expression could not be used to predict the instability strain in tension since it is seen that there is a large discrepancy between theoretical and experimental curves at low values of strain.

The experimental instability strain in tension for half-hard aluminium was found to be 0·03 and from the expression $\bar{\sigma} = 22{,}200(0{\cdot}222 + \bar{\varepsilon})^{0{\cdot}25}$ the theoretical value is $(n - B) = 0{\cdot}028$. It was to be expected that the theoretical value would give the lower figure since elastic strains are neglected. If the equation $\bar{\sigma} = C\bar{\varepsilon}^m$ is to be used the constants C and m must be re-determined.

REFERENCES

1. R. HILL, *Phil. Mag.* **41**, 1133 (1950).
2. H. W. SWIFT, *J. Mech. Phys. Solids* **1**, 1 (1952).
3. P. B. MELLOR, *J. Mech. Phys. Solids* **5**, 41 (1956).
4. P. B. MELLOR, *Engineer, Lond.* In press (1959).
5. D. G. B. THOMAS, *British Iron and Steel Research Association, Research Report* MW/B/4/54 (1954).
6. N. A. WEIL, *J. Franklin Inst.* **265**, 97 (1958).
7. N. L. SVENSSON, *J. Appl. Mech.* **25**, 89 (1958).

Int. J. Mech. Sci. Pergamon Press Ltd. 1960. Vol. 1, pp. 229–252. Printed in Poland

AN UPPER-BOUND APPROACH TO PLANE-STRAIN FORGING AND EXTRUSION—II

H. KUDO

Aeronautical Research Institute, Tokyo University

(*Received* 12 *January* 1959)

Summary – The upper-bound approach method as developed in Part I[1] of this work is applied to various types of plane-strain extrusion and forging of rigid–perfectly plastic material with closed dies and the results are seen to be of sufficient accuracy despite the little labour required for calculation.

The steady-state extrusion and piercing pressures agree with those derived from slip-line theory by the other investigators to within an error of 10 per cent, for a range of reductions 0·2 to 0·95. The most suitable velocity fields which give the minimum upper bounds resemble essentially the corresponding slip-line fields.

Extrusion pressures for a three-orifice extrusion and a sideways extrusion are found exactly or nearly equal to those for the usual extrusion having the same total reduction.

In a stepped extrusion, the working pressure is found to be a little higher than that of the usual extrusion having an identical reduction.

In the extrusion-forging and piercing-forging of short slugs, the working pressures vary with the thickness of the slug and in a manner depending on the condition of lubrication. These pressures and the most suitable velocity fields show good agreement with slip-line solutions. The most suitable velocity fields also give a good explanation of the formation of extrusion defects. Some opposed extrusion-forgings, with both top and bottom dies having orifices, are analysed and their working pressures are found to be lower than those of the usual one-way extrusion-forging.

A method of estimating the coining pressure with perfectly closed dies is proposed, using the velocity fields for extrusion and piercing.

Vol. 1
1960

INTRODUCTION

IN PART I[1] of this work a method of obtaining a good upper bound for the mean working pressure has been proposed by using a rigid-triangle velocity field and the concept of a unit rectangular deforming region. In this part, this method is applied to various types of forging and extrusion problems in which the material is deformed in closed dies so that their processes will be understood. Some of the results will be compared with known slip-line solutions to ascertain the reliability of the method adopted.

EXTRUSION AND PIERCING

The steady-state extrusion and piercing of long billets is now treated. The extrusion die and piercing punch are assumed to have flat working surface, Fig. 1.

Proceeding along the lines already described in connexion with Fig. 31, Part I, the upper bound for the mean working pressure ratio per unit area

of billet is, from a modification of equation (13) Part I, given by

$$\frac{\bar{p}}{2k} = (e_1 + e_2)R \tag{1}$$

where e_1 and e_2 refer to regions [1] and [2] respectively in Fig. 1, and R is the reduction defined by

$$R = 1 - W_e/W_c, \text{ for extrusion} \tag{2}$$

and

$$R = W_p/W_c, \text{ for piercing.}$$

Equation (1) holds when the container is smooth or when the extrusion is of backward type. The only difference between the constrained indentation, Fig. 31, Part I, and the extrusion or piercing processes, Fig. 1,

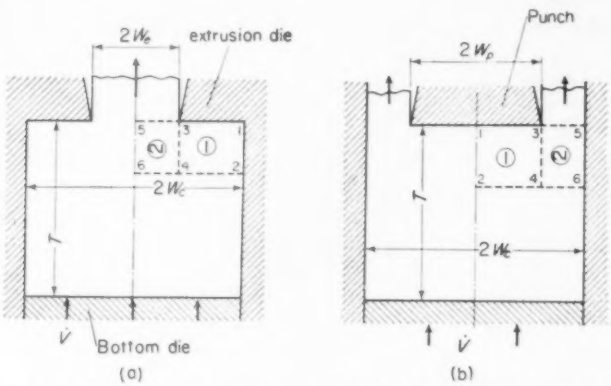

FIG. 1. Division of work-piece into unit deforming regions and rigid region for the upper-bound analysis of extrusion and piercing.
(a) Extrusion,
(b) Piercing.

is that the top surface of region [2] is free in the former, while it is constrained by the material already extruded in the latter.

For extrusion, therefore, the boundary condition for region [2] is denoted by *rrsr* (i), Table 1, Part I. That for region [1] is *ssrr* (i) with smooth dies and container, while it is *srrr* (i) for rough dies and a smooth container. Taking the values of e_1 and e_2 from the e versus a diagrams, with the aid of equation (15), Part I, and by minimising equation (1) with respect to G, upper-bound solutions for the extrusion pressure and velocity field easily follow. The upper bounds for the extrusion pressure ratio are shown in Fig. 2 by the solid line curves I and II. When the container is smooth, the results for smooth and for rough dies coincide for reductions of less than 0·58. As a special case, when the die is smooth, equation (16), Part I, holds again for $R \geqslant 0{\cdot}6$. The broken line curves in Fig. 2 represent the

slip-line field solutions after HILL[2]* and JOHNSON[3]. It will be seen that these upper-bound solutions differ from the exact solutions by no more than 3 per cent for $0{\cdot}45 < R < 0{\cdot}85$ and by no more than 10 per cent for $0{\cdot}20 < R < 0{\cdot}95$.

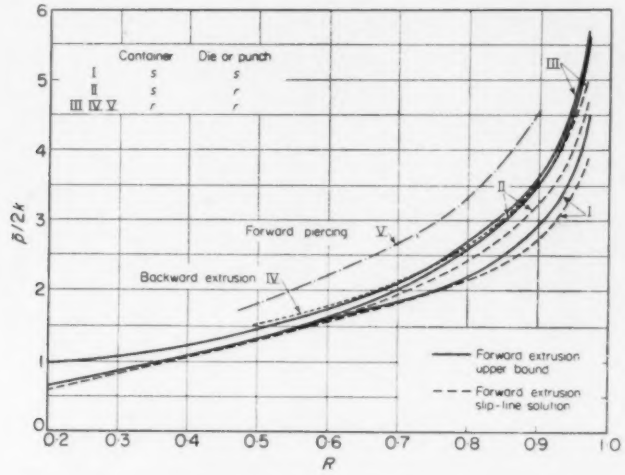

FIG. 2. Relations between mean extrusion and piercing pressures and reduction as determined from the upper bound analysis and the slip-line theory (HILL, JOHNSON).

The present upper bounds are, following the manner of JOHNSON, expressed by the empirical formula

$$\frac{\bar{p}}{2k} = 0{\cdot}50 - 1{\cdot}11\ln(1-R) \tag{3}$$

for smooth dies and container, and

$$\frac{\bar{p}}{2k} = 0{\cdot}30 - 1{\cdot}47\ln(1-R) \tag{4}$$

for a smooth container and rough dies, in the range $0{\cdot}3 < R < 0{\cdot}97$, with an accuracy of ± 5 per cent. The depth of the deforming region as determined by the most suitable rigid-triangle velocity field are plotted in Fig. 3.

Similarly, the upper bounds for backward extrusion with rough dies and container can be calculated and are shown in Fig. 2; the related depth of the deforming region is given in Fig. 3.

When the container is rough and the billet is pushed forward by the bottom die through the stationary container and against the stationary

* The values were taken from his chart for piercing punch pressure. His chart for mean extrusion pressure does not seem to be exact in the range of low reduction.

extrusion die, the energy dissipation on the container surface has to be taken into account so that

$$\frac{\bar{p}}{2k} = (e_1 + e_2)R + f_c \frac{T-G}{W_c} \tag{5}$$

where $\bar{p}/2k$ refers to the mean pressure on the bottom die face and f_c denotes the slip resistance ratio on the container surface.

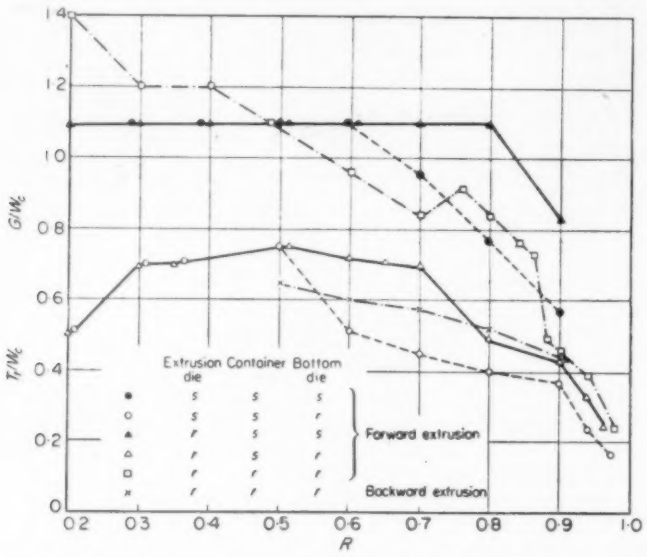

FIG. 3. Depths of stationary deforming region G and transition points T from steady to non-steady stage as obtained from the upper-bound analysis.

The boundary conditions for regions [1] and [2] when the die and container are both rough, are represented as *rrrr* (ii) and *rrsr* (i) respectively. Minimizing equation (5) with respect to G as before, the upper bounds for the bottom die pressure during forward extrusion are obtained as a function of T. In Fig. 2, for convenience, the upper bound for the mean pressure acting on the bottom surface of the stationary deforming region 246, Fig. 1, is shown by the solid line III. Its coincidence with the corresponding slip-line field solution (the broken line III) is again good. The upper bound can be expressed by

$$\frac{\bar{p}}{2k} = 0{\cdot}48 - 1{\cdot}41\ln(1-R) \tag{6}$$

for the same range of reduction and with same accuracy as equations (3) and (4).

In Fig. 4 are shown comparisons of the most suitable rigid-triangle velocity fields and the slip-line field. The general character of deformation

and the exact deforming region derived from the two methods are quite similar. However, for the forward extrusion with rough die and container, the depth of the deforming region, as in Fig. 3, is seen to differ conside-

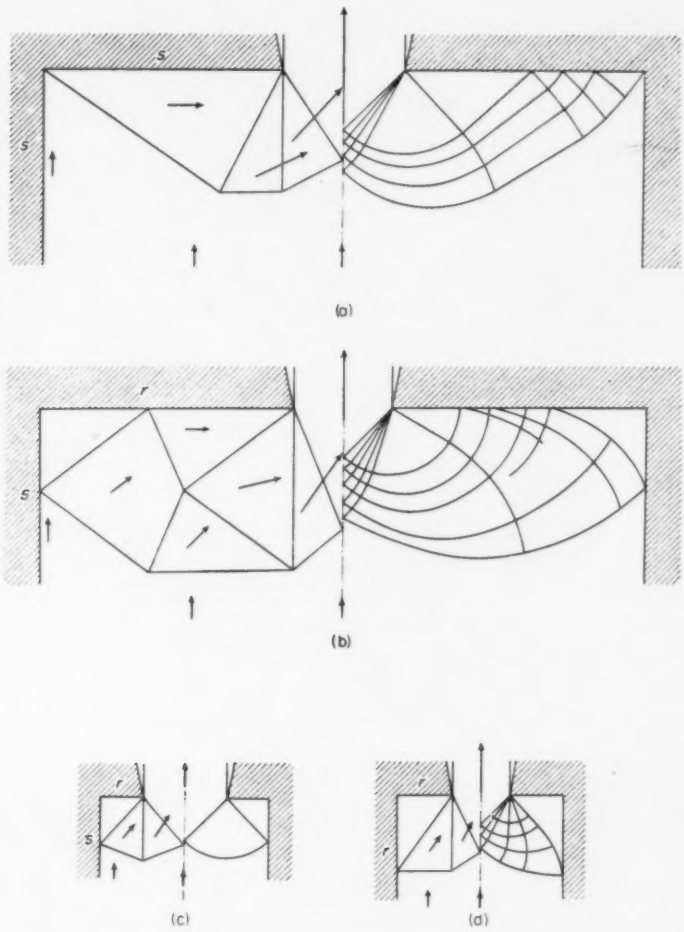

FIG. 4. Comparisons of the most suitable rigid-triangle velocity fields with slip-line fields (Hill and Johnson).
(a) Smooth die and container, $R = 0{\cdot}79$.
(b) Rough die and smooth container, $R = 0{\cdot}84$.
(c) Rough die and smooth container, $R = 0{\cdot}50$.
(d) Rough die and container, forward, $R = 0{\cdot}65$.

rably from the results given by JOHNSON[4], especially when the reduction is large.

The piercing process carried out in a smooth container is completely equivalent to the extrusion process in a smooth container, provided the

Vol. 1
1960

frictional condition of the piercing punch and extrusion die is identical. The solid lines, I and II, in Fig. 2, therefore, are also applicable to piercing.

The upper bounds for punch pressure taken from Fig. 2 are plotted against reduction in Fig. 5. The symmetrical character of the curve about

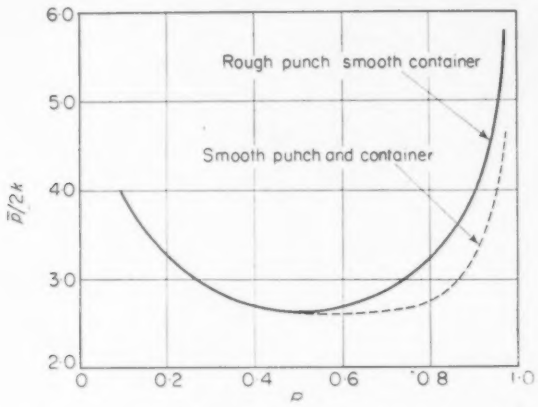

FIG. 5. The upper bounds for mean punch pressure in piercing.

$R = 0{\cdot}5$ for a rough punch is seen to reflect the equivalence of extrusion and piercing referred to; the velocity boundary conditions for an extrusion with a reduction ratio R are the same as those for piercing with the reduction ratio $(1-R)$ except for their signs.

When the container is rough, the effect of friction on the container surface should again be taken into account. The upper bound for the pressure on the bottom surface of the deforming region in forward piercing with a rough punch and container is given in Fig. 2; its value is seen to be considerably higher than that for forward extrusion with rough tools. This fact underlines the importance of lubrication in piercing practice, especially for high reductions.

It is to be noted that from the point of view of energy dissipation, the material extruded through the clearance between punch and container does not proceed in the vertical direction, but in an oblique direction when the container is rough and the extruded material is longer supported by the tool. Such a phenomenon has already been observed in an experimental work with plasticine by GREEN[5].

SOME SPECIAL EXTRUSIONS

The present section deals with such special problems as extrusion through a die having three orifices, Fig. 6(a), unsymmetrical piercing, Fig. 6(b), stepped extrusion, Fig. 8, and sideways extrusion, Fig. 9.

Slip-line solutions for plane-strain extrusion through dies having multiple orifices have already been given by DODEJA and JOHNSON[6]

and by JOHNSON *et al.*[7] In this work a three-orifice extrusion in which the side orifices are symmetrically situated with respect to the centre axis, Fig. 6(a) is examined in order to show the effectiveness of the present method of analysis. Some unsymmetrical piercing problems, Fig. 6(b), can be solved at the same time.

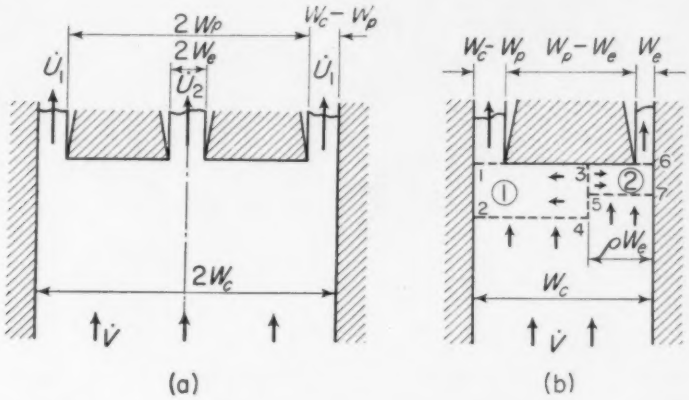

FIG. 6. Extrusion with three-orifice die and unsymmetrical piercing.
(a) Three-orifice extrusion.
(b) Unsymmetrical piercing.

A good upper bound can easily be obtained by dividing the deforming material into two unit extrusion regions [1] and [2], partitioned by the neutral plane 34. With the use of notations

$$R_1 = \frac{W_p}{W_c}, \quad R_2 = 1 - \frac{W_e}{W_c} \tag{7}$$

the reduction ratios for both unit extrusions are

$$r_1 = \frac{R_1 - \varrho}{1 - \varrho}, \quad r_2 = \frac{\varrho - 1 + R_2}{\varrho} \tag{8}$$

respectively, where ϱ defines the position of the neutral plane. Denoting the upper bound for the stationary extrusion pressure ratio for the two units by $\bar{p}_1/2k$ and $\bar{p}_2/2k$ respectively, and assuming either that the container is smooth or that the extrusion is a backward process, the upper bound for the mean extrusion pressure in the present problem is then given by

$$\frac{\bar{p}}{2k} = \frac{\bar{p}_1}{2k}(1 - \varrho) + \frac{\bar{p}_2}{2k}\varrho \tag{9}$$

where $\bar{p}_1/2k$ and $\bar{p}_2/2k$ are the function of r_1 and r_2 respectively.

It has already been observed that in extruding through a smooth die at high reductions, the most suitable velocity field under the die face is that shown in Fig. 4(a). This type of field when applied to regions [1]

and [2] yields no interference between them and, accordingly, the upper-bound values as determined for the extrusion with a single orifice are at once applicable to each extrusion unit.

If the container is smooth in Fig. 6(a), or if both sides of the container are equally smooth in Fig. 6(b), it transpires that $\bar{p}_1/2k$ and $\bar{p}_2/2k$ are the same function of reduction r_1 and r_2 respectively. Equation (9), therefore, has a minimum value

$$\frac{\bar{p}}{2k} = \left(\frac{\bar{p}_1}{2k}\right)_{r_1=R_t} \tag{10}$$

when

$$r_1 = r_2 = R_t \text{ or } \varrho = \frac{1-R_2}{1-R_t} \tag{11}$$

if $\bar{p}_1/2k$ and $\bar{p}_2/2k$ are concave with respect to reduction. In the above equations

$$R_t = R_1 + R_2 - 1 \tag{12}$$

represents the total reduction in the present problem. Equation (10) indicates that the extrusion pressure depends only on the total reduction when the container is smooth. An example of a velocity field for a smooth container and die is shown in Fig. 7(a).

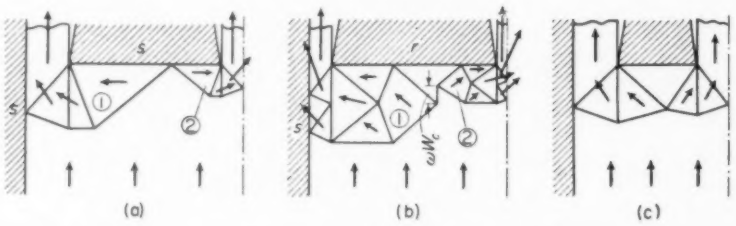

FIG. 7. Most suitable velocity fields in three-orifice extrusion.
(a) Smooth die and container.
(b) Rough die and smooth container.
(c) Small reduction.

When the die is rough, the application of the most suitable velocity field as determined already for single orifice extrusion, Fig. 4(b), requires a slight modification of equation (9) owing to the relative slip between the two unit regions, Fig. 7(b). The correction term which is added to equation (8) is $\omega/2$ and is very small when R_t is large. The same conclusion regarding equations (10) and (11), therefore, also holds for the present case with a high total reduction if the container is smooth in the case of Fig. 6(a), or if both sides of the container have a frictional resistance identical with that in case Fig. 6(b). When the reduction is small, a velocity field of the type shown in Fig. 7(c) results in a better upper bound.

The speeds of flow of the material through the orifices are given by, respectively,

$$\dot{U}_1 = \frac{1-\varrho}{1-R_1}\dot{V} \quad \text{and} \quad \dot{U}_2 = \frac{\varrho}{1-R_2}\dot{V}. \tag{13}$$

When ϱ is found from equation (11), it follows that

$$\dot{U}_1 = \dot{U}_2. \tag{14}$$

For a stepped extrusion as shown in Fig. 8 an upper bound for the steady working pressure is easily obtained if the whole vertical surface

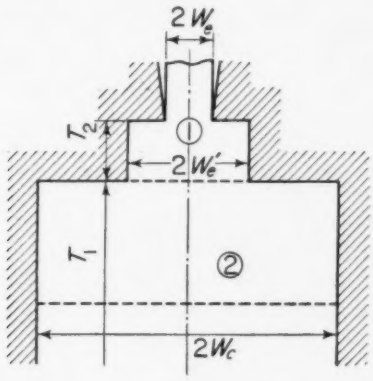

FIG. 8. Stepped extrusion.

of the container is smooth and if the depth of step T_2 is large compared with the width of the first die hole W_e'. In such cases, the whole process is regarded as two independent extrusion processes, of reduction $R_1 = 1-(W_e/W_e')$ and $R_2 = 1-(W_e'/W_c)$. Denoting the upper bounds for the extrusion pressure ratio in the two extrusion units by $\bar{p}_1/2k$ and $\bar{p}_2/2k$ respectively, an upper bound for the present stepped extrusion is easily shown to be given by

$$\frac{\bar{p}}{2k} = \frac{\bar{p}_1}{2k} + \frac{\bar{p}_2}{2k}. \tag{15}$$

As has been seen already, the relation of normal stationary extrusion pressure to reduction is expressed approximately by

$$\frac{\bar{p}_1}{2k} = m - n\ln(1-R). \tag{16}$$

If the frictional conditions on the first and second die surfaces are identical, $\bar{p}_2/2k$ is also expressed by equation (16) using R_2 instead of R_1. It follows then that

$$\frac{\bar{p}}{2k} = 2m - n\ln(1-R) \tag{17}$$

where R_t denotes the total reduction, $1-(W_e/W_c)$. Thus, $\bar{p}/2k$ exceeds that for stepless extrusion with the same reduction R_t by an amount in m which ranges between 0·3 and 0·5. This excess appear to reduce as the depth of step T_2 decreases below a certain amount.

Several sideways extrusion problems have been treated by GREEN[5] and JOHNSON *et al.*[7] In the present study a simple treatment of sideways extrusion will be illustrated for a case in which the orifice is located at the end of the container. This process, as shown in Fig. 9,

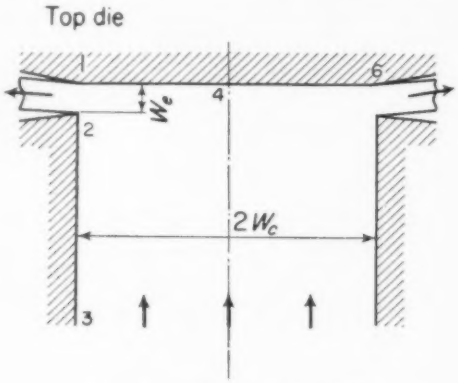

FIG. 9. Sideways extrusion.

will be seen to be quite similar to that of reverse-heading which has been discussed in Part I. The only difference lies in the condition of constraint at the orifice. However, from Figs. 19 and 21, Part I, the most suitable velocity field for the initial stage of heading, with its related upper bound, can be taken over for the present problem without modification.

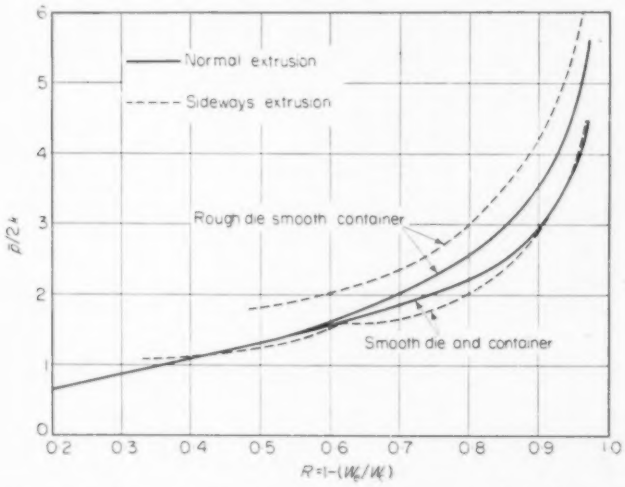

FIG. 10. Comparison of pressures for sideways and end extrusions.

Regarding $\{1-(W_e/W_c)\}$ as the sideways extrusion reduction, the upper bound solution for the container and top die smooth as well as for the container smooth and the top die rough are graphed in Fig. 10. The upper bounds for ordinary extrusion with the equivalent frictional conditions are also reproduced in the figure. It is interesting to see that the upper bounds for the sideways and ordinary extrusion nearly coincide for a given reduction and frictional condition.

EXTRUSION-FORGING

In this section the extrusion and piercing of comparatively short slugs, Fig. 11(a) and (b), are treated. Such processes are found in the final stages

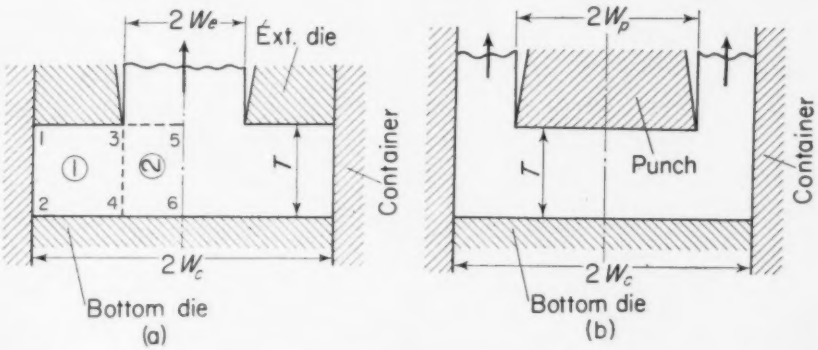

FIG. 11. Extrusion- and piercing-forging and division of work-piece into unit deforming regions.
(a) Extrusion-forging.
(b) Piercing-forging.

of extruding and piercing long billets, when the operations are no longer ones of steady state. The term "extrusion-forging" was first given to these processes by Sachs. Here the term "piercing-forging" will also be used in order to distinguish (b) from (a) in Fig. 11, when necessary.

Proceeding in the manner described before concerning Fig. 31(b) Part I, the upper bound for the mean working pressure for various conditions of friction, reductions and height–width ratios are easily calculated from equation (1) with the aid of Table 5, Part I. The results are graphed in Figs. 12 or 17. These diagrams can also be regarded as pressure-ram or die-stroke diagrams during extrusion. The solid circles in these figures indicate the transition point between steady and nonsteady flow stages. In Fig. 3, this transition point is plotted against reduction. It is to be noted that the height of the slug at this point equals the depth of the deforming region in the stationary stage when the bottom die is rough. The mode of variation of $\bar{p}/2k$ with T/W_c in the non-steady stage will be seen to vary considerably with the frictional conditions.

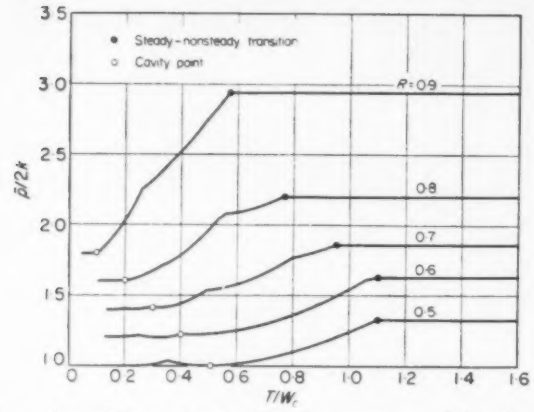

FIG. 12. Upper bound for extrusion-forging pressure. All tools are smooth.

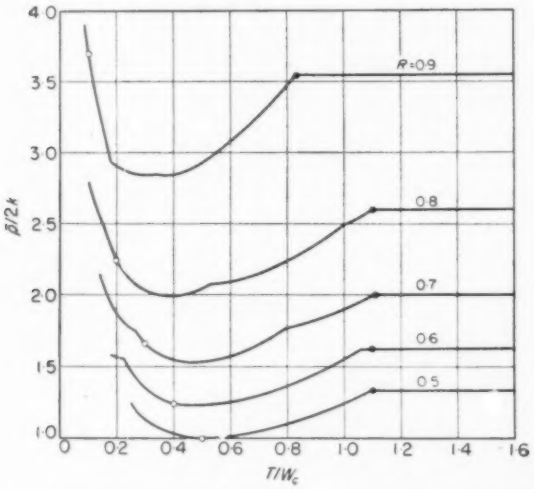

FIG. 13. Upper bound for extrusion-forging pressure. Rough extrusion die and smooth container and bottom die.

Comparison of upper-bound and slip-line field solutions for the working pressure is made in Figs. 14, 15 and 16(a); JOHNSON's[4] results and those of WANG[8] are inserted. The difference between the upper-bound results and those of JOHNSON is generally small and only about 12 per cent at most. Several results after WANG, however, differ considerably from the present upper bounds. There exists also a large discrepancy in the location of the transition points as determined by JOHNSON and the author, for forward extrusion with a rough container, top die and bottom die. The reason for this discrepancy is not yet clear.

In Fig. 18, comparisons are made between the shapes of the most suitable rigid-triangle velocity fields and the slip-line field after JOHNSON for a rough bottom die. The general agreement between them will be seen

to be very good. For values of T/W_c less than those indicated by the hollow circles in Figs. 12–17, the velocity fields in which part of the bottom surface 46, immediately below the orifice, separates from the bottom die,

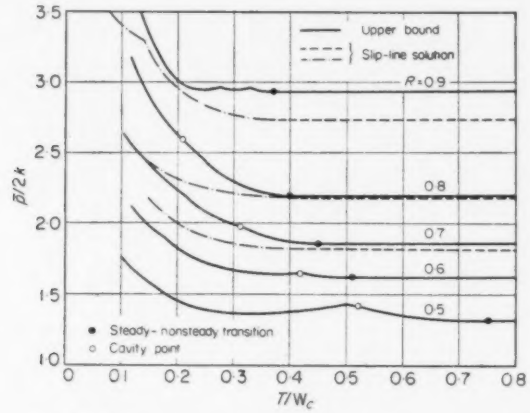

FIG. 14. Upper bound for extrusion-forging pressure. Smooth extrusion die and container and rough bottom die.

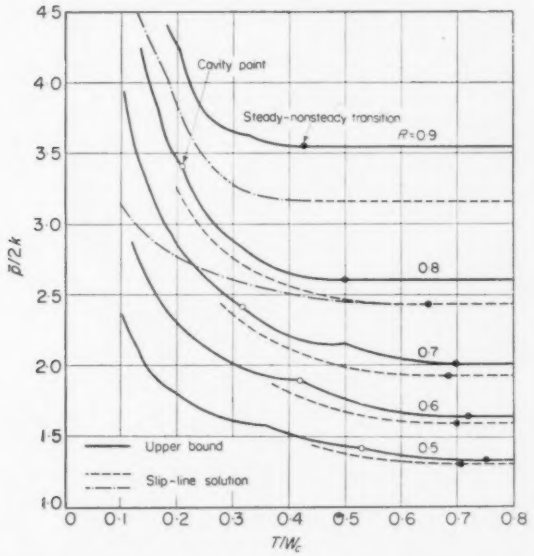

FIG. 15. Upper bounds for extrusion-forging pressure. Smooth container and rough dies.

require a lower rate of energy dissipation. More such velocity fields are illustrated in Fig. 19 and well explain the cavity formation on the bottom of extruded bars as well as the rounding-off at the bottom edge of pierced shells, the latter phenomena being pointed out by FUKUI, KUDO and

Vol. 1
1960

SEIXO[9] *. JOHNSON[10] has also given an explanation of the cavity formation in sheet extrusion in essentially the same direction.

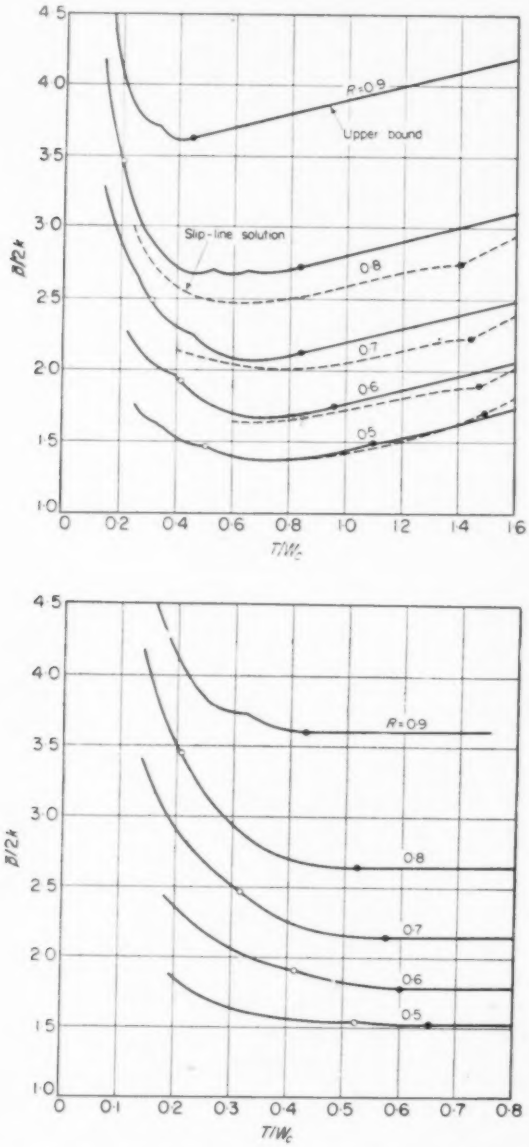

FIG. 16. Upper bound for extrusion-forging pressure. All tools are rough.
(a) Forward extrusion.
(b) Backward extrusion.

* Also observed experimentally by CHANG[11] and explained by Johnson in terms identical with these in the discussion on the paper by WATKINS *et al.*[12]

From the type of velocity field (a) in Fig. 19, where the bottom die is perfectly smooth, it will also be seen that the bottom surface skin of the work-piece is included in the centre of the body during non-steady-state flow before the onset of cavity formation and thus results in the inclusion

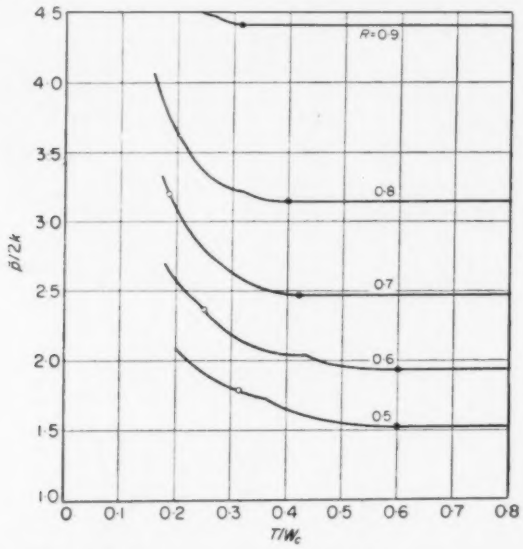

FIG. 17. Upper bound for backward piercing-forging pressure. All tools are rough.

defect of extruded products. This explanation has also been given by JOHNSON[13] independently of the author. An experimental verification of this explanation has been performed by the author. In experiments on the cold extrusion of round aluminium bar, this type of inclusion was not observed when a rough bottom die was used, but it was found with a thoroughly lubricated bottom die.

SPECIAL EXTRUSION-FORGING

The present section covers some special extrusion-forging, e. g. extrusion-forging between top and bottom dies which both have orifices, Figs. 20 and 23, and that between a top die which has three orifices and a flat bottom die, Fig. 26. The former will be termed "opposed extrusion-forging".

In the opposed extrusion-forging, the process is considered as two independent steady extrusion processes in the neighbourhood of the top and bottom dies, provided the billet is sufficiently long. These two processes, however, interact when the billet length is reduced; the process is then no longer steady.

In the symmetrically opposed extrusion-forging in Fig. 20, the process can be regarded as two symmetrically opposed normal extrusion-forgings,

Vol. 1
1960

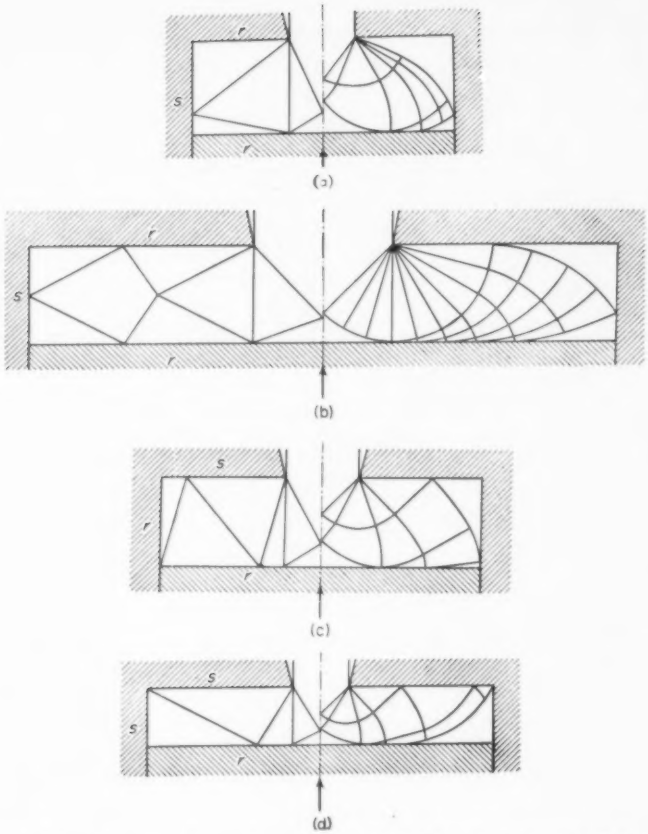

FIG. 18. Comparisons of most suitable rigid-triangle velocity fields with slip-line fields (Johnson) in extrusion-forging with rough bottom die.
(a) Rough extrusion die and smooth container, $R = 0{\cdot}76$, $T/W_c = 0{\cdot}73$.
(b) Rough extrusion die and smooth container, $R = 0{\cdot}78$, $T/W_c = 0{\cdot}49$.
(c) Smooth extrusion die and rough container, $R = 0{\cdot}71$, $T/W_c = 0{\cdot}42$.
(d) Smooth extrusion die and container, $R = 0{\cdot}84$, $T/W_c = 0{\cdot}33$.

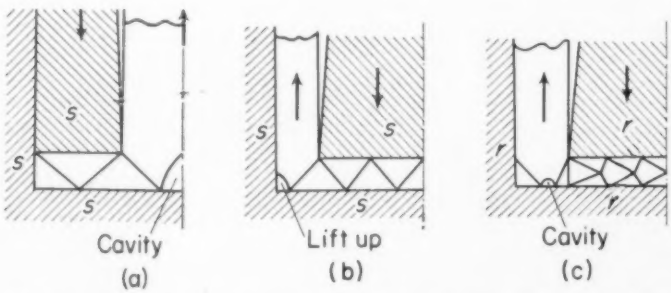

FIG. 19. Cavity formation on the bottom of the work-piece at the final stage of extrusion and piercing-forging.

Fig. 11, with a smooth flat bottom die. The upper bounds are then easily obtained and are shown in Figs. 21 and 22. Also given in these figures

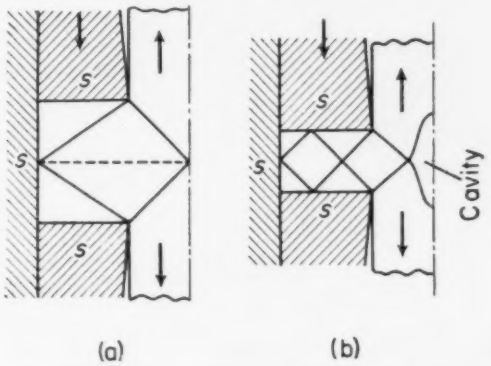

FIG. 20. Symmetrically opposed extrusion-forging and the most suitable velocity fields when all tools are smooth.

are the upper bounds when one of the two orifices is closed. The comparison of these two bounds in the figures shows the pressure drop effect when the second orifice is used in conjunction with the first. The two curves, however, become one if the value of T in the opposed extrusion-forging is regarded as half the distance between the top and the bottom dies, as long as the cavity formation point is not reached. This point is denoted by a hollow circle in Figs. 21 and 22. For values of T/W_c smaller than

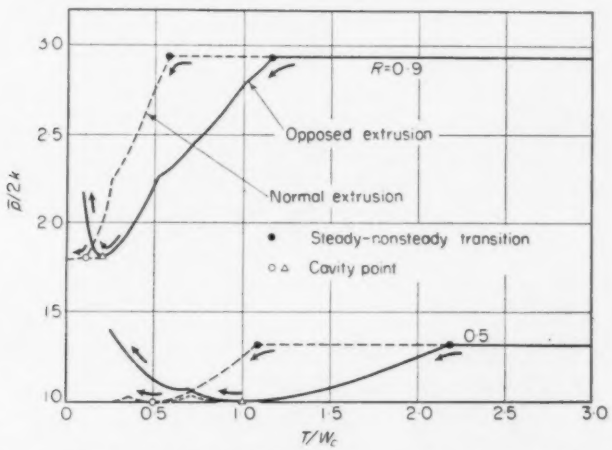

FIG. 21. Upper bounds for working pressure in symmetrically opposed extrusion-forging with smooth tools.

those represented by this point, a difference between these two will appear, since in opposed extrusion-forging cavity formation is usually prevented. If a crack is allowed to develop inside the material for the expenditure of a very small amount of energy, a cavity may be formed at the centre

of the material to reduce the internal rate of energy dissipation required for plastic deformation of material, see Fig. 20(b). The upper bound is then as given by the dotted line in Figs. 21 and 22, the triangle indicating the point of crack formation. This type of crack was actually found by the author in opposed extrusion experiments on round bar with aluminium, copper and brass. As was to be expected from this velocity field, a defect due to skin inclusion along the horizontal broken line in Fig. 20(a) has been observed in experiment.

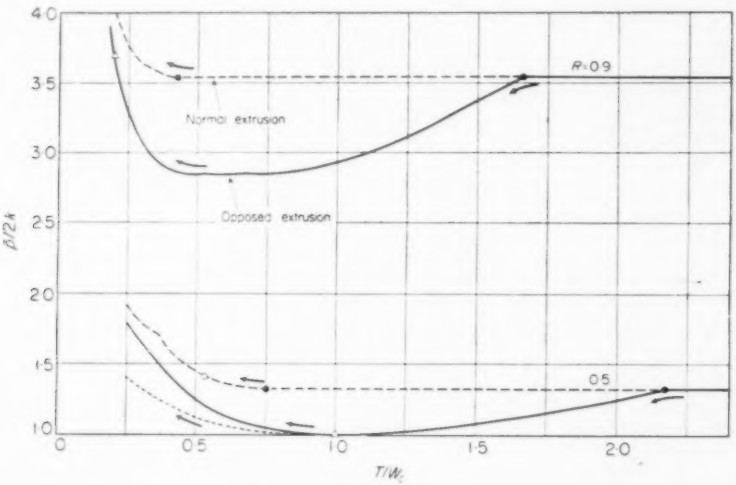

FIG. 22. Upper bounds for working pressure in symmetrically opposed extrusion-forging with rough dies and smooth container.

In the same manner, the upper bound and the most suitable velocity field for symmetrically opposed piercing-forging can be determined. In this case, the development of a crack on the outer surface of the product is predictable. Such crack formation, however, will be strongly constrained in the piercing process, if the extruded material is subject to a frictional resistance at the container wall. An alternative velocity field which results in a necking on the outer surface is given by JOHNSON[13].

In the case of opposed extrusion-piercing-forgings, good upper bounds are obtained by using the velocity fields shown in Fig. 23. When the billet is comparatively deep, the type of velocity field given in Fig. 23(a) is found to yield the best results. The deforming regions are then assumed to consist of four rectangular unit regions [1], [2], [3] and [4]; the regions 236′7 and 2′3′67 are assumed to be rigid. Using the directions shown in the figure, the height–width ratio, the pressing area and the pressing speed for each unit region can be listed as in Table 1, where

$$R_1 = \frac{W_p}{W_c}, \qquad R_2 = 1 - \frac{W_e}{W_c}. \tag{18}$$

R_1 and R_2 are the reductions when the orifice provided either in the bottom die or the top die, is closed.

From equation (6), Part I, the upper-bound ratio is given by

$$\frac{\bar{p}}{2k} = (e_1+e_2)(R_1-\varrho)+(e_3+e_4)(\varrho-1+R_2)\,. \tag{19}$$

When the container is smooth, e_1 and e_4, e_2 and e_3 are identical functions of the height–width ratio respectively. Equation (19), then, can be proved to have a minimum value given by

$$\frac{\bar{p}}{2k} = \{(e_1)_{a=\frac{(1-R_l)W_c}{T}} + (e_2)_{a=\frac{T}{R_l W_c}}\}\, R_l \tag{20}$$

when

$$\varrho = \omega = \frac{1-R_2}{1-R_l} \tag{21}$$

and where R_l is again defined by equation (12) and can be regarded as the total reduction for this process.

Vol. 1
1960

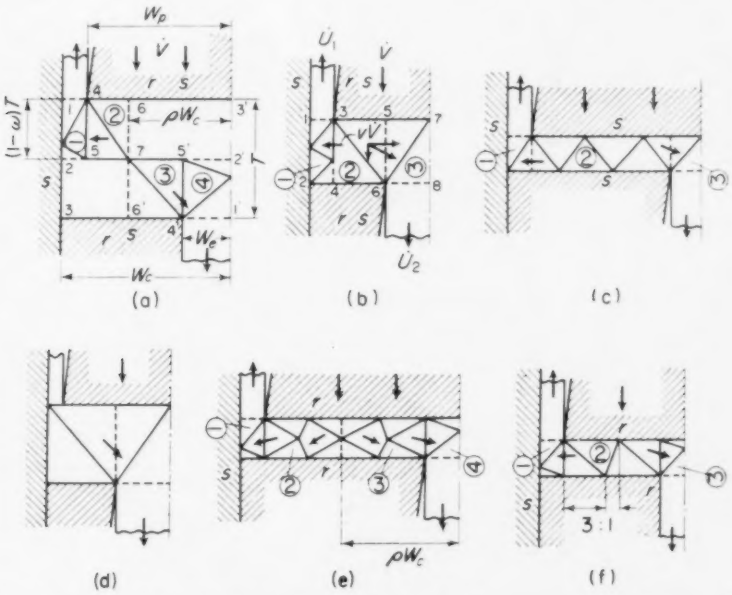

FIG. 23. Opposed extrusion-piercing-forging with smooth container. Its division into unit regions and examples of the most suitable velocity fields.

Equation (21) indicates that the velocity fields in the two unit extrusion regions are similar. Fig. 23(a) shows the most suitable velocity field taken from Table 1, Part I, corresponding to the boundary conditions imposed on each unit region. According to equation (21) the two surfaces of velocity discontinuity 47 and 4′7 form one straight line. This velocity

field can often be used as the most suitable field whether the dies be smooth or rough.

For smaller T/W_c, the kinds of velocity fields in Fig. 23(b) and (c) result in a lower rate of energy dissipation when the tools are all smooth. Thus, by dividing the whole of the slug between the dies into three unit rectangular deforming regions and by denoting the leftward velocity of the boundary plane 34 as $v\dot{V}$, the expression for the upper-bound ratio

$$\frac{\bar{p}}{2k} = e_1 \frac{T}{W_c} v + e_2 R_t + e_3 \left(R_t - \frac{T}{W_c} v \right) \tag{22}$$

is obtained.

When $R_1 = R_2$, equation (22) becomes independent of v, and

$$\frac{\bar{p}}{2k} = (e_1 + e_2) R_t \,. \tag{23}$$

From Table 1, Part I, it is seen that when one or both of a_1 and a_3 are less than unity, then $e_1 > e_3$ for $R_1 > R_2$ and $e_1 < e_3$ for $R_1 < R_2$. Equation (23), therefore, becomes least when $v = 0$ or $v = R_t W_c/T$. This indicates

TABLE 1. HEIGHT–WIDTH RATIO, PRESSING AREA AND SPEED FOR EACH INDIVIDUAL UNIT RECTANGULAR DEFORMING REGION IN OPPOSED EXTRUSION-PIERCING-FORGING

Region	Height–width ratio a_i	Pressed area A_i	Pressing speed $\dot{V}_i$
[1]	$\dfrac{(1-R_1)W_c}{(1-\omega)T}$	$(1-\omega)T$	$\dfrac{(R_1-\varrho)W_c}{(1-\omega)T}\dot{V}$
[2]	$\dfrac{(1-\omega)T}{(R_1-\varrho)W_c}$	$(R_1-\varrho)T$	$\dot{V}$
[3]	$\dfrac{\omega T}{(R_2+\varrho-1)W_c}$	$(R_2+\varrho-1)W_c$	$\dot{V}$
[4]	$\dfrac{(1-R_2)W_c}{\omega T}$	ωT	$\dfrac{(R_2+\varrho-1)W_c}{\omega T}\dot{V}$

that no positive extrusion of material is done from the narrower orifice. At the narrower orifice, then, the speed of flow relative to the die or punch is $\dot{V}$. When both a_1 and a_3 are greater than unity, the conclusion obtained for the case of $R_1 = R_2$ also holds, since $e_1 = e_3$, from Table 1, Part 1, and because of cavity formation.

In Fig. 24 are illustrated the upper bounds for the mean working pressure with smooth tools by a solid line. The dotted line curves represent the upper bounds for the corresponding normal extrusion-forgings. When $R_1 = R_2 = 0{\cdot}9$, $R_1 = R_2 = 0{\cdot}75$ and $R_1 = 0{\cdot}8$, $R_2 = 0{\cdot}7$, the velocity field of type (a), Fig. 23, gave the best upper bound between the solid circle (the transition point between steadv and non-steady stage) and the cross. For T/W_c smaller than that represented by the cross, the

type (b) and then (c) yields the best results. For $R_1 = 0{\cdot}85$ and $R_2 = 0{\cdot}95$, however, the type (a) was never the most suitable velocity field; the hollow circle and triangle indicate the cavity formation points.

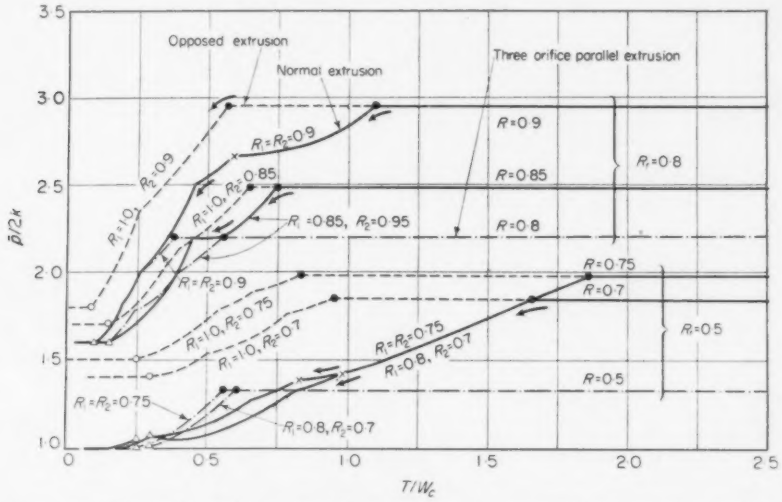

FIG. 24. Upper bounds for working pressure in opposed extrusion-piercing-forging, and three-orifice parallel extrusion-forging with smooth tools.

When the difference between R_1 and R_2 is very large, it will also be possible that the velocity field of type (d), Fig. 23, in which no outward flow takes place at the narrower orifice, gives a better upper bound.

When the dies are rough, the upper bound can be obtained with the

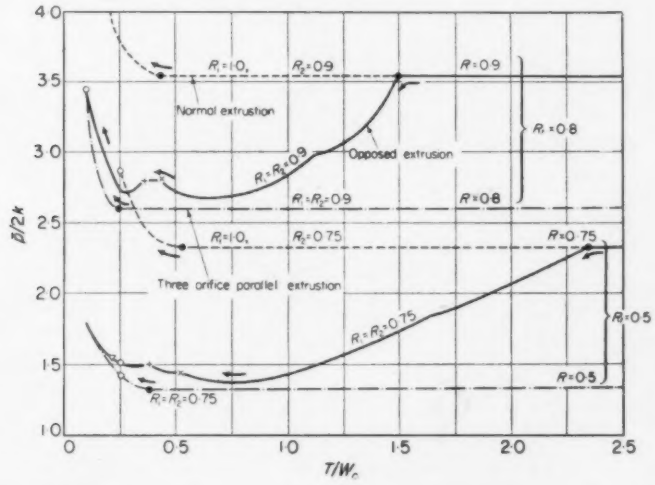

FIG. 25. Upper bounds for mean working pressure in opposed extrusion-piercing-forging, and three-orifice extrusion-forging, with rough dies and smooth container.

use of velocity fields shown in Fig. 23(e) and (f). In Fig. 25, however, only results for $R_1 = R_2$ and a smooth container are given. For this case, the position of the neutral plane $\varrho \overline{W}_c$ should be $0{\cdot}5\,W_c$ different from the case of smooth tools. In Fig. 25, the most suitable velocity fields for $R_1 = R_2 = 0{\cdot}90$ were the type (a), Fig. 23, between the solid circle and the cross, the type (f) between the crosses and the plus, and the type (e) for values of T/W_c smaller than that represented by the plus. When $R_1 = R_2 = 0{\cdot}75$, type (a) lies between the solid circle and the cross; the type analogous to (b) lies between the crosses and the pluses, and type (f) between the pluses and the triangle; the type (e) lies below the triangle.

The broken line curves in the figure indicate the upper bounds for the extrusion-forging, in which one of the orifices is closed. From Figs. 24 and 25 the marked pressure reducing effect of the second orifice added to the first orifice is seen.

Another type of combined extrusion-forging problem is that in which three orifices are provided in the top die, (symmetrical with respect to the axis of extrusion) the bottom die being flat and having no orifice (Fig. 26). The upper bounds obtained are shown in Figs. 24 and 25.

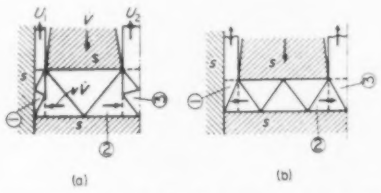

FIG. 26. The most suitable velocity fields in three-orifice extrusion-forging.

CLOSED-DIE COINING

An attempt is now made to treat approximately the process of "edging" associated with closed die coining: see Figs. 27 and 28. It is the final stage of closed-die coining and usually serves to form sharp edges on pre-forged parts.

Firstly, the simple case shown in Fig. 27 will be considered, being the final stage of upsetting in a closed die. If the horizontal non-contiguous length C_1 at the edge is large as compared with the vertical non-contiguous length C_2 and if it is very small compared with the width of the container W_c, the most suitable velocity field already obtained for constrained indentation, Fig. 31, Part 1, or the piercing problem Figs. 1(b) and 11(b) with a punch having a width $2(W_c - C_1)$, can be considered as giving a good upper bound for the present problem, Fig. 27(a).

On the other hand, when $C_2 > C_1$, the velocity field adopted for the heading process, Fig. 18, Part I, will be suitable if C_2 is regarded as the height of the unsupported part of the work-piece, Fig. 27(b). As was

seen from Fig. 10, the upper bounds for piercing (or extrusion) and heading were approximately equal for a given reduction. From this it follows that the edging pressure for deep rectangular work-pieces depends mainly on the frictional condition of the tool and the ratios C_1/W_c and C_2/W_c. This holds also for work-pieces having a small height–width ratio.

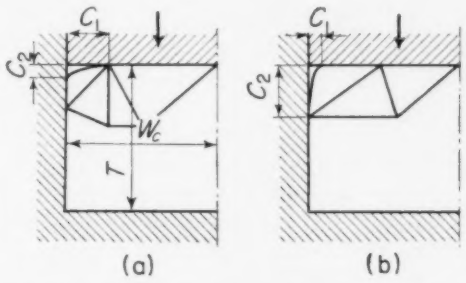

FIG. 27. Coining with flat, smooth closed-dies.

In practice, the non-contiguous lengths C_1' and C_2'' or C_2' and C_2''' at the left and right corners are usually not equal, i. e. the process is not symmetrical with respect to the centre axis. According to the discussion stated above concerning unsymmetrical piercing, Fig. 6, the upper bound for such an unsymmetrical edging process is seen to be given, approximately, by that for the corresponding stationary extrusion pressure with the reduction ratio $\{1-(C_1'+C_1'')/2W_c\}$ or $\{1-(C_2'+C_2'')/2W_c\}$, when the work-piece is deep.

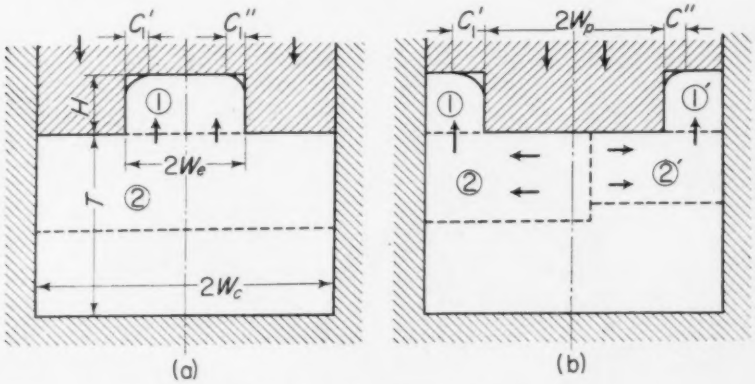

FIG. 28. Coining with recessed closed-dies.

A coining process in which the die contains a cavity, Fig. 28, may be treated similarly by dividing the work-piece into two unit extrusion regions [1] and [2]. From the discussion above concerning stepped extrusions, Fig. 8, it will be seen that the upper bound for the coining pres-

Vol. 1
1960

sure is again not much higher than that for the corresponding extrusion process with the reduction ratio $\{1-(C_1'+C_1'')/2W_c\}$ or $\{1-(C_2'+C_2'')/2W_c\}$.

The necessary pressure to fill all corners to within a given maximum allowable non-contiguous length is least when $C_1' = C_1''$ or $C_2' = C_2''$. Alternatively, the edging pressure is least when all corners are filled simultaneously.

REFERENCES

1. H. KUDO, *Int. J. Mech. Sci.* **1**, 57 (1959).
2. R. HILL, *J. Iron St. Inst.* **158**, 177 (1948).
3. W. JOHNSON, *J. Mech. Phys. Solids* **4**, 191 (1956).
4. W. JOHNSON, *J. Mech. Phys. Solids* **5**, 202 (1957).
5. A. P. GREEN, *J. Mech. Phys. Solids* **3**, 189 (1955).
6. L. C. DODEJA and W. JOHNSON, *J. Mech. Phys. Solids* **5**, 267 (1957).
7. W. JOHNSON, P. B. MELLOR and D. M. WOO, *J. Mech. Phys. Solids* **6**, 203 (1958).
8. J. WANG, *Chin. J. Mech.* **1**, 95 (1957).
9. S. FUKUI, H. KUDO and T. SEINO, *Rep. Inst. Sci., Tokyo* **11**, 91 (1957).
10. W. JOHNSON, *Appl. Sci. Res., Hague* **8** A, 228 (1959).
11. T. M. CHANG, *MERL Plasticity Report No.* 54 (1951).
12. M. T. WATKINS, K. ASHCROFT and J. MCKENZIE, *Proc. Inst. Mech. Engrs., Lond.* Preprint (1958).
13. W. JOHNSON, *Appl. Sci. Res., Hague* **8** A, 52 (1959).

Vol. 1
1960

Int. J. Mech. Sci. Pergamon Press Ltd. 1960. Vol. 1. pp. 253–281. Printed in Poland

Vol. 1
1960

WAVE ACTION IN THE EXHAUST SYSTEM OF A SUPERCHARGED TWO-STROKE-ENGINE MODEL

R. S. BENSON * and W. A. WOODS †

(*Received* 9 *April* 1959)

Summary — The paper describes a theoretical and experimental investigation of wave action in a supercharged two-stroke-engine model. The theoretical analysis, by the method of characteristics, showed that for an infinite pipe the basic wave form consisted of two pulses, one due to the exhaust blowdown and the other due to the supercharge air. For a finite pipe the wave form was dependent on the fixings at the open end. The theory and the experiments showed that in a pipe with a plain open end the infinite pipe wave form was superseded by strong wave action with residual waves. With a nozzle at the open end the wave action was damped out, the residual waves were suppressed and the infinite pipe basic wave form was observed with some modifications due to reflected waves from the nozzle end.

A study of the boundary conditions at the pipe ends showed that the flow into the pipe under unsteady conditions was different from the flow under steady conditions. At the outlet end the flow under steady and unsteady conditions was approximately the same.

INTRODUCTION

IN SUPERCHARGED engines it is desirable to utilize the maximum energy available in the exhaust gases to drive the turbo-charger. For this purpose wave action in the exhaust pipe should be controlled in order that the energy content of the pressure waves can be usefully converted into kinetic energy at the turbine nozzle. In a two-stroke-cycle engine the problem of wave action in the exhaust pipe is important if the scavenging and charging processes are to be efficiently performed. With the possibility of high-pressure charging of engines in the near future an investigation was carried out to study the pressure wave phenomenon in the exhaust pipe of a two-stroke-cycle engine operating under these conditions.

The analytical methods used in the paper are based on the methods of characteristics. Since this subject has been extensively discussed, only the basic formulae and the corresponding boundary equations are given in the paper.

* Department of Mechanical Engineering, University of Liverpool.
† Rolls Royce Ltd., Derby.
Formerly Munitions Committee Fellow, University of Liverpool.

APPARATUS

A special exhaust-pulse generator was constructed to simulate the cycle of events in a high-pressure-charged two-stroke-cycle engine (Fig. 1).

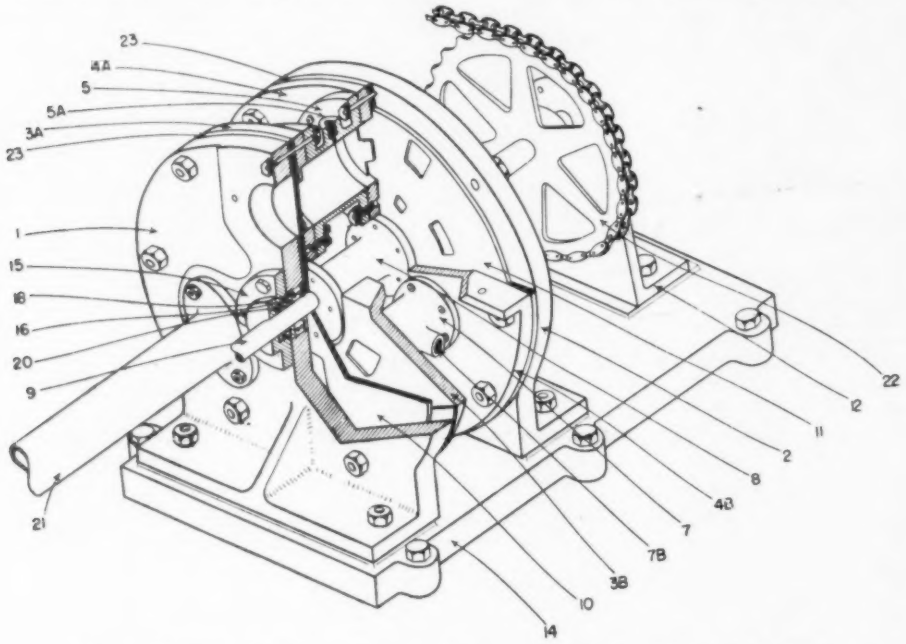

Fig. 1. Exhaust pulse generator. 1. Exhaust end plate. 2. Inlet end plate. 3A. Exhaust annular plate top. 3B. Exhaust annular plate bottom. 4A. Inlet annular plate top. 4B. Inlet annular plate bottom. 5. Large cylinder (3 in. dia.). 5A. Indicator boss. 6. Medium cylinder (2·55 in. dia.). 7. Small cylinder (2 in. dia.). 7B. Indicator boss. 8. Hub. 9. Shaft. 10. Exhaust shutter. 11. Inlet shutter. 12. Bearing bracket. 13. Bearing housing. 14. Bed plate. 15. Thrust-bearing housing. 16. Thrust washer. 17. Inlet-bearing retaining plate. 18. Exhaust-end bearing. 19. Inlet-end bearing. 20. Thrust bearing. 21. Exhaust pipe. 22. Chain wheel 23. Spacer.

Three cylinders of different internal diameter were mounted radially between two end plates, into which ports were machined. High-pressure air, to simulate the cylinder gas, and supercharge air were admitted at one end of the cylinder and "exhaust gas" was discharged at the other end. The timing of these operations is shown in Fig. 2. The ports were controlled by slotted rotating shutters so arranged to give a linear port-area–"crank"-angle relationship. One revolution of the shutters corresponded to three working cycles, this was obtained by machining three sets of slots in the shutters. The shutters were driven by an electric motor through a chain drive with a three to one speed reduction. A Farnboro indicator was coupled directly to the motor, thus one revolution of the Farnboro drum corresponded to one working cycle.

Vol. 196

With the above arrangements it was possible to achieve high cycle speeds (engine rev/min) at fairly low shutter speeds. The tests described in this paper are concerned with the small diameter (2 in.) cylinder only.

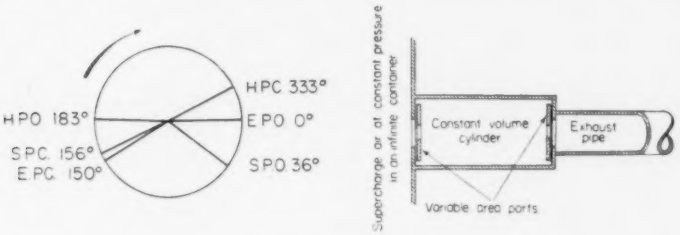

FIG. 2. Cycle of events of equivalent ideal engine.
E. P. O. exhaust port opening.
S. P. O. supercharge air port opening.
H. P. O. high pressure air port opening.
E. P. C. exhaust port closure.
S. P. C. supercharge air port closure.
H. P. C. high-pressure air port closure.

High-pressure air was supplied to the unit from a compressor at pressures up to 100 lb/in² gauge. The supercharge air was taken from the same line at a lower pressure. Fitted in the low-pressure line was a large air receiver located as near to the exhaust-pulse generator as possible, the pressure in the receiver being maintained constant at 15 lb/in² gauge.

Pressure measurements were taken in the cylinder and at several points in the pipe. A modified Farnboro indicator with diaphragm type pressure pick-ups and thyratron relay (HEMPSON and ROACH[1], BENSON[2]) was used for this purpose. Transient gas velocities were measured with a total head pick-up unit (BENSON and WOODS[3]).

The exhaust turbine supercharged system was simulated by fitting a nozzle at the outlet end of the exhaust pipe, similar to JENNY[4]. Several pipe sizes and nozzles were used, and tests were also carried out with plain open-ended pipes. The nozzle profiles were made to B. S. S. 1042: 1943.

NOTATION

General symbols

a = speed of sound
$\bar{a}$ = datum speed of sound
d = pipe diameter
f = D'Arcy friction coefficient
p = pressure
s = entropy
t = time
u = particle velocity
x = co-ordinate of length
c_p = specific heat at constant pressure
F_p = cross-sectional area of exhaust pipe

F_t = effective area of exhaust port
L = pipe length
N = engine speed rev/min
V = volume
W = mass
γ = isentropic index (assumed to be 1·4)
ϱ = density

General suffixes

q = equivalent port
qt = throat of equivalent port
t = throat of exhaust port or throat of nozzle
A = atmospheric
C = cylinder
CO = cylinder stagnation
E = exhaust port
P = in pipe at inlet end or nozzle end
PA = pipe atmospheric
S = supercharge air
SO = supercharge air stagnation

Parameters

$$\varphi = \frac{\text{effective nozzle area}}{\text{pipe cross-sectional area}}$$

$$\Phi_E = \frac{\text{effective exhaust-port area}}{\text{cylinder cross-sectional area}}$$

$$\Phi_q = \frac{\text{effective equivalent port area}}{\text{cylinder cross-sectional area}}$$

$$\Phi_S = \frac{\text{effective supercharge port area}}{\text{cylinder cross-sectional area}}$$

$$\psi = \frac{\text{effective exhaust-port area}}{\text{pipe cross-sectional area}}$$

$$\psi_q = \frac{\text{effective equivalent port area}}{\text{pipe cross-sectional area}}$$

Characteristic non-dimensional parameters

Isentropic flow

$$A = \frac{a}{a_{PA}} = \left(\frac{p}{p_A}\right)^{1/7}$$

$$U = \frac{u}{a_{PA}}$$

$$X = \frac{x}{L}$$

$$Z = \frac{a_{PA}t}{L}$$

a_{PA} = speed of sound corresponding to isentropic expansion from pipe pressure p to atmospheric pressure p_A. Constant through field of flow.

Non-isentropic flow

$$A = \frac{a}{a_A} = \left(\frac{p}{p_A}\right)^{1/7}$$

$$U = \frac{u}{a_A}$$

$$X = \frac{x}{L}$$

$$Z = \frac{\bar{a}t}{L}$$

a_A = speed of sound corresponding to isentropic expansion from pipe pressure p to atmospheric pressure p_A. Variable through field of flow.

METHOD OF CHARACTERISTICS AND BOUNDARY CONDITIONS

The unsteady flow conditions in the exhaust pipe can be represented by the characteristic equations as given by JENNY[4], BENSON[5] and others, which for isentropic flow are ($\gamma = 1{\cdot}4$)

State equation

$$\frac{dA}{dU} = \frac{d(p/p_A)}{d(u/a_{PA})} = \mp\frac{\gamma-1}{2} = \pm\frac{1}{5}. \tag{1}$$

Position equation

$$\frac{dX}{dZ} = U \mp A \tag{2}$$

$$A = \frac{a}{a_{PA}} = \left(\frac{p}{p_A}\right)^{1/7};\ U = \frac{u}{a_{PA}};\ Z = \frac{a_{PA}t}{L};\ X = \frac{x}{L}.$$

The corresponding equations for unsteady flow with friction are given in Appendix 1.

The pulse generator and pipe system were designed to represent as far as possible a one-dimensional flow system. For this arrangement the sudden-enlargement theory (COLE and MILLS[6]) may be used to establish the boundary conditions at entry to the pipe. The equations relating the pressures in the cylinder and pipe and the particle velocity in the pipe are: ($\gamma = 1{\cdot}4$)

$$\left(\frac{u_P}{a_{CO}}\right)^2 - \frac{5}{6}\left[\frac{1}{\psi}\left(\frac{a_t}{a_{CO}}\right)^2\frac{a_{CO}}{u_t} + \frac{7}{5}\left(\frac{u_t}{a_{CO}}\right)\right]\frac{u_P}{a_{CO}} + \frac{5}{6} = 0, \tag{3}$$

$$\left(\frac{p_P}{p_{CO}}\right)^{1/7} = \left(\frac{a_t}{a_{CO}}\right)^{5/7}\left[\psi\frac{u_t}{a_{CO}}\left(\frac{a_{CO}}{u_P} - \frac{u_P}{5a_{CO}}\right)\right]^{1/7}. \tag{4}$$

Sonic flow in ports

$$\left(\frac{p_P}{p_{CO}}\right)^{1/7} = \left[\psi\left(\frac{5}{6}\right)^3\left(\frac{a_{CO}}{u_P} - \frac{u_P}{5a_{CO}}\right)\right]^{1/7}. \tag{5}$$

For outflow from the pipe with a plain open end the pressure at the end of the pipe equals the outside pressure. For a nozzle the boundary conditions are similar to discharge from a cylinder direct to atmosphere (BENSON[5]). These are for $\gamma = 1{\cdot}4$:

Vol. 1
1960

subsonic flow in nozzle

$$\left(\frac{u_P}{a_{PA}}\right)^2 = \frac{5\left[\left(\frac{a_P}{a_{PA}}\right)^2 - 1\right]}{\left(\frac{a_P}{a_{PA}}\right)^{10} \varphi^{-2} - 1}, \tag{6}$$

sonic flow in nozzle

$$\frac{u_P}{a_{PA}} = \frac{a_P}{a_{PA}} \varphi \left(\frac{a_t}{a_P}\right)^6_{cr}. \tag{7}$$

The ratio $\left(\frac{a_t}{a_P}\right)_{cr}$ corresponds to the critical pressure ratio across the nozzle, i. e. $\left(\frac{a_t}{a_P}\right) = \left(\frac{p_t}{p_P}\right)^{1/7}_{cr}$. This will vary with nozzle size and is given by

$$\varphi^2 = \left(\frac{a_P}{a_t}\right)^{10}_{cr} \left[6 - 5\left(\frac{a_P}{a_t}\right)^2_{cr}\right]. \tag{8}$$

If the change in entropy of a gas particle as it enters the pipe is neglected, and the flow in the pipe is isentropic, a_{PA} corresponds to the speed of sound at atmospheric pressure, following isentropic expansion from the pipe pressure p_P to pressure p_A.

In a two-stroke-cycle engine the gas exchange process is carried out in three phases, namely, exhaust blowdown, scavenging and charging. In the first two phases the exhaust ports are open to the exhaust pipe. In the experiments discussed below these two phases will be referred to as the exhaust blowdown and the supercharging phases. In the exhaust-blowdown phase the cylinder is in communication with the exhaust pipe only and the pressure change in the cylinder can be calculated by equating the mass change in the cylinder with the mass flow through the ports. These are given by:

Mass change in a cylinder of constant volume:

$$\frac{dW_C}{dp_{CO}} = \frac{V_C}{a^2_{CO}}. \tag{9}$$

Mass flow through the ports:

Sonic flow in ports

$$\frac{dW_C}{dt} = -\frac{7}{5} F_t \frac{p_{CO}}{a_{CO}} \left(\frac{5}{6}\right)^3, \tag{10}$$

Subsonic flow in ports

$$\frac{dW_C}{dt} = -\frac{7}{5} F_P \frac{p_P}{a^2_P} u_P. \tag{11}$$

During the supercharge phase both the air ports and exhaust ports are open at the same time. One method of calculating the upstream pressures in the cylinder is to consider both the mass balance and heat

balance equations (JENNY[4], BENSON[7]). An alternative method, used in non-supercharged engine calculations, may be adopted. In this method the supercharge air and exhaust ports are replaced by an equivalent port.

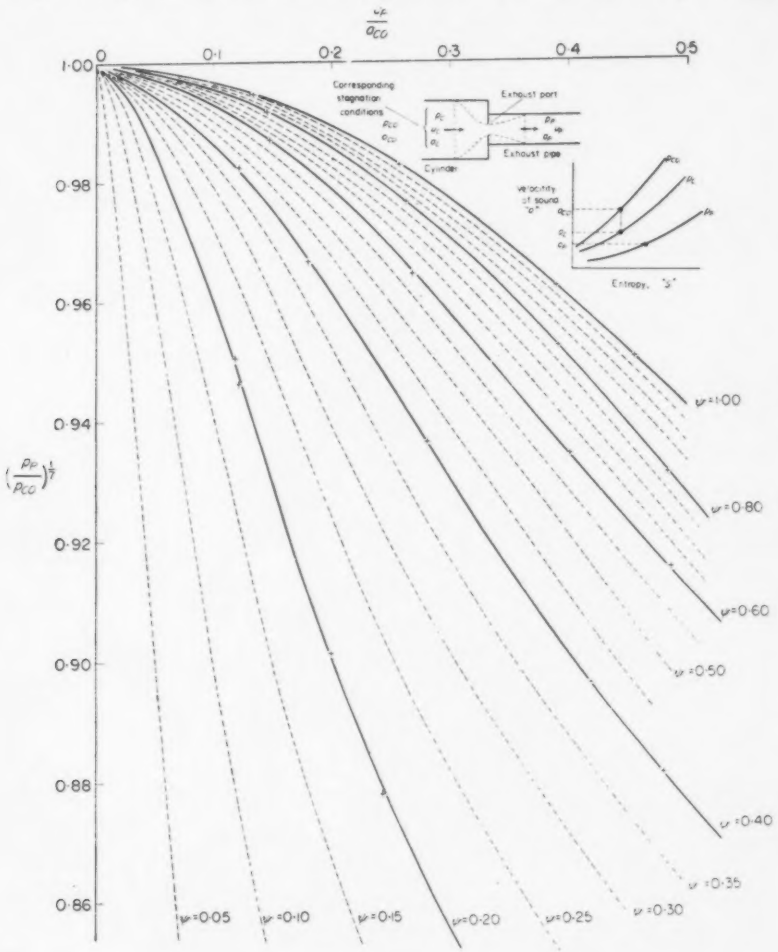

FIG. 3. Boundary chart. Flow into 1 in. diameter pipe (experimental results).

$\psi = \left(\dfrac{\text{geometric area of exhaust port}}{\text{cross-sectional area of exhaust pipe}}\right)$.

p_p = static pressure in exhaust pipe near inlet end.

a_{CO} = speed of sound in cylinder corresponding to stagnation conditions.

p_{CO} = total head pressure in cylinder.

u_p = gas velocity in exhaust pipe near inlet end.

The port area of the equivalent port (called the reduced port area) is calculated by assuming the air and exhaust ports are in series and the flow is at constant density. This method due to HOLD[8] gives the reduced area as

$$\Phi_q = \left(\Phi_E^{-2} + \Phi_S^{-2}\right)^{-1/2} \tag{12}$$

where $\Phi = \dfrac{\text{effective port area}}{\text{cylinder cross-sectional area}}$

suffix S refers to supercharge air port.
E refers to exhaust port.
q refers to equivalent port.

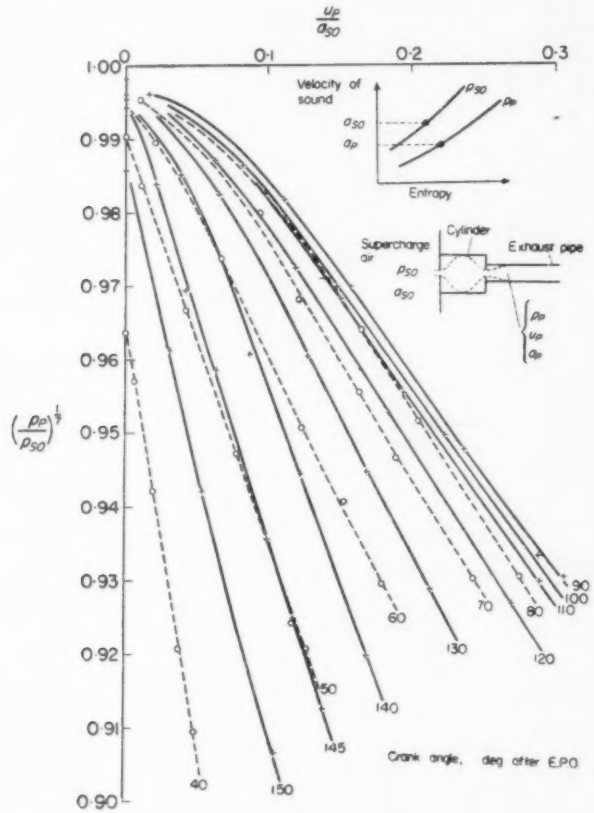

Fig. 4. Boundary curves for supercharge pulse period. Obtained by experiment for flow in 1 in. diameter pipe.

E. P. O. exhaust port opening.

p_P = static pressure in exhaust pipe near inlet end.

p_{SO} = total head pressure of supercharge air.

u_P = gas velocity in exhaust pipe near inlet end.

a_{SO} = speed of sound corresponding to stagnation conditions of supercharge air.

a_P = speed of sound in exhaust pipe near inlet end.

To calculate the pressure conditions at entry to the exhaust pipe it is considered that flow takes place from the supercharge air system directly across the equivalent port to the exhaust pipe. The boundary conditions

are developed assuming the sudden enlargement theory. Equations similar to (3), (4) and (5) can be derived for this case, but $a_{CO}, p_{CO}, u_t, a_t, \psi$ will be replaced by $a_{SO}, p_{SO}, u_{tq}, a_{tq}, \psi_q$, where suffix *so* refers to supercharge air stagnation conditions, *tq* to conditions at the throat of the

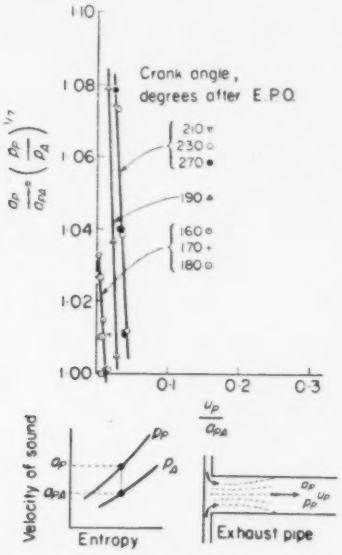

FIG. 5. Leakage boundary curves.

E. P. O. exhaust port opening.

p_P = static pressure in exhaust pipe near inlet end.

p_A = atmospheric pressure.

u_P = gas velocity in exhaust pipe near inlet end.

a_P = velocity of sound in exhaust pipe near inlet end.

a_{PA} = velocity of sound following isentropic expansion from pressure p_P and velocity of sound a_P to atmospheric pressure.

equivalent port and ψ_q is the ratio of the effective area of the equivalent port to the exhaust pipe cross-sectional area.

Characteristic plotting techniques have been described elsewhere (JENNY[4] and BENSON[9]). In practice computations have limited quantitative value unless the effective port areas are known. These may be evaluated under steady or unsteady flow conditions. In order to ascertain whether flow at the pipe ends corresponded to the conditions given above, the boundary curves were established by steady-flow experiments. By using these steady-flow boundary curves the pressure changes in the exhaust pipe were calculated and compared with the measured indicator diagrams. The experimental boundary curves corresponding to flow from the cylinder to the pipe for the 1 in. pipe are given in Fig. 3; the boundary curves for flow from the supercharge air system through the supercharge port and exhaust port into the 1 in. pipe are given in Fig. 4. Since there

was some leakage when both the supercharge air port and exhaust port were closed, the leakage rate was determined and the results plotted in the form of a boundary chart as shown in Fig. 5. The nozzle boundary curves obtained from equations (6) and (7) are given in Fig. 6.

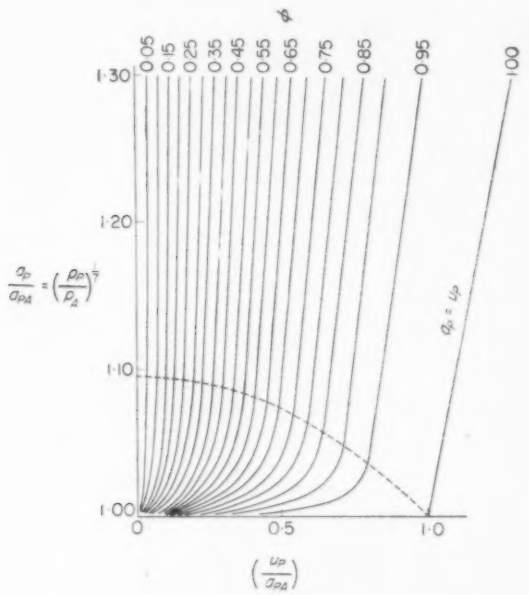

Fig. 6. Theoretical outflow boundary chart.

φ = $\left(\frac{\text{effective area of nozzle throat}}{\text{cross-sectional area of exhaust pipe}}\right)$.

u_P = gas velocity in exhaust pipe near nozzle.

a_P = velocity of sound in pipe near nozzle.

a_{PA} = velocity of sound following isentropic expansion from pressure p_P and velocity of sound a_P to atmospheric pressure.

p_P = static pressure in exhaust pipe near nozzle.

p_A = atmospheric pressure.

WAVE ACTION IN THE EXHAUST PIPE UNDER SUPERCHARGE CONDITIONS

It is not possible to obtain generalized solutions by the method of characteristics, since the method is essentially numerical. In order to discuss the flow development in a general manner unit processes can be used. By a combination of numerical solutions and unit processes it is possible to examine theoretically the wave development in the pipe. In this section, flow into an infinite pipe will be discussed, then the effect of the end fixings at the open end will be examined.

Infinite pipe

A number of calculations were carried out with the experimental

boundary curves to establish the fundamental wave form in the exhaust pipe without wave reflection. A typical result is shown in Fig. 7. It will be seen that there are two pronounced pulse forms in the pipe. The first is due to the exhaust blowdown and the second due to the supercharge air.

Finite pipe

With a finite pipe the reflected waves will influence the pressure development in the exhaust pipe. Space precludes a numerical examination in detail of the effect of the reflected waves on the pulse forms shown

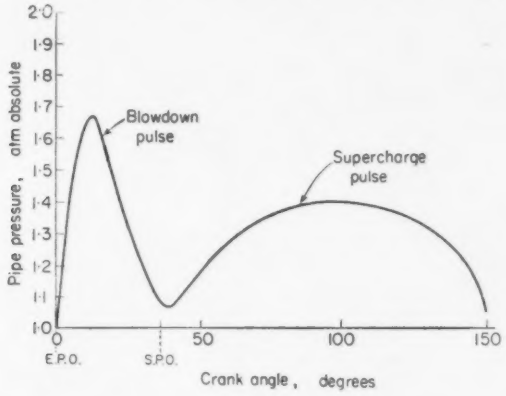

FIG. 7. Theoretical indicator diagram.
E. P. O. exhaust port opening.
S. P. O. supercharge air port opening.

in Fig. 7. It is possible however to examine the wave action in the pipe by considering the effect of the end fixings on a simple wave propagated along the pipe. In Fig. 8 the passage of an incident wave 01 up and down the pipe is considered. For the sake of simplicity it is assumed that on arrival back at the inlet end the port is closed. In the case of the plain open end the "Borda tube" effect for return flow is neglected.* It will be clearly seen that with a plain open end a strong "standing" wave system is established. Depending on the length of the pipe the pressure at the commencement of each working cycle may be greater or less than atmospheric. The persistance of these waves in the pipe after one working cycle causes the formation of residual waves. It will take a number of cycles before equilibrium conditions are established.

By fitting a nozzle at the end of the pipe the wave action is damped down, the pressure in the pipe drops and for short pipes no residual waves will be present at the commencement of a subsequent exhaust cycle.

* The "Borda effect" produces a drop in pressure at the closed end after each wave reflection at the open end. This "secondary damping" effect is, however, small compared with nozzle damping, except for large nozzle-area—pipe-area ratios.

Vol. 1
1960

From the practical view point the damping action of the nozzle simplifies characteristic calculations since only one cycle need be calculated to establish the pressure changes in the pipe.

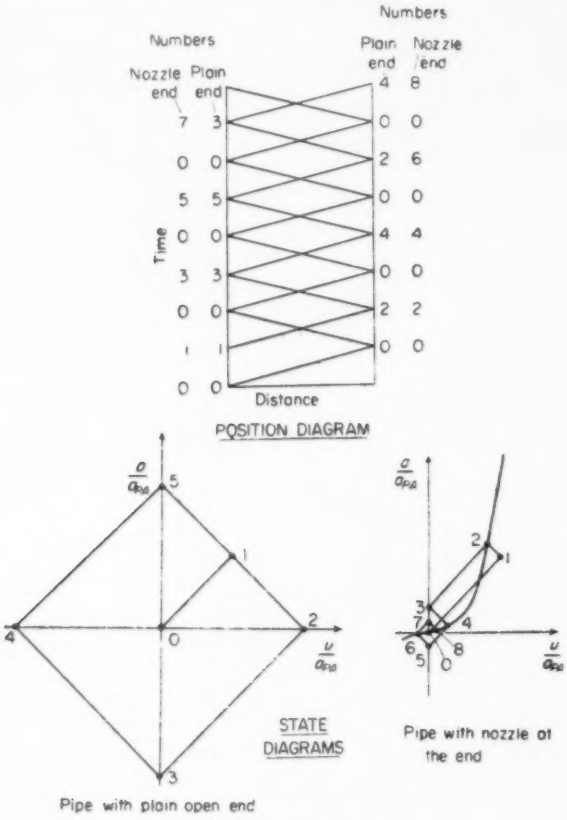

FIG. 8. Illustration of the wave damping effect caused by fitting a nozzle to a pipe.

a = velocity of sound in exhaust pipe.
u = gas velocity in exhaust pipe.
a_{PA} = velocity of sound in exhaust pipe following isentropic expansion to atmospheric pressure.

In the above example the port is considered to be closed when the reflected wave arrives at the inlet end. In the practical case the port be open when the first reflected wave arrives at the inlet end. The magnitude of the reflected wave will influence the pressure at the inlet end of the pipe. The effect of the nozzle size on the magnitude of the pressure at the inlet end of the pipe is illustrated in Fig. 9. We will neglect here the variation in time of arrival of the reflected wave and we will assume that the port area and cylinder pressure are the same for each size nozzle when the reflected wave arrives at the inlet end. The boundary curve

corresponding to a given port area (ψ) and cylinder pressure is shown by a dotted line on the state diagram. Once again a simple incident wave 01 is examined. The wave point 1 is reflected at the nozzle end at 3 and

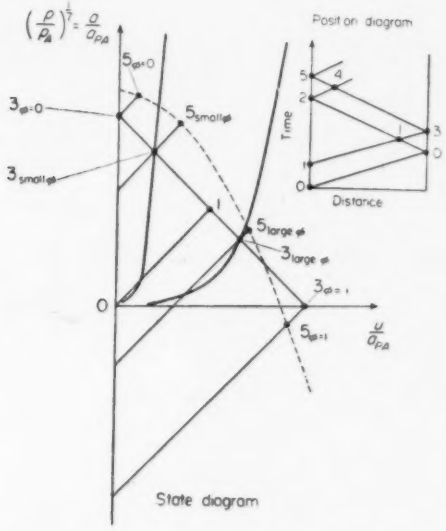

FIG. 9. Effect of nozzle size on amplitude of subsequent pulse.

φ = $\left(\dfrac{\text{effective area of nozzle throat}}{\text{cross-sectional area of exhaust pipe}}\right)$.

p = static pressure in exhaust pipe.

p_A = atmospheric pressure.

a = velocity of sound in exhaust pipe.

a_{PA} = velocity of sound in exhaust pipe following isentropic expansion to atmospheric pressure.

u = gas velocity in exhaust pipe.

arrives at the inlet end at 5. The value of $A\{=(p/p_A)^{1/7}\}$ at 5 increases as the nozzle size is reduced from a plain open end ($\varphi = 1$) to a closed end ($\varphi = 0$).

The magnitude of the reflected wave will depend on the pressure of the incident waves as well as the nozzle area. This will be seen in Fig. 10. It will be observed that as the magnitude of the incident wave increases so the pressure of the subsequent wave at the inlet end increases. Although in general a compression wave will be reflected as a compression wave at the nozzle, for low incident pressures there might be reflected expansion waves; this will be noted in Fig. 10. for the point 1*B*.

These general features illustrate the complexity of the wave action. By utilizing these simple unit processes it is possible to obtain a general conception of the wave action and hence to interpret the results obtained in the experiments described in the next section.

Vol. 1
1960

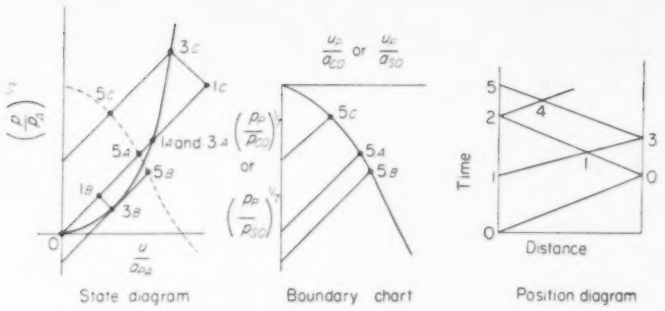

Fig. 10. Effect of incident-pulse amplitude on amplitude of subsequent pulse.

p = static pressure in exhaust pipe.
p_P = static pressure in exhaust pipe near inlet end.
p_A = atmospheric pressure.
p_{CO} = total head pressure in cylinder.
p_{SO} = total head pressure of supercharge air.
u = gas velocity in exhaust pipe.
u_P = gas velocity in exhaust pipe near inlet end.
a_{PA} = velocity of sound in exhaust pipe following isentropic expansion to atmospheric pressure.
a_{CO} = velocity of sound in cylinder corresponding to stagnation conditions.
a_{SO} = velocity of sound corresponding to stagnation conditions of supercharge air.

EXPERIMENTAL INVESTIGATION

The experimental investigation consisted of three parts:

1. Steady-flow tests to establish the boundary conditions at entry to the pipe and the nozzle end.

2. A detailed analysis of the pressure changes in the pipe and cylinder.

Table 1. Test group numbering (Each number represents a series of three tests at nominal release pressures of 50, 40, 30, lb/in² gauge)

Nozzle details	Speed (rev/min)	Pipe length 40 in.			Pipe length 120 in.		
		$d = 1$ in.	$d = 1\frac{1}{2}$ in.	$d = 2$ in.	$d = 1$ in.	$d = 1\frac{1}{2}$ in.	$d = 2$ in.
Nozzle ratio φ = 0·563 for $d = 1$ in., 0·34 for $d = 1\frac{1}{2}$ in., 0·191 for $d = 2$ in.	750	1	13	25	37	49	61
	1000	2	14	26	38	50	62
	1250	3	15	27	39	51	63
	1500	4	16	28	40	52	64
Nozzle ratio φ = ·25	750	5	17	29	41	53	65
	1000	6	18	30	42	54	66
	1250	7	19	31	43	55	67
	1500	8	20	32	44	56	68
No nozzle	750	9	21	33	45	57	69
	1000	10	22	34	46	58	70
	1250	11	23	35	47	59	71
	1500	12	24	36	48	60	72

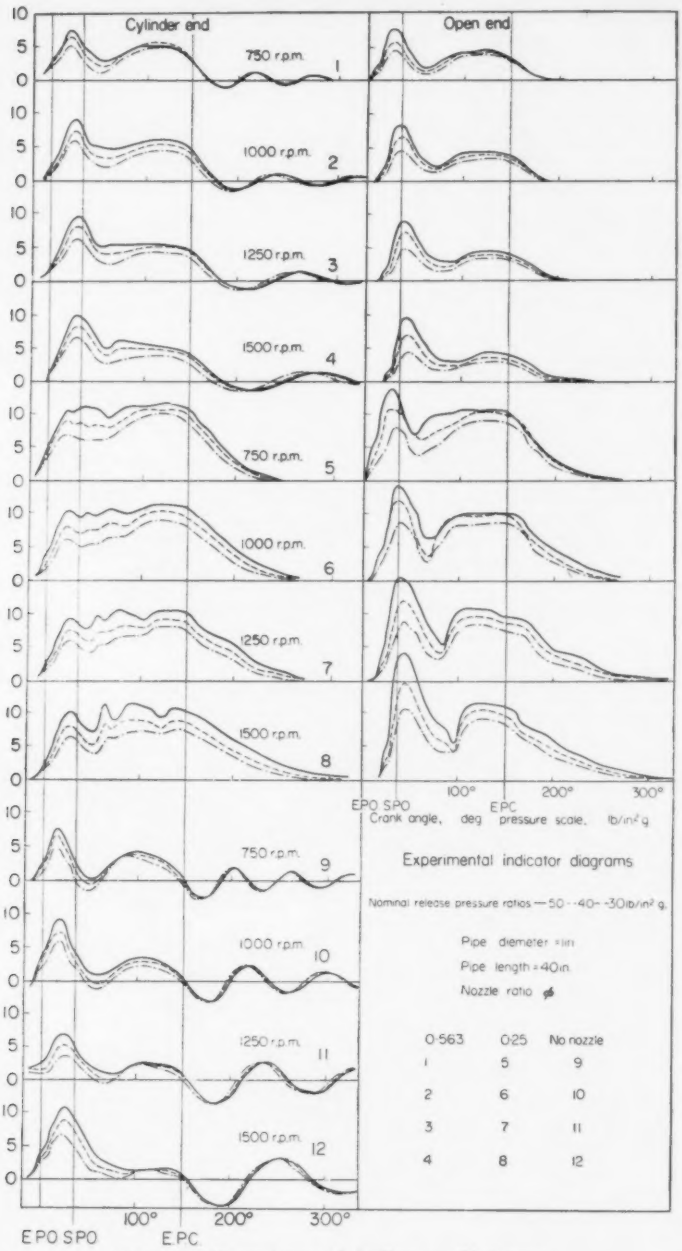

FIG. 11. Experimental indicator diagrams.
E. P. O. exhaust-port opening.
S. P. O. supercharge air port opening.
E. P. C. exhaust-port closure.

$$\varphi = \left(\frac{\text{geometric area of nozzle throat}}{\text{cross-sectional area of exhaust pipe}}\right).$$

3. A systematic investigation of the wave action in the exhaust pipe at various speeds, release pressures, with pipes of different diameter and length and nozzles of various sizes. A constant supercharge pressure of 15 lb/in² gauge was maintained in all these tests. A summary of the test programme is given in Table 1 and the pipe indicator diagrams are shown in Figs. 11–14.

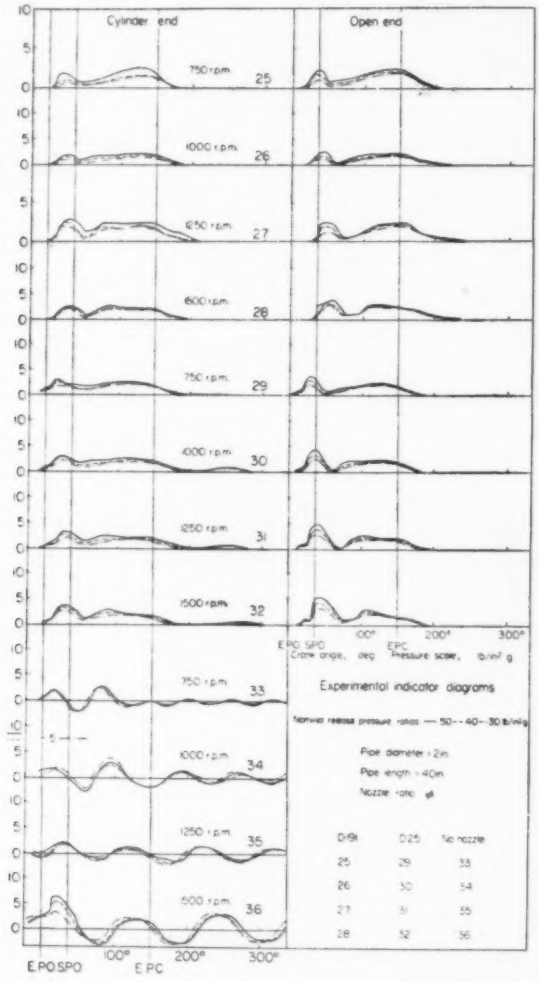

Fig. 12. Experimental indicator diagrams.

E. P. O. exhaust-port opening.

S. P. O. supercharge air port opening.

E. P. C. exhaust-port closure.

$$\varphi = \left(\frac{\text{geometric area of nozzle throat}}{\text{cross-sectional area of exhaust pipe}} \right).$$

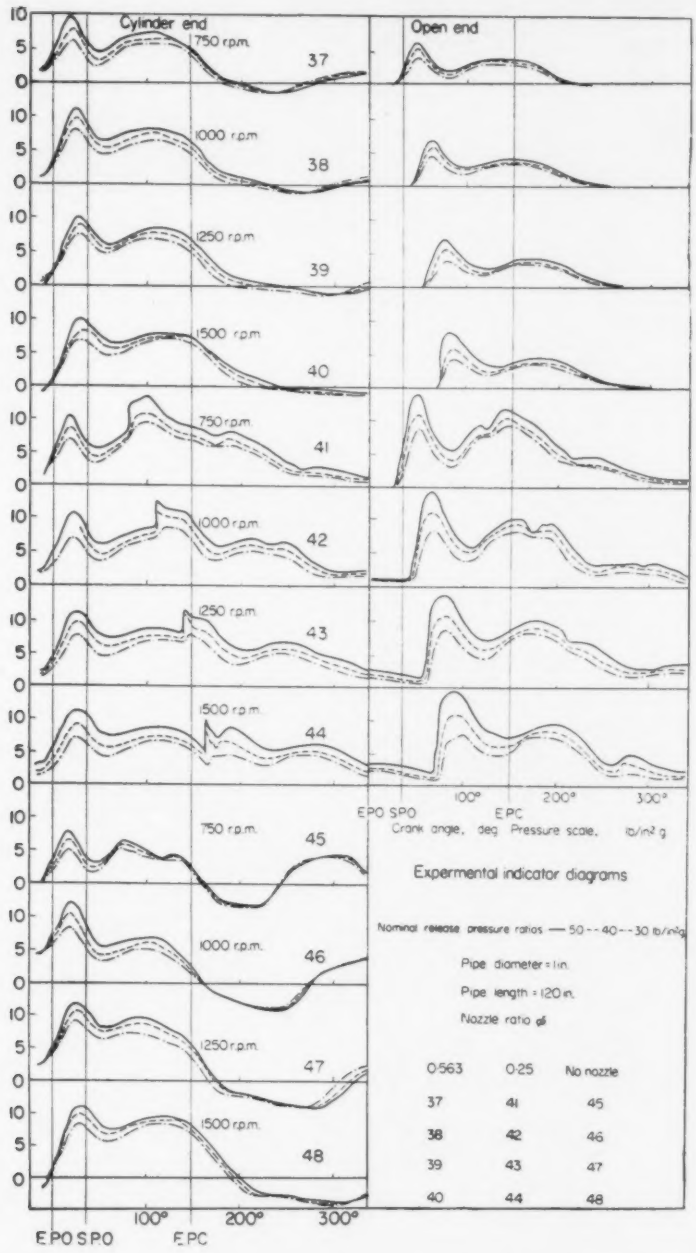

FIG. 13. Experimental indicator diagrams.
E. P. O. exhaust-port opening.
S. P. O. supercharge air port opening.
E. P. C. exhaust-port closure.

$$\varphi = \left(\frac{\text{geometric area of nozzle throat}}{\text{cross-sectional area of exhaust pipe}} \right).$$

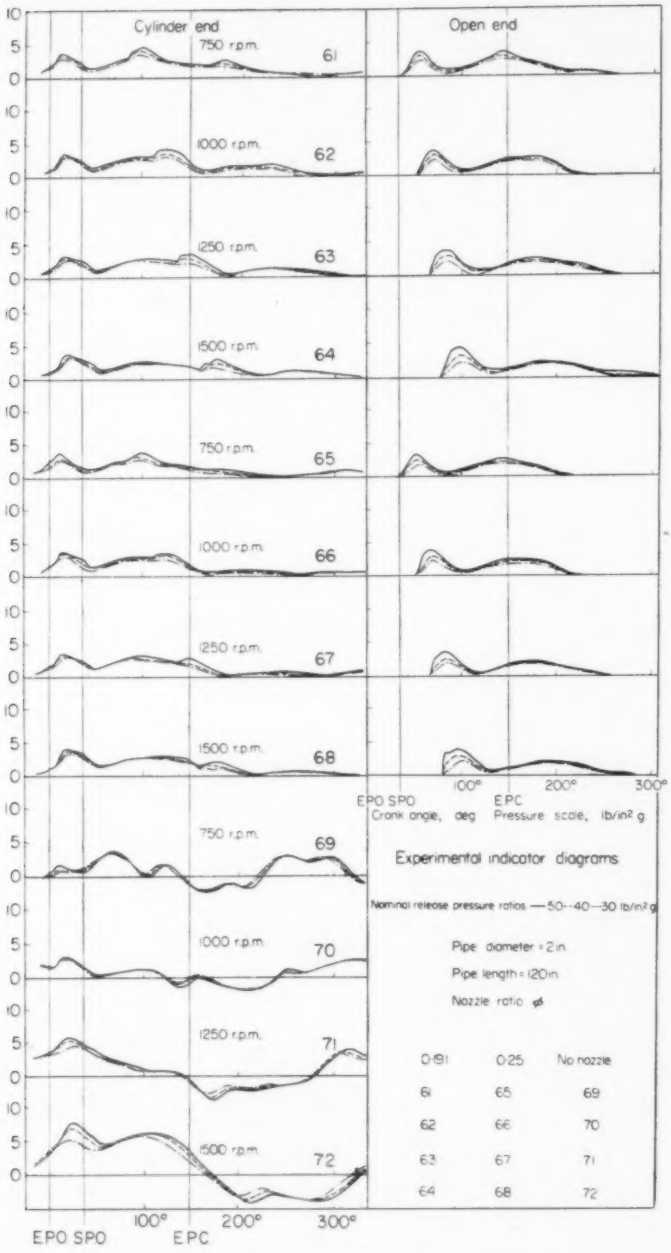

FIG. 14. Experimental indicator diagrams.
E. P. O. exhaust-port opening.
S. P. O. supercharge air port opening.
E. P. C. exhaust-port closure.

$$\varphi = \left(\frac{\text{geometric area of nozzle throat}}{\text{cross-sectional area of exhaust pipe}}\right).$$

COMPARISON OF CHARACTERISTIC CALCULATION AND MEASURED PRESSURE IN THE EXHAUST PIPE

The results of the characteristic calculations based on the steady-flow boundary curves (Figs. 3–5) are shown in Figs. 15 together with the measured diagrams. It will be seen that although there is fair agreement as regards

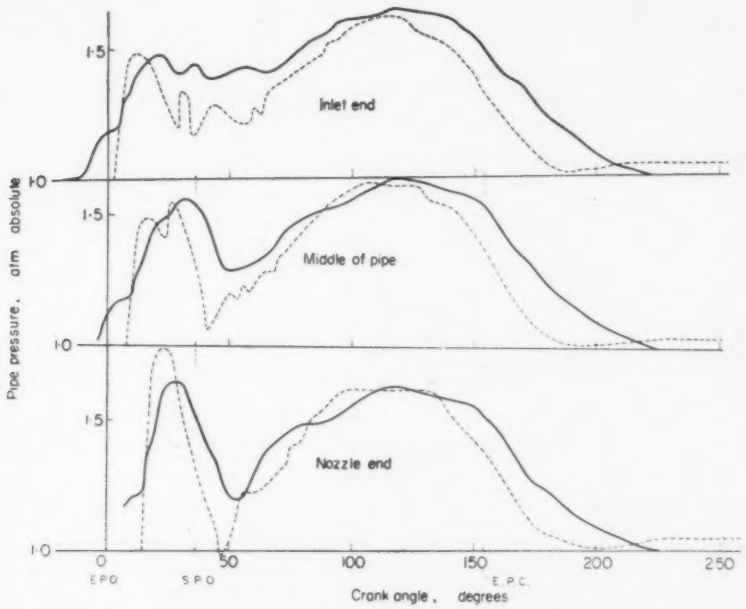

FIG. 15. Measured and calculated indicator diagrams. I.
E. P. O. exhaust-port opening.
S. P. O. supercharge air port opening.
E. P. C. exhaust-port closure.
—— measured diagram.
- - - - calculated diagram.

the trends in the curves the results are not as good as might be expected. Although friction effects will contribute to some of the differences between measured and calculated diagrams the major difference is due to the assumptions associated with the steady-flow boundary curves.

In the steady-flow experiments it was observed that the location of the point of pressure recovery varied (i) with the ratio of the port area to pipe area and (ii) with the upstream pressure. The well-known "ejector" action was observed immediately downstream of the ports and the pressure at this point was well below atmospheric pressure for small port openings. In the unsteady flow test no sub-atmospheric pressures were measured at the same position. It was evident that the flow at the pipe entry was different under unsteady conditions from that under steady conditions. This was clearly illustrated by a simple experiment performed in a shallow

water tank (Fig. 16). This experiment indicated that when unsteady flow was initiated through a sudden enlargement, a hemi-spherical wave was propagated from the smaller pipe. The pressure wave rapidly filled the enlargement and a short distance downstream a plane wave was formed.

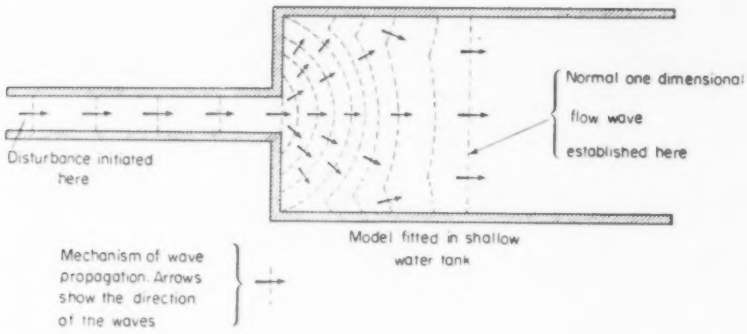

Fig. 16. Two-dimensional shallow water wave analogy for a sudden enlargement.

It would appear from this experiment that the recovery zone was shortened under unsteady flow conditions.

For outflow through the nozzle at the open end the transient total head pressure was measured with an impact tube located just downstream of the nozzle. The impact tube was calibrated under steady-flow conditions. By assuming steady flow between a plane just upstream of the nozzle and the impact tube a comparison was made between the measured total head downstream of the nozzle and the total head calculated from the indicator diagram taken upstream of the nozzle, (Benson and Woods[3]), using the nozzle steady-flow boundary curves. The results are shown in Fig. 17. It will be seen that the assumption of steady flow across the nozzle is reasonable.

On the basis of the above tests further calculations were made using the indicator diagram at the cylinder end of the pipe to obtain the boundary conditions at the pipe entry. The steady-flow boundary curves were used for the open end. The results of these calculations are shown in Fig. 18 where both the measured and calculated pressures are shown for the mid-point in the pipe.

From this analysis we may conclude that the conditions at pipe entry are different under steady flow from those under unsteady flow. At the pipe outlet the nozzle boundary curves for steady flow give good agreement with the unsteady-flow measurements. This latter conclusion confirms experiments by Benson[10] where it was shown that for large pipe-length/diameter ratios the steady-and unsteady-flow coefficients of discharge are very close.

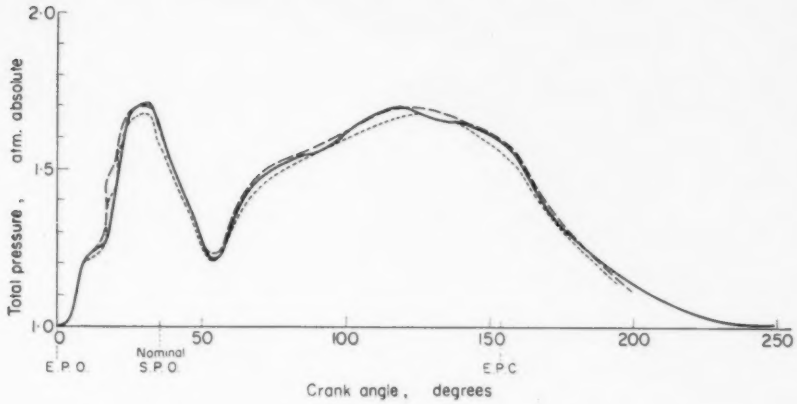

FIG. 17. Total head pressure indicator diagrams at nozzle outlet.
E. P. O. exhaust-port opening.
S. P. O. supercharge air port opening.
E. P. C. exhaust-port closure.
(a) ——— Diagram measured with "total head pressure unit apparatus". (b) – – – Diagram calculated from an indicator diagram taken in exhaust pipe upstream of nozzle. (c) — — Diagram calculated from the indicator diagram used in (b) together with an allowance for blockage caused by the "total head pressure unit apparatus".

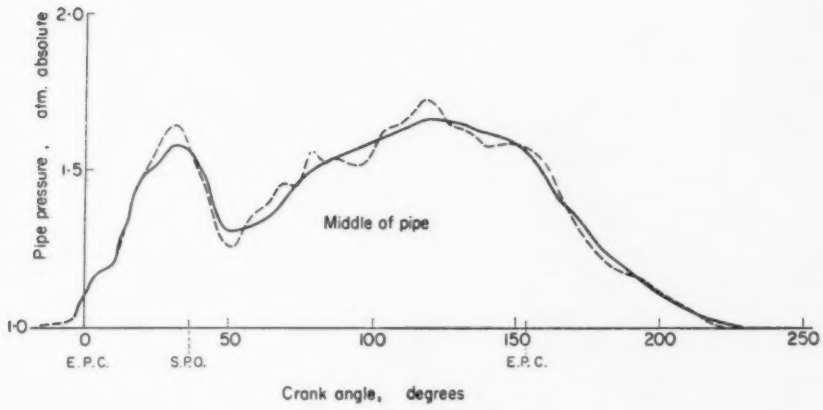

FIG. 18. Measured and calculated indicator diagrams. II.
E. P. O. Exhaust-port opening.
S. P. O. Supercharge air port opening.
E. P. C. Exhaust-port closure.
—— Measured diagram.
- - - - Diagram calculated using measured diagram at the cylinder end for boundary conditions.

Vol. 1
1960

DISCUSSION OF RESULTS

Inspection of the pipe indicator diagrams, Figs. 11–14, shows two characteristic wave forms in the exhaust pipe. One wave pattern is associated with the plain open-ended pipe and the other with a partially open-ended pipe (i. e. nozzle). The strong wave action in the pipe with a plain open end is clearly seen. The influence of the residual waves on the pressure development in the pipe is illustrated qualitatively in Fig. 19. In this figure the results of the plain open-end tests at different speeds are combined together. The shaded area shows

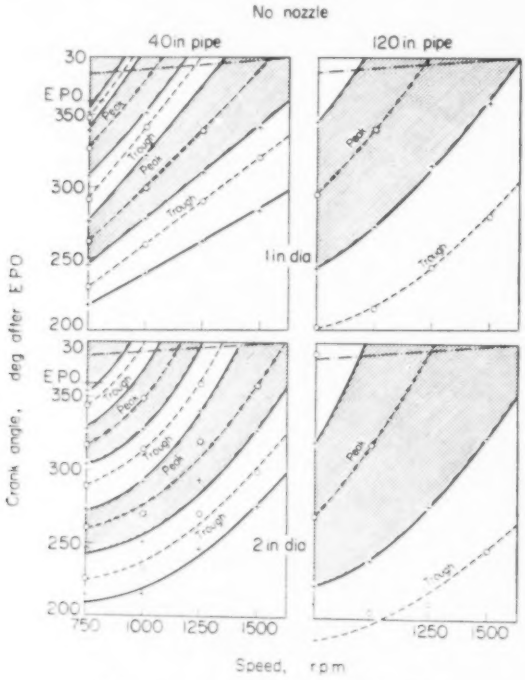

Fig. 19. Residual wave diagrams.

E. P. O. Exhaust port opening.
– – – Locus of pulse peaks and troughs.
——— Locus of atmospheric pressure.
· – · – Approximate locus of the peak of blowdown pulse under conditions of no residual and no reflected waves.
The shaded areas represent positive pressure pulses.

the positive pressures and the plain area the negative pressures. The peaks and troughs are shown as broken lines. A vertical line will give the qualitative pressure distribution at any one speed. On the same diagram the point of maximum blowdown pulse pressure without open-end reflection is shown by a chain dotted line. If this peak coincides with a positive residual wave the blowdown pulse will increase in amplitude; if it is asso-

ciated with a negative residual wave it decreases in amplitude. An arrow shows a typical result at 1250 rev/min in the 1 in. × 40 in. pipe in which the peak pressure was lower at 1250 rev/min than at 1000 rev/min.

The basic effects of a plain open end on the wave action are given in Table 2.

TABLE 2. GENERAL EFFECTS OF A PLAIN OPEN-ENDED PIPE

Variable increase	Respondent	
	Increase	Decrease
Release pressure	Wave-action amplitude	Angular wave travel time (slight)
Speed	Wave-action timing, amplitude and wave length.	
Pipe length	Wave-action timing and wave length.	
Pipe diameter	Prominence of superimposed secondary waves.	Wave-action amplitude.

Vol. 1
1960

By fitting a nozzle at the open end the residual waves are suppressed even when high supercharge air pressures are used. The conditions in the pipe at the commencement of exhaust blowdown are quasi-steady. Hence, except for very long pipes, the assumption of zero particle velocity before discharge may be used. Since the residual waves are suppressed the wave profile is similar to that given for the infinite pipe although the magnitudes of the pressure pulses will depend on the reflected wave effects.

The basic wave-action effects of a system with a nozzle fitted at the pipe outlet are given in Table 3.

TABLE 3. GENERAL EFFECTS OF A PIPE WITH NOZZLE AT OUTLET END

Variable increase	Respondent	
	Increase	Decrease
Release pressure	Pulse pressure	Angular wave travel time (slight)
Speed	Pulse pressures and angular wave travel time	
Pipe length	Angular wave travel time	Pulse amplitude at the nozzle.
$\frac{\text{Nozzle area}}{\text{Pipe area}} = \varphi$		Pulse amplitude at nozzle end.

The effects referred to in Tables 2 and 3 can be predicted by the use of unit processes in characteristic calculations as pointed out earlier in the paper.

Pipe friction

In the theoretical discussion pipe friction was neglected. The effect of pipe friction is to produce a train of diffusion waves running in the opposite direction to the primary wave. Calculations were made of the effect of friction on the pressure at the nozzle end. The friction factor for the pipe was determined by steady-flow tests and the pressures calcu-

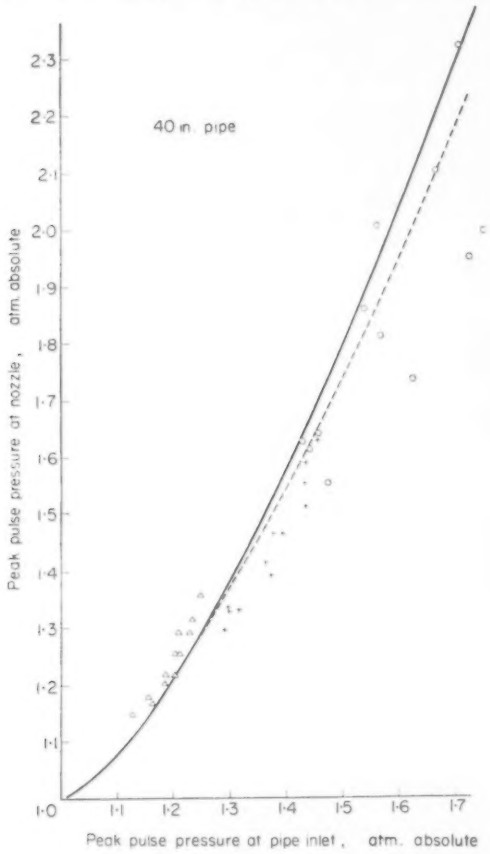

Fig. 20(a). Peak pulse pressures at inlet end – nozzle end.

$$\left(\frac{\text{Area of nozzle throat}}{\text{Cross-sectional area of exhaust pipe}}\right) = 0{\cdot}25.$$

o results from 1 in. diameter exhaust pipe.
\+ results from 1½ in. diameter exhaust pipe.
△ results from 2 in. diameter exhaust pipe.
—— theoretical relationship without friction.
– – – theoretical relationship with friction for 1 in. diameter pipe.

lated by the method of characteristics (Appendix I). A comparison of the measured peak pressures at the open end and the peak pressures at the cylinder end of the exhaust pipe are given in Fig. 20(a) and 20(b). On

the same graph the theoretical curves without friction and, for the 1 in. diameter pipe with friction, are given. As would be expected the effect of friction is more marked in the smaller-diameter pipe and with the longer lengths.

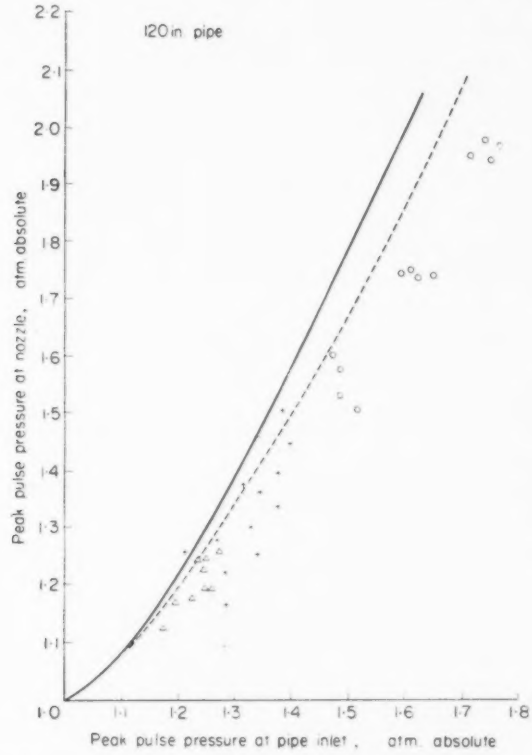

FIG. 20(b). Peak pulse pressures at inlet end — nozzle end.

$$\left(\frac{\text{Area of nozzle throat}}{\text{Cross-sectional area of exhaust pipe}}\right) = 0{\cdot}25.$$

o results from 1 in. diameter exhaust pipe.
+ results from 1½ in. diameter exhaust pipe.
△ results from 2 in. diameter exhaust pipe.
——— theoretical relationship without friction.
– – – theoretical relationship with friction for 1 in. diameter pipe.

Shock-wave formation

As the compression waves travel along the pipe the wave front steepens. The reflection of the compression wave at the nozzle end produces a compression wave which is propagated back along the pipe. If the pipe is long enough shock waves will form. Calculations showed that these might be expected in the small-diameter long pipes and this was confirmed in the experiments. It will be seen that in tests 41–44 (Fig. 13) shock waves were recorded at both the cylinder and nozzle ends of the exhaust pipe.

Vol. 1
1960

CONCLUSIONS

The wave profiles in the exhaust pipe of a turbocharged two-stroke-engine model showed two basic pulses one corresponding to the exhaust blowdown and the other to the supercharge air. These profiles were modified by the pipe dimensions (length and diameter), engine speed and nozzle size.

With a plain open-ended pipe under the same supercharge air conditions the basic wave form described above was superceded by a strong wave system. This produced residual waves. With this system a number of cycles are required before the wave form is in equilibrium. The effect of a nozzle at the open end is to damp out these residual waves.

The method of characteristics may be used to calculate the pressure development in the exhaust pipe. For accurate calculations unsteady-flow boundary curves are required for the entry to the pipe. For outflow through nozzles, steady-flow boundary curves may be used and for systems incorporating a nozzle-ended pipe equilibrium conditions are established in one cycle.

Acknowledgements – The tests described in this paper were carried out at the Walker and Harrison-Hughes Laboratories of the University of Liverpool. The authors wish to acknowledge with thanks the help given by Professor W. J. Kearton in providing the facilities. The authors also wish to thank Mr. W. Miller, Superintendent of the Laboratories, Mr. J. Cowie and Mr. E. Hobson for their help and advice.

Appendix

UNSTEADY PIPE FLOW WITH FRICTION

The basic equations for unsteady flow with friction (Jenny[4] and Shapiro[11]) for a constant-area pipe are

Continuity equation

$$\frac{\partial \varrho}{\partial t} + u\frac{\partial \varrho}{\partial x} + \varrho\frac{\partial u}{\partial x} = 0 . \tag{A1}$$

Euler's momentum equation

$$\frac{\partial u}{\partial t} + u\frac{\partial u}{\partial x} + \frac{1}{\varrho}\frac{\partial p}{\partial x} + F = 0 \tag{A2}$$

where

$$F = \frac{4fu^2 u}{2d\,|u|} , \tag{A3}$$

f = D'Arcy friction coefficient.

Energy equation

$$\frac{\partial p}{\partial t} + u\frac{\partial p}{\partial x} - a^2\frac{\partial \varrho}{\partial t} - a^2 u\frac{\partial \varrho}{\partial x} = (\gamma - 1)\varrho u F . \tag{A4}$$

The characteristic solutions expressed in non-dimensional form are:

Disturbance characteristic direction condition

$$\frac{dX}{dZ} = \frac{u}{\bar{a}} \pm \frac{a}{\bar{a}} \tag{A5}$$

$Z = \dfrac{\bar{a}t}{L}$; $X = \dfrac{x}{L}$; $\bar{a}$ = datum speed of sound, i. e. a constant.

Disturbance characteristic compatability condition

$$dU = \mp \frac{2}{\gamma - 1} dA - U \frac{da_A}{a_A} - \frac{4fL}{2d} \frac{u}{|u|} U^2 \left[1 \mp \frac{U}{A} (\gamma - 1) \right] \frac{a_A}{\bar{a}} dZ \tag{A6}$$

where

$$A = \frac{a}{a_A} = \left(\frac{p}{p_A} \right)^{1/7}, \qquad U = \frac{u}{a_A}$$

a_A = speed of sound at atmospheric pressure following isentropic expansion from pressure p (see below).

Path line characteristic direction condition

$$\frac{dX}{dZ} = \frac{u}{\bar{a}}. \tag{A7}$$

Path line characteristic compatability condition

$$\frac{da_A}{a_A} = \frac{\gamma - 1}{2} \cdot \frac{4fL}{2d} \cdot \frac{a_A}{\bar{a}} \cdot \frac{u}{|u|} \cdot U^3 \cdot \frac{dZ}{A^2} \tag{A8}$$

Entropy change

$$\frac{da_A}{a_A} = \frac{dS}{2c_P}. \tag{A9}$$

The non-dimensional forms given in equations (A5)–(A8) are slightly different from those suggested by JENNY[4]. By selecting an arbitrary datum contidion $\bar{a}$ in the position diagram and a variable reference condition a_A in the state diagram only one boundary curve need be plotted for the nozzle conditions. It should be noted that the value a_A will vary along the path line owing to friction and corresponds to the change in entropy, equation (A9).

PLOTTING PROCEDURE

Equation (A6) can be rewritten in form

$$dU = \mp \frac{2}{\gamma - 1} dA - \Delta_1 - \Delta_2 \tag{A10}$$

where

$$\Delta_1 = U \frac{da_A}{a_A} \tag{A11}$$

$$\Delta_2 = \frac{4fL}{2d} \frac{a_A}{\bar{a}} \frac{u}{|u|} U^2 \left[1 \mp \frac{U}{A} (\gamma - 1) \right]. \tag{A12}$$

For a wave travelling to the right the suffix R is used and to the left suffix L.

The application to the case of an incident wave 01 reflected at a nozzle is illustrated below.

Vol. 1
1960

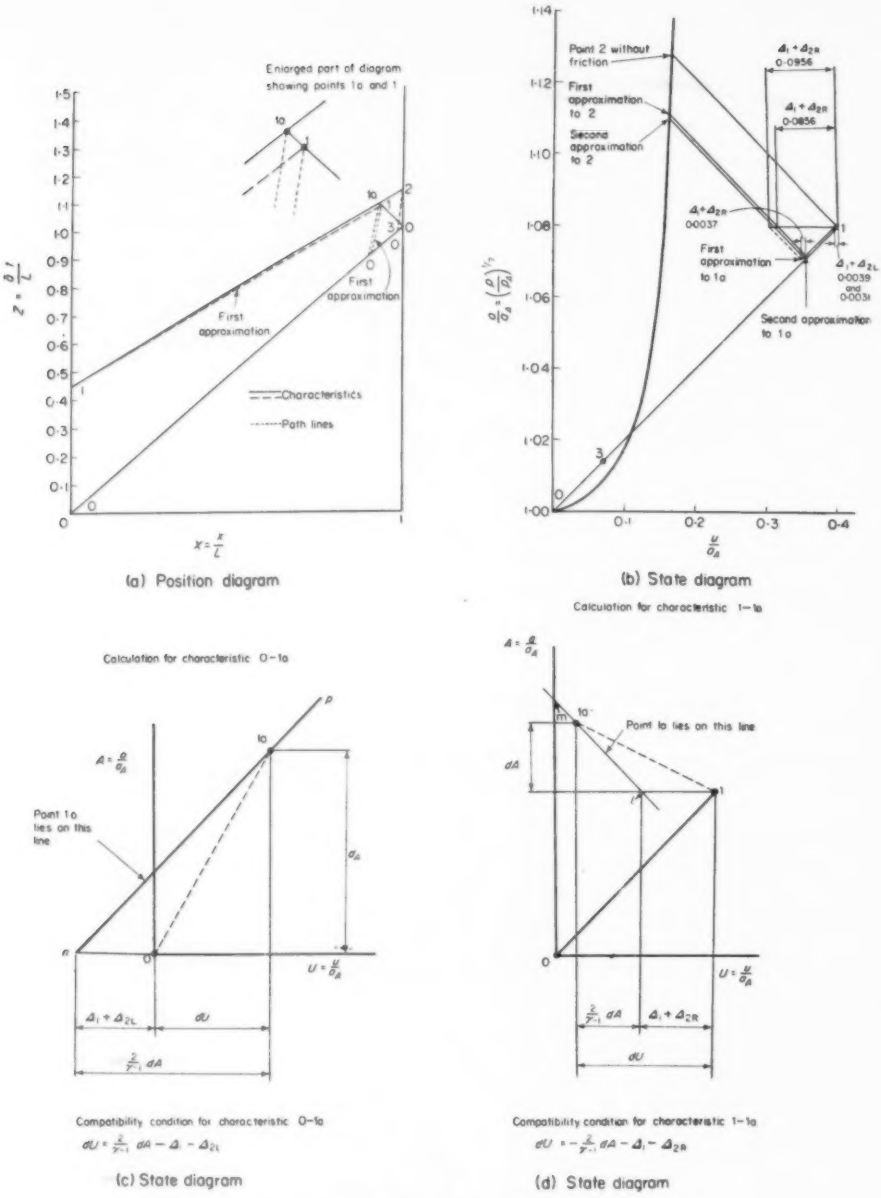

FIG. 21. Calculation with friction.

t = Time. $Z = \bar{a}t/L$ dimensionless time. x = Cartesian co-ordinate distance along pipe. $X = x/L$ dimensionless length. L = Length of pipe. $\bar{a}$ = Reference velocity of sound (i. e.) speed of sound at atmospheric pressure on the reference isentrope. a = Velocity of sound in pipe. a_A = Velocity of sound at atmospheric pressure following isentropic expansion from pressure p and velocity of sound a. u = Particle velocity of gas. p = Static pressure in pipe. p_A = Atmospheric pressure. Δ_1, Δ_{2R} and Δ_{2L} = characteristic displacement factors.

Isentropic flow

A simple incident wave 01, Fig. 21(a) and (b), is reflected at the nozzle end to the point 2 (without friction). The slope of the position characteristics being obtained by the substitution of the mean values of $a/\bar{a}$ and $u/\bar{a}$ along a characteristic into equation (A5).

Flow with friction

Starting with isentropic points 0, 1, 2 the displacement factors Δ_1 and Δ_2 are applied to allow for friction. Referring to Fig. 21(a) let the point $1A$ (with friction) be the same as point 1. Using the mean values of A and U for the characteristic 0–1 [Fig. 21(b)] the pathline 0–$1A$ is drawn and the entropy change da_A/a_A evaluated from equation (A8). The first approximation to point $1A$ in the state diagram is then obtained as follows:

Characteristic 0–$1A$

$$dU = +\frac{2}{\gamma-1}dA - \Delta_1 - \Delta_{2L}$$

Calculate the numerical values of $\Delta_1+\Delta_{2L}$ from the mean values of A, U and da_A/a_A along 01. From point 0 [Fig. 21(c)] set off $0n = \Delta_1+\Delta_{2L}$ and draw np with slope $\frac{dA}{dU} = +\frac{\gamma-1}{2}$, the point $1A$ will lie on this line.

Characteristic 1–1A

$$dU = -\frac{2}{\gamma-1}dA - \Delta_1 - \Delta_{2R}$$

As before calculate numerical value of $\Delta_1+\Delta_{2R}$ from the mean value of A, U and da_A/a_A along 1–1. From point 1 [Fig. 21(d)] set off $1l = \Delta_1+\Delta_{2R}$ and draw lm with slope $\frac{dA}{dU} = -\frac{\gamma-1}{2}$, the point $1A$ will lie on this line. Intersection of np and lm locates $1A$ to the first approximation.

The correct position of $1A$ in the position diagram is now obtained and the procedure repeated with $1A$ replacing 1 to obtain a closer approximation. The orders of magnitude of the successive approximations for a typical calculation are given in Fig. 21(b).

REFERENCES

1. W. J. R. Roach and J. G. G. Hempson, B. S. R. A. Report No. 130 (1954).
2. R. S. Benson, *Enginer, Lond.* **203**, 946 (1957).
3. R. S. Benson and W. A. Woods, *J. Roy. Aero. Soc.* **63**, 317 (1959).
4. E. Jenny, *Berechnungen und Modelversuche über Druckenwellen grosser Amplituden in Auspuff Leitungen*. Doctor's Thesis. Eidgen. Techn. Hosch., Zürich (1949).
5. R. S. Benson, *Engineer, Lond.* **199**, 546 (1955).
6. B. N. Cole and B. Mills, *Proc. Inst. Mech. Engrs., Lond.* **1B**, 364 (1952).
7. R. S. Benson, *J. Roy. Aero. Soc.* **62**, 132 (1958).
8. P. Hold, *Mat. tech. Z.* **3**, 83 (1941).
9. R. S. Benson, *Trans. Lpool. Engng.* Soc. **76**, 88 (1957).
10. R. S. Benson, *Proc. Inst. Mech. Engrs., Lond.* **173** (1959).
11. A. H. Shapiro, *The Dynamics and Thermodynamics of Compressible Fluid Flow*, Ronald Press, New York (1953).

Vol. 1
1960

Int. J. Mech. Sci. Pergamon Press Ltd. 1960. Vol. 1, pp. 282–300. Printed in Poland

SOME ASPECTS OF PRESS FORGING

S. KOBAYASHI,* A. G. MACDONALD,† and E. G. THOMSEN †

(*Received* 13 *April* 1959)

Summary – Axially symmetric billets in the form of cylinders of commercially pure lead (99·9 per cent) were forged between flat parallel dies and in closed dies at low hydraulic press-ram speeds of the order of 0·10 in/min. It was found that average forging pressures predicted by approximate theories based on simplified states of stress were in substantial agreement with the experimental observations. Local pressure measurements were also made by the use of pressure sensitive elements imbedded in the forging dies. It was found that the local pressure distribution in the deformed cylinders between flat dies was also in substantial agreement with the simplified theories, but that adjustments by plastic flow appeared to equalize the local pressures in the body of the forgings in the closed dies.

INTRODUCTION

THE problem of press forging of slabs and discs between parallel dies or platens as in up-setting or in edging and fullering has been discussed by a number of investigators. The important theoretical papers are those of PRANDTL[1], HILL, LEE and TUPPER[2], GREEN[3] and SHIELD[4], while more approximate treatments are given by SIEBEL[5], SACHS[6], STONE and GREENBERGER[7] and SCHROEDER and WEBSTER[8]. Comparisons of approximate solutions with slip-line solutions in plane strain are given by ALEXANDER[9], and by BISHOP[10] who extended the analysis to include such shapes as cylinders and squares. Experimental verification of some of the theories are due to WATTS and FORD[11] for overlapping slabs, and to KOBAYASHI *et al.*[12] and KOBAYASHI and THOMSEN[13] for more complex forging processes of slabs and cylinders. It is the purpose of the present investigation to extend the comparison of experimental data with theories and to include local pressure distributions for the compression of cylinders of commercially pure lead (99·9 per cent) between parallel dies (up-setting) and for forging of cylinders in closed dies.

FORGING OF CYLINDERS BETWEEN FLAT DIES

Shaping of cylinders into discs between flat and overlapping dies is called up-setting and is one of the simpler forging operations. In spite of the simplicity of the operation, however, this problem has defied analysis and apparently no exact solution has been found. It is for this reason that a number of investigators as for example, SIEBEL[5], STONE and

* Dept. of Mechanical Engineering, Doshisha University, Kyoto, Japan, and presently University of California, Berkley, California.

† University of California, Berkeley, California.

GREENBERGER[7], HILL[2], and SCHROEDER and WEBSTER[8], have simplified the problem and have considered approximate solutions. These solutions were recently critically reviewed by BISHOP[10] who came to the conclusion that theoretically the approximate solutions are possible. BISHOP bases his conclusion on the following reasoning.

The approximate equation describing equilibrium in the radial direction, is given by

$$\frac{d\sigma_r}{dr} = -\frac{2\mu\sigma_z}{h} \tag{1}$$

where μ is the coefficient of friction on the die surfaces, h is the instantaneous height of the disc and σ_r and σ_z are the radial and axial stress components respectively. The solution seems valid when μ is small, since it is reasonable to assume that the axial hoop stress component σ_θ from consideration of symmetry is equal to the radial stress component σ_r. Hence the yield condition to be satisfied reduces to $\sigma_z - \sigma_r = -\bar{\sigma}$ where $\bar{\sigma}$ is the instantaneous yield stress and is not a function of z and r; it follows at once that $\frac{\partial\sigma_z}{\partial r} = \frac{\partial\sigma_r}{\partial r}$. Consequently, equation (1) can readily be integrated and, by analogy of similar results for the plane strain case with slip-line solutions, one can infer that this solution is valid to at least a first approximation.

For the case where the friction force at the die surface is large, the foregoing criterion breaks down and some modification of equation (1) is required. Thus when sticking occurs at the die surface, the shearing stress at $z = \pm\frac{h}{2}$ reaches a critical constant magnitude and $\frac{\partial\sigma_r}{\partial r} = \frac{\partial\sigma_z}{\partial r}$ is again satisfied. In this case, μ takes on a value of 0·577 according to the SCHROEDER and WEBSTER [8] criterion or a value of 0·39 in accordance with the Haar–Karman hypothesis. At the mid-section of the disc, where $z = 0$, $\sigma_\theta = \sigma_r$ at $r = 0$ and $\sigma_\theta \cong \sigma_r$ at $r = r_f$, where r_f is the radius of the disc. It is evident then, that for the yield condition $\sigma_z - \sigma_r = \bar{\sigma}$, the relationship $\frac{\partial\sigma_z}{\partial r} = \frac{\partial\sigma_r}{\partial r}$ must be substantially true at $z = 0$ for all values of r. Consequently it cannot be too incorrect to assume that $\frac{\partial\sigma_z}{\partial r} = \frac{\partial\sigma_r}{\partial r}$ is not only true for all values of r at $z = 0$ and $z = \pm\frac{h}{2}$, but for all values of z as well.

Equation (1) under the foregoing assumptions can be integrated to yield the axial stress component in dimensionless form

$$-\frac{\sigma_z}{\bar{\sigma}} = \exp\left[\frac{2\mu}{h}(r_f - r)\right] \tag{2}$$

Vol. 1
1960

for the case of sliding between the surfaces of the dies and the disc, when $r_0 \leqslant r \leqslant r_f$ and $\mu < 0{\cdot}577$.

The radius $r = r_0$ provides the condition under which metal sticking occurs, which is given by

$$r_0 = r_f - \frac{h}{2\mu} \ln\left(\frac{1}{\mu\sqrt{3}}\right). \tag{3}$$

Hence the axial pressure distribution for the condition of sticking, i. e. $0 \leqslant r \leqslant r_0$ is given by

$$-\frac{\sigma_z}{\bar{\sigma}} = \frac{2}{h\sqrt{3}}(r_0 - r) + \frac{1}{\mu\sqrt{3}}. \tag{4}$$

From these equations the average forging pressure p_a can be readily evaluated in the following manner:

$$\left.\begin{aligned} \frac{p_a}{\bar{\sigma}} &= \frac{1}{2}\left(\frac{h}{\mu r_f}\right)^2\left[\exp\left(\frac{2\mu r_f}{h}\right) - \frac{2\mu r_f}{h} - 1\right] \quad \text{for} \quad r_0 \leqslant 0 \\ \text{and} \\ \frac{p_a}{\bar{\sigma}} &= \frac{1}{2}\left(\frac{h}{\mu r_f}\right)^2\left[\left(\frac{2\mu r_0}{h} + 1\right)\exp\left\{\frac{2\mu}{h}(r_f - r_0)\right\} - \frac{2\mu r_f}{h} - 1\right] \\ &\quad + \left(\frac{r_0}{r_f}\right)^2\left(\frac{1}{\mu\sqrt{3}} + \frac{2\sqrt{3}}{9}\frac{r_0}{h}\right), \quad \text{for} \quad 0 < r_0 \leqslant r_f. \end{aligned}\right\} \tag{5}$$

In order to illustrate the rise of the average forging pressure with increase of the ratio of the radius to the height of the disc, equations (5)

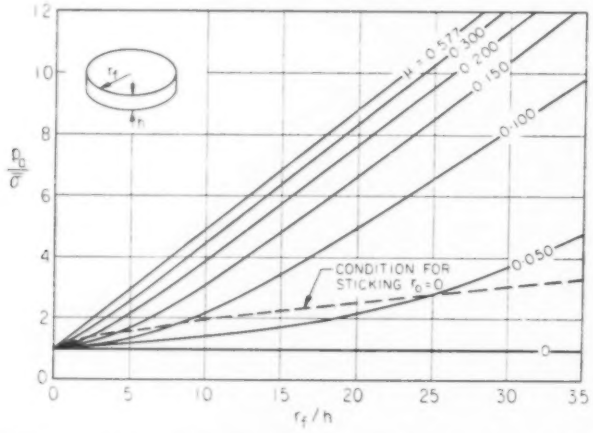

FIG. 1. Theoretical dimensionless average forging pressure as function of radius to height ratio of disc, forged between flat parallel dies.

for several μ are shown in Fig. 1 in graphical form. It is of interest to note that the criteria, $\mu = 0{\cdot}577$ and $\mu = 0{\cdot}39$, lead to almost identical limiting lines. Hence, it appears that there is little choice between these two limit

criteria; this is so, especially in view of the fact that SCHROEDER and WEBSTER[8] showed that some of their experimental points fell beyond the $\mu = 0{\cdot}577$ line.

There appears to be little or no experimental confirmation for the approximate equation of Fig. 1. The data of SCHROEDER and WEBSTER[8] previously referred to, showed some agreement but because of the fact that the data for continuous tests at constant μ were not included, a critical comparison is not possible. It is for this reason that the experimental investigation to be discussed was undertaken. The experimental equipment consisted of hardened parallel flat dies lapped to a finish of 3 μ in. r. m. s. values of roughness. The lower die, as shown in Fig. 2, was equipped with pressure sensing elements in order to determine not only average

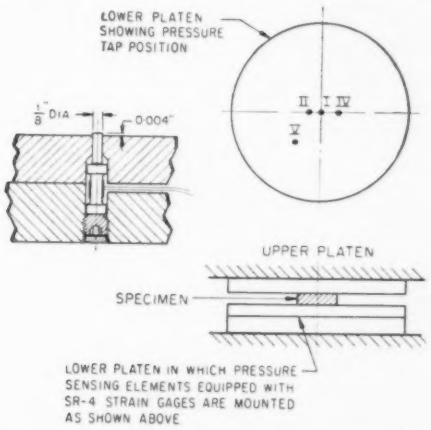

FIG. 2. Diagrammatic sketch of forging dies for up-setting lead cylinders.

but also local forging pressures. The pressure sensing elements were calibrated with both a rubber pad and a commercially pure lead billet under hydrostatic conditions. A typical calibration curve during a test run with continuously increasing pressure is shown in Fig. 3. The curve for lead with decreasing pressure is not shown, but would be below that for increasing pressure since the pressure sensing element will not respond until the plasticity conditions are reached. As a consequence of this, a complete calibration test would show a hysteresis loop. Furthermore the position of the pin of the pressure sensing element is of importance for assigning a zero reference reading to the instrument. If the pin of the pressure element extends beyond the surface, as shown in Fig. 3, the lead calibration curve at the start is below the rubber curve; the converse is true if the pin is below the surface of the die. In the disc experiments to be discussed, all pins extended at zero load a distance of 0·004 in. above the die surface.

The commercially pure lead billets, which were tested in the present

investigation, were prepared from 6 in. castings which were extruded at atmospheric temperature into $2\frac{1}{4}$ in. diameter round bars in order to break up the cast structure. These bars were then machined to 2 in. diameter specimens having four initial heights ranging from $\frac{1}{2}$ to 2 in. The

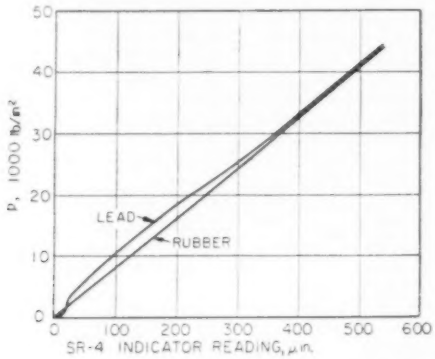

FIG. 3. Typical calibration curve of pressure sensitive element installed in forging dies to measure local pressures.

die surface and specimens before each test were either completely cleaned of all foreign matter and washed with acetone in order to induce appreciable friction or they were well lubricated with petroleum jelly in order to reduce the frictional drag between specimen and dies. The specimens were centered on the flat forging dies and a load was applied at an approximate crosshead speed of 0·10 in/min. The load was then increased at approximately constant speed to a maximum load of approximately

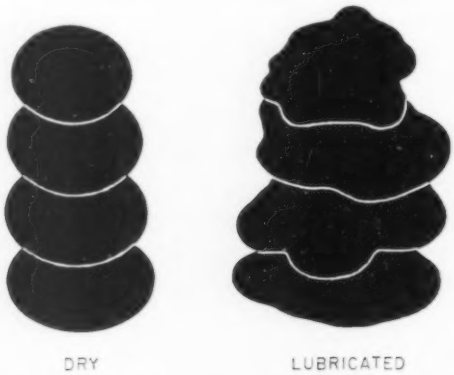

FIG. 4. Photographs of 2 in. diameter lead cylinders forged between overhanging flat and parallel dies.

190 tons. The final shapes resulting from the forging of the cylinders of varying initial heights are shown in the photographs of Fig. 4. The discs at the left, which are circular in shape, were the result of forging the lead cylinders at high friction, while those to the right having shapes of

varying configuration were those obtained with low friction. It is evident from this photograph that the degree of friction can affect greatly the behaviour of metals in a forging operation. It is of interest also to observe, that all cylinders were forged at an approximately equal final load, hence the varying sizes of the final forgings give a pictorial story of the effect of h and μ on the forging pressure.

The results of the foregoing experiments with lubricated and unlubricated cylinders are shown as maximum or final conditions in Table 1, while each complete test with running average forging pressure ratios $p_a/\bar{\sigma}$

TABLE 1. FORGING OF 2-IN. DIAMETER CYLINDERS OF COMMERCIALLY PURE LEAD (99·9 PER CENT PURE, EXTRUDED CASTINGS) BETWEEN PARALLEL AND FLAT DIES. DIE SURFACES WERE FINISH-LAPPED TO A ROUGHNESS OF 3μ IN. R. M. S. VALUES

No. of specimen	Lubrication	Initial height h_o (in.)	Final height h(in.)	Equivalent final radius r_f(in.)	Maximum load (lb)	Maximum $p_a/\bar{\sigma}$	Maximum r_f/h
1	petroleum jelly	2·0815	0·144	3·76	355,000	4·78	25·6
1	,,	1·5365	0·094	4·05	380,000	4·47	43·1
1	,,	1·010	0·0775	3·62	380,000	5·53	47·0
1	,,	0·516	0·0635	2·85	340,000	6·46	44·9
1	dry	2·081	0·212	3·14	380,000	7·08	14·8
1	,,	1·538	0·165	3·06	377,000	7·78	18·6
1	,,	1·0115	0·122	2·88	390,000	8·64	23·6
1	,,	0·517	0·081	2·53	380,000	11·20	31·2

r_f are calculated values by use of heights h and refer to radii of equivalent areas of circular discs for the lubricated dies.

as a function of r_f/h is shown graphically in Fig. 5. All experimental points throughout the paper are shown by symbols. The effective stress $\bar{\sigma}$ at each forging condition of strain and strain rate was evaluated from typical compression tests of 1 in. diameter by 1 in. long cylinders at various constant strain rates shown in Fig. 6. The test cylinders were provided with concentric grooves at their end surfaces to retain the lubricant and did not barrel during compression. Each test was carried out in such a way that the speed of the testing machine was continuously adjusted to maintain a constant strain rate. The undulations in the resulting curves shown by way of example were thought to be due to alternating effects of cold work and recrystallization and required averaging of the curves as shown. The effective stresses $\bar{\sigma}$ were then evaluated from the corresponding strains and strain rates as computed from the forging tests. A typical test run of the instantaneous height of the forging as function of time and the computed values of $\bar{\epsilon}$, $\dot{\bar{\epsilon}}$ and $\bar{\sigma}$ is shown in Fig. 7.

Vol. 1
1960

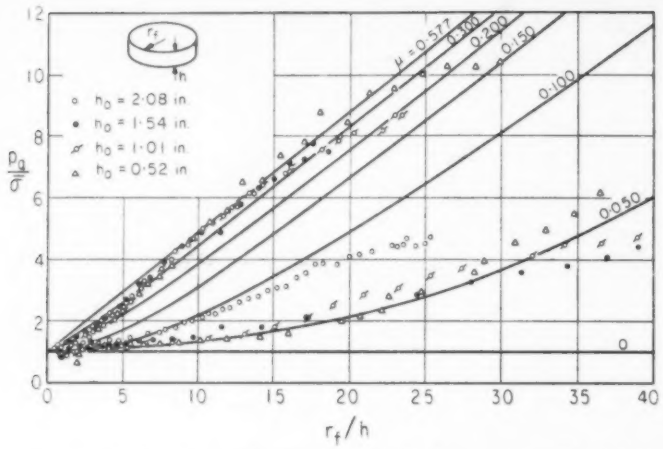

FIG. 5. Theoretical and experimental dimensionless average forging pressure as function of radius to height ratio for commercially pure lead.

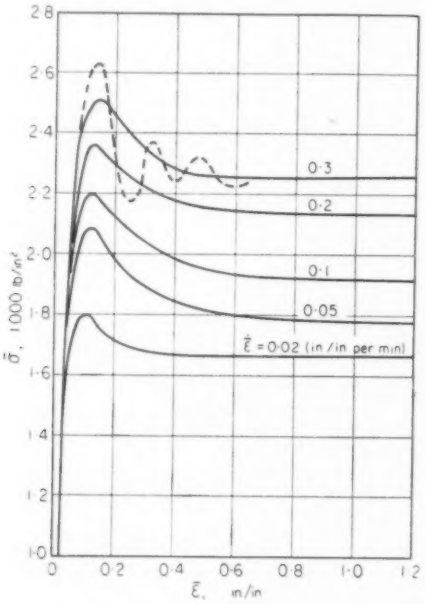

FIG. 6. Typical effective stress vs. effective strain curves of commercially pure lead at relatively low strain rates.

In comparing the average experimental forging pressure ratios $p_a/\bar{\sigma}$ with the approximate theory (see Fig. 5) it is evident that agreement is generally good, except at the beginning of each test, where some barreling occurs, if it is assumed that $\mu \cong 0{\cdot}05$ and $\mu \geqslant 0{\cdot}2$ with lubricated and unlubricated surfaces respectively. This was confirmed in an independent friction test (see KOBAYASHI *et al.*[12]) where it was found that μ was 0·08 and 0·21 for the two test conditions respectively.

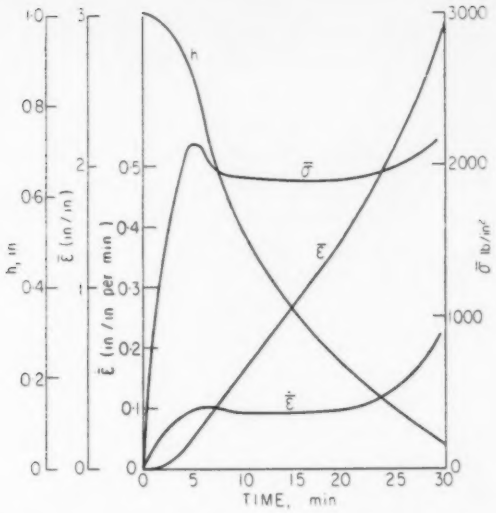

FIG. 7. Typical test run of 2 in. diameter lead cylinder forged dry between parallel dies.

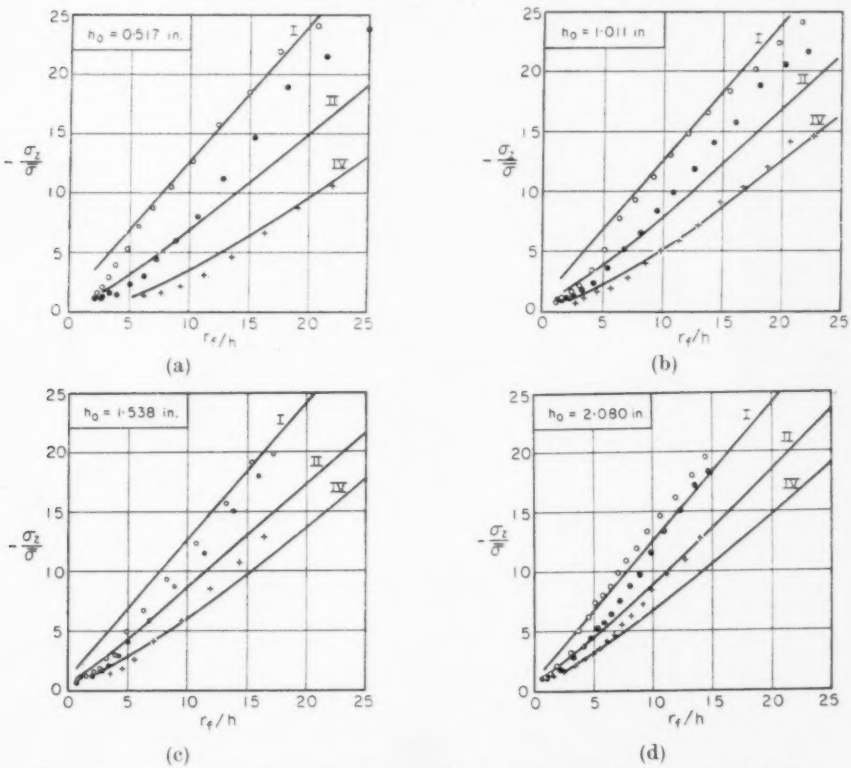

FIG. 8. Local axial pressure distribution for the condition of forging 2 in. cylinders dry between overlapping flat and parallel dies. (Roman numerals refer to location of local pressure sensitive element shown in Fig. 2.)

In order to compare the individual gauge pressures $-\sigma_z/\bar{\sigma}$ during the several tests without lubrication, it was necessary to plot equations (1), (3) and (4) as function of r_f/h as shown in Fig. 8(a–d) respectively. The roman numerals identifying the individual curves refer to the radial positions of the individual pressure sensing elements (see Fig. 2) where the measurements of the local pressures, $-\sigma_z$, were made. It is apparent that the local pressures of the individual test runs for the four test conditions ($h_0 \cong 2{\cdot}0$ to $0{\cdot}5$ in.) evaluated, agree quite well with the approximate theory as given by the limiting line, $\mu = 0{\cdot}577$, which closely approximates the line $\mu = 0{\cdot}2$.

FORGING OF CYLINDERS IN CLOSED DIES

KOBAYASHI *et al.*[12] suggested that a complex forging in closed dies when making a final impression could be analyzed by a simplified scheme. They suggested that, instead of dealing with the complex body of the forging itself, an approximate solution could be obtained by treating the forging as a fictitious disc. Thus for example in the over-lapping dies of Fig. 9 shown schematically, the major deformation is assumed to take

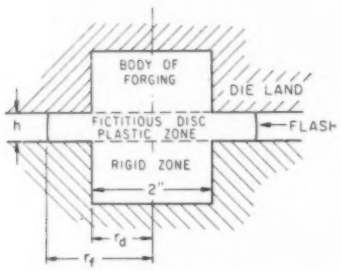

FIG. 9. Schematic diagram of fictitious disc during press forging of cylinder.

place in the flash which extends into the body of the forging and is enclosed between the dotted lines. The remainder of the body of the forging, except for small adjustments of contour occurring in actual practice, can be imagined to remain rigid. Experimental incremental forging steps were made and it was shown that this assumption is approximately correct.

In the development of the approximate theory it was assumed that the deformation process was not unlike that assumed for the process of forging a disc between flat and overlapping dies, but that the condition of friction at the boundary between the rigid body of the forging and that of the fictitious disc was that of shear deformation under a maximum shearing stress. Hence this is similar to the problem of deforming a disc under the conditions (1) sticking up to the die radius r_d and (2) sliding in the flash between $r_d \leqslant r \leqslant r_f$. The equations developed by KOBAYASHI *et al.*[12] are given below,

$$\frac{p_a}{\bar{\sigma}} = \frac{1}{2}\left(\frac{h}{\mu r_f}\right)^2\left[\left(\frac{2\mu r_d}{h}+1\right)\exp\left\{\frac{2\mu}{h}(r_f-r_d)\right\}-\frac{2\mu r_f}{h}-1\right] + \left(\frac{r_d}{r_f}\right)^2\left[\exp\left\{\frac{2\mu}{h}(r_f-r_d)\right\}+\frac{2\sqrt{3}}{9}\frac{r_d}{h}\right]. \tag{6}$$

In the event that the frictional resistance in the flash becomes so great that sticking occurs, then equation (6) reduces to those for a disc given by equations (5). Typical experimental data for forging a $1\frac{1}{16}\frac{5}{6}$ in. diameter lead cylinder, having an initial height of 1·50 in., are compared with theoretical curves in Fig. 10, and were reported earlier by Ko-

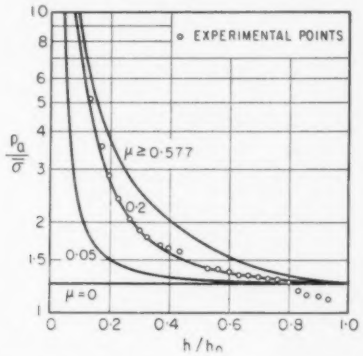

FIG. 10. Dimensionless average forging pressure as function of instantoneous height to initial height ratio.

BAYASHI and THOMSEN[13]. It is seen at once that the theory predicts average forging pressures which appear to be in good agreement with experimental observations.

In a complex forging, such as that under discussion, it would be of interest to study (i) the local pressures, similar to that of the discs forged between flat dies, and (ii) the effect of fixed flash radius on the local and average forging pressures. The latter condition is one that is encountered in practice and causes overhanging of the flash metal since the die lands are usually of a given width. Consequently, excess metal is allowed to flow beyond the die lands into the so-called relief trough in order to permit continued ejection of metal without increasing the total flash area. A schematic diagram of the experimental set-up which was used in the present investigation is shown in Fig. 11. The same platen containing the pressure sensing elements, such as was used earlier with the flat die forging tests, was also used here. This permitted the location of two pins of the pressure sensing element in the body of the forging and one in the flash. An additional element was located so as to measure the wall pressure. The whole assembly of air hardened dies (with three-part-die-shrink assemblies for future tests with work-hardening metals) are

Vol. 1
1960

mounted in an anti-friction die set for accurate alignment. In order to study the local pressure distribution as a function of distance from the interface of the fictitious disc, with the rigid body of the forging, removable hardened spacers and gauge pins were inserted in order to permit pressure measurements at variable heights. The spacers are shown in the diagram of Fig. 11. It was possible thereby to make pressure determinations at distances of 1/8 in., 7/8 in. and $1\frac{3}{4}$ in. from the interface.

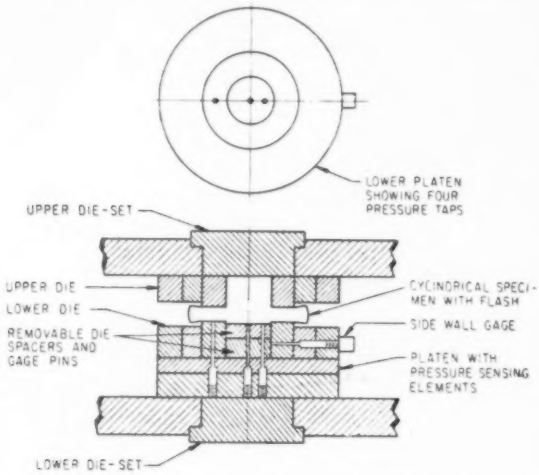

FIG. 11. Diagrammatic sketch of closed-forging dies.

In the event that an overhanging flash develops, it is necessary to modify the average forging pressures given by equation (6). This can be accomplished by considering the following. If the radial stresses and hoop stresses are assumed to be zero at the instant when the flash of the forging reaches the die-land edge at radius r_F, then the radial pressure must rise gradually from zero since the excess metal leaving the die induces a hoop tension stress. This pressure should not at any time become larger than the effective stress $\bar{\sigma}$, since a condition for yielding would then be satisfied in a different co-ordinate direction at the radius r_F by the fact that the maximum shearing stress is now at 45° to the axial direction z and the radial direction r. It appears that this latter condition requiring relatively large values of h_0/h will probably not be reached, since, as actually observed in the experiments, the radial stress relieves itself by buckling of the flash. The correction term for the total pressure is approximately given by

$$-\left(\frac{\sigma_r}{\bar{\sigma}}\right)_{r_F} \cong \frac{1}{2}\left[\left(\frac{3\frac{h_F}{h}-1}{\frac{h_F}{h}+1}\right)^{1/4}-1\right] \tag{7}$$

where $h = h_F$, when $r_f = r_F$, which results in the following equation

$$\frac{p_a}{\bar{\sigma}} = \left[1 - \left(\frac{\sigma_r}{\bar{\sigma}}\right)_{r_F}\right]\left\{\frac{1}{2}\left(\frac{h}{\mu r_f}\right)^2\left[\left(\frac{2\mu r_d}{h}+1\right)\exp\left(\frac{2\mu}{h}(r_f - r_d)\right) - \frac{2\mu r_f}{h} - 1\right]\right.$$
$$\left. + \left(\frac{r_d}{r_f}\right)^2 \exp\left(\frac{2\mu}{h}(r_f - r_d)\right)\right\} + \frac{2\sqrt{3}}{9}\left(\frac{r_d}{r_f}\right)^2 \frac{r_d}{h}. \qquad (8)$$

In order to illustrate the theoretical relationships, the average pressures were calculated and are shown in Fig. 12 as function of h_0/h for three conditions of forging and for two values of μ. Curves (a) are those applicable to overhanging dies and were calculated by means of equation (6). These are the same calculated values as shown in Fig. 10, but given there as semi-logarithmic co-ordinates of $\log p_a/\bar{\sigma}$ vs. h/h_0, instead of log-log coordinates of $\log p_a/\sigma$ vs. $\log h_0/h$. The present method of representation was chosen since it has the advantage of flattening the curves at larger values of h_0/h. Curves (c) were also calculated from equation (6), but under the assumption that the hoop stress and the radial stress components were zero. It is to be noted that the curves (a) and (c) depart from each other at $h_0/h = 3{\cdot}06$, for the particular die dimensions employed in the present investigation. This is due to the fact that the flash-land radius $r_F = 1{\cdot}75$ in., and the die radius $r_d = 1{\cdot}0$ in.; hence $h_0/h = (r_F/r_d)^2 = 3{\cdot}06$. Finally curves

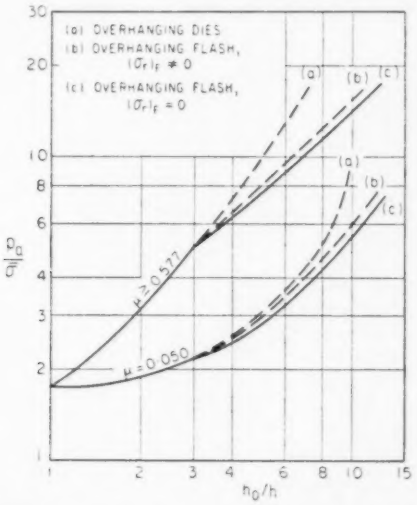

FIG. 12. Theoretical approximate forging pressures for two conditions of surface friction, for $h_0 = 0{\cdot}516$ in.

(b) were obtained by applying the corrections given by equation (8). It is seen that the curves (b) and (c) for overhanging flash depart appreciably from those of overlapping dies given by curves (a), but that the difference between (b) and (c) is relatively inconsequential. Hence, all experimental data to follow are only compared with type (c) theoretical curves.

Vol. 1
1960

The results of the present investigation using the forging shapes shown in Fig. 11 are summarized in Table 2 for the maximum condition of load and pressure encountered in each of the tests. In all cases duplicate tests

TABLE 2. FORGING OF 2-IN. DIAMETER CYLINDERS OF COMMERCIALLY PURE LEAD (99·9 PER CENT PURE EXTRUDED CASTINGS) IN CLOSED DIES

No. of specimen	Initial height h_0 (in.)	Final height h (in.)	Maximum load (lb)	Maximum $P_a/\bar{\sigma}$
2	2·080	0·106	190,000*	10·3
2	1·539	0·063	270,000	14·2
2	1·011	0·050	270,000	13·6
2	0·516	0·049	270,000	15·0

Note: All specimens lubricated with petroleum jelly.

* Maximum load was limited because flash expelled from die lands contacted die surfaces.

were made for each test condition and are compared with the prediction based on the approximate theories in Figs. 13–16 inclusive. It is evident at

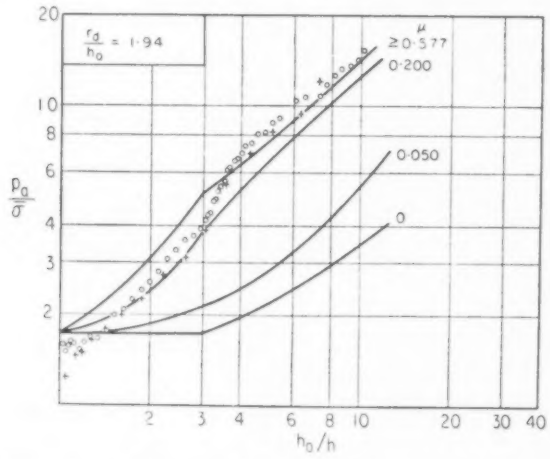

FIG. 13. Dimensionless average forging pressures as function of initial height to instantaneous height ratio of flash, for $h_0 = 0{\cdot}516$ in.

once that the correlation is good but not perfect. Much of the departure of the experimental points from the theory, however, can be attributed to barrelling of the flash at the beginning of each test. This condition is minimized when the initial height of the flash, h_0, is small. In this case the agreement in the first part of each test with the theory is relatively good. It is also to be noted that the condition of $\mu = 0{\cdot}2$, which as seen

in Fig. 10, correlated with the theory for overlapping dies, while in the present case agreement for the condition of $\mu = 0{\cdot}2$ does not exist for the entire test. This anomaly may be due to the fact that the corrections

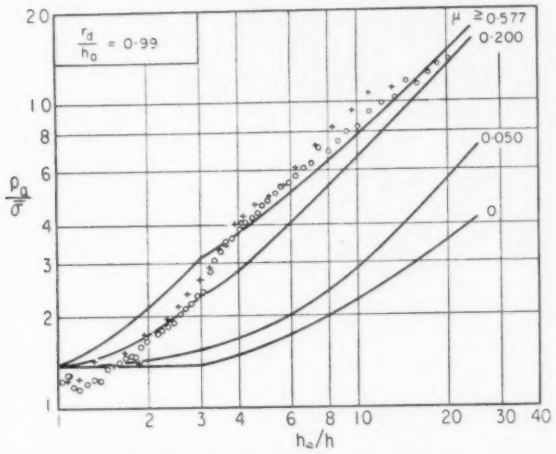

FIG. 14. Dimensionless average forging pressures as function of initial height to instantaneous height ratio of flash, for $h_0 = 1{\cdot}011$ in.

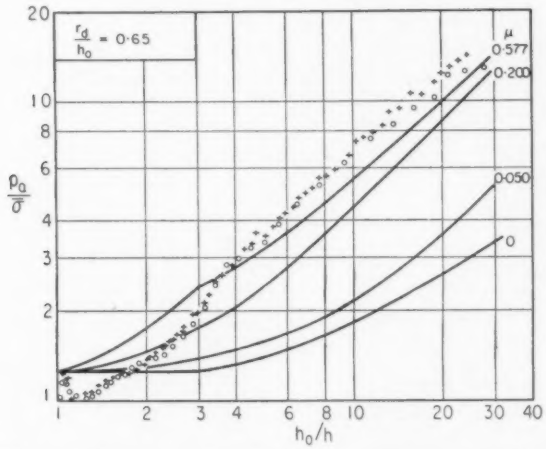

FIG. 15. Dimensionless average forging pressures as function of initial height to instantaneous height ratio of flash, for $h_0 = 1{\cdot}539$ in.

applied to the forging pressure because of the overhanging flash are not entirely sufficient, or that the petroleum jelly was not as effective throughout a test as was assumed.

In order to compare the experimental local forging pressures with the approximate theory, the following equations are applicable

Vol. 1
1960

$$\left.\begin{aligned} -\frac{\sigma_z}{\bar{\sigma}} &= \exp\left[\frac{2\mu}{h}(r_f - r)\right] \quad \text{for} \quad r_d \leqslant r \leqslant r_f \\ -\frac{\sigma_z}{\bar{\sigma}} &= \frac{2}{h\sqrt{3}}(r_d - r) + \exp\left[\frac{2\mu}{h}(r_f - r_d)\right] \quad \text{for} \quad 0 \leqslant r \leqslant r_d \end{aligned}\right\} \tag{9}$$

and when sticking occurs in the flash, equations (2)–(4) must be used. These calculations have been carried out and the theoretical curves

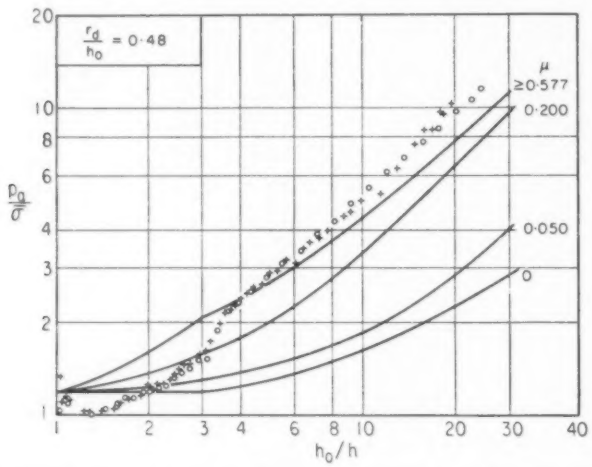

FIG. 16. Dimensionless average forging pressures as function of initial height to instantaneous height ratio of flash, for $h_0 = 2{\cdot}080$ in.

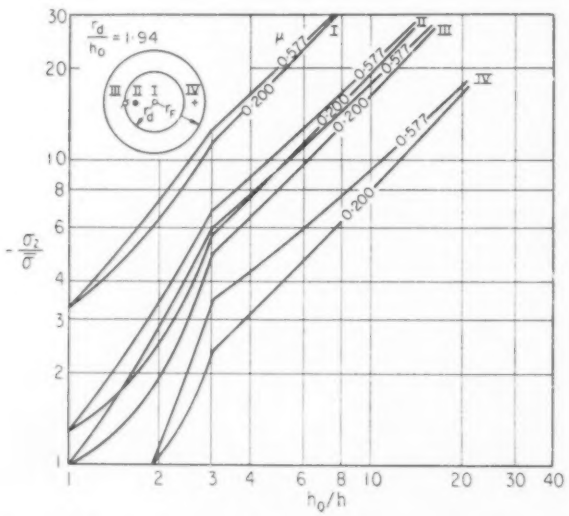

FIG. 17. Local theoretical dimensionless pressure distribution as function of height ratio for $h_0 = 0{\cdot}516$ in. and two coefficients of friction.

(not corrected for overhang) for the four gauge positions are shown in Figs. 17 and 18 for $r_d/h_0 = 0{\cdot}48$ and $1{\cdot}94$, and $\mu = 0{\cdot}2$ and $0{\cdot}577$. It is evident from these curves that the local pressures increase as one travels from

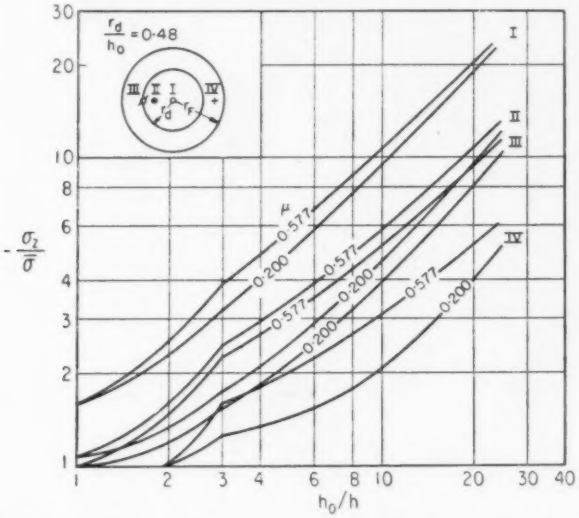

FIG. 18. Local theoretical dimensionless pressure distribution as function of height ratio for $h_0 = 2{\cdot}080$ in. and two coefficients of friction.

the flash toward the center of the forging and that for high friction between $\mu = 0{\cdot}2$ and $0{\cdot}577$ relatively little variation in pressure results. It is for this reason that it seems advisable to compare the experimental results with theoretical pressures for $\mu = 0{\cdot}577$ only. The results are shown in Figs. 19(a–d) inclusive. It is seen that the local pressures in the flash (gauge IV) are in agreement with theoretical predictions, while in the center of the forging the several pressure readings are more or less uniform and do not increase toward the center as predicted. This anomaly is attributable to the fact that the material in the body of the forging is not rigid and that readjustments by plastic deformation occur, which appear to have the effect of equalizing the pressures. This is of course a fortunate circumstance, since it is most desirable from a practical standpoint that a uniform pressure distribution in the die cavity prevail in order that a good impression of the dies may be obtained.

The experimental results for the pressure distribution obtained with a spacing of only 1/8 in. between the fictitious disc and the bottom of the die are shown in Fig. 20. The method of changing the depth of the die cavity employed is shown in Fig. 11 and consisted of inserting die spacers and gauge pins. It is seen that moving the gauge pins closer to the fictitious disc did not result in a substantial variation in local pressure in the forging. It must be concluded from this that the local pressures

Vol. 1
1960

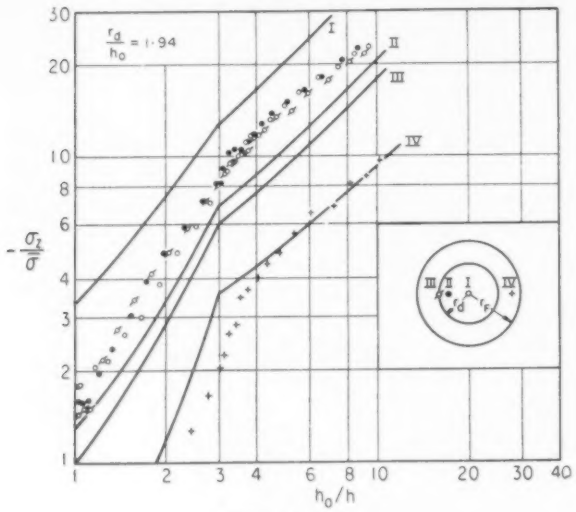

Fig. 19. (a)

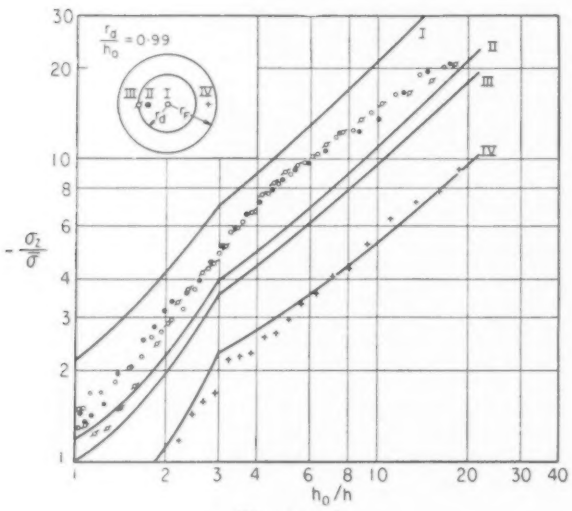

Fig. 19. (b)

FIG. 19. Local dimensionless pressure distribution as function of height ratio for several test conditions.

in the die cavity of a forging tend to equalize as long as there is sufficient bulk of material available to permit such readjustments.

CONCLUSIONS

A comparison of the average and local forging pressures of commercially pure lead cylinders compressed between flat parallel dies as in up-setting are in good agreement with a simplified forging theory. Hence, the theore-

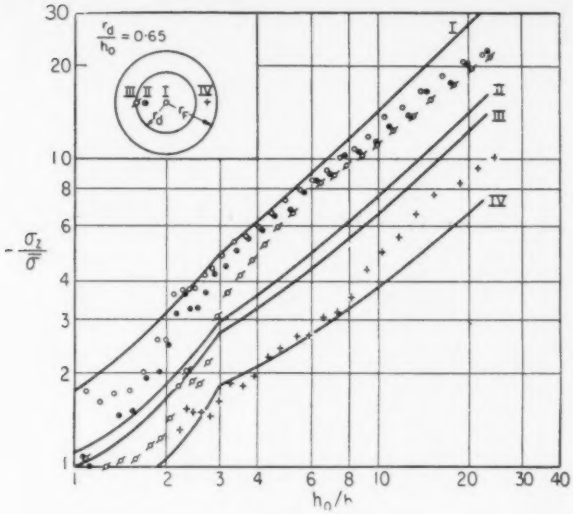

Fig. 19. (c)

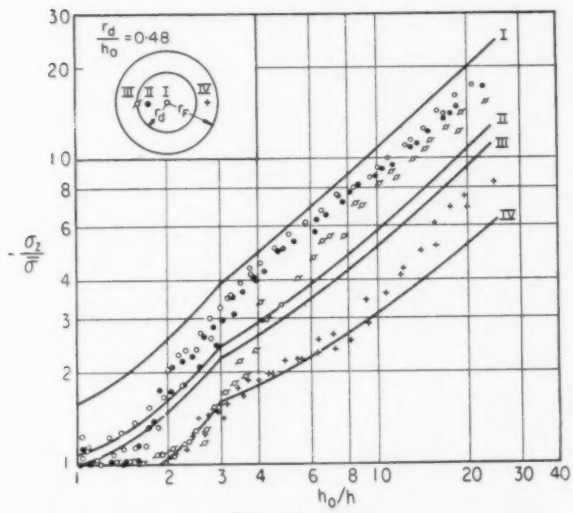

Fig. 19. (d)

tical proofs that BISHOP[10] advanced for the applicability of a simplified theory are appararently substantiated.

Similar comparisons of average forging pressures with theoretical values based on a disc theory for forging of cylinders in closed dies also show substantial agreement. The reasons for departure of the experimental forging pressures from the theory were thought to be due to bulging of the flash, failure of lubricant to retain its lubricating ability throughout a test, and possible failure to correct completely for stresses due to flash overhang. The local pressure distributions in the flash appear to be

Vol. 1
1960

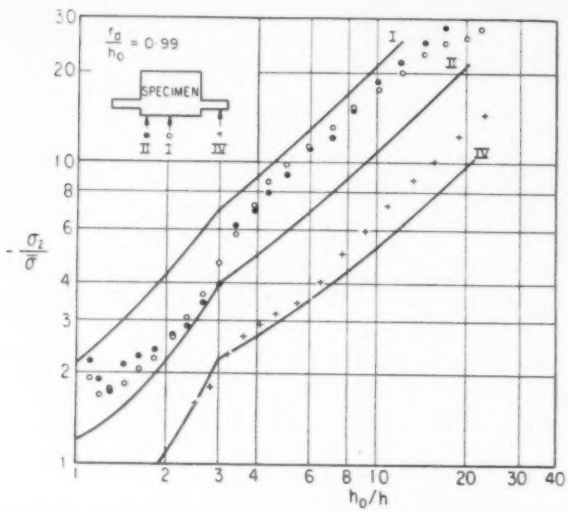

FIG. 20. Local dimensionless pressure distribution as function of height ratio, with pressure sensitive elements located 1/8 in. from fictitious disc, for $h_0 = 1{\cdot}010$ in.

as predicted by the theory, but adjustment by plastic flow of the metal within the body of the forging apparently permits readjustment of the local pressure to yield a more or less uniform pressure distribution.

Acknowledgements – The authors wish to thank the National Science Foundation for its support of the present investigation by its Grant to the University of California, as well as the University of California for the use of laboratory space and equipment. They further wish to thank Messrs. EGGLESTON, HALL, HARRIS, MILLER, SAYLOR and THOMETZ, students in Engineering, for assisting with the experimental phase of the investigation and reduction of data, Mr. KOT for preparing the drawings and Miss MATSUMOTO for typing the manuscript.

REFERENCES

1. L. PRANDTL, *Z. angew. Math. Mech.* **3**, 401 (1923).
2. R. HILL, E. H. LEE and S. J. TUPPER, *J. Appl. Mech.* **18**, 46 (1951).
3. A. P. GREEN, *Phil. Mag.* **42**, 900 (1951).
4. R. T. SHIELD, *Proc. Roy. Soc.* A. **233**, 267 (1955).
5. E. SIEBEL, *Stahl u. Eisen, Düsseldorf* **43**, 1295 (1923).
6. G. SACHS, *Mitt. Dtsch. MatPrüfAnst.* Suppl. **16** (1931).
7. M. D. STONE and J. T. GREENBERGER, *Iron Steel Eng.* **20**, 61 (1943).
8. W. SCHROEDER and D. A. WEBSTER, *J. Appl. Mech.* **16**, 289 (1949).
9. J. M. ALEXANDER, *J. Mech. Phys. Solids* **3**, 233 (1955).
10. J. F. BISHOP, *J. Mech. Phys. Solids* **6**, 132 (1958).
11. A. B. WATTS and H. FORD, *Proc. Inst. Mech. Engrs., Lond.* **1**B, 448 (1952).
12. S. KOBAYASHI, R. HERZOG, J. T. LAPSLEY, Jr. and E. G. THOMSEN, *Trans. Amer. Soc. Mech. Engrs.* **81**B, 228 (1958).
13. S. KOBAYASHI and E. G. THOMSEN, *Trans. Amer. Soc. Mech. Engrs.* **81**B, 217 (1958).

Int. J. Mech. Sci. Pergamon Press Ltd. 1960. Vol. 1, pp. 301–308. Printed in Poland

THE DESIGN OF PRESSURE VESSELS SUBJECTED TO THERMAL STRESS—III
THERMAL SHOCK*

E. WHALLEY and R. F. MACKINNON

Division of Applied Chemistry, National Research Council, Ottawa, Canada

(*Received* 19 *May* 1959)

Summary – The design of pressure vessels that are subjected to a sudden maintained change of temperature at one wall is discussed.

Vol. 1
1960

1. INTRODUCTION

IN THE first paper of this series (WHALLEY[1]), the mechanical behaviour of spherical and cylindrical vessels under the action of both pressure and thermal stresses was discussed for an arbitrary temperature distribution. In the second paper (WHALLEY[2]) the theory was applied to a steady-state temperature distribution, and design curves were given for pressure vessels made both of brittle and of ductile materials. During the build-up of a steady temperature gradient in a vessel, transient thermal stresses are obtained that must at some time be greater than the steady-state thermal stresses. Consequently, it is desirable to investigate transient stresses and to determine the effect they will have on the use of a pressure vessel.

In this paper we consider the behaviour of a vessel initially at constant temperature that is subjected to a sudden temperature change at one wall. It was shown in Ref. 1 that the ultimate pressure is independent of the thermal stress. The proof of this assumes, that, among other things, elastic waves caused by the application of stress can be neglected. This may no longer be true when elastic waves must be considered, particularly if the material is not perfectly ductile, but it is retained in this paper to avoid excessive complication. We here discuss a sudden thermal shock; in practice the shocks are never quite sudden, but the possibility that elastic waves may cause cracking must always be borne in mind, and the shock should be as gentle as practicable. Only experience will guide one in this matter.

The yield condition and the shakedown condition are important. The yield condition is readily calculated from the stresses in an elastic vessel. The stresses in a partly plastic vessel would be very difficult to calculate for transient temperatures, but fortunately, as was shown in Ref. 1, if the vessel had no residual stresses before the temperature and pressure

* N.R.C. No. 5565.

were applied, and if the maximum residual stress occurs at the same place as the maximum working stress, then the conditions for shakedown are the conditions for yielding with twice the tensile yield stress substituted for the tensile yield stress. It is, therefore, necessary to calculate the stresses of only an elastic vessel. Only cylindrical vessels are treated.

The conditions for fracture yield or shakedown will be calculated. For use in design the yield stresses and the ultimate stresses in the equations will usually be replaced by the stress multiplied by an appropriate safety factor. The discussions of Refs. 1 and 2 are also relevant to this paper.

2. THE STRESSES

We consider a concentric cylindrical vessel that is sufficently long that end effects are unimportant. It is subjected to pressure p_i inside and p_0 outside, is initially at temperature T and has no residual stresses. It is subjected to a temperature increase of ΔT applied suddenly to either the outer wall or the inner wall. The application of the temperature does not change either p_i or p_0. No heat is lost from the wall that is not heated. The inside radius is a and the outside is b and

$$k = b/a\,. \tag{2.1}$$

(i) *Shock at the outside wall*

Let the outside wall be suddenly heated at time $t = 0$ to ΔT above the rest of the vessel and maintained at this temperature, and let no heat be lost from the inner wall. The maximum thermal stresses are at the outside wall at time zero, and are obtained by inserting the conditions

$$\begin{aligned} T &= T + \Delta T \quad \text{at } r = b\,, \\ T &= T \qquad\quad \text{at all other } r \end{aligned} \tag{2.2}$$

into the general equations.[1,3] We find for the radial, tangential and longitudinal stresses at the outer wall, σ_{r0}, σ_{t0} and σ_{l0} respectively, when the end load due to the pressure is carried by the walls,

$$\sigma_{r0} = -p_0\,, \tag{2.3}$$

$$\sigma_{t0} = \frac{2p_i}{k^2-1} - p_0\frac{k^2+1}{k^2-1} - \beta\,, \tag{2.4}$$

$$\sigma_{l0} = \frac{p_i - k^2 p_0}{k^2-1} - \beta\,, \tag{2.5}$$

where

$$\beta = \alpha E \Delta T/(1-\nu)\,, \tag{2.6}$$

α is the thermal expansivity, E is Young's modulus, ν is Poisson's ratio and the subscripts 0 and i refer to the outer and inner wall respectively.

The thermal stresses are a maximum at the outer wall at zero time, and frequently the total stress will be a maximum at this point. However, the maximum pressure stresses are at the inner wall and it is possible that the sum of the pressure and thermal stresses at the inner wall may become greater than the stresses at the outer wall. It is necessary, therefore, to examine the stresses at the inner wall. According to JAEGER[4] the thermal tangential stress at the inner wall at time t is

$$\sigma_{ti} = \beta \sum_{s=1}^{\infty} \exp\left\{-x_s^2\left(\frac{\varkappa t}{b^2}\right)\right\} G(x_s)\left\{\frac{2k^2}{k^2-1} H_1(x_s) - H_0(x_s)\right\}, \tag{2.7}$$

where $\pm x_s$, $s = 1, 2, 3 \ldots$, are the roots (all real and simple) of the equation

$$J_0(x)\, Y_1(x/k) - J_1(x/k)\, Y_0(x) = 0\,, \tag{2.8}$$

and hence are dependent only on k; $\varkappa$ is the thermal diffusivity,

$$G(x_s) = \pi J_0(x_s) J_1(x_s/k) / \{J_0^2(x_s) - J_1^2(x_s/k)\}\,, \tag{2.9}$$

$$H_1(x_s) = \{J_1(x_s)\, Y_1(x_s/k) - J_1(x_s/k)\, Y_1(x_s)\}/x_s\,, \tag{2.10}$$

$$H_0(x_s) = J_0(x_s/k)\, Y_1(x_s/k) - J_1(x_s/k)\, Y_0(x_s/k)\,, \tag{2.11}$$

where J_0 and J_1 are Bessel functions of the first kind, zeroth and first order respectively, and Y_0 and Y_1 are Bessel functions of the second kind, zeroth and first order respectively. It should be noted that because the size of the vessel and the thermal diffusivity enter only in the term $\varkappa t/b^2$ the maximum stress is independent of the size of the vessel and of its thermal diffusivity.

TABLE 1. SOLUTIONS TO THE EQUATION $J_0(x)\, Y_1(x/k) - J_1(x/k)\, Y_0(x) = 0$

s \ k	1·25	1·5	2	3	4	5	6
1	8·212	5·104	3·588	2·879	2·668	2·574	2·523
2	23·689	14·281	9·603	7·311	6·580	6·232	6·036
3		23·649	15·818				

The roots of equation (2.8) were obtained numerically and graphically for various values of k and are given in Table 1. Solutions could not be obtained for $k < 1{\cdot}25$ because tables of the Bessel functions[5] stop at $x = 25$ and the solutions x_2 to equation (2.8) could not be obtained. We write the maximum value of σ_{ti} as

$$\sigma_{ti}(\max) = p_i \frac{k^2+1}{k^2-1} - \frac{2p_0 k^2}{k^2-1} + \beta f_{1k}\,. \tag{2.12}$$

Values of f_{1k} obtained numerically and graphically using the values of x_s in Table 1, are given in Table 2.

Vol. 1
1960

TABLE 2. VALUES OF f_{1k} FOR OUTSIDE HEATING

k	1·25	1·5	2	3	4	5	6
f_{1k}	0·34$_2$	0·347	0·374	0·401	0·419	0·433	0·440

(ii) *Shock at the inside wall*

Let the inside wall be suddenly heated at time $t = 0$ to ΔT above the rest of the vessel and let no heat be lost from the outer wall. The maximum thermal stresses are at $r = b$, $t = 0$, and are obtained in the same way as for outside shock. When the end load is carried by the pressure the stresses are

$$\sigma_{ri} = -p_i\,, \tag{2.13}$$

$$\sigma_{ti} = p_i\frac{k^2+1}{k^2-1} - \frac{2p_0k^2}{k^2-1} + \beta\,, \tag{2.14}$$

$$\sigma_{ti} = \frac{p_i - p_0k^2}{k^2-1} + \beta\,, \tag{2.15}$$

where the subscript i indicates the inner wall. At the outer wall the thermal stresses reach a maximum at some later time, and it is necessary to examine the stresses at the outer wall because they may become greater than those at the inner wall. According to JAEGER[4] the thermal tangential stress at the outer wall at time t for inside shock is

$$\sigma_{t0} = \beta\sum_{s=1}^{\infty}\exp\left\{-x_s^2\left(\frac{\varkappa t}{b^2}\right)\right\}L(x_s)\left\{\frac{k^2}{k^2-1} - \frac{4}{\pi x_s^2} + M_0(x_s)\right\}, \tag{2.16}$$

where

$$L(x_s) = \pi J_1^2(x_s)/\{J_1^2(x_s) - J_0^2(x_s/k)\}\,, \tag{2.17}$$

$$M_0(x_s) = J_0(x_s)\,Y_0(x_s/k) - Y_0(x_s)J_0(x_s/k)\,, \tag{2.18}$$

and x_s, $s = 1, 2, \ldots$, are the roots of the equation

$$J_1(x)\,Y_0(x/k) - J_0(x/k)\,Y_1(x) = 0\,. \tag{2.19}$$

At the time when the tangential stress given by equation (2.16) is a maximum we can write

$$\sigma_{t0}(\max) = \frac{2p_i}{k^2-1} - p_0\frac{k^2+1}{k^2-1} - f_{2k}\beta\,, \tag{2.20}$$

where f_{2k} is a function of k only and is equal to the maximum of the summed term in equation (2.16). For $k = 1{\cdot}25$, x_1 and x_2 were found numerically and graphically to be

$$x_1 = 7{\cdot}5, \qquad x_2 = 23{\cdot}45\,,$$

and from equations (2.16)–(2.19),

$$f_{2k} = 0{\cdot}28\,.$$

We shall see later that there is no need to be concerned with f_{2k} for higher values of k.

3. DESIGN FOR OUTSIDE SHOCK

The pressure and thermal stresses at any given surface can either reinforce or oppose. If they reinforce at one surface then they oppose at the other surface, and vice versa. Consequently, when discussing design it is convenient to discuss first conditions that must always hold, and then discuss further conditions that must hold when pressure and thermal stresses reinforce at the surface that is shocked, and when they oppose.

(i) *Brittle vessels*

Brittle vessels are assumed to fracture when the maximum principal stress reaches the fracture stress in tension or compression. For most brittle materials the fracture stress in tension is numerically quite different from that in compression. In the following equations the numerical value of the fracture stress will depend upon whether failure is occurring in tension or in compression, and this must be determined by inspection.

For simplicity we will consider that the outside pressure is zero. All vessels must, of course, obey the condition that fracture (at the inside surface) does not occur under the influence of pressure alone. Consequently, from equation (2.12) with $\beta = 0$, the condition that

$$p_i < \sigma_u(k^2-1)/(k^2+1) \tag{3.1}$$

must hold, independently of the thermal stress.

(a) When the pressure and thermal stresses act in the same sense at the outer surface, i. e. when the outer surface is cooled, the condition that fracture does not occur at the outer surface must be imposed. From equations (2.3)–(2.5) the maximum principal stress at the outer surface is the tangential, and consequently,

$$\frac{2p_i}{k^2-1} - \beta < \sigma_u\,. \tag{3.2}$$

If equation (3.2) holds then fracture will not occur under the thermal stress alone because the thermal stress is necessarily less than the ultimate stress. At the inner surface the thermal stress opposes the pressure stress and so no account need be taken, other than by equation (3.1), of the stresses at the inner surface.

(b) When the pressure and thermal stresses act in opposite senses at the outer wall, i. e. the outer surface is warmed, the stress at the outer wall when both act is less than when either act alone. So we must set

the maximum thermal stress as that that will cause fracture in the absence of pressure stresses, i. e.

$$|\beta| < |\sigma_u| \,. \tag{3.3}$$

Equation (3.1) will, of course, also hold. When the pressure and thermal stresses are in opposite senses at the outer wall they are in the same sense at the inner wall. So we must insert the condition that fracture does not occur at the inner wall, i. e. from equation (2.12),

$$p_i(k^2+1)/(k^2-1)+f_{1k}\beta < \sigma_1 \,. \tag{3.4}$$

(ii) *Ductile vessels*

A ductile material is assumed to yield without strain-hardening when the maximum shear stress τ reaches a limiting value τ_y. It is necessary that yield (at the inner surface) does not occur under the influence of pressure alone. Consequently, since

$$\tau = |\sigma_t - \sigma_r| \,, \tag{3.5}$$

σ_r is given by equation (2.12) with $\beta = 0$, and $\sigma_{ri} = -p_i$, the condition

$$|\Delta p| < \tau_y(k^2-1)/k^2 \,, \tag{3.6}$$

where

$$\Delta p = p_i - p_0 \,, \tag{3.7}$$

must hold independently of the thermal stress. The maximum shear stress at the outside surface, τ_0, is, from equations (2.3)–(2.5),

$$\tau_0 = |\Delta p/(k^2-1) - \tfrac{1}{2}\beta| \,. \tag{3.8}$$

(a) When the pressure and thermal stresses act in the same sense at the outer surface, i. e. when Δp and β are of opposite signs, the condition for no yielding at the outer surface is, from equation (3.8),

$$|\Delta p/(k^2-1) - \tfrac{1}{2}\beta| < \tau_y \,. \tag{3.9}$$

Equation (3.6) must, of course, also hold.

(b) When the pressure and thermal stresses act in the opposite senses at the outer surface, i. e. when Δp and β are of the same sign, the shear stress when both act is less than when either act alone. So we must set the maximum thermal stress as that that will cause yielding in the absence of pressure, i. e.

$$|\beta| < \tau_y \,, \tag{3.10}$$

and equation (3.6) will also hold. As well as ensuring that equations (3.6) and (3.10) hold, we must ensure that yielding does not occur at the inner surface. The maximum shear stress at the inner surface is easily obtained from equation (2.12) and the radial stress at the inner wall, $-p_i$. If yielding is not to occur at the inner wall then

$$|\Delta p k^2/(k^2-1) + \tfrac{1}{2} f_{1k}\beta| < \tau_y \,. \tag{3.11}$$

As was shown in Ref. 1, if one wishes to calculate the conditions for shakedown it is necessary only to substitute $2\tau_y$ (or σ_y, where σ_y is the yield stress in tension) for τ_y in equations (3.6)–(3.11).

4. DESIGN FOR INSIDE SHOCK

(i) *Brittle vessels*

We again consider for simplicity that the outside pressure is zero. The maximum principal stress is the tangential, so, from equation (2.14), fracture will occur when

$$p_i(k^2+1)/(k^2-1)+\beta = \sigma_u\,. \tag{4.1}$$

(a) If the thermal and pressure stresses act in the same sense at the inner wall, i. e. the inner wall is heated, then equation (4.1) is a sufficient condition for defining fracture.

(b) If the pressure and thermal stresses act in opposite senses we must usually ensure that neither pressure nor thermal stresses acting alone will cause fracture. Consequently both equations (3.1) and (3.3) hold. It is also necessary to ensure that fracture will not occur at the outer surface since at $t > 0$ the pressure and thermal stresses are in the same sense there. The maximum tangential stress that is consistent with equations (3.1) and (3.3) is obtained by putting equations (3.1) and (3.3) into (2.20). We find

$$\sigma_{t0}(\max) = \sigma_u\{2/(k^2+1)+f_{2k}\}\,, \tag{4.2}$$

where we have assumed that the maximum stresses allowed in tension and in compression are the same. For $k = 1{\cdot}25$, the quantity in brackets in equation (4.2) is 1·06, and as k increases it decreases rapidly. The stresses are usually less than the fracture stress by a large safety factor, and consequently, condition (4.2) is unimportant for $k > 1{\cdot}25$. Consequently the limiting conditions are equations (3.1) and (3.2) only. If these hold then fracture will not occur at the outer surface.

(ii) *Ductile vessels*

The maximum shear stress at the inside wall occurs at $t = 0$ and is, from equations (2.13)–(2.15)

$$\tau_i(\max) = |\Delta p k^2/(k^2-1)+\tfrac{1}{2}\beta|\,. \tag{4.3}$$

(a) If pressure and thermal stresses act in the same sense at the inside wall, i. e. if Δp and β have the same sign, then this is the maximum stress that occurs in the vessel. The necessary and sufficient condition for no yielding is then

$$|\Delta p k^2/(k^2-1)+\tfrac{1}{2}\beta| < \tau_y\,. \tag{4.4}$$

(b) If the pressure and thermal stresses act in the opposite sense at the inside wall, i. e. Δp and β have opposite signs, it is usually necessary to

Vol. 1
1960

ensure that yielding does not occur when either pressure or thermal stresses are present alone, i. e. conditions (3.6) and (3.10) hold. It is also important that no yielding should occur at the outer surface. From equation (2.16), substituting into it equations (3.6) and (3.10) and $\sigma_r = -p_0$, we find

$$\tau_0 > \tau_y \left(\frac{1}{k^2} + \frac{1}{2} f_{2k} \right) . \tag{4.5}$$

The quantity in brackets in equation (4.5) is always less than unity, at least for $k > 1{\cdot}25$, so T_0 must always be less than T_y. Consequently there is no need, if equations (3.6) and (3.10) hold, to consider yielding at the outer wall.

In order to facilitate reference, the numbers of the equations that are to be used for design for the various conditions are summarized in Table 3.

TABLE 3. DESIGN EQUATIONS FOR THERMAL SHOCK

Surface of shock	Inside		Outside	
Sense of stresses at surface of shock	Same	Opposite	Same	Opposite
Brittle	4·1	3·1, 3·3	3·1, 3·2	3·1, 3·3, 3·4
Ductile	4·4	3·6, 3·10	3·6, 3·9	3·6, 3·10, 3·11

REFERENCES

1. E. WHALLEY, *Canad. J. Tech.* **34**, 268 (1956).
2. E. WHALLEY, *Canad. J. Tech.* **34**, 291 (1956).
3. S. TIMOSHENKO and J. N. GOODIER, *Theory of Elasticity* p. 412. McGraw-Hill, New York (1951).
4. J. C. JAEGER, *Phil. Mag.* **36**, 418 (1945).
5. Functions of order zero and unity. *Bessel Functions Part* 1. British Association Mathematical Tables, Vol. XI. Cambridge University Press (1950).

Int. J. Mech. Sci. Pergamon Press Ltd. 1960. Vol. 1, pp. 309–311. Printed in Poland

BOOK REVIEWS

Power Reactors 1959. A.S.M.E. Nuclear Reactor Plant Data, Volume One. McGraw-Hill, New York, 1959. 126 pp., 29s.

THE A. S. M. E. 1959 edition of Power Reactors presents information about types of reactor plant and their experimental prototypes which are intended to produce electrical power. The edition of 1958 referred only to U. S. reactor plants, but the current one contains both revised data concerning twenty-one U. S. plants and data on eleven others; these are made up of six British, three French, one Canadian and one Swedish.

This very useful reference volume presents its data, i. e. statements of sizes and magnitudes, etc. under the following heads: Power Data, Nuclear Data, a System Flow Diagram, details about the Fuel Elements and Blankets and the Reactors, Reactor Control, Primary and Secondary Coolant Systems, Steam Systems, Description of Plant Containment and Miscellaneous Remarks.

W. J.

Proceedings of the Third U.S. National Congress of Applied Mechanics. Pergamon Press, London, 1958. 864 pp., 120s.

THE aim of this series of conferences is to maintain U. S. interest in applied mechanics in the intervals between international conferences. This aim has apparently been realized, for this volume contains, in addition to four general lectures, ninety-seven technical papers. These are divided into four sections:

(i)	Dynamics, Vibrations and Elastic Waves	(23 papers)
(ii)	Elasticity and Elastic structures	(30 papers)
(iii)	Plasticity, Viscoelastic Flow & Fracture	(27 papers)
(iv)	Fluid Flow, Aerodynamics & Heat Transfer	(18 papers)

The first general lecture, "Linear Thermodynamics and the Mechanics of Solids", by M. A. BIOT, is an extremely interesting exposition on a subject not generally treated in books on solid mechanics. The concepts of irreversible thermodynamics for systems departing slightly from equilibrium are first discussed. These concepts are then applied to the subjects of thermoelasticity and linear viscoelasticity. As a by-product of these studies the relations between the adiabatic and isothermal moduli in elasticity theory are clarified.

A review of boundary layers in subsonic and supersonic flow is given by H. L. DRYDEN in the second general lecture, followed by a well-presented survey of theories of creep buckling by N. J. HOFF. In the latter paper the defects of linearized theories for predictions of useful life are pointed out.

The final general lecture, on "Rotationally Symmetric Problems in the Theory of Thin Elastic Shells" by E. REISSNER, contains, as one would expect, an interesting set of problems and their solutions.

Clearly, it is impossible to give a survey of every paper presented. The following three were among those that interested the reviewer. A paper on the Application of Root-Locus Methods to Vibration Analysis, by R. H. CANNON, JR., represents a welcome diffusion of a well-established method of analysis in one technology (control theory) to another field.

The "Response of Tall buildings to Random Earthquakes", by A. C. ERINGEN includes an analysis of the motion of a ten-storey building. Indications of a method for assessing

Vol. 1
1960

the probable number of times the stresses in the structure will exceed safe values are given.

SHIELD and DRUCKER's paper on the "Limit Strength of Standard ASME Thin-walled Pressure Vessels" points out that for pressures below 40 lb/in² where a possibility of brittle fracture exists, the standard ASME torispherical head is apparently unsafe.

In a publication of this kind one notices occasional unwitting duplication of earlier efforts. However, the whole forms an interesting volume and the standard of work is, in the main, high.

R. I. T.

High Temperature Effects in Aircraft Structures. Pergamon Press, London, 1958. 357 pp., 70s.

PROFESSOR HOFF is the editor of a very useful and interesting volume devoted to the effects in aircraft structures of aerodynamic heating accompanying supersonic flight.

The book is published for and on behalf of the Advisory Group for Aeronautical Research and Development of N. A. T. O. with the aim of disseminating information on this particular topic. It consists of sixteen chapters, each having its own author, whose duty has been to write a review article primarily for the use of other researchers.

Essentially the material falls into four major groups; these are: heat transfer, the description of material behaviour at elevated temperatures, stress analyses and experimental methods available for investigation in this field.

The scope of the volume is best indicated however, by quoting the chapter titles and their authors:

External Sources of Heat	MARTIN H. BLOOM
Heat Transmission in the Structure	FREDERICK V. POHLE
Materials for High-temperature Aircraft Structures	POL DUWEZ
Non-metallic Structural Materials at High Temperatures	C. GURNEY
Glass-like Structural Materials at High Temperatures	IVAN PEYCHES
Creep and Relaxation in Metals	N. P. ALLEN
Creep and Stress Relaxation of Plastics	WILLIAM N. FINDLEY
Fatigue of Structural Materials at High Temperature	B. J. LAZAN
Thermal Stresses	L. BROGLIO and P. SANTINI
Buckling Caused by Thermal Stresses	A. VAN DER NEUT
Stress Distribution in the Presence of Creep	N. J. HOFF
Creep Buckling	B. FRAEIJS DE VEUBEKE
Influence of Aerodynamic Heating of Aeroelastic Phenomena	R. L. BISPLINGHOFF and JOHN DUGUNDJI
Experimental Methods in High-temperature Structural Research	J. TAYLOR
Models and Analogues	RICHARD R. HELDENFELS

The standard of each contribution is uniformly high and the material presented should appeal to a far wider audience than that section engaged directly in problems of aircraft structures. The book embodies results which are new and which have, hitherto, not been published. It gives concise summaries of information which is in general widely scattered and known only to the specialist.

W. J.

J. SMALL: **First Steps in Heat Transfer.** Blackie and Sons, Glasgow, 1959. 86 pp., 12s. 6d.

PROFESSOR SMALL has produced a short book of notes to introduce the subject of heat transfer to students and designers who have not hitherto studied it.

With the aid of numerous examples, the customary elements of thermal conductivity, convection and radiation are presented in a commendably clear, simple and straightforward manner.

The subject matter of the book might have been carried further at several points, still retaining its character of "first steps": e. g., Schmidt's graphical method for finding temperature distribution in a wall in unsteady heat flow. It may be that, owing to the rapid growth in importance of this subject, to-day's first steps may prove rather short for future readers. The fact remains that this book contains an amount of knowledge which is the minimum that any engineering graduate should possess, and presents it with admirable clarity.

W. J.

Vol. 1
1960

Vol.
196

BLANK
PAGE

Int. J. Mech. Sci. Pergamon Press Ltd. 1960. Vol. 1, pp. 313–321. Printed in Great Britain

ON THE THEORY OF VENTILATED WIND TUNNELS

L. C. Woods
University of New South Wales, N.S.W., Australia

(*Received* 9 *July* 1959)

Summary—This paper gives a new and more accurate treatment of the theory of rectangular wind tunnels that are ventilated by means of longitudinal slots on one pair of opposite walls. An aerofoil is placed at zero incidence midway between the slotted walls. The cross-flow, which is induced by the slots on the basic two-dimensional flow, is calculated accurately. This permits an averaged boundary condition to be obtained which is more accurate than those previously published.

In the final section of the paper the wake and solid blockage caused by the slotted walls is calculated. Let the slots have a width $2\sigma a$ and be spaced $2a$ apart and let the tunnel height be H. Then the theory yields the σ, $2a/H$ relation for zero blockage without any limit on the ratio $2a/H$, which in earlier treatments is required to be small.

1. INTRODUCTION

The exact mathematical treatment of the flow past aerofoils in "two-dimensional" wind tunnels, ventilated by means of longitudinal slots in the walls, is rather difficult. This is because the gaps or slots render the flow three-dimensional by imposing a periodic circulating "cross-flow" on the basic two-dimensional flow. This is illustrated in Fig. 1, which shows a symmetrical

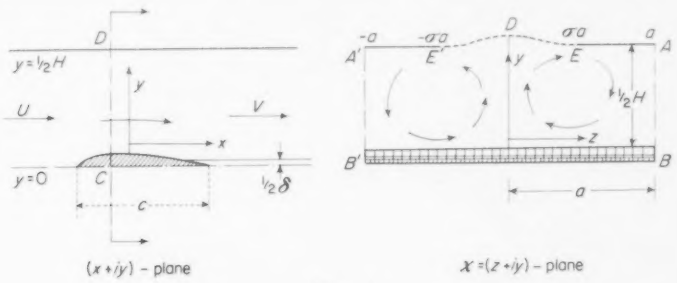

Fig. 1.

aerofoil at zero incidence on the axis of a slotted tunnel. The slots are uniformly spaced on the roof and floor of the tunnel, and this induces a flow pattern which is periodic in the z-direction. Efforts have been made to find exact solutions of this three-dimensional problem,[1] but even for the simple case shown in Fig. 1 the result is a very complicated set of equations which require numerical methods for their exact solution.

A much simpler treatment of the problem can be obtained if it is assumed that the flow is quasi-plane, i.e. that the cross-flow produced by the slots is only a small perturbation of the basic two-dimensional flow. These flows are assumed to be independent, except for a linking through the boundary conditions at the wall. The method thus has much in common with slender-body

theory. When the cross-flow problem has been solved an average boundary condition for the mean or basic two-dimensional flow can be deduced. Several authors have given various derivations of this averaged boundary condition (see Maeder and Wood,[2] who give references to the work of Guderley, Goethert, Davis and Moore on this topic; also see Baldwin *et al.*[3]), but these derivations are not very satisfactory for the following reason. The averaged boundary condition is calculated on the assumption that $2a/H \approx 0$, where $2a$ is the distance from the centre of one slot to the next, and H is the tunnel height (this assumption is wrongly accepted by some authors as being essential to the validity of using averaged boundary conditions), but later this boundary condition is used to derive a relation involving $2a/H$ and σ, the ratio of open to total boundary (see Fig. 1). We shall give a new derivation, which overcomes this defect.

2. MATHEMATICAL FORMULATION

Let the axes Ox, Oy, Oz be chosen as shown in Fig. 1, and let (u, v, w) be the velocity components in these directions. The velocity upstream at infinity will be U, and that downstream at infinity, V. We shall adopt linear perturbation theory and ignore second-order terms in $u-U$, v and w. In steady irrotational three-dimensional flow we have

$$\frac{\partial u}{\partial x}+\frac{\partial v}{\partial y}+\frac{\partial w}{\partial z}+\frac{1}{\rho}\left(u\frac{\partial \rho}{\partial x}+v\frac{\partial \rho}{\partial y}+w\frac{\partial \rho}{\partial z}\right)=0, \tag{1}$$

$$\frac{\partial v}{\partial x}=\frac{\partial u}{\partial y}, \quad \frac{\partial w}{\partial x}=\frac{\partial u}{\partial z}, \quad \frac{\partial w}{\partial y}=\frac{\partial v}{\partial z}, \tag{2}$$

$$u=\frac{\partial \phi}{\partial x}, \quad v=\frac{\partial \phi}{\partial y}, \quad w=\frac{\partial \phi}{\partial z} \tag{3}$$

and

$$\frac{dp}{\rho}=\frac{a^2}{\rho}d\rho=-q\,dq, \tag{4}$$

where ρ, p, q and a are the density, pressure, fluid speed and sound speed respectively. In linear perturbation theory the last two terms of (1) can be ignored, while by (4) the fourth can be written

$$\frac{u}{\rho}\frac{\partial \rho}{\partial x}=-\frac{u}{2a^2}\frac{\partial q^2}{\partial x}\simeq-\frac{u}{2a^2}\frac{\partial u^2}{\partial x}\simeq-\frac{U^2}{a_a^2}\frac{\partial u}{\partial x}=-M_a^2\frac{\partial u}{\partial x},$$

M_a being the Mach number upstream at infinity. Therefore, with $\beta_a^2=1-M_a^2$, (1) becomes

$$\beta_a^2\frac{\partial u}{\partial x}+\frac{\partial v}{\partial y}+\frac{\partial w}{\partial z}=0. \tag{5}$$

As we are assuming the slots to be all of equal width, and to be uniformly distributed across the tunnel wall, the flow pattern must be periodic in the Oz-direction. Let $(\bar{u}, \bar{v}, \bar{w})$ denote average values over one period $-a \leqslant z \leqslant a$, i.e.

$$\bar{u}=\frac{1}{2a}\int_{-a}^{a}u\,dz, \quad \bar{v}=\frac{1}{2a}\int_{-a}^{a}v\,dz, \quad \bar{w}=\frac{1}{2a}\int_{-a}^{a}w\,dz, \tag{6}$$

then these quantities will depend only on x and y. It is clear from Fig. 1 that if we chose the Oz-axis to lie on a line of symmetry passing through the centre

of a slot, then w will be an odd function of z. Thus

$$\bar{w} = 0. \tag{7}$$

If the first of (2) and (5) are now averaged over one period the result is

$$\frac{\partial \bar{v}}{\partial x} - \frac{\partial \bar{u}}{\partial y} = 0, \quad \beta_a^2 \frac{\partial \bar{u}}{\partial x} + \frac{\partial \bar{v}}{\partial y} = 0. \tag{8}$$

Let

$$\tau \equiv \Omega + i\theta = \beta_a\left(1 - \frac{\bar{u}}{U}\right) + i\frac{\bar{v}}{U}, \tag{9}$$

then as $\bar{u} \simeq \bar{q}$, Ω and θ are the speed parameter and the flow direction of the mean two-dimensional flow, and it follows from (8) and (9) that for this flow

$$\tau = \tau(Z), \quad (Z = x + i\beta_a y). \tag{10}$$

This equation, plus the corresponding averaged boundary conditions, determine the mean flow. However, before these boundary conditions can be obtained it is necessary to calculate the cross-flow.

To find a suitable equation for the cross-flow, let

$$u = \bar{u} + \tilde{u}, \quad v = \bar{v} + \tilde{v}, \quad w = \tilde{w}, \quad \phi = \bar{\phi} + \tilde{\phi}. \tag{11}$$

Substituting these into (5), and taking (8) into account, we get

$$\beta_a^2 \frac{\partial \tilde{u}}{\partial x} + \frac{\partial \tilde{v}}{\partial y} + \frac{\partial \tilde{w}}{\partial z} = 0. \tag{12}$$

We now introduce the approximation that $\partial\tilde{u}/\partial x$ is small compared with $\partial\tilde{v}/\partial y$ and $\partial\tilde{w}/\partial z$. This is the usual approximation of slender-body theory, and is valid if a typical downstream distance is much greater than a typical cross-stream distance, e.g. if $2a/H$ is small. In the present case, however, this restriction is not really essential; this can be shown as follows. The velocity u has two distinct components, viz. u_a due to the aerofoil alone, i.e. with the walls at infinity, and u_w the increment to u caused by the walls. This increment u_w can be written $u_w = \bar{u}_w + \tilde{u}$ as u_a is obviously independent of z. With walls that are either completely solid or completely open, $\partial u_w/\partial x$ is a very small quantity over the aerofoil surface. In fact, if C_D is the aerofoil drag coefficient and c is the chord length, this gradient can be expressed as $k(\pi c U C_D/\beta_a^3 H^2)$, where $k = \frac{1}{12}$ with solid walls and $\frac{1}{48}$ with open "walls". Thus with slotted walls the variations in $\partial u_w/\partial x$ with z will certainly not exceed $(\pi c U C_D/16\beta_a^3 H^2)$, and will, in fact, be a good deal less. This means that $\partial\tilde{u}/\partial x$ is quite small, regardless of the magnitude of the ratio $2a/H$, and as the variations we have described are greater at the aerofoil than elsewhere in the tunnel, this remark applies generally.

We are now able to replace (12) by

$$\frac{\partial \tilde{v}}{\partial y} + \frac{\partial \tilde{w}}{\partial z} = 0,$$

which by (3) and the last of (12) is equivalent to

$$\frac{\partial^2 \bar{\phi}}{\partial y^2} + \frac{\partial^2 \bar{\phi}}{\partial z^2} = 0. \tag{13}$$

This is the equation governing the cross-flow.

Vol. 1
1960

The boundary conditions for the cross-flow are:
(i) On the solid sections of the walls, $0 = v = \partial\phi/\partial y = \partial(\bar{\phi}+\tilde{\phi})/\partial y$, or

$$\frac{\partial\tilde{\phi}}{\partial y} = -\frac{\partial\bar{\phi}}{\partial y}. \tag{14}$$

(ii) In the gaps the pressure is constant, hence $q = U$, or ignoring second-order terms, $u = \partial(\bar{\phi}+\tilde{\phi})/\partial x = U$. Let the origins of ϕ and x coincide, then this boundary condition can be written

$$\tilde{\phi} = -\bar{\phi} + Ux. \tag{15}$$

(iii) On $z = \pm a$ the periodicity of the flow (see Fig. 1) and resulting symmetry requires that $w = \tilde{w} = 0$, so

$$\frac{\partial\tilde{\phi}}{\partial z} = 0. \tag{16}$$

(iv) On the aerofoil surface $v = U\theta_s$, where θ_s is the slope of the surface. But as θ_s is independent of z, $\bar{v} = U\theta_s$, whence $\tilde{v} = 0$, or

$$\frac{\partial\tilde{\phi}}{\partial y} = 0. \tag{17}$$

This completes the mathematical formulation of the problem.

3. THE MEAN BOUNDARY CONDITIONS

The first step in determining the mean boundary conditions is to calculate the cross-flow. Fig. 2 shows the $\Delta(= z+iy)$ plane, and the boundary conditions in this plane. It will be noticed that the normal derivative is specified everywhere, except on the gap $E'E$.

The Δ-plane is mapped on to the upper half of the t-plane shown by

$$t = \mathrm{sn}(\lambda\Delta, k), \tag{18}$$

where the modulus k and parameter λ are determined by

$$\lambda = \frac{K}{a} = \frac{K'}{\frac{1}{2}H}. \tag{19}$$

At E, $t = t_0$ and $\Delta = \sigma a + (i/2)H = \sigma a + iK'/\lambda$, so

$$t = \sin(\lambda\sigma a + iK') = \frac{1}{k}\,\mathrm{ns}(\lambda\sigma a) = \frac{1}{k}\,\mathrm{ns}(K\sigma), \tag{20}$$

The t-plane is mapped into the ζ-plane shown in Fig. 2 by

$$t = t_0 \sin\tfrac{1}{2}\zeta, \tag{21}$$

as is readily verified from the Schwarz–Christoffel mapping theorem. Combining (18) to (21) we now have

$$\sin\tfrac{1}{2}\zeta = k\,\mathrm{sn}(K\sigma)\,\mathrm{sn}(K\Delta/a). \tag{22}$$

The points B and A at $\Delta = a$ and $\Delta = a + iK'a/K$ map on to $\zeta = \gamma_0$ and $\zeta = \gamma_1$, and hence

$$\sin\tfrac{1}{2}\gamma_0 = k\,\mathrm{sn}(K\sigma) \tag{23}$$

and

$$\sin\tfrac{1}{2}\gamma_1 = \mathrm{sn}(K\sigma). \tag{24}$$

Let $\tilde{\psi}$ be the harmonic conjugate of $\tilde{\phi}$, then (25)

$$\tilde{\phi}+i\tilde{\psi}=\frac{\cos\frac{1}{2}\zeta}{2\pi}\left\{\int_{-\pi}^{\pi}\frac{\tilde{\psi}(\gamma)\,d\gamma}{\sin\frac{1}{2}\gamma-\sin\frac{1}{2}\zeta}+\int_{0}^{\infty}\left(\frac{\tilde{\phi}^{+}(\eta)}{\cosh\frac{1}{2}\eta-\sin\frac{1}{2}\zeta}+\frac{\tilde{\phi}^{-}(\eta)}{\cosh\frac{1}{2}\eta+\sin\frac{1}{2}\zeta}\right)d\eta\right\}$$

(see Woods[4]). Now on $\gamma=\pm\pi$ both $\tilde{\phi}^{+}(\eta)$ and $\tilde{\phi}^{-}(\eta)$ have the value $-\bar{\phi}+Ux$, which is independent of η. Substituting this value in (25), and integrating the first term by parts, we get

$$\tilde{\phi}(\gamma^{*})=-\frac{1}{\pi}\int_{-\pi}^{\pi}\left(\frac{\partial\tilde{\psi}}{\partial\gamma}\right)\ln\left|\frac{\sin\frac{1}{4}(\gamma-\gamma^{*})}{\cos\frac{1}{4}(\gamma+\gamma^{*})}\right|d\gamma-\bar{\phi}+Ux, \tag{26}$$

at a point $\gamma=\gamma^{*}$ on $\eta=0$.

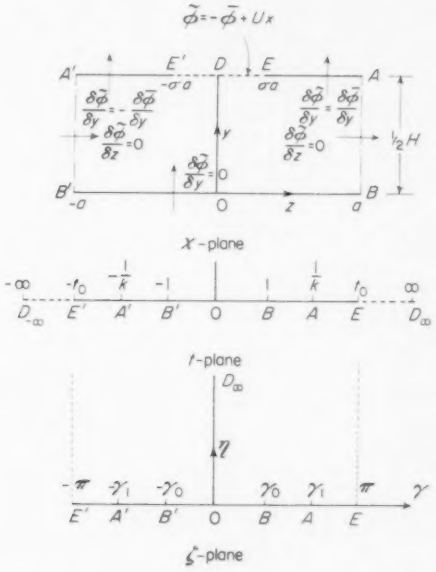

FIG. 2.

By a Cauchy–Riemann equation, on $\eta=0$, we have

$$\frac{\partial\tilde{\psi}}{\partial\gamma}=-\frac{\partial\tilde{\phi}}{\partial\eta}=-\frac{\partial\bar{\phi}}{\partial n}\left(\frac{\partial n}{\partial\eta}\right),$$

where n is measured along the normal to the boundary in the x-plane. It is apparent from Fig. 2 that $\partial\tilde{\psi}/\partial\gamma$ vanishes except in $-\pi<\gamma<-\gamma_1$, $\gamma_1<\gamma<\pi$, where

$$\frac{\partial\tilde{\psi}}{\partial\gamma}=\frac{\partial\bar{\phi}}{\partial y}\times\frac{\partial y}{\partial\eta}.$$

Differentiation of (22) gives

$$\frac{d\Delta}{d\zeta}=\frac{a\,\mathrm{ns}\,(K\sigma)\cos\frac{1}{2}\zeta}{2Kk\,\mathrm{cn}\,(K\Delta/a)\,\mathrm{dn}\,(K\Delta/a)} \tag{27}$$

and on $\zeta=\gamma$, $\Delta=x+\frac{1}{2}iH$, this becomes

$$\frac{\partial y}{\partial\eta}=-\frac{a\,\mathrm{ns}\,(K\sigma)}{2K}\frac{\cos\frac{1}{2}\gamma}{\mathrm{ds}\,(Kx/a)\,\mathrm{cs}\,(Kx/a)},$$

Vol. 1
1960

where by (22) and (24) $\mathrm{ns}\,(Kx/a) = \sin\frac{1}{2}\gamma/\sin\frac{1}{2}\gamma_1$. Hence

$$\frac{\partial\tilde{\psi}}{\partial\gamma} = -\frac{\partial\bar{\phi}}{\partial y}\frac{a\,\mathrm{ns}\,(K\sigma)}{2K}\frac{\cos\frac{1}{2}\gamma}{\left\{\left(\frac{\sin\frac{1}{2}\gamma}{\sin\frac{1}{2}\gamma_1}\right)^2-k^2\right\}^{\frac{1}{2}}\left\{\left(\frac{\sin\frac{1}{2}\gamma}{\sin\frac{1}{2}\gamma_1}\right)^2-1\right\}^{\frac{1}{2}}}.$$

Substituting this value in (26), we obtain

$$\tilde{\phi}(\gamma^*) = -\bar{\phi}+Ux+A(\gamma^*)\frac{\partial\bar{\phi}}{\partial y}, \tag{28}$$

where

$$A(\gamma^*) \equiv \frac{a\,\mathrm{ns}\,(K\sigma)}{2\pi K}\int_{\gamma_1}^{\pi}\frac{\cos\frac{1}{2}\gamma\ln\left|\frac{\cos\frac{1}{2}\gamma-\cos\frac{1}{2}\gamma^*}{\cos\frac{1}{2}\gamma+\cos\frac{1}{2}\gamma^*}\right|}{\left\{\left(\frac{\sin\frac{1}{2}\gamma}{\sin\frac{1}{2}\gamma_1}\right)^2-k^2\right\}^{\frac{1}{2}}\left\{\left(\frac{\sin\frac{1}{2}\gamma}{\sin\frac{1}{2}\gamma_1}\right)^2-1\right\}^{\frac{1}{2}}}d\gamma. \tag{29}$$

From the definition of $\tilde{\phi}$ its average value over $-a<z<a$ is zero, so the average of (28) with respect to z is

$$\bar{A}\frac{\partial\bar{\phi}}{\partial y}-\bar{\phi}+Ux = 0, \tag{30}$$

where

$$\bar{A} = \frac{1}{2a}\int_{-\gamma_0}^{\gamma_0}A(\gamma^*)\frac{dz}{d\gamma^*}d\gamma^*$$

$$= \frac{\mathrm{ns}\,(\sigma K)}{4Kk}\int_{-\gamma_0}^{\gamma_0}\frac{A(\gamma^*)\cos\frac{1}{2}\gamma^*\,d\gamma^*}{\left\{1-\left(\frac{\sin\frac{1}{2}\gamma^*}{\sin\frac{1}{2}\gamma_0}\right)^2\right\}^{\frac{1}{2}}\left\{1-k^2\left(\frac{\sin\frac{1}{2}\gamma^*}{\sin\frac{1}{2}\gamma_0}\right)^2\right\}^{\frac{1}{2}}}, \tag{31}$$

by (23), (24) and (27).

The required averaged boundary conditions now follow by differentiating (3) with respect to x

$$\bar{A}\frac{\partial\bar{v}}{\partial x}+U-\bar{u} = 0,$$

or by (9)

$$\lambda\frac{\partial\theta}{\partial x}-\Omega = 0, \tag{32}$$

where

$$\lambda \equiv -\beta_a\bar{A}. \tag{33}$$

The published work cited in the second paragraph of the introduction applies only to the limiting case $2a/H = 0$. By (19) this is the limit $K/K' = 0$, $K = \pi/2$, $k = 0$ and $\mathrm{sn}\,\sigma K = \sin(\pi\sigma/2)$. It now follows from (23), (24), (31) and (29) that in this limit

$$\lambda = -\beta_a\bar{A} = -\beta_a A(0)$$

$$= \beta_a\frac{a\sin\frac{1}{2}\gamma_1}{\pi^2}\int_{\gamma_1}^{\pi}\cot\tfrac{1}{2}\gamma\frac{\ln\{(1+\cos\frac{1}{2}\gamma)/(1-\cos\frac{1}{2}\gamma)\}}{\{\sin^2\frac{1}{2}\gamma-\sin^2\frac{1}{2}\gamma_1\}^{\frac{1}{2}}}d\gamma,$$

whence

$$\lambda = \frac{2a\,\beta_a}{\pi}\left|\ln\sin\frac{\pi\sigma}{2}\right|. \tag{34}$$

A more useful special case is obtained by assuming σ to be small, for it is shown in the next section that the values of σ which eliminate tunnel blockage are always less than 0·1 regardless of the value of $2a/H$. If σ is small it follows from (13) and (14) that γ_0 and γ_1 are small. Then by (29) and (31), $\bar{A} = A(0)$,

which reduces to the same integral as obtained in the derivation of (34), except that $K \neq \pi/2$ and $\frac{1}{2}\gamma_1 \simeq K\sigma$. Thus in this case

$$\lambda = \frac{a\beta_a}{K} |\ln \sigma K|. \tag{35}$$

4. BLOCKAGE IN A SLOTTED TUNNEL

The problem of determining the flow past an aerofoil in a slotted tunnel is now reduced to that of finding $\tau(Z)$ in the strip $-\infty < x < \infty$, $0 < y < \frac{1}{2}H$, subject to the boundary conditions

$$\theta = \theta_0(x) \text{ on } y = 0, \quad \lambda\left(\frac{\partial\theta}{\partial x}\right)_h - \Omega_h = 0 \text{ on } y = \tfrac{1}{2}H, \tag{36}$$

where the subscripts 0 and h denote values on the tunnel axis and wall respectively. This problem is readily solved by the Laplace transform method.

We shall put $q = U$ at $x = -\infty$, so that $\Omega_{-\infty} = 0$. Now (see Woods[4, 5])

$$\Omega_0(x^*) = \frac{1}{2b}\int_{-\infty}^{\infty} \left\{\theta_0(x)\,\mathrm{cosech}\,\frac{\pi}{2b}(x-x^*) + \Omega_h(x)\,\mathrm{sech}\,\frac{\pi}{2b}(x-x^*)\right\} dx \tag{37}$$

and

$$\theta_h(x^*) = \frac{1}{2b}\int_{-\infty}^{\infty} \left\{\theta_0(x)\,\mathrm{sech}\,\frac{\pi}{2b}(x-x^*) + \Omega_h(x)\,\mathrm{cosech}\,\frac{\pi}{2b}(x-x^*)\right\} dx \tag{38}$$

where

$$b \equiv \tfrac{1}{2}\beta_a H.$$

Let $\mathscr{L}$ denote the two-sided Laplace transform introduced by van der Pol and Bremmer,[6] i.e.

$$\mathscr{L}\{f(x); p\} \equiv p\int_{-\infty}^{\infty} \mathrm{e}^{-pt} f(t)\,dt,$$

then from results given by these authors it follows that

$$\mathscr{L}\left\{\mathrm{sech}\,\frac{\pi x}{2b};\ p\right\} = 2p\sec pb$$

and

$$\mathscr{L}\left\{\mathrm{cosech}\,\frac{\pi x}{2b};\ p\right\} = p\mathscr{L}\left\{\int_{-\infty}^{x} \mathrm{cosech}\,\frac{\pi x}{2b}\,dx;\ p\right\}$$

$$= \frac{2pb}{\pi}\mathscr{L}\left\{\ln\left|\tanh\frac{\pi x}{4b}\right|;\ p\right\} = -2pb\tan pb.$$

With these and with the aid of the convolution theorem we can transform (37) into

$$\mathscr{L}\{\Omega_0(x);\ p\} = \tan pb\,\mathscr{L}\{\theta_0(x);\ p\} + \sec pb\,\mathscr{L}\{\Omega_h(x);\ p\},$$

$$\mathscr{L}\{\theta_h(x);\ p\} = \sec pb\,\mathscr{L}\{\theta_0(x);\ p\} + \tan pb\,\mathscr{L}\{\Omega_h(x);\ p\}.$$

The second boundary condition in (36) transforms into

$$p\lambda\mathscr{L}\{\theta_h(x);\ p\} - \mathscr{L}\{\Omega_h(x);\ p\} = 0.$$

On eliminating Ω_h and θ_h we get

$$\mathscr{L}\{\Omega_0(x);\ p\} = \mathscr{L}\{\theta_0(x);\ p\}\left\{\frac{p\lambda + \tan pb}{1 - p\lambda\tan pb}\right\}$$

$$= -\frac{|p|}{p}\mathscr{L}\{\theta_0(x);\ p\} + \frac{1}{p}\mathscr{L}\{\theta_0(x);\ p\}\,\mathscr{L}\{F(x);\ p\}, \tag{39}$$

Vol. 1
1960

where

$$F(x) = \frac{1}{2\pi i}\int_{c-i\infty}^{c+i\infty} e^{px}\left\{\frac{|p|}{p} + \frac{p\lambda + \tan pb}{1 - p\lambda \tan pb}\right\} dp, \tag{40}$$

c being a real constant chosen so that the integral converges. Van der Pol and Bremmer[6] give $\mathscr{L}\{1/x;\, p\} = \pi|p|$; consequently on inverting (39) we obtain

$$\Omega_0(x) = \frac{1}{\pi}\int_{-\infty}^{\infty} \frac{\theta_0(x^*)\,dx^*}{x - x^*} + \int_{-\infty}^{\infty} \theta_0(x^*)\,F(x - x^*)\,dx^*. \tag{41}$$

As the first term on the right-hand side is the well known result for an aerofoil in an infinite stream, the second term must represent the increment to Ω_0 due to the slotted wall.

Equation (40) for $F(x)$ can be expressed in real form as follows. The real numbers c and $\mathscr{R}p$ must be chosen to secure the convergence of the integral, otherwise they are arbitrary. Let $c = 0$, and $p = -i\omega/b$, where ω is real, then (40) can be transformed into

$$F(x) = \frac{1}{\pi b}\int_0^{\infty} \frac{(b - \omega\lambda)\, e^{-\omega} \sin \omega x/b}{b\cosh\omega + \omega\lambda \sinh\omega}\, d\omega. \tag{42}$$

The "blockage factor" ϵ at a point x on the aerofoil surface is defined by $\epsilon = (\tilde{q} - \tilde{q}^*)/U$, where $\tilde{q}^*$ is the value $\tilde{q}$ would have at the same point x in an infinite stream, i.e. with $H = \infty$. Hence from (9) and (40),

$$\epsilon(x) = -\frac{1}{\beta_a}\int_{-c/2}^{c/2} \left(\frac{dy}{dx^*}\right)_0 F(x - x^*)\,dx^*,$$

on replacing θ_0 by $(dy/dx^*)_0$. Integration by parts gives

$$\epsilon(x) = \frac{\delta}{2\beta_a} F\left(\frac{c}{2} - x\right) - \frac{1}{\beta_a}\int_{-c/2}^{c/2} y_0(x^*)\, F'(x^* - x)\,dx^*, \tag{43}$$

as $y = 0$ at $x = -\frac{1}{2}$ and $y_0 = \delta/2$ at $x = c/2$ where δ is the wake displacement thickness $c/2C_D$ (see Fig. 1).

A useful approximation for $\epsilon(x)$ can be found by expanding the integrand in (43) in a series in $(x - x^*)/H$ and ignoring terms $0(H^{-3})$. The result is

$$\epsilon(x) = \frac{GA}{\beta_a^3 H^2} + \frac{\delta}{2\beta_a} F\left(\frac{c}{2} - x\right), \tag{44}$$

where from (38) and (42) G is a function of λ/b given by

$$G = -\frac{\beta_a^2 H^2}{2} F'(0) = \frac{2}{\pi}\int_0^{\infty} \frac{\omega(\omega\lambda/b - 1)\, e^{-\omega}\, d\omega}{\cosh\omega + \omega(\lambda/b)\sinh\omega}. \tag{45}$$

By (33) and (38) the ratio λ/b is $2(-\bar{A})/H$, and is therefore independent of the compressibility factor β_a. With small slots it follows from (35) that

$$\frac{\lambda}{b} = \left(\frac{2a}{H}\right)\frac{|\ln \sigma K|}{K}. \tag{46}$$

With completely solid walls $\sigma = 0$, so by (23), (24) and (31) $\gamma_0 = \gamma_1 = 0$, and $-\beta_a \bar{A} = \lambda = \infty$. Hence

$$G = \frac{2}{\pi}\int_0^{\infty} \frac{\omega\, e^{-\omega}}{\sinh\omega}\, d\omega = \frac{\pi}{6}.$$

Vol. 1
1960

While with completely open "walls", $\sigma = 1$, so (23), (24) and (29) give $\gamma_0 = \gamma_1 = \pi$, and $-\beta_a \bar{A} = \lambda = 0$. Thus

$$G = -\frac{2}{\pi}\int_0^\infty \frac{\omega\, e^{-\omega}}{\cos \epsilon\omega}\, d\omega = -\frac{\pi}{12}.$$

The corresponding forms of (44) are the well known standard results.

Zero average blockage can be obtained by choosing λ/b so as to make $\epsilon(0)$ vanish. Suppose C_D is negligible, then the wake blockage term in (44) can be ignored, and the condition for zero blockage reduces to $G = 0$. This equation can be solved numerically; let its solution be $\lambda/b = r$. If σ is small, this value can be substituted in (46) to give

$$\sigma = \frac{1}{K} e^{-rK(H/2a)} = \frac{1}{K} e^{-rK'}, \tag{47}$$

by (19). From a graph given by Baldwin *et al.*[3] it appears that $r \approx 1{\cdot}2$.

With this value of r in (47) we arrive at the σ, $2a/H$ relationship outlined in the following table:

$2a/H$	$\frac{1}{8}$	$\frac{1}{4}$	$\frac{1}{2}$	1	2	4
σ	0·0000	0·0003	0·0143	0·084	0·047	0·024
σ^*	0·0000	0·0003	0·0147	0·097	0·255	0·423

The value σ^* shown in the table is derived similarly from equation (34) which is valid only if $2a/H$ is small.

There are three conclusions to be drawn from this table: firstly, that the approximate theory of previous authors (which gives σ^*) fails for $2a/H > \frac{1}{2}$; secondly, that a remarkably small value of σ is required to eliminate the blockage effect regardless of the value of $2a/H$; and finally that σ has a maximum value at $2a/H \approx 1$.

REFERENCES

1. R. C. Tomlinson, *The Theoretical Interference Velocity on the Axis of a Two-dimensional Wind Tunnel with Slotted Walls.* Current Paper No. 181, Aeronautical Research Council, London (1954).
2. P. F. Maeder and A. D. Wood, *Z. angew. Math. Phys.* **7**, 177 (1956).
3. B. S. Baldwin, J. B. Turner and F. D. Knechtel, *Tech. Notes Nat. Adv. Comm. Aero., Wash.*, No. 3176 (1954).
4. L. C. Woods, *Appl. Sci. Res., Hague*, A **6**, 351 (1957).
5. L. C. Woods, *Proc. Roy. Soc.* A **233**, 74 (1955).
6. B. van der Pol and H. Bremmer, *Operational Calculus Based on the Two-sided Laplace Integral.* Cambridge University Press (1950).

Vol. 1
1960

Int. J. Mech. Sci. Pergamon Press Ltd. 1960. Vol. 1, pp. 322–335. Printed in Great Britain

THE DETERMINATION OF THE VALUE OF THE COLLAPSE LOAD FOR STATICALLY INDETERMINATE SYSTEMS UNDERGOING PLASTIC DEFORMATION*†

A. A. Gvozdev

TRANSLATOR'S PREFACE

The article by Professor A. A. Gvozdev which is the subject of this translation contains what appears to be the earliest proof of the theorems of limit analysis for proportional loading. In the course of his presentation, Gvozdev introduces many concepts now familiar in plasticity theory, notably generalized forces and displacements, the principle of maximum plastic work and the equivalent normality condition for strain rates at yield.

The article appeared in a slim volume entitled *Proceedings of the Conference on Plastic Deformations, December* 1936, which was issued by the Academy of Sciences of the U.S.S.R. in 1938, under the general editorship of Academician B. G. Galerkin.‡ Only fifteen hundred copies were made in the first printing and the document appears to have remained unnoticed outside the U.S.S.R., although frequently referred to by Russian authors.§

Gvozdev's paper is especially notable because of his use of generalized forces and displacements. This concept was employed in 1952 by Prager[8] when establishing a general theory of limit design, and Hodge[9] has given it a central place in his recent text on the plastic analysis of structures. Thus the paper is essentially modern in approach, despite its age, and this, together with the simple and direct manner of presentation of the material, is considered to make a full translation worthwhile.

Professor Gvozdev has written mainly on aspects of reinforced concrete construction. The Additional Bibliography (B) contains all articles by him which the translator has seen mentioned in the Russian literature.

* *Proceedings of the Conference on Plastic Deformations, December* 1936, p. 19. Akademiia Nauk SSSR, Moscow–Leningrad (1938).

† Translated from the Russian by Professor R. M. Haythornthwaite, Brown University, Providence, R.I. (Now at University of Michigan, Ann Arbor, Michigan.)

‡ See Additional Bibliography (A).

§ In the case of Gvozdev's paper, recognition appears to have come rather late even in Russia and in fact it coincided with a great outpouring of work on similar lines in Britain and the U.S.A. When reviewing developments in plasticity in the U.S.S.R. for the period 1917–47, Ishlinskii[1] dismisses the entire subject with the single sentence (p. 244) "The general idea of the carrying capacity of structures and the method of computation at the limit load was given by A. A. Gvozdev". Meanwhile neither Sokolovsky[2] nor Leibenson[3] had made any mention of his work in their books on the theory of plasticity. Nor did Kachanov[4] or Markov[5] recognize the limit theorems as derivable from the variational principles when specialized to proportional loading. Later on, writers interested in structural applications, such as Bezukhov[6] and Rzhanitsyn[7], have given considerable prominence to this and other papers by Gvozdev.

1. GENERAL APPROACH

One problem of structural construction which must occupy a central position is the computation of the carrying capacity, i.e. the determination of the largest live load which a structure can carry. Only in the case of brittle materials which obey Hooke's law almost to fracture can this problem be solved completely by the methods of the theory of structures and of elasticity. Of greater practical importance is the determination of the carrying capacity of structures composed of elements which yield on reaching a certain stress state.

It is more convenient to formulate the plastic relations in terms of the elements from which the parts of the structure are composed rather than for the material itself, i.e. for an element of length of a beam, for an element of a plate obtained by cutting through the entire thickness, for an element of a body, for a beam of a framework, etc. Thanks to this approach, the field of application of the theory under consideration is broadened appreciably.

The approach becomes particularly clear when applied to a segment of a reinforced concrete beam in bending. It would be incorrect to say that the material of such a beam can yield—yielding is possible only in the reinforcement. However, the relationship between the value of the bending moment M and the angle of relative rotation $\Delta\phi$ of the ends of the section (Fig. 1) shows that, when the moment reaches a certain value $M = \bar{M}$, the magnitude of the deformation increases almost without change in the loading. In the graph there is a typical yield zone ab. In reality, when the moment reaches the value $M = \bar{M}$, the *reinforcement* starts to yield, but in the *concrete* a crack opens, progressively diminishing the height of the compression zone. The moment M can be determined by a formula due to A. F. Loleit. The equality, $M = \bar{M}$, is suggested as the condition of yield for the reinforced concrete beam in bending.

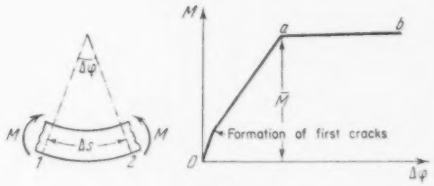

FIG. 1.

In what follows it will be necessary to define what is meant by the state of collapse of the structure. If for known conditions the elements of a structure are able to yield, then the structure can be considered as disabled as soon as the *displacements of the system can increase solely on account of the plastic deformation of its elements*. This state will be referred to below as the state of collapse, and the corresponding intensity of the live loading as the collapse load.

2. CHARACTERISTICS OF THE ELEMENTS

The methods of calculation of the value of the collapse load must be adapted to a wide class of structural forms, so the relationships which are to be written for an element of a structure should be formulated in a sufficiently

general manner. On the other hand, idealization of the properties of the material is unavoidable in order that our calculations should not be excessively complex. This leads, for example, to ignoring strain hardening and also to eliminating entirely the factor of time from the calculations.

For materials such as reinforced concrete, the relation between the deformations and the tractions up to the state of yield is exceedingly complex; therefore a new simplification is in order and for the plastic state we will introduce the most elementary relations in the spirit of Saint-Venant and von Mises.

The following characteristics will be attributed to the elements of the structure:

(a) For an element under the influence of constant forces, perceptible deformation is impossible except in the state of yield. In reality, reinforced concrete structures can deform continuously under the action of a constant load, due to the creep of the concrete; however, the magnitude of such deformation is of quite another order from the magnitude of the deformation at collapse, as defined above.

(b) In the state of yield, the generalized displacement (deformation) of an element can increase indefinitely for a constant value of the corresponding generalized force.

(c) For each possible mode of plastic deformation, the corresponding generalized force has a specified constant value. The set of generalized forces corresponding to all possible modes of deformation determines the yield condition, i.e. the relationship satisfied by the forces acting on the elements when in a state of yield.

The characteristics (a) and (b) can be considered as defining an ideally plastic body or element.

In the example of the reinforced concrete beam bent in one plane, which has been considered above, the value of the moment producing plastic deformation was found to be $M = \bar{M}$, where for definiteness we shall set $M > 0$.

If the beam has double reinforcement, then for bending in the opposite sense the corresponding value of the moment producing yield is found to be $M = \underline{M}$ where $\underline{M} < 0$. Consequently, possible values of the bending moment in the beam must satisfy the condition $\underline{M} \leqslant M \leqslant \bar{M}$. Such conditions, indicating that by virtue of the plastic characteristics of an element the load acting can change only within set limits, will be referred to as *limit conditions*.

If, as in the example considered, the stressed state of the element is determined by only one generalized force, the yield conditions (and hence the limit conditions) are particularly simple. Often, however, the stressed state of the element is characterized by values of several linearly unrelated generalized forces, for example, a longitudinal force N and bending moments M_x and M_y in a beam, or six stresses $(\sigma_x, \sigma_y, \sigma_z, \tau_{xy}, \tau_{yz}, \tau_{zx})$ on the sides of an elementary cube with sides perpendicular to the co-ordinate axes x, y, z, or, on the other hand, three principal stresses $(\sigma_1, \sigma_2, \sigma_3)$ on the sides of a correspondingly orientated elementary cube. For such cases the yield condition must be studied in more detail.

The deformation of the element can be described with the aid of the generalized displacements corresponding to the generalized forces which have been selected. For the sake of convenience, we select as generalized forces values of identical dimension, for example in the case of a beam, the moments about three axes which do not intersect at a point but which lie in the plane of the section. For this the generalized displacements will have identical dimensions.

We shall now obtain in a convenient fashion a geometrical interpretation which is often used for the study of strength theory. In a space of n dimensions, where n is the number of generalized forces necessary to define the stressed state of the element, we set out along the axes of one set of co-ordinates the values of the generalized forces $s_1, s_2, s_3, \ldots, s_n$, and along the axes of another, the values of the corresponding generalized displacements, $e_1, e_2, e_3, \ldots, e_n$. The corresponding forces and displacements are set out parallel and in one and the same direction (Fig. 2).

Vol. 1
1960

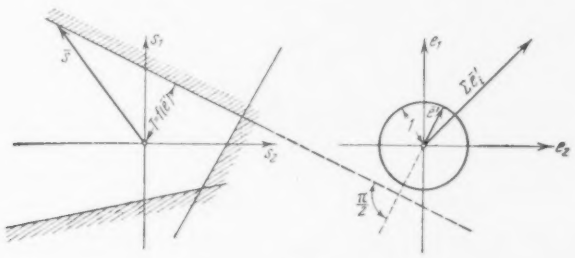

FIG. 2.

Any stressed state of an element is then represented by the vector **s** with components s_i $(i = 1, 2, \ldots, n)$, and the plastic deformation of the element by the vector **e** with the components e_i $(i = 1, 2, \ldots, n)$. Since, however, the deformation for a plastic state can increase indefinitely, the length (magnitude) of the vector **e** is indeterminate. This vector determines only the direction in space, whereas the vector **s** determines a point. Therefore, in place of the vector **e** it is more convenient to obtain the corresponding unit vector **e′**, i.e. the vector the length (magnitude) of which equals unity.

The property of the ideally plastic element given under (c) above can now be stated as: for each possible deformation, represented by the unit vector **e′**, where

$$\mathbf{e}' = \mathbf{e} \Big/ \sum_{i=1}^{i=n} e_i^2,$$

there corresponds an expenditure of work

$$T = \mathbf{e}'\,\mathbf{s} = f(\mathbf{e}').$$

All the vectors **s** the ends of which lie on a linear $(n-1)$-dimensional manifold ("plane") orthogonal to **e′** and distant $T = f(\mathbf{e}')$ from the origin of co-ordinates satisfy this condition (Fig. 2).

The equation of this linear manifold has the analytic form*

$$\Sigma e'_i s_i = f.$$

The set of such $(n-1)$-dimensional manifolds for all possible modes of deformation (of vectors $\mathbf{e}'$) produces a convex body in the n-dimensional space. The points of the surface (of the boundary) of this body satisfy the yield condition; all points of the body satisfy the limit condition.

If only discrete modes of deformation are possible,† the yield condition determines a polygon, the boundaries of which are orthogonal to the corresponding vectors $\mathbf{e}'$. If the possible vectors $\mathbf{e}'$ form an analytic manifold, then at the yield conditions they satisfy the points of an $(n-1)$-dimensional manifold (of a "surface") skirting a family of linear $(n-1)$-dimensional manifolds ("planes") corresponding to all possible vectors $\mathbf{e}'$. Thus in this case the deformation corresponding to the stress state represented by any point A of the boundary of the convex body, i.e. the plastic deformation, is represented by the vector $\mathbf{e}'_A$, parallel to the normal to the surface of the body at the point A (Fig. 3).

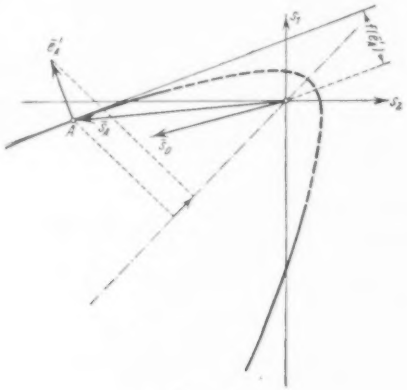

FIG. 3.

The origin of co-ordinates (the unstressed state) always satisfies the yield condition. Since the work being expended in the plastic deformation is always positive, the vector $\mathbf{e}'_A$ is directed along the outwards normal of the yield surface at the point A. Thus the following results are deduced from the definition of an ideally plastic element given above:

Result I. In the space $(s_1, s_2, \ldots, s_n)$, the yield condition gives an $(n-1)$-dimensional manifold ("surface") which is a limiting convex body, referred to as body B.

Result II. For each stressed state represented by a point A lying on the boundary of the body B (i.e. a state of yield) there corresponds a deformation represented by a vector $\mathbf{e}'_A$ directed along the outwards normal to the boundary of the body B at the point A.

* Translator's note—The original is $\Sigma e_i s_i = f$, which appears to be a misprint.

† Translator's note—This statement is unnecessarily restrictive. If any two modes of deformation occur at the same stress state, a polygonal form will result; however, certain linear combinations of the modes are then also possible.[10]

If $F = 0$ represents the yield condition, then the second result is written in the analytical form

$$e_i = C\partial F/\partial s_i \quad (i = 1, 2, \ldots, n),$$

where C is a positive quantity depending on the co-ordinates and on time but independent of the indices i.

This shows that the function F represents the potential of the flow, as introduced in the theory of plasticity by von Mises in 1928. It is necessary, however, to remark that von Mises's result possesses an entirely formal character. Von Mises wrote the function F as a quadratic which did not change with variations of the hydrostatic pressure and he sought to obtain an expression for the deformation in the form of linear functions of the stresses which again were to be independent of the hydrostatic pressure. Here, on the other hand, the role of the function F as a potential of the flow is derived directly from the definition of the ideally plastic material and is unrelated to the analytic expression for the condition of yielding and displacement.

Vol. 1
1960

From the definition of the ideally plastic material at the yield condition, the points lie on a convex body; hence it is easy to deduce the following result.

Result III (Fig. 3). The work $T = \mathbf{e}_A \mathbf{s}_A$ being expended on the plastic deformation of an element is not less than the virtual work $T' = \mathbf{e}_A \mathbf{s}_D$ which would be performed for the same deformations by combinations of any loadings (stresses) on the element which are permitted by the limit conditions.

We shall now clarify by means of examples what we understand by possible modes of plastic deformation. Suppose that for an element of some isotropic material only plastic deformation representing slip is possible, i.e. pure shear in the direction of one of the three principal shearing directions. In all there will be six possible modes of deformation (counting the sign of the deformation). All six of the possible vectors $\mathbf{e}$ lie in the plane $e_1 + e_2 + e_3 = 0$. In view of the similarity of the axes s_1, s_2 and s_3, the yield conditions define in this case a regular hexagonal prism (maximum shear stress hypothesis).

If not only pure shearing but also all deformation which does not change the volume of the element is possible, and if the work $T = \mathbf{e}'\mathbf{s}$ is constant, i.e. does not vary with the direction of $\mathbf{e}'$, then the yield conditions define a cylinder (Hencky–von Mises theory).

For concrete and rock, the condition of plasticity defines the boundary of a body which is broadening in the direction of increase in the hydrostatic pressure (Fig. 3). Evidently in this case the vector $\mathbf{e}$ is always projected in the positive direction of the axis* $1\mathbf{e}'_1 + 1\mathbf{e}'_2 + 1\mathbf{e}'_3$, i.e. the plastic deformation must be accompanied by an increase in the volume of the element.

This theoretical prediction is confirmed by the results of tests. In the University of Illinois, Richart, Brandtzaeg and Brown† subjected concrete cylinders to longitudinal compression and simultaneous hydrostatic pressure on the lateral surfaces. At the start of the test, the volume of the concrete

* Translator's note—See Fig. 3. The octahedral axis is meant.

† Translator's note—The author probably has in mind F. E. Richart, A. Brandtzaeg and R. L. Brown, *A Study of the Failure of Concrete under Combined Compressive Stress*, Bull. 185, University of Illinois Engineering Experimental Station (1928).

decreased owing to the smallness of Poisson's ratio. With increasing load, the reduction in volume slowed down and when the concrete started to flow it increased in volume; however, in many samples the original size remained the largest even up to the conclusion of the test.

Often the expressions for the limit conditions prove to be rather complicated. The following two examples show how they can be simplified for the purpose of practical calculations.

For an element of length of a metal I-beam subjected to the action of a longitudinal force and bending in the plane of the web, it is easy to construct the limit conditions for any position of the neutral axis, recalling that all that part of the section lying on one side of this axis is stressed to the yield limit in compression and the remaining part of the section is stressed to the yield limit in extension. The lens-shaped limit curve [Fig. 4(a)] is constructed from two parabolas having common tangents at the points C_1, C_2, C_3 and C_4.

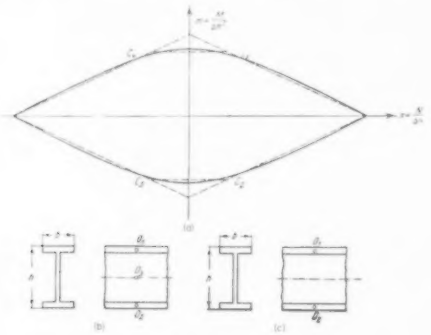

FIG. 4.

As is evident from the graph in the figure, it can be approximated closely with the aid of a hexagon (or allowing rather large error, by means of a rhombus). This corresponds to the substitution of a fictitious effective cross-section for which only discrete positions of the neutral axis are possible, as shown in Fig. 4(b) for the case of the hexagon and in Fig. 4(c) for the case of the rhombus.

For the reinforced concrete section with double reinforcement, as shown in Fig. 5, the limit moments for the upper and lower reinforcement are computed in accordance with the draft of technical specifications and standards for reinforced concrete construction (1936). In the case of eccentric extension, of pure bending and of eccentric compression with large eccentricity, the yield curve is composed of two line segments.* Only in the range of small eccentricities, i.e. at the approach to brittle fracture, does the yield curve depart from

* Translator's note—M_0 and M_0' are the bending moments associated with the axial forces when considered acting at O and O' respectively. The energy dissipation is always given by $D = \theta M_0 + \theta' M_0'$, where θ and θ' are the rotations taken about whichever bar is not extending: hence M_0 and M_0' are true generalized stresses. Note that, if both bars extend, θ and θ' are both non-zero, the values being obtained by allowing opening of the joint first about one bar and then about the other. Negative rotations, i.e. rotations opposite in sense to the corresponding moments, are not permissible.

these lines. If we restrict ourselves to cases far from brittle fracture, the limit conditions can be given approximately in the form $M' \leqslant \bar{M}; M \geqslant \underline{M}$. Two modes of plastic deformations correspond to this: (1) The lower reinforcement yields, the element opens and its parts rotate about an instantaneous centre lying at the level of the upper reinforcement. (2) The upper reinforcement yields, and opening of the element proceeds, by the turning of its parts about an instantaneous centre lying at the level of the lower reinforcement.

Thus in these two examples it appears to be sufficient for practical purposes to consider only two or three modes of deformation instead of the infinite number of modes which actually exists.

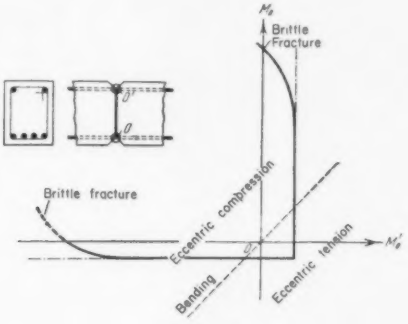

FIG. 5.

3. LIMITATIONS ON THE APPLICATION OF THE THEORY

Before passing on to an explanation of the principles and methods of calculation, it is necessary to make several reservations.

In all that follows, it is presupposed that, up to the instant of collapse, the deformations and the displacements remain sufficiently small so that one can ignore the change in the geometric quantities (angles, lever arms, spans, etc.) entering the equations of equilibrium of the elements and also the kinematical constructions and calculations. Such a restriction is usually made in the calculation of elastic systems, but in our case it is evidently more troublesome because the restriction is carried to very late stages of loading of the structure. None the less, for structures which are sufficiently rigid, as will usually be the case in construction, the restriction which has been referred to seems to be appropriate.

A danger which appears to be a more serious limitation on the application of the theory is that the structure might lose stability in whole or in part before reaching what is being designated here as the collapse load. This limitation is important in the case of metal construction,* but it plays hardly any role for reinforced concrete. However, for the latter material it is necessary to consider the possibility of brittle fracture prior to collapse due to yielding.

* Author's note—The question of loss of stability has decisive significance for compressed beams in metal frameworks, even when their flexibility is not very large. The author has, incidentally, given a diagram for the approach to failure in such beams.[11]

Vol. 1
1960

The possibility of prior collapse by instability or by brittle fracture requires individual verification and, for design, a strengthening of the elements involved.

In the following presentation of the theory, these questions are not touched upon; it will be assumed that the possibility of collapse by instability or by brittle fracture has been eliminated with the aid of appropriate constructional measures.

4. THE PROBLEM OF THE DETERMINATION OF THE COLLAPSE LOAD. LIMITING EQUILIBRIUM

The state of collapse, as it has been defined above, is the state of limiting equilibrium of a system under the action of (1) a dead load of given intensity and (2) a live load of intensity P.

Our problem becomes the determination of the value of the parameter P. For this purpose, it is assumed that the dead load is insufficient to cause the collapse of the system. The directions of the forces comprising the live loading are given; therefore only positive values of the parameter P are of interest.

For the state of collapse, two groups of conditions must be fulfilled:

Group I. The forces in all elements of the system must satisfy: (a) the conditions of equilibrium; (b) the limit conditions.

Group II. The configuration of the yield zones and the mode of possible deformations of the elements belonging to these zones must allow displacements of the points of the system. In this connection, the elements which are not in a state of yield are considered as not being deformed.

Every state of the system which meets the conditions of Group I will be called state I and the corresponding intensity of the live loading will be denoted by P_{I}. A set of states I exists to which a set Π_{I} of the values P_{I} corresponds. For example, those states through which the system passes when loaded from $P = 0$ up to collapse belong to this set. Evidently the set Π_{I} is bounded from above; we shall denote its upper limit by $\bar{P}_{\mathrm{I}}$.

Every state that meets the conditions of Group II will be called state II. It is possible to construct (mentally at least) the set of states for which the conditions of Group II are satisfied.

Each state II can be brought into correspondence with some intensity of the live loading P_{II}, as determined in the following manner: we give the system II an indefinitely small displacement which permits deformations of its plastic zones and we denote by $T_{\mathrm{II,\,II}}$ the work being expended in the elements of the system for the deformation corresponding to this displacement. We will compute also the work T_g done by the dead loading and the work T_p done by a unit live loading on the same displacement. We determine the value P_{II} from the equality

$$P_{\mathrm{II}} = \frac{T_{\mathrm{II,\,II}} - T_g}{T_p},$$

which meets the condition

$$P_{\mathrm{II}} T_p + T_g = T_{\mathrm{II,\,II}}.$$

Evidently fulfilment of this condition is necessary for the equilibrium of a system in state II. Since we are interested in the states for which $P_{II} > 0$, then*

$$T_p > 0.$$

This follows from the assumption that the dead load is insufficient for collapse of the system and hence,

$$T_{II,II} - T_g > 0.$$

This analysis will be needed below.

We will consider the set Π_{II} of positive values P_{II}. The lower bound of this set will be denoted by $\underline{P}_{II}$. Since in the state of collapse both condition I and condition II must be fulfilled, the intensity of the collapse load P lies simultaneously in both sets Π_I and Π_{II} (their intersection). Hence

$$\bar{P}_I \geqslant P \geqslant \underline{P}_{II}.$$

We shall now show that $\bar{P}_I$ is not larger than $\underline{P}_{II}$. Suppose that this is not so and

$$\bar{P}_I > \underline{P}_{II};$$

then it would be possible to take values P'_I and P'_{II} such that

$$P'_I > P'_{II}.$$

The state I′ is a state of equilibrium, therefore the work done by the forces of this state on any possible displacements must be equal to zero.† From the possible displacements we select the displacements of the state II′, with the aid of which the load P'_{II} is determined. Denoting by $T_{I,II}$ the work done by the forces acting on the elements of the system in state I′ for the deformations of the elements in state II′, we write

$$P'_I T_p + T_g = T_{I,II}.$$

The condition determining P'_{II} has the form

$$P'_{II} T_p + T_g = T_{II,II},$$

and so

$$P'_{II} - P'_I = \frac{T_{II,II} - T_{I,II}}{T_p}.$$

In accordance with Result III deduced from the definition of an ideally plastic element, the numerator of the right-hand side is not less than zero; and since

$$T_p > 0, \quad \text{then} \quad P'_{II} \geqslant P'_I.$$

We have arrived at a contradiction. Hence it follows that $\bar{P}_I$ is not larger than $\underline{P}_{II}$ and so *the collapse load P is the largest of the loads for which the conditions of Group* I *can be satisfied*; *and at the same time is the smallest of the loads for which the conditions of Group* II *are satisfied*

$$P_{I\max} = P = P_{II\min}.$$

* Translator's note—This is equivalent to restricting states II to displacements in which the live loading does positive work on the structure.

† Translator's note—This is the principle of virtual work for rigid bodies.

Thus the establishment of the collapse load may be approached either by a determination of $P = P_{\text{I max}}$ or by a determination of $P = P_{\text{II min}}$. A combination of these two methods is also possible. Now it is easy to show that factors producing internal stresses in the system (for example, removal of supports, residual deformations caused by previous cycles of loading, change of temperature, etc.) do not influence the value of the collapse load, provided, however, that the corresponding displacements are small and that it is possible to ignore changes in the mechanical properties of the material brought about by these factors. Actually, neither the conditions of equilibrium nor the limit conditions change, unless the loads involve the induced internal stresses as factors.

The fundamentals of the method of determining the collapse load will be illustrated briefly by two examples.

5. DETERMINATION OF THE COLLAPSE LOAD $P = P_{\text{I max}}$ FOR STATICALLY INDETERMINATE BEAM SYSTEMS WITH n UNKNOWNS

Making use of the conditions of equilibrium, it is possible to represent any force s_k in a statically indeterminate system as a linear function of the load P_1 and the statically indeterminate parameters $X_1, X_2, \ldots, X_n$

$$s_k = s_{kg} + P_1 s_{kp} + \sum_{i=1}^{i=n} s_{ki} X_i. \tag{1}$$

Here s_{kg} is the force system in the primary structure due to the dead loading; s_{kp} is the force system in the primary structure due to unit live loading, and s_{ki} the force system in the primary structure due to the forces $X_i = 1$.

The forces in the statically indeterminate system must, moreover, satisfy the limit conditions. Therefore the conditions which the load intensity P_1 must satisfy can be obtained by substituting the expression (1) for the force s_k into the yield conditions.

As was shown above, the limit conditions can be represented in the form of the union of expressions of the form

$$\sum_{j=1}^{j=m} e'_j s_j \leqslant f, \tag{2}$$

where s_j $(j = 1, 2, \ldots, n)$ are the forces characterizing the stressed state of the element and m the number of these forces.

After substitution of the expression for s_j from (1), the condition (2) takes the form

$$P_1 \Sigma e'_k s_{kp} + \Sigma e'_k s_{kg} + \Sigma x_i \Sigma e'_k s_{ki} \leqslant f$$

or, using the notation $\Sigma e'_k s_{kp} = \delta_p$, $\Sigma e'_k s_{kg} = \delta_g$, $\Sigma e'_k s_{ki} = \delta_i$,

$$P_1 \delta_p + \delta_g + \Sigma X_i \delta_i \leqslant f. \tag{3}$$

The condition (3) has a simple mechanical meaning: it is easy to see that the coefficients δ_p, δ_g and δ_i represent displacements (generalized), which arise in the basic structure in the direction of the corresponding live loading, the dead loading and the unknowns X_i when the element for which this condition arises undergoes unit deformation $\mathbf{e}'$.

Vol. 1
1960

Thus the condition (3) shows that the work done by the external forces applied to the basic structure on the displacements corresponding to the deformations $\mathbf{e}'$ of the element being considered does not exceed the work expended in the deformation $\mathbf{e}'$ of the element. It is indeed possible to consider the coefficient δ as an influence coefficient.

Using this interpretation, the conditions (3) can be written immediately without resource to equation (1) or condition (2). Each possible deformation of each of the elements of the system corresponds to a new form (3) and the problem can be solved by a consideration of the union of these conditions.

The basic structure as a whole can now be considered as an element. To each of the possible deformations of the element there corresponds a condition of the form (3). The union of these conditions determines the relation between the forces $P_{\mathrm{I}}, X_1, X_2, \ldots, X_n$ acting on the basic structure.

In an $(n-1)$-dimensional space with co-ordinates $X_1, X_2, \ldots, X_n, P_{\mathrm{I}}$, the union of conditions (3) determines a convex body B. To the internal points of the body correspond the states of the system for which the yield condition for the single element is not met. Each point A of the boundary of the convex body B lies on at least one of the n-dimensional manifolds determined by the condition (3). Therefore, for the state of the system represented by the point A of the boundary, there exists an element or elements the stressed state of which allows plastic deformation of the type defined.

If, however, point A corresponds to $P_{\mathrm{I}} < P_{\mathrm{I\,max}}$, then deformations of the systems, as has been shown already, cannot result from the consideration of the individual plastic deformations.

If for conciseness of language it is agreed that the positive direction of the axis P_{I} is directed upwards, then the determination of the collapse load is reduced to finding the segment of the upper supporting plane of the convex body (3) which cuts the axis P_{I}.

6. DETERMINATION OF THE COLLAPSE LOAD $P_{\mathrm{II\,min}}$ FOR A REINFORCED CONCRETE PLATE

We will consider as an example an annular reinforced concrete plate, supported along the inside and outside edges, with radially symmetric reinforcement above and below and loaded with a radially symmetric vertical load [Fig. 6(a)].

It is easy to explain the manner of its collapse. For possible plastic deformations of the elements, as understood above, one can take opening of cracks above and below, accompanied by rotation of the parts of the elements with respect to the horizontal axes, at the level of the upper and lower reinforcement. Owing to the axial symmetry of the plate and the loading, the cracks must be circumferential and radial. It is easy to convince oneself that collapse without circumferential cracks is impossible. However, a circumferential crack must be accompanied by radial cracks extending from the circumferential crack to the external boundary of the plate. The cracks which have been enumerated are formed on one (the lower) side of the plate [Fig. 6(b)]. If there were no other cracks, then the plate would rise at the external edge

Vol. 1
1960

and that is clearly impossible. Therefore radial cracks also appear on the upper surface from the internal to the external edge of the plate [Fig. 6(c)]. Only the combination of these two deformations satisfies the conditions of the specification, and for this it is not difficult to arrange a relationship between these two modes of deformation [Fig. 6(d)]. The collapse scheme is settled with precision to within the parameter determining the position of the circumferential crack. After this it is easy to form the work equation

$$P_{\text{II}} T_p + T_g = T_{\text{II, II}}.$$

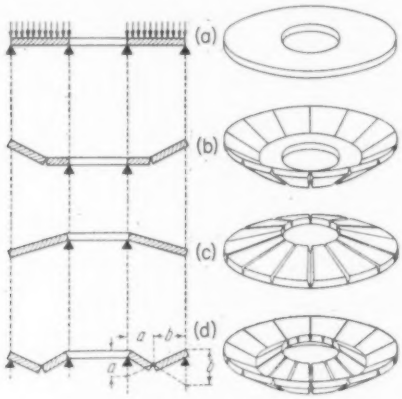

FIG. 6.

From this equation the value of P_{II} is determined as a function of the position of the circumferential crack. The usual minimum problem remains to be solved.

A circumstance meriting attention is that both the upper and lower circumferential reinforcement must yield from the circumferential crack to the external edge. Thus the outer part of the plate is subject to extension in the circumferential direction. Hence the internal part of an annular plate behaves like a clamped structure up to the moment of collapse. This result is perhaps somewhat unexpected and is, it seems to us, of considerable interest from the point of view of developing suitable designs for reinforcement.

REFERENCES

1. A. IU. ISHLINSKII, *Mechanics in the U.S.S.R. during the Thirty Years* 1917–1947, p. 244. GITTL, Moscow (1950).
2. V. V. SOKOLOVSKY, *Theory of Plasticity*. Akademiia Nauk SSSR, Moscow (1946).
3. L. S. LEIBENSON, *Elements of the Mathematical Theory of Plasticity*. Moscow (1943). (Translation: Note RMB19 of the Graduate Division of Applied Mathematics, Brown University, 1947.)
4. L. M. KACHANOV, *Prikl. Mat. Mekh.* **6**, 187 (1942). (Translation: Note RMB7 of the Applied Mathematics Group, Brown University, 1946.)
5. A. A. MARKOV, *Prikl. Mat. Mekh.* **11**, 339 (1947). (Translation: Note A11-T3 of the Graduate Division of Applied Mathematics, Brown University, 1948.)
6. N. I. BEZUKHOV, *The Theory of Elasticity and Plasticity*. GITTL, Moscow (1953). See also his article in: *Structural Mechanics in the U.S.S.R.*, 1917–1957 (edited by I. M. RABINOVICH) p. 233. Stroiizdat, Moscow (1957).

7. A. R. Rzhanitsyn, *Calculations of Structures taking account of the Plastic Properties of Materials* (2nd Ed.). Stroiizdat, Moscow (1954).
8. W. Prager, Sectional Address at the *Eighth International Congress of Theoretical and Applied Mechanics, Istanbul.* 1952 (1955).
9. P. G. Hodge, *The Plastic Analysis of Structures.* McGraw-Hill, New York (1959).
10. D. C. Drucker, *A More Fundamental Approach to Plastic Stress–Strain Relations.* A.S.M.E. (1952). Proceedings of the First U.S. National Congress of Applied Mechanics, 1951, p. 487.
11. A. A. Gvozdev, *Proekt i stand.* (1934).

ADDITIONAL BIBLIOGRAPHY

(A). *Proceedings of the Conference on Plastic Deformations, December,* 1936 (edited by B. G. Galerkin). Akademiia Nauk SSSR, Moscow–Leningrad (1938).
Contents:
A. A. Il'iushin, *On the Question of Visco-Plastic Flow of Material.*
A. A. Gvozdev. This paper.
S. A. Bernshtein, *The Computation of Statically Indeterminate Beams in the Plastic Range.*
B. N. Gorbunov, *On the Question of the Factor of Safety for Computations by the Theory of Plastic Deformation.*
S. A. Bernshtein and V. S. Turkin, *Experimental–Theoretical Investigations of the Elasto-Plastic Action of Continuous Steel Beams.*
K. S. Zavriev, *The Computation of Metal Structures for Critical Conditions, taking account of Plasticity.*
A. G. Nazarov, *The Application of the Concept of an "Ideal Profile" to the Analysis of the Carrying Capacity of Statically Indeterminate Systems.**
N. M. Beliaev, *Theories of Plastic Deformation.*†

(B). A. A. Gvozdev, *Stroitel'naia promyshlennost'* Vol. 10, No. 1 (1932); Vol. 11, No. 1 (1933); Vol. 12, Nos. 5, 6 (1934); Vol. 17, No. 3 (1939); Vol. 21, Nos. 1, 2 (1943); *Vest. VIA* No. 30 (1940); *Izv. Akad. Nauk SSSR, OTN* **9**, **10** (1943); **4** (1953); *Prestressed Concrete Structures* (edited by V. E. Ratts). Stroiizdat, Moscow (1947); *Inzh. sborn.* **5** (1948); **5** (1949); *Computation of the Carrying Capacity of Structures by the Method of Limiting Equilibrium.* Stroiizdat, Moscow (1949); *Questions of Contemporary Reinforced Concrete Construction* (edited by A. A. Gvozdev). Stroiizdat, Moscow (1952).
A. A. Gvozdev and M. S. Borishanskii, *Proekt i stand.* No. 6 (1934).
A. A. Gvozdev and V. I. Murashev, *Directions for the Computation of Reinforced Concrete Bents and Frames.* Stroiizdat, Moscow (1932).
A. A. Gvozdev, V. I. Murashev, V. N. Gornov and V. Z. Vlasov, *Directions for the Design and Computation of Monolithic Thin-walled Roofs and Floors.* TsNIPS, Moscow (1937).

* Nazarov is referring to an ideal sandwich section. He uses a piecewise linear moment–curvature relation.

† Beliaev's paper also appeared in *Izv. Akad. Nauk SSSR, OTN* **1** (1937), and a translation of the latter appeared as Note RMB–14 of the Applied Mathematics Group, Brown University, 1946.

Vol. 1
1960

Int. J. Mech. Sci. Pergamon Press Ltd. 1960. Vol. 1, pp. 336–341. Printed in Great Britain

THE COMPRESSION OF RIGID–PERFECTLY-PLASTIC MATERIAL BETWEEN ROUGH PARALLEL DIES OF UNEQUAL WIDTH

W. JOHNSON* and H. KUDO†

(*Received* 16 *June* 1959)

Summary—The results are given of calculations of the pressure to compress plastically, ideal material between perfectly rough parallel plates of variously unequal widths which do not overhang the material and in which the die width exceeds the material thickness. The rate of approach of the dies is also stated for certain die parameters. A particular solution is also given for the case when there is less than shearing friction between the material and the plates.

1. INTRODUCTION

THE major problem treated below is one which has attracted considerable attention in the form of the compression of material between perfectly rough dies of equal width. It has been discussed at length by Hill.[1] The first analysis of this problem was made by Prandtl[2] in which he proposed his well known cycloidal solution. Further analysis was contributed by Nadai[3] and a slip-line field solution was proposed by Hill *et al.*[4] Interest in this problem appears to stem from its physical similarity to that of rolling, witness Alexander's[5] approach in his treatment of the hot rolling process. Experimental confirmation of the analysis was offered by Nye[6] and more recently, van Rooyen and Backofen[7] have provided striking experimental evidence of the existence of a pressure plateau near the plate edges, as required by slip-line field theory, though not by the cycloidal solution.

This short paper presents a solution of the slightly more general problem of compression when the plates are not of equal width. This problem appears to be not easily approached by the usual analytical means—Siebel's analysis—as is the case when the plates are of equal width. The employment of a comparatively easy slip-line field solution in this instance demonstrates its superiority over a purely algebraic solution. In conclusion the particular case when the coefficient of friction between the platens and the material is 0·16 is discussed. Alexander[8] has produced particular solutions for cases such as this when the plates are of equal width.

2. SLIP-LINE FIELD

The solution used is a modification of that given by Hill *et al.*[4]

(i) The starting slip lines for the plastic–rigid boundary between the deforming material and the overhanging material are assumed to be two

* University of Manchester, Manchester, 13.

† Aeronautical Research Institute, Tokyo University.

straight lines of equal length, starting from the die edges and perpendicular to each other. This choice satisfies the stress equilibrium condition necessary for the overhanging material.

(ii) The die edges O_1 and O_2 are assumed to be stress singularity points.

Fig. 1 shows a particular slip-line solution drawn using a 15° equiangular net. Points A_1, B_2, C_3 are the equiangular points of intersection of the α- and β-lines at which they make an angle of 45° with vertical or horizontal lines. They can be chosen as the centre point of the compressed block, i.e. the point which lies on a vertical axis of symmetry. When one of them is chosen as the centre point, the region surrounded by the die faces and α-, β-lines which meet at this point can be considered as the rigid regions. This means that $A_1, B_2, \ldots$ are the possible common vertices of the upper and lower dead-metal zones which attach themselves to the top and bottom dies respectively.

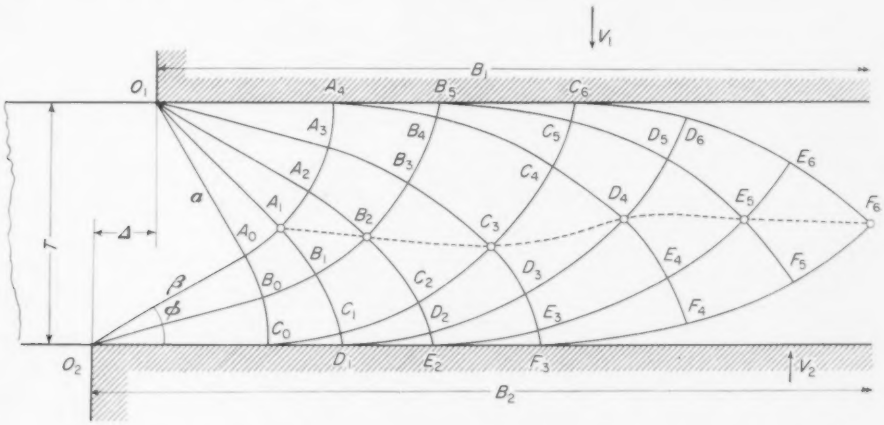

FIG. 1. Slip-line field for compression between perfectly rough plates of unequal width; $\phi = 30°$.

3. PRESSURE CALCULATIONS

From equilibrium considerations, the hydrostatic component of pressure at A_0 (the intersection of the starting α- and β-lines) is k. Using Hencky's equation, the pressure is determined along the surfaces of the top and bottom dies as well as along the surfaces of the two dead-metal regions. The total compressive force on the top and bottom dies are compared in several cases and they were found to differ by no more than 0·8 per cent. Mean top-die (i.e. the smaller one) pressures can thus be calculated and are graphed by full lines in Fig. 2 against B_1/T, ϕ being a parameter.

The meaning of the various quantities will be obvious from Fig. 1.

4. HODOGRAPHS

Fig. 3 illustrates a hodograph corresponding to the slip-line field of Fig. 1. The form of the hodograph is identical with a portion of a certain particular slip-line field for the compression of a material between two rough parallel plates of equal width. The speeds of the extruded overhanging rigid

material are indicated by the hollow circles (for instance, F_6' represents the speed when F_6 in Fig. 1 is chosen as the centre point) from which the relative speed of indentation V_2/V_1 of the bottom and top dies is obtained; this is shown in Fig. 4. When $\phi = 45°$, the process is of course symmetric, i.e. compression between two equal dies takes place and $V_2/V_1 = 1$. On the other hand, when $\phi = 0°$, $V_2/V_1 = 0$, i.e. when the bottom die extends outside the top die by an

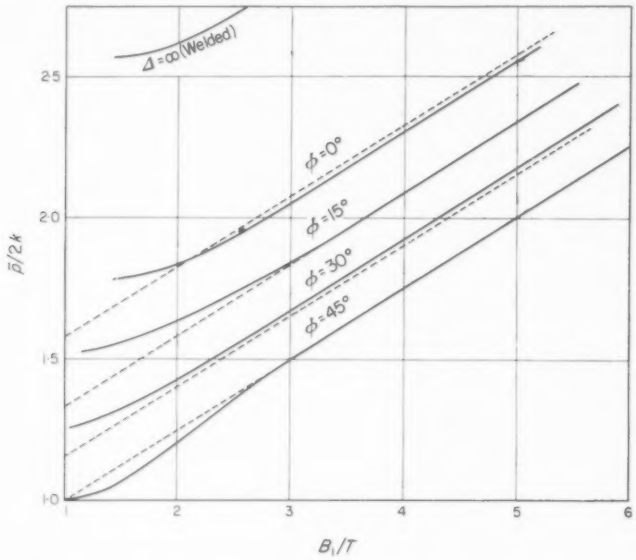

FIG. 2. Variation of $\bar{p}/2k$ with B_1/T. B_1 is upper die width, and T material thickness.

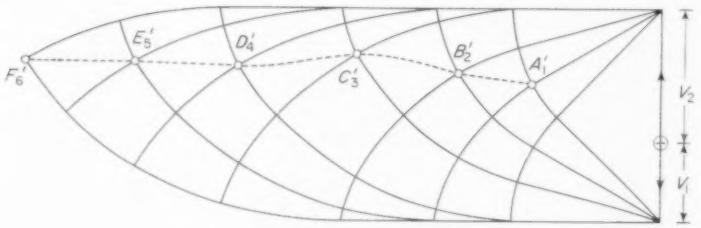

FIG. 3. Hodograph to Fig. 1.

amount larger than the plate material thickness and no indentation by the bottom die has taken place. For $\phi = 15°$ and $30°$, V_2/V_1 is between 0 and 1, and tends to a constant value for a given ϕ for large B_1/T. As B_1/T approaches close to unity, V_2/V_1 tends to increase.

5. DISCUSSION

Fig. 2 indicates the effect of the inequality of the top and bottom die widths. The mean compression pressure of the narrower die is affected by the width of the wider die. The wider the bottom die is the higher the top die mean pressure becomes. The results can well be approximated for B_1/T larger

than 2 by adapting Hill's[1] formula thus

$$\bar{p}/2k = (0{\cdot}75 + 0{\cdot}58\Delta/T) + 0{\cdot}25(B_1/T),$$

where Δ stands for half the amount by which the bottom die overhangs the top die. This formula is plotted in Fig. 2 as the broken line.

When $\Delta > T$, two cases may be considered:

(i) *Material not welded to the bottom die.* As no vertical pressure acts on the surface O_2O_2' of the bottom die [see Fig. 5(a)], it is probable that no shearing stress acts there either. In this case, $\bar{p}/2k$ for $\phi = 0°$ in Fig. 2 is applicable for all $\Delta > T$.

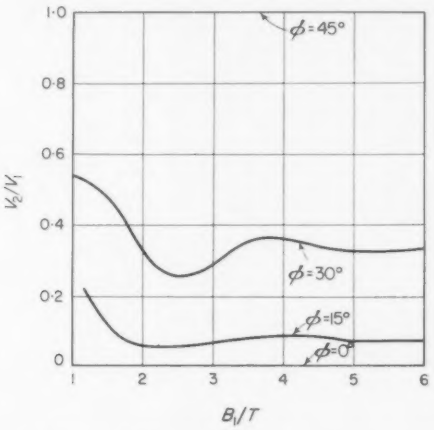

FIG. 4. Variation of V_2/V_1 with B_1/T; V_2/V_1 denotes ratio of bottom to top die-speed indentation.

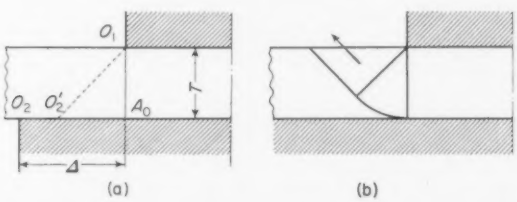

FIG. 5. (a) Material not welded to bottom die. (b) Slip-line field for material welded to bottom die when $\Delta/T > 2{\cdot}57$.

(ii) *Material welded to the bottom die.* If Δ is not very much larger than T, the material to the left of O_1A_0 will move out as a rigid body, against the action of shearing stress k over the surface A_0O_2. A hydrostatic pressure increment of $k(\Delta/T - 1)$ is thus superimposed on the pressure distribution obtained for $\phi = 0$.

For Δ/T larger than 2·57, a type of solution shown in Fig. 5(b) exists. This leads to a hydrostatic pressure increment of $k\pi/2$ on material within the plastic boundary. Accordingly, $\bar{p}/2k$ in this case is obtained by the addition of $\pi/4$ to the result for $\phi = 0°$ in Fig. 2.

6. COMPRESSION BETWEEN PARTLY ROUGH DIES

The problem of compression between plates of unequal width when their roughness is not such that there is shearing between the metal and the plates is more difficult to analyse and a particular solution for only one simple case is presented. This solution is particular because, for a given coefficient of friction μ between the material and the platens, it is only applicable for certain ranges of B/T or breadth to thickness ratio.

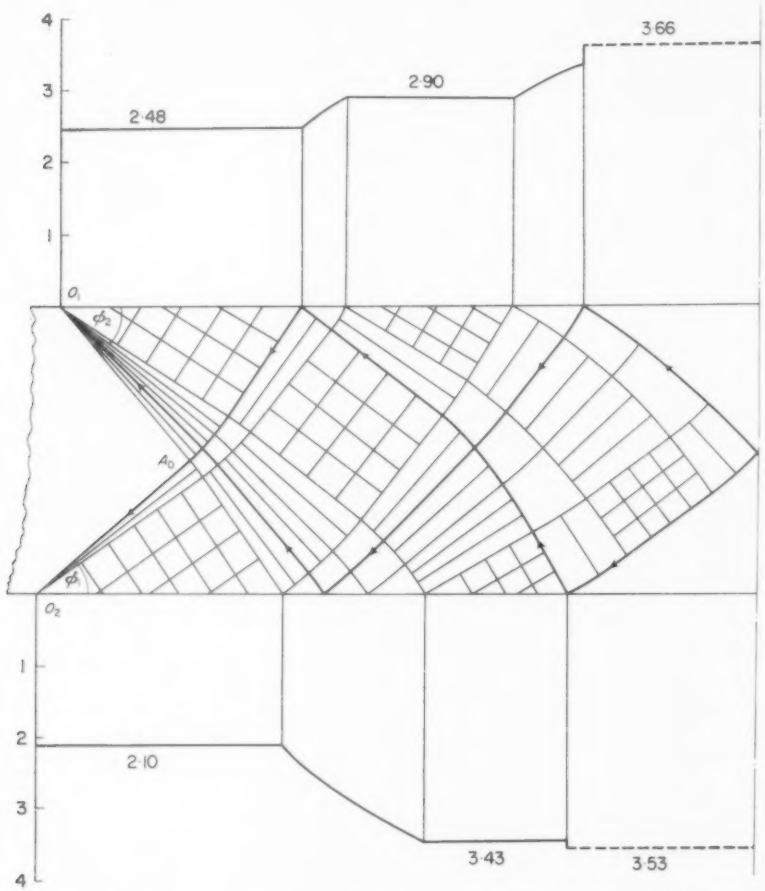

FIG. 6. Compression between partly rough plates; $\mu = 0{\cdot}16$; $B_1/T = 2{\cdot}45$; $B_2/T = 2{\cdot}53$. Also showing pressure distribution over both plates.

As in previous cases, the slip-line field is started by drawing a right-angled isosceles triangle $O_1 A_0 O_2$ on the line joining the singular points O_1 and O_2. The slip-line field is then extended from $O_1 A_0$ and $O_2 A_0$ in the usual way. The assumption that the starting slip lines are straight must, if μ is given, be discarded for certain B/T ratios; the problem then becomes much more complex, and whilst similar to Green's[9] solution for compression between perfectly smooth plates for non-integral B/T ratios, is yet more complicated owing to

both the inequality of the platen lengths and the fact that the slip lines meet both platens at non-constant angles.

When μ is given, in the instance shown in Fig. 6 $\mu = 0{\cdot}16$, angles ϕ_1 and ϕ_2 easily follow; a certain amount of guessing is essential to obtain reasonably accurate values of both ϕ_1 and ϕ_2. The right-angle triangles, hinged on O_1 and O_2 respectively and adjoining the plates, are thus determined. The field is then extended in the usual manner, a trial and error method being necessary to decide the angles of intersection of the slip lines with the platens as the field progresses along them. The field shown in Fig. 6 is concluded at an appropriate point where the α- and β-slip lines intersect at 45° to the direction of the platens; this point is then, by symmetry, on the centre-line of the block.

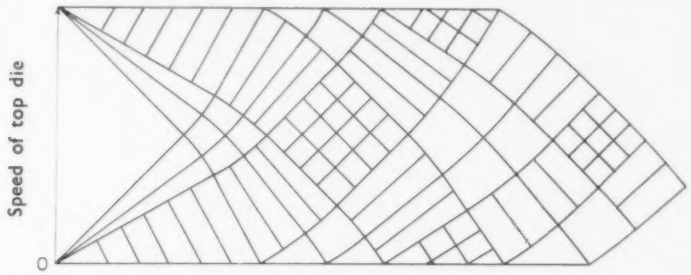

FIG. 7. Hodograph to Fig. 6.

The procedure for the subsequent analysis of the problem is adequately described in the paper by Alexander[8] dealing with compression between two parallel, partly rough plates of equal size. The problem here discussed is simple once the starting slip lines are recognized, but the solution is more tedious to evaluate than Alexander's because the angles of intersection of the slip lines on the top and bottom platens are not the same.

Fig. 7 shows the hodograph to Fig. 6. The problem was solved without recourse to the use of Prager's cycloid in the stress plane. Fig. 6 also displays several pressure plateaux, each extending over a different length of plate. As a check on the accuracy of the solution, a comparison of the force on the bottom and top plates, as determined by using the Hencky equations, was made and found to agree to within 1 per cent.

REFERENCES

1. R. HILL, *Mathematical Theory of Plasticity*. Clarendon Press, Oxford (1950).
2. L. PRANDTL, *Z. angew. Math. Mech.* **3**, 401 (1923).
3. A. NADAI, *Plasticity* Chap. 17. McGraw-Hill, New York (1931).
4. R. HILL, E. H. LEE and S. J. TUPPER, *Proc. 6th Int. Congr. Appl. Mech., Paris* (1946).
5. J. M. ALEXANDER, *Proc. Inst. Mech. Engrs., Lond.* **169**, 1021 (1955).
6. J. F. NYE, Ministry of Supply, A.R.D., Rep 39/47 (1947).
7. G. T. VAN ROOYEN and W. A. BACKOFEN, *J. Mech. Phys. Solids* **7**, 163 (1959).
8. J. M. ALEXANDER, *J. Mech. Phys. Solids* **3**, 233 (1955).
9. A. P. GREEN, *Phil. Mag.* **42**, 900 (1951).

Vol. 1
1960

Int. J. Mech. Sci. Pergamon Press Ltd. 1960. Vol. 1, pp. 342–349. Printed in Great Britain

ON THE DYNAMICS OF HIGH-SPEED CAM PROFILES

FERDINAND FREUDENSTEIN
Department of Mechanical Engineering, Columbia University, New York

(*Received* 20 *August* 1959)

Summary—An exact expression for the maximum output acceleration of a two-mass-and-spring cam system is developed for zero damping and dwell–rise–dwell profiles. A family of high-speed cam profiles having minimum components in the higher harmonics and similar in shape to Neklutin's "modified trapezoids" is suggested. One simple formula applies to the whole profile. General considerations on optimization of cam profiles (for minimum force on follower) and limitations on ultimate performance are presented.

1. INTRODUCTION

IN RECENT times an abundance of literature has appeared, ably presented and discussed by Rothbart,[1] on the design of cam profiles suitable for high speeds. Realizing the necessity of accommodating the masses, compliances and vibrational characteristics of the follower system, designers have progressed from the constant-acceleration or "gravity" cam profile to those less severe in the rate of force application, such as the cycloidal, higher-degree polynomials (the polydynes) and many others, including combinations, such as the modified trapezoids.[2, 3] These profiles have been rated by the computation of velocity, acceleration and shock factors, defined as maximum velocity, acceleration and shock, based on unit rise in unit time, as computed from the cam diagram, relating time (or cam rotation) to follower lift. Owing to the elasticity of the follower system, however, relative motion exists between the roller (say) contacting the cam profile and the output mass. The output mass, therefore, at the end of the follower system, has a different motion than that given by the cam diagram and can be considered as corresponding to the cam diagram multiplied by a dynamic amplification factor (C_D), which includes the effects of elasticity. A true measure of cam performance, thus, is the actual maximum force on the follower, per unit output mass M, per unit rise, per unit time. In symbols: $F^* = C_A MC_D L/T^2$ where L is lift, T is total rise time, C_A is an acceleration factor computed from the cam diagram, C_D is a dynamic amplification factor—the ratio of maximum output mass acceleration to maximum follower acceleration—and F is the maximum force on the follower (see Figs. 1 and 2).

It is desirable, therefore, to minimize the *dynamic acceleration factor* ($C_A C_D$) which is a true measure of the maximum force on the cam follower. Such considerations were employed in the cam analysis made by Hrones[4] on a differential analyzer machine; results were presented graphically and confirmed experimentally by Mitchell[5] in 1950. Disregarding damping, Hrones's model consists of a mass-and-spring as in Fig. 1. By adding a mass at the

cam-follower contact, as in Fig. 2, higher penalties are given to shock loading and this is the model used in this paper. Dudley's model[6] probably comes closer to reality than either Figs. 1 and 2—especially in the case of automotive valves—but Fig. 2 was chosen because, for more complicated models, the analysis becomes very much more cumbersome, although eventually it is realized that such models will and should be investigated.

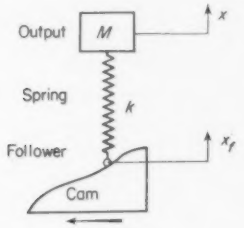

FIG. 1.

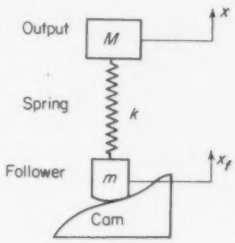

FIG. 2.

FIG. 1. Single-mass-and-spring model of cam system. M is output mass, x is output-mass motion, k is a spring constant and x_f is follower displacement.

FIG. 2. Two-mass-and-spring model of cam system. M is output mass, x is output-mass displacement, k is a spring constant, m is the follower mass at the cam and x_f is its displacement.

2. ASSUMPTIONS, METHODS, LIMITATIONS

It is assumed that the dynamic acceleration factor will be essentially minimized when the acceleration curve, derived from the cam diagram, is symmetrical about the mid-point (point 3, Fig. 3) and the quarter-point (point 2, Fig. 3). This assumption can be substantiated by symmetry arguments.

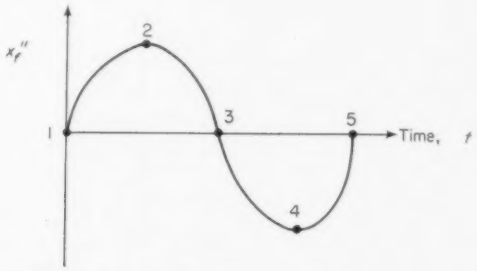

FIG. 3. Cam-follower acceleration diagram. The diagram is "symmetrical" about points 2 and 3 so that

$$x_f'' = \sum_{k=1,3,5}^{n} C_k \sin \omega k t$$

Thus the cam-acceleration diagram for the follower can be characterized by a Fourier sine series with only odd multiples of the fundamental frequency

$$a_f = \frac{d^2 x_f}{dt^2} = a_1 \sin \omega_1 t + a_3 \sin \omega_3 t + a_5 \sin \omega_5 t + \ldots = \sum_{n_{\text{odd}}} a_n \sin \omega_n t \qquad (1)$$

Vol. 1
1960

where $\omega_n = 2\pi n/T$; t is time, assumed proportional to cam rotation, x_f is the follower displacement, and a_i are coefficients, or numbers, characterizing the shape of the cam profile. Note that $a_f = 0$ at points 1, 3, 5 (Fig. 3) for all values of the a_i's; damping is neglected. This is reasonable for many mechanical systems and was pointed out in the course of the discussion on the paper by Hrones.[4] The conclusions which follow are limited to *D–R–D* cams. It is realized that the behavior of the cam as a periodic motion, of 360° period, is the only correct one and that the behavior outside the rise portion is affected by the rise, and vice versa. Owing to the uncertainty of damping, indexing and vibrations during dwell, as well as the mathematical difficulties involved, it was decided that a profile good in the rise region would probably be good in the dwell region also provided the acceleration was zero at the rise terminals and the shock finite. All the profiles considered satisfy this requirement. For this reason the results of this investigation do not apply to rise-return and other cams, where zero shock at the rise terminal may be required. It is believed, however, that the analysis could be extended to such cases.

3. CALCULATION OF DYNAMIC ACCELERATION FACTOR, $C = C_A C_D$

In Fig. 2,

$$M\frac{d^2x}{dt^2} + k(x - x_f) = 0, \tag{2}$$

$$m\frac{d^2x}{dt^2} + k(x_f - x) = F^*, \tag{3}$$

where F^* is force on cam-follower due to cam profile, F is F^*/M, force on follower per unit output mass, x is displacement of output mass, x_f is follower displacement, m is follower mass at cam, $\lambda = m/M$, and k is the spring constant. Let $\Omega^2 = k/M$, $\omega^2 = k/m$ and r be a resonant harmonic, such that r is assumed odd and of form $(4p+3)$ where p is an integer. Also, let $\omega_n = 2\pi n/T = n\omega_1$, $\Omega = r\omega_1$ and $F(0) = x(0) = x'(0) = x''(0) = 0$, where a single prime is equivalent to d/dt. From equations (2) and (3),

$$F + \frac{1}{\Omega^2}F'' = (1+\lambda)x_f'' + \frac{1}{\omega^2}x_f''''. \tag{4}$$

Using the Laplace transform, and confining ourselves to the interval $0 \leqslant t \leqslant T$, we can solve for F, obtaining after a certain amount of algebra,

$$F = \left\{ \sum_{\substack{n \\ (n \neq r)}} a_n\left(\lambda + \frac{1}{1 - n^2/r^2}\right) \right\} \sin \omega_n t - (\sin \Omega t) \sum_{\substack{n \\ (n \neq r)}} \left(\frac{a_n(n/r)}{1 - n^2/r^2}\right) + \tfrac{1}{2}a_r(\sin \omega_r t - \omega_r t \cos \omega_r t). \tag{5}$$

The dynamic acceleration factor

$$C = \frac{F_{\max}}{(L/T^2)} = \frac{2\pi F_{\max}}{(L/T^2)}. \tag{6}$$

The generality of the conclusions is not expected to be substantially affected if we assume that the resonant harmonic is odd, of form $(4p+3)$, where p is an integer, and that the resonant harmonic r is absent from the cam contour—i.e. that $a_r = 0$—provided that the resonant frequency is considerably higher than the cam rotational frequency (revolutions per second); this will enable

us to derive an exact expression for the dynamic acceleration factor. When $a_r = 0$ and $r = 4p+3$ (p a positive integer), it can be shown (Appendix I) that F becomes a maximum when $\omega_1 t = 90°$, for most "reasonable" looking cam profiles. Rearrangement of F in equation (5) under these circumstances reduces to

$$C = 2\pi \sum_{\substack{n=1,3,5 \\ (n \neq r)}} \left\{ \alpha a_n \left(\lambda + \frac{1}{1-\alpha n/r} \right) \right\} \Bigg/ \sum_{\substack{n=1,3,5 \\ (n \neq r)}} \frac{a_n}{n}; \qquad \begin{matrix} (\alpha = +1,\ n = 1,5,9,13,\ldots) \\ (\alpha = -1,\ n = 3,7,11,15,\ldots) \end{matrix} \tag{7}$$

This is a general expression for the dynamic acceleration factor which can be evaluated when the acceleration profile is known.

4. DISCUSSION OF DYNAMIC ACCELERATION FACTOR, EQUATION (7)

When $m = 0$ and $x_f'' = a_1 \sin \omega_1 t$, we obtain the well known cycloidal profile. For this profile, equation (7) yields $C = 2\pi r/(r-1)$. If the resonant frequency of the cam-follower system is 15 times the cam speed (rev/sec), $C = 1{\cdot}07$, which confirms one result of Hrones[4]. Furthermore, it is seen that the dynamic acceleration factor depends on the *natural frequency* of the cam-follower system and varies, therefore, (a) with the shape of the profile and the same follower system, and (b) with the *same* profile and different follower systems. This also complicates the question as to what might be an "optimum" profile. Any cam-follower system tends to vibrate at its natural frequency, thereby superimposing on the cam diagram a "wiggle" or oscillation. If then, we specify the output motion x to be smooth, without wiggles and with least maximum acceleration (or least squared integrated acceleration, etc.), we *reintroduce* this wiggle as a *counter-wiggle* in the cam-acceleration diagram, as is evident from the complementary function in equation (4). Such a profile would be clearly impractical, being much too sensitive and uncertain in its operation; for instance, in polydyne cam design it is neglected (or considered negligible).

What, then, shall be a criterion for optimum performance, if the criterion of least acceleration, least squared integrated acceleration and similar criteria are impractical, because the strict execution of this requirement leads to the reintroduction of the wiggle in the cam-acceleration diagram? It is difficult, if not impossible, to improve on the comments of Routh in his treatise:* "A disturbing force can produce a large forced vibration in any coordinate only if there be in that coordinate a free vibration of nearly the same period and containing the same real exponential." This can be seen when $n \approx r$, in equations (5) and (7). We may infer, qualitatively, then, that the chances of C being large are increased if there are sizeable higher harmonics in the neighborhood of a resonant frequency, the severity of the disturbance being a function of the amplitude a_r of the resonant harmonic and its order number r. This is not to deny the validity of the polydyne principle or any other principle,

* E. J. Routh, *The Dynamics of a System of Rigid Bodies* (6th Ed.), pp. 244–248, discussion on how a disturbing force is magnified (1905).

Vol. 1
1960

based on the sound idea of adding the flexibility displacements to the output displacements to deduce the cam profile. It would be reasonable then to consider for the output cam profile a class of profiles having minimum higher harmonics, or minimum "overtones", to borrow a phrase from acoustics. Clearly the cycloidal is the optimum in that direction having but a fundamental in the acceleration. The degree of reduction of overtones depends on the value of "r", the resonant frequency ratio. Two limiting conditions are apparent: (a) When $r \to \infty$ (i.e. the spring is infinitely stiff or rigid), there is no relative motion between follower and output mass and the gravity profile is optimum. (b) When $r \to 1$ (the spring is very flexible), resonance between cam and follower system is of very low frequency and it is essential to have minimum overtones, and the cycloidal suggests itself.

Any real cam, being generally between these two extreme conditions, could be optimized with a profile curve, intermediate between the cycloidal and the gravity—but with *minimum overtones*. Curves which have been suggested, and somewhat similar to these, are the modified trapezoids of Neklutin[2, 3] and it is thus seen that these curves have a sound theoretical basis, as is well known. The profiles suggested herein differ from the modified trapezoids in that they have *minimum overtones*, which also permits these curves to be represented by one continuous function.

5. CAM PROFILES HAVING MINIMUM HIGHER HARMONICS

Consider the cam-acceleration diagram (Fig. 3),

$$x_f'' = \sum_{k=1}^{n} a_k \sin k\omega_1 t,$$

where a_n is the last term of a *finite* Fourier series. For $n = 1$, we obtain

$$x_f = \frac{L}{T}\left(t - \frac{T}{2\pi}\sin\frac{2\pi t}{T}\right),$$

the well known cycloidal contour. For $n > 1$, we can progressively flatten out the sine wave of the cycloidal acceleration curve, until in the limit, with $n \to \infty$, it approaches the square wave corresponding to the gravity cam. After considerable investigation, it was found that the most convenient way to accomplish this is to require the tangent at the point 2 in Fig. 3 to be horizontal to the nth order in the acceleration diagram. This condition leads to a system of simultaneous equations in the a_i's and the following result:

Theorem. For a cam-acceleration diagram given by equation (1), with the highest harmonic the nth harmonic, and with $a_1 = 1$, the terms a_k are given by

$$a_k = \frac{1}{k^2}\prod_{m=3,5,7}^{n}\left|\frac{m^2-1}{m^2-k^2}\right|, \quad m \neq k^* \text{ and } n \geq 5.$$

C can now be computed from equation (7).

* This leads to the theorem that if k is any odd integer (*not necessarily* ≥ 5) then

$$|k| = \prod_{\substack{m=3,5,7 \\ m \neq k}} (m^2-1)/(m^2-k^2)$$

as has been proved by Professor A. E. Livingstone, University of Washington, Seattle, Washington, and shown to the author in a private communication.

Thus, for $n = 3$,

$$a_1 = 1, \quad a_3 = 1/9 \quad \text{and} \quad C = \frac{5{\cdot}386}{1-1/r}\left(\frac{1+3{\cdot}5/r}{1+3/r}\right).$$

Appendix II shows the various curves up to $n = 9$, their displacements, velocities, accelerations, shocks and the various corresponding factors. Note the presence of the dynamic amplification factor, C_D, a function of the resonant harmonic r. The velocity factor, for a static rate of force application, is the same for all profiles and is equal to 2·0. In any given application it would probably be wise to select a cam profile whose highest harmonic is not greater than 10 per cent of r and whether or not it pays to refine the cycloidal profiles, by considering the higher harmonics which reduce the maximum (static) acceleration, depends upon the individual application. To some extent the law of diminishing returns operates here. The limit approached by C $(r \to \infty)$ is 4 (gravity) and $a_k \to 1/k$. The reduction in C between 1 and 3 terms is about 14 per cent, whereas between 3 and 5 terms it is only an additional $2\frac{1}{2}$ per cent. Here, as in all phases of design, the judgement of the designer is the determining factor.

Vol. 1
1960

The curves are easily differentiated and integrated and are believed to be useful high-speed profiles; they are not supposed to be the only ones possible, rather they are offered as an additional type of family to be used, as a possible alternative to the polynomials, or when the circumstances demand minimization of the higher harmonics.

6. CONCLUSION

By means of various assumptions and idealizations, the dynamic acceleration factor has been derived and analyzed for a simple model and on the basis of the results, a series of "harmonic" profiles, with minimum overtones, has been suggested.

REFERENCES

1. H. Rothbart, *Cams*. John Wiley, New York (1956).
2. C. N. Neklutin, *Mach. Design* **24**, 143 (1952).
3. V. Bilaisis, *Mach. Design* **29**, 135 (1957).
4. J. A. Hrones, *Trans. Amer. Soc. Mech. Engrs.* **70**, 473 (1948).
5. D. B. Mitchell, *Mech. Engng., N.Y.* **72**, 467 (1950).
6. W. Dudley, *S.A.E. Quart. Trans.* **2**, 19, 51 (1948).

APPENDIX I

Proof that F reaches maximum at $2\pi t/T = \pi/2$.

We shall prove the assertion for $m = 0$; for m finite the only change is the added term $\Sigma\lambda a_k \sin \omega_k t$ which clearly possesses the required maximum. When $m = 0$,

$$F = \sum_k C_k \sin k\omega t - C_r \sin r\omega t \quad (k \neq r) \quad \omega = w_1 = \frac{2\pi t}{T}$$

$$r = 4p+3, \; p \text{ a positive integer}$$

$$C_k = \frac{a_k}{1-k^2/r^2}; \quad C_r = \sum_k \frac{a_k(k/r)}{1-k^2/r^2} \quad (k \neq r).$$

At $\omega t = \pi/2$, $dF/dt = 0$; hence an *extreme* value of some type exists for F.

At $\omega t = \pi/2$, $\dfrac{1}{\omega^2}\dfrac{d^2F}{dt^2} = -\sum_k \left(\dfrac{r^2 a_k k}{r - \alpha k}\right) \quad k \neq r, \quad \begin{matrix} \alpha > 0 \text{ at } k = 1, 5, 9, \ldots \\ \alpha < 0 \text{ at } k = 3, 7, 9. \end{matrix}$

Since all $a_k > 0$, d^2F/dt^2 is negative whenever $k < r$. Hence for profiles in which $n < r$, F reaches a maximum at $\omega t = \pi/2$. If the curve is a reasonable one we may infer that this is an absolute rather than a local maximum.

APPENDIX II

Properties of Family of Cam Profiles minimizing the Higher Harmonics

Follower acceleration $= \sum_{k=1,3,5}^{n} a_k \sin \dfrac{2\pi k t}{T}$

T = rise time
L = total lift
n = highest harmonic ($< r$)

Let $$S = \frac{1}{\sum_{k=1}^{n} \frac{a_k}{k}}$$

$$x_f = \frac{L}{T}t - \frac{LS}{2\pi}\sum_{k=1}^{n}\left[\frac{a_k}{k^2}\sin\frac{2\pi k}{T}t\right]$$

$$x_f' = \frac{L}{T}\left(1 - S\sum_{k=1}^{n}\frac{a_k}{k}\cos\frac{2\pi k t}{T}\right)$$

$$x_f'' = \frac{2\pi L}{T^2}S\sum_{k=1}^{n} a_k \sin\frac{2\pi k}{T}t$$

$$x_f''' = \frac{4\pi^2 L}{T^3}S\sum_{k=1}^{n} k a_k \cos\frac{2\pi k}{T}t$$

For $n \geq 5$ $$a_k = \frac{1}{k^2}\prod_{m=1,3,5}^{n}\left|\frac{m^2-1}{m^2-k^2}\right| \quad (m \neq k).$$

Performance factors for static case (force applied at very slow rate).

Velocity factor, $C_V = 2$

Acceleration factor, $C_A = 2\pi S\sum_{k=1}^{n}\alpha a_k$

Shock factor, $C_S = (2\pi)^2 S\sum_{k=1}^{n} k a_k$ $\quad \alpha = +1, k = 1, 5, 9, 13, \ldots$ $\quad \alpha = -1, k = 3, 7, 11, 15, \ldots$

Dynamic acceleration factor. $(m = 0)$

$$C = 2\pi S\sum_{k=1}^{n}\frac{a_k}{\alpha - k/r}$$

Dynamic amplification factor $C_D = \dfrac{\sum_{k=1}^{n}\frac{a_k}{\alpha - k/r}}{\sum_{k=1}^{n}\alpha a_k}$

Coefficients a_k vs. n (highest harmonic) if $a_1 = 1$.

$n = 1$,	$a_1 = 1$				
$n = 3$,	$a_1 = 1$,	$a_3 = 1/9$			
$n = 5$,	$a_1 = 1$,	$a_3 = 1/6$,	$a_5 = 1/50$		
$n = 7$,	$a_1 = 1$,	$a_3 = 1/5$,	$a_5 = 1/25$,	$a_7 = 1/245$	
$n = 9$,	$a_1 = 1$,	$a_3 = 2/7$,	$a_5 = 2/35$,	$a_7 = 1/98$,	$a_9 = 1/1134$
$n = \infty$,	$a_k = 1/k$.				

Highest harmonic n	$n = 1$	$n = 3$	$n = 5$
x_f Follower displacement	$\frac{L}{T}\left(t - \frac{T}{2\pi}\sin\frac{2\pi t}{T}\right)$	$\frac{L}{T}t - \frac{L}{2\pi}\left(\frac{27}{28}\sin\frac{2\pi t}{T} + \frac{1}{84}\sin\frac{6\pi t}{T}\right)$	$x_f = \frac{L}{T}t - \frac{LS}{2\pi}\left[\sin\frac{2\pi t}{T} + \frac{1}{54}\sin\frac{6\pi t}{T} + \frac{1}{1250}\sin\frac{10\pi t}{T}\right]$: $S = \frac{1125}{1192} = 0{\cdot}943792$
x'_f Follower velocity	$\frac{L}{T}\left(1 - \cos\frac{2\pi t}{T}\right)$	$\frac{L}{T}\left[1 - \frac{27}{28}\cos\frac{2\pi t}{T} - \frac{1}{28}\cos\frac{6\pi t}{T}\right]$	$\frac{L}{T}\left[1 - S\left\{\cos\frac{2\pi t}{T} + \frac{1}{18}\cos\frac{6\pi t}{T} + \frac{1}{250}\cos\frac{10\pi t}{T}\right\}\right]$
x''_f Follower acceleration	$\frac{2\pi L}{T^2}\sin\frac{2\pi t}{T}$	$\frac{2\pi L}{T^2}\left[\frac{27}{28}\sin\frac{2\pi t}{T} + \frac{3}{28}\sin\frac{6\pi t}{T}\right]$	$\frac{2\pi L}{T^2}S\left\{\sin\frac{2\pi t}{T} + \frac{1}{6}\sin\frac{6\pi t}{T} + \frac{1}{50}\sin\frac{10\pi t}{T}\right\}$
x'''_f Follower shock	$\frac{(2\pi)^2 L}{T^3}\cos\frac{2\pi t}{T}$	$\frac{4\pi^2 L}{T^3}\left[\frac{27}{28}\cos\frac{2\pi t}{T} + \frac{9}{28}\cos\frac{6\pi t}{T}\right]$	$\frac{4\pi^2 L}{T^3}\left\{\cos\frac{2\pi t}{T} + \frac{1}{2}\cos\frac{6\pi t}{T} + \frac{1}{10}\cos\frac{10\pi t}{T}\right\}$
Velocity factor C_V (static)	2	2	2
Acceleration factor C_A (static)	2π	$2\pi\left(\frac{6}{7}\right) = 5{\cdot}386$	5·060
Shock factor C_S (static)	$4\pi^2$	$(4\pi^2)\left(\frac{9}{7}\right) = 5{\cdot}14\pi^2$	$(4\pi^2)\frac{8}{5} = 6{\cdot}4\pi^2$
Dynamic acceleration C $(m = 0)$	$\frac{2\pi}{1 - \frac{1}{r}}$	$\frac{5{\cdot}386\left(1 + \frac{3{\cdot}5}{r}\right)}{\left(1 - \frac{1}{r}\right)\left(1 + \frac{3}{r}\right)}$	$5{\cdot}060\frac{\left(1 + \frac{39}{32r} - \frac{149}{8r^2}\right)}{\left(1 - \frac{1}{r}\right)\left(1 + \frac{3}{r}\right)\left(1 - \frac{5}{r}\right)}$
Dynamic amplification factor C_D $(m = 0)$	$\frac{1}{1 - \frac{1}{r}}$	$\frac{\left(1 + \frac{3{\cdot}5}{r}\right)}{\left(1 - \frac{1}{r}\right)\left(1 + \frac{3}{r}\right)}$	$\frac{\left(1 + \frac{39}{32r} - \frac{149}{8r^2}\right)}{\left(1 - \frac{1}{r}\right)\left(1 + \frac{3}{r}\right)\left(1 - \frac{5}{r}\right)}$
Remarks	Cycloidal	"1–3" harmonic	"1–3–5" harmonic

Int. J. Mech. Sci. Pergamon Press Ltd. 1960. Vol. 1, pp. 350–355. Printed in Great Britain

THE EFFECT OF SMALL CHANGES IN MASS AND STIFFNESS ON THE NATURAL FREQUENCIES AND MODES OF VIBRATING SYSTEMS

R. P. N. JONES
Engineering Laboratory, University of Cambridge

(*Received* 7 *August* 1959)

Summary—Exact equations are obtained for the changes in the natural frequencies and modes of an n-degree-of-freedom system, as a result of changes in the masses and elastic constants. These equations are in a form suitable for solution by successive approximation when the changes in the modes are small. A numerical example on a 5-mass flexural system is given.

1. INTRODUCTION

IT IS usually found necessary to introduce small modifications during the design and development of a structure or mechanism. In many cases, the design calculations will include a determination of the natural frequencies and modes of vibration of the system, and considerable labour can be saved if the effect of small changes can be determined directly, so that the frequencies and modes need not be calculated afresh when the design is modified.

An approximate solution of this problem has been given by Rayleigh,[1] who considers the effect of small changes in the coefficients of the kinetic and strain energy functions, when expressed in terms of normal co-ordinates. Particular problems have also been considered by Tuplin,[2] Head[3] and Mahalingam[4, 5].

In the present paper the effect of changes in mass and stiffness of an n-degree-of-freedom system is considered, and exact equations are obtained for the corresponding changes in the natural frequencies and modes. These equations can be solved conveniently by successive approximation when the modifications do not result in a large change in the normal modes of the system.

We consider first the "original" system, whose natural frequencies and modes of vibration are (it is assumed) completely known. The deflection co-ordinates of the system will be denoted by y_i $(i = 1, 2, 3, \ldots, n)$, and, for simplicity, it will be assumed that these co-ordinates are suitably chosen to avoid dynamic coupling, and that such coupling is not introduced in subsequent modifications to the system.*

Let the deflections $y_{i(r)}$ specify the rth normal mode of vibration, whose associated natural circular frequency is ω_r. For free vibrations in this mode we may write

$$y_i = y_{i(r)} \sin \omega_r t \tag{1}$$

* When these assumptions are not satisfied it is necessary to use a more general quadratic expression for T in place of equation (2).

where t denotes time. The maximum kinetic energy of this vibration is given by the expression

$$T_r = \tfrac{1}{2}\omega_r^2 \sum_{i=1}^{n} m_i y_{i(r)}^2 \tag{2}$$

where the quantities m_i are the effective masses. The maximum strain energy V_r may be expressed as a quadratic function of the deflections, i.e.

$$V_r = \frac{1}{2} \sum_{i=1}^{n} \sum_{j=1}^{n} k_{ij} y_{i(r)} y_{j(r)} \tag{3}$$

where the quantities k_{ij} are elastic constants of the system. The energies T_r and V_r are of course equal.

It is well known that any arbitrary deflection of a system may be expressed in terms of the normal modes, i.e.

$$y_i = \sum_{s=1}^{n} \phi_s y_{i(s)} \tag{4}$$

Vol. 1
1960

where the quantities ϕ_s are normal co-ordinates. It is also known that the total kinetic and strain energies of the system may be expressed as the sums of squares of $d\phi_s/dt$ or ϕ_s, and it may be shown that

$$\frac{1}{2} \sum_i m_i \left(\frac{dy_i}{dt}\right)^2 = \sum_s \frac{T_s}{\omega_s^2} \left(\frac{d\phi_s}{dt}\right)^2 \tag{5}$$

$$\frac{1}{2} \sum_i \sum_j k_{ij} y_i y_j = \sum_s T_s \phi_s^2. \tag{6}$$

2. EFFECT OF CHANGE IN MASS AND STIFFNESS

Suppose that the masses and elastic constants are changed by given amounts $\Delta m_i, \Delta k_{ij}$, and it is required to determine the resulting changes in the natural frequencies and modes. Using the same deflection co-ordinates y_i, let $\bar{y}_{i(r)}$ and $\bar{\omega}_r$ denote the rth mode and frequency of the modified system. We write

$$\bar{y}_{i(r)} = y_{i(r)} + \Delta y_{i(r)},$$

$$\bar{\omega}_r^2 \;\; = \omega_r^2 + \Delta(\omega_r^2).$$

The new mode may be expressed in terms of the normal modes of the original system, i.e.

$$\bar{y}_{i(r)} = \sum_s \phi_{s(r)} y_{i(s)} \tag{7}$$

where the quantities $\phi_{s(r)}$ are to be determined. Since the absolute values of the modal deflections may be chosen arbitrarily, we may take $\phi_{r(r)} = 1$.

Therefore

$$\Delta y_{i(r)} = \sum_{s \neq r} \phi_{s(r)} y_{i(s)} \tag{8}$$

where the summation extends to all values of s except $s = r$. For free vibrations in the rth mode, we may write

$$y_i = \bar{y}_{i(r)} \sin \bar{\omega}_r t, \tag{9}$$

and from equations (7) and (4)

$$\phi_s = \phi_{s(r)} \sin \bar{\omega}_r t. \tag{10}$$

The kinetic energy of the modified system is

$$\frac{1}{2}\sum_i (m_i+\Delta m_i)\left(\frac{dy_i}{dt}\right)^2 \tag{11}$$

and, by using (5), (9) and (10), it may be shown that the maximum kinetic energy of the free vibration is

$$T'_r = \bar{\omega}_r^2 \sum_s \frac{T_s}{\omega_s^2}\phi_{s(r)}^2 + \tfrac{1}{2}\bar{\omega}_r^2 \sum_i \Delta m_i \bar{y}_{i(r)}^2. \tag{12}$$

Similarly, the maximum strain energy is

$$V'_r = \sum_s T_s \phi_{s(r)}^2 + \frac{1}{2}\sum_i \sum_j \Delta\kappa_{ij}\bar{y}_{i(r)}\bar{y}_{j(r)}. \tag{13}$$

Equating T'_r and V'_r, we have

$$(\bar{\omega}_r^2-\omega_r^2)\frac{T_r}{\omega_r^2} + \sum_{s\neq r}\phi_{s(r)}^2(\bar{\omega}_r^2-\omega_s^2)\frac{T_s}{\omega_s^2} + \tfrac{1}{2}\bar{\omega}_r^2\sum_i \Delta m_i \bar{y}_{i(r)}^2 - \frac{1}{2}\sum_i\sum_j \Delta k_{ij}\bar{y}_{i(r)}\bar{y}_{j(r)} = 0. \tag{14}$$

Equation (14) gives the natural frequency $\bar{\omega}_r$ of the modified system, provided the corresponding mode of vibration $\bar{y}_{i(r)}$ is known. To determine $\bar{y}_{i(r)}$ we may apply Rayleigh's Principle, which states that the value of $\bar{\omega}_r$ is stationary for small variations of $\bar{y}_{i(r)}$ from the true normal mode. In choosing $\bar{y}_{i(r)}$ we have at our disposal the quantities $\phi_{s(r)}$ $(s\neq r)$, and Rayleigh's Principle therefore gives $(n-1)$ equations of the form

$$\frac{\partial\bar{\omega}_r}{\partial\phi_{s(r)}} = 0 \quad (s\neq r). \tag{15}$$

Now, from equation (7),

$$\frac{\partial\bar{y}_{i(r)}}{\partial\phi_{s(r)}} = y_{i(s)}. \tag{16}$$

Also, since the elastic constants obey the reciprocal property

$$k_{ij} = k_{ji}, \quad \Delta k_{ij} = \Delta k_{ji},$$

it may be shown that

$$\sum_i\sum_j \Delta k_{ij}\, y_{i(s)}\bar{y}_{j(r)} = \sum_i\sum_j \Delta k_{ij}\, y_{j(s)}\bar{y}_{i(r)}. \tag{17}$$

If we differentiate equation (14) with respect to $\phi_{s(r)}$, and make use of (15), (16) and (17), we obtain, for $s\neq r$,

$$2\phi_{s(r)}(\bar{\omega}_r^2-\omega_s^2)\frac{T_s}{\omega_s^2} + \bar{\omega}_r^2\sum_i \Delta m_i \bar{y}_{i(r)}y_{i(s)} - \sum_i\sum_j \Delta k_{ij}\bar{y}_{i(r)}y_{j(s)} = 0. \tag{18}$$

Equation (14), together with the $(n-1)$ equations (18), provides n simultaneous equations for determining the n quantities $\bar{\omega}_r$, $\phi_{s(r)}$ $(s\neq r)$.

Equation (14) may be put in a simpler form, as follows. If we multiply (18) by $\frac{1}{2}\phi_{s(r)}$, and add together the equations so obtained for all values of $s\neq r$, we obtain the further equation

$$\sum_{s\neq r}\phi_{s(r)}^2(\bar{\omega}_r^2-\omega_s^2)\frac{T_s}{\omega_s^2} + \tfrac{1}{2}\bar{\omega}_r^2\sum_i \Delta m_i\bar{y}_{i(r)}\Delta y_{i(r)} - \frac{1}{2}\sum_i\sum_j \Delta k_{ij}\bar{y}_{i(r)}\Delta y_{j(r)} = 0 \tag{19}$$

and subtracting (19) from (14), this gives

$$(\bar{\omega}_r^2 - \omega_r^2)\frac{T_r}{\omega_r^2} + \tfrac{1}{2}\bar{\omega}_r^2 \sum_i \Delta m_i \bar{y}_{i(r)} y_{i(r)} - \frac{1}{2}\sum_i \sum_j \Delta k_{ij} \bar{y}_{i(r)} y_{j(r)} = 0. \tag{20}$$

Equations (18) and (20) now provide the required solution. It should be noted that these equations are valid only if $\Delta y_{i(r)}$ satisfies (8). The absolute magnitudes of $\bar{y}_{i(r)}$ are fixed in relation to those of the original mode $y_{i(r)}$. The latter may, of course, be chosen arbitrarily.

3. APPROXIMATE SOLUTION

Equations (18) and (20) are exact, irrespective of the magnitude of the changes $\Delta m_i, \Delta k_{ij}$. A simple approximate solution of these equations may be obtained if the change in the mode of vibration is small. This will usually be true when the modifications do not result in a large change of distribution of mass or stiffness, unless the system has two or more frequencies which are nearly equal.

Putting $\bar{y}_{i(r)} \simeq y_{i(r)}$ in (20), we have

$$(\bar{\omega}_r^2 - \omega_r^2)\sum_i (m_i + \Delta m_i) y_{i(r)}^2 \simeq \sum_i \sum_j \Delta k_{ij} y_{i(r)} y_{j(r)} - \omega_r^2 \Sigma \Delta m_i y_{i(r)}^2, \tag{21}$$

and similarly from (18),

$$\phi_{s(r)}(\bar{\omega}_r^2 - \omega_s^2)\Sigma m_i y_{i(s)}^2 \simeq \sum_i \sum_j \Delta k_{ij} y_{i(r)} y_{j(s)} - \bar{\omega}_r^2 \sum_i \Delta m_i y_{i(r)} y_{i(s)}. \tag{22}$$

Equation (21) gives a first approximation to $\bar{\omega}_r$, whilst (22) gives the approximate values of $\phi_{s(r)}$, from which the new mode $\bar{y}_{i(r)}$ may be calculated by substitution in (7).

A more accurate solution may be obtained by successive approximation, the first approximations to $\bar{\omega}_r$ and $\bar{y}_{i(r)}$ being substituted in (20) and (18) to obtain the second approximations, and so on.

4. NUMERICAL EXAMPLE

As an illustrative example, a flexural system having five degrees of freedom has been chosen. The system consists of five equal masses (m), equally spaced at distances l on a light uniform beam, simply supported at each end. The total length of the beam is $6l$, and its flexural rigidity is EI. Because of its simplicity the natural frequencies and modes of this system are easily determined, and the results are given in Table 1.

TABLE 1

Mode No. (r)	$y_{1(r)}$	$y_{2(r)}$	$y_{3(r)}$	$y_{4(r)}$	$y_{5(r)}$	$\omega_r^2\, ml^3/EI$
1	$\frac{1}{2}$	$\frac{1}{2}\sqrt{3}$	1	$\frac{1}{2}\sqrt{3}$	$\frac{1}{2}$	0·075153
2	1	1	0	−1	−1	1·2
3	1	0	−1	0	1	6
4	1	−1	0	1	−1	18
5	$\frac{1}{2}$	$-\frac{1}{2}\sqrt{3}$	1	$-\frac{1}{2}\sqrt{3}$	$\frac{1}{2}$	36·848

The foregoing theory will now be used to determine the change in the fundamental mode and frequency as a result of a 20 per cent increase in mass (1), the beam stiffness and other masses remaining unchanged. We have, therefore

$$\Delta m_i = \begin{cases} 0{\cdot}2m & (i = 1), \\ 0 & (i = 2, 3, 4, 5), \end{cases}$$

$$\Delta k_{ij} = 0.$$

The first approximations given by (21) and (22) are

$$\begin{aligned} \bar{\omega}_1^2 - \omega_1^2 &= -0{\cdot}001232EI/ml^3, \\ \bar{\omega}_1^2 &= 0{\cdot}07392EI/ml^3, \\ \phi_{2(1)} &= 1{\cdot}641 \times 10^{-3}, \\ \phi_{3(1)} &= 4{\cdot}157 \times 10^{-4}, \\ \phi_{4(1)} &= 1{\cdot}030 \times 10^{-4}, \\ \phi_{5(1)} &= 3{\cdot}350 \times 10^{-5}. \end{aligned}$$

By substitution in (7) we obtain

$$\begin{aligned} \bar{y}_{1(1)} &= 0{\cdot}5022\ (0{\cdot}5024), \\ \bar{y}_{2(1)} &= 0{\cdot}8675\ (0{\cdot}8679), \\ \bar{y}_{3(1)} &= 0{\cdot}9996\ (1{\cdot}0000), \\ \bar{y}_{4(1)} &= 0{\cdot}8645\ (0{\cdot}8648), \\ \bar{y}_{5(1)} &= 0{\cdot}4987\ (0{\cdot}4989). \end{aligned}$$

The bracketed figures are obtained by scaling up the values of $\bar{y}_{i(r)}$ to give unit deflection of the central mass.

By comparison with a more exact solution it may be shown that the solution given above is correct to four significant figures. By substituting the values of $\bar{y}_{i(r)}$ (not the bracketed figures) in equations (20) and (18), a second approximation correct to six significant figures may be obtained.

In the case of the fundamental mode the convergence of the successive approximation is rapid, and an accurate solution is easily obtained. In the case of the higher modes there are greater changes, and the convergence of the process is slower. Thus, for the fifth mode, a fourth approximation must be calculated to obtain the mode correct to four significant figures.

5. DISCUSSION

To obtain an accurate solution by successive approximation it is desirable that the changes in the normal modes should be small. Clearly, these changes will depend on the distribution of the mass and stiffness changes as well as on their magnitudes. The change in any mode will also depend on the value of its frequency in relation to those of the other modes of the system. If, for simplicity, we consider a system in which there are small changes in the masses only, then equation (22) shows that $\phi_{s(r)}$ depends partly on the factor $\bar{\omega}_r^2/(\bar{\omega}_r^2 - \omega_s^2)$. This factor is small if $\omega_s \gg \bar{\omega}_r$, approximately unity if $\bar{\omega}_r \gg \omega_s$, and large if $\bar{\omega}_r \simeq \omega_s$. Thus, in a system having widely spaced natural frequencies (such as a flexural system), any change in mass distribution should have little effect on the fundamental mode, since the quantities $\phi_{s(1)}$ are small. This will not be true, however, for the higher modes. On the other

hand, in a system such as an equi-frequency flexible suspension, having two or more natural frequencies approximately equal, a small change in mass distribution is likely to produce large changes in the corresponding modes.

A practical disadvantage of the theory given in this paper is that it requires a knowledge of all the natural frequencies and modes of the original system. From (21) we can calculate a first approximation to $\bar{\omega}_r$ merely from a knowledge of the corresponding mode $y_{i(r)}$. However, to determine $\phi_{s(r)}$ it is necessary to know both $y_{i(s)}$ and $y_{i(r)}$. If all the modes of the original system are not known, we can obtain only approximate values for the changes in the known modes.

The numerical example given above indicates a useful application of the theory, that is, to determine the frequencies and modes of a system which departs but slightly from a simple, regular form whose frequencies and modes are easily calculated.

The theory may easily be extended to continuous systems by the use of appropriate integral expressions for kinetic and strain energy in place of equations (2) and (3).

Vol. 1
1960

REFERENCES

1. Lord Rayleigh, *The Theory of Sound*. Vol. 1, p. 114. Macmillan, London (1894).
2. W. A. Tuplin, *Phil. Mag.* **21**, 1097 (1936).
3. J. W. Head, *Proc. Inst. Mech. Engrs., Lond.* **169**, 253 (1955).
4. S. Mahalingham, *J. Appl. Mech.* **25**, 618 (1958).
5. S. Mahalingham, *J. Aero. Sci.* **26**, 46 (1959).

Int. J. Mech. Sci. Pergamon Press Ltd. 1960. Vol. 1, pp. 356–365. Printed in Great Britain

TORSION OF COMPOUND BARS—A RELAXATION SOLUTION

J. F. Ely and O. C. Zienkiewicz
Northwestern University, Illinois

(*Received* 30 *June* 1959)

Summary—This paper deals with a finite-difference solution of the torsion problem of nonhomogeneous and compound prismatic bars. General, governing equations for both problems are developed and the boundary conditions for an interface between parts composed of homogeneous but different materials are stated. The case of multiply connected regions is discussed and integral conditions, analogous to the conditions in multiply connected homogeneous bars, are developed.

Examples illustrating various types of problems are worked out and the accuracy of the method demonstrated by comparison with some known solutions.

NOTATION

xyz	co-ordinates
uvw	displacement components in xyz direction
τ_{xz}, τ_{yz}	shear stresses
θ	twist per unit length
G	modulus of rigidity
ϕ	Prandtl's stress function
T	torque
s, n	tangent and normal directions to curve
α	ratio of G_2 to G_1

1. INTRODUCTION

The increasing use of geometrically complicated composite sections in practice has prompted this investigation of the torsion of composite bars. Composite sections are used in reinforced concrete and aircraft, as well as other more specialized applications, and the methods presented here should prove useful in solving the torsion problem in these fields.

Several problems on the torsion of compound prismatic bars have been solved analytically by Muskhelishvilli,[1] Gorgidze,[2] Mitra,[3] Takeyama,[4] Suhareviki,[5] Sherman,[6] Cowan,[7] Craven[8] and others. The problems solved generally dealt with cross-sectional shapes that could be mapped conformally, with relative ease.

While these analytical solutions of the torsion problem for both homogeneous as well as composite bars are exceedingly important, it is necessary to use relaxation methods to solve the problem of even a homogeneous bar when the geometry of the cross-section becomes complicated as instanced by numerous publications by Southwell,[9] Shaw,[10] Allen,[11] Dobie[12] and others[13–16]. Since the homogeneous bar can be easily treated by relaxation methods, it

seemed logical to attempt to extend these methods to cover the case of simply and multiply connected composite bars when the geometry of the cross-section is complicated. Indeed, the treatment of this more general case also turns out to be simple.

It should be pointed out that the purpose of the examples which were chosen for this paper is to illustrate how the method can be applied to the various general classes of problems, and not to illustrate the handling of especially complicated boundaries. More complex boundary shapes can be dealt with as usual by using a finer mesh size which will require more time to obtain the required solutions. It is anticipated that any digital computer programmes available for solution of the Poisson equation could be easily adapted to the type of problems discussed.

Equations will be developed for simply connected cross-sections, where the material has a continuously varying G, and then for those that are composed of two distinct materials joined together, without slipping, at an interface. The additional conditions required in the case of a multiply connected cross-section will also be derived, and examples will be shown for each class of problem. Finally, the membrane analogy will be discussed in detail and other analogies pointed out.

Vol. 1
1960

2. GOVERNING EQUATIONS FOR CONTINUOUSLY VARYING G

Consider Fig. 1 and a material which has a continuously varying G in cross-section, but whose G is independent of z, i.e.

$$G = G(x, y). \tag{1}$$

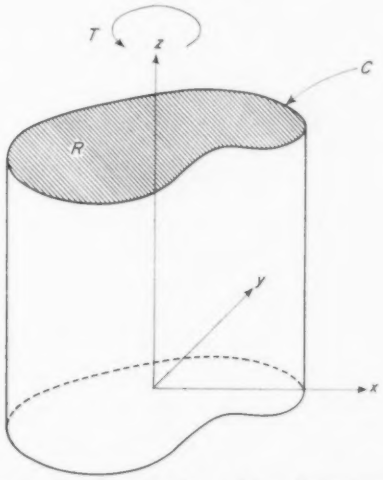

FIG. 1. Torsion of a bar. Co-ordinates used.

Following the notation used by Timoshenko and Goodier,[17] and using Prandtl's stress function ϕ, which defines the two stress components by

$$\tau_{xz} = \frac{\partial \phi}{\partial y}, \quad \tau_{yz} = -\frac{\partial \phi}{\partial x}, \tag{2}$$

and, with the other stresses equal to zero, we find that the equilibrium equations are automatically satisfied. If, in addition, we take the displacement components given by

$$u = -\theta yz, \quad v = \theta xz,$$

$$\frac{\partial w}{\partial x} = \frac{1}{G}\frac{\partial \phi}{\partial y} + \theta y, \quad \frac{\partial w}{\partial y} = -\frac{1}{G}\frac{\partial \phi}{\partial x} - \theta x, \tag{3}$$

all the relations between stresses and strains are determined correctly. To ensure continuity of the axial displacement w, we have, by differentiating the final two expressions of (3), that

$$\left\{\frac{\partial^2 \phi}{\partial x^2} + \frac{\partial^2 \phi}{\partial y^2}\right\} - \frac{1}{G}\left\{\frac{\partial \phi}{\partial x}\frac{\partial G}{\partial x} + \frac{\partial \phi}{\partial y}\frac{\partial G}{\partial y}\right\} = -2G\theta,$$

or

$$\frac{\partial}{\partial x}\left(\frac{1}{G}\frac{\partial \phi}{\partial x}\right) + \frac{\partial}{\partial y}\left(\frac{1}{G}\frac{\partial \phi}{\partial y}\right) = -2\theta. \tag{4}$$

In the case of constant G this reduces to the familiar Poisson equation

$$\nabla^2 \phi \equiv \frac{\partial^2 \phi}{\partial x^2} + \frac{\partial^2 \phi}{\partial y^2} = -2G\theta. \tag{4a}$$

As the shear stress normal to the external boundary must be zero, it follows from the definition (2) that the stress function on this boundary must have a constant value. This constant can be arbitrarily fixed as zero. The sufficient and necessary boundary condition on the external boundary C becomes

$$\phi = 0. \tag{5}$$

To determine the torque T acting on the section, we integrate

$$T = \iint_R \{x\tau_{yz} - y\tau_{xz}\}\, dx\, dy,$$

which, by substitution of (2) and (5), yields

$$T = 2\iint_R \phi\, dx\, dy. \tag{6}$$

For purposes of computation it is convenient to rewrite the above relationships in a non-dimensional form. Substituting

$$x = x'L, \quad y = y'L, \quad G = G'G_0, \quad \phi = \phi'(G_0\theta L^2),$$

in which L represents some typical dimension of the section, and G_0 some typical value of G, we have, in place of (4) and (5),

$$\left\{\frac{\partial^2 \phi'}{\partial x'^2} + \frac{\partial^2 \phi'}{\partial y'^2}\right\} - \frac{1}{G'}\left\{\frac{\partial \phi'}{\partial x'}\frac{\partial G'}{\partial x'} + \frac{\partial \phi'}{\partial y'}\frac{\partial G'}{\partial y'}\right\} = -2G', \tag{7}$$

$$\phi' = 0 \quad \text{or} \quad G. \tag{8}$$

The stresses and the torque are given by

$$\tau_{s'z} = -(G_0\theta L)\frac{\partial \phi'}{\partial n'}, \tag{9}$$

$$T = 2G_0\theta L^4 \iint_R \phi'\, dx'\, dy'. \tag{10}$$

3. GOVERNING EQUATIONS FOR A DISCONTINUOUS G

We shall now consider the section shown in Fig. 2, where a discontinuity occurs in the variation of G at the interface C_2, which separates regions R_1 and R_2. Clearly, if G_1 and G_2 refer to the values of G in the respective regions, two functions, ϕ_1 and ϕ_2, satisfying equation (4) in their domains, are required.

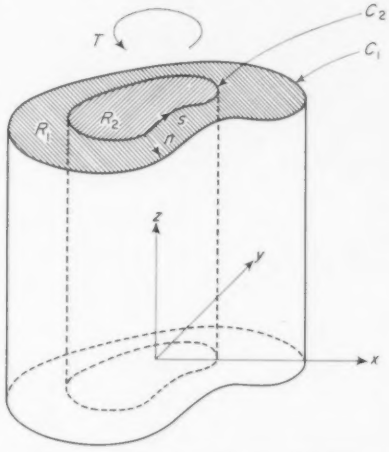

FIG. 2. Torsion of a composite bar.

On the external boundary, whether C_2 cuts it or not, the boundary condition (5) still has to be imposed. However, to specify the problem completely, additional requirements have to be imposed on the interface. These conditions must ensure that: (a) the shear stresses normal to the interface are the same in each region; and (b) the axial displacements are compatible on the interface. The first of these can be expressed as

$$\frac{\partial \phi_1}{\partial s} = \frac{\partial \phi_2}{\partial s} \quad \text{on} \quad C_2, \tag{11}$$

which can be satisfied by making

$$\phi_1 = \phi_2 \quad \text{on} \quad C_2, \tag{11a}$$

as the addition of arbitrary constants does not affect the results.

The second condition is satisfied if

$$\frac{\partial w_1}{\partial s} = \frac{\partial w_2}{\partial s} \quad \text{on} \quad C_2, \tag{12}$$

which by the use of (3) can be shown to be equivalent to

$$\frac{1}{G_1}\frac{\partial \phi_1}{\partial n} = \frac{1}{G_2}\frac{\partial \phi_2}{\partial n} \quad \text{on} \quad C_2, \tag{12a}$$

n being the direction of the normal to C_2.

It can be seen that the stress function will be continuous across the interface, but its derivatives will in general be discontinuous there. The problem thus becomes very similar to those encountered in porous media flow, or in

the determination of magnetic fields, when the permeabilities differ abruptly. It is well known that phenomena of refraction of the flow lines occur in such instances.

Considering the case of a bar made of two materials, each having constant elastic properties, and using the non-dimensional notation of the previous section, we have

$$\nabla^2 \phi_1' = -2 \quad \text{in} \quad R_1, \tag{13}$$

$$\nabla^2 \phi_2' = -2\alpha \quad \text{in} \quad R_2, \tag{14}$$

with $\phi' = 0$ on external boundary and

$$\phi_1' = \phi_2', \tag{15}$$

$$\alpha \frac{\partial \phi_1'}{\partial n'} = \frac{\partial \phi_2'}{\partial n'}$$

on interface, in which arbitrarily

$$G_1 = G_0$$

and

$$\alpha = \frac{G_2}{G_1}.$$

These relations will be used in the illustrative examples shown later.

It should be noted that the methods of the previous section, using a continuously varying G, could be used to solve this problem of a discontinuous G at an interface, by approximating to the discontinuity in G by a continuous but steep, variation. This is particularly easy to do in finite-difference treatment, and will be illustrated later. The results obtained by using this procedure, however, are not as accurate (for a given mesh size) as those obtained by assuming the G discontinuous, as does the method of this section.

4. MULTIPLY CONNECTED CROSS-SECTIONS

In the problems examined so far the condition of single-valued displacements is automatically satisfied, as could be shown by integration of the expressions (3). If, however, referring to Fig. 2, the region enclosed by C_2 were empty, an additional condition would be required. Such a condition, usually expressed in a form of a line integral, is well known for the problem of torsion of multiply connected, homogeneous sections (see Timoshenko and Goodier[17]). For the problem on hand, where G_1 may be variable, an equivalent condition has to be established. We shall derive this by taking the case of a hole as a limiting case of the problem discussed in the previous section. Now we shall take G_2 as being equal to a constant k in R_2, and let this constant tend to zero.

Clearly, one of the conditions on the "interface" now is that ϕ_1 is equal to a constant. Condition (12a) becomes insufficient in the limit, merely giving $\partial\phi_2/\partial n = 0$, which is already implicit, no condition being imposed on $\partial\phi_1/\partial n$. However, integrating (12a) around the interface C_2, we have

$$\oint_{C_2} \frac{1}{G_1} \frac{\partial \phi_1}{\partial n} = \oint_{C_2} \frac{1}{G_2} \frac{\partial \phi_2}{\partial n},$$

where G_2 is a constant, while G_1 is a function of x and y. Applying Green's Theorem in two dimensions to the right-hand side, we obtain

$$\oint_{C_1} \frac{1}{G_1} \frac{\partial \phi_1}{\partial n} = \frac{1}{G_2} \iint_{A_{C_1}} \left(\frac{\partial^2 \phi_2}{\partial x^2} + \frac{\partial^2 \phi_2}{\partial y^2} \right) dx\, dy,$$

where A_{C_1} is the area inside the curve C_2. Since G_2 is constant, equation (4a) applies inside and on C_2. Therefore we obtain after substitution

$$\oint_{C_1} \frac{1}{G_1} \frac{\partial \phi_1}{\partial n} = \frac{1}{G_2} \iint_{A_{C_1}} (-2G_2\theta)\, dx\, dy$$

$$\oint_{C_1} \frac{1}{G_1} \frac{\partial \phi_1}{\partial n} = -2\theta A_{C_1}. \tag{16}$$

It can be seen that this equation reduces to the familiar form when G_1 is a constant; namely,

$$\oint_{C_1} \frac{\partial \phi_1}{\partial n} = -2G\theta A_{C_1}.$$

A sufficient number of boundary conditions is now available for a unique solution of multiply connected sections.

It can be observed that as G_2 tends to zero, ϕ_2 must become constant in region R_2 to satisfy the governing equation (4), and the analogy of the "floating disc" is again applicable, as it is in the case of homogeneous sections.

5. MEMBRANE AND OTHER ANALOGIES

It has been pointed out that the torsion problem of a homogeneous bar is analogous, mathematically, with several other physical problems. These include the membrane under constant pressure, the problem of viscous flow of fluid in a tube, flow of a current in a conductor of variable thickness, and in general any of the physical problems which satisfy Poisson's or Laplace's equation. These analogies can be extended to the case of a composite bar in torsion with rewarding results. We shall discuss only one of these, namely, the membrane analogy. It is well known that the deflections of a membrane subjected to a constant pressure and tension satisfy the equation

$$\nabla^2 z = -\frac{q}{T}$$

(in which q is a pressure, T the membrane tension and Z the deflection). It can easily be shown that in the case of a membrane with variable tension the equivalent expression is

$$\frac{\partial}{\partial x}\left(T \frac{\partial z}{\partial x} \right) + \frac{\partial}{\partial y}\left(T \frac{\partial z}{\partial y} \right) = -q.$$

The analogy with equation (4) is now obvious if

$$T \equiv \frac{1}{G}, \quad q \equiv 2\theta, \quad z \equiv \phi.$$

Vol. 1
1960

Discontinuous variation of G can be interpreted as a discontinuous variation of the membrane tension and because

$$\oint T \frac{\partial z}{\partial n} = -Aq$$

by statics, all the other relationships for interface conditions, as well as for multiply connected regions, can be deduced. It should be observed that the variation of T implies existence of distributed forces parallel to the xy planes—which in the case of an interface becomes a line force. As a possible experimental solution the membrane analogy does not appear practicable.

6. EXAMPLES

The governing equations and their respective boundary conditions can be easily transformed into suitable finite-difference relationships and a solution can then be obtained by application of relaxation methods. As the techniques of both are well known and described in many texts (e.g. Allen[11]) it is not

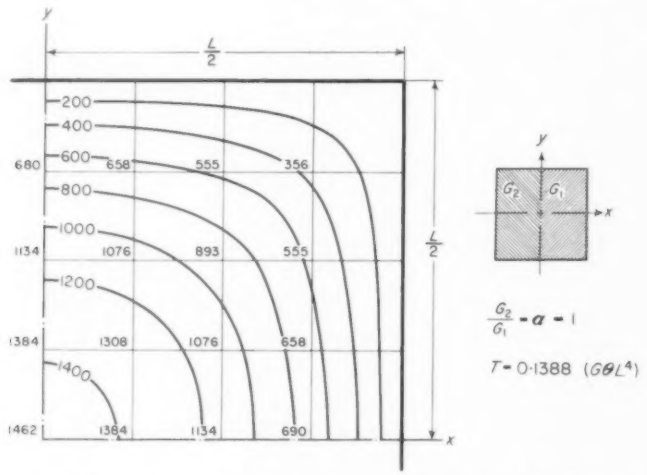

Fig. 3(a). Example A. Torsion of a square composite bar; $\alpha = 1$; values of $\phi' \times 10^4$.

proposed to elaborate on these matters here. The general treatment of Poisson's equation is now virtually standard for the usual Neumann and Dirichlet boundary conditions and the main problems encountered here are those pertaining to the interface between the two materials. Again, as the conditions at the interface are essentially similar to those encountered in the treatment of seepage or magnetic field problems in media of different permeabilities, techniques or relaxation treatment are well known. These, used for the first time by Christopherson,[18] are excellently described in Allen's text, and no special difficulty was encountered in their application in the examples solved.

Examples A and B (Figs. 3(a–c) and 4) show problems in which straight and curved interfaces between two materials occur respectively. The accuracy

of the relaxation solution can be seen from the table below, in which the stiffness of the bars of example A obtained from a relatively coarse mesh solution are compared with values computed by a series solution developed by Muskhelishvilli[1].

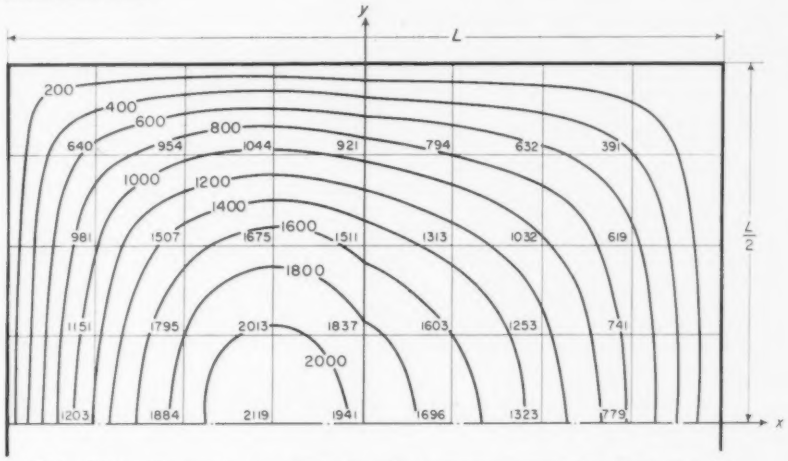

FIG. 3(b). Example A. Torsion of a square composite bar; $\alpha = 2$; $T = 0{\cdot}1941\ (G\theta L^4)$; values of $\phi' \times 10^4$.

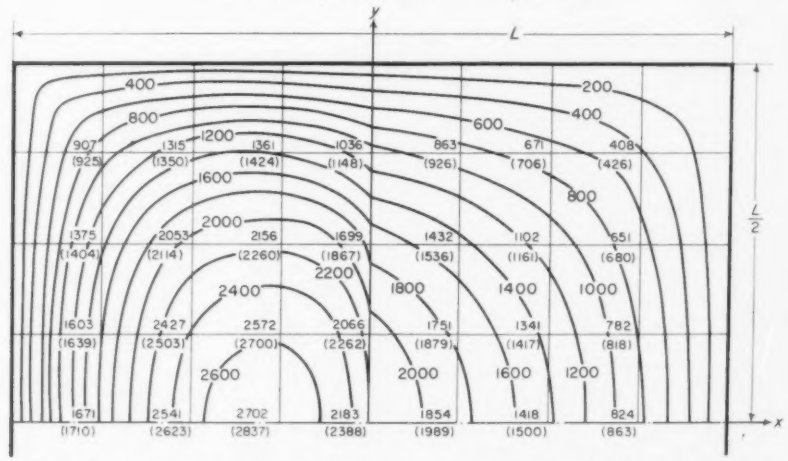

FIG. 3(c). Example A. Torsion of a square composite bar; $\alpha = 3$; $T = 0{\cdot}2358\ (G_0\theta L^4)$; values of $\phi' \times 10^4$.

$$T = D(G_0\theta L^4)$$

Values of	Torsional rigidity, D			
	By relaxation	Timoshenko	Muskhelishvilli*	(% discrepancy)
$\alpha = 1$	0·1388	0·1406	0·1407	1·28
$\alpha = 2$	0·1941		0·1972	1·57
$\alpha = 3$	0·2358		0·2399	1·71

* Only two terms of the series solution were used, and these values are always greater than the true value. The error increases with increasing α.

Vol. 1
1960

To test the alternative method of satisfying the interface conditions, in one of the examples [see Fig. 3(c)], G was assumed to vary in a continuous way from G_1 to G_2 within a distance of one mesh length. The finite difference expression of equation (4) can now be used directly at all mesh points. Values in parentheses, [Fig. 3(c)], refer to an assumed continuous variation of G, while the others are for a discontinuous variation of G.

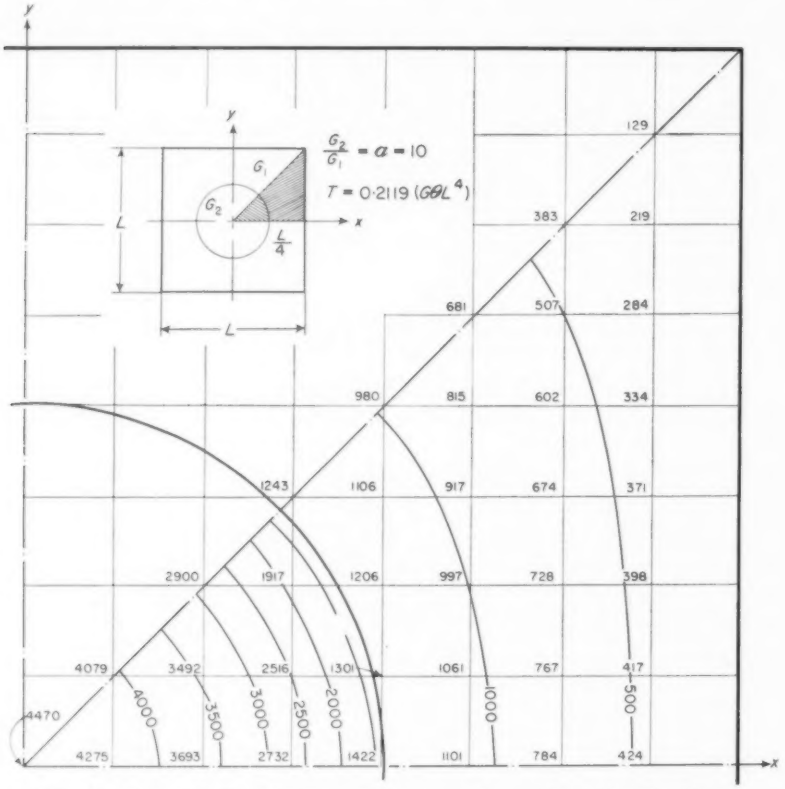

Fig. 4. Example B. Torsion of a square bar with a circular insert; $\alpha = 10$; values of $\phi' \times 10^4$.

The coarseness of the mesh resulted in an error of about 6 per cent in the final stiffness as compared with the exact solution, i.e. it proved to be less accurate than the method employing the correct interface conditions. The procedure may, however, be advantageous when numerous curved interfaces occur.

In example C (Fig. 5) the case of a multiply connected region is considered in which the interface between two materials cuts the hole boundary. The procedure followed here was essentially the same as described by Shaw[10] for the treatment of multiply connected, homogeneous shafts. Solutions with a constant and arbitrary value of the stress function on the hole boundary are first obtained using the governing equation (4) and excluding the non-homogeneous term. Then a solution of the full equation with a zero value of

the stress function of the hole boundary is computed, and the final solution obtained by a linear combination of these. This combined solution satisfies the integral condition (16). Again no special difficulties were encountered.

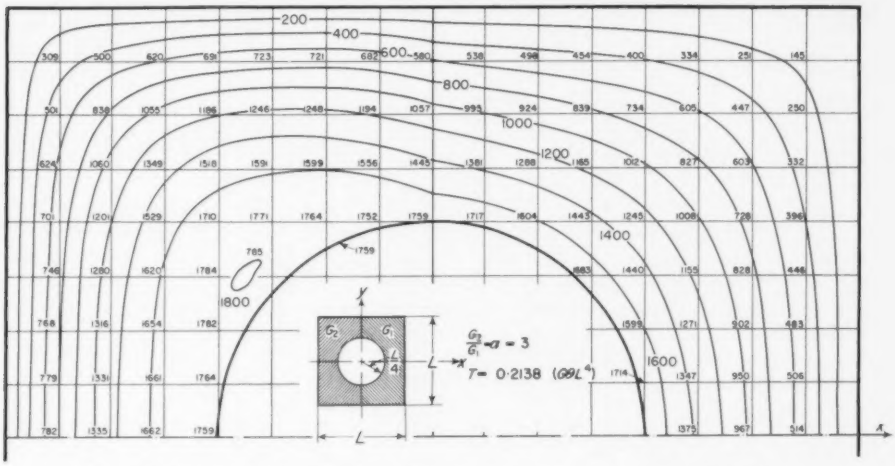

FIG. 5. Example C. Torsion of a composite bar with a circular hole.

REFERENCES

1. N. I. MUSKHELISHVILLI, *Some Basic Problems of the Mathematical Theory of Elasticity* p. 561. Noordhoff, Groningen (1953).
2. A. YA. GORGIDZE, *Trudy Tbiliss Math. Inst. Razmadze* **17**, 95 (1949).
3. D. N. MITRA, *Bull. Calcutta Math. Soc.* **47**, 191 (1955).
4. HISAO TAKEYAMA, *J. Soc. Appl. Mech., Japan* **2**, 88 (1949).
5. I. V. SUHAREVIKI, *Inzh. sborn. Akad. Nauk SSSR* **19**, 107 (1954).
6. D. I. SHERMAN and M. Z. NARODETSKII, *Inzh. sborn. Akad. Nauk SSSR* **6**, 17 (1950).
7. H. J. COWAN, *Appl. Sci. Res., Hague* (A) **3**, 344 (1952).
8. A. H. CRAVEN, *Mathematika* **1**, 96 (1954).
9. R. V. SOUTHWELL, *Relaxation Methods in Theoretical Physics* p. 85. Clarendon Press, Oxford (1946).
10. F. S. SHAW, *The Torsion of Solid and Hollow Prisms in the Elastic and Plastic Range by Relaxation Methods.* Austral. Counc. Aeronaut. Rep. ACA-11,38 (1944).
11. D. N. DE G. ALLEN, *Relaxation Methods* p. 198. McGraw-Hill, London (1955).
12. W. B. DOBIE and A. R. GENT, *Struct. Engr.* **30**, 203 (1952).
13. H. J. COWAN, *Civ. Engng. Lond.* **48**, 567, 827, 950 (1953).
14. W. B. DOBIE, *Struct. Engr.* **30**, 34 (1942).
15. T. J. HIGGINS, *J. Appl. Phys.* **14**, 469 (1943).
16. L. E. PAYNE, *Iowa St. Coll. J. Sci.* **23**, 381 (1949).
17. S. TIMOSHENKO and J. N. GOODIER, *Theory of Elasticity.* McGraw-Hill, New York (1951).
18. D. G. CHRISTOPHERSON and R. V. SOUTHWELL, *Proc. Roy. Soc.* A **168**, 317 (1936).

Vol. 1
1960

Int. J. Mech. Sci. Pergamon Press Ltd. 1960. Vol. 1, pp. 366–368. Printed in Great Britain

AN UPPER-BOUND APPROACH TO PLANE-STRAIN FORGING AND EXTRUSION—III

HIDEAKI KUDO
Aeronautical Research Institute, Tokyo University

(*Received* 12 *January* 1959)

Summary—Flow patterns on sections of lead billets during various plane-strain forging and extrusion operations are photographed and presented. These are compared with predicted most suitable velocity fields obtained by the method described in Parts I and II of this series of papers. The agreement is satisfactory and the proposed upper-bound-approach method is thus found to be simple and reliable for practical purposes.

1. INTRODUCTION

THE purpose of this part of the investigation is to examine whether or not the upper-bound solutions derived in Parts I[1] and II[2] of this work do in fact give good approximations to the actual behaviour of material. Flow patterns of pure lead work-pieces in the plane of flow are taken and compared with the most suitable rigid-triangle velocity fields which yield the minimum upper bounds for working pressure.

The distortion of square grids which follows from a rigid-triangle velocity field is calculable following Hodge[3]. Here, however, this calculation is not carried out and only qualitative comparisons are made.

2. EXPERIMENTAL APPARATUS AND PROCEDURE

The flow patterns, as revealed by the distortion of grid-lines scratched on the blackened section-surface of lead billets, were photographed in a special apparatus developed by the author,[4] Fig. 1, through a thick glass plate directly and continuously during a working process carried out at a speed of 0·01 mm/sec.

In this apparatus, however, the working pressure could not be measured with satisfactory accuracy because of the high frictional resistance on the sliding die; it was necessary to press the sliding die strongly against the glass plate to prevent flash development between it and the tool. In addition, the thickness of the billet perpendicular to the plane of flow (10 mm) was not large enough as compared with the width of billet (20 mm). In the present work, therefore, the working pressures were measured as a reference only.

The test billets were either lubricated with lanoline or degreased with benzine and trichlorethylene according to whether the condition required was "smooth" or "rough". These boundary-surface conditions, however, were not perfectly realized. Even with the best lubricating technique some friction is inevitably present and, on the other hand, even a trace of grease functions as lubricant.

The mean uniaxial yield stress of the lead at a low strain-rate was 1·94 kg/mm^2 as determined by a compression test; its compressive yield stress, $2k$, in plane strain with a Mises yield criterion is then 2·24 kg/mm^2.

Fig. 2 shows the flow pattern during the compression of a rectangular work-piece between two parallel rough dies. The condition "rough", however, seems to be almost realized in compression with degreased dies, and shows good agreement with the calculated velocity field. But the fact that the flow pattern in this figure is unsymmetrical also indicates imperfection in trying to attain the condition "rough". It is to be noted that the discrepancy between the experimental and predicted results also proceeds from work-hardening and the viscosity of the actual metal.

Figs. 3–5 show open-die extrusion-forging. Satisfactory agreement between the photographed and the predicted velocity fields will be seen from the figures. Among them, it is clear that the region underlying the die opening did not deform during working when the tools were lubricated—as was expected from the analysis.

The results and comparisons for the heading process are illustrated in Figs. 6–9. In this case, again, the general agreement is good. The discrepancies between the experimental and predicted results are attributable mainly to the facts that (i) the experiments were carried out by regarding the axis of symmetry as a container and (ii) that there was a relatively wide clearance between the bottom die and container, see Fig. 6(b). The discrepancy which is seen in Fig. 8 seems to be caused also by the use of an improper assumption in obtaining the most suitable velocity field, namely that the boundary plane 456 in Fig. 18(b), Part I, moves uniformly leftward. It seems from the experimental results that the velocity field in which the plane 45 moves faster than the plane 56 gives a better result, Fig. 8(b).

Figs. 10–12 refer to the indentation of a rectangular block of finite dimensions.

The common extrusion and extrusion-forging processes with the reduction $R = 0{\cdot}25$, $0{\cdot}50$ and $0{\cdot}75$ are shown in Figs. 13–17. Here the agreement between the analysis and experiment can be regarded as satisfactory if some allowance is made for the effects of friction and work-hardening. Comparison of Figs. 13 and 14 clearly indicates the effect of friction on the lubricated surface of the container. That is, a marked dead metal is seen in the forward extrusion, Fig. 14, as is expected from analysis, while it is not the case in the backward extrusion, Fig. 13, under otherwise identical conditions.

Figs. 18–22 show the flow patterns and predicted velocity fields for some piercing and piercing-forging configurations. The transition points from steady to non-steady stages as determined from photographs of the flow pattern taken continuously throughout the extrusion and piercing experiments, and from the calculations, also agree well.

Results concerning unsymmetrical piercing and piercing-forging are illustrated in Figs. 23–25. This process can be regarded also as a three-orifice extrusion, Fig. 6, Part II, if the container surface is perfectly smooth. The agreement between the experimental and the predicted results will again be seen to be satisfactory. It is interesting to note that the relation between the extruded lengths from the left- and right-hand orifices differs according to the condition of friction on the die surfaces, Figs. 24 and 25.

Figs. 26–28 refer to experiments concerning opposed extrusion-piercing-forging. The working pressures and the lengths of the extruded parts as determined from experiment and analysis are given in Fig. 29. The experimental values of pressure are considerably higher than those predicted broken lines for the reason stated in the preceding section. However, the points of transition from deformation-mode (a) to (b), Fig. 23, Part II, as represented by the hollow circle (experiment) and cross (theory), as well as the extruded lengths, agree well.

An example of unsymmetrically opposed extrusion-forging is given in Fig. 30 though the velocity field was not calculated for this case. However, the rigid-triangle field, such as is given on the right-hand sides of Fig. 30(a) and (c) are seen to be good approximations to the experimental results. The velocity field of type (a) agrees with that proposed by Johnson[5]. In this experiment, the ratio of the speed of the material flowing from the narrower orifice to that from the wider orifice, decreased as the process advanced until it became zero, Fig. 31.

A number of examples of flow patterns in the edging process are shown in Figs. 32–34, the bevelled specimens being compressed between parallel dies. These patterns show no clear plastic–rigid boundaries because of the small strains involved, but they are likely to have resulted from the predicted velocity fields shown on the right-hand side of the figures.

Fig. 35 indicates the mean edging-pressure as determined by experiment and that determined by an upper-bound calculation. In this case, it is to be noted that the calculated value was always higher than the experimental value, contrary to other experimental results. The reason for this is likely to arise from the low yield-stress of the lead since the strain and strain-rate in the material during such edging processes are small. The ratios between horizontal and vertical non-contiguous lengths C_1/C_2, Fig. 27, Part II, which were obtained from the experiment are plotted in Fig. 35 and are seen to have remained almost constant throughout the deformation—as was expected from the most suitable velocity field.

Fig. 36 illustrates a coining or forging-edging process. It is seen that in its final stage, the edging process is taking place near the top surface of the die cavity.

Acknowledgements—The author wishes to thank Professor S. Fukui of the University of Tokyo, for his helpful advice and encouragement throughout the work. He also wishes to thank Mr. J. Seino and Mr. I. Takita of the Institute of Aeronautical Research at the University of Tokyo, and Mr. M. Kametani of Iwasaki Communication Apparatus Co. Ltd. for their kind assistance with the experiments, calculations and the preparation of the manuscript. Acknowledgement is also made to Mr. W. Johnson for his kind help in preparing the paper for publication.

This work was supported by the Fund for Scientific Research, provided through the Ministry of Education, Japan.

REFERENCES

1. H. KUDO, *Int. J. Mech. Sci.* **1**, 57 (1960).
2. H. KUDO, *Int. J. Mech. Sci.* **1**, 229 (1960).
3. P. G. HODGE, *J. Appl. Mech.* **17**, 257 (1950).
4. H. KUDO, *Rep. Inst. Sci.* **11**, 148 (1957).
5. W. JOHNSON, *Proc. Inst. Mech. Engrs., Lond.* **173**, 61 (1959).

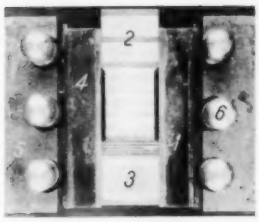

FIG. 1. Apparatus and tools for direct and continuous observation of internal metal flow: 1—lead billet; 2—top die or punch; 3—bottom die; 4—container; 5—housing; 6—fastening bolt for thick glass plate.

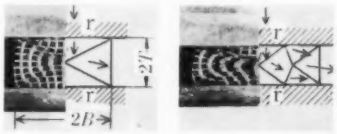

(a) (b)

FIG. 2. Compression between parallel degreased dies.

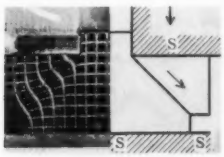

FIG. 3. Open-die extrusion-forging with lubricated dies, $W/B_0 = 0{\cdot}31$, $T_0/B_0 = 0{\cdot}625$.

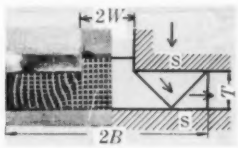

FIG. 4. Open-die extrusion-forging with lubricated dies, $W/B_0 = 0{\cdot}31$, $T_0/B_0 = 0{\cdot}62$.

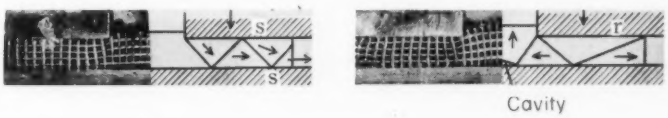

(a) (b)

FIG. 5. Open-die extrusion-forging, $W/B_0 = 0{\cdot}28$, $T_0/B_0 = 0{\cdot}28$. (a) Both dies lubricated. (b) Top die degreased, bottom die lubricated.

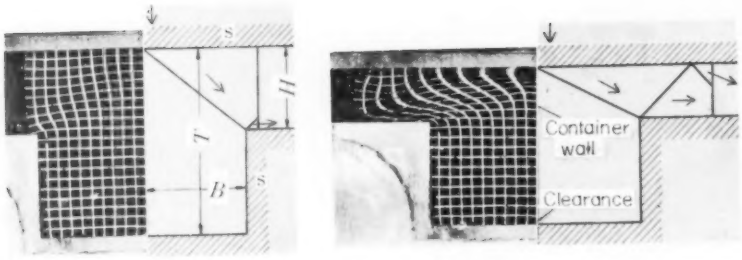

(a) (b)

FIG. 6. Heading with lubricated tools, $T_0/B = 1{\cdot}99$, $H_0/B = 1{\cdot}00$.

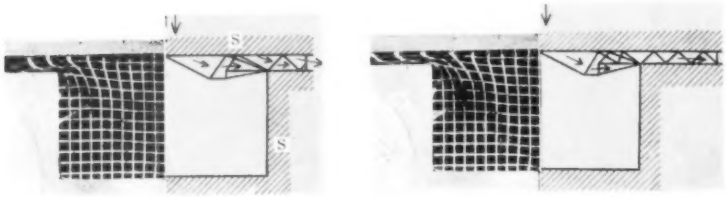

(a) (b)

FIG. 7. Heading with lubricated tools, $T_0/B = 1{\cdot}50$, $H_0/B = 0{\cdot}50$.

(a) (b)

FIG. 8. Heading with lubricated tools, $T_0/B = 0{\cdot}30$, $H_0/B = 0{\cdot}15$.

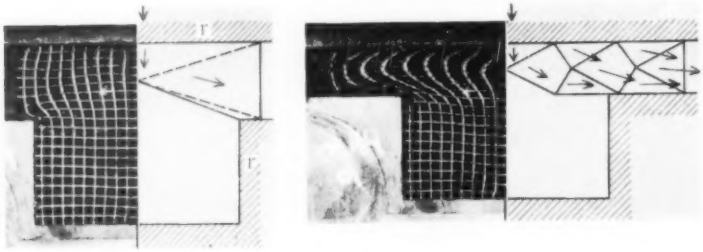

(a) (b)

FIG. 9. Heading with degreased tools, $T_0/B = 1{\cdot}98$, $H_0/B = 0{\cdot}95$.

Plate II

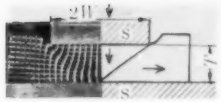

FIG. 10. Flat indentation with lubricated tools, $T_0/W = 1{\cdot}00$.

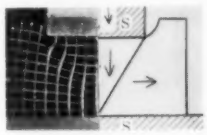

FIG. 11. Flat indentation with lubricated tools, $T_0/W = 2{\cdot}00$.

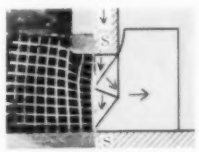

FIG. 12. Flat indentation with lubricated tools, $T_0/W = 4{\cdot}00$.

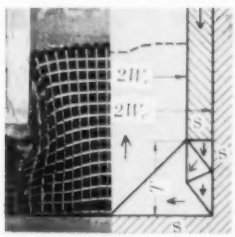

FIG. 13. Backward extrusion with lubricated tools, $R = 0{\cdot}25$, $T_0/W_c = 1{\cdot}43$.

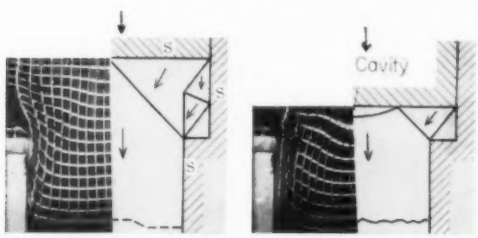

(a) (b)

FIG. 14. Forward extrusion with lubricated tools, $R = 0{\cdot}25$, $T_0/W_c = 1{\cdot}45$.

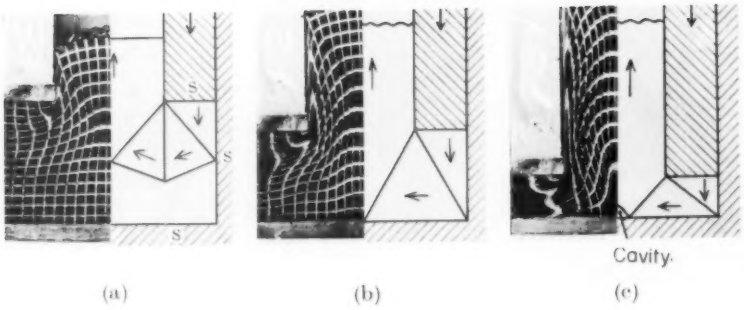

(a) (b) (c)

FIG. 15. Backward extrusion with lubricated tools, $R = 0{\cdot}50$, $T_0/W_c = 1{\cdot}47$.

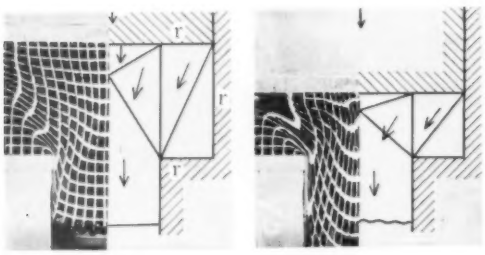

(a) (b)

FIG. 16. Forward extrusion with degreased tools, $R = 0{\cdot}50$, $T_0/W_c = 1{\cdot}45$.

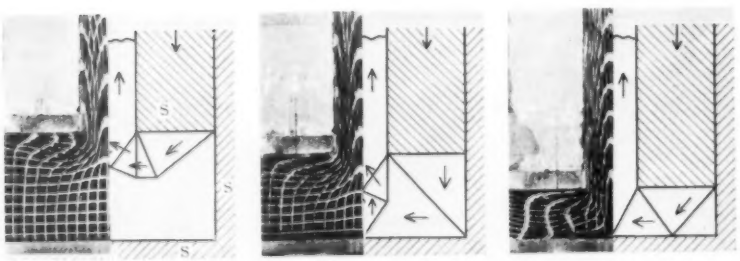

(a) (b) (c)

FIG. 17. Backward extrusion with lubricated tools, $R = 0{\cdot}75$, $T_0/W_c = 1{\cdot}46$.

Plate IV

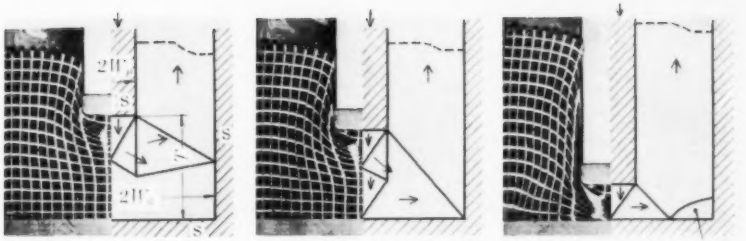

FIG. 18. Backward piercing with lubricated tools,
$R = 0{\cdot}25$, $T_0/W_c = 1{\cdot}45$.

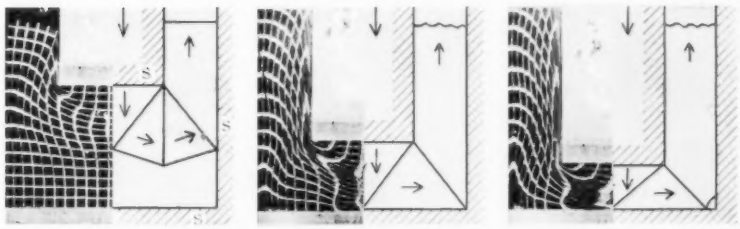

FIG. 19. Backward piercing with lubricated tools,
$R = 0{\cdot}50$, $T_0/W_c = 1{\cdot}47$.

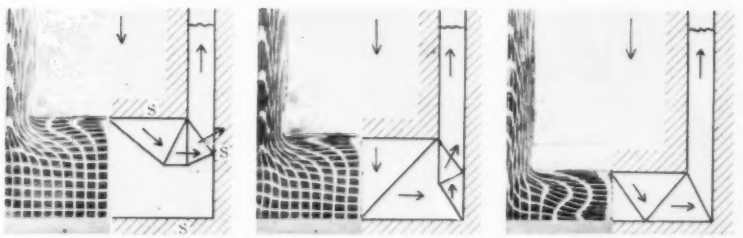

FIG. 20. Backward piercing with lubricated tools,
$R = 0{\cdot}75$, $T_0/W_c = 1{\cdot}47$.

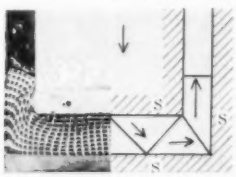

FIG. 21. Backward piercing with lubricated tools,
$R = 0{\cdot}75$, $T_0/W_c = 0{\cdot}49$.

Plate V

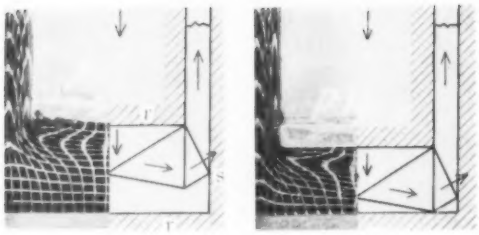

(a) (b)

FIG. 22. Backward piercing with degreased punch, bottom die and lubricated container, $R = 0{\cdot}75$, $T_0/W_c = 1{\cdot}30$.

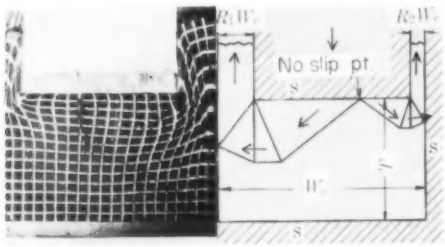

(a)

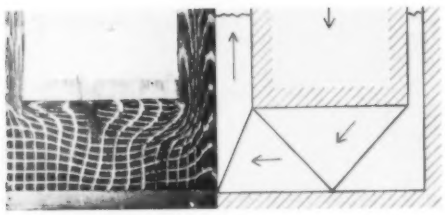

(b)

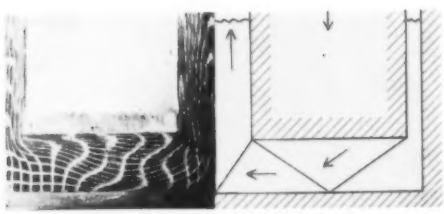

(c)

FIG. 23. Unsymmetrical backward piercing with lubricated tools, $R_i = 0{\cdot}75$, $R_1 = 0{\cdot}83$, $R_2 = 0{\cdot}92$, $T_0/W_c = 0{\cdot}68$.

Plate VI

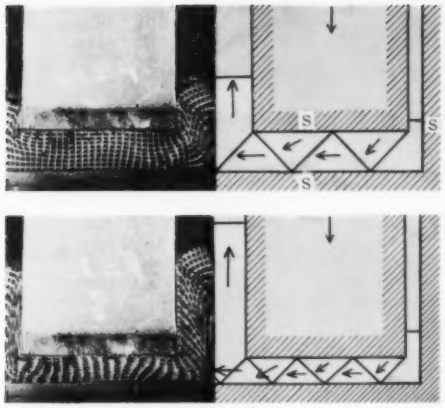

FIG. 24. Unsymmetrical backward piercing with lubricated tools, $R_t = 0{\cdot}75$, $R_1 = 0{\cdot}83$, $R_2 = 0{\cdot}92$, $T_0/W_c = 0{\cdot}49$.

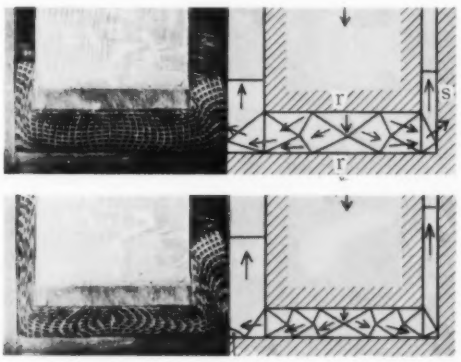

FIG. 25. Unsymmetrical backward piercing with degreased punch, bottom die and lubricated container, $R_t = 0{\cdot}75$, $R_1 = 0{\cdot}83$, $R_2 = 0{\cdot}92$, $T_0/W_c = 0{\cdot}49$.

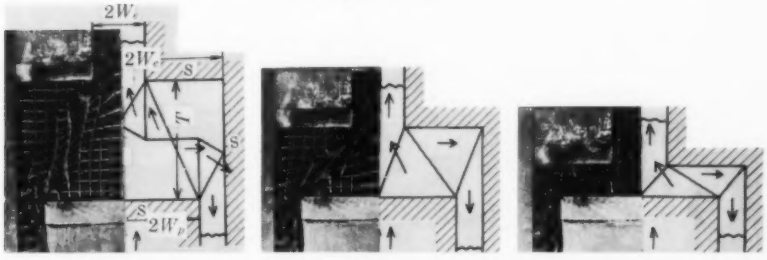

FIG. 26. Opposed extrusion-piercing with lubricated tools, $R_1 = R_2 = 0{\cdot}75$, $T_0/W_c = 1{\cdot}47$.

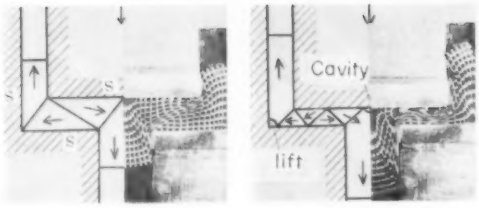

FIG. 27. Opposed extrusion-piercing with lubricated tools, $R_1 = R_2 = 0{\cdot}75$, $T_0/W_c = 0{\cdot}49$.

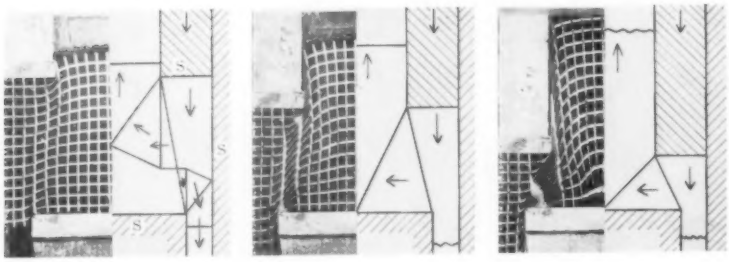

FIG. 28. Opposed extrusion-piercing with lubricated tools, $R_1 = 0{\cdot}50$, $R_2 = 0{\cdot}75$, $T_0/W_c = 1{\cdot}46$.

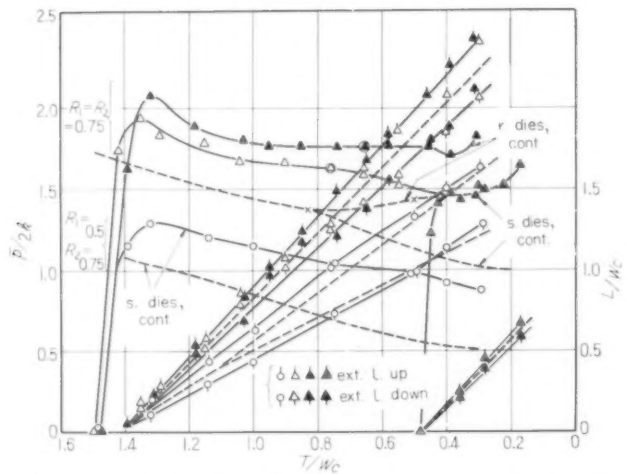

FIG. 29. Autographic diagram for pressure and extruded length in opposed extrusion-piercing of lead. ———— experimental result. — — — — calculated result. ○, ×, observed and calculated beginning point for overall deformation.

Plate VIII

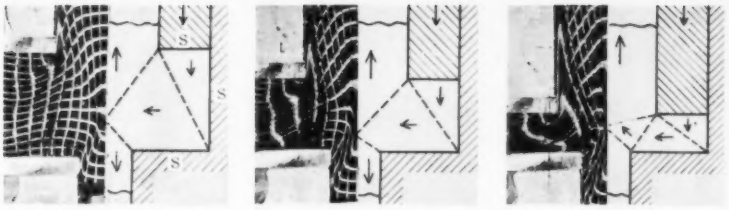

FIG. 30. Unsymmetrically opposed extrusion with lubricated tools, $R_1 = 0{\cdot}50$, $R_2 = 0{\cdot}25$, $T_0/W_c = 1{\cdot}45$.

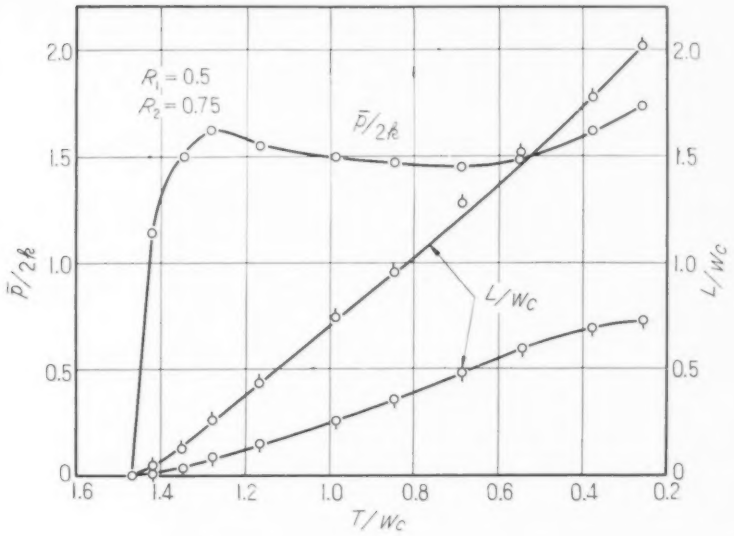

FIG. 31. Autographic diagram for pressure and extruded length in unsymmetrically opposed extrusion with lubricated tools.

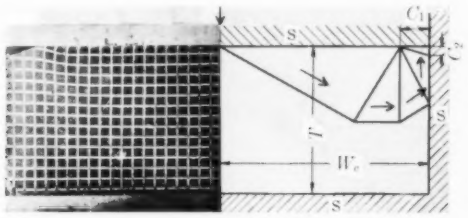

FIG. 32. Edging with lubricated tools, $C_{10}/C_{20} = 2{\cdot}75$, $T_0/W_c = 0{\cdot}72$.

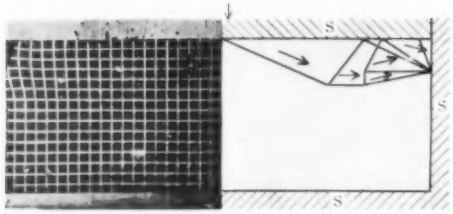

FIG. 33. Edging with lubricated tools, $C_{10}/C_{20} = 0{\cdot}37$, $T_0/W_c = 0{\cdot}74$.

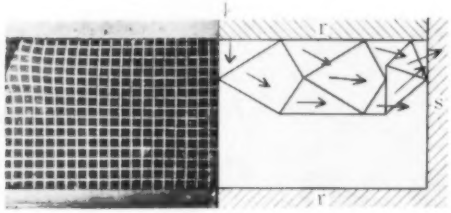

FIG. 34. Edging with degreased top and bottom dies and lubricated container, $C_{10}/C_{20} = 3{\cdot}35$, $T_0/W_c = 0{\cdot}75$.

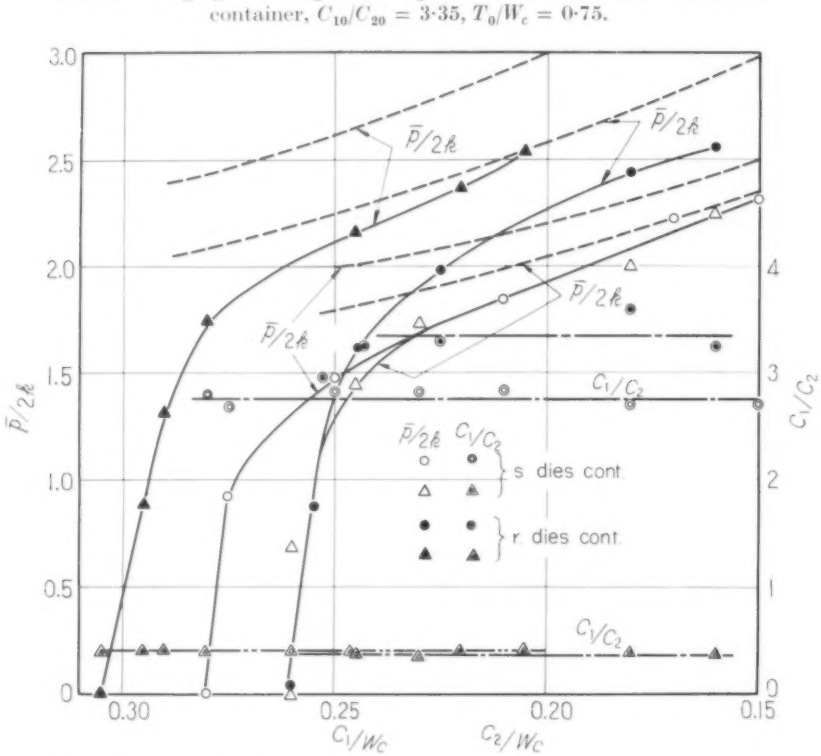

FIG. 35. Edging pressure and C_1/C_2 during edging, as observed experimentally and calculated analytically.

Plate X

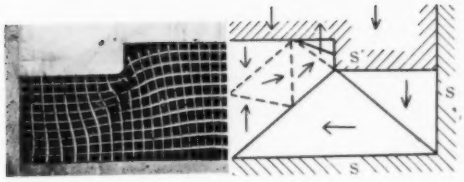

(a)

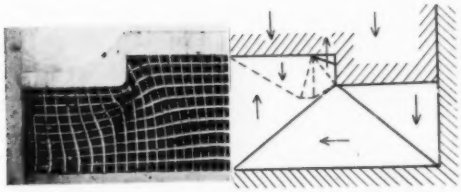

(b)

FIG. 36. Closed-die coining with lubricated tools.
$W_e/W_c = 0{\cdot}5$, $T_0/W_c = 0{\cdot}50$.

Vol
196

Int. J. Mech. Sci. Pergamon Press Ltd. 1960. Vol. 1, pp. 369–378. Printed in Great Britain

THE DESIGN OF PRESSURE VESSELS SUBJECTED TO THERMAL STRESS—IV

MULTILAYER VESSELS*

E. WHALLEY and S. MORRIS

Division of Applied Chemistry, National Research Council, Ottawa, Canada

(*Received* 27 *May* 1959)

Summary—A theoretical investigation has been made of the design of multilayer cylindrical pressure vessels subjected to combined pressure and steady-state thermal stresses. The criterion used to pick the best design is that the maximum working stresses in the component cylinders are equal; this necessitates that all the cylinders have the same diameter ratio. The number and size of the components required for any given pressure and temperature difference may be determined with the aid of formulae and graphs presented.

Vol. 1
1960

1. INTRODUCTION

IT HAS in recent years become increasingly desirable to design pressure vessels capable of withstanding both pressure and thermal stresses. The general theory for monoblock vessels is contained in Part I[1] of this series, in Part II[2] the theory is applied to the steady-state temperature distribution, and in Part III[3] it is applied to transient thermal stresses. The present paper describes the design of multilayer cylindrical pressure vessels to withstand a given pressure and a given steady-state temperature difference across the walls.

The design of multilayer pressure vessels that are at uniform temperature has been discussed by Manning[4, 5] who used the criterion that the maximum value under load of the maximum shear stress within each layer is the same for all layers. He showed that the diameter ratio should be the same for each component cylinder, and that the required interference per unit radius is constant for a given vessel. Manning's theory is extended in this paper to include thermal as well as pressure stresses. Because thermal and pressure stresses may add or subtract at any point within the vessel the theory is somewhat more complex than if only pressure stresses are present. The more important combinations of pressure and thermal stress are considered in detail.

In a multilayer vessel residual stresses are intentionally formed, usually by shrinkage, in order to increase the elastic range of the vessel under the required load. Consequently, plastic flow does not usually occur, and we will be concerned with only elastic deformations.

2. THEORY

(i) *The diameter ratios*

We consider a multilayer cylinder made of m component cylinders of identical material and numbered $1, 2, \ldots, m$. The properties of any cylinder n are denoted by the subscript n, the subscript is omitted from symbols for

* N.R.C. No. 5587.

properties of the complete vessel, a and b are the inner and outer radii, $K = b/a$ is the radius ratio of the complete vessel, $k_n = b_n/a_n$ is that of component cylinder n, T is the temperature at radius r, subscripts i and o denote the inner and outer faces of the vessel, and subscripts in and on denote the inner and outer faces of component n.

The steady-state temperature distribution is (equation II, 3.4)*

$$T = T_i - \Delta T \ln (r/a)/\ln k, \tag{2.1}$$

where T is the temperature at radius r,

$$\Delta T = T_i - T_o, \tag{2.2}$$

and T_i and T_o are the temperatures at the inner and outer surfaces of the complete vessel. The temperature T at radius r within the nth component is related to the temperature at the inside T_{in} and outside T_{on} of that component, thus

$$T = T_{in} - (T_{in} - T_{on}) \ln (r/a_n)/\ln k_n. \tag{2.3}$$

We also have

$$T_{in} = T_{in-1} - (T_{in-1} - T_{on}) \ln k_{n-1}/\ln k_n. \tag{2.4}$$

In order to calculate the maximum shear stress τ_n at radius r within the nth component we insert the values of the tangential and radial principal stresses, σ_t and σ_r respectively obtained from equations (II, 3.6)† and (II, 3.7), into the equation for the maximum shear stress τ,

$$\tau = \tfrac{1}{2} |\sigma_t - \sigma_r|, \tag{2.5}$$

and obtain

$$\tau_n = \left| \frac{p_{in} - p_{on}}{k_n^2 - 1} \frac{b_n^2}{r^2} - \frac{\alpha E (T_{in} - T_{on})}{2(1-\nu)} \left(\frac{b_n^2/r^2}{k_n^2 - 1} - \frac{1}{2 \ln k_n} \right) \right|, \tag{2.6}$$

where p_{in} and p_{on} are the contact pressures at the inner and outer faces respectively of the nth cylinder, α is the thermal expansion coefficient, E is Young's modulus and ν is Poisson's ratio. The maximum shear stress may be a maximum within component n at either the inner wall or the outer wall; it cannot be a maximum between the walls because, from equation (2.6), $\partial \tau_n / \partial r$ cannot be zero since it varies as r^{-3}. We consider the maximum stress at each wall in turn, taking first the condition that the maximum stress is at the inner wall, and we assume that if this is so for one

* Equation (II, 3.4) denotes equation (3.4) of Part II.

† Equation (II, 3.6) should read

$$\sigma_t = \frac{-p_i}{k^2-1} \left(\frac{b^2}{r^2} - 1 \right) - \frac{p_i k^2}{k^2-1} \left(1 - \frac{a^2}{r^2} \right) - \tfrac{1}{2} \beta \left(\frac{k^2}{k^2-1} \left(1 - \frac{a^2}{r^2} \right) - \frac{\ln r/a}{\ln k} \right);$$

equation (II, 2.3) should read

$$Q = 4\pi\lambda\Delta T(k-1);$$

equation (II, 2.5) should read

$$T = T_i \pm \frac{k\Delta T}{k-1} \left(1 - \frac{a}{r} \right);$$

equation (II, 3.3) should read

$$Q = 2\pi\lambda\Delta T/\ln k;$$

equation (II, 2.4) should read

$$T = T_i - T_0$$

and a negative sign should precede the term that includes β in equations (II, 2.9) and (II, 2.10).

component then it will be so for all components. The maximum shear stress at the inner surface of the nth cylinder is obtained by substituting $r = a_n$ in equation (2.6). We find

$$\tau_{in} = \left| \frac{(p_{in} - p_{on})\, k_n^2}{k_n^2 - 1} - \frac{\alpha E (T_{in} - T_{on})}{2(1-\nu)} \left(\frac{k_n^2}{k_n^2 - 1} - \frac{1}{2 \ln k_n} \right) \right|. \tag{2.7}$$

The criterion we now introduce[4] is that the value of τ_{in} is the same in each layer. The condition $\tau_{in-1} = \tau_{in}$ gives for p_{in}, using equations (2.7) and the corresponding equation for the $(n-1)$th layer and writing

$$k_n\, k_{n-1} = X, \tag{2.8}$$

$$(2X^2 - k_{n-1}^2 - k_n^2)\, p_{in} = p_{in-1}(k_n^2 - 1)\, k_{n-1}^2 + p_{on}(k_{n-1}^2 - 1)\, k_n^2 + \frac{\alpha E}{2(1-\nu)} \frac{(T_{in-1} - T_{on})}{\ln X} \{k_n^2 (k_{n-1}^2 - 1) \ln k_n - k_{n-1}^2 (k_n^2 - 1) \ln k_{n-1}\}. \tag{2.9}$$

On eliminating p_{in} between equations (2.7) and (2.9), we obtain

$$\tau_{in} = \left| \frac{X^2}{2X^2 - k_{n-1}^2 - k_n^2} \left\{ (p_{in-1} - p_{on}) - \frac{\alpha E}{2(1-\nu)} (T_{in-1} - T_{on}) \right\} + \frac{\alpha E}{1-\nu} \frac{(T_{in-1} - T_{on})}{4 \ln X} \right|. \tag{2.10}$$

We seek the value of a_n that will minimize τ_{in}. This is obtained by putting $\partial \tau_{in} / \partial a_n = 0$ while holding constant the pressures, temperatures and radii of all interfaces other than that at $r = a_n$. We have, therefore,

$$\frac{\partial \tau_{in}}{\partial k_{n-1}} = a_{n-1} \frac{\partial \tau_{in}}{\partial a_n} = 0. \tag{2.11}$$

This occurs when $(2X^2 - k_{n-1}^2 - k_n^2)$ is a maximum, i.e. when

$$k_n = k_{n-1}. \tag{2.12}$$

This result holds for all n, so, for the minimum value of the maximum shear stress under load, all component cylinders have the same radius ratio, and we may write

$$k_n = k$$

for all components. By inserting this condition into equation (2.9) we find

$$p_{in} = \tfrac{1}{2}(p_{in-1} + p_{on}), \tag{2.13}$$

and by inserting it into equation (2.4), we find

$$T_{in} = \tfrac{1}{2}(T_{in-1} + T_{on}). \tag{2.14}$$

That is, both the temperatures and the contact pressures of the interfaces under full load are in arithmetic progression. Therefore,

$$T_{in} - T_{on} = \Delta T / m, \tag{2.15}$$

$$p_{in} - p_{on} = \Delta p / m, \tag{2.16}$$

where
$$\Delta p = p_i - p_o. \tag{2.17}$$

Also,
$$k = K^{1/m}. \tag{2.18}$$

Vol. 1
1960

These conditions, except for (2.15), are those obtained by Manning for an isothermal vessel, and it is pleasing to find that the presence of steady-state thermal stresses does not alter the simple requirement of geometrical similarity of the components.

Inserting equations (2.15) and (2.16) into (2.6), we obtain

$$\tau_n = \left| \Delta p \frac{b_n^2/r^2}{m(k^2-1)} - \tfrac{1}{2}\beta\left\{\frac{b_n^2/r^2}{m(k^2-1)} - \frac{1}{2m\ln k}\right\}\right|, \tag{2.19}$$

where $$\beta = \alpha E \Delta T/(1-\nu).$$

The maximum value of τ_n is obtained by putting $r = a_n$, and we find

$$\max \tau_{in} = \left| \Delta p \frac{k^2}{m(k^2-1)} - \tfrac{1}{2}\beta\left\{\frac{k^2}{m(k^2-1)} - \frac{1}{2m\ln k}\right\}\right|. \tag{2.20}$$

It was pointed out above that the maximum value of the maximum shear stress within a cylinder may occur at the outer surface of the cylinder. From equation (2.19) we find that τ_n is a maximum at the inner surface except when Δp and β have the same sign and

$$\tfrac{1}{2}|\beta| > |\Delta p| > \tfrac{1}{2}|\beta|\left\{1 - \frac{(k^2-1)}{(k^2+1)\ln k}\right\}, \tag{2.21}$$

in which case τ_n is a maximum at the outer surface. When this occurs, by following a similar procedure to that for τ_n a maximum at the inner surface, i.e. by equating the values τ_n at the outer surfaces of each component and minimizing as we did above, we find conditions identical to those above, equations (2.13–19). The maximum value of τ_n is obtained by putting $r = b_n$ in equation (2.19). We find

$$\tau_{on} = \left| \Delta p \frac{1}{m(k^2-1)} - \tfrac{1}{2}\beta\left\{\frac{1}{m(k^2-1)} - \frac{1}{2m\ln k}\right\}\right|. \tag{2.22}$$

(ii) *The interference*

The radial displacement u_n under load at any radius r within the nth cylinder is obtained by substituting the appropriate boundary conditions into the derivation of u.[6] For a steady-state temperature distribution the expression for u_n becomes

$$\begin{aligned}\frac{u_n}{r} = {} & \frac{p_{in}}{E}\frac{(1-\nu)+(1+\nu)b_n^2/r^2}{k^2-1} - \frac{p_{on}}{E}\frac{(1-\nu)k^2+(1+\nu)b_n^2/r^2}{k^2-1} \\ & + \alpha T_{on} + \frac{\alpha(T_{in}-T_{on})}{2(1-\nu)}\left\{\frac{(1-\nu)+(1+\nu)\ln b_n/r}{\ln k} - \frac{(1-3\nu)+(1+\nu)b_n^2/r^2}{k^2-1}\right\} \\ & - \frac{\nu\sigma_{ln}(p)}{E},\end{aligned} \tag{2.23}$$

where $\sigma_{ln}(p)$ is the longitudinal stress in the nth layer caused by the pressure.

The interference δ_{nn+1} between the nth and $(n+1)$th cylinders is given by

$$\delta_{nn+1} = u_{in+1} - u_{on}. \tag{2.24}$$

In order to determine δ_{nn+1} the value of $\sigma_l(p)$ must be specified. If the end load is taken external to the vessel, then

$$\sigma_l(p) = 0 \tag{2.25}$$

for all layers, and when equation (2.23) is substituted into (2.24), then $\sigma_i(p)$ cancels. It should be noted that implicit in equation (2.23) is the assumption that there is no friction between layers; if there is friction, then a longitudinal stress must be applied to each layer, a different stress for each layer, to satisfy the condition that the longitudinal strain is the same for each layer. It does not seem worthwhile to discuss this condition.

By putting equation (2.23) into (2.24) and using (2.25), we find

$$\delta_{nn+1} = 2(\Delta p - \tfrac{1}{2}\beta)/mE. \tag{2.26}$$

When β is put equal to zero the same equation as found by Manning[4] is obtained. It should be noted from equation (2.26) that an interference is required between the components only if $\Delta p > \frac{1}{2}\beta$. Otherwise, a clearance must be left between the cylinders. As Manning points out, the interference between consecutive components is based on their dimensions before, and not during, the assembly. Southwell[7] discusses the problem of calculating the interference required for assembly after the cylinder has been partly assembled.

Vol. 1
1960

(iii) *The residual stresses*

In the preceding sections we have shown that the radius ratio of all components should be the same, in order to ensure that the maximum working shear stresses in each layer are as small as possible; we have calculated these stresses, and we have calculated the interference required between each layer in order to realize these stresses. It is important that the residual stresses left when the pressure and the temperature gradient are removed, and the stresses when either pressure or temperature stresses are applied alone, are not higher than the maximum allowable stress. The problem of calculating these stresses is considered in this section.

The residual contact pressure p'_{on} at radius b_n is obtained from the relation

$$p'_{on} = p_{on} + \sigma_{ron}, \tag{2.27}$$

where σ_{ron} is the radial stress at radius b_n in a monoblock vessel of the same size as the compound cylinder and under the same conditions of temperature and pressure. It is calculated from equation (II, 3.6). Since the contact pressures under full load are in an arithmetic progression, then

$$p_{on} = p_i - n\Delta p/m. \tag{2.28}$$

Substituting σ_{ron} and equation (2.28) into (2.27), we find

$$p'_{on} = (\Delta p - \tfrac{1}{2}\beta)\left(\frac{K^2 - K^{2(1-n/m)}}{K^2 - 1} - \frac{n}{m}\right). \tag{2.29}$$

In order to obtain the residual maximum shear stress τ_{Rn} within the nth cylinder the residual contact pressures from equation (2.29) are substituted into equation (2.6) and T_{in} is put equal to T_{on}. There results

$$\tau_{Rn} = \left|\frac{b_n^2}{r^2}(\Delta p - \tfrac{1}{2}\beta)\left\{\frac{1}{m(k^2-1)} - \frac{K^{2(1-n/m)}}{K^2-1}\right\}\right|. \tag{2.30}$$

It may happen that the stress produced when temperature or pressure acts alone is greater than the stress when both are present; consequently, we calculate these stresses. The shear stresses that act within the nth cylinder when temperature or pressure alone is applied are denoted by τ_{Tn} and τ_{pn} respectively. They are obtained by superposing upon the residual stress the stress that would result within the entire vessel if it were a monoblock cylinder and if only the temperature or pressure difference were acting upon it. We find

$$\tau_{Tn} = \left| \Delta p \left(\frac{b_n^2/r^2}{m(k^2-1)} - \frac{K^2}{K^2-1} \frac{b_n^2/r^2}{k^{2n}} \right) - \tfrac{1}{2}\beta \left(\frac{b_n^2/r^2}{m(k^2-1)} - \frac{K^2}{K^2-1} \left(\frac{b_n^2/r^2}{k^{2n}} - \frac{b^2/r^2}{K^2} \right) - \frac{1}{2\ln K} \right) \right|, \tag{2.31}$$

$$\tau_{pn} = \left| \Delta p \left(\frac{b_n^2/r^2}{m(k^2-1)} - \frac{K^2}{K^2-1} \left(\frac{b_n^2/r^2}{k^{2n}} - \frac{b^2/r^2}{K^2} \right) \right) - \tfrac{1}{2}\beta \left(\frac{b_n^2/r^2}{m(k^2-1)} - \frac{K^2}{K^2-1} \frac{b_n^2/r^2}{k^{2n}} \right) \right|. \tag{2.32}$$

3. DESIGN OF VESSEL

There are two main points upon which the design of a vessel is based. The first is that the maximum shear stress must always be less than the yield stress. The second is that, in order to obtain the most efficient use of material, the maximum tensile and compressive stresses that are obtained during the normal use of the vessel should be equal or nearly equal. The maximum shear stress is said to be a tensile stress when $\sigma_t > \sigma_r$, and a compressive stress when $\sigma_t < \sigma_r$. The stresses considered are those under full load, under pressure alone, under thermal gradients alone and under no load. They are given by equations (2.19), (2.32), (2.31) and (2.30) respectively. Since the relative values of the stresses depend greatly upon the values of Δp and β, this section is subdivided as follows:

(i) Interference is required between the component cylinders; i.e. from equation (2.26),

$$\Delta p > \tfrac{1}{2}\beta.$$

The following subdivisions are considered separately,

(a) $\beta < 0 < \Delta p$,

(b) $0 < \tfrac{1}{2}\beta < \Delta p$,

(c) $\tfrac{1}{2}\beta < \Delta p < 0$.

(ii) Clearance is required between the component cylinders; i.e. from equation (2.26),

$$\Delta p < \tfrac{1}{2}\beta.$$

(i) $\Delta p > \tfrac{1}{2}\beta$

Interference is required between the components. Under this condition, equation (2.30) shows that the residual maximum shear stress has its maximum value at the inner surface of the inner cylinder, where it is compressive. Its value, τ_{Ri1}, is

$$\tau_{Ri1} = (\Delta p - \tfrac{1}{2}\beta) \left(\frac{K^2}{K^2-1} - \frac{k^2}{m(k^2-1)} \right). \tag{3.1}$$

(a) $\beta < 0 < \Delta p$. For this condition it is seen from equation (2.19) that the maximum working maximum shear stress is at the inner surface of each cylinder and is

$$\tau_{in} = \Delta p \frac{k^2}{m(k^2-1)} - \tfrac{1}{2}\beta\left\{\frac{k^2}{m(k^2-1)} - \frac{1}{2m\ln k}\right\}. \tag{3.2}$$

This is a tensile stress and it is the maximum tensile stress that the cylinder experiences. The maximum compressive stress that is obtained is at the inner surface of the inner component under no load. It is given in equation (3.1).

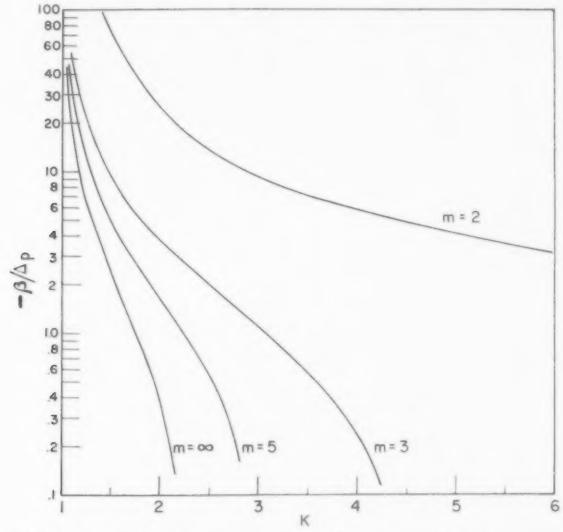

FIG. 1. $-\beta/\Delta p$ vs. k for various values of m according to equation (3.5).

The condition

$$\tau_{in} = \tau_y = \tfrac{1}{2}\sigma_y \tag{3.3}$$

where τ_y is the yield stress in shear and σ_y is the yield stress in tension, gives

$$\frac{2\Delta p_y}{m\sigma_y} = \frac{k^2-1}{k^2} + \frac{\beta_y}{m\sigma_y}\left\{1 - \frac{k^2-1}{2k^2\ln k}\right\}, \tag{3.4}$$

where Δp_y and β_y are values of Δp and β that together just cause yielding. Equation (3.4) is plotted against k in Fig. 4 of Part II if the ordinate is replaced by $2\Delta p_y/m\sigma_y$ and the curve parameter by $\beta/m\sigma_y$. The relation $\tau_{in} = \tau_{Rti}$ gives the equation

$$-\frac{\beta}{\Delta p} = 2\left\{\frac{2k^2/m(k^2-1) - K^2/(K^2-1)}{K^2/(K^2-1) - 2k^2/m(k^2-1) + 1/2\ln K}\right\}. \tag{3.5}$$

This is plotted in Fig. 1.

When designing a vessel for given conditions of temperature and pressure the first step will usually be to decide the radius ratio of the complete vessel because, to a first approximation, the ultimate pressure of a multilayer vessel does not depend upon the number of layers, but only on the radius ratio K.[4] The value of K can be chosen by any of a number of empirical, semi-empirical or theoretical, methods, so that the vessel will operate at a given fraction of

Vol. 1
1960

its calculated ultimate pressure. Having chosen K, it is necessary to choose the number of layers. The minimum value of m that will ensure that the residual stress is equal to or less than the working stress is obtained from Fig. 1. For example, if $-\beta/\Delta p$ is 2 and K is 3, then the minimum value of m is 3, i.e. that corresponding to the neighbouring curve with higher m. Having chosen m, it is then necessary to determine whether the working stresses are greater than the yield stresses. This is most easily done by using equation (3.4) in graphical form, using Fig. 4 of Part II with the ordinate and the curve parameter changed as described above.

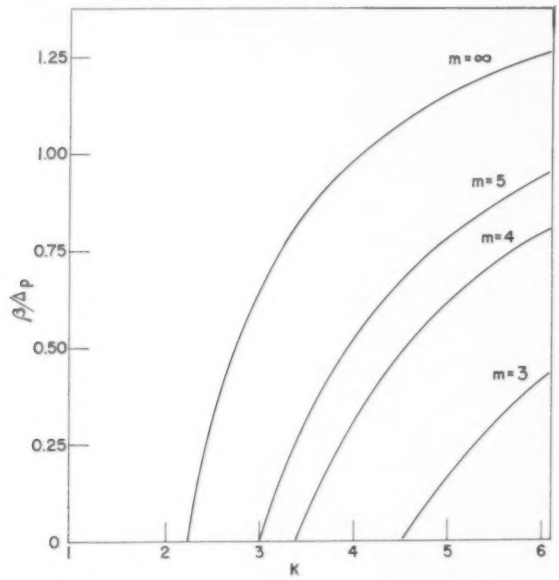

FIG. 2. $\beta/\Delta p$ vs. k for various values of m according to equation (3.6).

(b) $0 < \frac{1}{2}\beta < \Delta p$. From equations (2.31), (2.32), (3.1) and (3.2) it is readily shown that the maximum tensile stress is that at the inner face of the inner component when pressure alone is acting, and the maximum compressive stress is that at the inner face of the inner component when temperature alone is acting. Equating these stresses, we obtain

$$\frac{\beta}{\Delta p} = -2\left\{\frac{2k^2/m(k^2-1) - K^2/(K^2-1)}{K^2/(K^2-1) - 2k^2/m(k^2-1) + 1/2\ln K}\right\}. \tag{3.6}$$

This is plotted in Fig. 2. Equation (3.6) is identical with (3.5); it is used in different ranges for the different conditions. K having been chosen, Fig. 2 is used in a similar manner to Fig. 1 to choose the value of m that will make the stresses with pressure alone and with temperature alone most nearly equal. Instead of choosing the value of m to be that appropriate to the higher neighbouring curve, it will frequently be best to choose that appropriate to the nearest curve because then the maximum stresses are most nearly equal. It is then necessary to ensure that the yield stress is not exceeded when

pressure alone and temperature alone is applied. The maximum stresses are calculated from equations (2.31) and (2.32) by putting $n = 1$, $r = a$.

(c) $\frac{1}{2}\beta < \Delta p < 0$. For these conditions the maximum shear stress in tension is easily shown to be that at the inner face of the inner component under temperature alone, and the maximum shear stress in compression is that at the inner face of the inner component under pressure alone. By equating these stresses we obtain again equation (3.6). Fig. 2 can be used as in sub-section (b) to choose the best value of m. Again it is necessary to ensure that the yield stresses are not exceeded, and equations (2.31) and (2.32) can be used for this as in sub-section (b) above by putting $n = 1$, $r = a$.

(ii) $\Delta p - \frac{1}{2}\beta < 0$

Clearance is required between the cylinders. There are no residual stresses because the component cylinders are not in contact. Consequently, only the working stresses need be considered. It is interesting to note that since there are no residual stresses they set no limit to the pressure that can be withstood. Consequently, a vessel can be designed to withstand any desired, frequently applied, external pressure without limit by making a multilayer vessel of an appropriate value of K and number of layers. This is in marked contrast to internal-pressure vessels for which, because there are necessary residual stresses, there is a definite limit to the pressure that can be applied frequently, and this is set by the yield strength of the material.[5]

Vol. 1
1960

It was shown in Section 2 that if β and Δp have the same sign and if

$$\tfrac{1}{2}|\beta| > |\Delta p| > \tfrac{1}{2}|\beta|\{1 - (k^2-1)/(k^2+1)\ln k\}, \tag{3.7}$$

then the maximum working stress occurs at the outer surface of each component. By setting this stress equal to the yield stress, we obtain for the conditions under which yielding just occurs,

$$\frac{\Delta p_y}{\sigma_y} + \frac{\beta_y}{2\sigma_y}\left\{\frac{k^2-1}{2\ln k} - 1\right\} = m(k^2-1). \tag{3.8}$$

If equation (3.7) does not hold, then the maximum stress is at the inner surface and is tensile. By putting it equal to the yield stress, we find

$$\frac{\Delta p_y}{\sigma_y} + \frac{\beta_y}{2\sigma_y}\left\{\frac{k^2-1}{2k^2\ln k} - 1\right\} = m\frac{k^2-1}{k^2}. \tag{3.9}$$

It is, of course, necessary that the vessel withstand both temperature gradients alone and pressure difference alone. For pressure alone the appropriate equations are obtained from equations (3.8) or (3.9) by putting $\beta = 0$, and for temperature alone, if the component cylinders are brought into contact, by putting $\Delta p = 0$. If the component cylinders are not brought into contact by temperature gradients alone, then the major temperature differences in the absence of pressure will usually occur in the gaps between the cylinders if the cylinders remain concentric, and so the thermal stresses in the material will be low. If the cylinders are not concentric and touch one another, then the thermal stresses formed are not readily calculated.

The methods of design considered above have been concerned only with minimizing the maximum stresses experienced by the vessel; in practice, other criteria will also be considered when designing a vessel. The cost of making the vessel will be important, and, because the cost will usually increase as the number of layers is increased, it will frequently be better to use a less efficient design, i.e. fewer layers, and perhaps a greater total thickness to save the cost of manufacture. The effect of inaccuracies in machining[4] must also be borne in mind. A vessel can be designed for optimum strength only for given pressure and temperature. If a vessel is to be used over a range of pressures and temperatures, then a design must be chosen that will be a suitable compromise.

REFERENCES

1. E. WHALLEY, *Canad. J. Tech.* **34**, 268 (1956).
2. E. WHALLEY, *Canad. J. Tech.* **34**, 291 (1956).
3. E. WHALLEY and R. MACKINNON, *Int. J. Mech. Sci.* **1**, 301 (1960).
4. W. R. D. MANNING, *Engineering, Lond.* **163**, 349 (1947).
5. W. R. D. MANNING, *Engineering, Lond.* **170**, 464 (1950).
6. S. TIMOSHENKO, *Strength of Materials* p. 230. Van Nostrand, Princeton (1956).
7. R. V. SOUTHWELL, *The Theory of Elasticity* p. 413. Oxford University Press (1941).

Int. J. Mech. Sci. Pergamon Press Ltd. 1960. Vol. 1, pp. 379–395. Printed in Great Britain

Vol. 1
1960

REVIEW

THE DESIGN OF PRESSURE VESSELS SUBJECTED TO THERMAL STRESS*

E. WHALLEY
Division of Applied Chemistry, National Research Council, Ottawa, Canada

(*Received* 6 *November* 1959)

1. INTRODUCTION

THE design of high-pressure vessels is usually based on either the yield pressure, i.e. the smallest pressure required to cause elastic failure, the ultimate pressure, i.e. the pressure at which the wall becomes unstable and expands without limit until it ruptures, or the shakedown pressure, i.e. the pressure that will just not cause cyclic plastic flow when it is applied and removed. It has been known for many years that the presence of thermal gradients causes thermal stresses, and that these may reach very high values, which may easily exceed the pressure stresses. Both the ASME Boiler and Unfired Pressure Vessel Code 1952 and the British Standard Code 1500 : 1949 for Fusion-Welded Pressure Vessels acknowledge that thermal stresses should be taken account of, but neither discusses how to do this.

The amount of work, both industrial and laboratory, that makes use of high pressures is rapidly increasing, and frequently both high pressures and high thermal gradients are used simultaneously. It is becoming increasingly desirable, therefore, to apply rational design to vessels for these conditions. The purpose of this paper is to review present knowledge of this field.

Much work has been done on thermal stresses in elastic solids, and in recent years a few authors have discussed the thermal stresses in elastic–plastic solids. We are concerned in this review with combined pressure and thermal stresses in either wholly elastic or elastic–plastic vessels; work that is not directly relevant to the design of pressure vessels is excluded from the survey. There is, unfortunately, no experimental work in this subject, and so we must rely entirely on theory for guidance. Theory deals with highly idealized solids, to which real solids may or may not approximate accurately. This must be remembered when a pressure vessel is being designed, and allowances made for the approximate theory.

2. GENERAL THEORY

2.1. *Properties of material*

The following assumptions are usually made.

(i) All materials are homogeneous and isotropic.

* N.R.C. No. 5615.

(ii) A brittle material is perfectly elastic up to the ultimate strength. It then fractures, without appreciable yielding, when the maximum principal stress equals the ultimate tensile strength.

This appears to be a fairly good approximation to the behaviour of a brittle material[1] and agrees quite well with the measurements of Cook and Robertson[2] and Popplewell[3] on cast-iron cylinders subjected to internal pressure.

(iii) A ductile material is perfectly elastic up to the yield point, and is then ductile above it. Plastic flow occurs when the maximum shear stress reaches a particular value, i.e. according to Tresca's criterion. Strain-hardening may or may not occur.

No real material is perfectly elastic up to its yield point, but most metals are nearly elastic. The von Mises yield criterion is more often used than the Tresca criterion. For the von Mises and Tresca theories, the maximum difference between the predicted yield stresses under multiaxial stress relative to that under simple tensile stress is about 15 per cent, and is for the relation between the shear and tensile yield stresses. It is not surprising, therefore, that a clear-cut distinction between them is difficult to obtain. Cook[4] and Steele and Young[5] found the Tresca theory adequate for cylindrical mild-steel vessels subjected to internal pressure, though Morrison[6] favoured the von Mises theory for low-alloy steels; however, none of the measurements distinguishes compellingly between the two theories. For a cylindrical vessel subjected to internal or external pressure, the stress system is easily shown to be a superposed hydrostatic pressure and simple torsion, and for this system the von Mises theory reduces to a particularly simple form. The stress system is more complicated when thermal stresses are present; the longitudinal stress is no longer the mean of the radial and tangential stresses and it must be calculated if von Mises's theory is to be used. This presents problems in the theory of plastic–elastic vessels that are not easily solved accurately; they are avoided if Tresca's theory is used because so long as the longitudinal stress is the intermediate principal stress (as it always is if only pressure stresses are present) it need not be known. For these reasons most of the theory so far developed has used Tresca's theory.

(iv) The temperature is everywhere low enough that creep is inappreciable.

(v) The effect of temperature and stress on the elastic moduli, the yield point, and the coefficient of thermal expansion is inappreciable.

(vi) Thermal and pressure stresses are applied slowly enough that stress waves are unimportant.

(vii) The displacements are everywhere small compared with the dimensions of the vessel.

This will be true in vessels with a radius ratio of less than about six in which the plastic deformation is contained, i.e. which is still partly plastic.

(viii) The Bauschinger effect (reduction of yield point due to previous plastic flow in the reverse direction) does not occur in a pressure vessel.

There is some experimental evidence[7, 8] that the Bauschinger effect is not as important in pressure vessels as in tensile bars.

(ix) There are no important stress-raisers present.

(x) Fatigue due to stressing below the elastic limit is unimportant.

It is unlikely that a vessel subjected to static pressure and thermal stresses will fail by this kind of fatigue but it may be important in, for example, pumps, in which the temperature of the fluid may change according to approximately adiabatic laws during the pumping.

In addition to the foregoing assumptions, other assumptions are required in order to discuss a vessel made of a strain-hardening material. The only work so far reported that is relevant to our subject is that of Bland[9]; the assumptions used are given in Sections 4.1 (iv) and 4.1 (v).

2.2 *Criteria of failure of vessel*

As well as having a theory of the material, it is necessary to have a criterion of failure of the vessel. Conditions that are judged to cause failure of a vessel will depend upon the material of the vessel, upon what it is to be used for, and to some extent upon the judgement of the designer. The three most important criteria that have been used for the design of pressure vessels are the following, together with appropriate safety factors:

Vol. 1
1960

(i) initial yield;

(ii) shakedown, i.e. the condition such that if the load is cycled in a prescribed manner it just does not cause repeated plastic deformation;

(iii) bursting.

For brittle materials criterion (i) using the maximum-principal-stress theory is probably the most useful because when elastic failure occurs the material cracks. For brittle materials, therefore, criteria (i) and (iii) are identical. The safety factor should usually be rather high and as high as 5 or 6 if possible. Care must be taken with glass vessels, which are probably best designed by this criterion: glass is rather treacherous, and the failure pressure depends greatly on the length of time the load is applied for, the pressure-transmitting fluid and many other factors. A glass vessel may fail at a pressure much lower than it has previously withstood.

The criterion to be used for ductile materials depends partly upon how the vessel is to be used. A small amount of plastic flow when pressure is first applied will be intolerable only when the original dimensions of the vessel must be maintained; then criterion (i) using either the Tresca or the von Mises theory should be used with an appropriate safety factor. At the same time the working pressure must be less than the ultimate pressure by the appropriate safety factor. If the vessel is to be used only a very few times there is no need to take account of the fatigue caused by successive plastic deformations on loading and unloading, so only the ultimate pressure need be considered; we shall see that in this case thermal stresses will have no effect on design. It should, however, be remembered that no material is perfectly ductile; plastic flow requires time to occur, and if a load is suddenly applied, as when a vessel is plunged into a hot or cold bath, the stresses may rise high enough to cause brittle fracture before they are readjusted by plastic flow. If the vessel is to be loaded many times, the maximum allowable load should be based on the required factor of safety for either bursting or shakedown, whichever gives the smaller load. A vessel

loaded thermally and with internal and external pressure will usually be required to withstand any two of these acting together, or any one of them alone. The strengthening effect obtained when the thermal and pressure stresses tend to cancel one another at the point of maximum stress should therefore not usually be taken into account. When pressure and thermal stresses are necessarily applied simultaneously, for example in guns, the strengthening effect may be useful.

2.3 *General equations*

There are several equations that must be obeyed by the vessel in any state of stress; we consider these now. We consider a symmetrical spherical or cylindrical hollow vessel with inside radius a and outside radius b. The pressures p_i and p_o act uniformly on the inside and outside surfaces respectively. The temperature of the walls is spherically or cylindrically symmetrical, and at any radius r within the wall it is T. The temperature of the inside surface is T_i and of the outside surface T_o. Also

$$\Delta p = p_i - p_o, \quad \Delta T = T_i - T_o \tag{2.1}$$

The principal stresses are a radial stress σ_r, a tangential stress σ_t and, in a spherical vessel, a second equal tangential stress σ_t or, in a cylindrical vessel, a longitudinal stress σ_l. Corresponding to each principal stress is a principal strain ϵ_r, ϵ_t and ϵ_l. The equation of equilibrium of the stress must always hold; by symmetry[10] for a spherical vessel

$$r d\sigma_r/dr = 2(\sigma_t - \sigma_r) \tag{2.2}$$

and for a cylindrical vessel

$$r d\sigma_r/dr = \sigma_t - \sigma_r \tag{2.3}$$

For small strains the strains ϵ_r and ϵ_t are everywhere related to the radial displacement u as follows:

$$\epsilon_r = du/dr, \quad \epsilon_t = u/r \tag{2.4}$$

for both spherical and cylindrical vessels. Since the total external axial force on a cylindrical vessel is usually zero the condition

$$2\pi \int_a^b \sigma_l r \, dr = \text{force exerted by the pressure on the ends} \tag{2.5}$$

must usually be obeyed.

In the elastic parts of a vessel Hooke's law is obeyed, i.e. for a cylindrical vessel

$$\epsilon_r - \alpha T = [\sigma_r - \nu(\sigma_t + \sigma_l)]/E \tag{2.6}$$

$$\epsilon_t - \alpha T = [\sigma_t - \nu(\sigma_r + \sigma_l)]/E \tag{2.7}$$

$$\epsilon_l - \alpha T = [\sigma_l - \nu(\sigma_r + \sigma_t)]/E \tag{2.8}$$

where α is the coefficient of thermal expansion, ν is Poisson's ratio, and E is Young's modulus. For a spherical vessel, equations (2.6)–(2.8) hold if σ_t is replaced by σ_l, when of course (2.7) and (2.8) become identical. These equations together with the general equations of the last paragraph and the boundary conditions that are described below are enough to define the stresses and strains in elastic regions of a vessel.

The onset of plasticity when the material is ductile is determined by the Tresca equation

$$\sigma_3 - \sigma_1 = \sigma_y \tag{2.9}$$

where σ_3 and σ_1 are the greatest and least principal stresses respectively and σ_y is the yield stress in tension. If we assume that the longitudinal stress in a cylindrical vessel is always the intermediate stress then for both spherical and cylindrical vessels, yielding just begins when

$$\sigma_t - \sigma_r = \pm \sigma_y \tag{2.10}$$

For a non-strain-hardening material σ_y is independent of the strain; for a strain-hardening material it depends upon the plastic strain.

A brittle material fractures when the maximum principal stress reaches a limiting value σ_u.

The various boundary conditions that must be applied to the foregoing equations are as follows:

(i) at $r = a$ $\quad \sigma_r = -p_i$ (2.11)

(ii) at $r = b$ $\quad \sigma_r = -p_o$ (2.12)

(iii) at an elastic–plastic boundary equation (2.10) holds, (2.13)

(iv) the radial stress and radial displacement are continuous across an elastic–plastic boundary. (2.14)

We have now assembled the tools for calculating the stresses. It is necessary only to choose the appropriate equations and boundary conditions for any given system and to solve them. It should be noted that all the foregoing equations are exact within the limits of the assumptions described in Section 2 above if the dimensions a, b and r, are those of the strained vessel. If the strains are small, little error is introduced by using the original values of a, b and r; otherwise, the strains in the plastic region must be calculated.

3. SPHERICAL VESSELS

3.1 *General temperature distribution*

(i) *Completely elastic vessels.* In a spherical vessel that is completely elastic it follows from equations (2.2) to (2.7) and boundary conditions (2.11) and (2.12) that[10, 11]

$$\sigma_r = -\frac{p_i}{k^3-1}\left(\frac{b^3}{r^3}-1\right) - \frac{p_o k^3}{k^3-1}\left(1-\frac{a^3}{r^3}\right) + \frac{2\alpha E}{1-\nu}\left\{\frac{1-a^3/r^3}{b^3-a^3}\int_a^b Tr^2\,dr - \frac{1}{r^3}\int_a^r Tr^2\,dr\right\} \tag{3.1}$$

$$\sigma_t = \frac{p_i}{k^3-1}\left(\frac{b^3}{2r^3}+1\right) - \frac{p_o k^3}{k^3-1}\left(1+\frac{a^3}{2r^3}\right) + \frac{2\alpha E}{1-\nu}\left\{\frac{1+a^3/2r^3}{b^3-a^3}\int_a^b Tr^2\,dr + \frac{1}{2r^3}\int_a^r Tr^2\,dr - \frac{1}{T}\right\} \tag{3.2}$$

where $k\,(=b/a)$ is the radius ratio. The stress system is of the form $(\sigma_r, \sigma_t, \sigma_t)$; consequently, it is equivalent to a hydrostatic stress (σ_t) with a superposed uniaxial stress $(\sigma_r - \sigma_t, 0, 0)$. The uniaxial stress is, from equations (3.1) and (3.2),

$$\sigma_r - \sigma_t = -\tfrac{3}{2}\Delta p \frac{b^3/r^3}{k^3-1} - \frac{3\alpha E}{1-\nu}\left\{\frac{a^3/r^3}{b^3-a^3}\int_a^b Tr^2\,dr + \frac{1}{r^3}\int_a^r Tr^2\,dr - \tfrac{1}{3}T\right\} \tag{3.3}$$

(ii) *Failure of brittle vessels.* The maximum principal stress is usually the tangential stress, and failure occurs when this first reaches the fracture stress σ_u. By putting the right-hand side of equation (3.2) equal to σ_u, it is seen that both the pressure required for fracture to occur and the position of fracture are dependent on the thermal stresses. The thermal stresses may be such as to oppose the pressure stresses and to increase the fracture pressure, or they may reinforce the pressure stresses and so decrease the fracture pressure. There are of course two values of σ_u, one positive and describing failure in tension, and one negative and describing failure in compression; the two values may be very different. More detailed discussion of an arbitrary temperature distribution is not very profitable.

(iii) *Failure of ductile vessels.* We have seen that the stress system in an elastic vessel is equivalent to superposed hydrostatic and uniaxial stresses. Consequently, all theories of yielding that predict no dependence of the yield stress on the hydrostatic pressure predict the same relation between the yield load and the yield stress in tension. Hence, both Tresca's and von Mises's theories predict that yielding occurs when the modulus of the right-hand side of equation (3.3) equals the yield stress σ_y. In the absence of a temperature gradient the maximum tensile stress $\sigma_r - \sigma_t$ is always at the inside surface and the yield pressure is given by

$$\pm\frac{\Delta p_y}{\sigma_y} = \frac{k^3-1}{\frac{3}{2}k^3} \tag{3.4}$$

The solution with the positive sign corresponds to $p_i > p_o$, and that with the negative sign to $p_i < p_o$. In the presence of temperature gradients, yielding can occur at any position within the walls, depending upon the values of the thermal and pressure stresses. A detailed discussion is given by Whalley[11].

(iv) *Partly plastic non-strain-hardening vessels.* If the stresses in a vessel made of a ductile material are increased beyond the yield point, plastic flow will occur and the stresses will be readjusted. The size of the plastic region will increase as the stresses are increased, and eventually the vessel will burst. There may be one or more plastic regions: for further details see Whalley[11]. However, it is possible to obtain a good deal of information without detailed analysis.

The maximum pressure that the vessel can withstand can be obtained from the following considerations. If the vessel is completely plastic, equations (2.2) and (2.10) hold throughout the vessel wall. When equation (2.2), with (2.10) substituted into it, is integrated with the boundary conditions (2.11) and (2.12), one obtains easily

$$\Delta p_u = \pm 2\sigma_y \ln k \tag{3.5}$$

The pressure Δp_u required to cause the whole wall just to become plastic is thus independent of the presence of any thermal stress. If Δp_u is positive it is the

maximum pressure the vessel will withstand, since subsequent expansion will cause k to decrease and hence Δp_u will decrease. It is, then, the ultimate, but not necessarily the bursting, pressure. If Δp_u is negative the wall will flow inwards and thicken until k is high enough to hold the applied pressure.

The shakedown load will be calculated assuming that the load cycle is from maximum load to zero. After at most a few applications of the loading cycle, no more plastic flow occurs, and the loading and unloading is completely elastic. The stress in the region in which plastic flow has occurred is

$$\sigma_t - \sigma_r = \pm \sigma_y$$

If the unloading is completely elastic the residual stress $(\sigma_t - \sigma_r)_{\text{res}}$ is given by

$$(\sigma_t - \sigma_r)_{\text{res}} = \pm \sigma_y - (\sigma_t - \sigma_r)_{\text{el}}$$

Vol. 1
1960

where $(\sigma_t - \sigma_r)_{\text{el}}$ is the stress caused by the load, calculated assuming the vessel to be elastic. Under shakedown conditions the maximum residual stress is the yield stress so that

$$\max (\sigma_t - \sigma_r)_{\text{el}} = \pm 2\sigma_y \tag{3.6}$$

If the position at which the maximum occurs is the same as that at which yielding began on loading, then the shakedown load is twice the load for initial yield.

If the position at which $|(\sigma_t - \sigma_r)_{\text{el}}|$ is maximum is not that at which yielding began, a more detailed analysis is required; this is given by Whalley[11].

3.2 *Steady-state temperature distribution*

With the temperature distribution in the steady state, when the inside wall is maintained at temperature T_i and the outside wall at temperature T_o, it is easily shown (see Whalley[12] and many other sources) that at any radius r the temperature T is

$$T = T_i - \Delta T \frac{k(1 - a/r)}{k - 1} \tag{3.7}$$

The thermal variable of primary interest may be either the temperature difference between the outside and inside walls, or the rate of heat transfer between the walls. It is convenient to define the variables

$$\beta = \alpha E \Delta T/(1 - \nu) \tag{3.8}$$

$$\gamma = \alpha E Q/[2\pi\lambda(1 - \nu)] \tag{3.9}$$

which are useful when discussing both spherical and cylindrical vessels. Q is the amount of heat conducted through the wall of the vessel divided by the outer radius of the vessel if it is spherical, or by its length if it is cylindrical, and λ is the thermal conductivity. It can be shown[12] that for spherical vessels

$$\beta = \gamma(k - 1) \tag{3.10}$$

and for cylindrical vessels $\beta = \gamma \ln k$

Equations will usually be written in terms of β; they are easily transformed into terms in the heat-transfer variable γ by using equation (3.10). By inserting (3.7) into equations (3.1)–(3.3) we find

$$\sigma_r = -\frac{p_i}{k^3-1}\left(\frac{b^3}{r^3}-1\right)-\frac{p_o k^3}{k^3-1}\left(1-\frac{a^3}{r^3}\right) + \beta\frac{k}{k^3-1}\left\{(k+1)\left(1-\frac{b}{r}\right)-\frac{a}{r}\left(1-\frac{b^2}{r^2}\right)\right\}, \tag{3.11}$$

$$\sigma_t = \frac{p_i}{k^3-1}\left(\frac{b^3}{2r^3}+1\right)-\frac{p_o k^3}{k^3-1}\left(1+\frac{a^3}{2r^3}\right) + \beta\frac{k}{k^3-1}\left\{(k+1)\left(1-\frac{b}{2r}\right)-\frac{a}{2r}\left(1+\frac{b^2}{r^2}\right)\right\}, \tag{3.12}$$

$$\sigma_r-\sigma_t = -\tfrac{3}{2}\Delta p\frac{b^3/r^3}{k^3-1}-\beta\frac{k}{k^3-1}\left\{\frac{b}{2r}(k+1)+\frac{a}{2r}\left(1-3\frac{b^2}{r^2}\right)\right\} \tag{3.13}$$

Even if we restrict ourselves to the steady-state temperature distribution and only internal pressure, a full discussion is complicated (see Derrington and Johnson[13]). However, for most design purposes the following discussion will suffice.

(i) *Failure of brittle vessels.* From equations (3.11) and (3.12) the maximum principal pressure stress is always the bore tangential stress, and the maximum principal thermal stress is also the bore tangential stress. If fracture first occurs at the inside surface it will do so at the internal pressure p_{iu} such that the tangential stress at $r = a$ (equation 3.12) is equal to the fracture stress σ_u, i.e. when

$$\sigma_u = p_{iu}\frac{\frac{1}{2}k^3+1}{k^3-1}-\tfrac{1}{2}\beta\frac{k(2k^2-k-1)}{k^3-1} \tag{3.14}$$

On rearrangement this gives

$$\frac{p_{iu}}{\sigma_u} = \frac{k^3-1}{\frac{1}{2}k^3+1}+\frac{\beta}{\sigma_u}\frac{k(2k^2-k-1)}{k^3+2} \tag{3.15}$$

The first term on the right-hand side of (3.15) gives the ultimate pressure in the absence of a temperature gradient. If β is positive the ultimate pressure is increased by the temperature gradient. It will, however, usually be unwise to use this strengthening in design, and when it occurs the maximum pressure of a vessel should usually be a chosen fraction of the ultimate pressure in the absence of temperature gradients, i.e. of

$$\frac{p_{iu}}{\sigma_u} = \frac{k^3-1}{\frac{1}{2}k^3+1} \tag{3.16}$$

If the thermal stresses weaken the vessel, i.e. if β is negative, the maximum allowable pressure should be based on equation (3.15). The maximum possible value of β is that which will just cause fracture in the absence of internal

pressure. This is obtained by putting $p_{iu} = 0$ in equation (3.15) to give

$$\max \frac{\beta}{\sigma_u} = -\frac{2(k^3-1)}{k(2k^2-k-1)} \tag{3.17}$$

It can easily be shown that if the maximum pressure is given by equation (3.16) and the maximum temperature difference by equation (3.17) the stress at the outside surface can never rise to the ultimate stress, so verifying the assumption that fracture occurs at the bore.

Kern[14] has suggested that high-pressure (100 atm) quartz lamps, in which heat is transferred to the outside, be designed so that the maximum shear stress at the inside wall is zero; this is possible because the stresses oppose one another at this place. Two criticisms can be levelled at this suggestion: (a) quartz is brittle and so the maximum principal stress seems more appropriate, and (b) it is more important to consider the maximum stress than the stress at a pre-chosen place.

(ii) *Failure of ductile vessels.* In the absence of thermal stresses the yield pressure is given by equation (3.4). In the absence of pressure stresses the value of β that causes first yielding is found from equation (3.13) to be

$$\pm \frac{\beta_y}{\sigma_y} = \frac{k^3-1}{k(k^2-\frac{1}{2}k-\frac{1}{2})} \tag{3.18}$$

If a vessel must not yield under the influence of either thermal or pressure stresses alone, then it can be shown[12] that yielding under the combined action of pressure and thermal stresses always occurs at the inside wall at a pressure given by

$$\pm \frac{\Delta p_y}{\sigma_y} = \frac{k^3-1}{\frac{3}{2}k^3} + \frac{\beta}{\sigma_y}\frac{2k^2-k-1}{3k^2} \tag{3.19}$$

If pressure and thermal stresses are necessarily applied together it may not be necessary to specify that the vessel withstand the stresses separately. Then, if the stresses are in the opposite senses, as they are if Δp and ΔT have the same sign, it may be possible for the vessel to withstand higher pressures with the temperature gradient than it would without. There is thus a possibility of "stress-saving", and this has been discussed in some detail by Derrington and Johnson[13]. As was shown in Section 3.1 (iv), the shakedown load for a load cycle from full load to zero load is twice the yield load; we find from equation (3.13) that if shakedown occurs at the inner surface, as it must if Δp is less than $2\Delta p_y$ given by equation (3.4) and β is less than $2\beta_y$ given by equation (3.18) then the shakedown pressure Δp_s is

$$\pm \frac{\Delta p_s}{\sigma_y} = \frac{k^3-1}{\frac{3}{4}k^3} \mp \frac{\beta}{\sigma_y}\frac{2k^2-k-1}{3k^2} \tag{3.20}$$

No calculations of the displacements in the plastic region under the combined action of thermal and pressure stresses appear to have been published.

4. CYLINDRICAL VESSELS

4.1 *General temperature distribution*

(i) *Completely elastic vessels.* In a cylindrical vessel that is completely elastic it follows from equations (2.3) to (2.8) and boundary conditions (2.11) and (2.12) that

$$\sigma_r = -\frac{p_i}{k^2-1}\left(\frac{b^2}{r^2}-1\right)-\frac{p_o k^2}{k^2-1}\left(1-\frac{a^2}{r^2}\right) + \frac{\alpha E}{1-\nu}\left\{\frac{1-a^2/r^2}{b^2-a^2}\int_a^b Tr\,dr-\frac{1}{r^2}\int_a^r Tr\,dr\right\}, \tag{4.1}$$

$$\sigma_t = \frac{p_i}{k^2-1}\left(\frac{b^2}{r^2}+1\right)-\frac{p_o k^2}{k^2-1}\left(1+\frac{a^2}{r^2}\right) + \frac{\alpha E}{1-\nu}\left\{\frac{1+a^2/r^2}{b^2-a^2}\int_a^b Tr\,dr+\frac{1}{r^2}\int_a^r Tr\,dr-T\right\}, \tag{4.2}$$

$$\sigma_l = \frac{p_i-k^2p_o}{k^2-1}+\frac{\alpha E}{1-\nu}\left\{\frac{2}{b^2-a^2}\int_a^b Tr\,dr-T\right\} \tag{4.3}$$

For the pressure stresses alone

$$\sigma_l = \tfrac{1}{2}(\sigma_r+\sigma_t)$$

and so the stress system is equivalent to a superposed hydrostatic stress $\frac{1}{2}(\sigma_t+\sigma_r)$ and a pure shear stress $[\frac{1}{2}(\sigma_t-\sigma_r), -\frac{1}{2}(\sigma_t-\sigma_r), 0]$. This simple stress system no longer holds when thermal and pressure stresses are superposed.

(ii) *Failure of brittle vessels.* It is possible, at least in principle, for either the radial, tangential or longitudinal stress to be the maximum principal stress, so a rigorous investigation of fracture for the general temperature distribution would involve much algebra. Specific temperature distributions are considered later.

(iii) *Failure of ductile vessels.* When no thermal stresses are present the longitudinal stress is always the intermediate stress; this is not necessarily true when thermal stresses are added. However, in order to simplify discussion, it has been assumed[9, 11] that the longitudinal stress is still the intermediate stress. It is likely that under most conditions of practical interest this will be true. Whether it is or not is easily investigated using equations (4.1) to (4.3).

According to the maximum-shear-stress theory, elastic failure will occur when $\sigma_t-\sigma_r = \pm\sigma_y$, i.e. substituting σ_t and σ_r from equations (4.1) and (4.2), when

$$\frac{2\Delta p}{k^2-1}\frac{b^2}{r^2}+\frac{2\alpha E}{1-\nu}\left\{\frac{a^2/r^2}{b^2-a^2}\int_a^b Tr\,dr+\frac{1}{r^2}\int_a^r Tr\,dr-\tfrac{1}{2}T\right\} = \pm\sigma_y \tag{4.4}$$

If only pressure stresses are present the maximum stress difference $(\sigma_t-\sigma_r)$ is at the inside wall, and yielding will begin there at the pressure

$$\frac{\Delta p_y}{\sigma_y} = \pm\frac{k^2-1}{2k^2}$$

If both pressure and thermal stresses are present yielding can begin anywhere in the walls. A detailed discussion is given by Whalley[11].

(iv) *Partly plastic non-strain-hardening vessels.* As with the spherical vessel, it is possible to obtain a good deal of information without analysing the various modes of yielding in detail. When the vessel is completely plastic, equations (2.3) and (2.10) hold, and when the combined equations are integrated with boundary conditions (2.11) and (2.12) we obtain

$$\Delta p_u = \pm \sigma_y \ln k \tag{4.5}$$

where Δp_u has the same significance as in Section 3.1 (iv). The ultimate pressure is thus independent of the thermal gradients. The shakedown load is, as with a spherical vessel, twice the yield load.

The radial and tangential stresses are easily obtained. The general equations for the stresses in the elastic region of the tube are, from Hooke's Law and the equation of equilibrium[10 (p. 409)],

$$\sigma_r = C_1 - \frac{C_2}{r^2} - \frac{\alpha E}{1-\nu}\frac{1}{r^2}\int_a^r Tr\,dr \tag{4.6}$$

$$\sigma_t = C_1 + \frac{C_2}{r^2} + \frac{\alpha E}{1-\nu}\left(\frac{1}{r^2}\int_a^r Tr\,dr - T\right) \tag{4.7}$$

where C_1 and C_2 are constants.

In the plastic region of the tube equations (2.3) and (2.10) hold; when they are combined and the resulting equation integrated we obtain

$$\sigma_r = \pm \sigma_y \ln r + C_3 \tag{4.8}$$

where C_3 is a constant of integration. σ_l is determined from equations (4.8) and (2.10). The boundary conditions that determine C_1, C_2 and C_3, are equations (2.11)–(2.14).

For most purposes of design for a non-strain-hardening material it is not necessary to know σ_l. This is the main advantage of Tresca's criterion over von Mises's: however, if one wishes to calculate displacements then it must be known. In order to calculate σ_l we need the flow rule for the plastic region.[9] Subject to σ_l's being the intermediate stress we have, if plastic flow occurs without change of volume,

$$d\epsilon_l^p = 0 \tag{4.9}$$

$$d\epsilon_r^p + d\epsilon_l^p = 0 \tag{4.10}$$

where $d\epsilon_l^p$, etc., are the increments of plastic strain. Then, if $d\epsilon_l$ and $d\epsilon_l^e$ are the increments of total and elastic strain respectively,

$$d\epsilon_l = d\epsilon_l^e + d\epsilon_l^p, \text{ etc.} \tag{4.11}$$

From equations (4.9) and (4.11)

$$d\epsilon_l = d\epsilon_l^e \tag{4.12}$$

and therefore

$$\epsilon_l = \epsilon_l^e \tag{4.13}$$

Thus equation (2.8) holds in both the elastic and plastic regions, and ϵ_l is independent of r. In order to calculate ϵ_l and σ_l we note that the total axial force P on any section is

$$P = 2\pi \int_a^b r\sigma_l\,dr \tag{4.14}$$

Vol. 1
1960

By eliminating σ_l between equations (2.3) and (2.8) we find

$$\sigma_l = E\epsilon_l + \nu d(r^2\sigma_r)/r\,dr - \alpha ET \tag{4.15}$$

By substituting this value of σ_l into equation (4.14) and integrating we find

$$P = \pi E\epsilon_l(b^2-a^2) + 2\pi\nu(b^2 p_o - a^2 p_i) - 2\pi\alpha E\int_a^b Tr\,dr \tag{4.16}$$

If the axial force is known, then ϵ_l is easily calculated. The most useful three cases are plane strain, $\epsilon_l = 0$; open-end tube, $P = 0$; and closed-end tube, $P = \pi(a^2 p_i - b^2 p_o)$. Thus, knowing ϵ_l from equation (4.16) and the axial force, and σ_r and $d\sigma_r/dr$ from equations (4.6), (4.8) and the appropriate boundary conditions, σ_l can be calculated using (4.15).

(v) *Partly plastic strain-hardening vessels.* In order to investigate a strain-hardening vessel it is necessary to calculate the plastic strain. This has been done by Bland[9]. It was assumed that the strain-hardening is a function of the equivalent plastic strain $\bar{\epsilon}^p$ defined by the equation

$$\bar{\epsilon}^p = \int d\epsilon^p = \sqrt{\frac{2}{3}}\int\{(d\epsilon_l^p)^2 + (d\epsilon_r^p)^2\}^{\frac{1}{2}} \tag{4.17}$$

Since, by equation (4.10) $d\epsilon_r^p = -d\epsilon_l^p$, equation (4.17) becomes

$$\bar{\epsilon}^p = \frac{2}{\sqrt{3}}\int|d\epsilon_l^p| \tag{4.18}$$

If $d\epsilon_l^p$ has the same sign throughout the deformation, then

$$\bar{\epsilon}^p = \frac{2}{\sqrt{3}}\epsilon_l^p \tag{4.19}$$

The value of ϵ_l^p can be obtained as follows. Since the dilation is purely elastic, then

$$\frac{du}{dr} + \frac{u}{r} + \epsilon_l = \frac{1-2\nu}{E}(\sigma_r + \sigma_t + \sigma_l) + 3\alpha T \tag{4.20}$$

On integration u is obtained, and from the relation $\epsilon_t = u/r$ we find ϵ_t. The plastic strain component ϵ_l^p is obtained by subtracting the elastic component and introducing the condition that in the plastic region $rd\sigma_r/dr = \sigma_y$, where σ_y may be a function of $\bar{\epsilon}^p$. We find

$$\epsilon_l^p = \frac{1-\nu^2}{E}\sigma_y - \alpha(1+\nu)\left\{\frac{2}{r^2}\int_a^r Tr\,dr - T\right\} + \frac{C}{r^2} \tag{4.21}$$

where C is a constant to be determined by the condition that the plastic strains are zero at the elastic–plastic boundary. From equation (4.17) $\bar{\epsilon}^p$ is $2/\sqrt{3}$ times equation (4.21). Since σ_y is a known function of $\bar{\epsilon}^p$ then equation (4.21) allows σ_y and $\bar{\epsilon}^p$ to be completely determined.

4.2. *Steady-state temperature distribution*

The steady-state temperature distribution is

$$T = T_i - \Delta T\frac{\ln r/a}{\ln k} \tag{4.22}$$

By inserting this into equations (4.1)–(4.3) we find that the stresses in a wholly elastic vessel are

$$\sigma_r = -\frac{p_i}{k^2-1}\left(\frac{b^2}{r^2}-1\right)-\frac{p_o k^2}{k^2-1}\left(1-\frac{a^2}{r^2}\right) - \tfrac{1}{2}\beta\left\{\frac{k^2}{k^2-1}\left(1-\frac{a^2}{r^2}\right)-\frac{\ln r/a}{\ln k}\right\}, \tag{4.23}$$

$$\sigma_t = \frac{p_i}{k^2-1}\left(\frac{b^2}{r^2}+1\right)-\frac{p_o k^2}{k^2-1}\left(1+\frac{a^2}{r^2}\right) - \tfrac{1}{2}\beta\left\{\frac{k^2}{k^2-1}\left(1+\frac{a^2}{r^2}\right)-\frac{\ln r/a}{\ln k}-\frac{1}{\ln k}\right\}, \tag{4.24}$$

$$\sigma_l = \frac{p_i - p_o k^2}{k^2-1} - \beta\left\{\frac{k^2}{k^2-1}-\frac{\ln r/a}{\ln k}-\frac{1}{2\ln k}\right\} \tag{4.25}$$

(i) *Failure of brittle vessels.* For simplicity we consider a vessel with internal pressure only. It is readily seen from equations (4.23)–(4.25) that the maximum principal pressure stress is always the bore tangential stress, and the maximum principal thermal stress is also the bore tangential stress. If the stress first reaches the fracture stress at the bore, fracture will occur at the pressure p_{iu} given by

$$\sigma_u = p_{iu}\frac{k^2+1}{k^2-1}-\beta\left\{\frac{k^2}{k^2-1}-\frac{1}{2\ln k}\right\} \tag{4.26}$$

This rearranges to give

$$\frac{p_{iu}}{\sigma_u} = \frac{k^2-1}{k^2+1}+\frac{\beta}{\sigma_u}\left\{\frac{k^2}{k^2+1}-\frac{k^2-1}{2(k^2+1)\ln k}\right\} \tag{4.27}$$

If the pressure and thermal stresses at the bore act in opposite directions the vessel may withstand a greater pressure if thermal stresses are present than if they are absent. However, it will usually be unwise to make use of this in design, because the vessel may have to withstand both pressure and temperature stresses separately as well as together. In the absence of thermal stresses the bursting pressure is

$$\frac{p_{iu}}{\sigma_u} = \frac{k^2-1}{k^2+1} \tag{4.28}$$

The maximum values of β and γ are those that will cause fracture. These are obtained by putting $p_{iu} = 0$ in equation (4.27) to give

$$\max\frac{\beta}{\sigma_u} = -\left\{\frac{k^2}{k^2-1}-\frac{1}{2\ln k}\right\}^{-1} \tag{4.29}$$

If the stresses are of opposite sign at the inside surface they will have the same sign at the outside surface, and so fracture may occur there. However, it can be shown that if the pressure and temperature differences are less than those given by equations (4.28) and (4.29) then fracture will never occur at the outer surface. Design curves based on equation (4.27) and the corresponding equations involving γ instead of β are given by Whalley[12].

Luster[15] has shown that for a given internal pressure and steady-state heat transfer there is a value of k that gives a minimum value of the maximum

Vol. 1
1960

principal stress at the bore, and suggested that this be used for design. It is probably better to ensure that the stresses are everywhere below a given value.

(ii) *Failure of ductile vessels.* As with spherical vessels,[13] the position of maximum stress can be anywhere in the wall, and a detailed discussion would follow similar lines to Derrington and Johnson's. If the vessel must be able to withstand both thermal and pressure stresses alone, then the results are fairly simple. The pressure difference must be less than the yield pressure Δp_y in the absence of thermal stress,

$$\frac{\Delta p_y}{\sigma_y} = \pm \frac{k^2-1}{2k^2} \tag{4.30}$$

and the maximum temperature difference must be less than the yield temperature difference,

$$\frac{\beta_y}{\sigma_y} = \mp \left\{ \frac{k^2}{k^2-1} - \frac{1}{2\ln k} \right\}^{-1} \tag{4.31}$$

Under these conditions, yielding always occurs first at the inside surface at a pressure difference given by

$$\frac{\Delta p_y}{\sigma_y} = \pm \frac{k^2-1}{2k^2} + \frac{\beta}{\sigma_y}\left\{ \frac{1}{2} - \frac{k^2-1}{4k^2 \ln k} \right\} \tag{4.32}$$

The yield pressure according to equation (4.32) can be obtained from the shakedown pressure plotted in Figs. 4–6 of Ref. 12 by means of the relation

$$\frac{\Delta p_y}{\sigma_y} = \frac{\Delta p_s}{\sigma_y} - \frac{1}{2}\frac{\Delta p_s^0}{\sigma_y} \tag{4.33}$$

where Δp_s^0 is the shakedown pressure in the absence of thermal stresses.*

(iii) *Partly plastic non-strain-hardening vessels.* The radial and tangential stresses in both the elastic and plastic regions are easily obtained from the equations and boundary conditions in subsections (4.1) (i) and (iv) and the temperature distribution, equation (4.22). (See Whalley[12] and Bland[9].) It is found that, in the elastic region when the elastic–plastic boundary is at radius ρ

$$\sigma_r = -\tfrac{1}{2}\sigma_y \frac{\rho^2}{b^2}\left(\frac{b^2}{r^2}-1\right) + \frac{\beta}{2\ln k}\left\{ \frac{1}{2}\frac{\rho^2}{b^2}\left(\frac{b^2}{r^2}-1\right) - \ln\frac{b}{r} \right\} - p_o \tag{4.34}$$

$$\sigma_t = \tfrac{1}{2}\sigma_y \frac{\rho^2}{b^2}\left(\frac{b^2}{r^2}+1\right) - \frac{\beta}{2\ln k}\left\{ \frac{1}{2}\frac{\rho^2}{b^2}\left(\frac{b^2}{r^2}+1\right) + \ln\frac{b}{r} - 1 \right\} - p_o \tag{4.35}$$

where $\rho \leqslant r \leqslant b$, and, in the plastic region,

$$\sigma_r = \sigma_y \ln r/a - p_i \tag{4.36}$$

$$\sigma_t = \sigma_r + \sigma_y \tag{4.37}$$

where $a \leqslant r \leqslant \rho$. By equating at $r = \rho$ the values of σ_r from equations (4.34) and (4.35), the pressure required to extend the plastic–elastic radius to ρ is shown to be given by

$$\frac{\Delta p}{\sigma_y} = \ln\frac{\rho}{a} + \frac{1}{2}\left(1-\frac{\rho^2}{b^2}\right) - \frac{\beta}{2\sigma_y \ln k}\left\{ \frac{1}{2}\left(1-\frac{\rho^2}{b^2}\right) - \ln\frac{b}{\rho} \right\} \tag{4.38}$$

* Equations (2.18) and (3.31) of Ref. 12 are in error.

This is easily arranged for ease of computation to

$$\frac{\Delta p/\sigma_y - \ln k}{1 - \frac{1}{2}\beta/\sigma_y \ln k} = \frac{1}{2}\left(1 - \frac{\rho^2}{b^2}\right) + \ln\frac{\rho}{b} \tag{4.39}$$

A graph of the right-hand side of equation (4.39) against ρ/b readily enables the left-hand side to be obtained for any value of ρ/b, or ρ/b to be obtained for any value of the thermal and pressure stresses. Such a graph is given by Prager and Hodge[16].

The shakedown pressures are readily calculated.[12] If the vessel must be able to withstand thermal and pressure stresses separately, then the maximum pressure is related to the shakedown pressure in the absence of thermal stresses

$$\frac{\Delta p_s}{\sigma_y} = \frac{k^2 - 1}{k^2} \tag{4.40}$$

and the maximum temperature difference (or heat-transfer rate) to the value of β for shakedown β_s, in the absence of pressure stresses,

$$\frac{\beta_s}{\sigma_y} = \left(\frac{k^2}{k^2 - 1} - \frac{1}{2\ln k}\right)^{-1} \tag{4.41}$$

It can be shown that if the pressure and temperature differences are less than given by equations (4.40) and (4.41) then shakedown will occur at the bore under the load

$$\frac{\Delta p_s}{\sigma_y} = \frac{k^2 - 1}{k^2} + \frac{\beta}{\sigma_y}\left(1 - \frac{k^2 - 1}{2k^2 \ln k}\right) \tag{4.42}$$

Charts of equation (4.42) are given by Whalley[12].

(iv) *Partly plastic strain-hardening vessels.* Bland[9] has discussed the theory of a strain-hardening vessel in which the material hardens according to the linear law

$$\sigma_y = \sigma_{yo}(1 + \eta\bar{\epsilon}^p) \tag{4.43}$$

Bland shows that the pressure difference required to cause the plastic–elastic boundary to progress from radius a to radius ρ is

$$\frac{\Delta p}{\sigma_{yo}} = \left(\frac{\Delta p}{\sigma_y}\right)_{\eta=0} + \phi\left\{\frac{1}{2}\left(\frac{\rho^2}{a^2} - 1\right) - \ln\frac{\rho}{a}\right\} \tag{4.44}$$

where $(\Delta p/\sigma_y)_{\eta=0}$ is given by equation (4.38), and

$$\phi = (1 + \beta/\sigma_{yo} \ln k)\{1 + \sqrt{(3)}\, E/2\eta\, \sigma_{yo}(1 - \nu^2)\}^{-1} \tag{4.45}$$

The stresses remaining when the load is removed, both with and without further plastic flow, were investigated numerically for a few special cases. Shakedown was not investigated. This would be quite complex in the general case because, if each cycle of plastic flow increases the hardness, then many cycles will have to be followed in order to obtain a general answer. The theory is restricted to small strains and is not suitable for investigating accurately the ultimate pressure of a strain-hardening vessel.

It can be said then that, though the non-strain-hardening vessel is reasonably well understood, and any condition not so far discussed explicitly can probably be discussed, at the cost of some algebra, in sufficient detail to facilitate the design of a vessel, the theory of the strain-hardening vessel requires a great deal more work before the effect of the strain-hardening on the performance can be calculated with reasonable completeness.

Vol. 1
1960

4.3 *Thermal shock*

Whalley and Mackinnon[17] have investigated pressure vessels subjected to thermal shock at either the inside or the outside surfaces. The principles are similar to those described above, and for details the original paper should be consulted.

4.4 *Multilayer vessels*

The design of multilayer pressure vessels that are at uniform temperature has been discussed by Manning,[18,19] who used the criterion that the maximum value under load of the maximum shear stress within each layer is the same for all layers. He showed that the diameter ratio should be the same for each component cylinder, and that the required interference per unit radius is constant for a given vessel. Manning's theory has been extended[20] to include thermal as well as pressure stresses. In a multilayer vessel residual stresses are intentionally formed, usually by shrinkage, in order to increase the elastic range of the vessel under the required load. Consequently, plastic flow does not usually occur and only elastic deformations need be considered.

It was shown that for a vessel with layers made of similar material subjected to pressure and to steady-state thermal gradients:

(i) all components have the same radius ratio;

(ii) the interference, δ, between each component calculated from the dimensions before assembly, is

$$\delta = 2(\Delta p - \tfrac{1}{2}\beta)/mE \tag{4.46}$$

(iii) the maximum shear stress $\tau_{\max}$ within each component is at the inner surface and is

$$\tau_{\max} = \left| \Delta p \frac{k^{2/m}}{m(k^{2/m}-1)} - \tfrac{1}{2}\beta\left\{\frac{k^{2/m}}{m(k^{2/m}-1)} - \frac{1}{2\ln k}\right\}\right| \tag{4.47}$$

where k is the radius ratio of the whole vessel;

(iv) the maximum residual, maximum shear stress obtained when no pressure or thermal stresses are present is at the inner wall of the inner component and is

$$\tau_{R_{\max}} = (\Delta p - \tfrac{1}{2}\beta)\left(\frac{k^2}{k^2-1} - \frac{k^{2/m}}{m(k^{2/m}-1)}\right) \tag{4.48}$$

if $\Delta p > \frac{1}{2}\beta$. The stresses given by equations (4.47) and (4.48) must, of course, be less than the shear yield stress of the material. If $\Delta p < \frac{1}{2}\beta$ there are no residual stresses because the components are not in contact. This is easily seen from equation (4.46) because under such conditions the interference is negative, i.e. is a clearance. There are some complications; it may be that the stresses are a maximum when pressure alone is applied or when the thermal gradient alone is applied. For further details see the original paper.

5. SOME PROBLEMS THAT REMAIN

A start on the problems of elastic–partly-plastic vessels has been made, though there is still much to be done that may be of interest to the designer. In particular, little has been done explicitly to calculate the displacements in the plastic region; and other temperature distributions may be important. It

seems unlikely that the theory of a solid that yields ideally according to von Mises's theory will be of enough interest to the designer to compensate for the complexity, though it may be interesting for other reasons. Some of the assumptions made in Section 2.1 are not always reasonably valid, and if large temperature differences are encountered then the variation of the physical properties of the material with temperature may be important. It is not unlikely that vessels will be operated such that the hotter parts are in the creep region and the cooler parts in the elastic–plastic region, and the theories of the behaviour of these vessels would be interesting. The effect of stress-raisers such as side openings may frequently be important.

Probably the most important theoretical problems at the present time concern work-hardening vessels. The ground-work of a fairly simple treatment has been laid, but the difficulties of following this through several cycles of the load until cycling causes no further work-hardening are formidable. Numerical work on any scale will probably rely upon electronic computers.

Vol. 1
1960

The effect of thermal stresses on the ultimate pressure of a work-hardening vessel is not known, neither has it been calculated for a non-work-hardening vessel in which the strains are not small compared with the dimensions of the vessel. Little work has been reported on the failure of pressure vessels by fatigue due to elastic stresses, and the effect of thermal stresses has not been taken into account at all.

Finally, in all this field there is no experimental work; this is badly needed to confirm or disprove the theoretical formulas.

REFERENCES

1. A. Nadai, *Theory of Flow and Fracture of Solids* (2nd Ed.). McGraw-Hill, New York (1951).
2. G. Cook and A. Robertson, *Engineering, Lond.* **92**, 786 (1911).
3. W. C. Popplewell, *Owen's College Calendar*, Appendix p. cclxix (1890).
4. G. Cook, *J. Instn. Mech. Engrs.* **126**, 407 (1934).
5. M. C. Steele and J. Young, *Trans. Amer. Soc. Mech. Engrs.* **74**, 355 (1952).
6. J. M. C. Morrison, *Proc. Inst. Mech. Engrs., Lond.* **159**, 81 (1948).
7. A. G. Warren, *Symposium on Internal Stresses in Metals and Alloys.* Institute of Metals (London) Monograph and Report Series No. 5, 209 (1948).
8. J. H. Faupel, *J. Franklin Inst.* **259**, 405 (1955).
9. D. R. Bland, *J. Mech. Phys. Solids* **4**, 209 (1956).
10. S. Timoshenko and J. N. Goodier, *Mathematical Theory of Elasticity* (2nd Ed.). McGraw-Hill, New York (1951).
11. E. Whalley, *Canad. J. Tech.* **34**, 268 (1956).
12. E. Whalley, *Canad. J. Tech.* **34**, 291 (1956).
13. M. G. Derrington and W. Johnson, *Appl. Sci. Res., Hague* A **7**, 408 (1958).
14. J. Kern, *Z. angew. Chem.* **3**, 321 (1951).
15. E. W. Luster, *Trans. Amer. Soc. Mech. Engrs.* **53**, 161 (1931).
16. W. Prager and P. G. Hodge, *Theory of Perfectly Plastic Solids* p. 106. John Wiley, New York (1951).
17. E. Whalley and R. F. Mackinnon, *Int. J. Mech. Sci.* **1**, 301 (1960).
18. W. R. D. Manning, *Engineering, Lond.* **163**, 349 (1947).
19. W. R. D. Manning, *Engineering, Lond.* **170**, 462 (1950).
20. E. Whalley and S. Morris, *Int. J. Mech. Sci.* **1**, 366 (1960).

Int. J. Mech. Sci. Pergamon Press Ltd. 1960. Vol. 1, pp. 396–397. Printed in Great Britain

LETTERS TO THE EDITOR

On the response of the singly free linear oscillator

(*Received* 18 *October* 1959)

CONSIDER the linear oscillator of Fig. 1 excited into harmonic motion by the sinusoidally varying displacement of the anchored end A of its spring mount

$$\left.\begin{aligned} m\ddot{x}+k(x-y)&=0\\ y&=y_0\cos\omega_1 t.\end{aligned}\right\} \tag{1}$$

Let this system be in motion at some frequency higher than resonant: then the response x will be antiphase to the movement y of the foundation. Since both ends of the spring are therefore in motion, there must exist a node somewhere within the spring [Fig. 2(a)]. Without change in the result, the spring may then hypothetically be thought to be separated at the node, and mounted there rigidly [Fig. 2(b)].

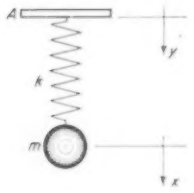

FIG. 1.

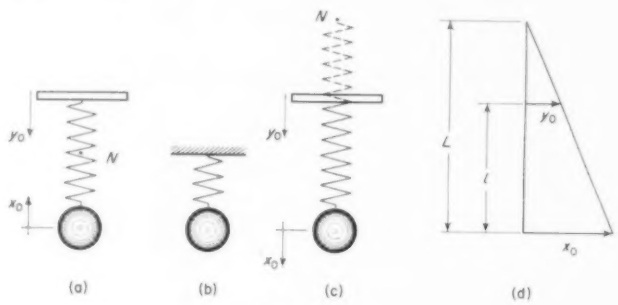

FIG. 2.

Can we still say the mass m is oscillating on a spring of stiffness k? The effectively shorter spring has a greater stiffness. The natural frequency may be regarded as a variable dependent on the node location.

Below resonance, mass and support move in phase together, but with different amplitudes. To locate the node here [Fig. 2(c)], an imaginary extension of the spring must be envisaged. To figure the spring stiffness in this case, the location of the node is reckoned from the proportion of the amplitudes of the motions x and y. Thus from the triangle [Fig. 2(d)], where l is the static length of the spring, and L the distance to the node

$$\frac{L}{l}=\frac{x_0}{x_0-y_0}.$$

Since

$$x_0=\frac{y_0}{1-(\omega_1/\omega_0)^2}\quad\text{(in which }\omega_0^2=k/m\text{)}$$

$$\frac{L}{l}=\left(\frac{\omega_0}{\omega_1}\right)^2.$$

The frequency of the mass m upon the effective spring of length L and stiffness k_1 is

$$\omega = \left(\frac{k_1}{m}\right)^{\frac{1}{2}} = \left(\frac{l}{L}\frac{k}{m}\right)^{\frac{1}{2}} = \left(\frac{\omega_1}{\omega_0}\right)\omega_0 = \omega_1.$$

Thus the position of the node continually shifts with changing excitation frequency in such a way that the natural frequency ω of the spring-mass system (measured from the node) agrees with its stimulating frequency.

As the frequency increases from nothing to resonant, the node, starting from a point infinitely far above, moves downward until it reaches point A. With further increase, it continues to move down, tending to reach the mass itself as the palpitation becomes exceedingly quick.

In every actual system the spring itself has mass, and the system discussed above is oversimplified. If a consideration of the spring's distributed mass is included, however, the conclusions above need be only slightly modified. At low speeds below the first resonant frequency, the node as before travels downward from the sky to the level A, as the stimulating frequency increases. Then, as the pulse quickens, the node continues to fall until, at the tempo defined as the second natural frequency, it reaches a point which may be calculated as the node location for this node by use of the partial differential equation. Thereafter this node continues downward as in the simplified theory. But a second node is to be observed, which first appears at the top and then, with the increasing beat of the stimulus, follows the first node downward. In succession then, more nodes arrive as eigenvalues are exceeded; but always the natural frequencies of both the segments of spring between its nodes and its end with the terminal mass are in agreement with each other and with the excitation.

F. R. E. Crossley
Ü. Germen

Yale University
New Haven
Connecticut

Vol. 1
1960

Comment on "Small vibrations of thin incomplete circular rings"

(*Received* 29 *March* 1960)

The paper by R. R. Archer (Small vibrations of thin incomplete circular rings, Vol. 1, p. 45) is an excellent example of the use of the separation-of-variables technique for solving a linear differential equation. However, I would like to point out that this technique can only be applied to the above problem when the damping coefficients for transverse and longitudinal motion of the ring element are equal. While it is mathematically legitimate to *assume* their equality in order to obtain a simple solution, this assumption can hardly correspond to reality.

R. I. Tanner

Mechanical Engineering Department
University of Manchester

Int. J. Mech. Sci. Pergamon Press Ltd. 1960. Vol. 1, pp. 398–400. Printed in Great Britain

BOOK REVIEWS

CHARLES DONALD SWIFT: **Steam Power Plants.** McGraw-Hill, New York, 1959. 100 pp., 89s.

THIS is a book which will appeal primarily to those who are concerned with the planning and operation of power stations.

It is comprehensive in scope, almost too comprehensive to enable any single aspect of power station working or plant construction to be treated fully, covering as it does nearly every subject, from the character traits which are desirable in turbine drivers to the methods of preventing fires in partly erected wooden cooling towers. It would have added to the value of the book if a bibliography could have been included so that some of the issues treated could be explored at greater length in the appropriate specialized papers.

The emphasis is severely practical, and in the reviewer's estimate the book would be improved by the inclusion of a little more theory. Here and there one may find a rather half-hearted appeal to fundamentals. Thus in the paragraph on steam turbines a Mollier diagram is shown and its use is quite correctly described, but no state-point loci are shown on the diagram by way of illustration. The reasons given for the use of condensers could be much more graphically illustrated by its use. It would also be of value to illustrate the ideas of steam consumption and efficiency. It should be possible, without lengthening the book, to provide a chapter at the beginning on simple background theory.

On occasion the reader is annoyed by statements of the obvious, e.g. "Water is a very essential element in the production of steam . . ." and it should hardly be necessary to state, concerning the steam plant operator, "that he must be able to control his actions so that he remains in good physical condition and can come on shift at the proper time in fit condition to work his shift". Statements like the following should be erased at the manuscript stage: "Most plants have to make their own steam, so they get some sort of closed vessel, put water in it, and heat it until the water is turned into steam".

In spite of the above criticisms, the book is by no means without merit. The author clearly writes from a wide and useful experience and a great deal of valuable practical information is included—information of a type which space limitations tend to preclude from the more academic texts. As such it will be a useful reference book for anyone concerned with steam station practice, and provide background reading for students and apprentices.

The elimination of banalities and attention to suggestions such as those given above would make a future edition a valuable book, in so far that it fills a gap in the existing literature of the subject.

D. J. RILEY

A. C. WILSON: **Industrial Thermal Insulation.** McGraw-Hill, New York, 1959. 70s.

THE book has obviously been compiled by an engineer with much experience in many aspects of the uses of thermal insulation, and this has resulted in an excellent guide to the practical work of such installations. Detailed descriptions are given of applications as widely varied as cold rooms for food storage, underground pipelines, high-pressure steam lines and boilers, turbine plant, etc. In most cases simple but typical examples of the type of insulation being considered are examined theoretically and the results presented in a form which can be used without further calculations being required. This marriage of the practical and theoretical aspects of so many different types of insulation should make the book of value to both the designer and user, particularly to the latter.

Although it is of use to the designer, it is felt that the theoretical aspects of heat transmission are dealt with in such a generalized and possibly over-simplified manner that the solving of a novel type of insulation problem may need a much more fundamental approach than is described in the chapter labelled "Principles of Heat Insulation". For instance, the book's frontispiece states that a brief introduction is given to the insulation of rockets and missiles, but this is quite misleading as the "brief" introduction consists only of one paragraph. However, thermal problems of missiles are of such a specialized nature that a book of this size and nature could not pretend to describe or to discuss such

problems. For the everyday, down-to-earth insulation problems the theoretical treatment is adequate, and the economic considerations of lagging are presented clearly and simply. For the practical engineer (as distinct from the scientist), the author considers a discourse on Reynolds or Nusselt numbers unwarranted, and these vital factors are never mentioned again. For a practical guide book of this kind the author's approach is probably the best one—after all there are many, many books on the "scientific" aspects of heat transmission already available.

One chapter which could be of great help to the design engineer is that giving typical specifications of twenty-six different applications of insulation. These are quite detailed and could be copied direct on to a firm's order form.

To the reviewer the book represents the condensation into one volume of the information at present contained in the scattered catalogues of several different commercial firms, plus several text-books, plus recommendations from the commercial and financial experts, and it can be recommended as a useful addition to any engineer's library.

A. Williams

T. M. Charlton: **Energy Principles in Applied Statics**. Blackie, Glasgow, 1959. 112 pp., 25s.

This is a book intended for engineers and, from its form, more particularly for students of structural engineering.

There are almost as many methods of structural analysis as there are structural engineers, and most practising engineers recognize several, while exhibiting a facility in one particular method (with personal short cuts) which enables them to convince themselves that the method is "best". Building codes too have been formulated in such a way that safe designs should arise from standard methods and economies have arisen mainly from standardization of fabrication. The underlying assumptions of such analyses have, for a long time, been forgotten, except in the aircraft industry where non-uniform shapes and unit design have shown the need for a more exact approach and where stress-office mechanization has opened the way for methods using purely automatic computation. In the last few years, "programmes" for digital computers have been prepared which permit the exact analysis of building structural frameworks, frequently including automatic stability checks and allowance for variation of stiffness with load. On the other hand, this has lately been matched by work in the universities to tabulate the main branches of structural analysis in a sort of family tree. The coincidence of these facts has led to considerable emphasis being laid recently on the basic ideas of energy, strain, complementary, potential and total.

Where before the primary need was for rapid methods based on approximation to conditions and a developed structural sense, it is obvious that nowadays it is essential to examine the structural assumptions much more carefully, since the computations are most likely to be carried out automatically, and structures are designed which appear to fall outside the scope of normal building codes.

This book covers in detail the derivation of ideas of energy in static systems and how various elementary concepts may be applied to the analysis of structures. In choosing for analysis a number of problems which are solved by strain and potential energy, by virtual work and by complementary energy, the differences, the advantages and the basic assumptions of each method are most clearly defined. Generally speaking, non-linear systems are not analysed, though characteristics which lead to non-linearity are clearly underlined so that the student is fully aware of the implications of non-linearity.

The last chapter of the book shows the development of flexibility coefficients and of stiffness coefficients and wherein the advantages of each lie. Unfortunately, the solution of the subsequent equations by matrices, the basis of computer work, is omitted, though, with the equations established, this may not have been thought necessary.

These energy principles are available in standard works, more briefly explained and often in a generalized form suitable for elasticians interested in non-linearity. But students of structural engineering will find a much fuller explanation in this book, suitably graded for study. They are also unlikely to encounter problems of a type whose solution is not contained here.

M. G. Derrington

Vol. 1
1960

R. S. PARADISE and G. A. CHURCH: **Problems in Strength of Materials**. Blackie, Glasgow, 1959. 278 pp., 25s.

THE authors claim to have covered in this book the syllabus for an engineering degree and for the examination of the Institution of Mechanical Engineers. They have taken sixteen chapter headings under which to provide 368 questions with 108 worked answers, the rest of the answers being given in the back of the book.

The examples are worked in considerable detail, but the usefulness of the book to students would have been increased by one or two pages in each chapter summarizing the facts and formulae required. Most of the questions are of a practical rather than a fundamental nature, seeming of more interest to technical college than university teachers. It is difficult to judge the full scope of this type of book, but most universities require a greater knowledge of such topics as membrane action, temperature stresses, torsion of various sections and some others than there is room for in this compact volume.

M. G. DERRINGTON

J. CLENDINNING: **Principles and Use of Surveying Instruments** (2nd Ed.). Blackie, Glasgow, 1959. 205 pp., 25s.

THERE has been something of a decline in the regard for surveying as a discipline in our schools of engineering during the past twenty years or so. At the same time, none of the recent innovations in surveying-instrument design is British in origin. It is perhaps going too far to suggest that there is any strong relationship here, but the former state of affairs may have some influence on the latter.

Many of the recent developments on the instrument side have been almost exclusively the work of the physicist or the optical scientist, while research into aerial surveying techniques is costly. Surveying as a whole does not appear to be such a fruitful field for our civil engineering research workers as it was at the turn of the century, and one result of this has been a tendency to curtail the time given in the curricula to surveying. There is thus a growing need for lucidly written texts designed to amplify for the student those more practical aspects of the subject which must necessarily receive cursory treatment in restricted lecture programmes.

Mr. Clendinning has written such a book on surveying instruments and the relatively short time in which this primer has run to a second edition indicates its success. An extra chapter has been added describing some of the innovations of the past decade, viz. self-aligning levels, wedge telemeters, split-image tacheometers and electronic methods of measuring distance. No reference is made to the swinging-prism compensators for vertical-circle reading now being fitted to certain theodolites, but this omission may be due to the small amount of space available to the author. This may also account for the shortness of the extra chapter, which is a pity, since few people are more fitted to write on modern developments in surveying than the Editor of the Empire Survey Review. The new instruments are simply and clearly explained, however, and the additions will increase still further the merit of this second edition.

S. RAYMOND

Vol. 1
1960